Synthetic, kinetic and electrochemical aspects of ferrocene- and ruthenocene-containing titanium(IV) complexes with biomedical applications

A dissertation submitted in accordance with the requirements of the degree

Philosophiae Doctor

in the

Department of Chemistry

Faculty of Science

at the

University of the Free State

by

Elizabeth Erasmus

Supervisor

Prof. J.C. Swarts

November 2005

Dankbetuigings

Aan God Almagtig, dankie vir U onuitspreeklike genade, krag en wysheid wat my deur hierdie studie gedra het. Aan U alleen kom al die eer toe!
2 Kor. 12:7 My genade is vir jou genoeg. My krag kom juis tot volle werking wanneer jy swak is.

Ek wil graag my promotor, Prof. J.C. Swarts, bedank vir sy uitstekende leiding, ondersteuning en al sy kosbare tyd wat hy afgestaan het gedurende die verloop van die studie. Sy vriendelikheid, positiewe houding en aansteeklike entoesiasme, word opreg waardeer. Hy is 'n ware inspirasie.

Die skrywer bedank: Prof. C.E.J. Medlen van die Departement Farmakologie, Universiteit van Pretoria, vir die uitvoer van die sitotoksiese toetse en die opstel van die oorlewingsgrafieke. Dr. A.J. Muller van die Departement Chemie, Universiteit van die Vrystaat, vir die uitvoer en oplos van die kristal struktuur. Prof. M.J. Cook van die Departement Chemie van University of East Anglia, in England vir die beskikbaarheid van die DSC apparaat en Prof. J.C. Swarts van die Departement Chemie, Universiteit van die Vrystaat, vir die uitvoer van die vloeistof-kristal eksperimente.

My dank gaan ook aan al my vriende, die studente en personeel van die Chemie Departement vir al hulle bystand, belangstelling en hulp hoe gering dit ook al was.

Aan my familie, in besonder my ouers, baie dankie vir al die liefde, gebede en ondersteuning. Sonder julle was dit nie moontlik nie.

Die skrywer erken die NRF vir finasiële bystand.

Elizabeth (Lizette) Erasmus

2005

Contents

CONTENTS

CONTENTS

List of Abbreviations

A	absorbance
Å	angstrom
acac	acetyl acetonato $(CH_3COCHCOCH_3)^-$
$AlCl_3$	Aluminium trichloride
ArN_2^+	aryl or alkyl diazonium salt
BuLi	*n*-butyllithium
Cc	cobaltocenium $[(C_5H_5)_2Co]^+$
$CHCl_3$	chloroform
CH_2Cl_2	dichloromethane
CH_3CN	acetonitrile
CH_3OH	methanol
CO	carbon monoxide or carbonyl
cod	cyclooctadienyl
Cp	cyclopentadienyl $(C_5H_5)^-$
CV	cyclic voltammetry
δ	chemical shift
DCM	dichloromethane
DME	dimethoxyethane
dme	dropping mercury electrode
DMSO	dimethyl sulfoxide
D_O	diffusion coefficient of the oxidized specie
D_R	diffusion coefficient of the reduced specie
ε	molecular extinction coefficient
E	applied potential
E^{01}	formal reduction potential
E_a	energy of activation
E_{pa}	peak anodic potential
E_{pc}	peak cathodic potential
ΔE_p	separation of peak anodic and peak cathodic potentials
Et	ethyl
eq	equivalents
F	Faraday constant (96485.3 C mol^{-1})

LIST OF ABBREVIATIONS

LIST OF ABBREVIATIONS

Fc	ferrocene [$(C_5H_5)_2Fe$] or ferrocenyl [$Fe(C_5H_5)(C_5H_4)$]-
$Hg(OAc)_2$	mercury acetate
i_{pa}	peak anodic current
i_{pc}	peak cathodic current
k_2	second-order rate constant
k_b	Boltzmann constant (1.381×10^{-23} J K^{-1})
k_{obs}	observed rate constant
k_s	rate constant of solvation
LDA	lithium diisopropylamide
λ_{exp}	wavelength at maximum absorbance
M	central metal atom
Me	methyl
n	number of electrons
NaOH	sodium hydroxide
$[NBu_4][PF_6]$	tetrabutylammonium hexafluorophosphate
$[NBu_4][B(C_6F_5)_4]$	tetrabutylammonium tetrakis[pentafluorophenyl]borate
NHE	normal hydrogen electrode
^1H NMR	nuclear magnetic resonance spectroscopy
Hrca	1-Ruthenocenyl-4-methylprop-1,3-dione, [RcCOCH2COCH$_3$]
Hrctfa	1-Ruthenocenyl-4,4,4-trifluorobutan-1,3-dione, [RcCOCH2COCF$_3$]
Hrcbz	1-Ruthenocenyl-4-phenylprop-1,3-dione, [RcCOCH2COPh]
o	ortho
Oc	osmocene, $[(C_5H_5)_2Os]$
Ph	phenyl, (C_6H_5)
phen	1,10-phenanthroline
pK_a	-log K_a, K_a = acid dissociation constant
ppm	parts per million
R	gas constant (8.314 J K^{-1} mol^{-1})
Rc	ruthenocene, $[(C_5H_5)_2Ru]$
S	solvent
ΔS^*	entropy of activation
SCE	saturated calomel electrode
SHE	standard hydrogen electrode
T	temperature
THF	tetrahydrofuran

LIST OF ABBREVIATIONS

UV/Vis	ultraviolet/visible spectroscopy
ΔV^*	volume of activation
ν(C=O)	infrared carbonyl stretching frequency
X	halogen
χ_R	group electronegativity (Gordy scale) of R group

List of Structures

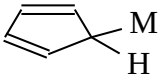

1

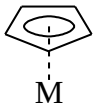

2

3

4

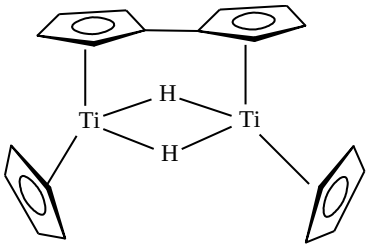

5

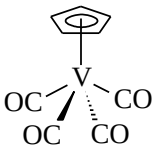

6

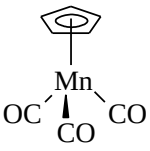

7

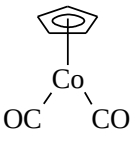

8

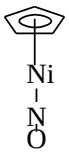

9

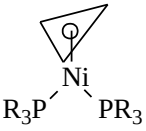

10

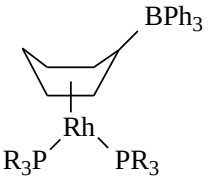

11

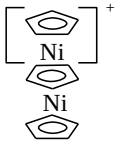

12

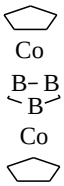

13

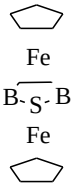

14

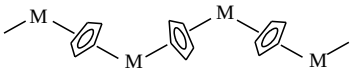

15

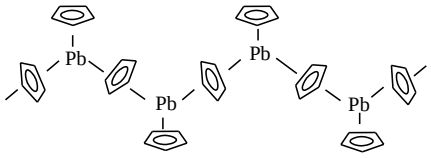

16

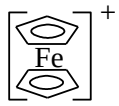

17

18

19

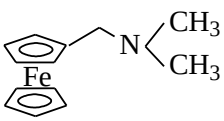

20

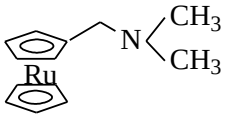

21

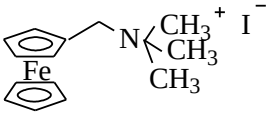

22

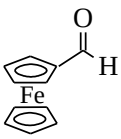

23

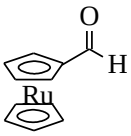

24

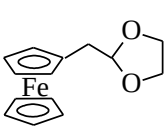

25

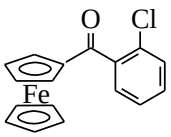

26

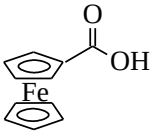

27

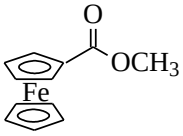

28

LIST OF STRUCTURES

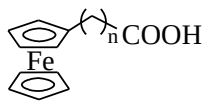

29 n = 0; 30 n = 1
31 n = 2; 32 n = 3

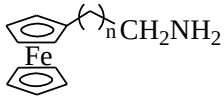

33 n = 0; 34 n = 1
35 n = 2; 36 n = 3

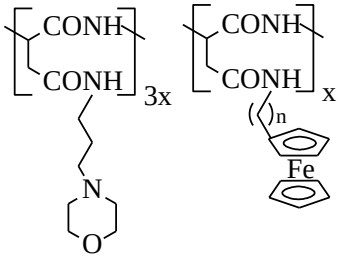

37 n = 0; 38 n = 1
39 n = 2; 40 n = 3

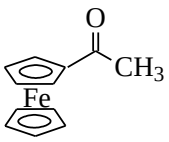

41

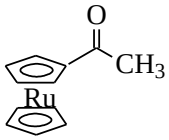

42

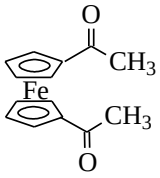

43

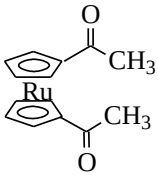

44

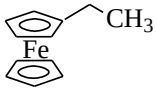

45

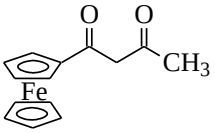

46

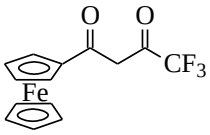

47

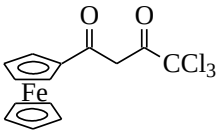

48

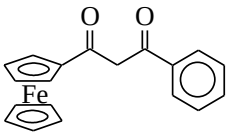

49

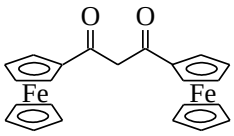

50

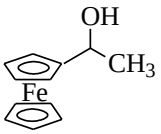

51

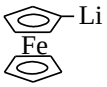

52

53

54

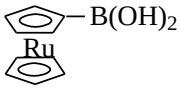

55

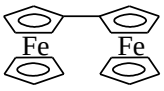

56

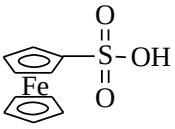

57

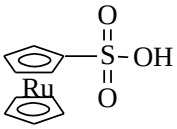

58

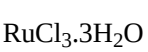

59

60

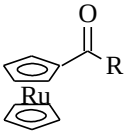

61

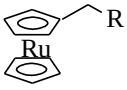

62

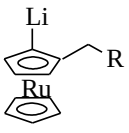

63

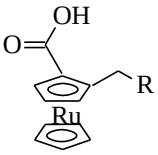

64

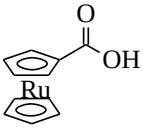

65

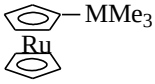

66

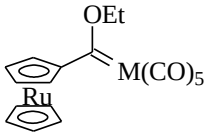

67

M = Si, Ge, Sn

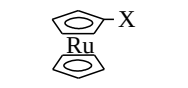

X = Cl, Br, I, OAc

68

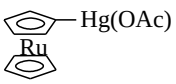

69

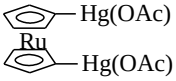

70

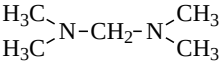

71

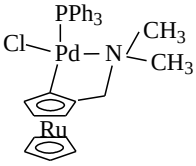

72

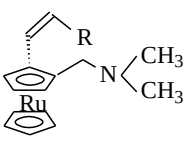

73

LIST OF STRUCTURES

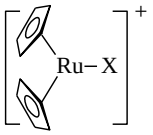

X = Cl, Br, I

74

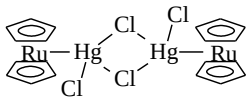

75

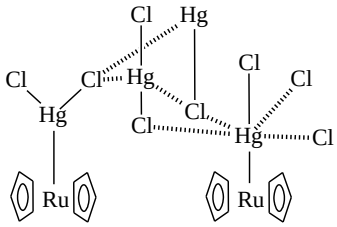

76

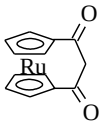

77

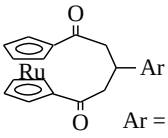

Ar = Ph, fc

78

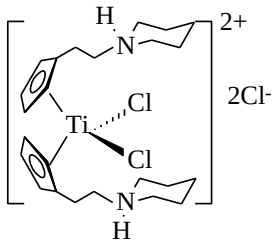

79

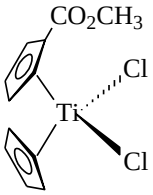

80

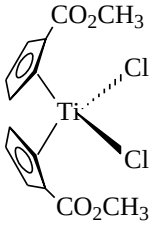

81

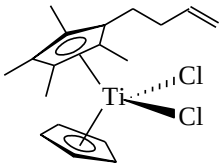

82

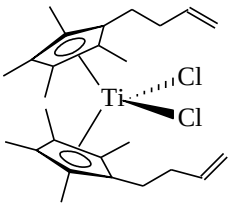

83

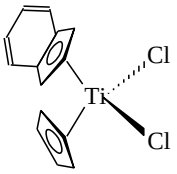

84

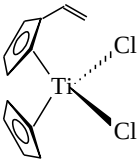

85

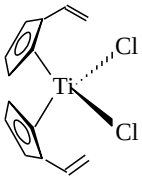

86

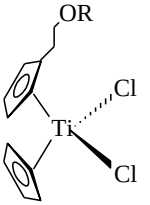

R = isobornyl, menthyl, fencyl and methyl

87

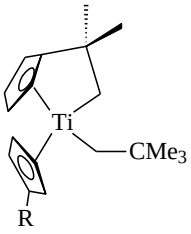

88

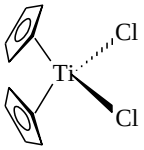

89

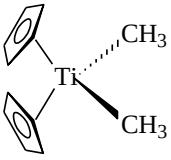

90

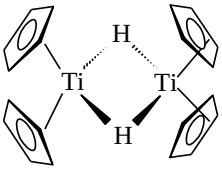

91

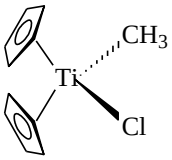

92

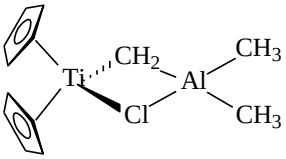

93

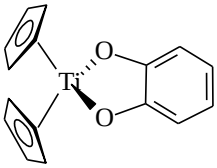

94

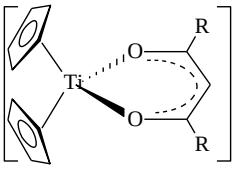

95

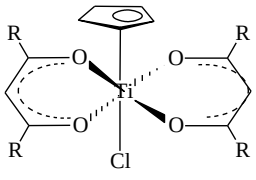

96

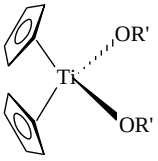

97

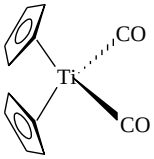

98

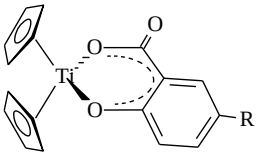

99 R = H, CHO, NH_2

LIST OF STRUCTURES

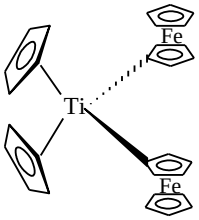

100

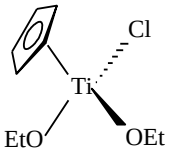

101

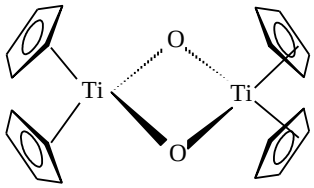

102

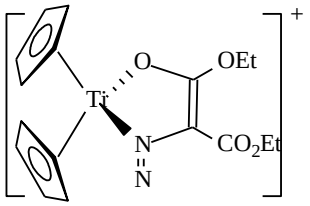

103

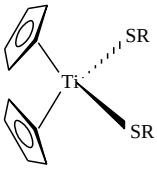

104

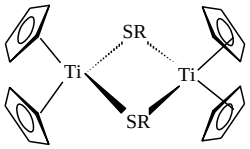

105

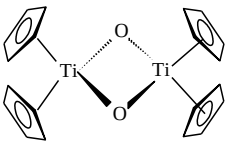

106

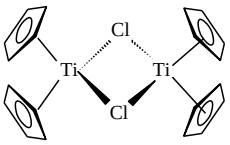

107

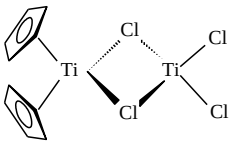

108

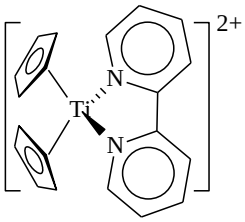

109

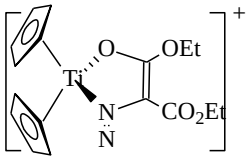

110

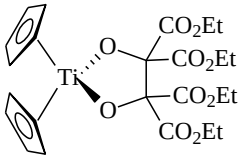

111

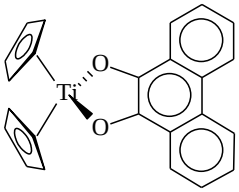

112

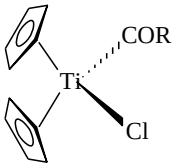

113

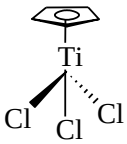

114

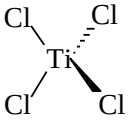

115

[CpTiCl(ASP)CpTiCl$_3$]

116

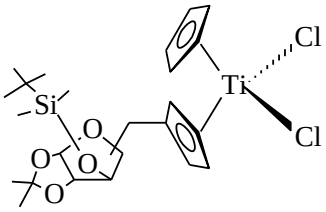

117

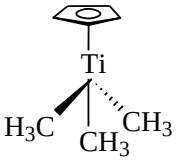

118

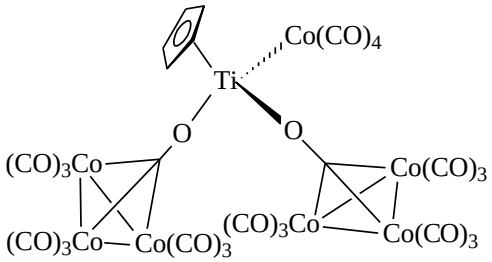

119

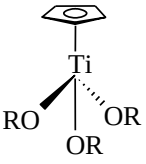

120

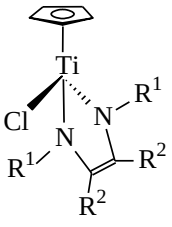

121

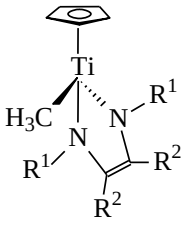

122

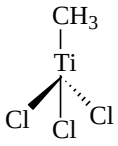

123

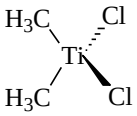

124

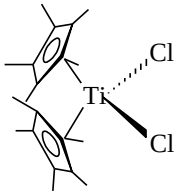

125

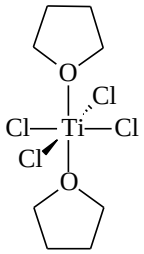

126

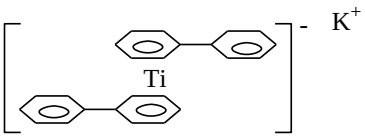

127

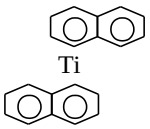

128

$[K(15\text{-Crown-}5)_2][Ti(C_{10}H_8)_2SnMe_3]$

129

$[NBu_4]_2[TiCl_6]$

130

$[NBu_4][\textit{trans}\text{-}TiCl_4(THF)_2]\cdot THF$

131

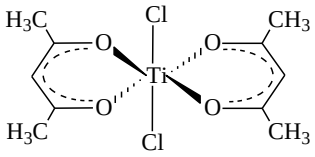

132

$[Ti(acac)_3][FeCl_4]$

133

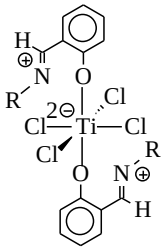

134

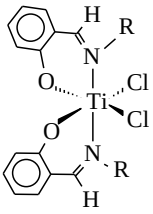

135

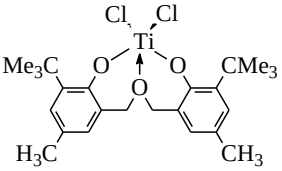

136

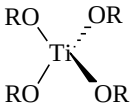

137

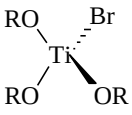

138

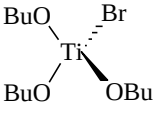

139

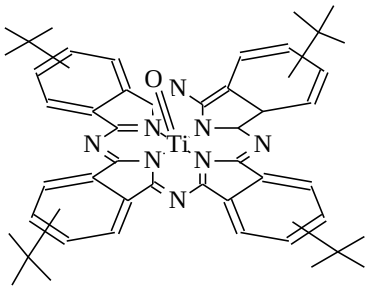

140

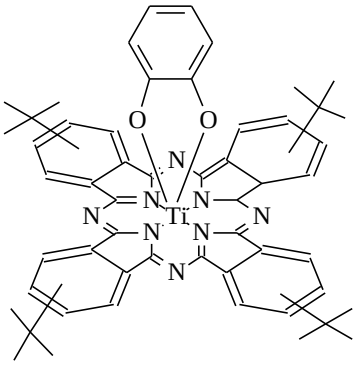

141

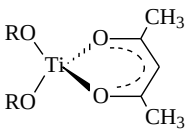

142

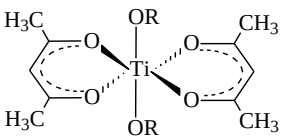

143

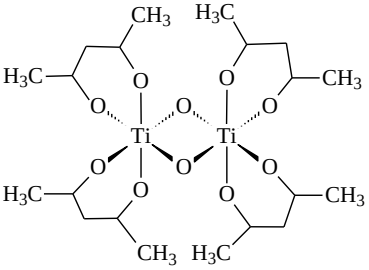

144

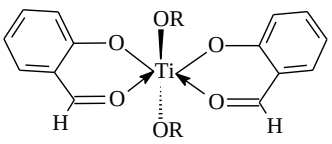

145

LIST OF STRUCTURES

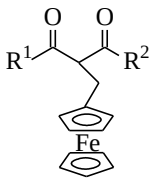

146

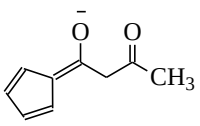

147

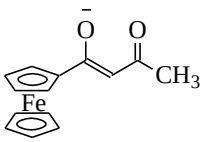

148

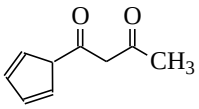

149

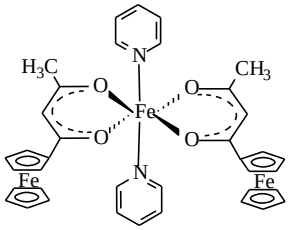

150

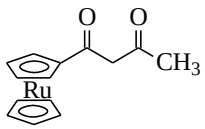

151

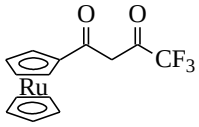

152

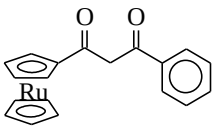

153

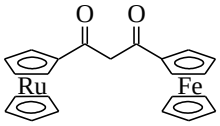

154

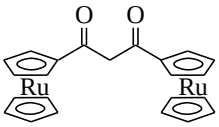

155

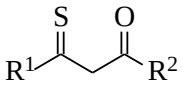

156

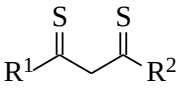

157

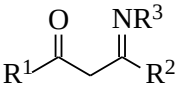

158

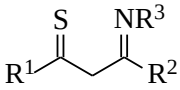

159

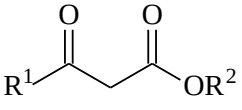

160

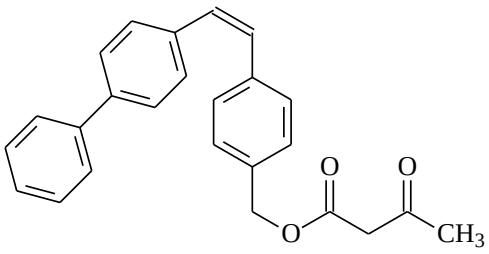

161

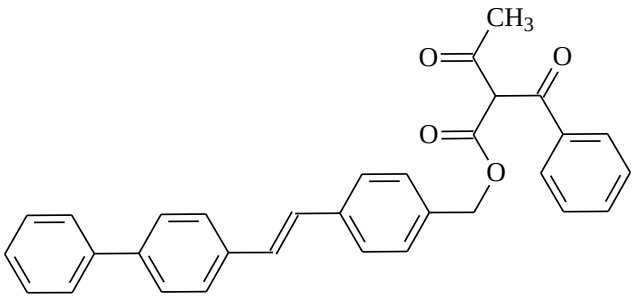

162

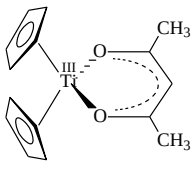

163

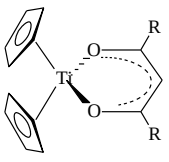

164

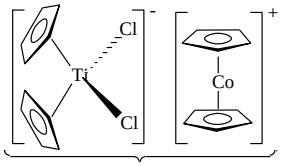

165

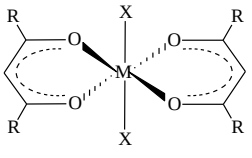

166

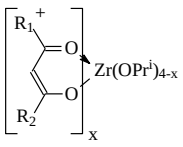

167

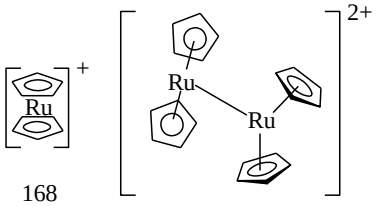

168

169

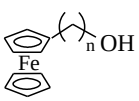

n = 1 (170), 2 (171),
3 (172) and 4 (173)

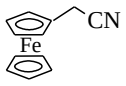

174

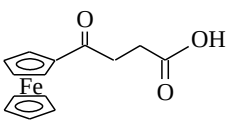

175

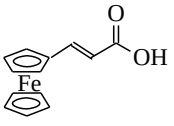

176

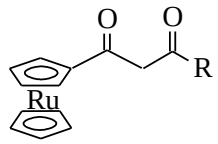

R = $C_{10}F_{21}$ (177), C_6F_5 (178) and $C_{10}H_{21}$ (179).

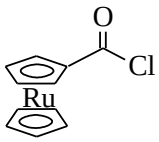

180

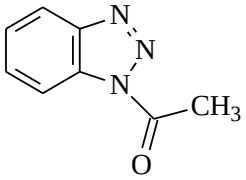

181

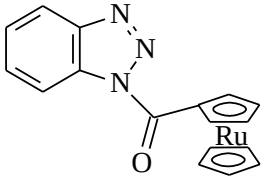

182

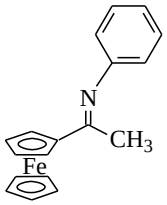

183

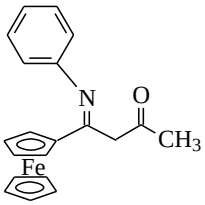

184

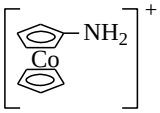

185

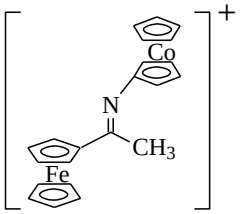

186

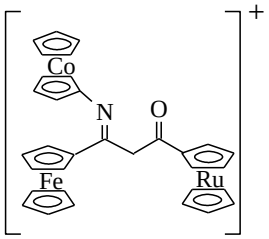

187

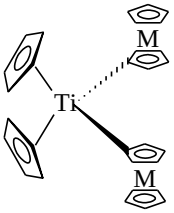

M = Fe (100)
Ru (188)
Os (189)

M = Fe (190)
Ru (191)
Os (192)

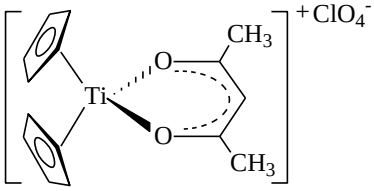

193

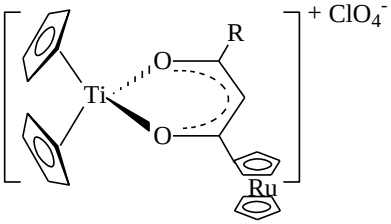

R = $C_{10}F_{21}$ (195), CF_3 (196), C_6F_5 (197), $C_{10}H_{21}$ (198), CH_3 (194), Rc (199) and Fc (200).

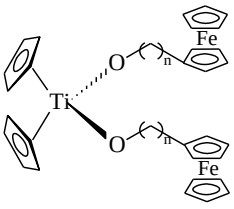

n = 1 (201), 2 (202)
3 (203), 4 (204).

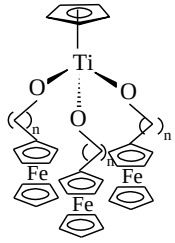

n = 1 (205), 2 (206)
3 (207), 4 (208).

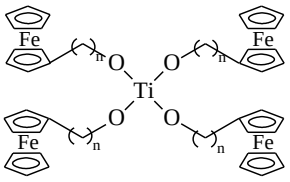

n = 1 (209), 2 (210)
3 (211), 4 (212).

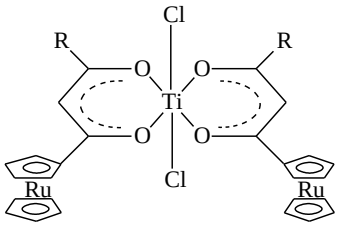

R = $C_{10}F_{21}$ (213), CF_3 (214), C_6F_5 (215), $C_{10}H_{21}$ (216), CH_3 (217), Rc (218) and Fc (219).

LIST OF STRUCTURES

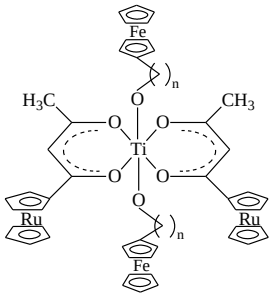

n = 1 (220), 2 (221), 3 (222), 4 (223)

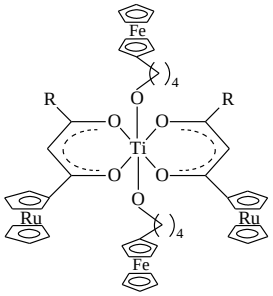

R = $C_{10}F_{21}$ (224), CF_3 (225), C_6F_5 (226), $C_{10}H_{21}$ (227), CH_3 (223), Rc (228) and Fc (229).

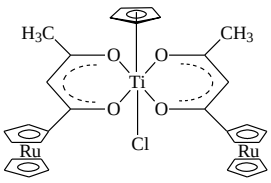

230

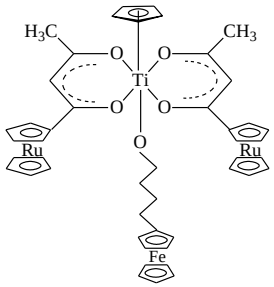

231

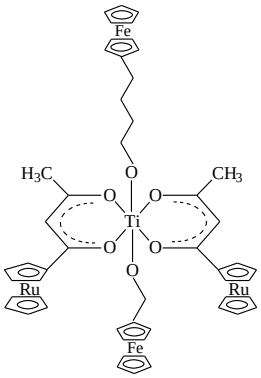

232

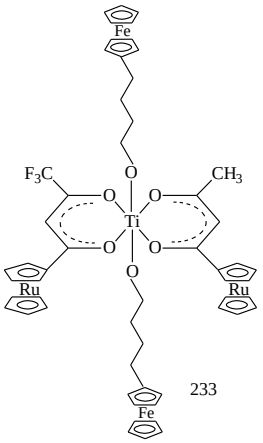

233

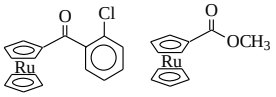

234

235

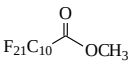

236

237

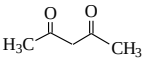

238

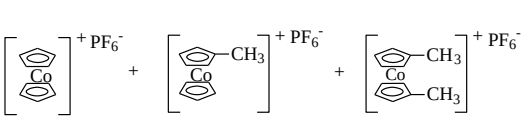

239

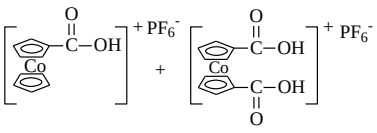

240

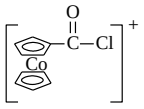

241

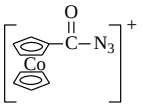

242

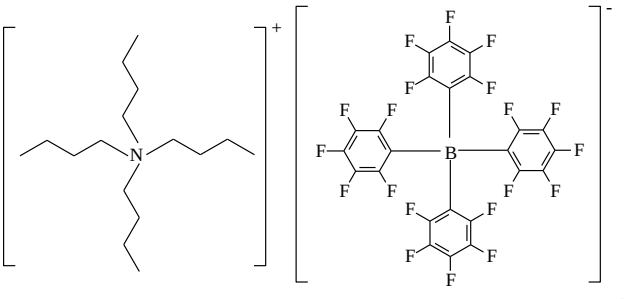

243

Chapter 1

Introduction and aim of study

1.1. Introduction

Metallocenes have a wide range of uses, varying from polymerisation catalysis,[1, 2, 3] organic synthesis catalysts,[4, 5] as well as being useful starting materials for preparation of various organometallic compounds.[6, 7]

In the medical field, metallocenes exhibit various biological activities.[8, 9, 10, 11, 12] Ferrocene acts as a mediator in the biosensoring of glucose,[13] and when anchored to a water-soluble polymer it shows enhanced antineoplastic activity.[14] Titanocene dichloride exhibits pronounced antiviral,[15] and anti-inflammatory activity.[16] Ruthenocene-containing chloroquine analogues have shown increased antimalarial activity to chloroquine-resistant strains of *P. falciparum*.[17]

With the introduction of cisplatin [*cis*-diamminedichloroplatinum(II)] as a chemotherapeutic drug in 1979, the possibility of developing new and improved metal-containing chemotherapeutic agents arose. New chemotherapeutic drugs acetylacetonatocycloocta-1,5-dienerhodium(I),[18] and ferrocenium salts,[19] exhibit improved cancerostatic properties against Ehrlich Ascites tumour cell lines, which are resistant to classical anti-tumour agents.[19, 20, 21, 22] Titanium(IV) complexes are being introduced as antineoplastic drugs, owing to their pronounced antitumor properties and low toxicity. Titanocene dichloride and budotitane [$Ti(H_3CCOCHCOC_6H_5)_2(OC_2H_5)_2$] show impressive cancerostatic activity,[23] and are currently in phase II clinical trials.[24, 25] Derivatives of titanocene were also found to have antitumor properties.[24]

This laboratory has investigated the synergistic effect of rhodium/ferrocenyl-,[26] and rhodium/ruthenocenyl β-diketonato complexes in anti-cancer drug research.[27] In some cases the mixed metal systems show improved antineoplastic effects over cisplatin. Metallocenes, especially those containing early transition metals such as Ti and Fe, exhibit lower toxicity than platinum compounds.[28] In order to complement previous studies in this laboratory,[26] the need has arisen to investigate possible synergistic effects in cancer therapy that can be obtained by using combinations of titanium, ferrocene and/or ruthenocene within the same mixed-metal complex.

The mechanism of the antitumor action of the titanium(IV) compound titanocene dichloride is still unknown.[29] What is clear is that the mechanism of cell interaction is very different to that of cisplatin. The mechanism by which titanocene kills cancer cells is thought to involve at least in part the interaction of a hydrolysed titanocene species with DNA. Metallocene complexes accumulate in nucleic acid-rich regions of the cell and hence nucleic acid synthesis, particularly DNA synthesis, is probably inhibited.[30] If this is indeed the case, the kinetic rate of the hydrolysis of these titanocene complexes is probably a key factor in the mechanistic pathway by which titanocene and other Ti(IV) derivatives kill cancer cells.

1.2. Aims of the study

With this background the following goals were set for this study:

(i) The synthesis and characterisation of new and known ruthenocene-containing β-diketones of the type $RcCOCH_2COR$ with R = CH_3, CF_3, Fc, Rc, C_6F_5, $C_{10}H_{21}$ and $C_{10}F_{21}$. These compounds were synthesised *via* new and known methods.

(ii) The synthesis of ferrocene-containing alcohols of the type $Fc(CH_2)_nOH$, n = 1, 2, 3 and 4.

(iii) The synthesis and characterisation of new complexes containing a titanocenyl or titanium(IV) centre coordinated to a ruthenocene-containing β-diketonato and/or ferrocenylalcohol ligands.

(iv) An electrochemical study utilising cyclic voltammetry, square wave- and linear sweep voltammetry on selected complexes to determine the electrochemical reversibility and the formal reduction potentials of the mixed metal redox active centre(s) of these complexes. This will also serve to quantify any intra-molecular communication between the redox active mixed metal centres.

(v) A kinetic study of the hydrolysis of some of the synthesised titanium(IV) complexes.

(vi) A cytotoxic study to determine whether the new titanium complexes exhibit antineoplastic activity against cancer cells from a human colorectral cancer cell line (CoLo) and a human cervix epitheloid cancer cell line (HeLa).

---

[1] G. Wilkinson, Editor, *Comprehensive Organometallic Chemistry*, vol. 3, Pergamon Press, Oxford, 1982, p. 475-545 and references therein.

[2] V.A.E. Barrios, A. Petit, F. Pla and R.H. Najera, *Eur. Polym. J.*, 2003, **39**, 1151.

[3] N.J. Long, *Metallocenes: An introduction to sandwich complexes*, Blackwell Science, London, 1998, p. 23.

[4] G. Wilkinson, Editor, *Comprehensive Organometallic Chemistry*, vol. 3, Pergamon Press, Oxford, 1982, p. 273-278 and references therein.

[5] F.N. Tebbe, G.W. Parshall and G.S. Reddy, *J. Am. Chem. Soc.*, 1978, **100**, 3611.

[6] N.J. Long, *Metallocenes: An introduction to sandwich complexes*, Blackwell Science, London, 1998, p. 148-154.

[7] G. Wilkinson, Editor, *Comprehensive Organometallic Chemistry*, vol. 3, Pergamon Press, Oxford, 1992, p. 331-426 and references therein.

[8] E.W. Neuse and F. Kanzawa, *Appl. Organomet. Chem.*, 1990, **4**, 19.

[9] P. Köpf-Maier, M. Leitner and H. Köpf, *J. Inorg. Nucl. Chem.*, 1980, **42**, 1789.

[10] P. Köpf-Maier, M. Leitner, R. Voigtlander and H. Köpf, *Z. Naturforsch.*, 1979, **34C**, 1174.

[11] P. Köpf-Maier, S. Grabowski, J. Liegener and H. Köpf, *Inorg. Chim. Acta*, 1985, **108**, 99.

[12] E. Meléndez, *Crit. Rev. Oncol.*, 2002, **42**, 309.

[13] N.J. Long, *Metallocenes: An introduction to sandwich complexes*, Blackwell Science, London, 1998, p. 258.

[14] J.C. Swarts, D. Swarts, D.M. Maree, E. W. Neuse, C. La Madeleine and J.E. van Lier, *Anticancer Res.*, 2001, **21**, 2033.

[15] P. Köpf-Maier and H. Köpf, *Metal Compounds in Cancer Therapy*, ed. S.P. Fricker, Chapman & Hall, London, 1994, p. 109.

[16] B.K. Keppler, C. Friesen, H. Vongerchten and E. Vogel, *Metal Compounds in Cancer Therapy*, ed. B.K. Keppler, VCH, Weinheim, 1993, p. 297.

[17] P. Beagley, M.A.L. Blackie, K. Chibale, J.R. Moss and P.J. Smith, *J. Chem. Soc., Dalton Trans.*, 2002, 4426.

[18] G. Sava, S. Zorzet, L. Perissin, G. Mestroni, G. Zassinovich and A. Bontempi, *Inorg. Chim. Acta*, 1987, **137**, 69.

[19] P. Köpf-Maier, H. Köpf and E.W. Neuse, *Cancer Res. Clin. Oncol.*, 1984, **108**, 336.

[20] P. Köpf, *Naturforsch. C. Biochem. Biophys. Biol. Virol.*, 1985, **40C**, 843.

[21] D. Osella, M. Ferrali, P. Zanello, F. Laschi, M. Fontani, C. Nervi and G. Caviviolio, *Inorg. Chim. Acta*, 2000, **306**, 42.

[22] P. Yang and M. Guo, *Coord. Chem. Rev.*, 1999, **185**, 189.

[23] H. Köpf and P. Köpf-Maier, *Angew. Chem.*, 1979, **18**, 477.

[24] M. Guo and P.J. Sadler, *J. Chem. Soc., Dalton Trans*., 2000, 7.

[25] J.R. Boyles, M.C. Baird, B.G. Campling and N. Jain, *J. Inorg. Biochem.*, 2001, **84**, 159.

[26] J.C. Swarts, C.E. Medlen, *European Patent.* EP 1 345 951 B1, bulletin 2004/34, 2004, pp 1-36.

[27] K.C. Kemp, M.Sc. Study, *Synthesis, electrochemical, kinetic and thermodynamic studies of new ruthenocene-containing betadiketonato rhodium(I) complexes with biomedical applications*, University of the Free State, R.S.A. 2004.

[28] N.J. Long, *Metallocenes: An introduction to sandwich complexes*, Blackwell Science, London, 1998, p. 260.

[29] G. Mokdsi and M.M. Harding, *J. Inorg. Biochem.*, 2001, **86**, 611.

[30] P. Köpf-Maier, *J. Struct. Biol.*, 1990, **105**, 35.

Chapter 2

Literature Survey

2.1. Metallocenes

2.1.1. Introduction

In organometallic chemistry, a metallocene is a compound consisting of a positively charged metal ion sandwiched between two negatively charged cyclopentadienyl anions.

Metallocenes,[1] are a series of organometallic compounds, some of which possess a good antineoplastic activity against various animal cancer cells. Fundamental differences exist between the platinum group metal complexes and the metallocenes, including their structure and mechanism of antineoplastic activity.

Metallocenes exist in various different structures. Metal derivatives of cyclopentadiene can be classified as either ionic cyclopentdienides or covalent cyclopentadienyl. The covalent structures are commonly described using the hapto (η) nomenclature system. In most texts, the monohapto (η^1) or σ type structure (**1**) and the pentahapto (η^5) or π type structure (**2**) are described as common for covalent cyclopentadienyl derivatives (Figure 2.1).

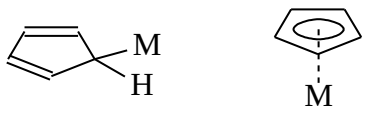

1 **2**

Figure 2.1. Structures of monohapto (η^1) or σ type structure (**1**) and the pentahapto (η^5) or π type structure (**2**).

There exist an enormous number of pentahaptocyclopentadienyl metal complexes (η^5-C_5H_5-M), which can be classified into different structural types:

- Parallel sandwich complexes such as ferrocene.[2]
- Bent or tilted sandwich complexes such as titanocene dichloride.[3]
- Half-sandwich complexes such as (η^5-cyclopentadienyl)dicarbonylcobalt(I).[4]
- Multi-decker sandwich complexes such as nickelocene.[5]

Relevant to this study are parallel sandwich complexes of ruthenocene and tilted sandwich complexes of titanocene dichloride.

2.1.1.1. Parallel sandwich complexes

These are the most common of the metallocene series of compounds. Group 8 metallocenes (Fe, Ru, Os) are the most stable members of the parallel series, due to the fact that all the bonding and non-bonding orbitals are filled.

The cyclopentadienyl ligands can rotate freely with two possible conformations often encountered: the fully staggered conformation (**3**), having D_{5d} symmetry or eclipse conformation (**4**), having D_{5h} symmetry (see Figure 2.2). In the solid state, rings are staggered only below the λ point (164 K). At room temperature there is rotational disorder, permitting neither D_{5d} nor D_{5h} symmetry.

3 **4**

Figure 2.2. Structures of the staggered (**3**) and eclipse (**4**) conformation having D_{5d} or D_{5h} symmetry respectively of the parallel sandwich dicyclopentadienyl complexes.

Single crystal X-ray studies have shown that the rings are staggered in solid ferrocene [Fc, $(C_5H_5)_2Fe$],[6] cobaltocene [$(C_5H_5)_2Co$],[7] and magnocene [$(C_5H_5)_2Mg$],[8] and eclipsed in solid ruthenocene [Rc, $(C_5H_5)_2Ru$].[9] The equilibrium ring conformation for the ferrocene in the vapour state, however, is eclipsed.[10] Electron diffraction data for vanadocene [$(C_5H_5)_2V$],[11] manganocene [$(C_5H_5)_2Mn$],[12] cobaltocene,[7, 13] nickelocene [$(C_5H_5)_2Ni$],[14, 15] magocene,[16] and ruthenocene,[10] vapour have also been interpreted as consistent with the presence of the eclipsed structure, although in all cases the presence of the staggered structure could not be ruled out.

Studies have been reported of a green form of titanocene [$(C_5H_5)_2Ti$],[17] zirconocene [$(C_5H_5)_2Zr$],[18] and hafnocene [$(C_5H_5)_2Hf$],[19] in which it was concluded that these three compounds have a structure with parallel, pentahapto rings. The green compound with the empirical formula $C_{10}H_{10}Ti$ (**5**), however, was observed to be dimeric and a proposed structure,[20] has been confirmed (see Figure 2.3).[21, 22]

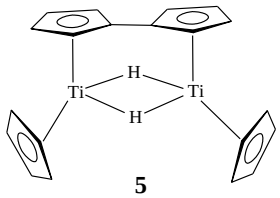

5

Figure 2.3. Structure of dimeric titanocene $[C_{10}H_{10}Ti]_2$ (**5**).

2.1.1.2. Bent or tilted sandwich complexes

In bent metallocenes the cyclopentadienyl rings are not parallel. This group of metallocenes usually feature *d*-block species involving group 4 and heavier groups 5-7 elements. Due to the electron-deficient nature of the complexes additional ligands that can contribute extra electrons are included in order to achieve the desired stable 18-electron configuration. However, structurally related complexes with 16 and 17 electrons also exist. The addition of the extra ligands give rise to geometry where the angle between the normals to the planes as defined by cyclopentadienyl rings is less than 180º (see Figure 2.4).[23] Due to the 18-electron rule, most metallocene complexes are restricted to metals with a low number of *d* electrons. In contrast, group 4 metallocenes prefer to form stable 16-electron species and bind only two single donating ligands. This leaves an unpaired central orbital, which can act as a Lewis acid.

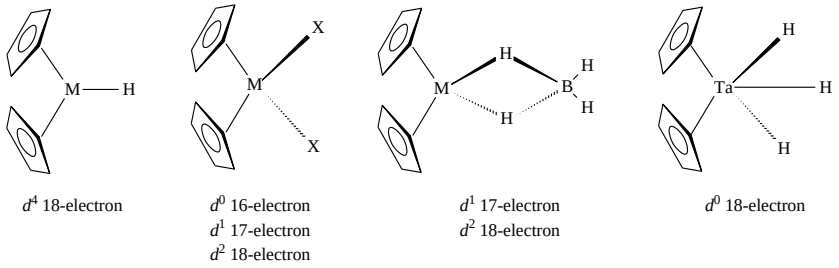

Figure 2.4. Structure of some bent metallocenes.

2.1.1.3. Half-sandwich complexes

Half-sandwich complexes of the general type $[(\eta^5\text{-}C_5H_5)ML_n]$ (n = 1, 2, 3, 4) represent a major class of transition metal organo derivatives. When L is a good π-acid ligand (CO or NO), the complexes follow the 18-electron rule. Figure 2.5 illustrates a typical series of this type (**6**, **7**, **8**, **9**).[24] When L is not such a good π-acceptor ligand (NH_3, PR_3 etc.) the 18-electron rule is not followed strictly, and complexes with 16 and 17 electrons can form (see Figure 2.5, no. **10**, **11**).[24] These complexes frequently have distorted geometries.

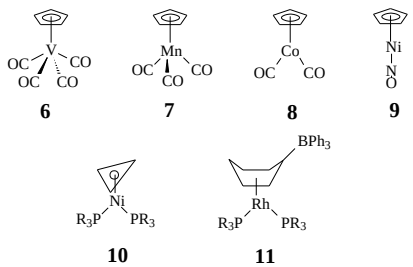

Figure 2.5. Structures of half sandwich complexes **6, 7, 8, 9, 10** and **11**.

As the cyclopentadienyl group is very firmly bound and generally inert to both nucleophilic and electrophilic reagents, it is often used as a stabilising ligand.

2.1.1.4. Multi-decker sandwich complexes

These complexes may also be viewed as metallocarboranes based on the pentagonal bipyrimid and their electronic structures. Stable derivatives of ferrocene and nickelocene $[(\eta^5\text{-}C_5H_5)_3Ni_2]^+$ (**12**)[5] have been isolated and characterised. A wide range of triple-decker sandwich compounds with 30 valence electrons based on carborane, azacarborane and thiocarborane are known (see Figure 2.6, no. **13** and **14**).[25, 26, 27]

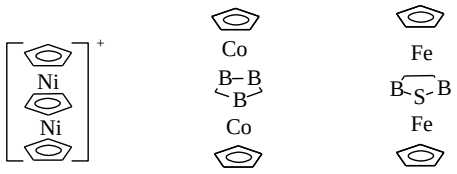

12 **13** **14**

Figure 2.6. Structure of triple-deckers **12, 13** and **14**.

Most triple-decker systems have 30 valence electrons but as different numbers of electrons can be accommodated, systems with 26 ranging to 34 valence electrons are known.

A polymeric structure with highly ionic $\mu\text{-}(\eta^5\text{-}\eta^5\text{-}C_5H_5)$ rings (**15**) has been found in single X-ray studies of C_5H_5In and C_5H_5Tl (see Figure 2.7).[28] Solid $(C_5H_5)_2Pb$ showed the presence of a polymeric structure (**16**) with each lead atom bonded to two $\mu\text{-}(\eta^5\text{-}\eta^5\text{-}C_5H_5)$ and one pentahapto rings (see Figure 2.7).[29]

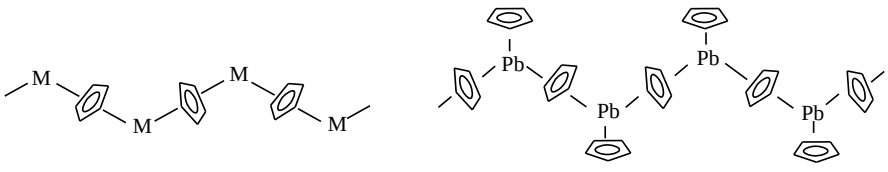

15 **16**

Figure 2.7. Structures of polymeric C_5H_5M (**15**) [M= In, Tl] and $(C_5H_5)_2Pb$ (**16**).

2.1.2. Synthesis of metallocene

There are three main routes that are normally followed in the formation of metallocenes. Figure 2.8 show the δ ^1H and δ ^{13}C NMR peak positions values for some diamagnetic metal sandwich compounds.

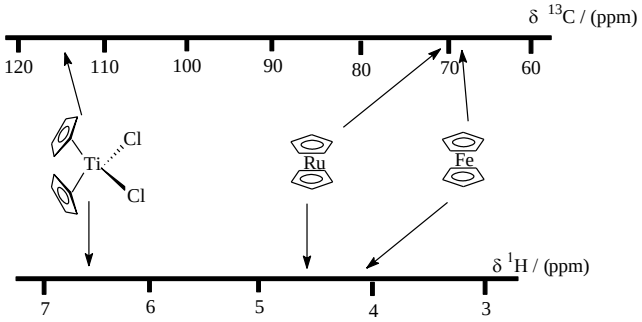

Figure 2.8. δ ^{1}H and δ ^{13}C values for some diamagnetic metal sandwich compounds.

2.1.2.1. Using a metal salt and cyclopentadienyl reagents

The normal starting point for metallocene synthesis is the 'cracking' of dicyclopentadiene. This involves a retro Diels-Alder reaction to produce the monomeric and fairly unstable C_5H_6 (abbreviated HCp). Because HCp is a weak acid (pK_a = 15), it can be deprotonated by alkali metals. Sodium cyclopentadienide (NaCp) is often the preferred intermediate for metallocene synthesis. In the final step of metallocene synthesis, the Cp^- from NaCp reacts with a metal salt or metal halide (Scheme 2.1).

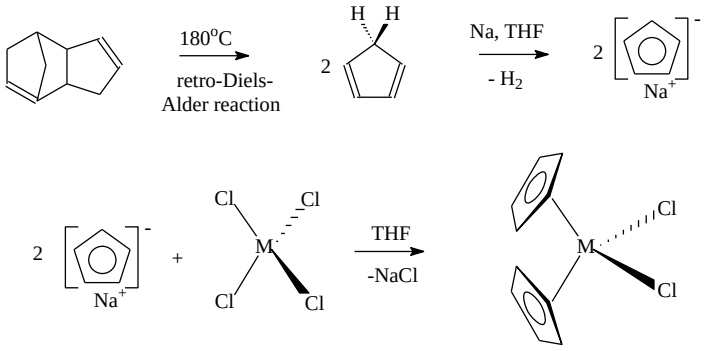

Scheme 2.1. Synthesis of metallocenes using a metal salt and cyclopentadienyl reagents.

2.1.2.2. Using a metal and cyclopentadiene

In this type of metallocene synthesis, the 'co-condensation method' is employed. It is possible to use vapours of transition metals as routine reagents in synthesis and catalysis.[30] The highly reactive metal or molecules are generated at high temperatures in a vacuum and then brought together with the chosen co-reactants on a cold surface. Complexes are then formed on warming the system to room temperature. The use of metal atoms in the vapour phase rather than the solid metal have also been used. Scheme 2.2 shows such a reaction to form a metallocene.

$$M + 2C_5H_6 \xrightarrow{500^oC} [(C_5H_5)_2M] + H_2$$

Scheme 2.2. Synthesis of metallocenes *via* the co-condensation method, M = Fe, Ru and Os.

2.1.2.3. Using a metal salt and cyclopentadiene

If the salt anion, such as Cl^- in $FeCl_2$, has poor basicity and cannot deprotonate cyclopentadiene, an auxiliary base can be utilised to generate the cyclopentadienyl anions *in situ*, which can sometimes be more convenient (Scheme 2.3).[31] Alternatively, a reducing agent is required.

$$FeCl_2 + 2C_5H_6 + 2C_2H_5NH \longrightarrow [(C_5H_5)_2Fe] + 2[(C_2H_5)_2NH_2]Cl$$

Reaction with reducing agent

$$Ru^{III}Cl_3(H_2O)_x + 3C_5H_6 + 3/2\ Zn \longrightarrow [(C_5H_5)_2Ru^{II}] + C_5H_8 + 3/2\ Zn^{2+}$$

Scheme 2.3. Synthesis of metallocenes using a metal salt and cyclopentadiene.

2.1.3. Ferrocene

Ferrocenium complexes are compounds that have shown that they have good chemotherapeutic properties in the treatment of cancer.[32] The ionic ferrocenium (**17**) is obtained by the oxidation of ferrocene (**18**) (see Figure 2.9). This process is reversible and numerous studies have been done on the oxidation of **18** and its derivatives.[33, 34]

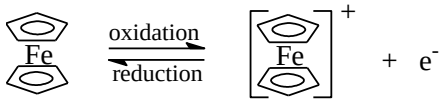

18 17

Figure 2.9. Oxidation of ferrocene (**18**) to give the ferrocenium cation (**17**).

2.1.3.1. Ferrocene Chemistry

Ferrocene is predictably the best documented of all metallocenes, many good reviews are available for the chemistry of ferrocene and its derivatives.[35, 36, 37, 38] The cyclopentadienyl rings are aromatic and due to its great stability and ability to maintain the ligand-metal bond, it is possible to carry out a wide variety of organic transformations on the cyclopentadienyl ligands. The outline of ferrocene (and ruthenocene) chemistry relevant to this study is shown in Scheme 2.4.

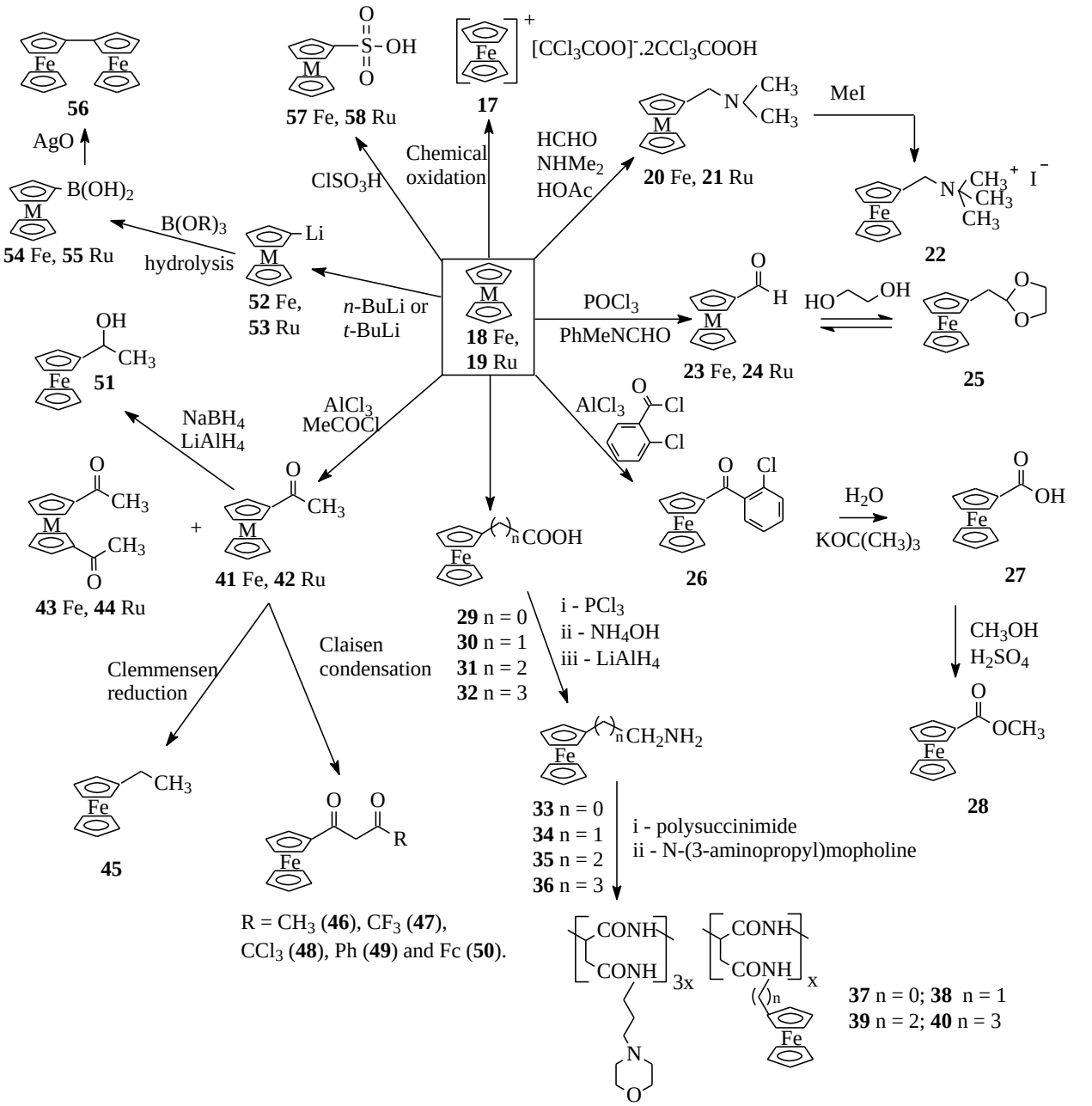

Scheme 2.4. Some organic reactions of ferrocene (M = Fe, **18**) and ruthenocene (M = Ru, **19**).

Ferrocenium salts are known for their antineoplastic activity against Ehrlich ascites tumor cell lines,[39] these ferrocenium salts (**17**) can be obtained by the oxidation of **18**. Aminomethylation (Mannich reaction) involves the condensation of **18** or **19** with formaldehyde and amines. Using dimethylamine gives dimethylaminomethylferrocene (**20**) or dimethylaminomethylruthenocene (**21**), a compound useful in the preparation of many other derivatives like **22**.[40] Ferrocene- (**23**) and rutheocenecarboxaldehyde (**24**)[41] is obtained by the Sommelet reaction, which involves the reaction between *N*-methylformanilide, phosphorus oxychloride and **18** or **19**.[42] Ethylene glycol converts **23** into the cyclic acetal (**25**), but **25** can hydrolyse back to **23** with extreme ease. (2-Chlorobenzoyl)ferrocene (**26**)[43] is prepared by a Friedel-Craft reaction between **18** and 2-chlorobenzoyl chloride. Ferocenecarboxylic acid (**27**)[43]

is obtained from **26**, due to the fact that non-enolizable ketones may be converted to carboxylic acids by potassium-*tert*-butoxide-water,[44] and that aryl 2-chlorophenyl ketones may be cleaved with loss of the 2-chlorophenyl group to give only one of the two possible acids.[45] The carboxylic acid **27** is converted to the ester methylferrocenoate (**28**) by a Fischer esterification, which is a conversion of a carboxylic acid directly into an ester by reaction with an alcohol in the presence of a mineral acid catalyst.[46]

Ferrocenoic acid (**29**) has been prepared in many ways,[37] the most important by oxidation of acetylferrocene (**41**),[37, 47] or *via* the chlorobenzoyl-chloro method.[48] Ferrocenylacetic acid (**30**) may be prepared from *N*,*N*-dimethylaminomethylferrocene methiode (**22**),[49, 50, 51] after cyanation followed by hydrolyses of the resulting ferroceneacetonitrile. 3-Ferrocenylpropanoic acid (**31**) is prepared from ferrocenylcarboxaldehyde (**23**) and malonic acid,[52] followed by the hydrogenation of the intermediate. 4-Ferrocenylbutanoic acid (**32**) is prepared by a Clemmensen reduction[53] of 3-ferrocenoylpropanoic acid.[54] After amination and Clemmensen reduction with aluminium hydride[55] of the appropriate ferrocenylcarboxylic acid (**29-32**), the appropriate ferrocenylamine (**33-36**) is reacted with polysuccinimide[56] to give the various polymers (**37-40**). **18** and **19** undergo Friedel-Craft catalysed acetylation very readily on one ring (acetylferrocene, **41;** acetyl ruthenocene, **42**) and less readily on both rings (1,1'-bisacetylferrocene, **43;** 1,1'-bisacetylruthenocene, **44**). If the two rings are free to rotate only one 1,1'-disubstituted compound is isolated, whereas three 1,1'disubstituted isomers could be formed in the absence of rotation. In practice, only one compound is isolated. The reaction can be catalysed by any Lewis acid, most commonly $AlCl_3$ but the use of H_3PO_4 as catalyst can be effective as it limits the amount of disubstituted product formed. **41** can undergo Clemmensen reduction to form ethylferrocene (**45**). Claisen condensation of **34** with the appropriated ester gives the various β-diketones (**46-50**).[57] A discussion on β-diketones and its reactions follows in paragraph 2.2. Reduction of **41** to an alcohol is obtained with sodium borohydride/lithium aluminiumhydride to give **51**.

Another reaction typical of aromatic systems is metallation. Lithiation reactions are thought to involve nucleophilic attack of the hydrocarbon portion of the Li-containing reagent on a hydrogen atom of the compound undergoing metallation and this proton must be relatively acidic. Mono-lithiated ferrocene (**52**) and mono-lithiated ruthenocene (**53**) can be prepared by treating **18** or **19** with stoichiometric quantities of *n*-BuLi or *t*-BuLi in hexane/ether.[58, 59] Alkali metal derivatives have found extensive application as intermediates in the synthesis of other ring-substituted species and lithium, sodium, mercury and boron derivatives can be usefully employed, for example reactions of **52** or **53** going to **54** or **55** and **56**.[40] Sulphonation cannot be carried out directly using concentrated sulphuric acid as this leads to ferrocene oxidation but the

use of chlorosulphonic acid in acetic anhydride or with the SO_3-dioxane complex gives good yields of **57** and **58**.[40]

2.1.4. Ruthenocene

Following the discovery of ferrocene, ruthenocene was one of the first organometallic compounds to be formed. However, much less attention has been paid to it, because it is more costly and synthetically more challenging. Ruthenocene (**19**) can be formed in a number of ways some of which include: treating ruthenium(III) acetylacetonate [$Ru(acac)_3$] with an excess of cyclopentadienylmagnesium bromide [$(C_5H_5)MgBr$];[60] the direct reaction of rutheniumtrichloride [$RuCl_3$] (**59**) and cyclopentadiene in ethanol in the presence of zinc (from this synthesis other cyclo-olefin complexes can also be formed, see Figure 2.10);[61] and a high yield synthesis involving $RuCl_{3.2}H_2O$ and silylated or stannylated cyclopentadienes.[62]

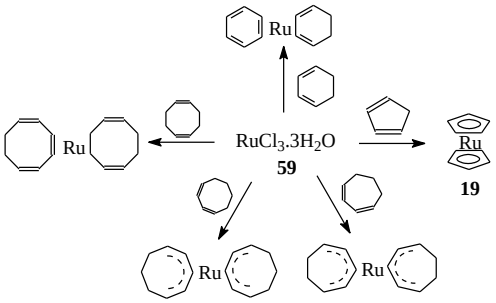

Figure 2.10. Formation of various cyclo-olefin ruthenium(III) complexes

The electronic structure and bonding is similar to that of ferrocene and the metal orbitals featured are 4*d*, 5*s* and 5*p*. The bigger and more diffuse orbitals of ruthenocene enables its valence electrons to approach the ring orbitals more closely than in ferrocene. Thus, this leads to a stronger metal-ring bond.

Ruthenocene (**19**) as well as derivatives of **19** normally have an eclipsed conformation (see Figure 2.11), which is confirmed by calculations to be thermodynamically the preferred conformation by 4.66 kJ mol^{-1}.[63]

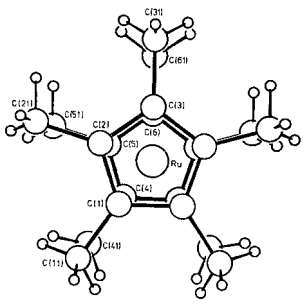

Figure 2.11. A perspective view of the crystal structure of a derivative of **19**, decamethylruthenocene.[63]

2.1.4.1. Ruthenocene Chemistry

The chemistry of ruthenocene (**19**) closely resembles that of ferrocene (**18**) (Scheme 2.4.), i.e. the cyclopentadienyl rings undergo the same type of aromatic transformations. However, there are some notable differences. For example, **19** is thermally more stable than **18**. The general reactivity is shown in Scheme 2.5. Friedel-Craft acetylation, metallation, arylation, formylation and sulphonation reactions are all possible but the degree of aromatic reactivity has been shown to be markedly lower for **19** than for **18**. The order of reactivity of the metallocenes is in agreement with the relative availability of metal electrons, or basicity: **18** > **19**. Under forcing conditions for acylation, **18** gives exclusively the di-substituted product whereas **19** gives a mixture of mono- and di-substituted products. This behaviour is explained by the different effective electronegativity at the ring carbon atoms, which is due to the different electronic structures and characteristics of the different metals. The increased ring-metal bond in **19** results in a lower π-electron density around the rings and accounts for the decreased electrophilic reactivity.[40]

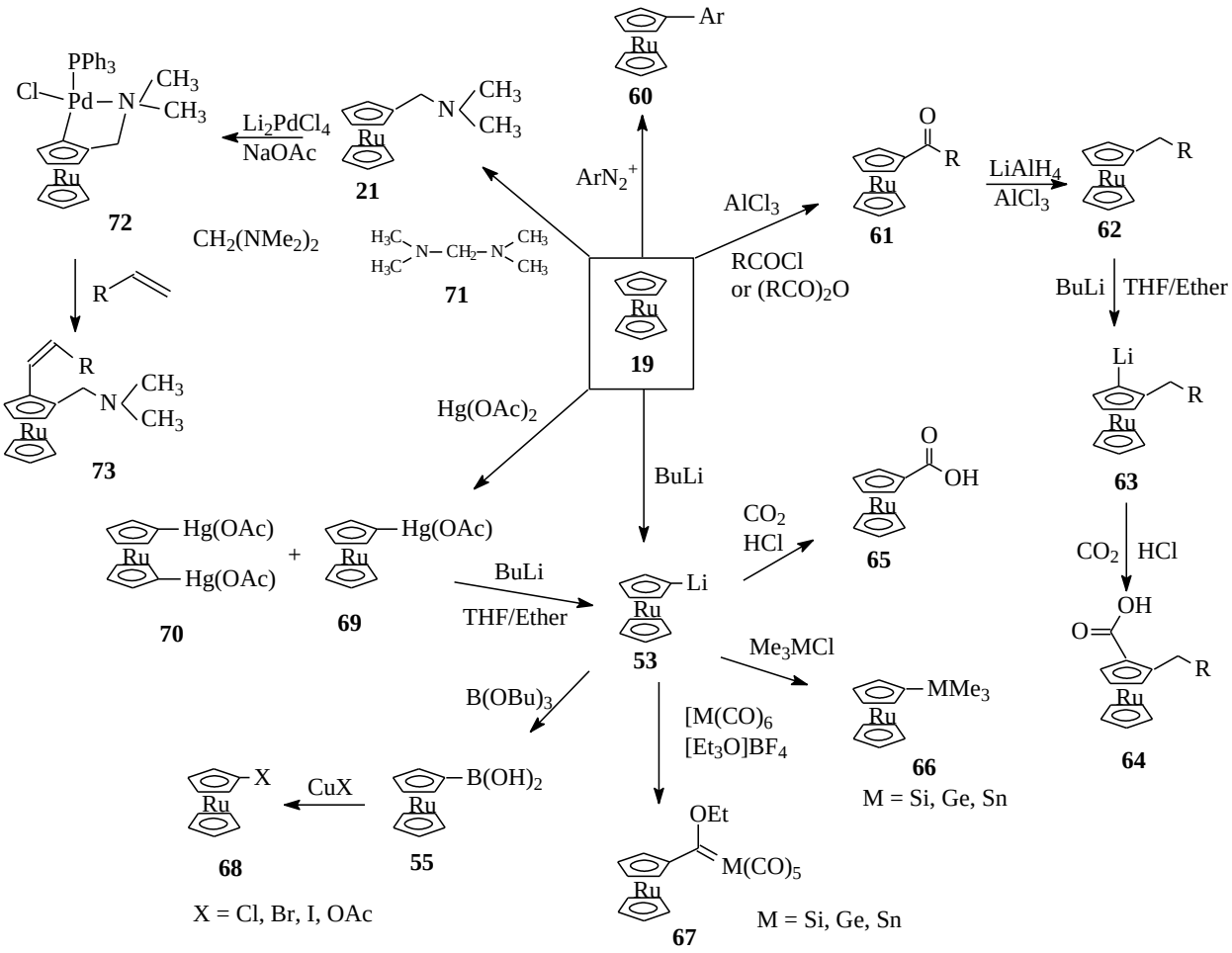

Scheme 2.5. Some organic chemistry of ruthenocene (**48**).

The aryl or alkyl-substituted (**60**) ruthenocene derivatives are obtained by reacting **19** with the appropriated diazonium salt.[41, 64] Acetylation of **19** with acid chlorides or anhydrides under Friedel-Craft conditions produce both mono- (**42**) and 1,1'-di-substituted (**44**) derivatives (Scheme 2.4), the latter being favoured by excess catalyst such as $AlCl_3$.[65] Examples of derivatives (**61**) formed are RcCONHPh and RcCOSMe.[65] Clemmenson reduction is demonstrated by the reduction of **61** to give **62**.[41] Hydrogen replacement of the mono-substituted ruthenocene of the substituted or non-substituted ring depends on the existing substituent. If the existing substituent is electron withdrawing, such as acetyl in **42**, it deactivates the substituted Cp ring of reference, leading almost exclusively to the heteroannular 1,1'-disubstituted product e.g. **44**. However, if the existing substituent is electron donating, such as alkyl in **62**, it activates the ruthenocene complex, and substitution takes place preferably on the same cyclopentadienyl ring that contains the activating substituent as shown in the lithiation of **62**, to give **63.** Compound **63** can be turned into a carboxylic acid, **64**. Reaction of **19** with *n*-BuLi results in a lithioruthenocene (**53**), which when treated with carbon dioxide followed by HCl, yields ruthenocenecarboxylic acid (**65**).[41, 64, 65] Lithioruthenocene is the source of many otherwise inaccessible derivatives, some of which are **66**, **67**, **55** and **68**.[40, 64] The mercurated ruthenocenes **69** and **70** were obtained by reacting **19** with mercury acetate in a methanol-ether solution.[64, 65] **19** can also undergo Mannich reactions with $CH_2(NMe_2)_2$ (**71**) to form **21**. Metallation of **21** with Li_2PdCl_4/NaOAc produces a substituted ruthenocenyl complex **72**,[40] which gives good yields of olefins **73** (R = COMe, COPh or Ph) following reaction with $RCHCH_2$.[40]

Chemical oxidation of **19** by halogens gives the bent compound **74** (Figure 2.12.) and a dication is formed from the direct reaction of **19** with $Hg(CN)_2$ in perchloric acid.[40]

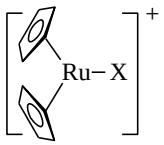

X = Cl, Br, I

74

Figure 2.12. Structure of the bent dicationic ruthenocene derivative **74**.

Ruthenocene has the ability to form donor-acceptor complexes with weak Lewis acids, it prefers to form adducts with species that accept an electron pair. For example, with HgX_2, **19** will produce stable complexes of defined composition 1:1 (**75**) or 1:3 (**76**) with excess $HgCl_2$ (Figure 2.13.). The 1:1 adduct (**75**) are simple halide-bridged compounds with a Ru-Hg bond whilst the extra molecules in the 1:3 adduct (**76**) are incorporated *via* Cl-Hg-Cl bridging bonds.

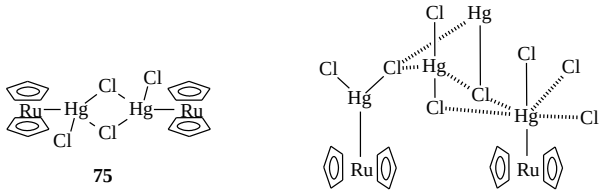

75 **76**

Figure 2.13. Structures of 1:1 (**75**) and 1:3 (**76**) ruthenocene mercury adducts

Internal Claisen condensation of corresponding acetyl ester derivatives of ruthenocene yields bridged derivatives e.g. ruthenocenophane-1,3-dione (**77**) and 3-arylruthenocenophane-1,5-dione (**78**) (Figure 2.14).[66]

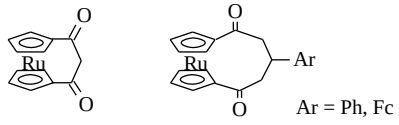

77 **78**

Figure 2.14. Structures of some ruthenocenophanes **77** and **78**.

2.1.5. Titanocene(IV) dihalide

The bent metallocenes, like titanocene dichloride are tetrahedral and possess a unique chemical structure where substituents or replacements at three different positions can be made to tailor diverse physical, chemical and biological properties (Figure 2.15). While still maintaining a tetrahedral structure the central metal atom (position A) can be varied using the metal ions Ti, Zr, Hf, V, Nb, Ta, Mo and W. Various substituents can be introduced into the cyclopentadienyl ring prior to forming the metallocene dihalide (position B) and different ligands can replace the two Cl^- ions coordinated to the central metal atom (position C).

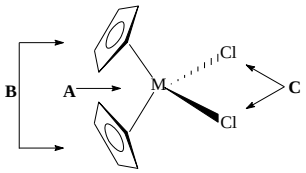

Figure 2.15. Structural flexibility of metallocene dichlorides for chemical design. Normally M = Ti, Zr, Hf, V, W and Mo.

Variation of the central metal atom (position A) leads to variations in the chemical and physical properties of the complexes. Also, the electron configuration of the central metal atom may influence toxicity but does not directly govern anticancer activity of the metallocene derivative.[67] It has been found that there exists a diagonal relation in the periodic table (Figure

2.16) of those central atoms, which effect strong cancerostatic properties in their metallocene complexes.

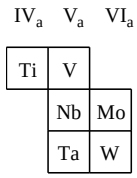

Figure 2.16. Position of early transition metal in the periodic table.[67]

2.1.5.1. Chemistry of cyclopentadienyl ring of titanocene(IV) dihalide

The cyclopentadienyl ring can be modified in a virtually unlimited number of ways in order to influence the electronic properties, steric and coordination environment of the metal by a static intramolecular coordination of the side chain.

In order to obtain substituted cyclopentadienyl rings, the substituents have to be introduced into the cyclopentadienyl ring prior to forming the titanocene dihalide. This could be obtained by either reacting the alkali metal or thallium salts of the substituted cyclopentadienyl ligand with either $TiCl_4$ (to form the di-substituted cyclopentadienyl complexes) or $TiCpCl_3$ (to form the mono-substituted cyclopentadienyl complex). The alkali metal salts of Li and Na are, however, not stable and decomposes quickly, the thallium salts can be stored for long periods and is formed by reacting the cyclopentadienyl ring (either substituted or not) with thallium-hydroxide.[68]

The following is a discussion regarding various substituents introduced onto the cyclopentadienyl ring of titanocene, its synthesis and some of its properties:

Recent studies done on amino-functionalised metallocenes showed that the metallocene can be functionalosed to have a terminal neutral amino group at the end of an aliphatic side chain (the amino function is not directly coordinated to metal center). The quaternisation of the pendant amino group can result in water-soluble species.[69] The reaction of a novel, high yield one-step synthesis of water stable and soluble titanocene dichloride dihydrochloride salts (**79**) from the direct reaction of neutral amino-substituted cyclopentadienes with $TiCl_4$ is shown in Scheme 2.6.[70]

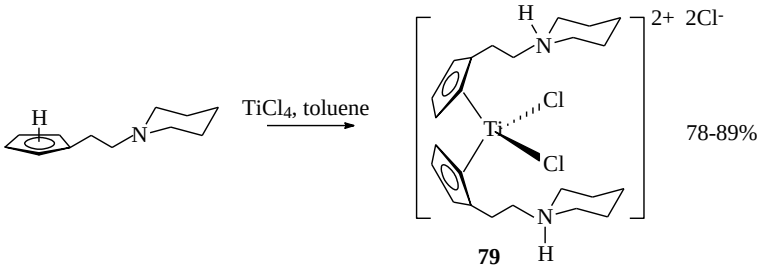

Scheme 2.6. Reagents and conditions for the synthesis of titanocene dichloride dihydrochloride salt (**79**).

Substitution also influences the antineoplastic activity of the titanocene dichloride derivatives. A decrease in antineoplastic activity has been observed when electron donating groups such as methyl, ethyl, trialkylsilyl and trialkylgermyl have been introduced onto the cyclopentadienyl ring.[71] However, cyclopentadienyl ring derivatives containing polar, electron-withdrawing groups such as carboxylic acids and esters have shown to be more effective than titanocene dichloride as an antineoplastic agent.[72] The compounds used for these tests were the carbometoxycyclopentadienyl derivatives of titanocene dichloride: the monosubstituted $(C_5H_5)(C_5H_4CO_2CH_3)TiCl_2$ (**80**) and the disubstituted $(C_5H_4CO_2CH_3)_2TiCl_2$ (**81**). The substitution of the carbomethoxy moiety to the cyclopentadienyl ring is introduced prior to formation of titanocene dichloride.[73, 74] This is achieved *via* a multi-step synthesis according to Scheme 2.7.

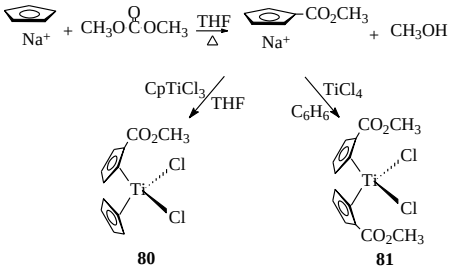

Scheme 2.7. Multi-step synthesis of the monosubstituted (η^5-C_5H_5) (η^5-$C_5H_4CO_2CH_3$)$TiCl_2$ (**80**) and the disubstituted (η^5-$C_5H_4CO_2CH_3$)$_2TiCl_2$ (**81**).

Titanium complexes containing either one or two of the substituted cyclopentadienyl rings, 1-(3-butenyl)-2,3,4,5-tetramethylcyclopentadienyl ligand [$C_5Me_4CH_2CH_2CHCH_2$], is synthesized by either $TiCl_4$ or $TiCl_3$ according to Scheme 2.8. Both the mono- (**82**) and the bis- (**83**) [$C_5Me_4CH_2CH_2CHCH_2$] titanium complexes can be converted to the dimethyl derivative.[75]

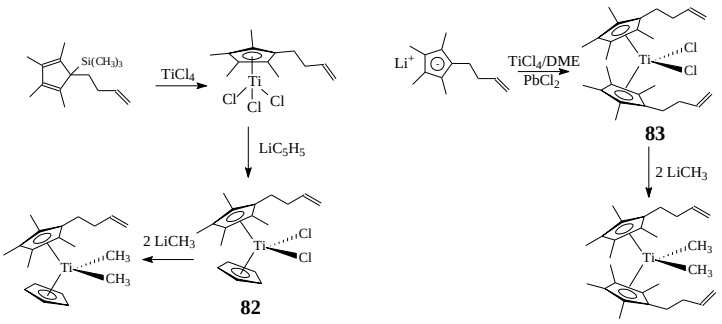

Scheme 2.8. Synthesis of the mono- (**82**) and the bis- (**83**) 1-(3-butenyl)-2,3,4,5-tetramethylcyclopentadieny titanium complexes.

A few other types of substituted cyclopentadienyl titanium complexes, **84**,[76] **85**,[77] **86**,[77] and **87,**[78] are shown in Figure 2.17, some of these subtituents can bond across to the titanium forming a 'tucked-in' titanocene complex, e.g. **88**.[79]

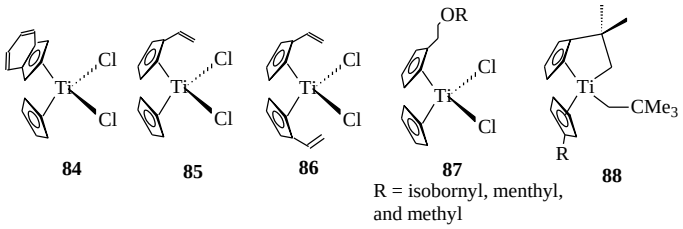

Figure 2.17. Structures of some substituted cyclopentadienyl titanium complexes.

Another way in modifying the cyclopentadienyl ring is the introduction of a linking group between the two cyclopentadienyl rings of the metallocene. This linkage is called an interannular bridge. Complexes with interannular cyclopentadienyl bridges were originally called metallocenophanes. Now, interannular cyclopentadienyl bridged bent-metallocene complexes of the early transition metals, lanthanide and main group metals are commonly referred to as *ansa*-metallocenes.[80] The multiple functions that the *ansa*-bridge serves include:[81]

- preventing free rotation, thus fixing the symmetry of the metallocene complexes;
- controlling the stereochemistry of metallocene formation by directing the orientation of the rings upon metallation;
- enforcing a bent-sandwich geometry between the rings thereby influencing the reactivity of the metal;
- increasing the electrophilicity of the metal and increasing the tilt of the rings on the metal causing an increase in the access of substrates to the equatorial wedge of the complex;
- providing an active site at which reversible metal ion binding, reversible bridge formation, ligand substitution and ring opening polymerisation chemistry can occur.

The standard synthetic method is reaction of the dilithium salt of the bridged dicyclopentadienyl anion with the metal tetrahalide, $TiCl_4$ or $[TiCl_3(THF)_3]$ followed by oxidation with aqueous HCl (Scheme 2.9).[40]

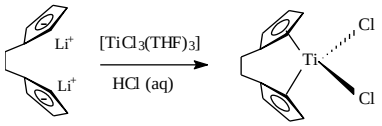

Scheme 2.9. Synthesis of an *ansa*-titanocene.

2.1.5.2. Chemistry of halide replacement of titanocene(IV) dihalide

Dicyclopentadienyl titanium halides are ideal starting materials for ligand exchange and redox reactions. It is a usefull site for molecular modification, because the chloride ligands on the central metal atom of the titanocene dichloride can be exchanged for any other halide or pseudohalide ligand without the loss of any anti-tumour activity.[82]

Many well-documented reviews on the chemistry of titanocenes are available.[3, 40] Only a few relevant points with respect to this study will, therefore, be mentioned here. The outline of this chemistry is shown in Scheme 2.10.

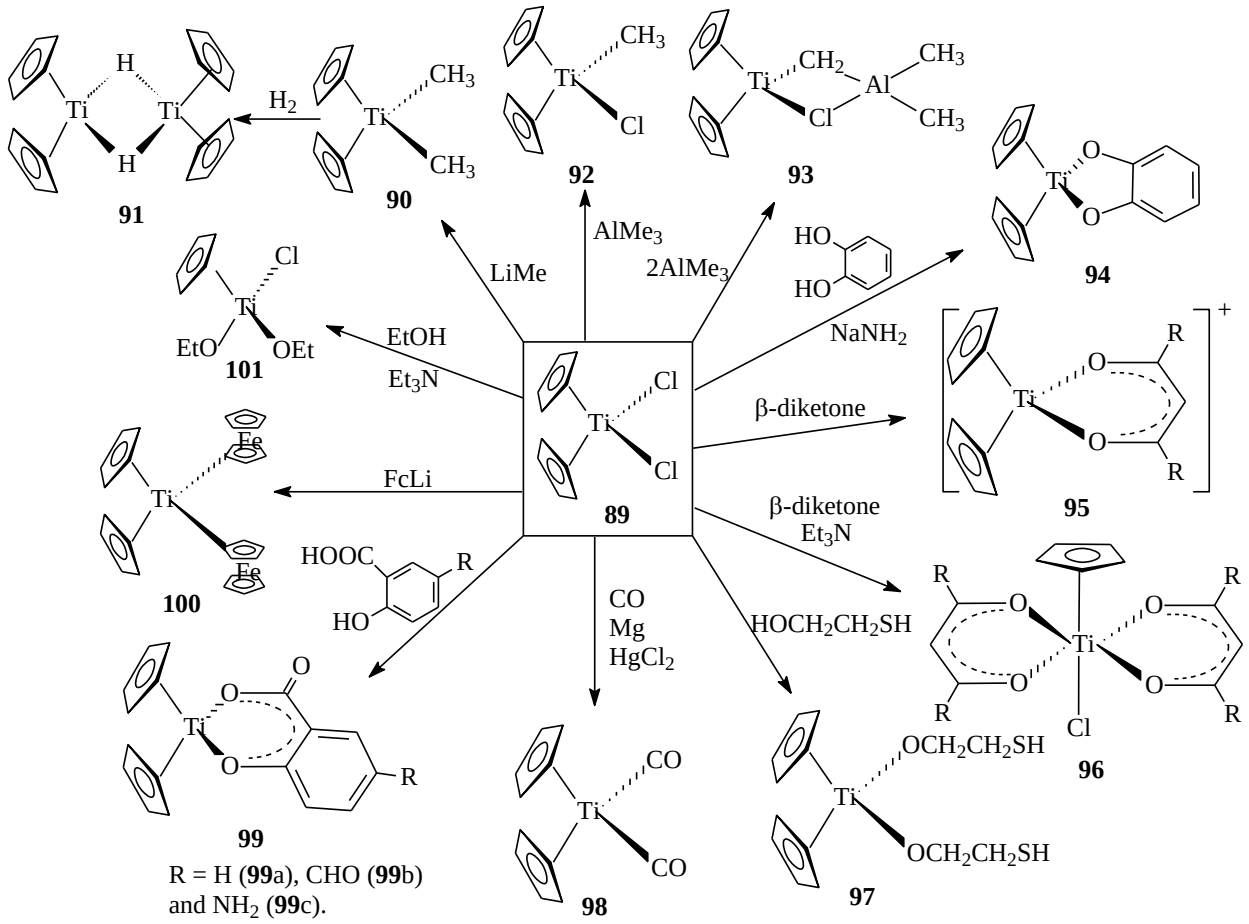

Scheme 2.10. Some halide replacement reactions of titanocene dichloride (**89**).

Reaction of methyl lithium with **89** yields di(cyclopentadienyl)-dimethyltitanium(IV) (**90**),[83] which is a very useful precursor to a large variety of different titanium(IV) complexes.[3] Under Schlenk conditions, the dimeric dihydrido-bis(dicyclopentadienyl)titanium(III) complex (**91**),[84] is formed by reaction of solid **90** with gaseous hydrogen. In contrast to the acidic character of the bridge hydrogen in other transition metal complexes, however, **91** behaves like a typical hydride. One equivalent of $AlMe_3$, reacts with **89** to yield the mono-methyl titanium(IV) complex (**92**),[40] whereas two equivalents of $AlMe_3$ yield Tebbe's reagent (**93**),[85] which is a useful alternative to the classical Wittig reagents for the conversion of an ester to a vinyl ether.[40] **89** can also react with bichelating ligands. Dialcohols (such as 1,2-benzenediol) normally react by splitting off one Cp-ring and one Cl^- ion,[86] but under the right conditions, such as in the presence of sodamide, $NaNH_2$, displacement of both Cl^- ions is achieved to yield titanocene catcholato complex (**94**) as the product.[87] Another bichelating ligand that can react with **89** is β-diketonates, and depending on reaction conditions, one of two types of titanium(IV) β-diketonates can be

formed, the mono-β-diketonate titanium complex (**95**)[88] or the bis-β-diketonate titanium complex (**96**).[89] Titanium(IV) β-diketonates will be discussed in paragraph 2.3.2. The reaction of **89** with mercaptoethanol in the presence of NEt_3 at room temperature yields the corresponding dialkoxide derivatives **97**.[90] Air-stable titanocene(IV) salt complexes can be synthesized by reacting **89** with phosphorous- or sulphur-based β-amino acid complexes in atmospheric conditions.[91] Each of these complexes contains two identical ligands with a terminal ammonium chloride group and either the phosphorous- or sulphur-based ester groups bonded directly to the titanium centre. Reduction of **89** to dicarbonyldi(cyclopentadienyl)titanium(II) (**98**) can occur *via* several methods including the aid of an activated magnesium amalgam in a carbon monoxide atmosphere.[92] A more recent method of reductive carbonylation, which is currently used in catalytic process, is the exposure of Ti(IV) to CO in an ionic liquid such as $AlCl_3$ and 1-ethyl-3-methylimidazolium chloride ($AlCl_3$-EMIC) melt.[93] It should be mentioned that the titanium in (**98**) is in the II oxidation state and the rest of the complexes discussed are in the IV oxidation state, and that titanium(III) dicarbonyl complexes are known and have a formula of $[TiCp_2(CO)_2]^+$.[93] Further reactions of **98** will be discussed in paragraph 2.1.5.3. To tie a titanocene moiety to a monomeric or polymeric carrier molecule, it must have an active, anchorable site. The salicylato complexes **99b** and **99c** of titanium(IV),[94] are anchorable to a suitable polymeric drug carrier *via* the aldehyde and amino groups. Treatment of **89** with ferrocenyllithium, yields dicyclopentadienyldiferrocenyltitanium (**100**) as an air-sensitive, dark-green crystalline solid.[95] Equimolar amounts of most alcohols react with **89**, resulting in the cleavage of the cyclopentadienyl ring in preference over the chloride ligand to yield the bisalkoxide **101**.[96] More forcing conditions yield the tetraalkoxides.[96]

2.1.5.3. Chemistry of dicarbonyl titanocene(II)

Some of the common oxidative additions and other reactions that the carbonyl complex **98** can undergo, are shown in Scheme 2.11.

Depending on the ratio of RSSR, either the titanium (IV) complex (**104**) or the titanium(III) complex (**105**) can be formed.[97] Complex **98** is extremely moisture- and oxygen-sensitive, giving various decay products, **106** being just one of them. **99** can react with **89** to give the titanium(III)chloro complex (**107**), which acts as a convenient precursor for many titanium(III) complexes.[98] Reaction of **98** with $TiCl_4$ on the other hand gives a complex very similar to **107**, namely bis[dichloro(cyclopentadienyl)titanium(III)] (**108**). **108** also acts as a convenient precursor for many titanium(III) complexes,[99] one of these being the bipyridyl titanium(III) complex (**109**),[100] which may also be prepared by reaction of **98** with bipyridyl.[101]

Titanocene dicarbonyl (**98**) reacts with diethyl diazomalonate (DEDM) by losing carbon monoxide and giving [$(C_5H_5)_2$Ti(DEDM)] (**110**), in which the diazo ligand is η^3-N,N,O bonded to the metal through both nitrogen atoms and one oxygen of the ester groups.[102] While **98** causes the disproportionation of CO_2,[103] it promotes the reductive coupling of CO_2-like molecules such as diethyl ketomalonate, DEKM. **98** reacts with DEKM in benzene to produce red-maroon crystals of **111**.[104] The phenatrenediolate complex (**112**) is formed when **98** reacts with 9,10-phentraquinone.[105] Addition of acyl halides to **98** would result in the formation of (**113**),[106] the Ti-COR bond is greatly distorted owing to a bond interaction between titanium and the carbonyl oxygen.

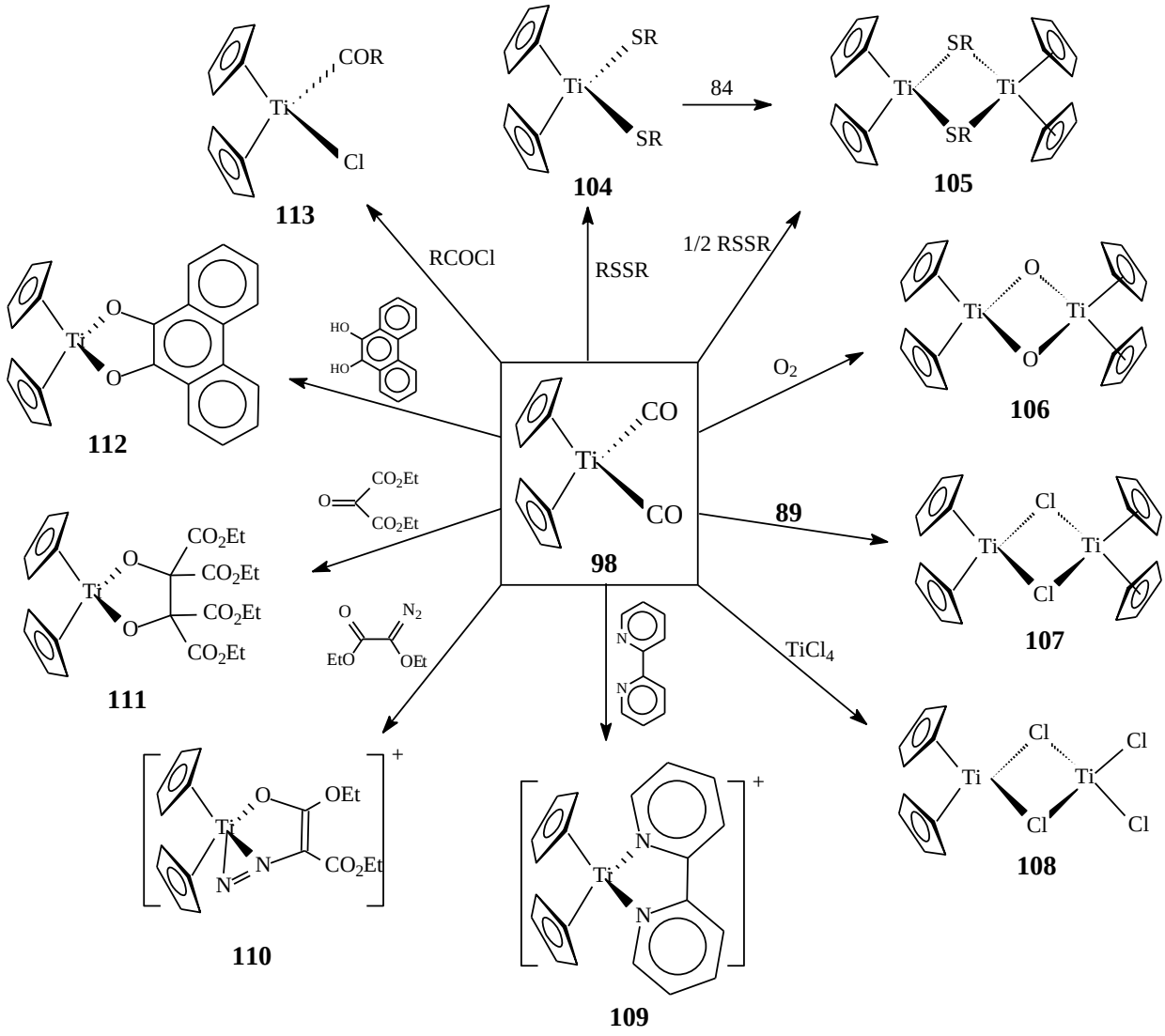

Scheme 2.11. Representative reactions of dicarbonyldi(cyclopentadienyl)titanium(II) (**98**).

2.1.5.4. Aqueous chemistry of titanocene(IV) dichloride

In aqueous media titanocene dichloride hydrolyse,[107, 108, 109, 110] according to Scheme 2.12. Marks studied the kinetics of some of the hydrolysis reactions of this compound and reported the

half-life of the loss of the second Cl^- to be approximately 50 minutes, whilst the first one's displacement is too fast to measure.[111]

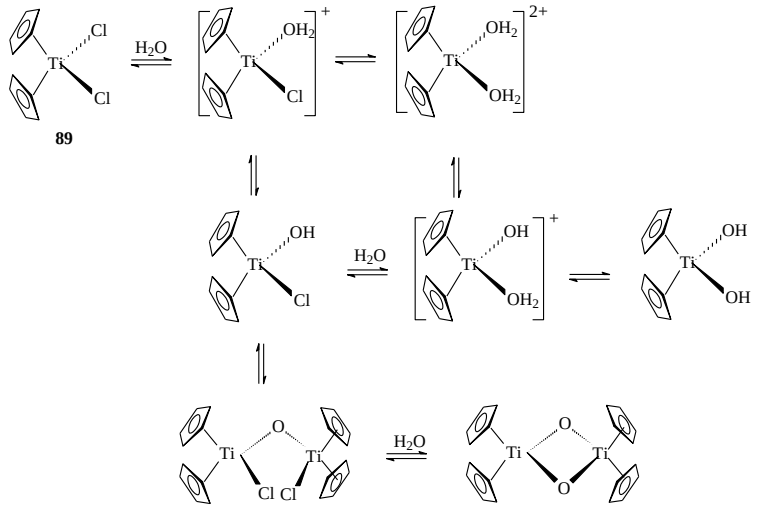

Scheme 2.12. Hydrolysis of titanocene dichloride **89**.

2.1.6. Cyclopentadienyltitanium(IV) trihalide

Cyclopentadienyltitanium(IV) trichloride (**114**) can be synthesized *via* a few different methods (Scheme 2.13.). The first method involves the reaction between magnesium cyclopentadienide and titanium tetrachloride, in a mol ratio of 1:2 $Mg(C_5H_5)_2$ to $TiCl_4$.[112] The second method involves the redistribution (scrambling) between titanocene dichloride (**89**) and titanium tetrachloride (**115**).[112] This represents the first known redistrubution reaction between an organometallic compound with delocalised bonds and a corresponding metal halide. Another method for preparing **114** involves the preferential cleavage of one of the cyclopentadienyl anions of **89** by chlorine.[113] To obtain optimum yields of **114** it is important not to expose the product to chlorine after one cyclopentadienyl anion from **89** has been removed since it has been demonstrated that **114** can be cleaved almost quantitatively to **115** under similar conditions.

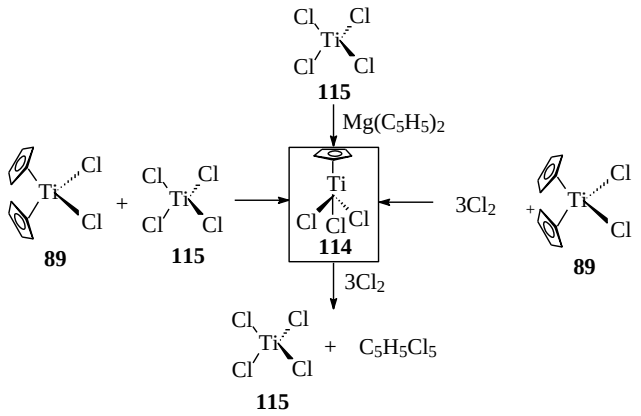

Scheme 2.13. Synthesis of cyclopentadienyltitanium(IV) trichloride (**114**).

Preparation for **114** by above mentioned methods is time consuming and the final product is obtained in low yields. In another method, described by Moorhouse, the desired compound can be obtained in a single step by the reaction shown in Scheme 2.14.A.[114] The reaction can be understood in terms of an electrophilic attack on the cyclopentadienyl group with cleavage of the silicon-carbon bond, see Scheme 2.14.B.

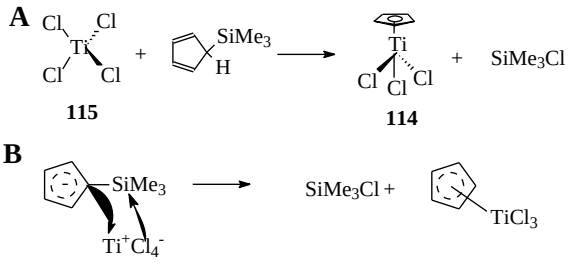

Scheme 2.14. Synthesis of **114** *via* silicon method.

2.1.6.1. Chemistry of Cyclopentadienyltitanium(IV) trihalide

Cyclopentadienyltitanium(IV) trichloride (**114**) is rather more sensitive to hydrolysis than the corresponding titanocene(IV) dichloride derivatives. In solution **114** is readily hydrolysed and appears to proceed in stages *via* $[TiCl_3Cp]_2O$,[113] to include a tetrameric oxo-bridged species.[115]

114 is a much weaker Lewis acid than $TiCl_4$ (**115**). Nevertheless, a few well-defined adducts have been reported, Scheme 2.15. shows a few.

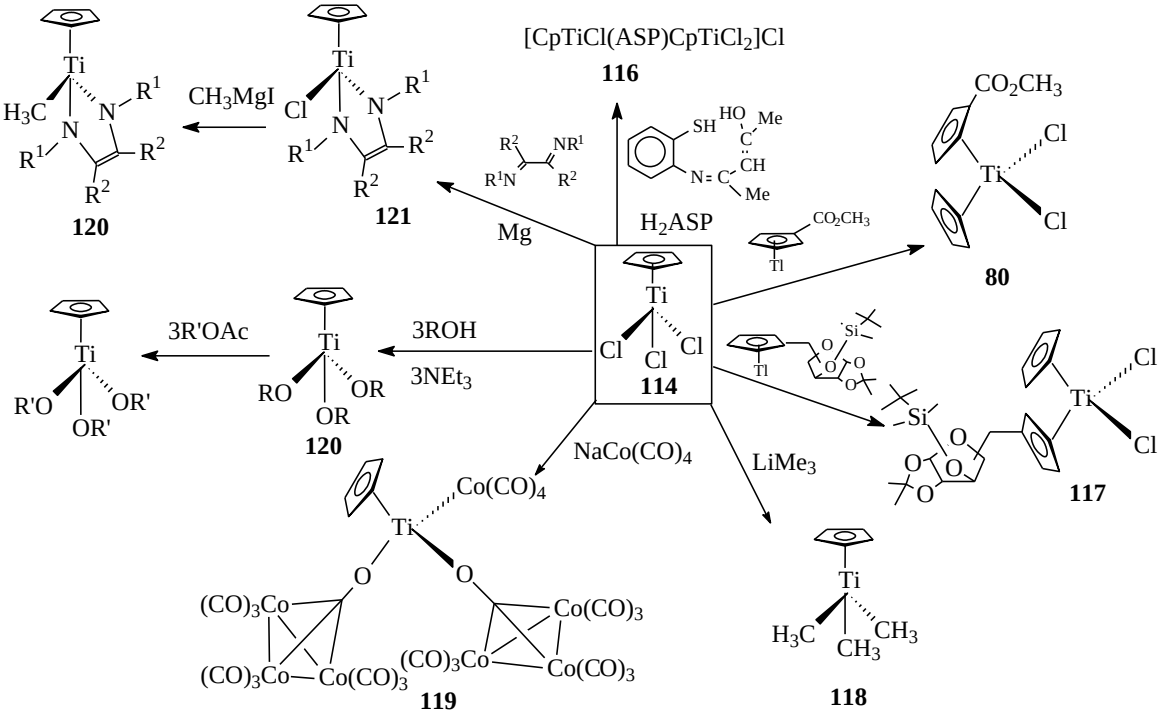

Scheme 2.15. Chemistry of Cyclopentadienyltitanium(IV) trichloride (**109**).

A complex adduct (**116**) was found during a reaction between **114** and acetylacetone-2-mercaptoanil, a potentially tridentate ligand.[116] Structural details are uncertain but IR evidence pointed to the possibility of association *via* chloride bridges. **114** is a useful starting material for the preparation of titanocene dichloride derivatives containing different cyclopentadienyl ligands, carbomethoxy- (**80**)[74] and carbohydrate-substituted (**117**)[117] titanocene dichloride derivatives. [$TiMe_3Cp$] (**118**) has been obtained from the reaction of **114** and methyllithium and readily isolated as a lemon crystalline solid.[118] **114** is a useful reagent for incorporating a titanium cyclopentadienyl into a variety of complex molecules. One example of these types of complex molecules is **119**, which is obtained by the reaction of **114** with $NaCo(CO)_4$.[119] The reactions of alcohols with **109** are complex and only in a few cases proceed to the trialkoxide (**120**).[120] A base, usually triethylamine, is normally required to remove hydrogen chloride. Exchange of the OR groups in **120** by reaction with R'OH is sometimes possible, but is generally limited to certain phenols (*m*- and *p*-fluoro substituted phenols and thiophenols),[121] and substituted cyclopentadienyl derivatives. Treatment of **114** with one equivalent magnesium in the presence of 1,4-diaza-1,3-dienes yields the monomeric titanium complex **121**.[122] Alkylation **121** with one equivalent of CH_3MgI affords the methyl derivative **122**.[122]

2.1.7. Titanium(IV) tetrachloride

Titanium(IV) tetrachloride (**115**) is a very useful starting material for obtaining many different complexes as well as for catalysis, conversions and formation of intermediate-containing titanium-carbons in alcoholysis/hydrolysis (Scheme 2.16).[118]

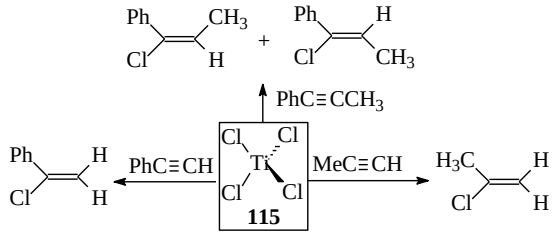

Scheme 2.16. Preparation of haloalkanes by alcoholysis/hydrolysis of reaction products by insertion of alkynes into the Ti-Cl bond of $TiCl_4$.

2.1.7.1. Chemistry of titanium(IV) tetrachloride

Many well-documented reviews on the chemistry of titanium tetrachloride are available.[118] A few points relevant to this study will, however, be highlighted. The outline of this chemistry is shown in Scheme 2.17.

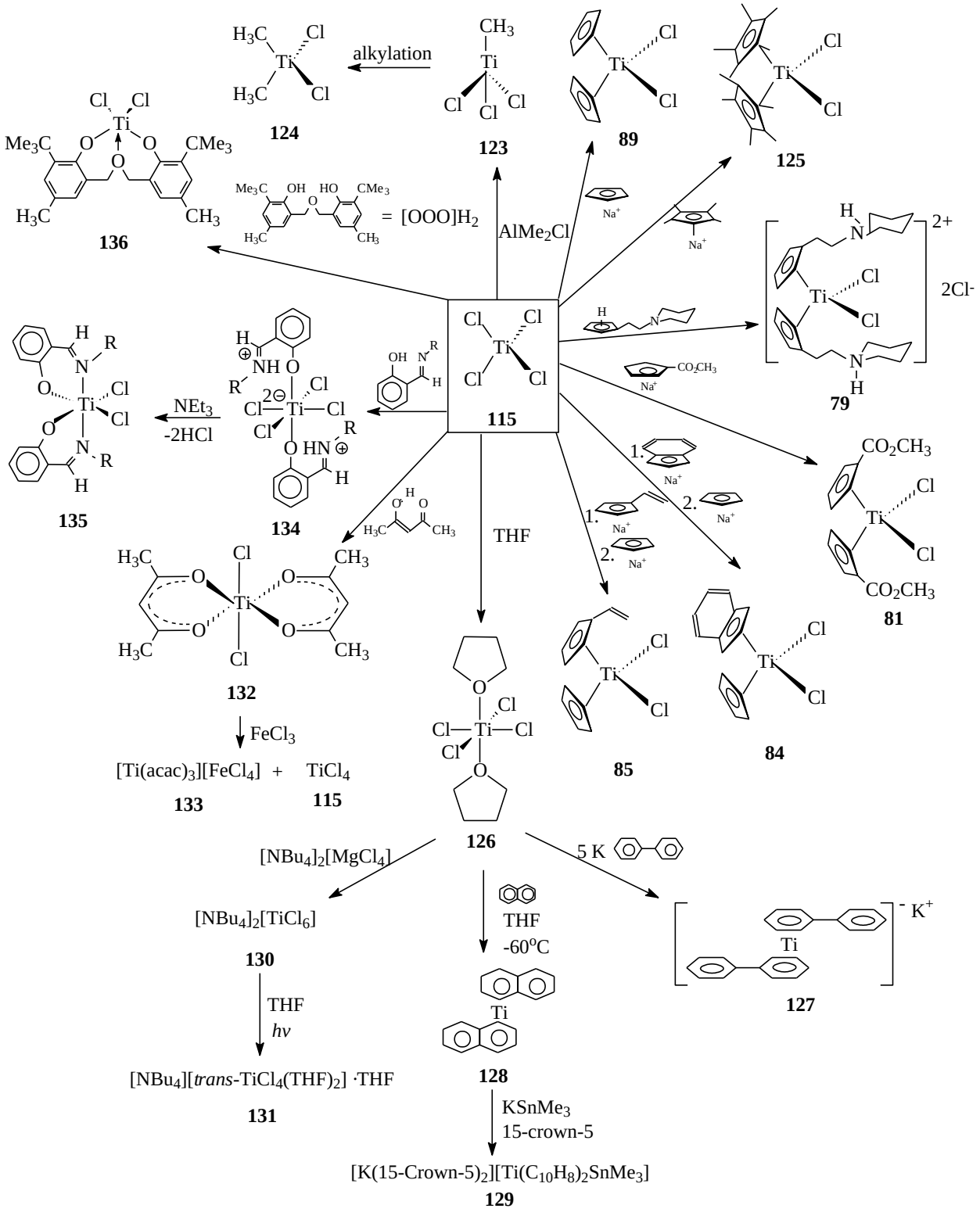

Scheme 2.17. Some chemistry of titanium tetrachloride (**115**).

The alkyltitanium(IV) halides are widely studied because of their relationship to Ziegler-Natta catalyst, the simplest member of the series being [$TiMeCl_3$] (**123**). **123** can be prepared by the reaction of **115** with $AlMe_2Cl$,[123] or **115** and MeMgBr suspended in hexane,[124] or from **115** and $ZnMe_2$.[125] Further alkylation of **123** with dimethylzinc or trimethylaluminium, gives a black complex [$TiMe_2Cl_2$] (**124**), which were found to be considerably less thermally stable than the

starting titanium compound. Titanocene(IV) dichloride (**89**) is prepared by reaction of anhydrous **115** with cyclopentadienylmagnesium halides or with cyclopentadienylsodium.[126] **115** can also be use to synthesize di-substituted cyclopentadienyl titanium derivatives, e.g. bis(methylcyclopentadienyl)titanium dichloride (**125**),[127] soluble titanocene dichloride dihydrochloride salts (**79**),[70] and the disubstituted $(C_5H_4CO_2CH_3)_2TiCl_2$ (**81**).[74] **115** can also be used for the synthesis of mono-substituted cyclopentadienyl titanocene dichloride derivatives, seeing as in some cases the trichloro complex **114** (Scheme 2.15) does not produce the desired complex due to extensive reduction. Two examples of this mixed cyclopentadienyl complexes are **84**[73] and **85**.[75] The compounds $TiCl_4{\cdot}O(CH_2CH_2)_2O$, $TiCl_4{\cdot}\ C_5H_{10}O$, $TiCl_4{\cdot}\ 2C_5H_{10}O$, $TiCl_4{\cdot}\ C_4H_8O$, $TiCl_4{\cdot}\ 2C_4H_8O$ (**126**) and $TiCl_4{\cdot}\ CH_3OC_6H_5$ have been prepared by the direct combination of **115** with the corresponding ether in carbon tetrachloride solution.[128] The only practical solvent for the tetrahydrofuran complex **126**, is THF itself. When dissolved in other solvents, the solvent molecule exchanges for THF in the coordination sphere. Because of their pronounced tendency to hydrate the THF-complex must be prepared and stored out of contact with the atmosphere.[129] Bis(arene)titanium complexes can be prepared by the reduction of **126** by arene anions, e.g. biphenyl to give **127**.[130] Bis(naphthalene)titanium complexes (**128**) can also be prepared by the reduction of **126**, which can undergo a further reaction with 15-crown-5 to yield **129**.[131] The reaction between **126** and $[NBu_4]_2[MgCl_4]$ in THF gave the compound $[NBu_4]_2[TiCl_6]$ (**130**).[132] Under the influence of light in THF **131** undergoes reduction to $[NBu_4][\textit{trans}\text{-}TiCl_4(THF)_2]{\cdot}THF$ (**131**).[132] Dichlorobis(acetylacetone)titanium(IV) (**132**) is prepared in high yield by reaction of acetylacetone and anhydrous **115** in DCM,[133] the benzoylacetonate and dibenzoylmethane can be prepared by the same method.[134] **132** can react with $[FeCl_3]$ to form an ionic complex **133** and **115**.[135] **115** forms a neutral 1:2 adduct (**134**) with *N*-(2,6,-diisopropylphenyl)salicylimine, two equivalents of HCl are removed from **134** by treatment with NEt_3 to yield the bis[*N*-2,6-diisopropylphenyl)salicylaldiminato]$TiCl_2$ (**135**).[136] 2-oxapropanediyl-1,3-bis(2-*tert*-butyl-4-methylphenol), $[OOO]H_2$, cleanly reacts with an equimolar amount of **115** to give the dichloro titanium complex $[OOO]TiCl_2$ (**136**) as pentane-soluble, microcrystals in virtually quantitative yields.[137] It is sensitive to moisture, decomposing within minutes in air.

2.1.8. Titanium(IV) alkoxide

Due to titanium's good ability to form Ti-O bond, many titanium(IV) alkoxides are known. Summarized in Scheme 2.18, is some of the titanium(IV) alkoxide's (**132**) chemistry.

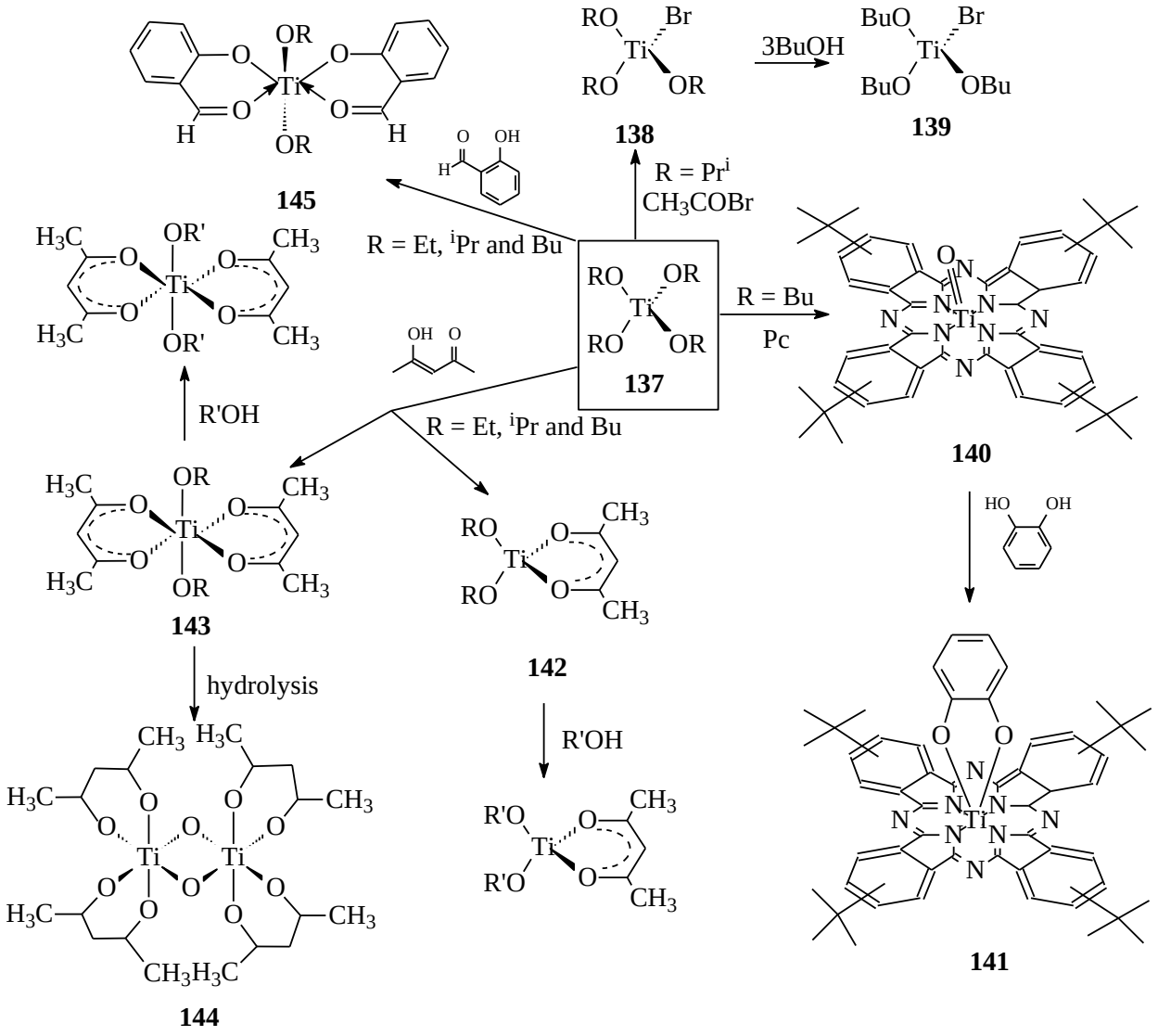

Scheme 2.18. Chemistry of some titanium(IV) alkoxide (**137**).

The reaction between the titanium alkoxide, titanium isopropoxide, and acetyl bromide gave the indicated product (**138**) in quantitative yields by using stoichiometric amounts of the reagents.[138] Further reaction of the mono-bromide (**138**) with a higher alcohol, such as butanol gave **139**.[138] Phthalocyaninatotitanium(IV) oxide (**140**) can form by reaction of the appropriate phthalocyanine (Pc) and **137**.[139] Donor ligands such as catechol possess good reactivity towards **140**, for axial ligand exchange to form **141**.[139] The reaction of **137** with acetylacetone have been found to yield two types of derivatives – dialkoxy titanium monoacetylacetonato (**142**) and dialkoxy titanium diacetylacetonato (**143**) whereas the latter does not react further with any acetylacetone, both have been shown to interchange completely their alkoxide groups with higher alcohols.[140] Hydrolysis of **143** yields a dimeric substance (**144**) with Ti-O-Ti bonds.[141] When equimolar amounts of salicylaldehyde and **137** are mixed at room temperature, heat evolves and after distilling alcohol off, the product **145** is obtained, similar reactions can be done with methyl salicylate and ethyl acetoacetate.[142]

2.2. β-Diketones

β-Diketones are well known as ligands of a variety of metals, as catalyst[143] and as antineoplastic reagents. They are also used for extracting metals in organic media. It has been shown that β-diketones complexes with rhodium(I) and derivatives of ferrocene show appreciable antineoplastic activity.[144]

2.2.1. Synthesis of β-diketones

β-Diketones are prepared in general by Claisen-condensation reactions.[145] In these reactions a ketone, which possesses an α-hydrogen, reacts with a suitable acylation reagent (ester, acid anhydride, acid chloride) in the presence of an appropriate base (Scheme 2.19).

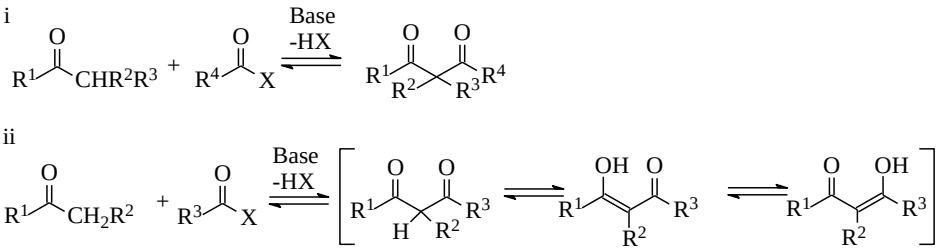

Scheme 2.19. The synthesis of β-diketones.

2.2.2. Mechanism

The mechanism of the Claisen-condensation is as indicated in Scheme 2.20. For this illustration the base lithium diisopropylamide (LDA) and the ester R^2COOEt are used.

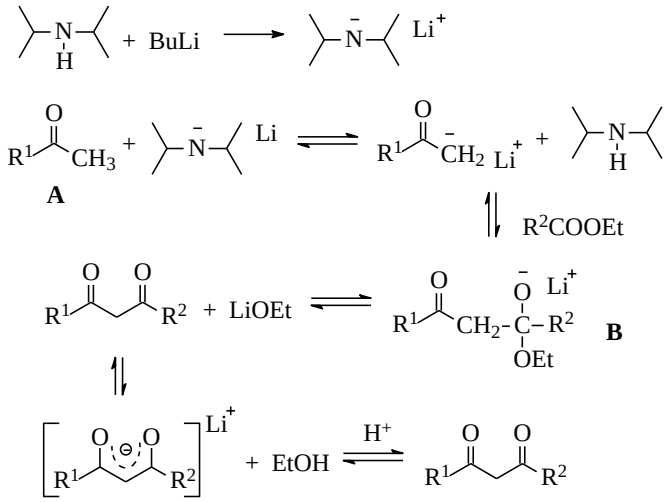

Scheme 2.20. Mechanism for the formation of a β-diketone.

2.2.3. Factors influencing the synthesis

Various aspects can influence the synthesis of a β-diketone, either positively or negatively. The pK_a of the starting ketone, **A**, determines the ease with which the α-hydrogen is removed by the base. In general the more electron donating R^1, R^2 and R^3 (Scheme 2.19), the stronger the base should be to remove the α-hydrogen. Steric factors influence the generation of the counter anion (Scheme 2.20, **B**). In general the rate of acelation of a ketone (Scheme 2.20) with a specific ester and base becomes slower for the R^1 groups (Scheme 2.19) according to the following series:[146]

(Fastest) $CH_3 > RCH_2 > R_2CH$ (slowest)

The most generally used bases are NaOH (weakest base), alkyloxides (R-OM, M = alkalimetal), hydrides, alkalimetals, simple amides (MNH_2, M = alkalimetals, strongest base) or sterically hindered bases such as lithiumdiisopropylamide (LDA). For ketones with strong electron donating R-groups (Scheme 2.19) β-diketone formation only occurs with the strong bases namely the amides.

The ease of acelation of a ketone is proportional to the rate of alkaline hydrolysis of the acelation reagent, RCOX, which is as follows:

(fastest) acidchloride > acid anhydride > ester (slowest)

Side reactions can influence the yield of the β-diketone negatively. A few side reactions that can occur during β-diketone synthesis are (see Scheme 2.21):

- Self condensation of the ketone (Aldol reaction), (i),[147]
- β-keto-ester formation, especially if the ketone which has to acelate, is unreactive, (ii),[148]
- Synthesis of bis-β-diketones from malon- and succinic acid esters sometimes leads to the Strobbe-reaction, (iii),[149]
- When the alkyl group of the ester and the alkyloxide is exchanged, the reactivity of the newly formed ester can be lowered to a point where no acelation of the ketone occurs, (iv),[150]
- Conversion of the ester to an amide, when using an amide as the base, terminates β-diketone formation, (v).[151] The use of the sterically hindered base, LDA, largely eliminates this side reaction.[152]

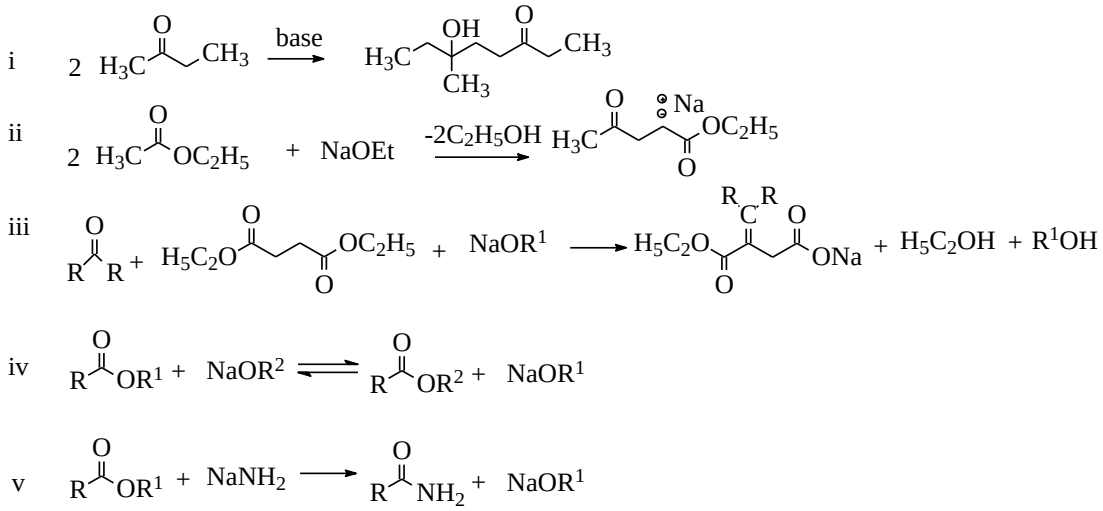

Scheme 2.21. Side reactions that can occur during the formation of β-diketones.

Seeing as β-diketone formation is an equilibrium process, synthesis can be forced to completion by either removal of ethanol from the reaction mixture,[153] or by precipitation of the anionic form of the β-diketone.

Stoichiometric amounts of base to reagent are also advantageous. The ratio of ketone: acelation reagent: sodium alkoxide should be 1:1:1, seeing as half of the alkoxide is generated in the second part of the reaction. For sodium, sodium amide or sodium hydride, however, a ratio of 1:1:2 gives better results.[154]

2.2.4. Other methods of preparation of β-diketones

The most common method for the synthesis of β-diketones is by Claisen condensation (described in paragraph 2.2.1-2.2.2). There are however, alternative routes that can be followed.

An alternative route to prepare β-diketones is by a Pinacol rearrangement of an α,β-epoxy ketone in the presence of $Pd(PPh_3)_4$ and 1,2-bis(diphenylphosphino)ethane (see Scheme 2.22. i).[155] β-Diketones are also co-formed when thioesters, containing a β-keto group in the alkyl position, is treated with a tertiary phosphine under basic conditions (see Scheme 2.22 ii).[156] Other methods include reactions which involves enzyme catalyzed reactions,[157] a solid-phase synthesis of β-diketones through the use of enamine methodology (see Scheme 2.22 iii),[158] and the use of *N*-acylbenzotriazoles as a *C*-acylation reagent for the synthesis of β-diketones (see Scheme 2.22 iv).[159] *N*-acylbenzotriazoles can also be used for the conversion of imines into enaminones (see Scheme 2.22 iv).[160]

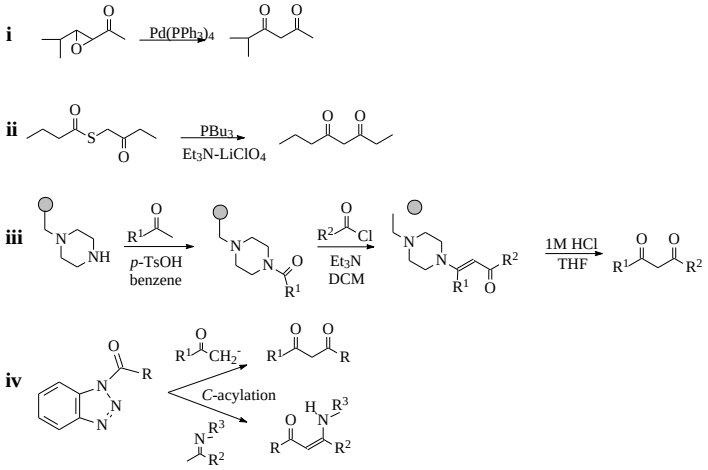

Scheme 2.22. Synthesis of b-diketone *via* different methods.

2.2.5. Keto-enol tautomerism of β-diketones

Proton transfer and hydrogen bonding are two important behavioural aspects regarding structure and reactivity of simple compounds,[161] and complex substances,[162] from water to DNA. β-Dicarbonylic compounds exhibit both features and they constitute one of the best examples of keto-enol tautomerism combining in many cases a slow proton transfer process and high concentration of the enol form which is stabilized by intramolecular hydrogen bonding.

Keto-enol tautomerism has been studied for many years by means of techniques such as bromine titration, infrared and ultraviolet spectroscopy. NMR, like other spectroscopic methods, provides the opportunity for investigating the tautomeric equilibrium without affecting the position of the equilibrium itself.[163]

The existence of keto-enol equilibria for pentane-2,4-diones (acetyl acetone) and related compounds has been recognized for a long time.[164] The position of the keto-enol equilibrium is influenced by several factors, particularly electronic and steric effects of the substituents and the nature of the solvent.[165, 166] The solvent influence on the position of the keto-enol equilibrium can be understood in the light of the strong tendency of the enol form to intramolecular H-bond, while the keto-form may bond to protic solvents *via* hydrogen bonding.

In cyclic β-diketones such as 1,3-cyclopentanodione, bulky substituents favoured the keto form, but primary alkyl groups favour the enol tautomer.[167]

Electron withdrawing subtituents lead to higher percentages of the enol tautomer in solution. ^{1}H NMR studies showed the ability of the trifluoromethyl group to attract electron density from the enolic ring by induction. It also revealed the ability of aromatic subsituents to supply electron density to the enolic ring by resonance.[168] Relevant ^{1}H and ^{13}C NMR data have been reported with regard to tautomerism of β-diketones.[169, 170, 171, 172]

The hydrogen bonding of the *cis*-enol tautomers of β-diketones is rather strong (50-100 kJ mol $^{-1}$), not very short (2.45-2.55 Å), non-centred and non-linear. The proton of this OHO bond finds itself in a double minimum potential energy well. This hydrogen bond is the key factor in determining many of the chemical properties of β-dicarbonylic compounds including the keto-enol equilibrium.[173] In general K_e is much more sensitive to the nature of the β-substituents for β-diketones than for the corresponding β-ketoester or β-ketoamides.[174]

β-Diketones have been subjected to some mass spectrometric studies. In cases where keto-enol tautomerism occur, it has been demonstrated that not only enolization regularly takes place before ionisation but it is also possible to assign certain fragmentations to specific tautomers.[175] This may also allow one to learn about their origins (from the molecule or the molecular ion) by examining the temperature effect on the g.c.-m.s. system.

Some studies on tautomeric structures of ketones,[176] and β-ketoesters,[177] give an indication of the capability of mass spectrometry to provide useful data regarding occurrence of enol forms.

2.2.6. β-diketones with a substituted 3 position

A β-diketone can be changed to have a substituent at the methine position by deprotonating both the keto and enol form of the β-diketone with a suitable base like sodium ethoxide in ethanol, to form the resonance-stabilize β-diketonato ions (Scheme 2.23). The final alkylate product is formed by nucleophilic attack of the enolate ion on the bromo-C-atom of e.g. *n*-C_4H_9Br.

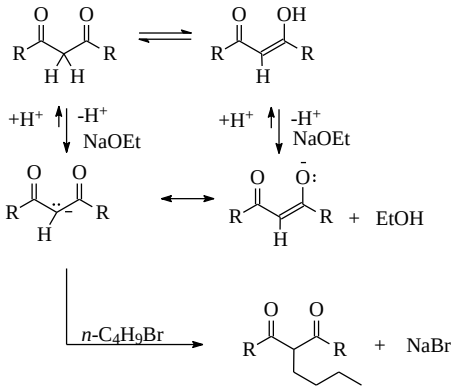

Scheme 2.23. The formation of a methine-substituted β-diketone.

2.2.7. Metal-containing β-diketones

Amongst the most widely studied coordination compounds are the complexes of β-diketones, which appear to have been investigated with virtually every metal and metalloid in the

periodic table. β-Diketones with a metal or organometallic substituent as part of the β-diketonato pseudo-aromatic structure are, however, not that well known and is still being investigated. Some of the better known metal-containing β-diketones are the ferrocene-containing β-diketones, CH_3 (**46**), CF_3 (**47**) and Ph (**49**) (see Schemes 2.4 and 2.2.4).

2.2.8. Ferrocene-containing β-diketones

The synthesis of the ferrocene-containing β-diketones compounds are basically the same as for normal β-diketone and is accomplished with the condensation of the acetylferrocene (**34**) with an appropriate ester. A few synthetic routes are available to obtain the ferrocene-containing β-diketones compounds (Scheme 2.24).[57] Ferrocene bis-β-diketones can be achieved by using the 1,1'-diacetylferrocene.

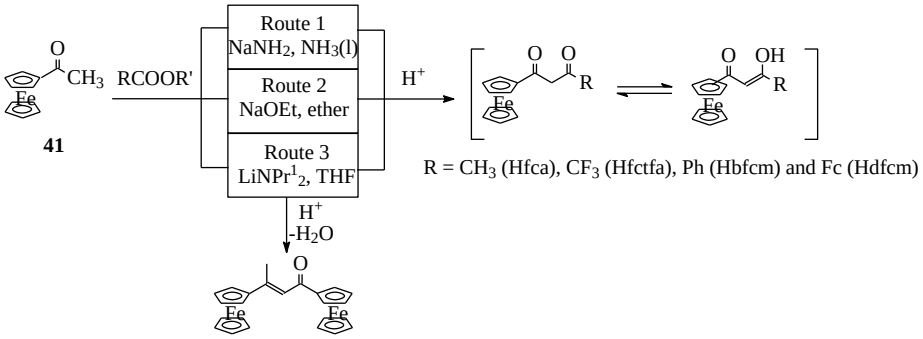

Scheme 2.24. Claisen condensation of acetylferrocene (**41**) and appropriate ester to yield a ferrocene-containing β-diketone.

Some of the physical properties such as pK_a' and % enol tautomer of the various ferrocene-containing β-diketones compounds are shown in Table 2.1.[176]

Table 2.1. pK_a' values and % enol tautomer of various ferrocene-containing β-diketones ($FcCOCH_2COR$).

R	pK_a'	% enol tautomer[216]
CF_3	7.15 (0.02)	97
CH_3	10.01 (0.2)	78
C_6H_5	10.41 (0.02)	91
Fc	13.1 (0.1)	67

Reaction of (ferrocenylmethyl)trimethylammonium iodide (**22**) with mono-sodium salts of a range of acidic 1,3-diketones leads to 2-(ferrocenylmethyl)1,3-diketones (**146**), but with the corresponding tetrabutylammonium salts deacylation occurs (Scheme 2.25).[178]

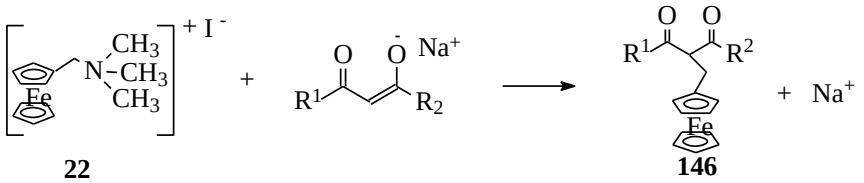

22 **146**

Scheme 2.25. Synthesis of 2-(ferrocenylmethyl)1,3-diketones.

Ferrocene-containing β-diketones can be complexed with many different metals including Pb^{2+},[179] UO_2^{2+},[179] Cu^{2+},[179] Co^{3+},[179] Fe^{3+},[179] Ni^{2+} [179] to give metal diketones. Metal complexes with different types of ligands, such as the complex [Rh(fca)(cod)],[180, 176] can also be synthesized. Another interesting reaction ferrocene-containing β-diketones can undergo is photo-induced ligand exchange (Scheme 2.26).[181] Ferrocenylacetyl acetone (**46**) in the presence of pyridine under radiation with visible light, undergo photo-induced charge transfer, resulting in the liberation of free Fe^{2+}, cyclopentadienylacetyl acetone (**147**) and a cyclopentadienyl ring. The second process involves proton-transfer from **46** to **147** and the cyclopentadienyl ring to yield **148** and **149**. The third process is complex formation, Fe^{2+} coordinates with **148** generating **150**.

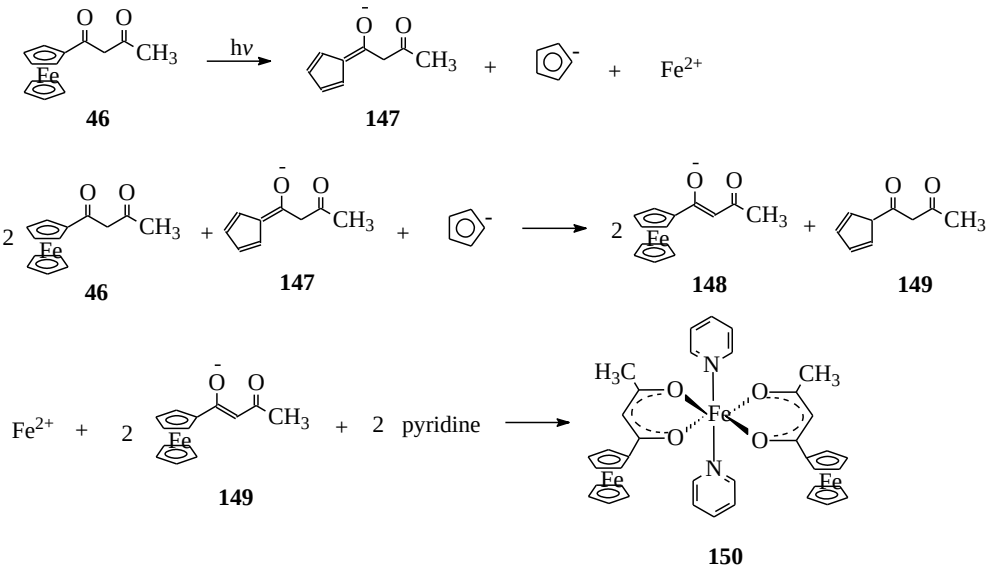

46 **147**

46 **147** **148** **149**

149

150

Scheme 2.26. Photo-induced ligand exchange of ferrocenylacetyl acetone (**46**).

2.2.9. Ruthenocene-containing β-diketones

In recent studies in this laboratory, five new ruthenocenyl-containing β-diketones were prepared by Claisen condensation of acetyl ruthenocene (**51**) and the appropriated ester.[182] These ruthenocenyl-containing β-diketones are shown in Figure 2.18. These compounds were then complexed with the rhodium dimer $[Rh_2Cl_2(cod)_2]$ to give mixed ligand rhodium complexes.

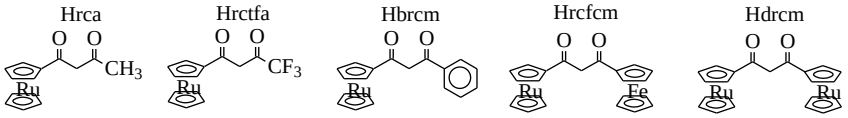

Figure 2.18. Structures of different ruthenocenyl-containing β-diketones.

Some of physical properties such as yields, pK_a' and % enol tautomer of the ruthenocenyl-containing β-diketones compounds are shown in Table 2.2.[182]

Table 2.2. Yields, pK_a' values and % enol tautomer of the ruthenocenyl-containing β-diketones.

β-diketone	% Yield	pK_a'	% enol tautomer
Hrctfa	83	7.36(3)	92.5
Hrca	27	10.22 (1)	68.5
Hbrcm	41	11.31 (4)	85
Hrcfcm	34	>13	47
Hdrcm	28	-	39.4

2.2.10. Derivatives of β-diketones

Different modifications on the basic skeleton of the β-diketone is possible, this yields completely new classes of compounds. Some of these new classes are the mono-thio-β-diketone (**156**), dithio-β-diketone (**157**), enaminone (**158**), β-enaminothione derivative (**159**) and β-keto-esters (**160**) (see Figure 2.19).

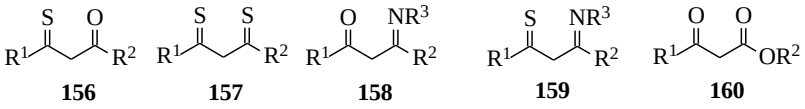

Figure 2.19. Structurally modified derivatives.

Relevant to this study are the enaminones (**158**). Various methods exist for the preparation of enaminoketones (**158**) such as reactions of α-metalated imines with esters,[183] reduction of β-amino ketones in the presence of triethyl amine promoted by Pd(II),[184] and a new method which starts from β-ketoesters or 1,3-diketones and primary amines in water to yield β-enamino ester or enaminoketones (Scheme 2.27).[185] Ketimines can be converted into enaminones by acylbenzotriazoles (Scheme 2.28).[186]

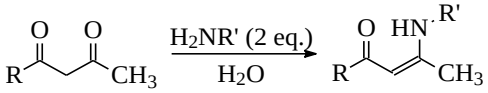

Scheme 2.27. Synthesis of β-enamino ester or enaminoketones.

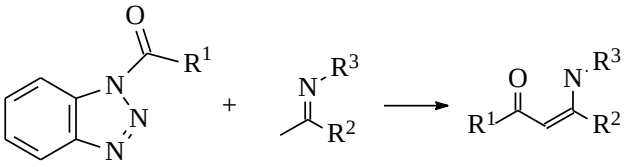

Scheme 2.28. Synthesis of enaminoketones *via* acylbenzotriazoles.

One of the simplest β-keto-esters is ethyl acetoacetate, which is prepared by reaction of 2 equivalents of ethyl acetate and sodium. Far more elaborate β-keto-esters exists like **161** shown in Figure 2.20.[187] **161** is prepared by treatment of a benzyl alcohol with diketone and a catalytic amount of *N*,*N*-dimethylamino pyridine. β-Ketoester **161** can be further reacted to yield the new β-keto-ester **162**.[187]

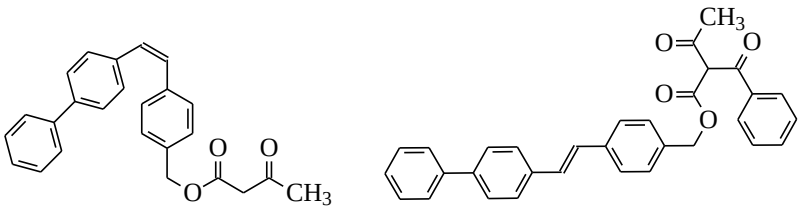

161 **162**

Figure 2.20. Structure of β-keto-esters **161** and **162**.

β-keto-esters can be synthesised with 100% regioselectivity by C-acylation of lithium enolates with methyl cyanoformate.[188] Certain β-keto-esters undergo Reformatsky-type Aldol reaction with aldehydes and ketones to yield δ-hydroxyl-β-ketoesters.[189]

2.3. Metal β-Diketonato complexes

The usual mode of bonding of β-diketone ligand is as β-ketoenolates forming a bidentate ligand. A metal cation replaces the enolic hydrogen of the ligand and a six-membered chelate ring is produced (see Figure 2.21).

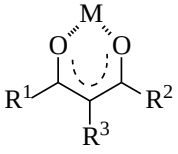

Figure 2.21. β-Ketoenolate as bidentate ligand.

Since the enolate ion carries a single negative charge, metal atoms can react with one or more enolate ions to give either neutral molecules or charged molecules depending on the coordination number and valency of the central metal atom.

2.3.1. Mono-β-diketonato titanium(III) complexes

In mono-β-diketonato metal complexes, the β-diketonato ligands are bidentate with the configuration about the metal (Ti for this study) approximately tetrahedral.[190] Acetylacetonatobis(cyclopentadienyl)titanium(III) (**163**) can be obtained *via* a few methods, one of which involves the vigorous stirring of a fourfold excess acetylacetone in a solution of $Cp_2Ti^{III}Cl$ in air-free water (Scheme 2.29).[191] Not all titanium atoms are in the III oxidation state; some of the titanium atoms are oxidized to titanium(IV) that was brought about by the protonation of the titanium(III) species by the hydrochloric acid produced in the initial step.

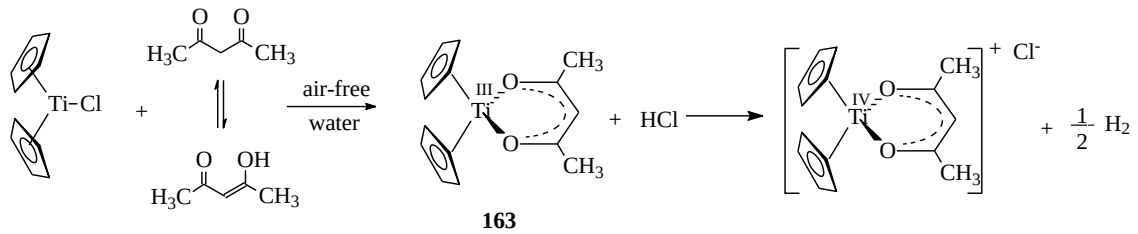

Scheme 2.29. Synthesis of acetylacetonatobis(cyclopentadienyl)titanium(III) (**163**).

An alternative approach in producing titanium(III) β-diketonato complexes **164**, involves the effective replacement of one chloride ligand in $[(C_5H_5)_2TiCl_2]$ by the β-diketone leading to the neutral paramagnetic titanocene(III)-β-diketonato complex.[192] A more efficient method of the above mentioned procedure is to start with titanocene dichloride and to reduce it with cobaltocene to form $[Co(C_5H_5)_2][(C_5H_5)_2TiCl_2]$ **165**, which reacts readily with the β-diketone and triethyl amine (Scheme 2.30).

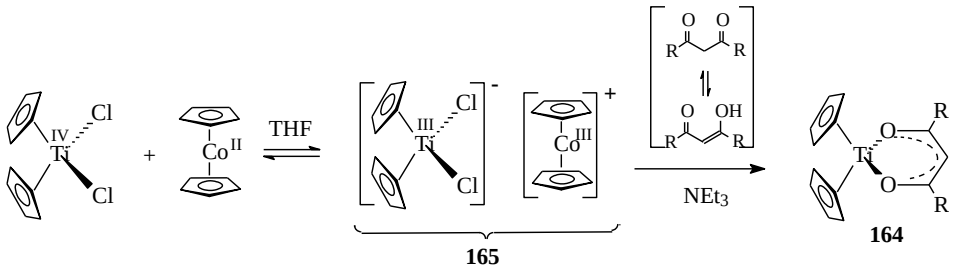

Scheme 2.30. Synthesis of titanium(III) β-diketonato complexes **164** by reduction with cobaltocene.

Crystallographic data obtained for the acetylacetonatobis(cyclopentadienyl)titanium(III) **163**,[192] shows it has a monoclinic lattice with a $P2_1/c$ space group, since the two cyclopentadienyl ligands are asymmetrically bonded. The structure was found to be slightly distorted, but the average Ti-C bond length of 2.37Å as well as the Cp-Ti-Cp angle of 134.4° are similar to values found for other titanocene(III),[193] and titanocene(IV) complexes.[194] The Ti-O bond length (2.07Å) and the O-Ti-O angle (84.3˚) are in agreement with similar complexes.

2.3.2. Mono-β-diketonato titanium(IV) and vanadium(IV) complexes

The synthesis of titanium(IV) β-diketonato complexes is usually based on an anion metathesis reaction, which is driven by precipitation of one of the products. Doyle and Tobias prepared titanocene(IV)-β-diketonato complexes *via* this procedure.[195] Titanocene dichloride dissolves in water with aquation to give cationic species and some polynuclear complexes also exist (Scheme 2.12). The product that forms is an ionic species with ClO_4^- as the counter ion. Addition of the β-diketonate reacts with the ionic specie to produce the titanocene(IV)-β-diketonato complexes (Scheme 2.31). It is important to note that even with very high concentrations of the chelating ligand it is impossible to obtain the bis chelate.

Indication that the β-diketonato ligand is chelating comes from both the infrared and NMR spectra, the complexes undoubtedly have a wedge-like sandwich structure with tetrahedral coordination about the titanium centre, which is the same coordination as for the titanocene dichloride.[196] The same synthetic strategy was used to synthesize vanadium(IV) mono-β-diketonato complexes.[197] It was found that the structural details of the vanadium and titanium β-diketonates are essentially the same. The infrared of the two compounds are almost identical and X-ray studies show that they are isomorphous.[197] The ease of preparation of these mono-β-diketonate complexes results from the very low solvation energy of the complex cation.

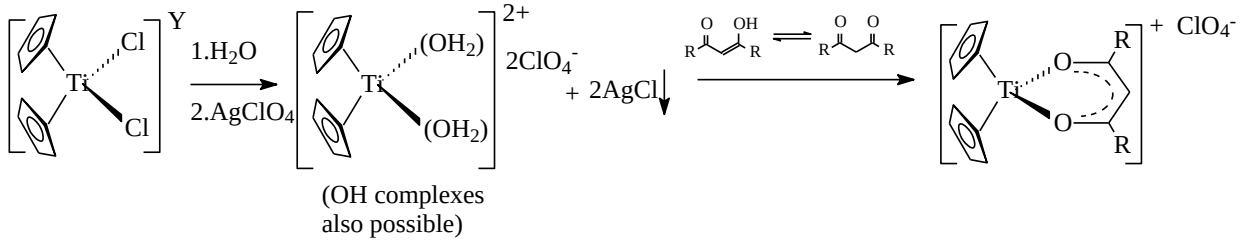

Scheme 2.31. Reaction and formation of the titanocene(IV)-β-diketonato complexes.

Metallocene(IV) complexes with various β-diketonates (Figure 2.22),[198] and different counteranions like $F_3CSO_3^-$, BF_4^- and $RR'NCS_2^-$ with R = Me, Et and *i*-Pr are known.[195, 199, 200]

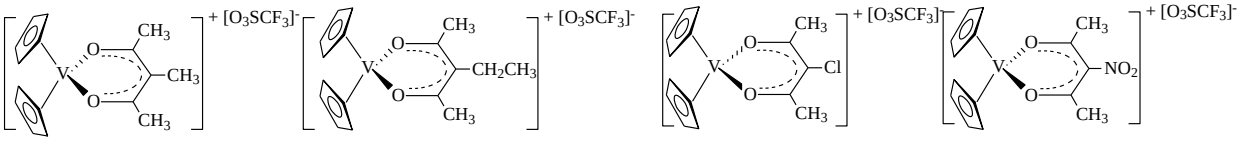

Figure 2.22. Chemical structure of vanadocene(IV) complexes with various β-diketones.

Although there is a very close parallel between the analogous bis(cyclopentadienyl)titanium(IV) and –vanadium(IV) compounds, the reaction with ethyl acetoacetate is one case where different products (Figure 2.23) are obtained. Conclusive evidence for this comes from comparing their infrared spectra.[201]

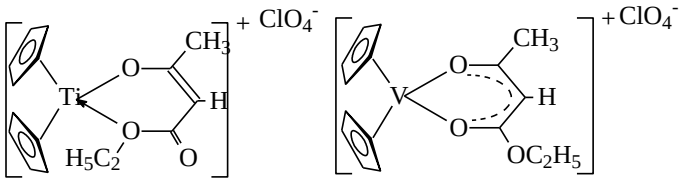

Figure 2.23. Different structures of titanocene(IV)- and vanadium(IV) ethyl acetoacetate .

2.3.3. Bis-β-diketonato metal complexes of Ti, Zr and Hf

The bis-β-diketonato complexes have an octahedral-coordination and can occur both in the *trans*- and *cis*-configuration (Figure 2.24). The *cis*-configuration is the most stable isomer for most cases, even though the *trans*-configuration may sometimes be preferred due to steric reasons. The higher stability of the *cis*-configuration is attributed to the π-back donation into the three metal *d*-orbitals (d_{xy}, d_{xz} and d_z^2), whereas for the *trans*-configuration only two *d*-orbitals (d_{xy} and d_{xz}) are involved.[202]

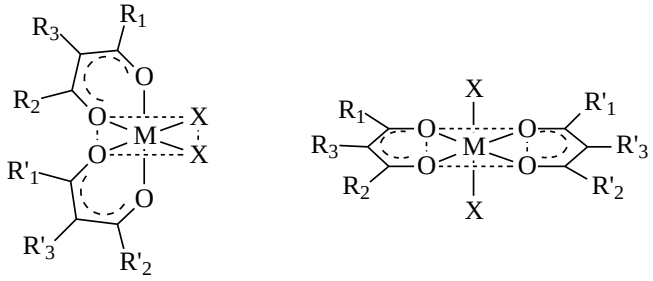

Figure 2.24. Structure of the bis-β-diketonato metal complexes, [M(bis-β-diketonato)$_2$X$_2$], in the *cis*- and *trans*-conformations, X = OR, Cl or $(C_5H_5)^-$, M = Ti^{IV} or Zr^{IV}.

Reaction of metallocene(IV) dichlorides (Ti, Zr) with β-diketonates in the presence of a hydrogen acceptor such as triethyl amine yields chlorocyclopentadienylbis(β-diketonato)metal(IV) and triethylammonium chloride (Scheme 2.32).[203] The titanium complex and the amine can be separated by extraction with benzene (or toluene). The chlorocyclopentadienylbis(β-diketonato)metal(IV) with metal = Ti, Zr and Hf are very susceptible to atmospheric moisture and can be readily hydrolysed (see Scheme 2.34 for products).

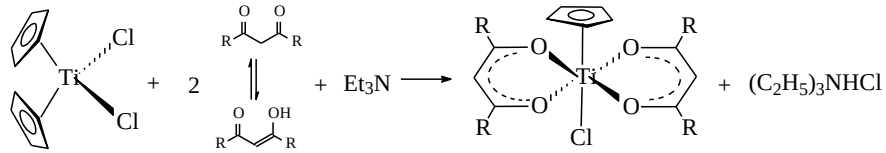

Scheme 2.32. Reaction and formation of the bis-β-diketonato titanium(IV) complexes.

Another type of bis-β-diketonato metal complex **166** (M = Ti, Zr, Hf, Ge and Sn) can be synthesized from the corresponding metal tetrahalogenides and the β-diketone in an organic solvent,[204] according to the Scheme 2.33. An exception to the rule is the corresponding molybdenum complexes, which have molybdenum pentachloride as its starting material.[204]

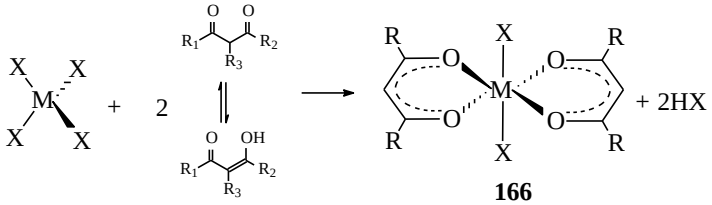

Scheme 2.33. General synthesis of [M(β-diketonato)$_2$X$_2$] complexes **166**, M = Ti, Zr, Hf, Ge and Sn, X = halogen or alkoxide.

The bis-β-diketonato metal complexes **166** hydrolyse according to Scheme 2.34.[205] The easily replaceable group, X, which is usually an alcohol or a halogen, is substituted by an aqueous group. Substitution of the group X occurs at a relatively rapid rate. The order of stability against hydrolysis, which depends on the hydrolysable group X; is:

$$OEt > F > Cl > Br > I$$

$$[M(\beta\text{-diketonato})_2X_2] \overset{H_2O}{\rightleftharpoons} [M(H_2O)(\beta\text{-diketonato})_2X]^+X^- \rightleftharpoons$$

$$[M(OH)(\beta\text{-diketonato})_2X] + HX \overset{H_2O}{\rightleftharpoons} [M(OH)(H_2O)(\beta\text{-diketonato})_2]^+X^- \rightleftharpoons$$

$$[M(OH)_2(\beta\text{-diketonato})_2] + HX \overset{-H_2O}{\rightleftharpoons} \text{polymers} \longrightarrow MO_2$$

Scheme 2.34. Hydrolysis of bis-β-diketonato metal complexes **166.**

2.3.4. Tris- and tetrakis- β-diketonato metal complexes

Although β-diketonato complexes are known for every early transition metal, zirconium and hafnium are unique in that in the Ti, Zr and Hf periodic table group, they are the only metals reported to form β-diketonates in which the metal exhibit six, seven and eight coordination numbers. The known compounds for the seven and eight coordinated species are of the type

[M(β-diketonato)$_3$Cl],[206] and [M(β-diketonato)$_4$],[206] with M = Zr, Hf and β-diketonato = dibenzoylmethanato, (PhCOCHCOPh)$^-$. Zirconium(IV) and hafnium (IV) chlorides and bromides react with a β-diketone under anhydrous conditions to yield substitution products plus hydrogen halide. In diethyl ether, the di-substituted products [M(β-diketonato)$_2$X$_2$] are obtained.[207] At higher temperatures, in refluxing benzene the reaction gives the tri-substituted product [M(β-diketonato)$_3$X].[207] The tetra-substituted product [M(β-diketonato)$_4$] cannot be prepared by reaction of M(IV) chloride with an excess of β-diketone, even after prolonged heating. However, heating of [M(β-diketonato)$_3$X] with the β-diketone (ratio 1:40) for 24 h at 80˚C, yielded [M(β-diketonato)$_4$] in 20% yield.[207]

Depending on the ratio of zirconium isopropoxide to β-diketones or β-ketoesters, a mono-, di, tri or tetra-substituted zirconium β-diketonato or β-ketoester **167** can form according to Scheme 2.35.[208]

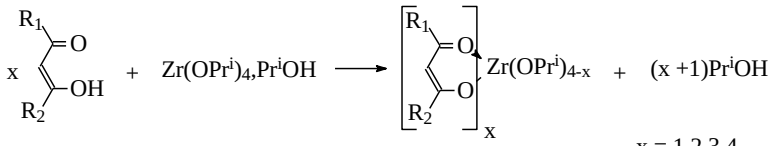

167

Scheme 2.35. The general synthesis of either a mono-, di, tri or tetra-substituted zirconium β-diketonato or β-ketoester **167**.

2.4. Acid dissociation constants

2.4.1. Introduction

In the process where a weak acid is ionised, the weak acid is in equilibrium with its corresponding conjugated base. The equilibrium constant of this process is known as the acid dissociation constant. From the following reaction, the equilibrium constant is determined by Equation 2.1.

$$HA(aq) + H_2O(l) \rightleftharpoons H_3O^+(aq) + A^-(aq)$$

$$K_c = \frac{[H_3O^+][A^-]}{[HA][H_2O]}$$

$$K_a = K_c[H_2O]$$

$$= \frac{[H^+][A^-]}{[HA]}$$

Equation 2.1.

Note $pK_a = -\log K_a$, thus for acids pK_a is given by Equation 2.2.

$$pK_a = pH + \log \frac{[HA]}{[A^-]}$$

Equation 2.2.

A large pK_a implicates a weak acid and thus a strong base. The acid dissociation constants can be used to predict the ease of reaction behaviour between two different acids and bases.

2.4.2. Methods of acid dissociation constant determinations

A few methods can be used to determine the acid dissociation constant of a compound. The most common methods used are the spectroscopic monitoring of acid base titration (for $1 < pK_a < 13$) and the conductometric method.

In the spectroscopic determination of the acid dissociation constant for β-diketones, absorbance data are collected as a function of pH. A least square fit of the absorbance/pH data into Equation 2.3 leads to the pK_a' value.[209]

$$A_T = \frac{A_{HA}10^{-pH} + A_A10^{-pKa'}}{10^{-pH} + 10^{-pKa'}}$$

Equation 2.3.

In Equation 2.3., A_T = total absorption, A_{HA} = absorption of the free β-diketone and A_A = absorption of the deprotonated (base) β-diketone.

2.4.3. Acid dissociation constants of β-diketones

Scheme 2.36 represents the reaction that takes place during the acid dissociation constant determination of β-diketones. Due to the difficulties to separate the pK_a values for the keto- and enol-tautomers of the β-diketone, the symbol pK_a' denoting the experimentally observed pK_a' value is used rather than the normal thermodynamic pK_a symbol.

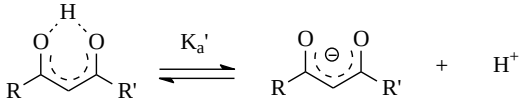

Scheme 2.36. The reaction that takes place during the acid dissociation determination of β-diketones.

Acid dissociation constants for ferrocene- and ruthenocenyl-containing β-diketones are given in Table 2.3.[182]

Table 2.3. Apparent acid dissociation constants (pK_a') of ferrocenyl- and ruthenocenyl-containing β-diketones ($FcCOCH_2COR$, $RcCOCH_2COR$) in 10% CH_3CN/H_2O mixture at 25ºC.

Ferrocenyl-containing β-diketone		Ruthenocenyl-containing β-diketone	
R	pK_a' [57]	R	pK_a' [182]
CF_3	6.53(3)	CF_3	7.36(3)
CH_3	10.01(2)	CH_3	10.22(1)
C_6H_5	10.41(2)	C_6H_5	11.31(4)
Fc	13.1(1)	Fc	>13

2.5. Group electronegativities

The ability of an atom in a molecule to attract electrons to itself, is known as electronegativity (χ) of that atom. Group electronegativities (χ_R) refer to the combined electronegativity of a specific side group, such as the CF_3 group, and not just one atom.

Electronegativity is an empirical value and is expressed especially on four different scales: the Pauling (χ_P);[210, 211] Allerd & Rochow (χ_{A+R});[210, 211] Allen (χ_{spec})[210] and Gordy (χ_G) scales.[211] With respect to this study, the Gordy scale is relevant. Figure 2.25 shows the linear relationship between the group electronegativity and the carbonyl stretching frequency (Figure 2.25) of esters of the type $RCOOCH_3$.[182]

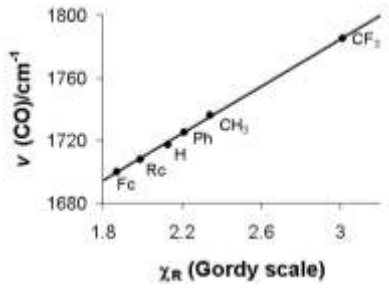

Figure 2.25. Graph of known carbonyl stretching frequencies *vs* Gordy scale group electronegativities, (χ_R) for a range of methyl esters, with R the side group when methyl ester has the structure $RCOOCH_3$.

2.6. Kinetics

2.6.1. Activation energy and activation parameters

Even though exothermic reactions are energetically (thermodynamically) favoured, not all of these reactions will proceed fast to their products. Some exothermic reactions occur readily

(almost instantaneous), whereas other reactions are slow, even to the point of being unobservable. This shows that an intermediate transition state must be involved (Figure 2.26). Every reaction in which bonds are broken will have a high energy transition state that must be reached before products can form. The energy needed to raise the reactant to the transition state energy level is called the activation energy, E_a.

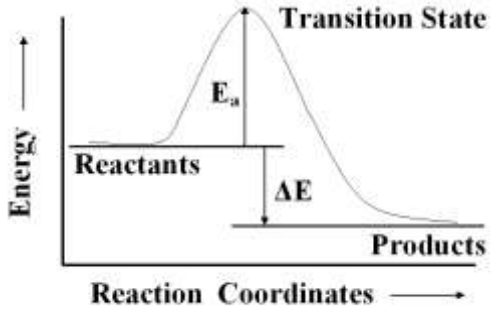

Figure 2.26. Activation energy of reactants, intermediates and products.

The rate of chemical reactions increases with temperature. Generally, the dependence of the rate constant k on temperature follows the Arrhenius equation (Equation 2.4).[212]

$$k = Ae^{(-Ea/RT)}$$

Equation 2.4.

Here E_a is the activation energy and is useful in determining the mechanism of the reaction. The higher the activation energy the slower the reaction at any given temperature.

Other activation parameters include ΔH^*, ΔS^*, $\Delta G^*$and ΔV^*. The sign and magnitude of these thermodynamic parameters also often indicate the mechanism of a reaction. The transition state theory postulates that an activated complex is in equilibrium with the reagent before the reaction takes place. The reaction rate is given by the rate of decomposition of the activated complex to form the products (Scheme 2.37). The rate constant is given by Equation 2.5 according to this theory.

$$A + B \underset{}{\overset{K_c^*}{\rightleftharpoons}} [A{\cdot}B]^* \xrightarrow{k} \text{products}$$

Scheme 2.37. General scheme illustrating the transition state theory.

$$k = (RT/Nh)K_c^*$$

Equation 2.5.

Here K_c^* = equilibrium constant, R = gas constant, h = Planck's constant, N = Avogadro's number and T = absolute temperature.

The information of this activated complex is governed by thermodynamic considerations similar to those of ordinary chemical equilibria. The free energy of activation is thus defined thermodynamically as shown in Equation 2.6.

$$\Delta G^{*} = -RT \ln K_c^{*}$$
$$= \Delta H^{*} - T\Delta S^{*}$$

Equation 2.6.

Combination of Equations 2.5 and 2.6 gives Equation 2.7.

$$\ln k = \ln [(RT)/(Nh)] + \Delta S^{*}/R - \Delta H^{*}/ RT$$

Equation 2.7.

The magnitude of ΔS^{*}, can be used to determine whether the mechanism of substitution is associative or dissociative of nature. A significantly positive ΔS^{*} value indicate a dissociative mechanism and a large negative ΔS^{*} value indicates an associative mechanism of substitution.

The volume of activation consists of two parts: an intrinsic part ΔV^{*}_{intr} and a solvation part ΔV^{*}_{solv}, and is defined in Equation 2.8.

$$\Delta V^{*} = \Delta V^{*}_{intr} + \Delta V^{*}_{solv}$$

Equation 2.8.

The volume changes that arises during the formation of the transition state due to the vibrations in bond lengths and angles are represented by ΔV^{*}_{intr}, while the change in solvation is reflected by ΔV^{*}_{solv}. For a dissociative mechanism ΔV^{*}_{intr} is positive due to bond cleavage and ΔV^{*}_{solv} is negative due to electrostriction, thus $\Delta V^{*}$is approximately zero for a dissociative mechanism.[213] For an associative mechanism on the other hand ΔV^{*} is large negative, due to the negative contribution from ΔV^{*}_{intr} (which arises from the bond formation) and only a minor contribution from ΔV^{*}_{solv}. Hence, a dissociative mechanism is indicated by positive ΔS^{*} (measured in J) and ΔV^{*} values, whereas large negative ΔS^{*} and ΔV^{*} values indicate an associative mechanism.

2.6.2. Isomerisation Kinetics

The chemistry of enols has traditionally attracted a great deal of attention. Particular interest has been focused on the enolic forms of β-diketones due to the tautomeric proton transfer equilibrium in solution between the keto- and two possible enol forms. It is possible to follow the

rate of keto- to enol-conversion (and *vice versa*) kinetically, provided the rate of conversion is slow.

In ^{13}C NMR studies done on *p*-substituted benzoylacetones, it was found that the tautomeric equilibrium between the enol forms is shifted towards the methyl keto form by electron withdrawing groups.[214] It has also been proved that solvents systems also affect the keto-enol equilibrium. Studies carried out on acetylacetone in different alcohol:water ratios, showed more alcohol in solution favours the enol isomer.[215]

^1H NMR studies on metallocene-containing (ferrocene[216] and ruthenocene[182]) β-diketones, revealed that the dominant enol isomer in solution was such that the C=O group is adjacent to the ferrocenyl or ruthenocenyl groups and that the enol C-OH group is adjacent to the R side group of Mc-CO-CH=C(OH)-R. Thermodynamic data of keto enol conversion for some ruthenocenyl-containing β-diketone's are given in Scheme 2.38 and Table 2.4.

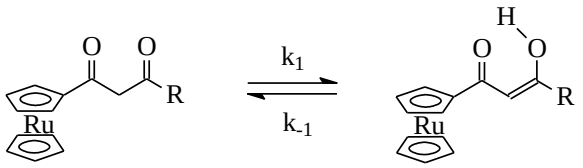

Dominant form

Scheme 2.38. The keto-enol tautomerization of the ruthenocene-containing β-diketones (R = CF_3, CH_3, Ph, Fc and Rc).

Table 2.4. Data of the keto-enol tautomerization of the ruthenocene-containing β-diketones (R = CF_3, CH_3, Ph, Fc and Rc) in $CDCl_3$ at 293K.

R-group	χ_R	% enol at equilibrium	K_c in $CDCl_3$ at 293K	ΔG (kJ mol^{-1})
CF_3	3.01	92.5	12.3	-6.11
CH_3	2.34	68.5	2.2	-2.6
Ph	2.21	85.0	5.7	-4.24
Fc	1.87	47.0	0.9	0.26
Rc	1.99	39.4	0.7	1.05

2.6.3. Substitution kinetics

Substitution reactions or ligand exchange is usually divided into three main groups: nucleophilic substitution, electrophilic substitution and oxidative addition followed by reductive elimination.[217] These substitution reactions involve the interaction between 18-electron and 16-

electron species. Factors that may influence the rate of substitution is the type and nature of all the ligands involved (entering, leaving and remaining), the central metal atom and the solvent.[218]

There are two main mechanisms of ligand substitution that can be identified, they are the dissociative mechanism and the associative mechanism.

2.6.3.1. The dissociative mechanism

The dissociative mechanism resembles S_N1 substitution in organic chemistry. Firstly the leaving monodentate ligand dissociates from the coordination sphere of the metal. The number of monodentate ligands bonded to the central metal atom is thus reduced. Secondly, the incoming (entering) ligand reacts with the transition state to form the final product. The intermediate transition state, $[L_nM]$, is coordinatively unsaturated and very reactive.

Slow step: $[L_nM - X] \xrightarrow{k,\ slow} [L_nM] + X$

Fast step: $[L_nM] + Y \xrightarrow{fast} [L_nM - Y]$

The kinetic rate law takes the form: rate = $k[L_nM - X]$ and the entropy of activation (ΔS^*) is positive because the transition state is less ordered than the starting materials. In a dissociative mechanism, the stereochemistry may be retained or racemization may take place. This depends on the rate at which the incoming ligand reacts with the intermediate $[L_nM]$.[219]

2.6.3.2. The associative mechanism

The associative mechanism resembles S_N2 substitution in organic chemistry. The incoming ligand initially binds to the metal centre, leading to an intermediated with an increased coordination number. This intermediate subsequently undergoes a further reaction, where the leaving group detaches to give the substituted product.

Slow step: $[L_nMX] + Y \xrightarrow{k,\ slow} [L_nM\langle^{X}_{Y}]$

Fast step: $[L_nM\langle^{X}_{Y}] \xrightarrow{fast} [L_nM - Y] + X$

A different kinetic rate law applies: rate = $k[L_nMX][Y]$. The activation entropy (ΔS^*) is negative, which implies that the transition state is more ordered than the starting materials. Electron-deficient complexes (*e.g.* 16 or 17 valence electron compounds) favour the associative mechanism, but some 18 electron compounds also follow the associative mechanism.[219] The

associative mechanism often involves solvolysis (Scheme 2.39), especially if the solvent is polar or has a tendency to solvate. If solvolysis takes place the kinetic rate law changes to:

$$\text{rate} = (k_s + k_2[Y])[L_nM - X] = k_{obs}[L_nM - X]$$

where $k_{obs} = k_s + k_2[Y]$, a pseudo first order rate constant, k_s = rate constant of solvent pathway and k_2 = rate constant of the direct pathway.

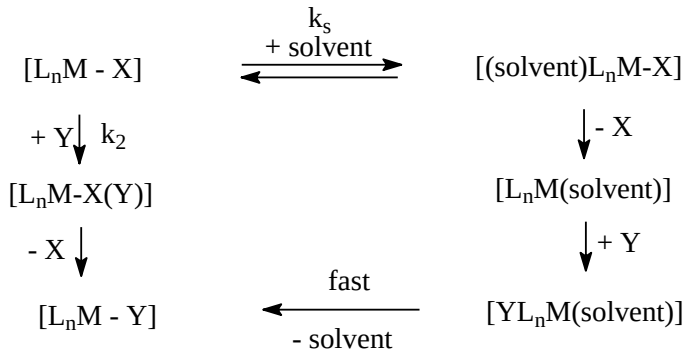

Scheme 2.39. Schematic representation of the direct and solvent pathway for the associative mechanism.

2.6.4. Ligand exchange between titanium(IV) complexes

Dihalo- and dialkoxybis(β-diketonato)titanium(IV) complexes undergo rapid ligand exchange reactions (redistribution reactions) which exchange both the monodenate axial halo or alkoxy ligands (equation 1) and the bidentate β-diketonato ligand (equation 2).[220]

$$Ti(\beta\text{-dik})_2(X)_2 + Ti(\beta\text{-dik})_2(Y)_2 \rightleftharpoons 2Ti(\beta\text{-dik})_2XY \quad ...1$$

$$Ti(\beta\text{-dik})_2(X)_2 + Ti(\beta\text{-dik}')_2(X)_2 \rightleftharpoons 2Ti(\beta\text{-dik})(\beta\text{-dik}')(X)_2 \quad ...2$$

^{1}H NMR spectra for a solution containing equimolar amounts of $Ti(acac)_2F_2$ and $Ti(acac)_2Br_2$ are shown in Figure 2.43(a). The resonance lines at the lowest and highest field were assigned to the methine protons of $Ti(acac)_2F_2$ and $Ti(acac)_2Br_2$, respectively, by reference of the pure parent compounds. The resonance at intermediate field was assigned to the mixed-ligand complex $Ti(acac)_2FBr$. Similar results were obtained for $Ti(acac)_2F_2$ and $Ti(acac)_2(OEt)_2$.

^{1}H NMR spectra for a solution containing equimolar amounts of $Ti(acac)_2F_2$ and $Ti(tfca)_2F_2$ are shown in Figure 2.27(b). The resonance at lowest and highest field are due to the parent complexes $Ti(acac)_2F_2$ and $Ti(tfac)_2F_2$, while the two lines at intermediate field were assigned to the mixed-ligand complex $Ti(acac)(tfac)F_2$.

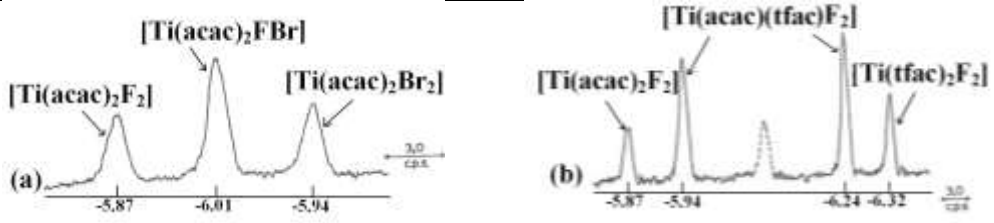

Figure 2.27. Methine proton of ^{1}H NMR of (a) $Ti(acac)_2F_2$ + $Ti(acac)_2Br_2$ and (b) $Ti(acac)_2F_2$ + $Ti(tfac)_2F_2$.

The exchange reactions of zirconium and hafnium trifluoroacetylacetone with the free ligand in benzene and chlorobenzene and of the metal acetylacetones with the free ligand in chlororbenzene are first order in both metal complex and free ligand.[221] The acetylacetone exchange in benzene has a different rate law. The order with respect to the metal complex is one; however, the order with respect to the free ligand increases as the acetylacetone concentration increases.

2.6.5. Hydrolysis kinetics of metal alkoxides

Metal alkoxides have strong reactivity toward water due to the difference of polarizabilities between metal and alkoxy groups. Hence, many kinds of metal alkoxides can be hydrolyzed with ease and transformed to metal oxides. The reaction of hydrolysis reaction mechanism of the metal alkoxides depend on the electron affinities, size and charges of the metal ions. The sizes and numbers of alkoxy groups play an important role in the hydrolysis reaction.

The mechanism of hydrolysis of $Ti(OEt)_4$ is thought to be in two stages. First $Ti(OEt)_4$ is hydrolysed to form Ti-OH bonds and in the second stage a condensation polymerization takes place to form Ti-O-Ti bonds, resulting in a three dimensional structure.[222] During the second stage the absorbance increases rapidly and makes it difficult to determine the absolute equilibrium point of absorbance. Therefore, the hydrolysis reaction stage, where absorbance increased gradually were used to determine the reaction rate constant. The rate of hydrolysis was found to be first order when Guggenheim's method was used.[222, 223] When Kivinen's equation was used,[224] second order rate constants, k_{exp}, could be determined. Two kinds of mechanisms were proposed: associative and interchange associative.

When dihalobis(β-diketonato)titanium(IV) complexes $[Ti(acac)_2(X)_2]$ were exposed to the atmosphere, the crystalline solids showed pitting of the crystal faces, loss of sharp extinction and loss of color.[133] It was found that the dibromo and dichloro- bis(acetylacetonato)titanium complexes converted to an opaque white powder, which was presumed to be titanium(IV) oxide. Different degrees of hydrolysis for $[Ti(acac)_2(X)_2]$ compounds were observed after the following

air exposure times: The dibromide was almost completely hydrolysed in 2h; the dichloride in *ca*. 5 days. Even after 10 days the difluoride was only partially hydrolysed. When these complexes $[Ti(acac)_2(X)_2]$ were in acetonitrile solution and treated with water, hydrolysed products of the dibromide and dichloride complexes precipitated immediately. The difluoride acetonitrile solution immediately became turbid.

When similar complexes such as, budotitane derivatives $[Ti(bzac)_2(X)_2]$, are mixed with cremophor and propylene glycol, micelles are formed when dissolved in water.[225] These micelles surround the substance, protecting it from hydrolysis and making it water-soluble. This cremophor-propylene glycol-budotinane mixture gives the complex stability over several hours.

2.7. Electronanalytical chemistry

2.7.1. Voltammetry

Voltammetry comprises a group of electroanalytical methods in which information about an analyte is derived from the measurement of current as a function of applied potential obtained under conditions that encourage polarization of a working electrode. It is widely used by inorganic, physical and biological chemists for characterisational purposes, including fundamental studies of oxidation and reduction processes in various media, adsorption processes on surfaces and electron transfer mechanisms at chemically modified electrode surfaces.

In voltammetry, a variable potential excitation signal is impressed upon an electrochemical cell containing an electrode. This excitation signal elicits a characteristic current response upon which the method is based. Three of the most common excitation signals are shown in Figure 2.28. With the triangular waveform (A), the potential is cycled between two values, first increasing linearly to a maximum and then decreasing linearly with the same numerical rate to its original value. This cyclic voltammetric process may be repeated numerous times with the current being recorded as a function of time. Square-wave voltammetry (B) is one of the types of two pulse excitation signals, where the currents are measured at various times during the lifetime of these pulses. From this type of voltammetry better resolution is gained, when the CV data does not clearly distinguish between multiple peaks. The linear sweep method (C) represents the classical voltammetry excitation signal, in which the dc potential applied to the cell increases linearly very slowly as a function of time. From an analytical point of view this type of voltammogram is advantageous because it can be used to accurately determine the relative amount of electrons, to flow in a particular electrochemical process (one in the Fe^{2+}/Fe^{3+}

system) compared to other electrochemical processes. Linear sweep voltammetry represents the first, forward wave of a CV, at very slow scan rates (2 mV s^{-1} maximum). Typical CV scan rates are 50 mV s^{-1} or faster, but it is dependent on active electrode area.

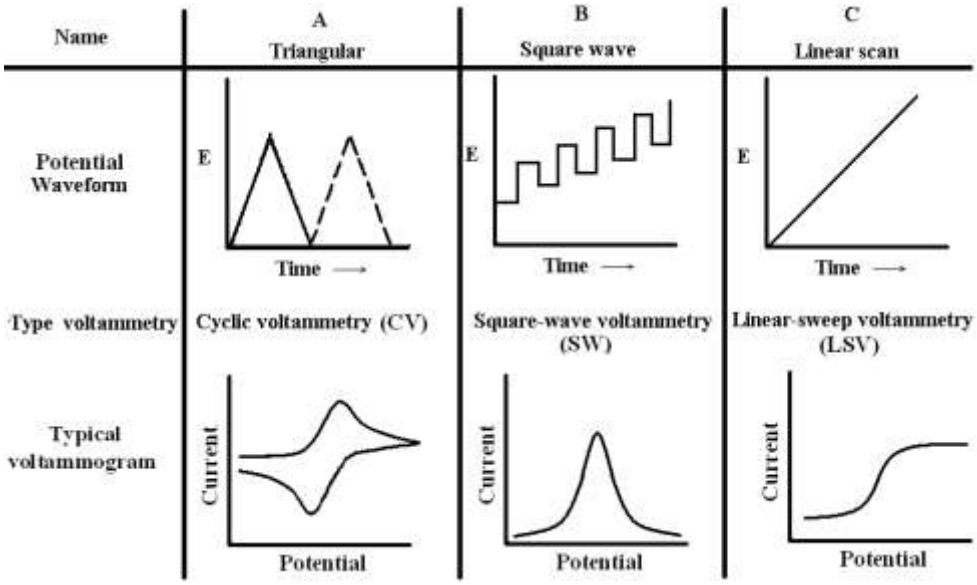

Figure 2.28. Potential excitation signals used in voltammetry.

2.7.1.1. Cyclic voltammetry

Cyclic voltammetry (CV) is possibly the simplest and most versatile electroanalytical technique for the study of electroactive species. The effectiveness of CV is its ability to probe the redox behaviour of an electroactive species fast over a wide potential range.[226] Cyclic voltammetry is a simple and direct method for the measurement of the formal reduction potential of a reaction when both oxidized and reduced forms are stable during the time when the voltammogram is taken.[227] Both thermodynamic and kinetic information are available in one experiment. Therefore, both reduction potential and heterogeneous electron transfer rates can be measured. The rate and nature of a chemical reaction coupled to the electron transfer step can also be studied. Knowledge of the electrochemistry of a metal complex can be useful in the selection of the proper oxidizing agent to oxidize the metal complex to an intermediate oxidation state.

The current response on a cyclic voltammogram (vertical axis) is plotted as a function of the applied potential (horizontal axis). Figure 2.29 shows a typical CV. Often there is very little difference between the first and successive scans. However, the changes that do appear on repetitive cycles are important in obtaining and understanding information about reaction mechanisms.

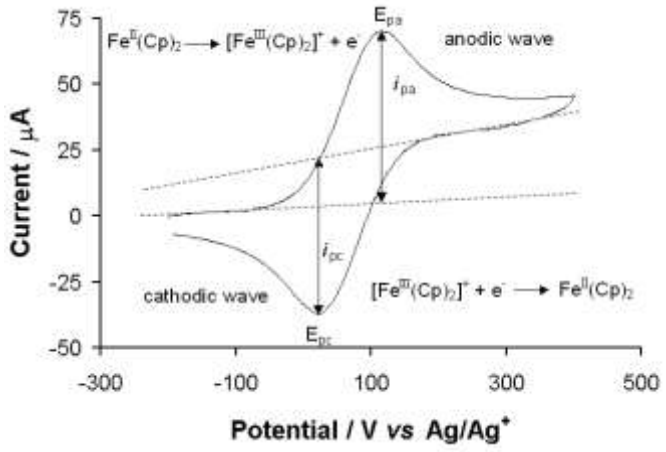

Figure 2.29. Cyclic voltammogram of a 3.0 mmol dm^{-3} solution of ferrocene measured in CH_3CN/0.1 mol dm^{-3} [NBu][PF_6] on a glassy carbon electrode at 25˚C, scan rate 100mV s^{-1}. Cp = $(C_5H_5)^-$.

2.7.1.2. Important parameters of cyclic voltammetry [226, 228]

The most important parameters of cyclic voltammetry are the peak anodic potentials (E_{pa}), peak cathodic potential (E_{pc}) and the magnitudes of the peak anodic current (i_{pa}) and peak cathodic current (i_{pc}) (Figure 2.29). One method of measuring i_p involves the extrapolation of a current baseline to eliminate background currents. Establishing the correct baseline is essential for accurate measurement of the peak currents.

A redox couple may or may not be electrochemically reversible. By electrochemically reversibility, it is meant that the rate of electron transfer between the electrode and substrate is fast enough to maintain the concentration of the oxidised and reduced species in equilibrium according to the Nernst equation at the electrode surface at the particular scan rate. The formal reduction potential for an electrochemically reversible redox couple is midway between the two peak potentials (Equation 2.9)

$$E^{01} = (E_{pa} + E_{pc})/2$$

Equation 2.9.

This E^{01} is an estimate of the polarographic $E_{1/2}$ value provided that the diffusion constants of the oxidised and reduced species are equal. The polarographic $E_{1/2}$ value can be calculated from E^{01} *via* Equation 2.10.

$$E_{1/2} = E^{01} + (RT/nF) \ln (D_R/D_O)$$

Equation 2.10.

Here D_R = diffusion coefficient of the reduced specie, D_O = diffusion coefficient of the oxidised specie. In cases where $D_R/D_O \approx 1$, $E_{1/2} \approx E^{01}$.

For electrochemical reversible couples the difference in peak potentials (ΔE_p) should be 59 mV at 25˚C for a one electron transfer process. The number of electrons (n) transferred in the electrode reaction for a reversible couple can be determined from the separation between the peak potentials from Equation 2.11.

$$\Delta E_p = E_{pa} - E_{pc} \approx (59\ mV)/n$$

Equation 2.11.

This (59 mV)/n separation of peak potentials is independent of the scan rate of the reversible couple, but slightly dependent on the switching potential and cycle number.[229] In practice, within the context of this research program, a redox couple with a ΔE_p value up to 90 mV will still be considered as electrochemically reversible. Peak separation increases due to slow electron transfer kinetics at the electrode surface, and also because of over potentials or high solvent resistence.

The peak current, i_p, is dependent on a few variables and is described by the Randle-Sevcik equation for the first sweep of the cycle at 25˚C (Equation 2.12).

$$i_p = (2.69 \times 10^5) n^{3/2} A D^{1/2} v^{1/2} C$$

Equation 2.12.

i_p = peak current (A), n = amount of electrons per molecule, A = working electrode surface (cm^2), C = concentration (mol cm^{-3}), v = Scan rate (V s^{-1}) and D = Diffusion coefficient (cm^2 s^{-1}).

The values of i_{pa} and i_{pc} should be identical for a reversible redox couple, which is not followed by any chemical reaction (Equation 2.13).

$$i_{pc}/i_{pa} = 1$$

Equation 2.13.

Systems can also be quasi-reversible or irreversible (Figure 2.30). An electrochemically quasi-reversible couple is where both the oxidation and reduction processes takes place, but the electrochemical kinetics are slow and theoretically $\Delta E_p > 59$ mV (practically within the context of this thesis 90 mV $\leq \Delta E_p \leq \pm$ 150 mV are considered to indicate an electrochemically quasi-reversible couple). A complete chemical irreversible system is one where only oxidation or reduction is possible.[230] In cases where the system is quasi-reversible or irreversible, Equations 2.10, 2.12 and 2.13 are not applicable.

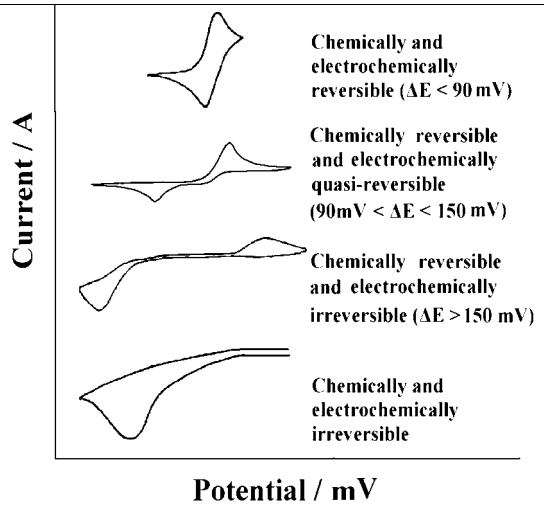

Figure 2.30. A schematic representation of the cyclic voltammogram expected from an electrochemical reversible, an electrochemical irreversible and a chemical irreversible system. The indicated potential limits are not theoretical predictions. Rather, they indicate limits that are used for classification purposes from practically determined values within the scope of this study.

2.7.1.3. Solvents, supporting electrolytes and reference electrodes

A suitable medium is needed for electrochemical phenomena to occur. This medium generally consists of a solvent containing a supporting electrolyte. The most important requirement of a solvent is that the electrochemical specie under investigation must be soluble and stable in it.[231] The electrochemical species under investigation must be soluble to the extent of at least 1 x 10^{-4} mol dm^{-3} and the electrolyte concentration must be at least 10 times but preferably 100 times that of the electrochemical specie under investigation. An ideal solvent should possess electrochemical and chemical inertness over a wide potential range, it should be a good solvent for both electrochemical species and electrolyte, and it should preferably be unable to solvate the electrochemical specie. Solvents that are often used are dipolar aprotic solvents, which have large dielectric constant ($\geq$ 10) and low proton availability. Acetonitrile (CH_3CN) has a dielectric constant of 37 and is most commonly used in anodic studies, THF is useful in cathodic studies. CH_3CN is an excellent solvent for both inorganic salts and organic compounds and is stable after purification. Dichloromethane (DCM) is used when a strictly non-coordinating solvent is required.

In the majority of electroanalytical and electrosynthetic experiments, a supporting electrolyte is used to increase the conductivity of the medium. Most of the current is carried by the ions of the supporting electrolyte. Tetrabutylammonium hexafluorophosphate, $[NBu_4][PF_6]$, is the most widely used supporting electrolyte, in organic solvents. A $[NBu_4][PF_6]$ solution in CH_3CN exhibits a wide potential range with positive (3.4 V) and negative decomposition potentials (–2.9 V) *vs* SCE.[232]

In the past, nearly al experimental papers, potentials of a reference electrode are specified *vs* normal hydrogen electrode (NHE) or saturated calomel electrode (SCE). However, IUPAC now recommend that all electrochemical data are reported *vs* an internal standard.[233] In organic media the Fc/Fc^+ couple (Fc = ferrocene) is a convenient internal standard. [234, 235] The Fc/Fc^+ couple exhibits E^{01} = 0.400 V *vs* NHE.[236] NHE and SCE are used for measurements in aqueous solutions. However, in many instances electrochemical measurements in water are impossible due to insolubility or instability. With non-aqueous solvents, an experimental reference electrode such as Ag/Ag^+ (0.01 mol dm^{-3} $AgNO_3$ in CH_3CN) or Ag/AgCl may be used.

Recent developments in the development of new supporting electrolytes and the use of non-traditional solvents have increased options in electrochemical studies. The use of the non-coordinating but very expensive supporting electrolyte tetrabutylammonium tetrakis(pentafluorophenyl)borate, $[NBu_4][B(C_6F_5)_4]$, improves electrochemistry results compared to electrochemistry results obtained by utilising the weak coordinating electrolyte tetrabutylammonium hexafluorophosphate.[237] It was shown that with the use of this new electrolyte, electrochemistry could be conducted in solvents of low dielectric strength and reversible electrochemistry could be obtained for compounds that are normally irreversible.[238] It was also shown that the peak separation between two very close oxidation peaks could be better analysed with the use of this electrolyte.[239]

2.7.1.4. Bulk electrolysis

While cyclic voltammetry, linear sweep voltammetry and square wave voltammetry only considers electrochemistry at the surface of an electrode, the bulk electrolysis technique involves the electrolysis of the bulk solution. The total amount of coulombs consumed during electrolysis is used to determine the amount of substance electrolysed. Alternatively the number of electrons (*n*) transferred per molecule can be determined of a known amount of substance.

During the process of bulk electrolysis (also known as controlled potential electrolysis or coulometry), the analyte is completely electrolysed by applying a fixed potential to an electrode. The solution is stirred and an electrode with a large surface area is used to minimize electrolysis time. The total amount of coulombs (Q) consumed during the experiment is determined by the integration of the current (*i*) (Equation 2.14) during the course of the experiment (Figure 2.31).

$$Q(t) = \int i(t) \partial t$$

Equation 2.14.

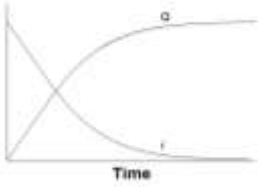

Figure 2.31. Current-time and charge-time response for controlled potential electrolysis.

When the electrolysis of the analyte is complete ($i \rightarrow 0$), the total charge is used to calculate the number of electrons (n) transferred per molecule for a known amount (N mol) of the analyte electrolysed by means of Faraday's law (Equation 2.15).

$$Q = nFN$$

Equation 2.15.

Q = the total amount of charge consumed during the experiment measured in coulombs, F = Faraday's number = 96485 C eq^{-1}, n = the number of electrons transferred per molecule (eq mol^{-1}) and N = amount of analyte (mol).

2.7.2. Electrochemistry of some metallocene complexes

2.7.2.1. Ferrocene

Ferrocene, with a formal reduction potential of 400 mV *vs* NHE,[236] can be used in CV experiments as an internal reference system in a wide range of non-aqueous solvents,[235] or when using different reference electrodes.[234] The Fc/Fc^+ couple is reversible and has a ΔE_p = 59 mV under ideal conditions. Different formal reduction potentials of Fc in solvents such as THF, DCM and CH_3CN referenced to the same reference electrode have been measured (Table 2.6, p 58). Irrespective of the shift in E^{01} (Fc/Fc^+) in different solvents, the formal reduction potential of another compound (e.g. $[IrCl_2(fctfa)(COD)]$) relative to Fc/Fc^+ as an internal standard, remains unchanged.[240] Complexes with two or three ferrocenyl ligands bound to it, showed different oxidation and reduction peaks for the different Fc moieties (Figure 2.48).[241, 242 243] The observed inequalities is due to the improbability of all ferrocenyl groups of the same molecule, coming simultaneously in reaction contact with the electrode to invoke three simultaneous one-electron transfer processes.[244, 245] This result implies mixed-valent intermediates are generated according to the following scheme:

$$(Fc)_3 \rightleftharpoons FcFc^+Fc + e^- \rightleftharpoons Fc^+Fc^+Fc + e^- \rightleftharpoons (Fc)_3^{3+} + e^-$$

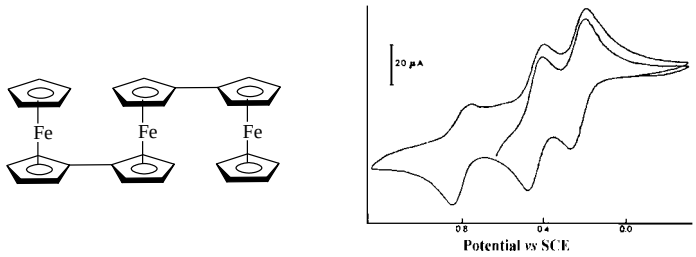

Figure 2.32. Left: Structure of 1,1'-terferrocene(1+). Right: Cyclic voltammogram of 1,1'-terferrocene(1+) in 1:1 CH_2Cl_2:CH_3CN containing 0.1 M $[NBu_4][PF_6]$ at scan rate 200 mV/s.

In the complexes where two ferrocenyl ligands are bonded covalently to each other *via* a methylene bridge bond, it could be either by one or two linkages (Figure 2.33).[246] This leads to quite a dramatic difference in their polarographic behaviour (Table 2.5), which can be related to cyclic voltametric behaviour *via* Equation 2.10 (p 52). In the bridged ferrocenes with two linkages, the Fe-atoms are kept very close to one another. Its CV data shows that the second one-electron oxidation step is more difficult than the first. Electron interaction can take place *via* two ways: 1) through the carbon skeleton of the ligands (i.e. conjugation), or 2) direct through-space metal-metal interaction (field effect). The CV results of the bridged ferrocenes with one linkage show that its second oxidation step is easier than that found for the doubly bridged ferrocenes, thus the potential of the two redox couples are closer to one another. This is attributed to the direct electrostatic field interaction between the Fe atoms, because due to steric reasons the mono bridged ferrocenes derivative can adopt a conformation in which the two Fe atoms are pseudo-*trans* to one another.

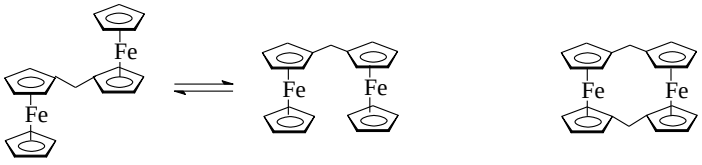

Figure 2.33. Ferrocene derivatives, which are either linked *via* one or two linkages.

Table 2.5. Polarographic half potentials of ferrocene derivatives, bridged ferrocenes that are either linked *via* one or two linkages.

Bridged ferrocenes	$E_{1/2}$ / V	$\Delta E_{1/2}$ / V relative to Fc (0.34 V)
One methylene linkage	0.30, 0.40	-0.04, 0.06
Two methylene linkages	0.25, 0.44	-0.09, 0.10

When ferrocene is bound in a complex like a β-diketone ($FcCOCH_2COR$), the E^{01} value of the Fc/Fc^+ couple is influenced by the group electronegativity of the R group (Figure 2.34, Table 2.6),[244] due to the good communication between the ferrocenyl ligand and the R group *via* the backbone of the pseudo-aromatic β-diketone core. With increasing

electronegativity of the R group on the β-diketone, the E^{01} value of the Fc/Fc^+ couple also increases since electron-density is withdrawn from it by R. There is also a linear relationship between the pK_a' of the β-diketone and the E^{01} value of the Fc/Fc^+ couple, and with increasing pK_a' there is a decrease in the E^{01} value of the Fc/Fc^+ couple.

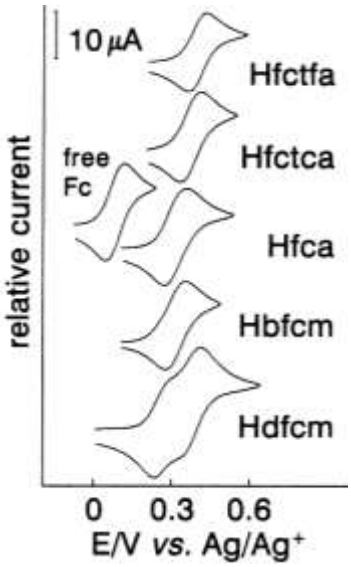

Figure 2.34. Cyclic voltammograms of 2 mmol dm^{-3} solutions of ferrocene (Fc) and ferrocene-containing-β-diketones measured in 0.1 mol dm^{-3} $[NBu_4][PF_6]/CH_3CN$ at a scan rate of 50 mV s^{-1} on a Pt working electrode at 25.0(1)°C *versus* Ag/Ag^+.

Table 2.6. E^{01} *vs* Ag/Ag^+, of the β-diketones of the type $FcCOCH_2COR$ R = CF_3, CCl_3, CH_3, Ph and Fc group electronegativities of the R groups on the β-diketones and pK_a' values of the β-diketones.

β-diketones	R groups on the β-diketones	E^{01} *vs* Ag/Ag^+ / mV[244]	Group electronegativities of the R groups[244]	pK_a' of the β-diketones[245]
Hfctfa	CF_3	0.394	3.01	6.53
Hfctca	CCl_3	0.370	2.76	7.15
Hfca	CH_3	0.313	2.34	10.01
Hbfcm	Ph	0.306	2.21	10.41
Hdfcm	Fc	0.265; 0.374	1.87	13.1

Other examples where the E^{01} value of the Fc/Fc^+ couple is influenced when ferrocene is part of a complex, is a series of ferrocenylcarboxylic acid **29-32**[247] and the polymer/ferrocene conjugates **37-40**.[248] It is observed that the closer the carbonyl group on **29-32** and **37-40** is to the ferrocenyl moiety the more positive the formal reduction potential of the ferrocenyl moiety

becomes. It is evident that the electron withdrawing property of the carbonyl group is masked very well when the spacer chain (-CH_2-) length become longer (Figure 2.35).

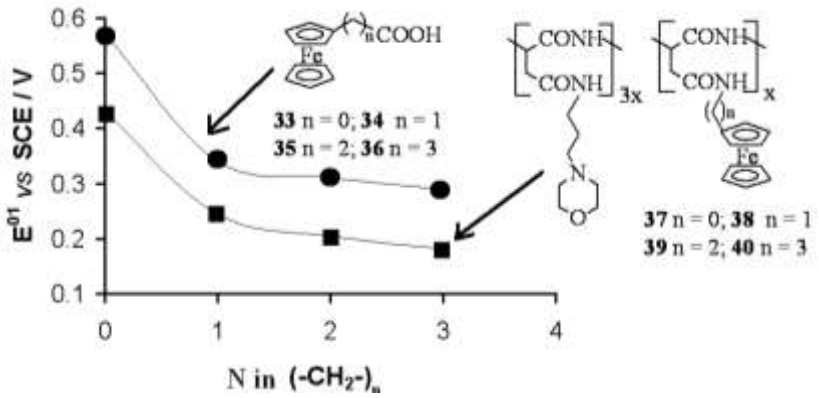

Figure 2.35. Relationship between formal reduction potential, E^{01}, and n, where n = number of CH_2 groups separating the carbonyl group from the ferrocenyl moiety for the acids series **29-32** (●) and the polymers **37-40** (■).

2.7.2.2. Ruthenocene

Despite the extensive use of ferrocene as a model redox system for nonaqueous studies, the electrochemistry of ruthenocene has been far less studied and remains less well understood. In an ethanol/dme (dropping mercury electrode) or tetrabutylammonium perchlorate system the oxidation of ruthenocene is reported to proceed by an irreversible, $2e^-$ process.[249, 250, 251 and 252.] A quasi-reversible $1e^-$ oxidation of ruthenocene has been observed in Lewis acid-base molten salts (Figure 2.36).[253] The solvent was a mixture of 0:8:1 $AlCl_3$:1-butylpyridinium chloride, into which the ruthenocene was dissolved. It was later shown that a 1 e^- reversible electrochemical process occurs, when a noncoordinating electrolyte {tetrabutylammonium tetrakis[3,5-bis(trifluoromethyl)phenyl]borate, $[NBu_4][B(C_6F_5)_4]$} and a noncoordinating solvent is used (Figure 2.36).[254]

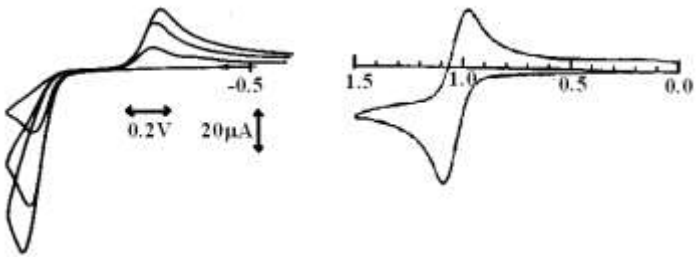

Figure 2.36. Left: Quasi-reversible $1e^-$ oxidation of ruthenocene in Lewis acid-base molten salts. Right: The 1 e^- reversible electrochemical process of ruthenocene in $[NBu_4][B(C_6F_5)_4]$ and CH_2Cl_2.

Geiger and co-workers have found that, the electrochemical oxidation of ruthenocene in $CH_2Cl_2/[NBu_4][B(C_6F_5)_4]$, gives the dimeric dication $[(C_5H_5)_2Ru]_2^{2+}$,(**164**), in equilibrium with

the 17 electron ruthenocenium ion $[(C_5H_5)_2Ru]^+$, (**165**) (Figure 2.37).[255] At room temperature the rapid equilibrium accounts for the quasi-Nernstian CV ($E_{1/2}$ = 0.41 V *vs* Fc). Direct electrochemical evidence for **164** is seen by CV and bulk electrolysis at 243K. **164** undergo a highly reversible 2 e^- cathodic reaction at E_{pc} = 0 V. At reduced temperature the oxidation displays decreased electrochemical reversibility and a new cathodic wave for a reaction product, ascribed to **164**, is observed (Figure 2.37).

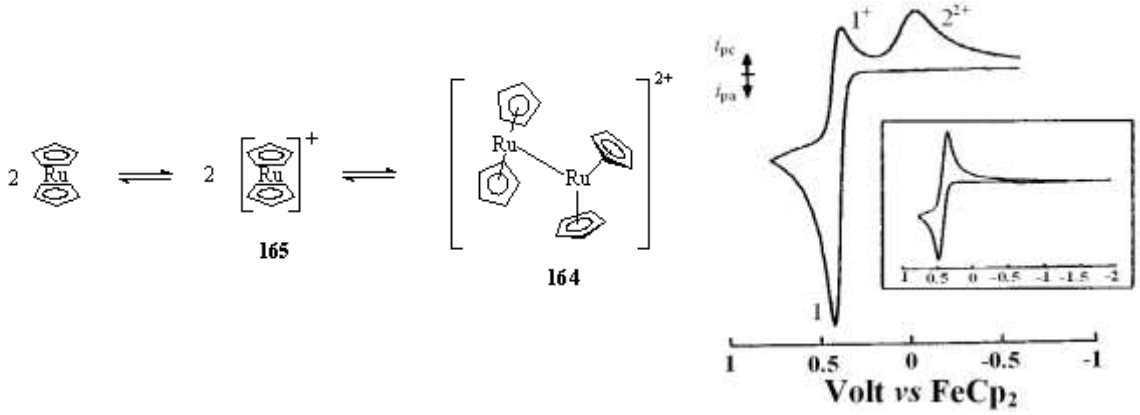

Figure 2.37. Left: Equilibrium between **164** and **165**. Right: CV of ruthenocene in $[NBu_4][B(C_6F_5)_4]$ and CH_2Cl_2, T = 243K, inset at ambient temperature.

Irreversible electrochemical behaviour has been found for binuclear ruthenocene compounds.[256] It was shown that in CH_2Cl_2/*n*-Bu_4NClO_4 the compound 1,4-bis (ruthenocenyl)benzene has two oxidation peaks at 0.42V and 0.56V *vs* Fc/Fc^+, the reduction peak occurred at 0.28V *vs* Fc/Fc^+ (Figure 2.38). The cyclic voltammetric behaviour of a novel ruthenocene surfactant (dimethylaminomethyl)ruthenocene) also shows two oxidation peaks at 0.74V and 0.91V, but no reduction peaks could be observed even at high scan rates (Figure 2.38).[257]

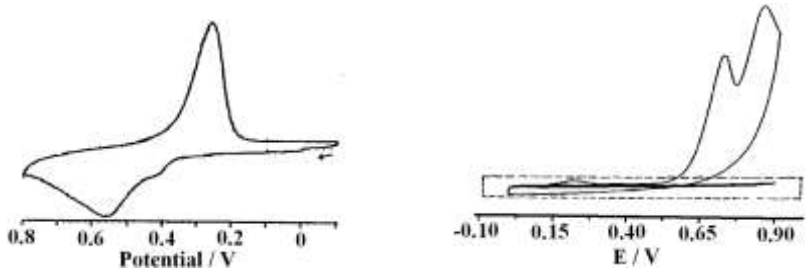

Figure 2.38. Left: Irreversible electrochemistry of the binuclear compound, 1,4-bis(ruthenocenyl)benzene Right: Irreversible electrochemistry of the ruthenocene surfactant, dimethylaminomethyl)ruthenocene.

The electrochemistry of ruthenocenyl-containing β-diketones, ($RcCOCH_2COR$, where R = CF_3, CH_3, Ph, Fc and Rc), in $CH_3CN/[NBu_4][PF_6]$ revealed irreversible electrochemical behaviour.[182] Except for R = CF_3, al the β-diketones showed two oxidation peaks, which were explained by the keto and enol forms of the β-diketones (Figure 2.39). It was also shown that

there exists a linear relationship between the group electronegativity of the R groups and the first oxidation peak of the ruthenocene-containing β-diketones (Figure 2.39).

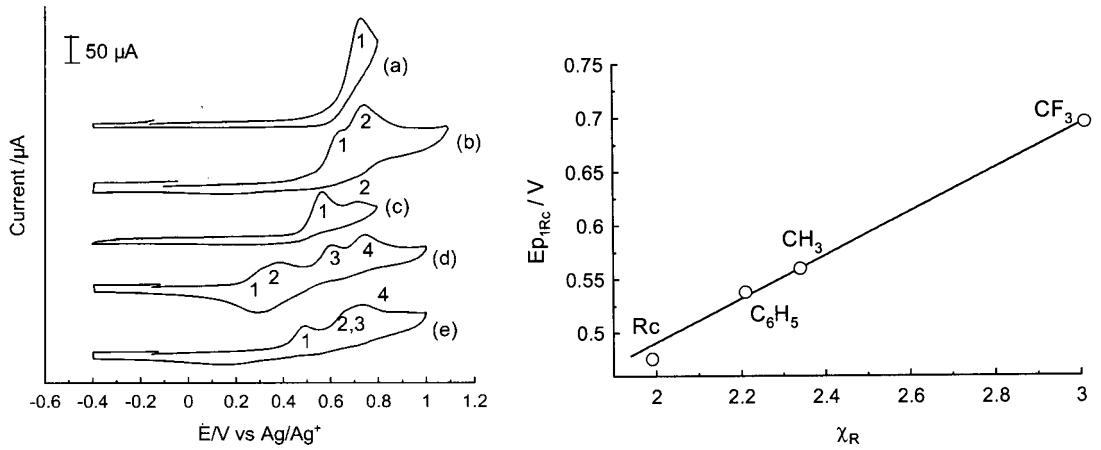

Figure 2.39. Left: Cyclic voltammograms of 2 mmol dm^{-3} solutions of ruthenocene-containing-β-diketones measured in 0.1 mol dm^{-3} $CH_3CN/[NBu_4][PF_6]$ at a scan rate of 250 mV s^{-1} on a glassy carbon working electrode, (a) Hrctfa R = CF_3, (b) Hrca R = CH_3, (c) Hbrcm R = Ph, (d) Hrcfcm R = Fc, (e) Hdrcm R = Rc. Right: The linear relationship between group electronegativity of the R groups and the first oxidation peak of the ruthenocenyl-containing β-diketones.

2.7.2.3. Titanocene dichloride

The redox properties of titanocene dichloride reveal a strong dependence on the solvent; in THF and DCM quasi-reversible redox character has been observed with i_{pa}/i_{pc} = 0.65-0.95 and ΔE_p = 90-100 mV, while in CH_3CN a small reoxidation peak, strongly shifted to the positive direction with ΔE_p = 400 mV, was observed (Table 2.7).[258] This can be interpreted within the framework of a 'square scheme' where the electrochemical reduction step is accompanied by the rapid substitution of one chloride ligand by the solvent molecule (Scheme 2.40). The back electron transfer follows the same reaction path for weakly coordinating media (THF, DCM) whereas this process is shifted to a more positive potential in the case of strong coordinating solvents (CH_3CN).

Several electrochemical studies on titanocene dichloride reported mutually consistent E^{01} values.[258, 259, 260] Electrochemical characterisation of a titanocene dichloride derivative, $[Cl_2TiCpC_5H_4(CH_2)_3NC_4H_4]$, (one of the cyclopentadienyl rings is functionalised with a pyrrolyl ring (Py)), revealed that the reduction and oxidation resemble the behaviour of the unsubstituted titanocene dichloride or Py (Table 2.7).[261] Reduction of this complex demonstrates a dependence on the solvent complexation ability, which gives rise to the quasi-reversible behaviour found in THF and DCM. In CH_3CN, on the other hand, irreversibility was found. The Ti^{4+}/Ti^{3+} transition leads to the substitution of one of the Cl^- ions by a solvent molecule.

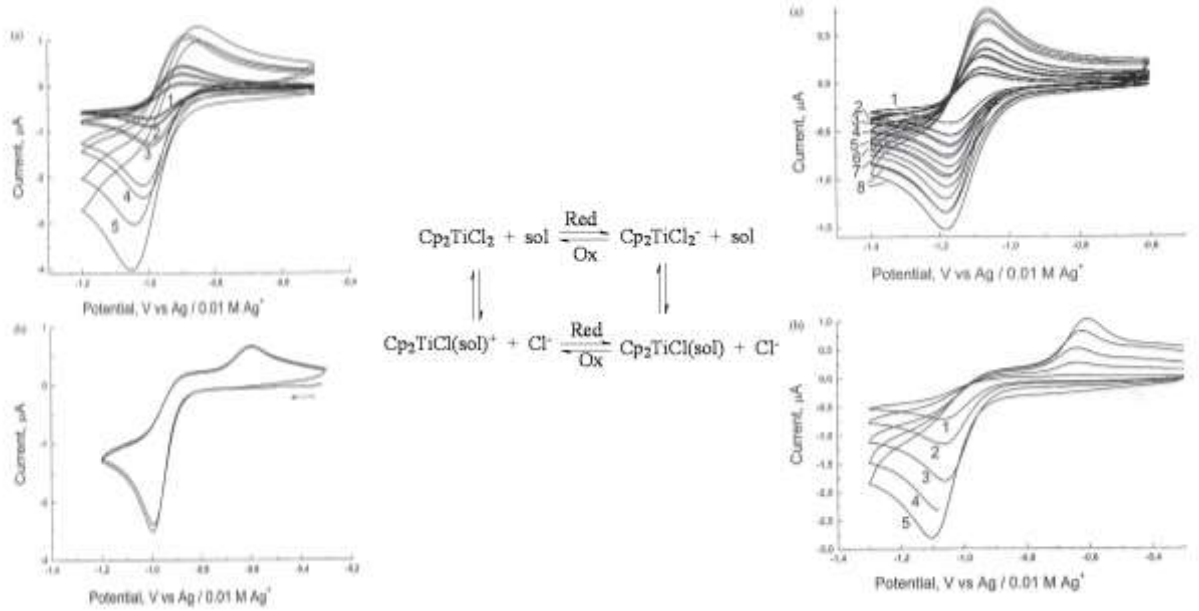

Scheme 2.40. Left: CV curves of titanocene dichloride ($TiCp_2Cl_2$) (a) DCM solution, v = 10, 20, 50, 200 or 500 mV s^{-1} (curves 1-5); (b) CH_3CN solution, v = 100 mV s^{-1} (two first cycles. Middle: The 'square scheme' illustrating the oxidation and reduction of titanocene dichloride. Right: CV curves of titanocene-pyrrole derivative ($TiCp_23Py$): (a) THF solution, v = 10, 20, 30, 50,70, 100, 140 or 160 mV s^{-1} (curves 1-8); (b) CH_3CN solution, v = 10, 30, 70, 120 or 200 mV s^{-1} (curves 1-5). (CV's taken from reference 261).

Table 2.7. Redox potentials in solutions *vs* Ag/Ag^+ and SCE (Pt electrode and supporting electrolyte 0.2 M $[NBu_4][PF_6]$ of Fc, $TiCp_2Cl_2$ and $[Cl_2TiCpC_5H_4(CH_2)_3NC_4H_4]$ ($TiCp_23Py$).[261]

Substance	Solution	E^{01} *vs* Ag/Ag^+ / V	E^{01} *vs* SCE / V	E^{01} *vs* Fc/Fc^+ / V	i_{pa}/i_{pc}	ΔE_p / V
Fc	THF	0.20	0.53	0.00	1.0	100
	DCM	0.21	0.43	0.00	1.0	100
	CH_3CN	0.10	0.43	0.00	1.0	80
$TiCp_2Cl_2$	THF	-1.08	-0.76	-1.28	0.-90-0.95	90
	DCM	-0.95	-0.73	-1.16	0.65-0.75	100
	CH_3CN	-0.80	-0.47	-0.90	-	400
$TiCp_23Py$	THF	-1.12	-0.79	-1.32	0.7-0.9	95
	DCM	-0.98	-0.76	-1.19	0.65-0.8	115
	CH_3CN	-0.845	-0.525	-0.945	-	425

As can be seen from Table 2.7, the E^{01} values as well as the reversibility (ΔE_p) of the complexes are highly dependent on the nature of the solvent and the supporting electrolyte used.[262] This is also confirmed by electrochemical studies done on another titanocene derivative, di(propylthiotetramethylcyclopentadienyl)titanium dichloride,[262] $[(C_5Me_4SCH_2CH_2CH_3)_2TiCl_2]$, whose electrochemical behaviour is analogous to that of titanocene dichloride. The first

reduction step of $[(C_5Me_4SCH_2CH_2CH_3)_2TiCl_2]$ depends strongly on the nature of the solvent and the supporting electrolyte.

Methyl-substituted titanocene dichlorides', $[(C_5H_{5-n}Me_n)_2TiCl_2]$ n = 0-5, CV data in THF revealed that the standard potential ($E^0{}_1$) shifts to more negative values proportionally to the number of methyl groups in the $[(C_5H_{5-n}Me_n)_2TiCl_2]$ n = 0-3, compounds, with an increment of 0.093 V per one methyl group.[263] A decline from this linear dependence is observed for $[(C_5HMe_4)_2TiCl_2]$ and a positive shift for $[(C_5Me_5)_2TiCl_2]$ (Table 2.8). These positive shifts can be brought about by a steric strain between the cyclopentadienyl ligands, which lower the dihedral angle between cyclopentadienyl ring planes.

Table 2.8. Cyclic voltammetry of titanocene dichloride complexes in THF, potentials were related to the standard redox potential of Fc/Fc^+ couple (0.203 V *vs* sat. Ag/AgCl in water).

Compound	ΔE_p / V	E^{01} *vs* Fc/Fc^+ / V
$(C_5H_5)_2TiCl_2$	0.090	-1.313
$(C_5H_4Me)_2TiCl_2$	0.083	-1.403
$(C_5H_3Me_2)_2TiCl_2$	0.093	-1.478
$(C_5H_2Me_3)_2TiCl_2$	0.079	-1.593
$(C_5HMe_4)_2TiCl_2$	0.081	-1.623
$(C_5Me_5)_2TiCl_2$	-	-1.573

2.7.2.4. Metallocene β-diketonato complexes

Electrochemical data obtained from the titanocene(III)-β-diketonato complex $[TiCp_2(LL')]$, where LL' = $acac^-$ or $bzac^-$, shows that both the metal as well as the β-diketonato ligand are electrochemically active (Figure 2.40).[192] The Ti(III) can be reversibly oxidized in a one electron process at a potential, which is apparently independent of the β-diketonato ligand. $[Ti^{III}Cp_2(acac)]$ E^{01} = -0.86 V and $[Ti^{III}Cp_2(bzac)]$ E^{01} = -0.85 V *vs* Fc/Fc^+ in butyronitrile (0.2 M $[NBu_4][PF_6]$). The author of this publication attributed the negligible influence of the β-diketonato ligand to the existence of a highly localized centred frontier orbital, which dominates the redox chemistry. This may be so, but is open to criticism. The group electronegativity of a CH_3 group and C_6H_5 group are almost identical, 2.34 and 2.21 respectively, Table 2.6. Therefore the electronic influence of $acac^-$ and $bzac^-$ on the redox properties of the Ti nucleus in $[Ti^{III}Cp_2(acac)]$ and $[Ti^{III}Cp_2(bzac)]$ should be almost identical. The peaks at ± -2.5 V is attributed to the β-diketonato ligand.

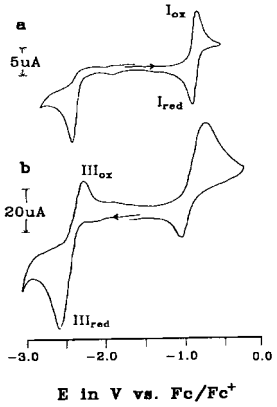

Figure 2.40. CV of [$Ti^{III}Cp_2$(bzac)] (2 mM) obtained in butyronitrile (0.2 M NBu_4PF_6) at scan rate 200 mV/s with a) 1 mm Pt disk electrode at 22˚C and b) a 5 mm glassy carbon disk electrode at -50˚C.[192]

2.8. Cytotoxic studies

Cisplatin (*cis*-$PtCl_2(NH_3)_2$) has been actively used in the treatment of cancer since its discovery in 1965.[264] However, due to the severe side-effects of cisplatin and some new generation platinum drugs,[265, 266] the search for new, better (more cytotoxic) cancer drugs having less negative side effects on healthy cells is still going on.

2.8.1. Ferrocene compounds in cancer therapy

It was found that free unsubstituted ferrocene (**18**) does not display any antitumor activity due to its insolubility in water. However, the ferrocenium salt (**17**) (Figure 2.9, p 9) does display antineoplastic activity against Ehrlich ascites tumor cell lines.[39] Other ferrocenyl complexes also showed good to excellent antineoplastic activity: ferrocenylacetic acid,[267] and ferrocene-containing β-diketones (**46-50**).[268, 269] The ferrocenylalcohols (**29-32**) have been tested *in vitro* against HeLa and CoLo DM320 cell lines.[270] A clear activity-structure correlation was observed. The activity of the alcohols improved with increase in methyl spacer that separates the ferrocenyl group and the alcohol group (Table 2.9). It was also evident that the more negative the formal reduction potential, E^{01}, values of the alcohol, the more pronounced antineoplastic activity was exhibited. This is consistant with a mechanism of action in killing cancer cells involving first oxidation of each ferrocenyl group by biological oxidising agents to the active ferrocenium species. The ferrocenium species then gets involved in electron transfer reactions that ultimately leads to cell death.[271]

Table 2.9. Formal reduction potentials, E^{01}, *vs* Ag/Ag^+ in CH_3CN and IC_{50} values of alcohol (**29-32**) against HeLa cell lines. IC_{50} = The concentration of an inhibitor that is required for 50% cell death.

Compound	E^{01} / V	IC_{50} / μM
$Fc(CH_2)OH$ (**29**)	0.111	>100
$Fc(CH_2)_2OH$ (**30**)	0.029	34.99
$Fc(CH_2)_3OH$ (**31**)	0.029	17.00
$Fc(CH_2)_4OH$ (**32**)	0.026	5.72

When anchoring antineoplastic ferrocene derivatives to water-soluble polymer, it was found that lower concentrations of drug units were needed for the same effectiveness than when the drug was administered in monomeric form.[272] As was found with the ferrocenyl alcohols, both the size of the spacer and E^{01} play a role in the drug activity. More methylene spacers and more negative formal reduction potentials both enhance the antineoplastic activity.

2.8.2. Ruthenocene compounds in cancer therapy

The radiopharmaceutical acetyl-(^{103}Ru)-ruthenocene has been used in the investigation of the affinity of acetylruthenocene for the adrenal glands of mice.[273] It was shown that the compound has an affinity for the regions in the adrenal gland where adrogen and glucocorticoid synthesis occurs. A study was conducted that demonstrates modification of organ distribution of the radiopharmaceutical acetyl-(^{103}Ru)-ruthenocene.[274] It was found that if the hormones can be controlled, the target of the acetylruthenocene can also be controlled.

Ruthenocene-containing β-diketones and their rhodium complexes have been tested against CoLo and HeLa cell lines and have proved to be very effective.[272]

2.8.3. Titanium compounds in cancer therapy

Titanocene derivatives and bis(β-diketonato)titanium(IV) complexes appear to have good antineoplastic activity. They do not follow the rationale and mechanism of action of the traditional platinum complexes.[82] Cisplatin acts by binding to DNA, after its chloride ions have been replaced by hydroxyl groups. This binding to the DNA, inhibits DNA replication and chain elongation, which is believed to be the main cause of its antineoplastic activity.[275] The mechanism of action of the titanium complexes is not clear. Nucleic acids have been proposed to

be target places in the cell, most likely suppressing the synthesis of RNA or DNA. At present, it is believed that transferrin could be a potential carrier of Ti(IV) into the target place.[276]

Diacido titanium complexes of type Cp_2TiX_2, where X = carboxylates, phenolates, dithiolenes and thiophenolates have shown anti-proliferative action.[71] Other mono-substituted complexes of formula Cp_2TiClX, where X = 1,3,5-trichlorophenolate, 1-aminothiophenolate, 1-methylphenolate and selenophenolate, have also exhibited similar anti-tumour activity.[71, 277]

Attempts aimed at improving the anti-tumour activity of cyclopentadienyl metal or metallocenyl complexes included the replacement of H of $C_5H_5^-$ for R (R = CH_3, C_2H_5 and $N(CH_3)_2$) groups ranging from mono- to deca-substitution. This modification of the Cp ligand on $(C_5H_5)Ti^{2+}$ showed a dramatic reduction in the anti-tumour activity, as the degree of H substitution increases.[71] However, substitution on the cyclopentadienyl ring(s) with carbomethoxy has shown increased anti-tumour action.[72]

Several ionic titanocene complexes of general formula $[Cp_2TiX]^+Y^-$ or $[Cp_2TiL_2]^{2+}[Y^-]_2$, where X is an anionic ligand and L is a neutral ligand, have been tested for anti-proliferative action. These species offer higher solubility in water than the neutral titanocene dihalides. Some representative examples of this type of complex are $[(C_5H_5)_2Ti(bipy)][CF_3SO_3]_2$, $[(C_5H_5)_2Ti(phen)][CF_3SO_3]_2$, $[(C_5H_5)_2Ti[o\text{-}S(NHCH_3)C_6H_4]^+I^-$ and $[(C_5H_5)_2Ti(Cl)NCCH_3]^+[FeCl_4]^-$.[71, 278, 279]

Budotitane and its derivatives (Figure 2.41) belongs to the class of bis(β-diketonato)metal complexes.[280] The M(β-diketonato)$_2X_2$ complexes are highly susceptible to hydrolysis and are relatively difficult to dissolve in water. Variation of the R groups (no. A-D) in Table 2.10 of the (β-diketonato) ligands in [M(β-diketonato)$_2X_2$] complexes can increase the anti-tumour activity; the anti-tumour activity of the compounds in Table 2.10 was found to be independent of the leaving group X .[225]

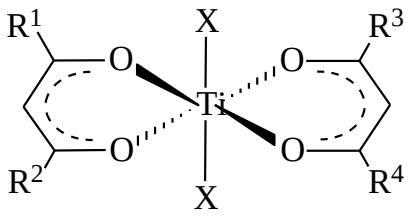

Figure 2.41. Structure of budotitane. Variations of X, R^1, R^2, R^3 and R^4 are shown in Table 2.12.

Table 2.10. Anti-tumour activity of Ti(β-diketonato)$_2$X$_2$. T/C(%) = (median survival time of treated animal *vs* median survival time of control animal) x 100.

Number	β-diketonato	X	T/C(%)
A	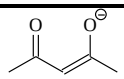	OEt	90-100
B	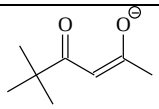	OEt	130-170
C	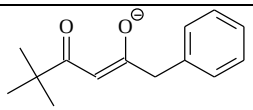	OEt	150-200
D	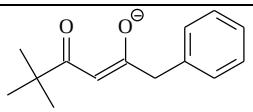	Cl	150-200
E	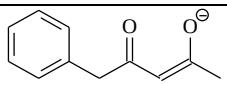	OEt	130-170
F	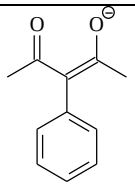	OEt	200-250
G	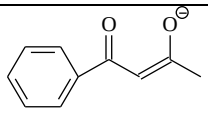	OEt	>300
H	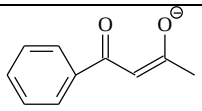	Cl	>300
I	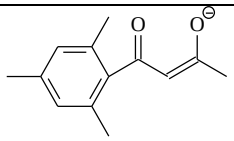	Cl	>300
J	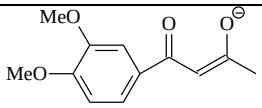	Cl	150-200
K	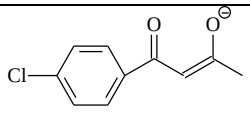	Cl	150-200
L	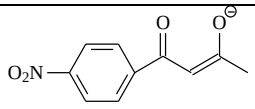	Cl	100-120

From the examination of the extent to which the aromatic groups (entries E-H in Table 2.10.) on the β-diketonato ligand in complexes of the type [M(β-diketonato)$_2$X$_2$] changes the anti-cancer efficiency of the complexes in mice, it is evident that when phenyl groups stand in

direct conjugation to the metal enolate pseudo-aromatic ring, the anti-tumour activity increase dramatically (entries G-H in Table 2.10).

Variations on the phenyl ring (entries I-L in Table 2.21) also affect the anti-tumour properties of the complexes. The introduction of methyl groups at the phenyl ring (I) does not alter anti-tumour activity, whereas methoxy, chlorine and nitro groups reduce anti-tumour activity (J-L).

2.9. Liquid Crystals

The melting of most crystalline solids involves the abrupt collapse of the position and orientation of the lattice array, which marks the onset of essentially free movement of molecules in the isotopic liquid phase. In contrast, for many compounds that have rod-like or disc-like shapes, this process occurs by way of one or more intermediate phases as the temperature increased (Figure 2.42, Right). This intermediary state is called the liquid crystal state or the mesomorphic state and compounds exhibiting mesophases are called mesogens.

In these mesophases, varying degrees of molecular order are retained. Mesophases have properties, which are intermediate between those of the fully ordered crystalline solid and an isotropic liquid. These mesophases can be divided into two main groups: (1) those which are produced by the action of heat on the crystal or cooling of the isotopic liquid are called Thermotropic Mesophases and (2) those that are generated by the action of a solvent on the solid crystal are called Lyotropic Mesophases. Thermotropic mesophases can be further divided and summarised as in Figure 2.42 (Left).[281]

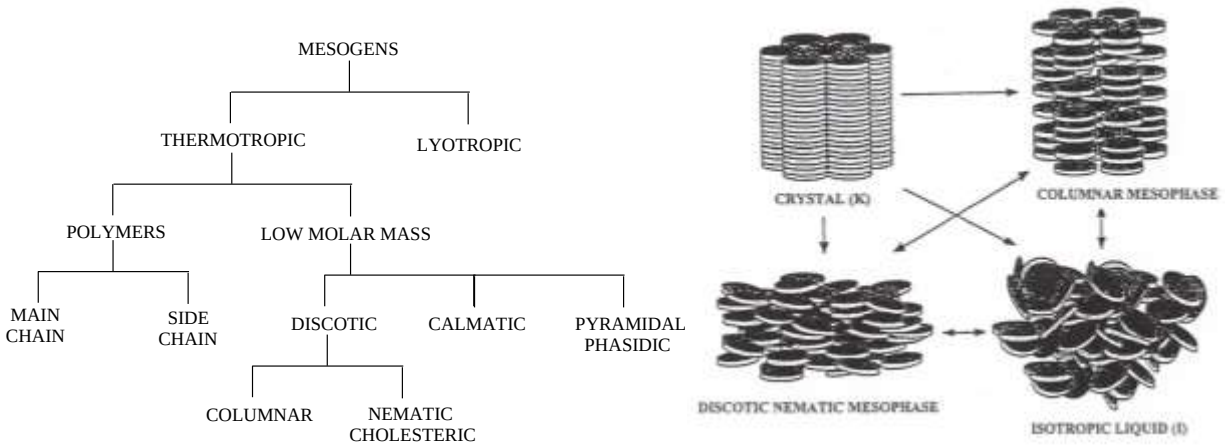

Figure 2.42. Left: Classification of mesophases. Right: Schematic representation of the possible melting processes of mesogenic discotic materials.

Columnar mesophases can interalia be obtained when attractive forces between aromatic cores of a compound causes a degree of stacking of molecules on top of each other. This would lead to a crystalline state (Figure 2.43). However, when long side chains are bound to the aromatic core, these may melt when heat is applied to the system without disturbing the order generated by the attractive forces keeping the aromatic cores stacked in a columnar fashion. This in essence would lead to a liquid crystal state. If the attractive forces between the aromatic cores are broken before side chain melting occurs no liquid crystal state will be observed. However, upon cooling the isotropic liquid state of such a system, phase changes may be observed at lower temperature than the melting point. This will be the result of different packing patterns of the side chains of the system at different temperature. Such apparent solid phase changes may also be the result of slow kinetics causing the long side chains of such a system first to freeze into an amorphous solid at the melting point before, at lower temperatures, and at a slow rate these side chains rearrange into a different crystal packing mode. It will manifest as a solid state phase change during a phase study. Such liquid crystal and solid state phase changes is conveniently observed by differential scanning calorimetry.

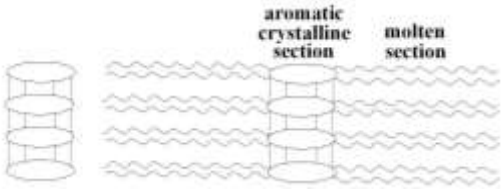

Figure 2.43. Diagram showing attractive forces between aromatic cores and co-existence of a crystalline and molten section in liquid crystal samples.

With respect to this study it becomes of interest to see if metallocene β-diketones and their titanium complexes may exhibit any thermotropic columnar mesophase or solid state phase change behaviour (Figure 2.44).

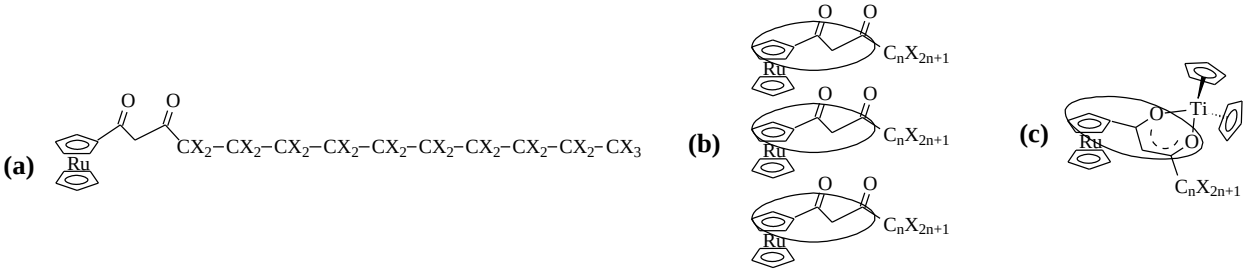

Figure 2.44. (a) Ruthenocene-containing β-diketone with X = H or F, showing the pseudo aromatic core that (b) may induce a thermotropic columnar mesophase. (c) Titanocene β-diketonato complexes that may show mesophase or solid state phase changes.

[1] P. Köpf-Maier and H. Köpf, *Chem. Rev.*, 1987, **87**, 1137.

[2] G. Wilkinson, Editor, *Comprehensive Organometallic Chemistry*, vol. 8, Pergamon Press, Oxford, 1982 and references therein.

[3] G. Wilkinson, Editor, *Comprehensive Organometallic Chemistry*, vol. III, Pergamon Press, Oxford, 1982 and references therein.

[4] W.P. Hart, D. Shihua and M.D. Rausch, *J. Organomet. Chem.*, 1985, **282**, 111.

[5] H. Werner and S. Salzer, *Aangew. Chem. Int. Ed. Engl.*, 1972, **11**, 930.

[6] J.D. Dunitz, L.E. Orgel and A. Rich, *Acta Crystallogr.*, 1956, **9**, 373.

[7] W. Bünder and E. Weiss, *J. Organomet. Chem.*, 1975, **92**, 65.

[8] W. Bünder and E. Weiss, *J. Organomet. Chem.*, 1975, **92**, 1.

[9] G.L. Hardgrove and D.H. Templeton, *Acta Crystallogr.*, 1959, 12, 28.

[10] A. Haaland and J.E. Nilsson, *Acta Chem. Scand.*, 1968, **22**, 2653.

[11] E. Gard, A. Haaland D.P. Novak and R. Seip, *J. Organomet. Chem.*, 1975, **88**, 181.

[12] A. Almenningen, A. Haaland and T. Motzfeldt, *Selected Topics in Structural Chemistry*, Universitetsforlaget, Olso, 1967, p. 105.

[13] A. Almenningen, E. Gard, A. Haaland and J. Brunvoll, *J. Organomet. Chem.*, 1976, **107**, 273.

[14] L. Hedberg and K. Hedberg, *J. Chem. Phys.*, 1970, **53**, 1228.

[15] I.A. Ronnova, D.A. Bochvar, A.L. Chaitjakov, Y.T. Struchkov and N.V. Alekseev, *J. Organomet. Chem.*, 1969, **18**, 337.

[16] A. Haaland, J. Lusztyk, J. Brunvoll and K.B. Starowieyski, *J. Organomet. Chem.*, 1975, **88**, 279.

[17] G.W. Watt, L.J. Baye and F.O. Drummond, *J. Am. Chem. Soc.*,1966, **88**, 1138.

[18] G.W. Watt and F.O. Drummond, *J. Am. Chem. Soc.*,1966, **88**, 5926.

[19] G.W. Watt and F.O. Drummond, *J. Am. Chem. Soc.*,1970, **92**, 826.

[20] H.H. Brintzinger and J.E. Bercaw, *J. Am. Chem. Soc.*,1970, **92**, 6182.

[21] L.J. Guggenberger and F.N. Tebe, *J. Am. Chem. Soc.*,1973, **95**, 7870.

[22] A. Davison and S.S. Wreford, *J. Am. Chem. Soc.*,1974, **96**, 3017.

[23] P.C. Wailes, R.S.P. Coutts and H. Weigold, *Organometallic Chemistry of Titanium, Zirconium and Hafnium*, Academic Press, New York, 1974.

[24] G. Wilkinson, Editor, *Comprehensive Organometallic Chemistry*, vol. I, Pergamon Press, Oxford, 1982.

[25] D.C. Beer, V.R. Miller, L.G. Sneddon, R.N. Grimes, M. Mathew and G.J. Palenik, *J. Am. Chem. Soc.*,1973, **95**, 3046.

[26] G.E. Herberich, J. Hengesbach, U. Kolle and W. Oschmann, *Aangew. Chem., Int. Ed. Engl.*, 1977, **16**, 42.

[27] W. Siebert and W. Rothermel, *Aangew. Chem., Int. Ed. Engl.*, 1977, **16**, 333.

[28] A. Almenningen, A. Haaland and T. Motzfeldt, *J. Organomet. Chem.*, 1967, **7**, 97.

[29] C. Panattoni, G. Bombieri and U. Croatto, *Acta Crystallogr*., 1966, **21**, 823.

[30] P.L. Timms and T.W. Turney, *Adv. Organomet. Chem.*, 1977, **15**, 53.

[31] G. Wilkinson, Editor, *Comprehensive Organometallic Chemistry*, vol. II, Pergamon Press, Oxford, 1982 and references therein.

[32] P. Köpf-Maier, H. Köpf and E.W. Neuse, *J. Cancer Res. Clin. Oncol..*, 1984, **108**, 336.

[33] T. Kuwana, D.E. Bublitz and G. Hoh, *J. Am. Chem. Soc.*, 1960, **82**, 4206.

[34] D.M. Knight and R.C. Schlitt, *Anal. Chem.*, 1965, **37**, 470.

[35] E.W. Neuse, *Metal-Containing Polymeric Systems* (Eds.: J.E. Sheats, C.E. Carraher and C.U. Pittman), Plenum Press, New York, 1985, p. 99.

[36] E.W. Neuse and M.S. Loonat, *J. Organomet. Chem.*, 1985, **286**, 329.

[37] E.W. Neuse, B.S. Mojapelo and J. Ensling, *Transition Met. Chem.*, 1985, **10**, 135.

[38] E.W. Neuse and F.B.D. Khan, *Transition Met. Chem.*, 1986, **11**, 70.

[39] P.Köpf-Maier, H. Köpf and E. Neuse, *Cancer Res. Clin. Oncol.*, 1984, **108**, 336.

[40] N.J. Long, *Metallocenes: An introduction to sandwich complexes*, Blackwell Science, London, 1998.

[41] O. Hofer and K. Schloegel, *J. Organomet. Chem.*, 1968, **13**, 443.

[42] C.L. Hewett, *J. Chem. Soc.*, 1940, 293.

[43] E.R. Biehl and P.C. Reeves, *Synthesis*, 1973, 360.

[44] G.A. Swan, *J. Chem. Soc.*, 1948, 1408.

[45] M. Derenberg and P. Hedge, *Tetrahedron Lett.*, 1971, 3825.

[46] J. McMurry , Editor, *Organic Chemistry*, 4th edition, Brooks/Cole Publishing Company, Pacific Grove, 1996 ,825.

[47] J. Conradie, G.J. Lamprecht, S. Otto and J.C. Swarts, *Inorg. Chim. Acta*, 2002, **328**, 191.

[48] D. Lednicer, J.K. Linsay and C.R. Hauser, *J. Org. Chem.*, 1958, **23**, 653.

[49] P.J. Graham, R.V. Lindsey, G.W. Parshall, M.L. Peterso and G.M. Whitman, *J. Am. Chem. Soc.*. 1957, **79**, 3416.

[50] E.W. Neuse and W.N. Mbonyana, *Inorganic and metal-Containing Polymeric Materials* (Eds.: J. Sheats et al.), Plenum Press, New York, 1970, vol 5.

[51] E.W. Neuse and W.N. Mbonyana, *Polym. Mater. Sci. Eng.* 1989, **61**, 94.

[52] M. Rosenblum, A.K. Barnerjee, N. Danieli, R.W. Fish and V. Schlatter, *J. Am. Chem. Soc.*, 1963, **85**, 316.

[53] K. Schögl, *Mh. Chem.*, 1957, **88**, 601.

[54] K. Schögl and H. Egger, *Mh. Chem.*, 1963, **94**, 376.

[55] P.D. Beer and D. K. Smith, *J. Chem. Soc., Dalton Trans.*, 1998, 417.

[56] P. Neri and G. Antoni, *Macromol. Synth.*, 1982, **8**, 25.

[57] W.C. du Plessis, T.G. Vosloo and J.C. Swarts, *J. Chem. Soc. Dalton Trans.*, 1998, 2507.

[58] F. Rebiere, O. Sameul and H.B. Kagan, *Tet. Lett.*, 1990, **31**, 3121.

[59] D. Guillaneux, H.B. Kagan, *J. Org. Chem.*, 1995, **60**, 2504.

[60] G. Wilkinson, *J. Am. Chem. Soc.*, 1952, **74**, 6146.

[61] P. Pertici and G. Vitulli, *J. Chem. Soc., Dalton Trans.*, 190, 1961.

[62] C.H. Winter, S. Prizad and D.H. Cao, *J. Chem. Soc., Chem. Commun.*, 1991, 1027.

[63] D.C. Liles, A. Shaver, E. Singleton and M.B. Wiege, *J. Organomet. Chem.*, 1985, **288**, C33.

[64] G. Wilkinson, Editor, *Comprehensive Organometallic Chemistry*, vol. IV, Pergamon Press, Oxford, 1982.

[65] M.D. Rausch, E. O. Fischer and H. Grubert, *J. Am. Chem. Soc.*, 1960, **82**, 76.

[66] S. Toma, M. Salisova and M. Goghova, *Chimia*, **34**, 1986.

[67] P. Köpf-Maier, M. Leitner and H. Köpf, *J. Inorg. Nucl. Chem.*, 1980, **42**, 1789.

[68] H. Meister, *Aangew. Chem.*, 1957, **69**, 533.

[69] S. Bradley, P.C. McGowan, K.A. Oughton, M. Thornton-Pett and M.E. Walsh, *J. Chem. Soc., Chem. Commun.*, 1999, 77.

[70] M.A.D. McGowan and P.C. McGowan, *Inorg. Chem. Commun.*, 2000, **3**, 337.

[71] P. Köpf-Maier and H. Köpf, *Struct. Bonding*, 1988, **70**, 103.

[72] J.R. Boyles, M.C. Baird, B.G. Campling and N. Jain, *J. Inorg. Biochem.*, 2001, **84**, 159.

[73] W.P. Hart, D. Shihua and M. D. Rausch, *J. Organomet. Chem.*, 1985, **282**, 111.

[74] M.D. Rausch, J.F. Lewison and W.P. Hart, *J. Organomet. Chem.*, 1988, **358**, 161.

[75] J. Okuda, K.E. du Plooy and P.J. Toscano, *J. Organomet. Chem.*, 1995, **495**, 195.

[76] S.L. Hart, D.J. Duncalf, J.J. Hastings, A. McCamley and P.C. Taylor, *J. Chem. Soc., Dalton Trans.*, 1996, 2843.

[77] M. Ogasa, D.T. Mallin, D. W. Maccomber and M.D. Rausch, *J. Organomet. Chem.*, 1991, **405**, 41.

[78] A.A.H. van der Zeijden and C. Mattheis, *J. Organomet. Chem.*, 1998, **555**, 5.

[79] H. van der Heijden and B. Hessen, *Inorg. Chim. Acta*, 2003, **345**, 27.

[80] J.A. Smith, J.V. Seyerl, G. Hutter and H.H. Brintzinger, *J. Organomet. Chem.*, 1979, **173**, 175.

[81] P.J. Shapiro, *Coord. Chem. Rev.*, 2002, **231**, 67.

[82] E. Meléndez, *Crit. Rev. Oncol.*, 2002, **42**, 309.

[83] P.C Wailes, H. Weigold and A.P. Bell, *J. Organomet. Chem.*, 1971, **33**, 181.

[84] J.E. Bercaw and H.H. Brintzinger, *J. Am. Chem. Soc.*, 1969, **91**, 7301.

[85] F.N. Tebbe, G.W. Parshall and G.S. Reddy, *J. Am. Chem. Soc.*,1978, **100**, 3611.

[86] R. Choukroun and Gervais, *J. Chem. Soc., Dalton Trans.*, 1980, 1800.

[87] K. Andrä, *J. Organomet. Chem.*, 1968, **11**, 567.

[88] G. Doyle and R.S. Tobias, *Inorg. Chem.*, 1967, **6**, 1111.

[89] M.J. Frazer and W.E. Newton, *Inorg. Chem.*, 1971, **10**, 2137.

[90] R. Fandos, C. Hernandez, A. Otero, A. Rodriguez, M.J. Ruiz and P. Terreros, *J. Organomet. Chem.*, 2000, **606**, 156.

[91] S.A. Shackelford, D.F. Shellhamer and V.L. Heasley, *Tetrahedron Lett.*, 1999, **40**, 6333.

[92] J.M. Shreeve, Editor, *Inorganic Synthesis*, vol. 24, John Wiley & Sons, New York, p 147, 1986.

[93] R.T. Carlin and J. Fuller, *Inorg. Chim. Acta*, 1997, **225**, 189.

[94] M.G. Meirim, E.W. Neuse, M. Rhemtula and S. Schmitt, *Trans. Met. Chem.*, 1988, **13**, 272.

[95] G.A. Razuvaev, G.A. Domrachev, V.V. Sharutin and O.N. Suvorova, *J. Organomet. Chem.*, 1977, **141**, 313.

[96] P.C. Bharara, *J. Organomet. Chem.*, 1976, **121**, 199.

[97] G. Fachinetti and C. Floriani, *J. Chem. Soc., Dalton Trans.*, 1974, 2433.

[98] L.E. Manzer, *J. Organomet. Chem.*, 1976, **110**, 291.

[99] L.E. Manzer, *J. Organomet. Chem.*, 1976, **110**, 291.

[100] M.L.H. Green and C.R. Lucas, *J. Chem. Soc., Dalton Trans.*, 1972, 1000.

[101] E.O. Fischer and R. Amtmann, *J. Organomet. Chem.*, 1967, **9**, 15.

[102] S. Gambarotta, C. Floriani, A. Chiesi-Villa and C. Guastini, *J. Am. Chem. Soc.*, 1982, **104**, 1918.

[103] G. Fachinetti, C. Floriani, A. Chiesi-Villa and C. Gaustini, *J. Am. Chem. Soc.*, 1979, **101**, 1767.

[104] M. Pasquali, C. Floriani, A. Chiesi-Villa and C. Guastini, *J. Am. Chem. Soc.*, 1979, **101**, 4740.

[105] G. Fachinetti, C. Floriani and H. Stoeckli-Evans, *J. Chem. Soc., Dalton Trans.*, 1977, 2297.

[106] C. Floriani and G. Floriani, *J. Chem. Soc., Chem. Comm.*, 1972, 790.

[107] K. Döppert, *J. Organomet. Chem.*, 1979, **178**, C3.

[108] Y.L. Page, *J. Organomet. Chem.*, 1980, **193**, 201.

[109] U. Thewalt and G. Schleussner, *Aangew. Chem.*,1978, **90**, 559.

[110] H. Köpf, S. Grabowski and R. Voigtlander, *J. Organomet. Chem.*,1981, **216**, 185.

[111] J.H. Toney and T.J. Marks, *J. Am. Chem. Soc.*, 1985, **107**, 947.

[112] C.L. Sloan and W.A. Barber, *J. Am. Chem. Soc.*, 1959, **81**, 1364.

[113] R.D. Gorsich, *J. Am. Chem. Soc.*, 1960, **82**, 4211.

[114] A.M. Cardoso, R.J.H. Clark and S. Moorhouse, *J. Chem. Soc., Dalton Trans.*, 1980, 1157.

[115] A.C. Skapski, P.G.H. Troughton and H.H. Sutherland, *Chem. Commun.*, 1968, 1418.

[116] E.C. Alyea and A. Male, *Inorg. Nucl. Chem. Lett.*, 1977, **13**, 587.

[117] A.C. Fernandes, C.C. Romao and B. Royo, *J. Organomet. Chem.*, 2003, **682**, 14.

[118] G. Wilkinson, Editor, *Comprehensive Organometallic Chemistry*, vol. III, Pergamon Press, Oxford, 1982.

[119] G. Schemid, B. Stutte and R. Boese, *Chem. Ber.*, 1978, **111**, 1239.

[120] A.N. Nesmeyanov, O.V. Nogina, N.A. Lazareva and V.A. Dubovitskii, *Bull. Acad. Sci. USSR, Div. Chem. Sci.*, 1976, 777.

[121] A.N. Nesmeyanov, O.V. Nogina, N.A. Lazareva, V.A. Dubovitskii and B.V. Lokshin, *Bull. Acad. Sci. USSR, Div. Chem. Sci.*, 1971, 2354.

[122] J. Scholz, G.A. Hadi, K.H. Thiele, H. Görls, R. Weimann, H. Schumann and J. Sieler, *J. Organomet. Chem.*, 2001, **626**, 243.

[123] C. Beerman, *Aangew. Chem.*, 1959, **71**, 195.

[124] K.H. Thiele and K. Jacob, *Z. Anorg. Allg. Chem.*, 1968, **356**, 195.

[125] R.J.H. Clark and M.A. Coles, *Inorg. Synth.*, 1976, **16**, 120.

[126] G. Wilkinson and J.M. Birmingham, *J. Am. Chem. Soc.*, 1954, **76**, 4281.

[127] L.T. Reynolds And G. Wilkens, *J. Inorg. Nucl. Chem.*, 1959, **9**, 86.

[128] P.M. Hamilton, R. McBeth, W. Bekebrede and H.H. Sisler, *J. Am. Chem. Soc.*, 1953, **75**, 2881.

[129] R.J. Kern, *J. Inorg. Nucl. Chem.*, 1962, **24**, 1105.

[130] D.W. Blackburn, D. Britton and J.E. Ellis, *Aangew. Chem. Int. Ed. Engl.*, 1992, **31**, 1495.

[131] J.E. Ellis, D.W. Blackburn, P. Yeun and M. Jang, *J. Am. Chem. Soc.*, 1993, **115**, 11616.

[132] P. Sobota, M.O. Mustafa and T. Lis, *Polyhedron*, 1989, **8**, 2013.

[133] R.C. Fay and R.N. Lowry, *Inorg. Chem.*, 1967, **6**, 1512.

[134] N. Serpone and R.C. Fay, *Inorg. Chem.*, 1967, **6**, 1835.

[135] M. Cox, J. Lewis and R.S. Nyholm, *J. Chem. Soc.*, 1964, 6113.

[136] J. Strauch, T.H. Warren, G. Erker, R. Fröhlich and P. Saarenketo, *Inorg. Chim. Acta*, 2000, **300**, 810.

[137] V. Reimer, T.P. Spaniol, J. Okuda, H. Ebeling, A. Tuchbreiter and R. Mulhaupt, *Inorg. Chim. Acta*, 2003, 345, 221.

[138] I.D. Verma and R. C. Mehrotra, *J. Less-Common Metals*, 1959, **1**, 263.

[139] M. Barthel, D. Dini, S. Vagin and M. Hanack, *Eur. J. Org. Chem.*, 2002, 3756.

[140] D.M. Puri and R.C. Mehrotra, *J. Less-Common Metals*, 1961, **3**, 253.

[141] A. Yamamoto and S. Kambara, *J. Am. Chem. Soc.*, 1957, **79**, 4344.

[142] [142] A. Yamamoto and S. Kambara, *J. Inorg. Nucl. Chem.*, 1961, **21**, 58.

[143] W.R. Cullen, S.J. Rettig and E.B. Wickenheizer, *J. Organomet. Chem.*, 1989, **370**, 141.

[144] G. Sava, S. Zorzet, L. Perissin, G. Menstroni, G. Zassinovich and A. Bontempi, *Inorg. Chim. Acta*, 1987, **137**, 69.

[145] C.R. Hauser, F.W. Swamer and J.T. Adams, *Organic reactions*, John Wiley & Sons, 1954, vol. 8, pp. 61-62.

[146] C.R. Hauser, F.W. Swamer and J.T. Adams, *Organic reactions*, John Wiley & Sons, 1954, vol. 8, pp. 65.

[147] A.T. Nielson and W.J. Houlihan, *Organic reactions*, Robert E. Krieger Publishing Company, Huntington, New York, 1975, vol. 16, pp. 20.

[148] R.T. Morrison and R.N. Boyd, *Organic Chemistry*, Allyn and Bacon Inc. 1987, 5th edition, pp. 922.

[149] W.S. Johnson and G.H. Daub, *Organic Reactions*, John Wiley and Sons, 1951, vol. 6, pp. 2.

[150] B.V. Bhide and J. Suchborough, *Indian Inst. Science*, 1925, **8A**, 89.

[151] C.R. Hause, R. Levine and R.F. Kibler, *J. Am. Chem. Soc.*, 1946, **68**, 26.

[152] W.R. Cullen and E.B. Wickenheiser, *J. Organomet. Chem.*, 1989, **370**, 141.

[153] C.R. Hauser, F.W. Swamer and J.T. Adams, *Organic reactions*, John Wiley & Sons, 1954, vol. 8, pp. 113.

[154] C.R. Hauser, F.W. Swamer and J.T. Adams, *Organic reactions*, John Wiley & Sons, 1954, vol. 8, pp. 111-114.

[155] M. Suzuki, A. Watanabe and R. Noyori, *J. Am. Chem. Soc.*, 1980, **102**, 2095.

[156] M. Roth, R. Dubs, E. Götschi and A. Eschenmoser, *Helv. Chim. Act*, 1971, **54**, 710.

[157] P.J. Chapman, G. Meerman, I.C. Gunlus, R. Srinivasan and K.L. Rinehart Jr., *J. Am. Chem. Soc.*, 1966, **88**, 618.

[158] K.H. Park and L.J. Cox, *Tetrahedron Lett.*, 2003, **44**, 1067.

[159] A.R. Katritzky and A. Pastor, *J. Org. Chem.*, 2000, **65**, 3679.

[160] A.R. Katritzky, Y. Fang, A. Donkor and J. Xu, *Synthesis*, 2000, 2029.

[161] M. Calvin and K.W. Wilson, *J. Am. Chem. Soc.*, 1945, **67**, 2003.

[162] R.H. Holm and F.A. Cotton, *J. Am. Chem. Soc.*, 1958, **80**, 5658.

[163] J.L. Burdett and M.T. Rogers, *J. Am. Chem. Soc.*, 1964, **86**, 2105.

[164] H.J. Jarries and G. Parry, *Inorg. Chim. Acta*, 1978, **31**, 233.

[165] H. Jarret, M. Sadler and J. Shoolery, *J. Chem. Phys.*, 1953, **21**, 2092.

[166] L. Reeves, *Can. J. Chem.*, 1957, **35**, 1351.

[167] R.L. Lindtvedt and H.F. Holtzclaw Jr, *Inorg. Chem.*, 1966, **5**, 239.

[168] R.L. Lindtvedt and H.F. Holtzclaw Jr, *J. Am. Chem. Soc.*, 1966, **88**, 2713

[169] N.N. Shapet'ko, S.S. Berestova, G.M. Lukovkin and Y.S. Bogachev, *Org. Mag. Res.*, 1975, **7**, 237.

[170] Gorodetshy, Z. Luz and Y. Mazur, *J. Am. Chem. Soc.*, 1967, **89**, 1183.

[171] D.C. Nonhebel, *Tetrahedron*, 1968, **24**, 1869.

[172] D. Isaazson and K.J. Morokuma, *J. Am. Chem. Soc.*, 1975, **102**, 4453.

[173] C. Haddon, *J. Am. Chem. Soc.*, 1980, **102**, 1807.

[174] J.W. Bunting, J.P. Kanter, R. Nelander and Z. Wu, *Can. J. Chem.*, 1995, **73** , 1305.

[175] L. Zamir, B.S. Jensen and E. Larsen, *Org. Mass Spectrom.*, 1969, **2**, 49.

[176] P.E. Allegretti, L. Gavernet., E. A. Castro and J.J.P. Furlong, *J. Mol. Struct. (Theochem)*, 532: 2000, **1-3**, 139.

[177] P.E. Allegretti, M.M. Schianovi, H.E. Di Loreto, C.O. Della Vedova and J.J.P. Furlong, *J. Mol. Struct.*, in press.

[178] C.M. Zakaria, C.A. Morrison, D. McAndrew, W. Bell and C. Glidewell, *J. Organomet. Chem.*, 1995, **485**, 201.

[179] C.J. Pedesen, N.J. Salem and V. Weinmayr, *U.S. Patent*, **2,875,223**, Feb. 24, 1959.

[180] J.C. Swarts, T.G. Vosloo, J.G. Leipoldt and G.J. Lamprecht, *Acta Crystallogr., Sect. C*, 1993, **49**, 760.

[181] D.J. Che, G. Li, X. L. Yau and D.P. Zou, *J. Organomet. Chem.*, 1998, **568**, 165.

[182] K.C. Kemp, M.Sc. Study, *Synthesis, electrochemical, kinetic and thermodynamic studies of new ruthenocene-containing betadiketonato rhodium(I) complexes with biomedical applications*, University of the Orange Free State, R.S.A., 2004.

[183] G. Bartoli, C. Cimarelli, G. Palmieri, M. Bosco and R. Dalpozzo, *Synthesis*, 1990, 895.

[184] S.I. Murahashi and Y. Tsumiyama, *Bull. Chem. Soc. Jpn.*, 1987, **60**, 3285.

[185] H.A. Stefani, I.M. Costa and D. de O. Silva, *Synthesis*, 2000, 1526.

[186] A.R. Katritzky, Y. Fang, A. Donkor and J. Xu, *Synthesis*, 2000, 2029.

[187] T. Bosanac and C.S. Wilcox, *Tetrahedron Lett.*, 2001, **42**, 4309.

[188] L.N. Mander and S.P. Sethi, *Tetrahedron Lett.*, 1983, **24**, 5425.

[189] Y. Wang and S. Zhu, *Tetrahedron Lett.*, 2001, **42**, 5741.

[190] D.A. White, *J. Inorg. Nucl. Chem.*, 1971, **33**, 691.

[191] R.S.P. Coutts and P.C. Wailes, *Aust. J. Chem.*, 1969, **22**, 1547.

[192] A.M. Bond, R. Colton, U. Englert, H. Hűgel and F. Merken, *Inorg. Chim. Acta*, 1995, **235**, 117.

[193] F. Bottomley, I.J.B. Lin and P.S. White, *J. Organomet. Chem.*, 1981, **212**, 341.

[194] H. Klein and U. Thewalt, *J. Organomet. Chem.*, 1980, **194**, 297.

[195] G. Doyle and R.S. Tobias, *Inorg. Chem.*, 1967, **6**, 1111.

[196] N.V. Alekseev and I.A. Ronova, *Zh. Strukt. Khim.*, 1966, **7**, 103.

[197] G. Doyle and R.S. Tobias, *Inorg. Chem.*, 1968, **7**, 2479.

[198] A.T. Kotchevar, P. Ghosh, D.D. DuMez and F.M. Uckun, *J. Inorg. Biochem.*, 2001, **83**, 151.

[199] A.K. Sharma and N.K. Kaushik, *Z. Naturforsch.*, 1984, **39b**, 604.

[200] U.B. Saxena, A.K. Rai, V.K. Mathur and R.C. Mehrotra, *J. Chem. Soc.*, 1970, 904.

[201] G. Doyle and R.S. Tobias, *Inorg. Chem.*, 1968, **7**, 2484.

[202] D.C. Bradley and C.E. Holloway, *J. Chem. Soc., Chem. Commun.*, 1965, 284.

[203] M.J. Frazer and W.E. Newton, *Inorg. Chem.*, 1971, **10**, 2137.

[204] H.J. Keller, B.K. Keppler and D. Schmähl, *A. Forsch.*, 1982, **32(8)**, 806.

[205] B.K. Keppler and M.E. Heim, *Drugs of the Future*, 1988, **3,** 638.

[206] L. Wolf and C. Tröltzch, *J. Prakt. Chem.*, 1962, **17**, 78.

[207] T.J. Pinnavalia and R.C. Fay, *Inorg. Chem.*, 1968, **7**, 502.

[208] U.B. Saxena, A.K. Rai, V.K. Mathur and R.C. Mehrotra, *J. Chem. Soc.*, 1970, 904.

[209] G. Schmitt and S. Ozman, *J. Org. Chem.*, 1976, **41**, 3331.

[210] P.R. Wells, *Progress in Physical Organic Chemistry*, 1968, **6**, pp 111-145.

[211] R.E. Kagarise, *J. Am. Chem. Soc.*, 1955, **77**, 1377.

[212] S. Arrhenius, *Z. Phys. Chem.*, 1889, **4**, 226.

[213] E. Whalley, *J. Chem. Phys.*, 1963, **38**, 1400.

[214] R.M. Cravero, M. Gonzalez-Sierra and A.C. Olivieri, *J. Chem. Soc. Perkin Trans. 2*, 1993, 1067.

[215] W. Blokzijl, J.B.F.N. Engberts and M.J. Blandamer, *J. Chem. Soc. Perkin Trans. 2*, 1994, 455.

[216] W.C. du Plessis, W.L. Davis, S.J. Cronje and J.C. Swarts, *Inorg. Chim. Acta*, 2001, **314**, 97.

[217] R.J. Cross, *Chem. Soc. Rev.*, 1985, **14**, 197.

[218] R.G. Wilkins, *Kinetics and Mechanisms of Reactions of Transition metal complexes*, 2nd Edition, VCH, Weinheim, 1991, pp. 103, 232-242.

[219] F. Mathey and A. Servin, *Molecular Chemistry of the Transition Elements*, John Wiley & Sons, Chichester, 1996, pp. 28-50.

[220] R. Fay and R.N. Lowry, *Inorg. Chem.*,1974, **13**, 1309.

[221] A.C. Adams and E.M. Larsen, *Inorg. Chem.*, 1966, **5**, 814.

[222] J.K. Park, J.J. Myoung, J.B. Kyong and H.K. Kim, *Bull. Korean Chem. Soc.*, 2003, **24**, 671.

[223] E.A. Guggenheim, *Phil. Mag.*, 1926, **2**, 538.

[224] A. Kivinen, *Acta Chem. Scand.*, 1965, **19**, 845.

[225] B.K. Keppler and M.E. Heim, *Drugs of the Future*, 1988, **13**, 637.

[226] P.T. Kissinger and W.R. Heineman, *J. Chem. Educ.*, 1983, **60**, 702.

[227] D.H. Evans, K.M. O'Connell, R.A. Peterson and M.J. Kelly, *J. Chem. Educ.*, 1983, **60**, 290.

[228] G.A. Mobbot, *J. Chem. Educ.*, 1983, **60**, 697.

[229] A.J. Bard and L.R. Faulknaer, *Electrochemical Methods: Fundamentals and Applications*, Wiley, New York, 1980, chapter 6.

[230] P.A. Christensen and A. Hamnett, *Techniques and Mechanisms in Electrochemistry*, Blackie Academic & Professional, London, 1994, pp. 55-67, 170-175.

[231] J.J. Van Benschoten, J.Y. Lewis, W.R. Heineman, D.A. Roston and P.T. Kissinger, *J. Chem. Educ.*, 1983, **60(9)**, 772.

[232] P.T. Kissinger and W.R. Heineman, *Laboratory Techniques in Electroanalytical Chemistry*, Dekker, New York, 1984, chapter 13.

[233] G. Gritzner and J. Kuta, *Pure Appl. Chem.*,1984, **56**, 461.

[234] R.R. Gagné, C.A. Koval and G.C. Lisensky, *Inorg. Chem.*, 1980, **19**, 2855

[235] G. Gritzener and J. Kuta, *Pure and Appl. Chem.*, 1984, **56**, 461.

[236] H.M. Koepp, H. Wendt and H. Stehlow, *Z. Electrochem.*, 1960, **64**, 483.

[237] L. Pospisil, B.T. King and J. Michl, *Electrochim. Acta*, 1998, **44**, 103.

[238] R.J. Le Suer and W.E. Geiger, *Aangew. Chem., Int. Ed. Engl.*, 2000, **39**, 248.

[239] W.J. Moore, *Physical Chemistry*, 4th Ed, Longman Group Limited, 1972, pp 333-334.

[240] J. Conradie, Ph.D. Study, University of the Orange Free State, R.S.A., 1999.

[241] C. LaVanda, D.O. Cowan, C. Leitch and K. Bechgaard, *J. Amer. Chem. Soc.*, 1974, **96**, 6788.

[242] W.H. Morrison, Jr., S. Krogsrud and D.N. Hendrickson, *Inorg. Chem.*,1973, **12**, 1998.

[243] G.M. Brown, T.J. Meyer, D.O. Cowan, C. LeVanda, F. Kaufman, P.V. Roling and M.D. Rausch, *Inorg. Chem.*, 1975, **14**, 506.

[244] W.C. du Plessis, J.J.C. Erasmus, G.J. Lamprecht, J. Conradie, T.S. Cameron, M.A.S. Aquino and J.C. Swarts, *Can. J. Chem.*,1999, **77**, 378.

[245] W.C. du Plessis, T.G. Vosloo and J.C. Swarts, *J. Chem. Soc., Dalton Trans.*, 1998, 2507.

[246] J.E. Gorton, H.L. Lentzner and W.E. Watts, *Tetrahedron*, 1971, **27**, 4353.

[247] N.F. Blom, E.W. Neuse and H.G. Thomas, *Transition Met. Chem.*, 1987, **12**, 301.

[248] J.C. Swarts, G.J. Lamprecht and E.W. Neuse, *J. Inorg. Organomet. Polym.*, 1994, **143**, 4.

[249] D.E. Bublitz, G. Hoh and T. Kuwana, *Chem. Ind. (London)*, 1959, **78**, 365.

[250] T. Kuwana, D.E. Bublitz and G. Hoh, *J. Am. Chem. Soc*, 1960, **82**, 5811.

[251] S.P. Gubin, L.I. Smirnova, L.I. Denisovich and A.A. Lubovich, *J. Organomet. Chem.*, 1971, **30**, 243.

[252] L.I. Denisovich, N.V. Zakurin, A.A. Bazrukova and S.P. Gubin, *J. Organomet. Chem.*, 1974, **81**, 207.

[253] R.J. Gale, R. Job, *Inorg. Chem.*,1981, **20**, 42.

[254] M.G. Hill, W.M. Lamanna and K.R. Mann, *Inorg. Chem.*, 1991. **30**, 4690.

[255] S. Trupia, A. Nafady and W.E. Geiger, *Inorg. Chem. Comm.*, 2003, **42**, 5480.

[256] M. Sato, G. Maruyama and A. Tanemura, *J. Organomet. Chem.*, 2002, **23**, 655.

[257] C. Jacobs, A.Y. Safronov, S. Wilson, H.A.O. Hill and T.F. Booth, *J. Electroana. Chem.*, 1997, **427,** 161.

[258] J. Langmaier, Z. Samec, V. Varga, M. Horacek, R. Choukroun and K. Mach, *J. Organomet. Chem.*, 1999, **584**, 323.

[259] G.V. Loukova and V.V. Strelets, *J. Organomet. Chem.*, 2000, **606**, 203.

[260] N. El Murr, A. Chaloyard and J. Tirouflet, *J. Chem. Soc. Chem. Comm.*, 1980, 446.

[261] M.A Vorotyntsev, M. Casalta, E. Pousson, L. Roullier, G. Boni and C. Moise, *Electrochim, Acta*, 2001, **46**, 4017.

[262] A. Vallat, R. Roulier and C. Bourdon, *J. Electroanal. Chem.*, 2003, **542**, 75.

[263] J. Langmaier, Z. Samec, V. Varga, M. Horacek, R. Choukroun and K. Mach, *J. Organomet. Chem.*, 1999, **579**, 348.

[264] M. Rozencweig, D.D. von Hoff, M. Slavik and F.M. Muggia, *Ann. Int. Med.*, 1977, **86**, 803.

[265] J.H. Burchenal, K. Kalaher, T. O'Toole and J. Chisholm, *Cancer Res.*, 1977, **37**, 3455.

[266] N.K. Kim, T. Kim, S. Shin, J.A. Lee, Y. Cho, K.H. Kim, D. Kim, D.S. Heo and Y. Bang, *Cancer (N.Y.)*, 2001, **91**, 1549.

[267] E.W. Neuse and F.Kanzawa, *Appl. Organomet. Chem.*, 1990, **4**, 19.

[268] J.C. Swarts, T.G. Vosloo, S.J. Cronje, W.C du Plessis, C.E.J. van Rensburg, E. Kreft, C. La Madeleine and J.E. van Lier, *Anticancer Res*., 2001, **21**, 2033.

[269] J. Ward, M.E. Grabin, E. Berlin, and D.M Young, *Cancer Res.*. 1977, **37**, 1238.

[270] R.F. Shago, M.Sc. Study, *Synthetic, spectroscopic, thermodynamic and electrochemical studies on multi-tetradesylated phthalocyanine-ferrocenylbutoxide conjugates with liquid crystalline properties*, University of the Orange Free State, R.S.A., 2002.

[271] D. Osella, M. Ferrali, P. Zanello, F. Lashi, M. Fontani, C. Nervi and G. Lavigiolio, *Inorg. Chim. Acta*, 2000, **306,** 42.

[272] J.C. Swarts, C.E. Medlin, *European Patent.* EP 1 345 951 B1, bulletin 2004/34, 2004, pp 1-36.

[273] R. Herken and M. Wenzel, *Eur. J. Nucl. Med.*, 1985, **10**, 56.

[274] J. Shani, T. Livshitz and M. Wenzel, *Int. J. Nucl. Med. Biol.*, 1985, **12**, 13.

[275] M. Crul, R.C.A.M. van Waardenburg, J.H. Beijen and J.H.M. Schellens, *Can. Treat. Rev.*, 2002, **28**, 291.

[276] E. Melendez, *Crit. Rev. Oncol./Hematol.*, 2002, **42**, 309.

[277] P. Köpf-Maier, T.P. Klapötke and H. Köpf, *Inorg. Chim. Acta*, 1988, **153**, 119.

[278] P.Köpf-Maier, *Eur. J. Clin. Pharmacol.*, 1994, **47**, 1.

[279] P.Köpf-Maier and H. Köpf, *Chem. Rev.*, 1987, **87**, 1137.

[280] M.J. Blandamer and J. Burgess, *Coord. Chem. Rev.*, 1980, **31**, 93.

[281] M.J. Cook, *Phthalocycnines: Introduction to Liquid Crystals-UEA report*, 1992.

Chapter 3

Results and Discussion

3.1. Introduction

The synthesis and characterization of a selection of new and known organometallic compounds, which include ferrocene, ruthenocene and titanium complexes, are presented (see Figure 3.1 for the structures). The ferrocene complexes include the series of ferrocenylalcohols ferrocenylmethanol, 2-ferrocenylethanol, 3-ferrocenylpropanol and 4-ferrocenylbutanol. The ruthenocene complexes are ruthenocene-containing β-diketones, $RcCOCH_2COR$ with R = $C_{10}F_{21}$, CF_3, C_6F_5, $C_{10}H_{21}$, CH_3, Rc and Fc. A few different types of titanium coordination complexes were synthesised, and involve different coordination combinations of the ferrocenylalcohols and/or ruthenocene-containing β-diketones.

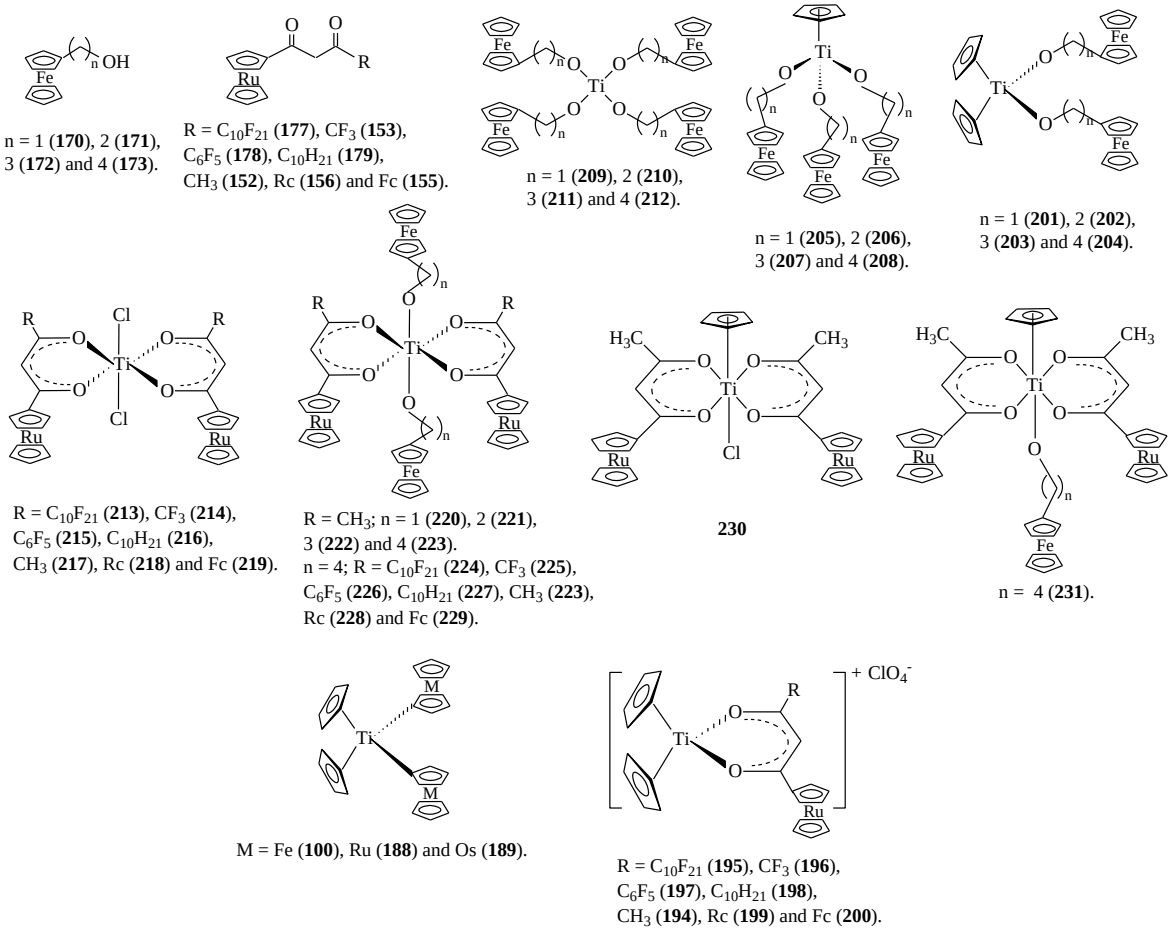

Figure 3.1. Structures of organometallic compounds that was synthesised during the course of this reseach program.

Spectroscopic characterization of these complexes was preformed by proton nuclear magnetic resonance (^{1}H NMR), infra red (IR) and ultra violet (UV/Vis) spectroscopy.

All synthesised complexes were electrochemically analysed (cyclic, Oster Young Square wave and linear sweep voltammetry) and the data are reported.

Kinetics results for the conversion of the β-diketones from enol- to keto-isomer are described. Ligand exchange and substitution kinetics performed on selected titanium complexes are reported. The hydrolyses kinetic results for a few selected titanium complexes are also presented.

Some cytotoxic properties of selected compounds on cancer cells are presented and phase study results by differential scanning, calorimetry of four complexes are reported.

The crystal structure of a titanium complex containing a ruthenocene-containing β-diketone are also reported.

3.2. Synthesis

3.2.1. Ferrocenylalcohols

The series of ferrocenylalcohols ferrocenylmethanol (**170**), 2-ferrocenylethanol (**171**), 3-ferrocenylpropanol (**172**) and 4-ferrocenylbutanol (**173**)] were synthesised according to Scheme 3.1.

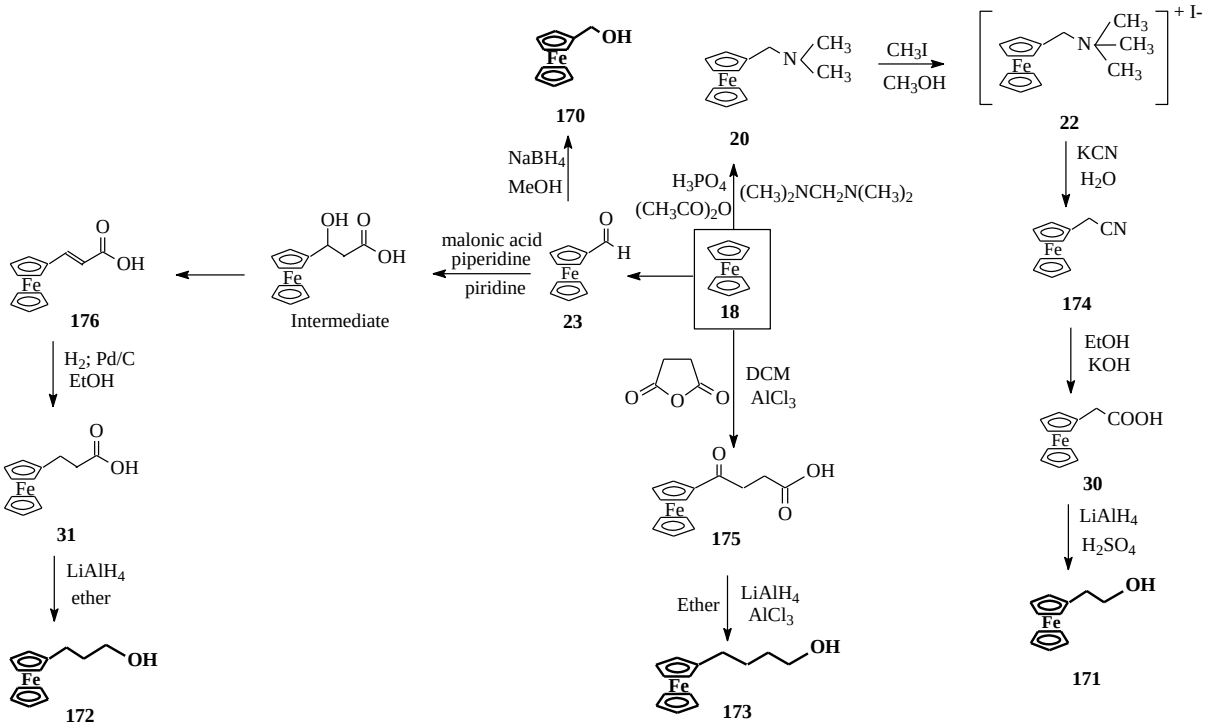

Scheme 3.1. Synthesis of ferrocenylalcohols **170-173.**

Ferrocenylcarboxaldehyde (**23**) was used as a precursor in the synthesis of ferrocenylmethanol (**170**) and 3-ferrocenylpropanol (**172**). Ferrocenylcarboxaldehyde (**23**) was prepared by the treatment of ferrocene (**18**) with phosphorus oxychloride and N-methylformanilide. The addition of sodium borohydride to **23** caused immediate reduction of the carbonyl group to form ferrocenylmethanol (**170**), and was accompanied by a colour change from red to yellow. This alcohol was found to be prone to slow decomposition and hence has to be purified by column chromatography prior to use. 2-Ferrocenylethanol (**171**) was synthesised in five steps from ferrocene (**18**). The first step involves the dimethylaminomethylation of **18** under inert atmosphere in the presence of acids to give dimethylaminomethylferrocene (**20**) in 77% yield. Thereafter, **20** was methylated almost quantitatively with methyl iodide to give the quaternary ammonium salt N,N-dimethylaminomethylferrocene methiodide (**22**). Ferrocenylacetonitrile (**174**) was prepared by cyanation of **22**, by refluxing it with sodium cyanide. This reaction was more troublesome, especially to isolate pure ferrocenylacetonitrile (**174**). With care **174** can be obtained in 98% yield. The saponification (hydrolysis) of **174** liberated ferrocenylacetic acid (**30**) in 66% yield after acidification and purification. Finally, acid **30** was reduced by excess lithium aluminiumhydride to give the desired 2-ferrocenylethanol (**171**) as a pale yellow solid in 93% yield. 3-Ferrocenylpropanol (**172**) is prepared in four steps, starting with the formation of **23**, the same starting material as for **170**. The second step involves the Michael addition of malonic acid in two-fold excess to yield ferrocenylacrylic acid (**176**). The precursor intermediate molecule of **176**, splits out water to give **176** in 18% yield. Low yield of **176,** shows that the removal of water from the intermediate molecule was not complete. Hydrogenation of **176** with hydrogen gas catalysed by palladium on activated charcoal gave 3-ferrocenylpropanoic acid. A standard reduction with five fold excess of lithium aluminium hydride gave the desired product 3-ferrocenylpropanol (**172**) as an orange liquid. For alcohol **175,** ferrocene (**18**) and succinic anhydride was reacted under standard Friedel-Craft acylation conditions to give 3-ferrocenoylpropionic acid (**175**). The alcohol, 4-ferrocenylbuthanol (**173**) was obtained as an dark orange liquid by the simultaneous reduction of the keto-group and the carboxylic acid with lithium aluminium hydride and aluminium trichloride.

The overall yields obtained for the four ferrocenylalcohols are shown in Table 3.1. Under indicated synthetic conditions there is a decrease in yield as the amount of methyl spacers between ferrocenyl moiety and the alcohol group increases. This is propably related to the increase in hydrophobicity as side chain length increases. It was subsequently found that the use of increased amounts of ethanol as co-solvent overcame this problem.[1]

Table 3.1. The overall yields obtained for ferrocenylmethanol (170), 2-ferrocenylethanol (171), 3-ferrocenylpropanol (172) and 4-ferrocenylbutanol (173).

Ferrocenylalcohol	Amount of methylene (-CH_2-) spacers between Fc- and -OH	% Yield
170: Ferrocenylmethanol	1	86
171: 2-Ferrocenylethanol	2	84
172: 3-Ferrocenylpropanol	3	69
173: 4-Ferrocenylbutanol	4	55

It is known that the alcoholic protons of **171** can form a hydrogen bond to iron (See Figure 3.2, Top Left).[2] **170**'s alkyl chain length is not long enough to form this kind of bond, however it has been shown by Swarts and co-workers,[1] utilising electrochemical techniques, a hydrogen bond can exist between two mixed valent molecules of **170** (Figure 3.2, Top Middel). The ^{1}H NMR of **170** shows an additional small doublet at 3.50 (see Figure 3.2, Bottom). This doublet could be the proof of the existence of the dimer. This dimer is not a mixed valent species and thus a different structure for the Fe^{II} dimer is proposed. See Figure 3.2, Top Right.

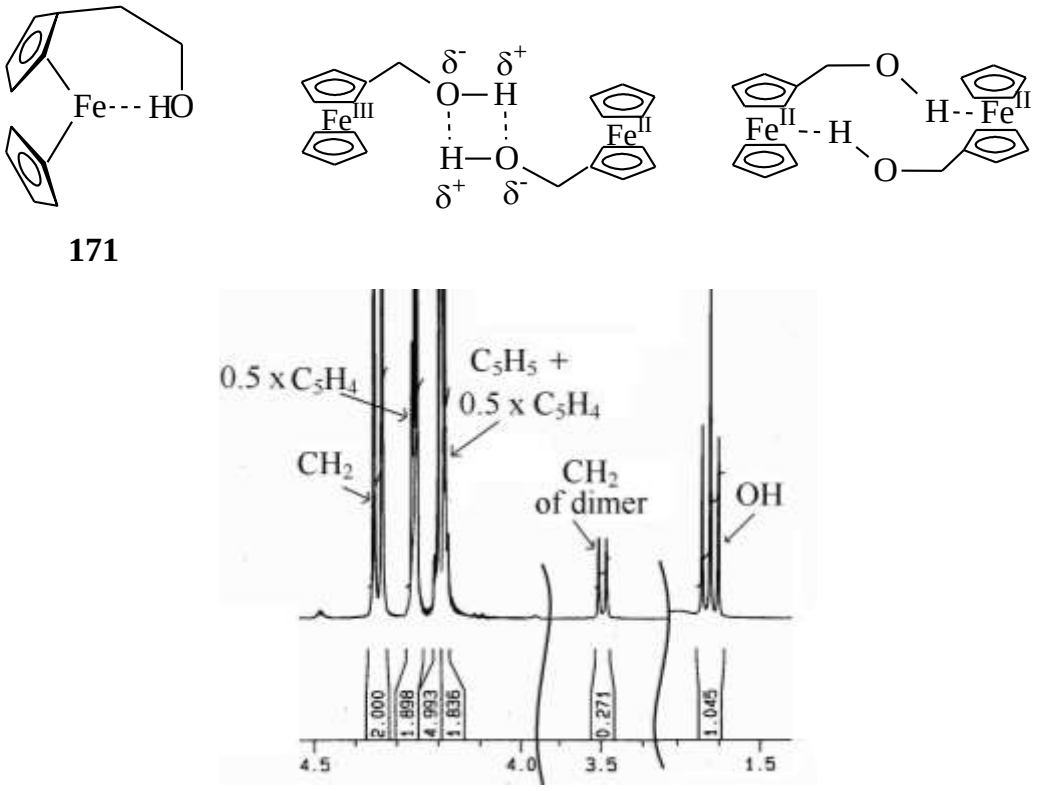

Figure 3.2. Top Left: Intermolecular hydrogen bonding of **171**. Top Middle: The hydrogen bonding between **170**-(**170**)$^+$. Top Right: Proposed hydrogen bonding between two molecules of **170**. Bottom: Patrial ^{1}H NMR of **170** (Full ^{1}H NMR is shown in Appendix, Spectrum 2).

3.2.2. Ruthenocene-containing β-Diketones

Three new and four known ruthenocene-containing β-diketones, $RcCOCH_2COR$ [where R = $C_{10}F_{21}$ (**177**), CF_3 (**152**), C_6F_5 (**178**), $C_{10}H_{21}$ (**179**), CH_3 (**151**), Rc (**155**) and Fc (**140**)] were prepared by Claisen condensation of acetylruthenocene and the appropriate ester, under the influence of the hindered base lithium diisopropylamide (LDA) according to Scheme 3.2.

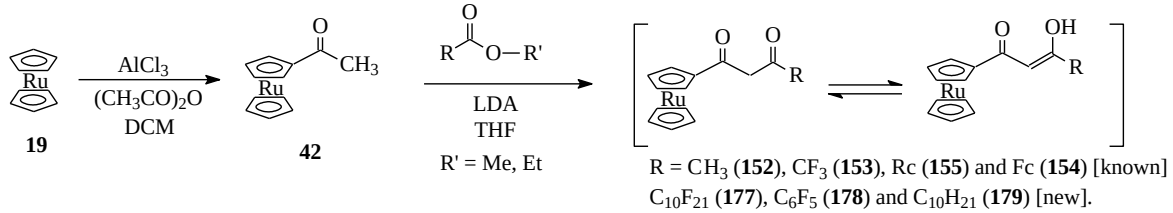

Scheme 3.2. Synthetic route utilized for preparation of the ruthenocene-containing β-diketones, $RcCOCH_2COR$.

The Friedel-Craft acetylation of ruthenocene (**19**) with 2.2 equivalents of aluminium trichloride in acetic anhydride gave acetylruthenocene (**42**).This reaction contrasts with ferrocene acylation which is effective with the much milder H_3PO_4 as Friedel-Craft catalyst. The synthesis of **42** was optimized from the known method,[3] just by doing the reaction under an inert atmosphere; this raised the yield by *ca* 30% to 96% yield.

The yields obtained for the β-diketones are shown in Table 3.2. The yields obtained varied but the general trend that was observed is that the greater the group electronegativity of the R group, the higher the yield obtained becomes. This can be explained by the fact that the more electron-withdrawing the R group is, the more positive charge will be generate on the carbonyl group. This in turn makes the ester more susceptible to attack from the *in situ* generated nucleophile $RcCOCH_2^-$. The low yield for **178** can be accounted for by the difficulty in isolating the product, which involves a few separations by coulomb chromatography.

Table 3.2. The yields obtained in the synthesis of the ruthenocene-containing β-diketones, $RcCOCH_2COR$ and group electronegativity of the R groups.

R group	χ_R	% Yield
177: $C_{10}F_{21}$	3.04	86
152: CF_3	3.01	85
178: C_6F_5	2.46	8.3
179: $C_{10}H_{21}$	2.43	23
151: CH_3	2.34	40
155: Rc	1.99	26
154: Fc	1.87	30

A new method of obtaining β-diketones, was also explored for the synthesis of these ruthenocene-containing β-diketones. The new method involved reaction of a carboxylic acid (or acid chlorides) with benzotriazole to giving an *N*-acylbenzotriazole. The obtained *N*-acylbenzotriazole can in turn be converted into a β-diketone.[4, 5]

1-Ruthenocenyl-4-methylprop-1,3-dione (**151**) was synthesised according to this new method by way of example. Both the acetylchloride and ruthenocenylchloride were reacted with benzotriazol to liberate the *N*-acylbensotriazol as **181** and **182** respectively in high yield. By reacting **181** and **182** with the correct ketone under basic conditions according to Scheme 3.3, β-diketone **151** was obtained.

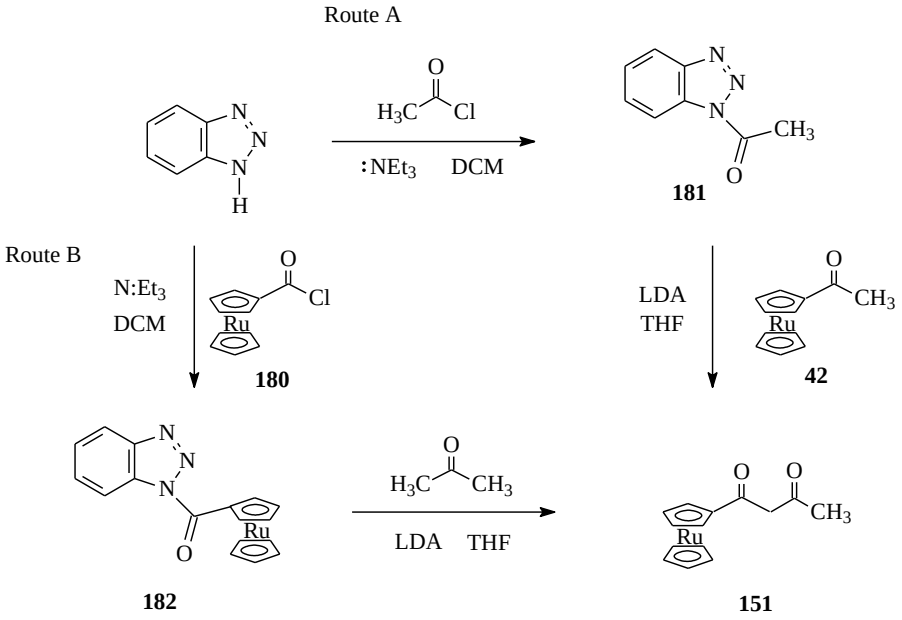

Scheme 3.3. Schematic representation of the new method of obtaining **151**.

The overall yield obtained for **151** *via* route A was 77% and the overall yield for route B was 76% based on ruthenocene. Both yields are much higher than the 43% overall yield from the Claisen condensation methods.

3.2.3. Enaminones

Ketimines can be converted into enaminones *via* acylbenzotriazole,[6, 5] utilizing the same method as described in section 3.2.2. for β-diketone synthesis.

In the model reaction, used here, acetyl ferrocene was reacted with aniline in the presence of $TiCl_4$ to give N-phenyl-N-(ferrocenylethylidene)amine (**183**) in 14% yield. **183** was further treated with **181** to give the enaminone 1-ferrocenylbutan-3-one-4-aniline (**184**) in 59% yield as a dark brown solid according to Scheme 3.4.

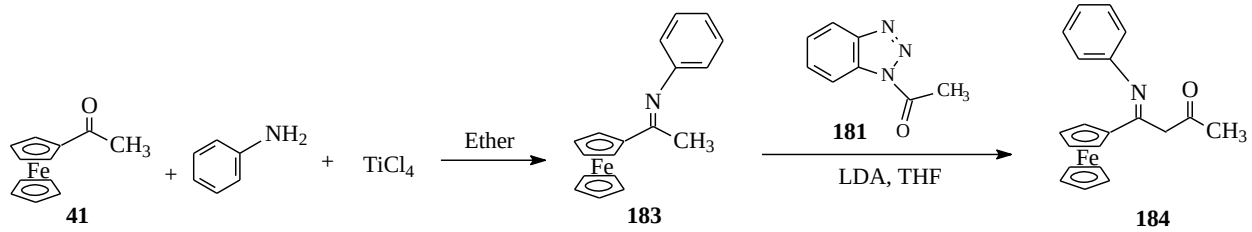

Scheme 3.4. The synthesis of enaminone **184**.

The formation of a multi-metal centered enaminone was achieved by utilising the *N*-acylbenzotriazol route. Acetyl ferrocene was reacted with the aminocobalticinium salt (**185**) to give the *N*-cobalticinium-*N*-(ferrocenylethylidene)amine salt (**186**) in 89% yield. **186** was further treated with **182** to give the enaminone 1-ferrocenyl-3-ruthenocenylpropan-1-one-3-*N*-cobalticiniumamine salt (**187**) in 46% yield according to Scheme 3.5.

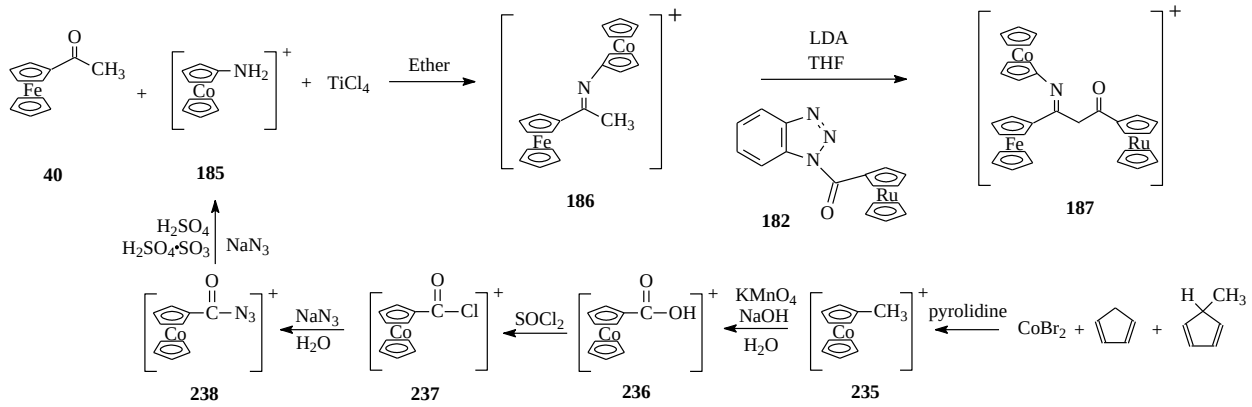

Scheme 3.5. The synthesis of the multi-metal-containing enaminone **187**. $TiCl_4$ is used as a catalyst in this reaction.

185 was synthesised according to Scheme 3.5.[7] A mixture of cobalticinium, methylcobalticinium (**235**) and 1,1'-dimethylcobalticinium hexafluorophosphate was prepared in 14% yield from equimolar amounts of cyclopentadiene, methylcyclopentadiene and cobaltbromide. Pyrrolidine, which is a stronger base and better solvent for $CoBr_2$, is used instead of diethylamine, which is normally used for metallocenes formation.[8] The methyl groups on **235** were oxidized to carboxylates by treatment with basic aqueous potassium permanganate. After acidification, a mixture of the mono- and bicarboxylic acid derivatives precipitated as hexafluorophosphate salts by addition of excess sodium hexafluorophosphate. The monocarboxylic acid (**236**) dissolved readily in acetone, whereas the bicarboxylic acid is virtually insoluble. The acyl chloride (**237**) was prepared from **236** and converted to the acyl azide **238**. Rearrangement of **238** in concentrated sulphuric acid at 130ºC produced **185** in 0.7% yield (literature reported 60% yield).

3.2.4. Titanium(IV) complexes

3.2.4.1. Bis(η^5-cyclopentadienyl)dimetallocenyl titanium(IV)

The titanium series **100, 188-189** were synthesized according to Scheme 3.6. The complexes dicyclopentadienyldimetallocenyl titanium(IV) $[(C_5H_5)_2Ti\{(C_5H_4)M(C_5H_5)\}_2]$ (M = Fe (**100**), Ru (**188**) and Os (**189**)) are synthesized by the treatment of the corresponding metallocenyllithium (FcLi, RcLi or OcLi) with titanocene(IV) dichloride (**89**) in THF. The lithiation reactions of the ferrocene and ruthenocene were preformed by using *t*-butyllithium at 0˚C for 30 min and 4 h respectively because *n*-butyllithium gives rise to dilithiated species.[3] Mono-lithiation is possible in low yield with *n*-butyllithium in ether as solvent, but *t*-butyllithium is much more effective for mono-lithiation. However, lithiation of osmocene needs special treatment and even then did not give good results. *n*-Butyllithium was used rather than *t*-butyllithium (which did not work at all) and reaction time was lengthened to overnight and room temperature, except during the addition of *n*-butyllithium, which was done at -78˚C. The metallocenylation of titanocene dichloride involved just the stirring of the corresponding metallocenyllithium (FcLi (**190**), RcLi (**191**) or OcLi (**192**)) with titanocene(IV) dichloride (**89**) in THF for an hour. Again the osmocene reaction needed a longer reaction time of 5 h. After washing and extraction, **100** and **188** were clean enough for further study but, **189** needed special treatment. Even after re-crystallization diosmocenyltitanocenyl still showed traces of unreacted osmocene. Unreacted osmocene could be removed by sublimation at 98˚C over 2h.

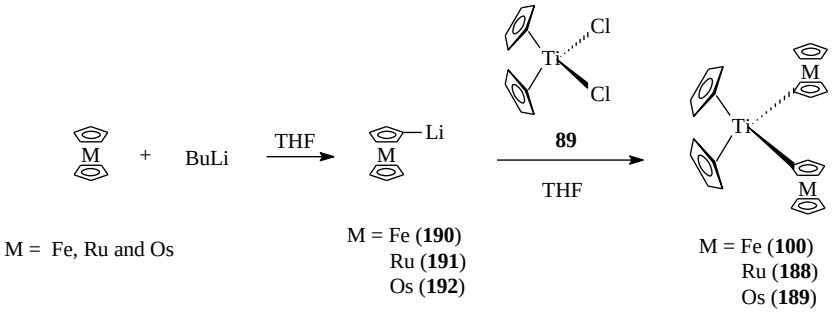

Scheme 3.6. Schematic representation of the synthesis of the different dicyclopentadienyldimetallocenyl titanium(IV) complexes $[(C_5H_5)_2Ti\{(C_5H_4)M(C_5H_5)\}_2]$ (M = Fe (**100**), Ru (**188**) and Os (**189**)).

The ^{1}H NMR spectra of chloroform-*d* solutions of $[(C_5H_5)_2Ti\{(C_5H_4)M(C_5H_5)\}_2]$ (M = Fe(**100**), Ru(**188**) and Os(**189**)) are simple and easily interpreted. From the ^{1}H NMR (Figure 3.3) it could be deduced that the protons on the cyclopentadienyl ring of the titanium are equivalent. The protons of cyclopentadienyl rings of the metallocenes (Fc, Rc and Oc) correspond to data for monosubstituted metallocenes. All the ^{1}H NMR spectra are as expected,

except for the ruthenocenyl derivative. It can be seen that one of the signals corresponding to C_5H_4 is at higher field than C_5H_5.

The position of the ^{1}H NMR signal of the cyclopentadienyl rings of the titanium, is influenced by the atomic electronegativity of the metal of the added metallocene [Fe (χ_{Fe} = 1.64), Os (χ_{Os} = 1.52) and Ru (χ_{Ru} = 1.42)]. The general trend is that with increased electronegativity of metal, there is an increase in ^{1}H NMR shift of the cyclopentadienyl protons bounded to the titanium to a lower field [Fe (6.48), Ru (6.32) and Os (6.36)]. This is expected, because the more electron-withdrawing the metal is, the more positive the titanium centre will become and thus the cyclopentadienyl protons bounded to the titanium will be deshielded, which will in turn lead to the ^{1}H NMR shift to a lower field.

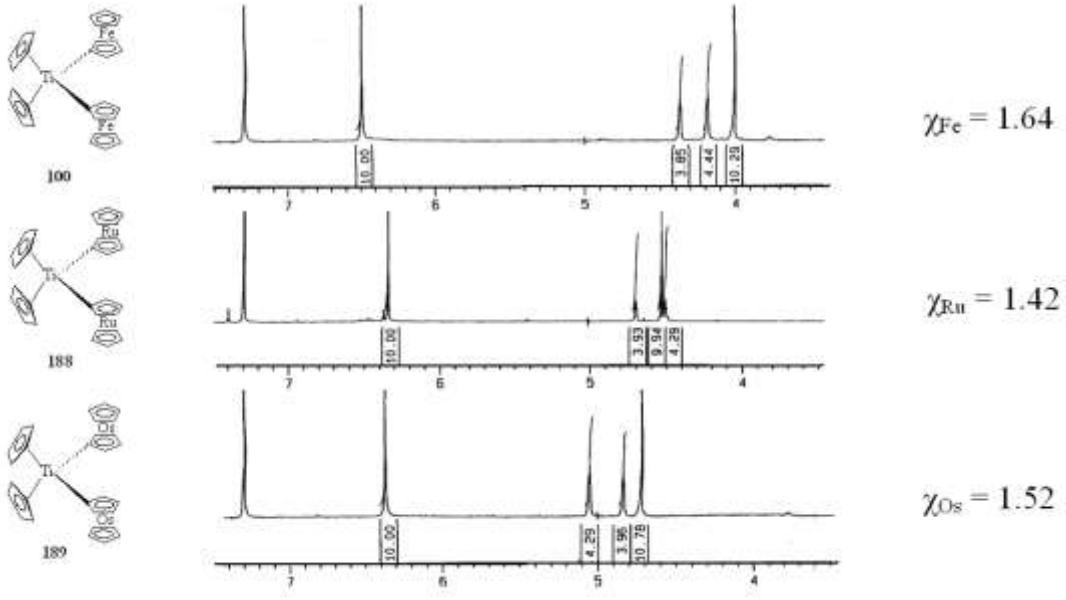

Figure 3.3. ^{1}H NMR of $[(C_5H_5)_2Ti\{(C_5H_4)M(C_5H_5)\}_2]$.

The $M(C_5H_4)(C_5H_5)$ with M = Fe, Ru and Os ^{1}H NMR signals appeared progressively more downfield in moving from M = Fe through to Ru to Os. This does not follow the trend predicted by $\chi_{Fe,\ Ru,\ Os}$, but it does follow the general ^{1}H NMR position trend of free ferrocene (C_5H_5 signal at 4.19 ppm), ruthenocene (C_5H_5 signal at 4.57 ppm) and osmocene (C_5H_5 signal at 4.74 ppm).

3.2.4.2. β-Diketonatobis(η^5-cyclopentadienyl)titanium(IV) perchlorate

The two $[(C_5H_5)_2Ti(\beta\text{-diketonato})]^+ClO_4^-$ complexes (**193-194**) were synthesized according to the general procedure as described by Doyle and Tobias (Scheme 3.7).[9] The

synthesis starts with the dissolving of $(C_5H_5)_2TiCl_2$ in water to give a complex aquated cationic species mixture (see Chapter 2, Scheme 2.12, page 22). Next follows the replacement of the now free Cl^- groups originally from the titanocene dichloride with perchlorate (ClO_4^-). This reaction is driven by the addition of $AgClO_4$ followed by the precipitation of AgCl. Chloride ion removal enhances the next step of the synthesis. Because ClO_4^- is a much poorer coordinating group than Cl^-, the substitution of the β-diketonate ligand onto the titanium centre is promoted. The product that forms is an ionic species with ClO_4^- as the counter ion. A base or hydrogen acceptor is not needed in this reaction due to the fact that the β-diketonate moiety has a keto-enol tautomer and the major form in solution is the enol form.[11] An important observation that was made from the synthesis of these complexes, is that if the $AgClO_4$ is in excess the yield decrease dramatically up to the point where the reaction does not work. This is probably due to side reaction catalysed by the excess silver in solution.

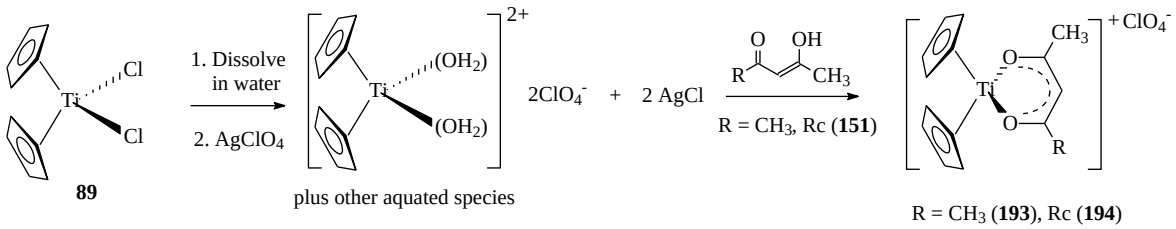

Scheme 3.7. Synthesis of the mono-β-diketonato titanocenyl complexes. Aqueous equilibrium of $(C_5H_5)_2TiCl_2$ is discussed in Chapter 2, Scheme 2.12. page 22.

The yields of **193** and **194** are 86% and 27% respectively. A new method of synthesis was developed to increase the yield of **194**, which was then used in further synthesis of similar complexes. A variety of $[(C_5H_5)_2Ti(\beta\text{-diketonato})]^+ClO_4^-$ complexes (see Table 3.3) were synthesized according to the general procedure as shown in Scheme 3.8.

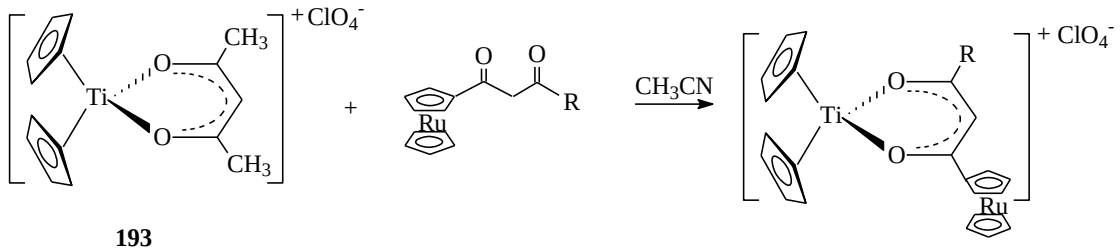

R = $C_{10}F_{21}$ (**177**), CF_3 (**152**), C_6F_5 (**178**), $C_{10}H_{21}$ (**179**), CH_3 (**147**), Rc (**155**) and Fc (**154**).

R = $C_{10}F_{21}$ (**195**), CF_3 (**196**), C_6F_5 (**197**), $C_{10}H_{21}$ (**198**), CH_3 (**194**), Rc (**199**) and Fc (**200**).

Scheme 3.8. Synthesis of the mono-β-diketonato titanocenyl complexes *via* 193.

Table 3.3. Charaterisation data of different mono-β-diketonato titanocenyl complexes of the type $[(C_5H_5)_2Ti(RcCOCHCOR)]^+ClO_4^-$. ^1H NMR data in $CDCl_3$.

R group	$(C_5H_5)_2$Ti- ^1H NMR position / ppm	methine ^1H NMR position / ppm	(C_5H_4)Ru- ^1H NMR position / ppm	(C_5H_4)Ru- ^1H NMR position / ppm	(C_5H_5)Ru- ^1H NMR position / ppm	% Yield	χ_R [a] / Gordy scale
195: $C_{10}F_{21}$		6.06				61%	3.04
196: CF_3	6.84	6.43	5.44	5.16	4.79	100%	3.01
197: C_6F_5	6.82	6.30	5.18	4.81	4.62	90%	2.46
198: $C_{10}H_{21}$	6.74	6.10	5.25	4.95	4.70	55%	2.43
194: CH_3	6.72	6.21	5.24	4.80	4.55	82%	2.34
199: Rc	6.70	6.24	5.18	4.94	4.66	63%	1.99
200: Fc	6.74	6.32	5.22	4.98	4.68	56%	1.87

a) χ_R (Gordy scale)[10, 11] apparent group electronegativity values.

The newly developed synthetic method for synthesis of $[(C_5H_5)_2Ti(RcCOCHCOR)]^+ClO_4^-$ complexes involves the substitution of the acetylacetonato ligand with the incoming ruthenocene-containing β-diketone. This substitution is able to occur because the group electronegativity of ruthenocene is lower than that of the methyl group and therefore the ruthenocene-containing β-diketone is in comparison a good nucleophile and acetyl acetonato is in comparison a good leaving group. Figure 3.4 (Left) shows the relationship of group electronegativity and yield under identical synthetic conditions. It can be seen that as the group electronegativity of the R-group increases the yield of the substitution product increases. Only R = $C_{10}H_{21}$ and $C_{10}F_{21}$ do not follow this pattern, and is propably due to the fact that the long chain raps around the molecule, or at least hamper access of these β-diketones to the Ti center of $[(C_5H_5)_2Ti(acac)]^+ClO_4^-$ making it sluggish to react.

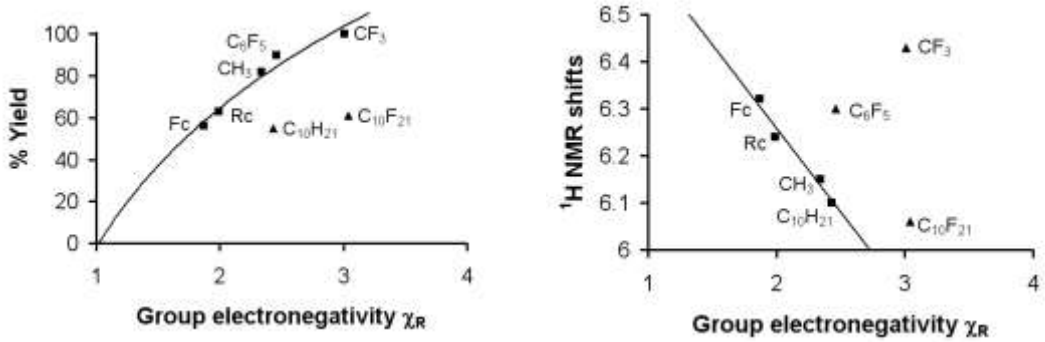

Figure 3.4. Left: Graph of group electronegativity *vs* yield of $[(C_5H_5)_2Ti(\beta\text{-diketonato})]^+ClO_4^-$ complexes. Right: Graph of group electronegativity *vs* ^1H NMR shift of the methine proton of $[(C_5H_5)_2Ti(\beta\text{-diketonato})]^+ClO_4^-$ complexes.

The ^{1}H NMR spectra of chloroform-*d* (acetone-d_6 as well) solutions of all the mono-β-diketonato titanocenyl complexes $[(C_5H_5)_2Ti(RcCOCHCOR)]^+ClO_4^-$ are simple and easily interpreted. All the spectra show three general signals: the titanium bonded cyclopentadienyl protons (counts for 10 protons) resonates at a low field (6.6-6.9 ppm) due to the cyclopentadienyl aromatic system; secondly the methine proton (counts for 1 proton) which resonates at a slightly higher field (6.0-6.5 ppm) but still in the aromatic region due to the pseudo aromatic system which is generated by the β-diketonato ligand coordinated to the Ti^{4+} cation; and thirdly the set of signals which belongs to the ruthenocenyl (C_5H_5 and 2 x C_5H_4) protons (4.5-5.2). The other signals that appear belonging to the R groups ($C_{10}F_{21}$, CF_3, C_6F_5, $C_{10}H_{21}$, CH_3, Rc and Fc) of the β-diketonato ligand $(RcCOCHCOR)^-$, varied in position in the different complexes. The change in the R group causes shifts in the position of the three first described sets of signals due to electronic communication through the C-C bonds *via* conjugation. Depending on the electron-donation or electron-withdrawing properties of the R group, the signals are moved either up or down field (Table 3.3).

From Figure 3.4 (Right), it can be seen that with increasing group electronegativity of the R group on the β-diketonato ligand there is a decrease in ^{1}H NMR peak position shift for the methine proton to a higher field. The methine signals are in the aromatic region. This is due to the pseudo-aromatic metallocyclic ring to which it is bonded. The complexes where the R group contains F ($C_{10}F_{21}$, CF_3, C_6F_5), does not fit in with this relationship. This could possibly be attributed to the fact that F can be involved in a type of back donation from the non-bonding electrons (similar back-donation from F has been observed in carbenium ions,[12] and aryl rings[13]), which could influence the ^{1}H NMR position of the methine proton.

3.2.4.3. Bis(cyclopentadienyl)di(ferrocenylalkoxy) titanium(IV)

The bis(cyclopentadienyl)di(ferrocenylalkoxy)titanium(IV) $[(C_5H_5)_2Ti(O(CH_2)_nFc)_2$, n = 1 (**201**), 2 (**202**), 3 (**203**), 4 (**204**)] (see Table 3.4, Section 3.2.4.4, p 91) were synthesised according to the general procedure as described by Fandos and co-workers (Scheme 3.9).[14] The synthesis involves the mixing of **89** with two equivalents of the base triethyl amine and two equivalents of the desired alcohol (**170-173**). After overnight stirring, the ammonium salt is separated (by filtration) to yield the crude product after solvent removal as brown crystals in low yields.

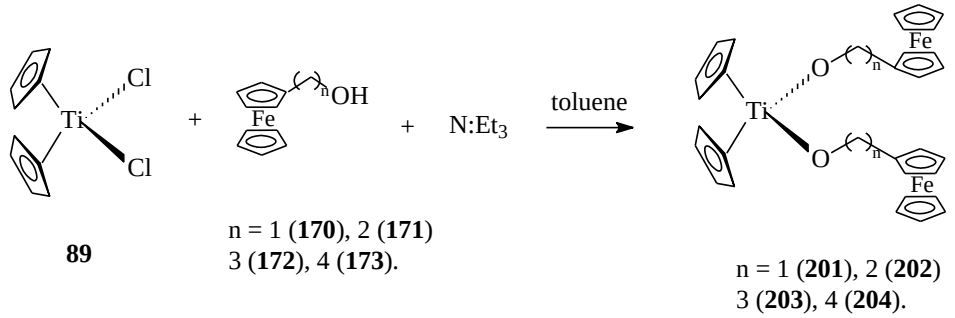

89

n = 1 (**170**), 2 (**171**)
3 (**172**), 4 (**173**).

n = 1 (**201**), 2 (**202**)
3 (**203**), 4 (**204**).

Scheme 3.9. Synthesis of the bis(cyclopentadienyl)di(ferrocenylalkoxy)titanium(IV) complexes.

The ^{1}H NMR spectra of chloroform-*d* solutions of all the bis(cyclopentadienyl)di(ferrocenylalkoxy)titanium(IV) complexes $[(C_5H_5)_2Ti(O(CH_2)_nFc)_2]$ are simple and easily interpreted. All the spectra show two general signals: the cyclopentadienyl protons of the titanocenyl moiety (counts for 10 protons), which resonates at a low field (~6.4 ppm) due to the high atomic electronegativity of Ti (χ_{Ti} = 1.32); secondly the cyclopentadienyl protons of the ferrocenyl moiety (counts for 9 protons) which resonates at a higher field (4.1-4.3 ppm) due to the influence of the Fe^{2+} (χ_{Fe2+} = 1.8)[15] metal 'sandwiched' between the two cyclopentadienyl rings. The other protons belong to the $(CH_2)_n$ protons. The amount of CH_2 signals depends on the amount of CH_2 spacers between the O-atom and the ferrocenyl moiety.

3.2.4.4. Cyclopentadienyltri(ferrocenylalkoxy)titanium(IV)

The series of cyclopentadienyltri(ferrocenylalkoxy)titanium(IV) $[(C_5H_5)Ti(O(CH_2)_nFc)_3$, n = 1 (**205**), 2 (**206**), 3 (**207**), 4 (**208**)] (see Table 3.4) was synthesised according to Scheme 3.10. The synthesis involves the mixing of **114** with three equivalents of the desired alcohol (**170-173**). After stirring overnight, with the evolution of HCl gas, the brown solid product was isolated by recrystallization.

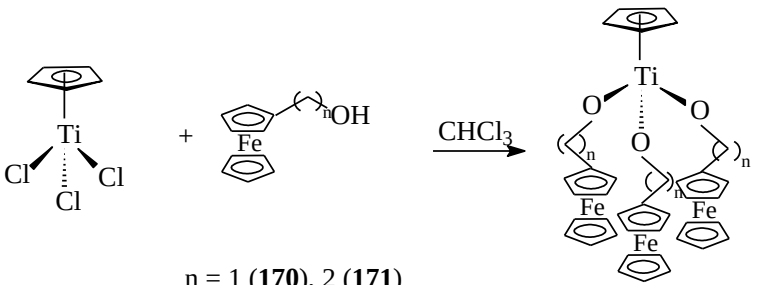

114

n = 1 (**170**), 2 (**171**)
3 (**172**), 4 (**173**).

n = 1 (**205**), 2 (**206**)
3 (**207**), 4 (**208**).

Scheme 3.10. Synthesis of the diferrocenylalkoxycyclopentadienyltitanium(IV) complexes.

Table 3.4. Synthetic yields of di(ferrocenylalkoxy)bis(cyclopentadienyl)titanium(IV) complexes of the type $[(C_5H_5)_2Ti(O(CH_2)_nFc)_2]$, cyclopentadienyltri(ferrocenylalkoxy)titanium(IV) complexes of the type $[(C_5H_5)Ti(O(CH_2)_nFc)_3]$ and tetra(ferrocenylalkoxy)titanium(IV) complexes of the type $[Ti(O(CH_2)_nFc)_4]$. Fc = ferrocenyl.

	$[(C_5H_5)_2Ti(O(CH_2)_nFc)_2]$				$[(C_5H_5)Ti(O(CH_2)_nFc)_3]$				$[Ti(O(CH_2)_nFc)_4]$			
n	201: 1	202: 2	203: 3	204: 4	205: 1	206: 2	207: 3	208: 4	209: 1	210: 2	211: 3	212: 4
% Yield	5	6	7	8	79	93	98	100	23	59	70	91

From Table 3.4 it can be seen that as the alkyl chain length of the ferrocenyl-containing alcohol group increases there is an increase in the yield of the product under identical synthetic condition. This may be because an increase in alkyl chain length increases the electron-donating property of the alcohol, which in turn makes the longer chain alcohols better nucleophiles.

The ^1H NMR spectra of chloroform-*d* solutions of all the cyclopentadienyltri(ferrocenylalkoxy)titanium(IV) complexes $[(C_5H_5)Ti(O(CH_2)_nFc)_3]$ are simple and easily interpreted. All the spectra show two general signals: the aromatic cyclopentadienyl protons of the cyclopentadienyl ring bound to titanium (counts for 5 protons) resonates at a low field (~6.65 ppm) due to the electron-withdrawing power of Ti^{4+} (χ_{Ti4+} exact value is not known but is published as "high")[16]; secondly the cyclopentadienyl protons of the ferrocenyl moiety (counts for 9 protons) which resonates at a higher field (4.0-4.5 ppm) (χ_{Fe2+} = 1.8). The other protons belong to the CH_2 protons. The amount of CH_2 signals depends on the amount of CH_2 spacers between the alkoxy moiety and the ferrocenyl moiety.

3.2.4.5. Tetra(ferrocenylalkoxide)titanium(IV)

The series of tetra(ferrocenylalkoxy)titanium(IV) $[Ti(O(CH_2)_nFc)_4$ with n = 1 (**209**), 2 (**210**), 3 (**211**), 4 (**212**)] (see Table 3.4, Section 3.2.4.4) was synthesised according to Scheme 3.11 The synthesis involves the mixing of **115** with four equivalents triethyl amine and four equivalents of the desired alcohol (**170-173**). After stirring overnight the ammonium salt is separated (by filtration) to yield the desired product after solvent removal and washing with hexane.

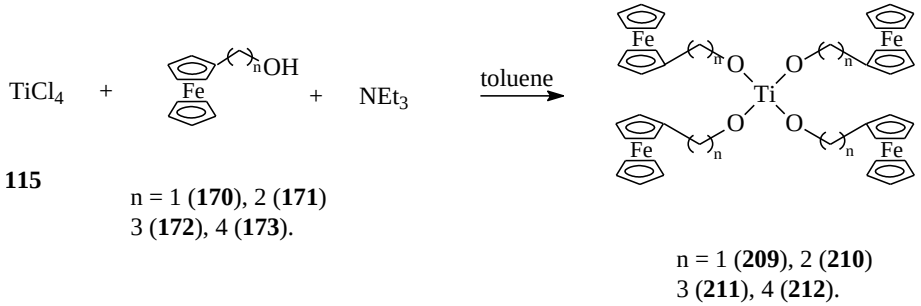

Scheme 3.11. Synthesis of the tetra(ferrocenylalkoxy)titanium(IV) complexes.

From Table 3.4 it can be seen that as the alkyl chain length of the ferrocenyl-containing alcohol group increases there is an increase in the yield of the product. As discussed for the synthesis of $[(C_5H_5)Ti(O(CH_2)_nFc)_3]$, this is because as the alkyl chain length increases, the electron-donating property of the alcohol increases, making it a better nucleophile.

The ^1H NMR spectra of chloroform-*d* solutions of all the tetra(ferrocenylalkoxy)titanium(IV) complexes $[Ti(O(CH_2)_nFc)_4]$ show the cyclopentadienyl protons of the ferrocenyl moiety (counts for 36 protons) which resonates at 4.0-4.4 ppm. The other protons belong to the methylene protons. The amount of methylene signals depends on the amount of CH_2 spacers between the oxygen moiety and the ferrocenyl group.

3.2.4.6. Dichlorobis(β-diketonato)titanium(IV) complexes

The series of dichlorobis(β-diketonato)titanium(IV) complexes $[TiCl_2(RcCOCHCOR)_2$, R = $C_{10}F_{21}$ (**213**), CF_3 (**214**), C_6F_5 (**215**), $C_{10}H_{21}$ (**216**), CH_3 (**217**), Rc (**218**) and Fe (**219**)] (see Table 3.5) was synthesised according to Scheme 3.12. The synthesis involves the mixing of **115** and the appropriate β-diketone, $RcCOCH_2COR$ short refluxing, partial solvent removal and product precipitation by addition of hexane.

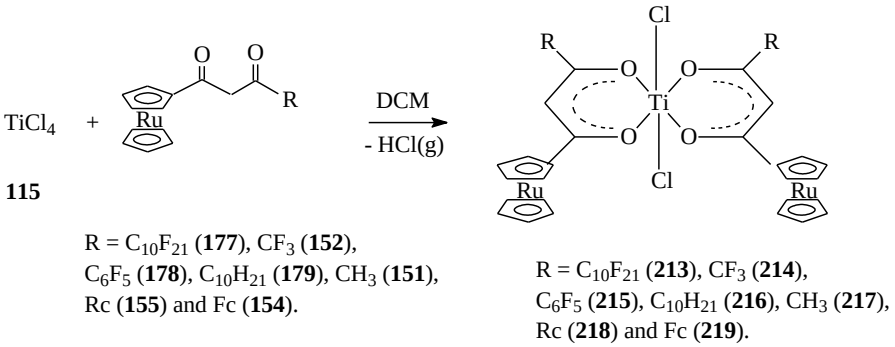

Scheme 3.12. Synthesis of the dichlorobis(β-diketonato)titanium(IV) complexes.

Table 3.5. Charaterisation data for the synthesis of the dichlorobis(β-diketonato)titanium(IV), $TiCl_2(RcCOCHCOR)_2$.

R group	χ_R	% Yield	Methine ^{1}H NMR position / ppm	(C_5H_4)Ru- ^{1}H NMR position / ppm	(C_5H_4)Ru- ^{1}H NMR position / ppm	(C_5H_5)Ru- ^{1}H NMR position / ppm
213: $C_{10}F_{21}$	3.04	62	6.06	5.21	4.94	4.63
214: CF_3	3.01	78	6.16	4.85-5.55		4.4-4.8
215: C_6F_5	2.46	99	6.27	5.25	5.02	4.75
216: $C_{10}H_{21}$	2.43	39	6.01	5.18	4.93	4.68
217: CH_3	2.34	99	6.05	5.21	4.91	4.71
218: Rc	1.99	30	6.17	5.17	4.83	4.62
219: Fc	1.87	54	6.20	4.2-5.5		

The products were obtained in yields varying from 30 to 99%. No meaningful relationship could be found between yield obtained and group electronegativity of the R-group on the β-diketone.

The ^{1}H NMR spectra of chloroform-*d* (acetone-d_6 as well) solutions of all the dichlorobis(β-diketonato)titanium(IV) complexes $TiCl_2(RcCOCHCOR)_2$ are not as simple and easy to interpret as the other titanium complexes (Figure 3.5, top, spectra of **219** shown as an example). The signals for the Rc and Fc group cannot individually be assigned at all, although four broadened peaks could be identified. At best, one can observe that the multiplet at 4.1-5.5 ppm counts the correct number of protons for the four metallocenyl groups, namely 36. The broad ferrocene- and ruthenocene- based multiplet can be accounted for by noting that at least four different possible isomers of the complex **219** (Figure 3.5, bottom) exist in the crude reaction mixture. It was not possible to separate these isomers. This causes different interactions (shielding effects) through space. However, the mixed multiplet signal is integrated for the correct amount of protons that **219** require.

All the spectra of $TiCl_2(RcCOCHCOR)_2$ show two general signals: the methine protons (counts for 2 protons) which resonates at a low field (6.0-6.3 ppm) but still in the aromatic region due to the pseudo aromatic system which is generated by the β-diketonato ligand coordinated to the Ti metal; and secondly the set of signals which belongs to the ruthenocenyl (C_5H_5 and 2 x C_5H_4) protons (4.5-5.2). The other signals that appear belong to the R groups ($C_{10}F_{21}$, CF_3, C_6F_5, $C_{10}H_{21}$, CH_3, Rc and Fc) of the β-diketonato ligand $(RcCOCHCOR)^-$, varied in position in the different complexes. The change in the R group causes shifts in the position of the two first described sets of signals due to electronic communication through the C-C bonds *via*

conjugation. Depending on the electron-donation or electron-withdrawing properties of the R group, the signals are moved either up or down field (Table 3.5).

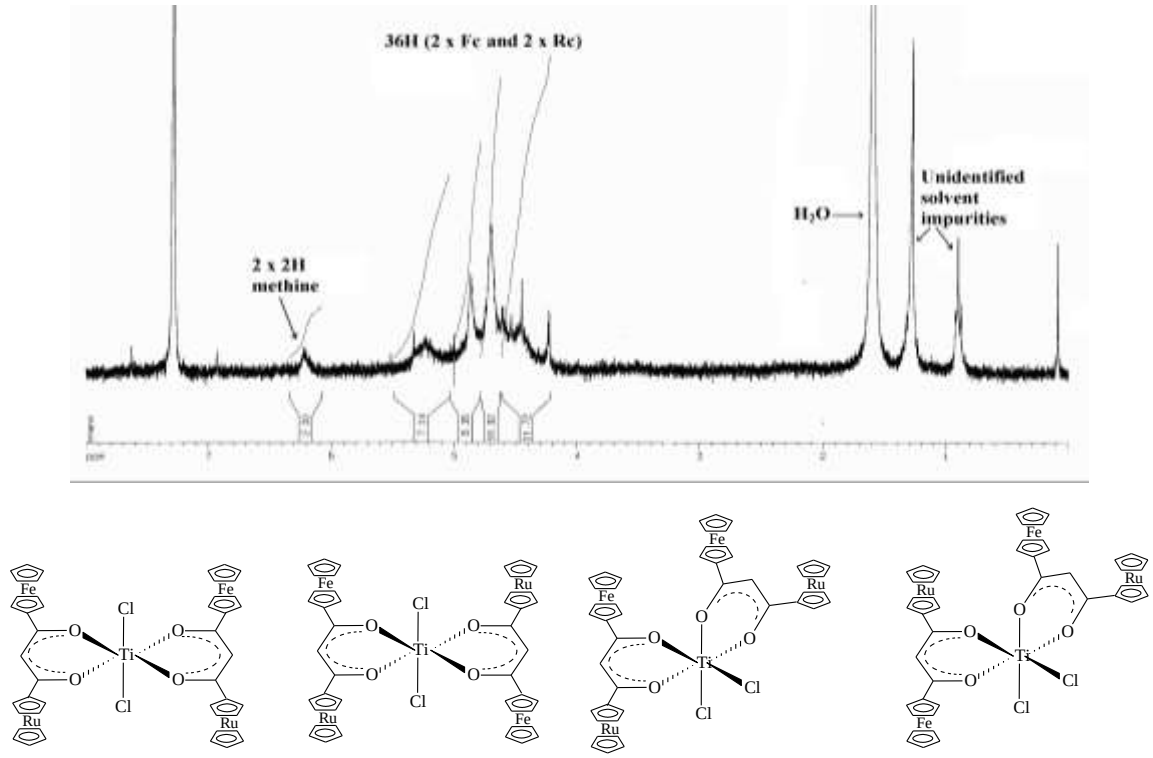

Figure 3.5. Top: ^{1}H NMR of **219** in chloroform-*d*. Bottom: Four possible isomers of **219**. Many other isomers may also exist, including isomers where the direction of ferrocenyl and ruthenocenyl protruding is reversed (i.e. up or down).

From Figure 3.6 it can be seen that with increasing group electronegativity of the R group on the β-diketonato ligand there is a shift in ^{1}H NMR methine proton position to a higher field. Complexes where the R group contains F ($C_{10}F_{21}$, CF_3, C_6F_5), does not fit in with this relationship. This could possibly be attributed to the fact that F can be involved in a type of back-donation from the non-bonding electrons (similar back-donation from F has been observed in carbenium ions,[12] and aryl rings[13]).

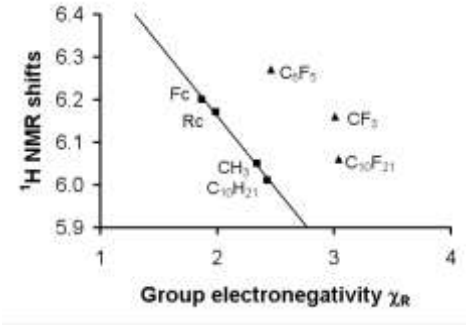

Figure 3.6. Graph of group electronegativity *vs* ^{1}H NMR shift of the methine proton of $TiCl_2(RcCOCHCOR)_2$ complexes.

3.2.4.7. Di(ferrocenylalkoxy)bis(β-diketonato)titanium(IV)

A series of di(ferrocenylalkoxy)bis(β-diketonato)titanium(IV) complexes $[Ti(O(CH_2)_nFc)_2(RcCOCHCOR)_2$ with n = 1 (**220**), 2 (**221**), 3 (**222**), 4 (**223**), R = CH_3 and n = 4, R = $C_{10}F_{21}$ (**224**), CF_3 (**225**), C_6F_5 (**226**), $C_{10}H_{21}$ (**227**), CH_3 (**223**), Rc (**228**) and Fc (**229**)] (see Table 3.6) were synthesised. The synthesis of $Ti(O(CH_3)_nFc)_2(RcCOCHCOR)_2$ can be achieved *via* two different routes and is illustrated in Scheme 3.13.

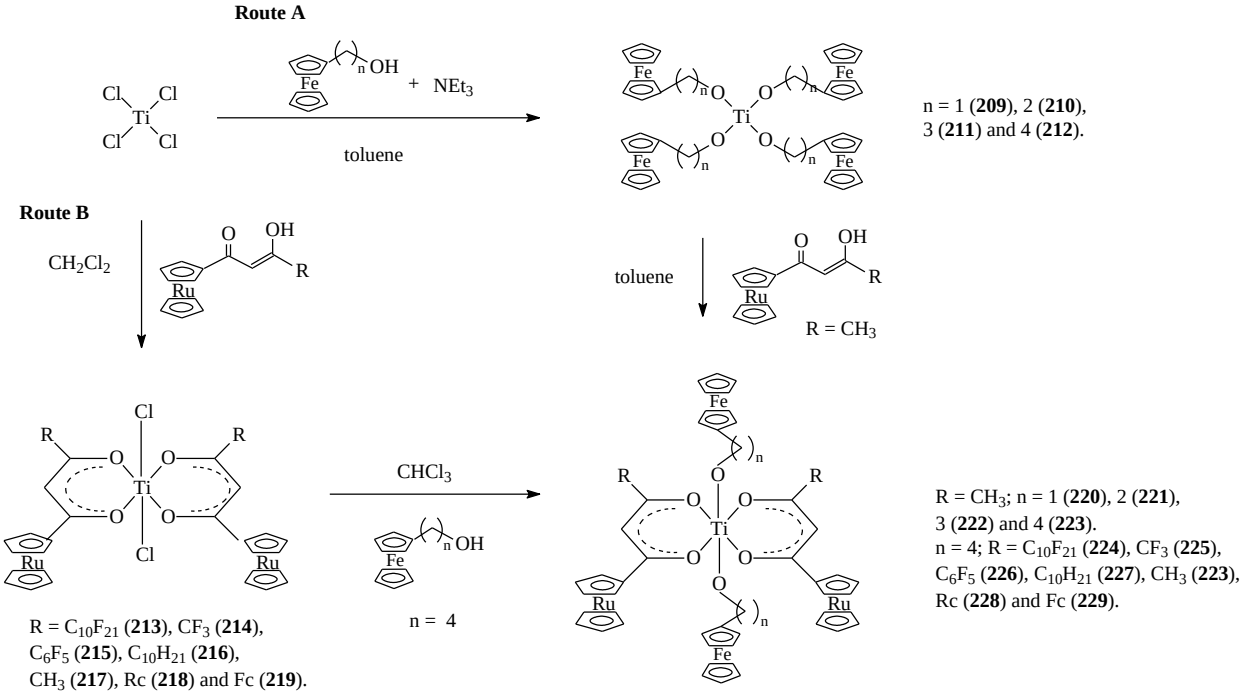

Scheme 3.13. Synthesis of the di(ferrocenylalkoxy)bis(β-diketonato)titanium(IV) complexes.

Table 3.6. Yields obtained for the synthesis of the di(ferrocenylalkoxy)bis(1-ruthenocenyl-3-methylprop-1,3-dionato)titanium(IV), $Ti(O(CH_2)_nFc)_2(RcCOCHCOCH_3)_2$ for different values of n (see Scheme 3.13) and di(4-ferrocenylbutoxy)bis(β-diketonato)titanium(IV), $Ti(O(CH_2)_4Fc)_2(RcCOCHCOR)_2$ for different R-groups (see Scheme 3.13)

n, R = CH_3	% Yield		R, n = 4	χ_R	% Yield
			224: $C_{10}F_{21}$	3.04	75
	Route A	Route B	225: CF_3	3.01	91
			226: C_6F_5	2.46	58
220: 1	24	8	227: $C_{10}H_{21}$	2.43	62
221: 2	27	12	223: CH_3	2.34	43
222: 3	29	27	228: Rc	1.99	37
223: 4	31	43	229: Fc	1.87	43

As can be seen from the data in Table 3.6, there is no direct relationship between the group electronegativity of the R-group on the β-diketonato and the yield obtained. However, the general trend that is observed in Figure 3.7 shows that as the group electronegativity increases the yield also increases. This can be explained by the fact that as χ_R increases, the titanium centre becomes more positive. This makes the chlorocomplexes better electrophiles and the titanium center more susceptible for nucleophilic attack by the ferrocene-containing alcohol.

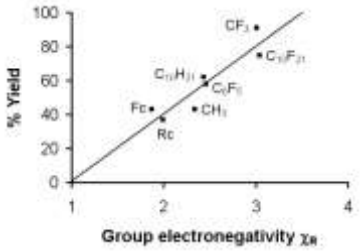

Figure 3.7. Graph of group electronegativity *vs* % Yield of the $Ti(O(CH_2)_4Fc)_2(RcCOCHCOR)_2$ complexes.

The ^{1}H NMR spectra of chloroform-*d* (acetone-d_6 as well) solutions of all the di(ferrocenylalkoxy)bis(β-diketonato)titanium(IV) complexes $Ti(O(CH_2)_nFc)_2(RcCOCHCOR)_2$ are rather difficult to interpret (Figure 3.8 gives the spectrum of **229** by way of example). The signals for the Rc and Fc group of the β-diketonato ligand cannot be resolved at all. At best, one can observe a broad multiplet at 4.2 -5.6 ppm that integrates for the correct number of protons, namely 36. The ferrocene- and ruthenocene- based multiplet as well as the multiplets observed for the other protons could be attributed to different possible isomers of the complexes similar to that shown for **219** in Figure 3.5 (p 94). This causes different through space interactions.

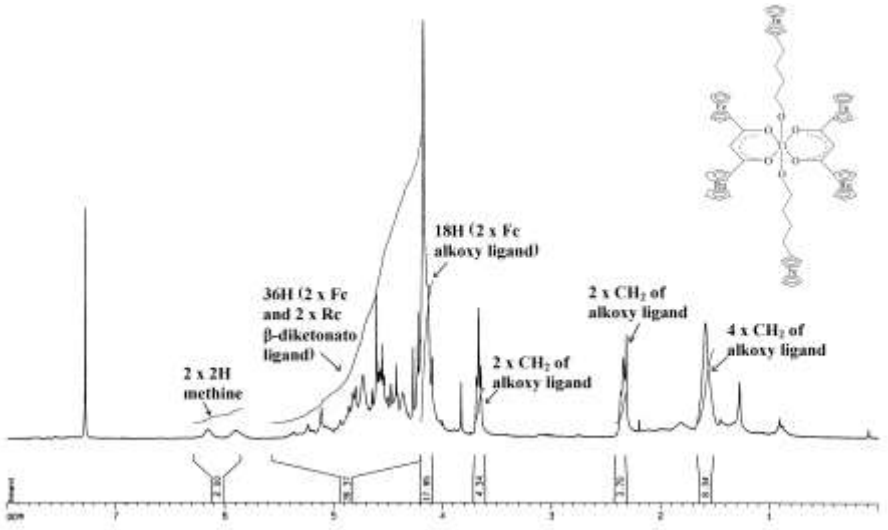

Figure 3.8. ^{1}H NMR of **229** in *d*-chloroform. Insert: One of the isomeric structures of **229**. Other isomers of **229** can also be shown as per Figure 3.5.

3.2.4.8. Chloro(cyclopentadienyl)bis(1-ruthenocenoylbutane-1,3-dionato) titanium(IV) and Cyclopentadienyl(ferrocenylbutoxy)bis(1-ruthenocenoylbutane-1,3-dionato)titanium(IV)

Chloro(cyclopentadienyl)bis(1-ruthenocenoylbutane-1,3-dionato)titanium(IV) (**230**), 26% yield and cyclopentadienyl(ferrocenylbutoxy)bis(1-ruthenocenoylbutane-1,3-dionato)titanium(IV) (**231**), 62% yield were synthesised as examples of ruthenocene-containing β-diketonato titanium(IV) complexes with a titanium coordination sphere of six having one cyclopentadienyl ligand coordinated to the Ti center. These complexes were made from titanocene (**89**) by elimination of one cyclopentadienyl ring. The synthesis of **230** and **231** are shown in Scheme 3.14.

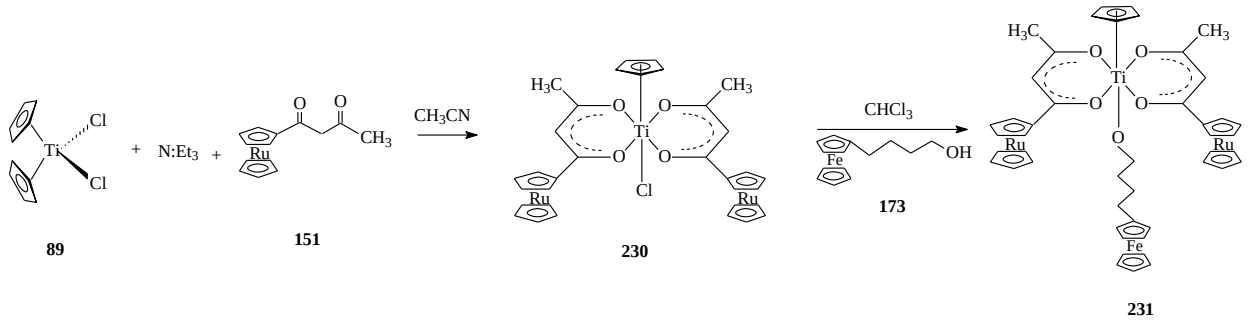

Scheme 3.14. Synthesis of Chloro(cyclopentadienyl)bis(1-ruthenocenoylbutane-1,3-dionato)titanium(IV) (**230**) and cyclopentadienyl(ferrocenylbutoxy)bis(1-ruthenocenoylbutane-1,3-dionato)titanium(IV) (**231**).

As was the case with the complexes in section 3.2.4.6 and 3.2.4.7, the ^{1}H NMR of **230** and **231** in *d*-chloroform are complicated and rather difficult to interpret. This is again due to the many different possible isomers that can be found for these complexes.

3.3. Group electronegativity (χ_R)

The group electronegativity of C_6F_5, $C_{10}H_{21}$ and $C_{10}F_{21}$ was obtained by inserting the value of the carbonyl stretching frequency for the methyl esters RCOOMe with R = C_6F_5, $C_{10}H_{21}$ and $C_{10}F_{21}$, into the linear plot of other known carbonyl stretching frequencies of RCOOMe esters *vs* previously determined Gordy scale group electronegativities (χ_R). The data used is tabulated in Table 3.7 and the plot (with the inserted values of C_6F_5, $C_{10}H_{21}$ and $C_{10}F_{21}$) is shown in Figure 3.9.

Table 3.7. IR carbonyl stretching frequencies of the methyl esters RCOOMe and Gordy group electronegativities (χ_R) of different R groups.

R	ν (C=O) / cm^{-1}	χ_R	R	ν (C=O) / cm^{-1}	χ_R
$C_{10}F_{21}$ this study	1786	3.04	CH_3	1736	2.34
CF_3[10]	1785	3.01	C_6H_5[11]	1725	2.21
Cl[10]	1780	2.97	H[10]	1717	2.13
CCl_3[10]	1768	2.76	Rc[17]	1708	1.99
C_6F_5 this study	1744	2.46	Fc[11]	1700	1.87
$C_{10}H_{21}$ this study	1741	2.43			

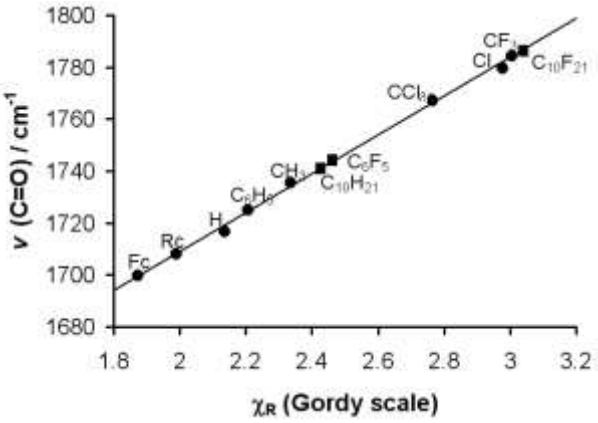

Figure 3.9. Calibration curve of known carbonyl stretching frequencies (●) *vs* Gordy scale group electronegativities (χ_R) for esters of the type $RCOOCH_3$. Unknown vales are ■ and was read off.

From Figure 3.9 the χ_R values of C_6F_5, $C_{10}H_{21}$ and $C_{10}F_{21}$ groups were read off and found to be χ_{C6F5} = 2.46, χ_{C10H21} = 2.43 and χ_{C10F21} = 3.04 respectively on the Gordy scale.

3.4. pK_a' Determinations

Apparent pK_a' of new β-diketones were determined, results apply to the equation shown in Scheme 3.15.

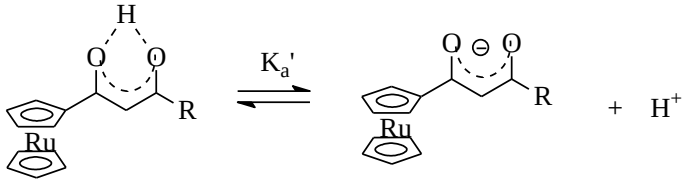

Scheme 3.15. The reaction that takes place in the determination of pK_a' showing the acid and conjugated basic form of the β-diketone.

The term "apparent" pK_a with symbol pK_a' is utilised because no effort was made to separate pK_a values for the keto- and enol isomer of each β-diketone.

Results are summerised in Table 3.8. Listed pK_a'-values were obtained from a least squares fit of the UV/Vis absorbance/pH data to Equation 3.1.[18] The wavelength at which each pK_a' was determined was decided upon by determining the biggest (or convenient) absorbtion difference of the deprotonated β-diketone and neutral β-diketone species in overlay spectra. The spectra of $RcCOCH_2COR$ and $[RcCOCHCOR]^-$ is shown in Figure 3.10.

$$A_T = \frac{A_{HA}10^{-pH} + A_A10^{-pKa'}}{10^{-pH} + 10^{-pKa'}}$$

Equation 3.1.

In equation 3.1, A_T = total absorption, A_{HA} = absorption of the free β-diketone and A_A = absorption of the deprotonated (basic) β-diketone.

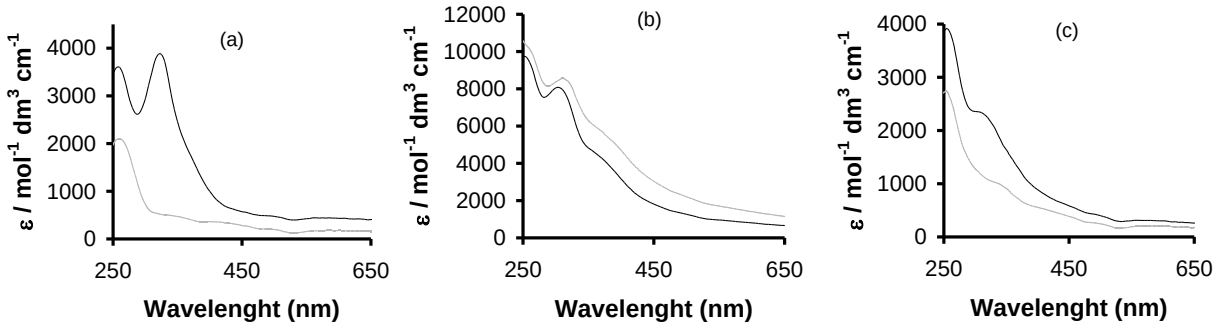

Figure 3.10. The electronic spectra of $RcCOCH_2COR$ (---) and $[RcCOCHCOR]^-$ (—) for R = C_6F_5 **177** (a), R = $C_{10}H_{21}$ **178** (b) and R = $C_{10}F_{21}$ **179** (c) in 10% CH_3CN/90% H_2O.

Table 3.8. pK_a' values (determined at λ_{exp}) and molar extinction coeffients ε (at λ_{max}) of $RcCOCH_2COCR$, R = C_6F_5, $C_{10}H_{21}$ and $C_{10}F_{21}$, in a 10% CH_3CN/90% H_2O mixture at 25˚C.

R	pK_a'	λ_{exp} / nm	ε / dm^3 mol^{-1} cm^{-1}	β-diketone λ_{max}	β-diketonato λ_{max}
C_6F_5	9.92(3)	320	2078	260	320
$C_{10}H_{21}$	10.06(2)	312	9809	250	250
$C_{10}F_{21}$	7.14(4)	307	3915	255	255
Fc	12.71[a]	-	-	-	-
Rc	12.14[a]	-	-	-	-

a) These pK_a' were determined by inserting their group electronegativity in the graph of χ_R *vs* pK_a' (Figure 3.11) and reading off the value.

All pK_a' values were determined in solvent mixtures containing 10% acetonitrile, 90% water with ionic strength maintained at 0.100 mol dm^{-3} [$NaClO_4$] with β-diketone concentration 0.2 mmol dm^{-3} at 25˚C. A 10% acetonitrile solvent system was used since the β-diketones are insoluble in pure water. Figure 3.11 (Left) shows the absorbance/pH profiles used for the pK_a' determinations of $RcCOCH_2COR$ (R = C_6F_5, $C_{10}H_{21}$ and $C_{10}F_{21}$). From Figure 3.11 (Right), it can be seen that as the group electronegativity of the R groups of the β-diketones increases, the pK_a' decreases. The pK_a' of $RcCOCH_2COR$ with R = Fc and Rc (previously unknown) was determined by inserting the electronegativity values in to Figure 3.11 and values are given in Table 3.8.

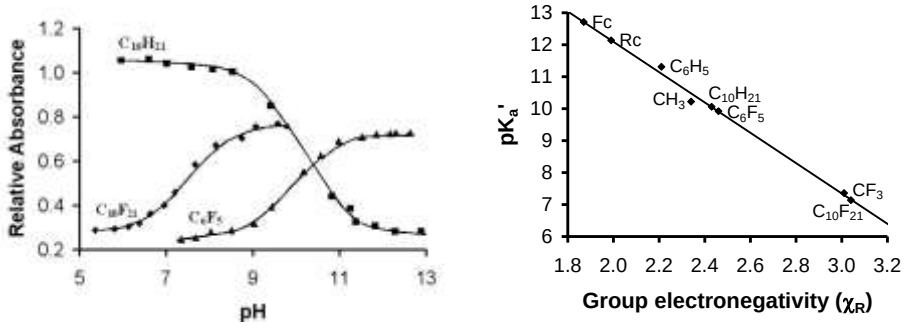

Figure 3.11. Left: Absorbance/pH profiles used for the pK_a' determinations of $RcCOCH_2COR$ (R = C_6F_5, $C_{10}H_{21}$ and $C_{10}F_{21}$) in 10% acetonitrile/90% water with ionic strength 0.100 mol dm^{-3} [$NaClO_4$] and β-diketone concentration 0.2 mmol dm^{-3} at 25˚C. Right: Graph of χ_R *vs* pK_a'.

3.5. Reaction Kinetics

3.5.1. Isomerisation kinetics between the keto- and enol-tautomers of β-diketones

It is found that directly after isolation of fluorine-containing β-diketones from an acidic aqueous solution, the enol form is present as the dominant tautomer. Other β-diketones, such as ruthenocenoylacetone, is enriched in the keto form. If the material is left in the solid state, it converts over weeks 100% to the enol form. When such a sample is dissolved in a suitable solvent, during a slow kinetic process, some of the enol isomer is converted to the keto isomer to eventually reach a solution equilibrium position.

The isomerisation kinetics between the keto- and enol-isomers of the β-diketone was followed by ^1H NMR in CD_3CN as solvent at 20˚C. The equilibrium studied is shown in Scheme 3.16. The ^1H NMR of the first spectra obtained 120 s after dissolving an aged solid sample and the equilibrium spectra are shown in Figure 3.12.

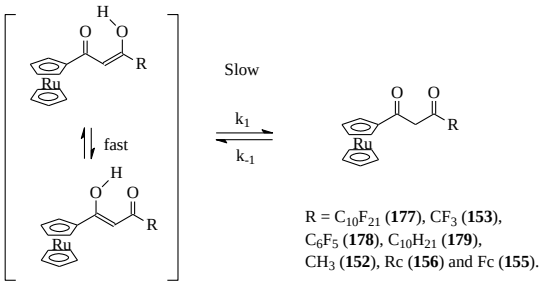

Scheme 3.16. The equilibrium between the keto- and enol-isomers of the ruthenocene-containing β-diketones that was studied. k_1 = rate constant for the forward reaction, k_{-1} = rate constant for the reverse reaction, $K_c = k_1/k_{-1}$ = equilibrium constant.

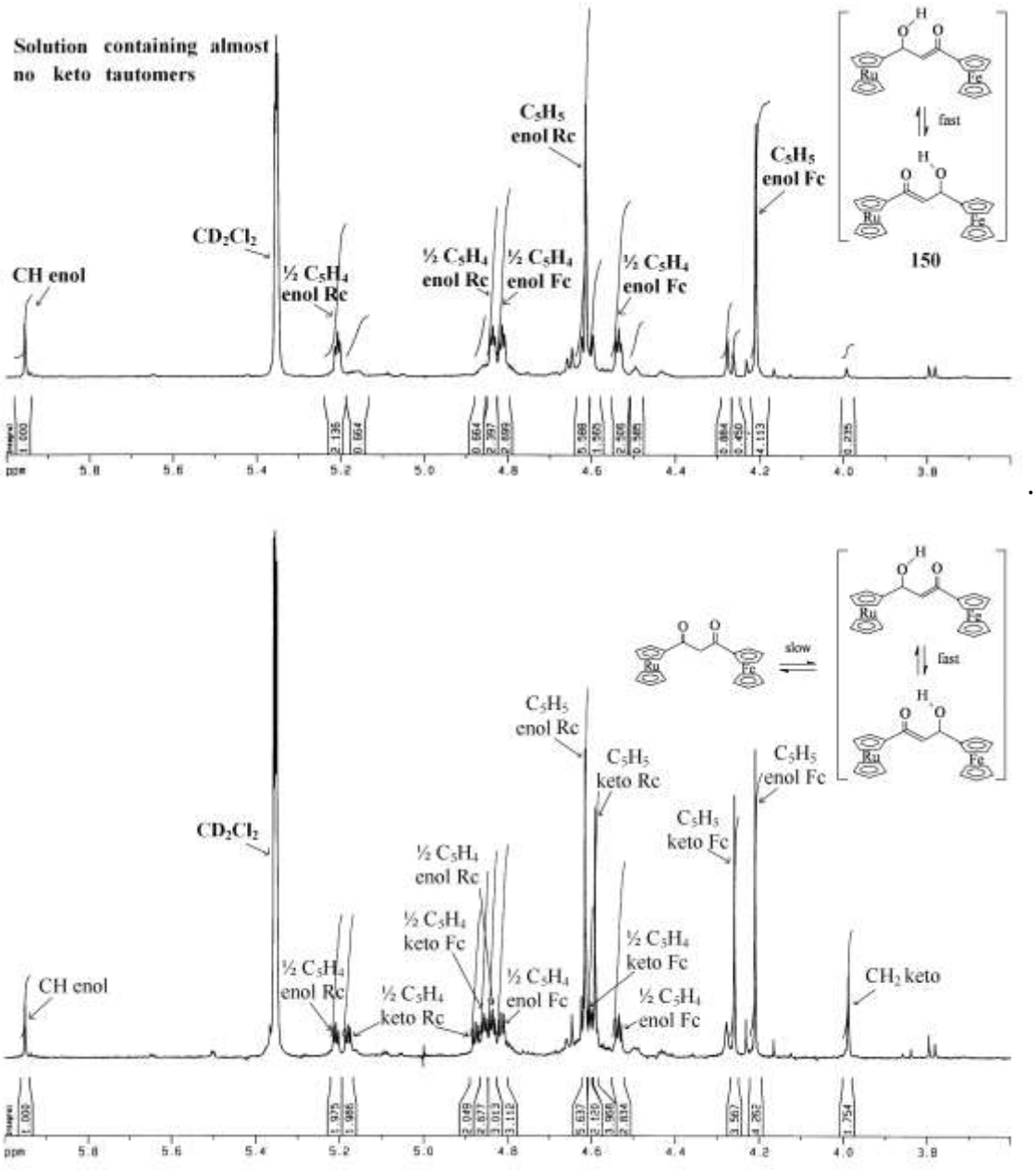

Figure 3.12. The ^{1}H NMR spectra of **154** in CD_2Cl_2 at 20˚C, 120 s after dissolving an aged sample in CD_2Cl_2 (Top) and at equilibrium (after 3 days) (Bottom).

In principle two enol isomers can exist in equilibrium. However, in practice only one set of enol tautomer signals is observed on the NMR. This implies that either the conversion from one enol tautomer to the other is fast on the NMR time scale, or that only one tautomer exist. Either way, upon interpreting NMR spectra of the enol tautomers, the measured integral values of the enol tautomers would be indicative of the total enol tautomers content in solution. This implies K_c could be determined conveniently by utilising integral values for suitable ^{1}H NMR signals (Equation 3.2).

$$K_c = \frac{\text{(integral value of } ^1\text{H NMR signal of a suitable keto molecular fragment)}}{\text{(integral value of } ^1\text{H NMR signal of a suitable enol molecular fragment)}}$$

Equation 3.2.

For example, the C_5H_5 signal integrals of the ferrocenyl group at 4.27 (keto) and 4.21 (enol) ppm could be use to obtained a K_c = (3.567)/(4.262) = 0.837. However, for evaluating kinetic data it was more convenient to use isomer percentages in determing rate constants (Equation 3.3).

$$K_c = (\%\text{ keto isomer})/(\%\text{ enol isomer}) = k_1/k_{-1}$$

Equation 3.3.

The percentage keto-isomer at any given time during the course of the conversion between the keto- and enol isomers can be calculated using Equation 3.4.

$$\%\text{ keto isomer} = [(\text{I of keto signal})*100]/[(\text{I of keto signal}) + (\text{I of enol signal})]$$

Equation 3.4.

I = integral value of the NMR signal. For example, using the C_5H_5 signals of the ferrocenyl group of $RcCOCH_2COFc$, **154**, the equilibrium % keto isomer = [3.567*100]/[4.262+3.567] = 45.6%. Thus using Equation 3.3 K_c = (45.6%)/(54.4%) = 0.838, which is for all practical purposes the same as the 0.837 found using Equation 3.2. From the calculated % keto isomer values, time traces showing the conversion rate from enol to keto tautomers can be constructed (see Figure 3.13 for **154**). From this graph the first order rate constant, k_{obs}, can be determined by application of Equation 3.5.[19] The observed rate constant, k_{obs}, is actually $k_{obs} = k_1 + k_{-1}$ rate constants for the forward and reverse steps shown in Scheme 3.16, i.e. $k_{obs} = k_1 + k_{-1}$.[19]

$$\ln\left[\frac{C_0 - C_\infty}{C_t - C_\infty}\right] = k_{obs}t \text{ with } k_{obs} = k_1 + k_{-1}$$

Equation 3.5.

C_0 = initial concentration expressed as % initial keto %, C_t = concentration at time (t) expressed as % keto content at time t.

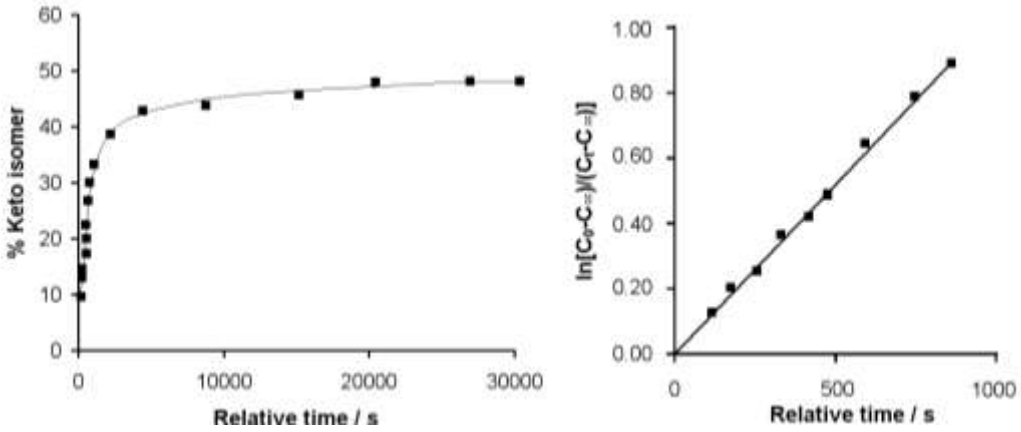

Figure 3.13. Time trace showing the conversion from enol- to keto tautomer for RcCOCHC(OH)Fc **154** at 20˚C in CD_2Cl_2. Insert: a kinetic plot of data for this process that leads to the observed first order rate constant $k_{obs} = k_1 + k_{-1}$.

By simultaneously solving equations $k_{obs} = k_1 + k_{-1}$ (Equation 3.5) and $K_c = k_1/k_{-1}$ (Equation 3.3), rate constants k_1 and k_{-1} can be separated. The kinetic data obtained for the β-diketones in the solvents, CD_3CN, $CDCl_3$ and CD_2Cl_2 is summarised in Table 3.9-3.10.

Table 3.9. Equilibrium constants, K_c, for the keto-enol equilibrium of $RcCOCH_2COR$ in CD_3CN at 20˚C. The first order rate constants, k_{obs}, k_1 for the keto to enol half reaction and k_{-1} for the enol to keto half reaction are also listed.

R-group	χ_R	$10^5\ k_{obs}$ / s^{-1}	$10^6\ k_1$ / s^{-1}	$10^5\ k_{-1}$ / s^{-1}	% enol at equilibrium	K_c in CD_3CN	ΔG^a / kJ mol^{-1}
177:$C_{10}F_{21}$	3.04	4.2(4)	4.23	3.78	89.9	0.112	5.42
153:CF_3	3.01	4.6(1)	2.93	4.31	93.6	0.068	6.66
178:C_6F_5	2.46	-[b]	-[b]	-[b]	>95[b]	<0.053[b]	>7.16[b]
179:$C_{10}H_{21}$	2.43	3.77(1)	5.77	3.19	84.7	0.181	4.23
152:CH_3	2.34	7.71(1)	39.9	3.72	48.3	1.070	-0.18
155:Rc	1.99	15.0(6)	86.2	6.38	42.6	1.351	-0.75
154:Fc	1.87	9.10(2)	38.7	5.23	57.5	0.739	0.11
154:Fc[c]	1.87	147(4)[c]	733.1[c]	73.6[c]	50.1[c]	0.996[c]	0.01[c]
Fc+elec[d]	1.87	128(3)[d]	637.9[d]	64.3[d]	50.2[d]	0.992[d]	0.02[d]

a) ΔG = Gibbs free energy applicable to Scheme 3.16.

b) % keto content at equilibrium to low for meaningful measurements.

c) In CD_2Cl_2 this ^1H NMR results is discussed in section 3.6.4. (p 145)

d) In CD_2Cl_2/$[NBu_4][B(C_6F_5)_4]$ ($[NBu_4][B(C_6F_5)_4]$ = 5[**154**] = 8.75 x 10^{-2} M), this ^1H NMR results is discussed discussed in section 3.6.4. (p 145)

Table 3.10. Equilibrium constants K_c for the keto-enol equilibrium of $RcCOCH_2COR$ in $CDCl_3$ at 25˚C. The first order rate constant, $k_{obs,}$ for the keto to enol half reaction and k_{-1} for the enol to keto half reaction are also listed.

R-group	χ_R	$10^5\ k_{obs}$ / s^{-1}	$10^5\ k_1$ / s^{-1}	$10^5\ k_{-1}$ / s^{-1}	% enol at equilibrium	K_c in $CDCl_3$	ΔG^a / kJ mol^{-1}
177:$C_{10}F_{21}$	3.04	26.06(3)	2.24	23.82	91.4	0.094	5.76
178:C_6F_5	2.46	23.13(2)	9.26	13.88	92.6	0.667	0.99
179:$C_{10}H_{21}$	2.43	1.39(5)	0.25	1.14	82.1	0.217	3.72

a) ΔG = Gibbs free energy applicable to Scheme 3.16.

The Gibbs free energy for the keto-enol isomerisation process can be obtained by utilising Equation 3.6.

$$\Delta G = -RT\ln K_c$$

Equation 3.6.

Relating to Tables 3.9 and 3.10 it is strikingly evident that ΔG becomes larger positive for the equilibrium $RcCOCHC(OH)R \rightleftharpoons RcCOCH_2COR$ as the group electronegativity, χ_R, becomes larger. This implies that thermodynamically, in solution,the enol isomer is the most stable species for electron-withdrawing R-groups such as CF_3. In contrast,electron-donating R-groups such as Fc or Rc stabilize the keto form in solution, as demonstrated by the negative ΔG values.

A detailed solvent study was not preformed. However, it was found that an increase in polarity and dielectric constant favours the enol form of $RcCOCH_2COR$ in Table 3.9 and Table 2.4 (p 46) for the solvent $CDCl_3$ (dielectric constant = 4.8), CD_2Cl_2 (dielectric constant = 8.9) and CD_3CN (dielectric constant = 37.5). Addition of a non-coordinating electrolyte such as tetrabutylammonium tetrakis(pentafluorophenyl)borate had virtually no influence on the equilibrium position of $RcCOCH_2COFc$ (Table 3.9).

The accuracy of ^1H NMR measurements prohibited accurate K_c measurements for R = C_6F_5 in CD_3CN in Table 3.9.

The general trend observed for the β-diketone in CD_3CN in Table 3.9 and $CDCl_3$ in Table 3.10, is that K_c increases as the group electronegativity decreases, i.e. that at equilibrium more of the keto tautomer is present. In both cases three exceptions were observed: $C_{10}F_{21}$, $C_{10}H_{21}$ and Fc. The fact that **177** and **179** does not follow the general trend can be explained by the long chain substituents, which could influence the equilibrium position. For **154**, no explanation can be given at this stage. In terms of how fast the equilibrium sets in, k_{obs} values in Tables 3.9 and 3.10 indicate that in CD_3CN (dielectric constant = 37.5) isomerisation rate is almost independent of R-group χ_R values. In CD_2Cl_2 (dielectric constant = 8.9), the forward and back reaction with

respect to $RcCOCH_2COFc$, **154**, becomes both faster, although the halflife of the overall process ($t_{½} = \ln 2/k_{obs}$) becomes longer.

3.5.2. Ligand exchange

3.5.2.1. Exchange of ferrocene-containing alkoxides in titanium(β-diketonato)$_2$(alkoxide)$_2$ complexes

Ligand exchange reactions of the mono-chelating ferrocene-containing alkoxy groups between **220** and **223** were studied spectroscopically by ^{1}H NMR and UV/Vis (see Scheme 3.17 for reactions) under second order conditions.

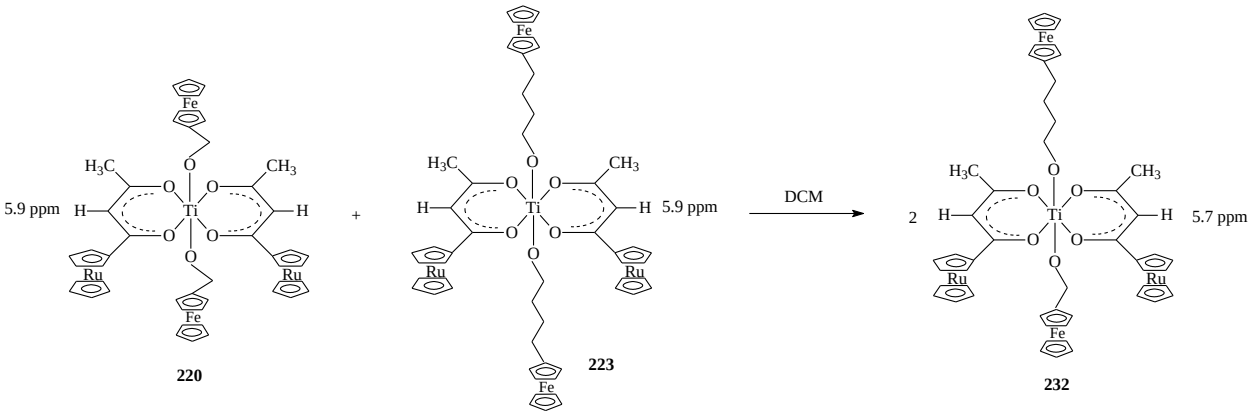

Scheme 3.17. Schematic representation of the ligand exchange reactions between **220** and **223**.

The reaction was made up as solutions containing equimolar amounts of **220** and **223** (i.e. [**220**] = [**223**]) in CD_2Cl_2 and the ^{1}H NMR was recorded at regular time intervals. It was found that the reaction between **220** and **223** yielding **232** went to completion. It is important to note that **220** and **223** have many different isomers similar to that shown in Figure 3.5 (p 94). The partial ^{1}H NMR spectra (of the methine region around 6 ppm) obtained 120 s after dissolving **220** and **223** in CD_2Cl_2 and at t = ∞ (about 3 days) are shown in Figure 3.14.

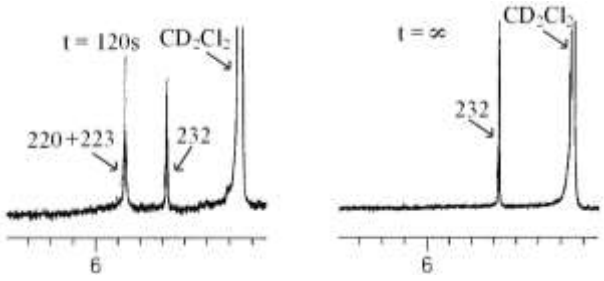

Figure 3.14. ^{1}H NMR of the ligand exchange reactions in CD_2Cl_2 at t = 120s and t = ∞ of **220** and **223**. [**220**] = [**223**] = 1.75 x 10^{-4} mol dm^{-3}.

The reaction between **220** and **223** with equal concentrations, is a second order reaction and therefore Equation 3.7 holds. To follow the reaction by ^{1}H NMR with time, the disappearance of the methine peaks at 5.9 ppm and the appearance of the peak at 5.7 ppm were monitored with time. Since the initial reactions concentrations and the final product concentration is known, the integral values of these peaks could be transformed to concentrations. A typical time trace of the results is shown in Figure 3.15. Kinetic data obtained by ^{1}H NMR are presented in Table 3.11.

$$\frac{1}{C_t} - \frac{1}{C_0} = k_2 t$$

Equation 3.7.

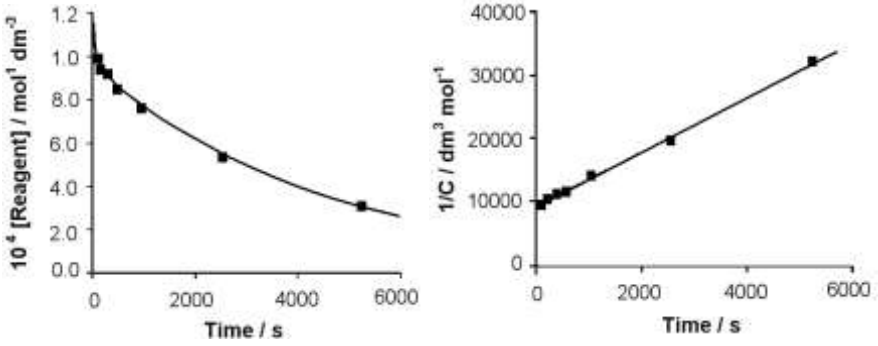

Figure 3.15. Graphs of the ligand exchange reaction between **220** and **223** in CD_2Cl_2 at 20˚C.

Table 3.11. Data for the ligand exchange reaction between **220** and **223** in CD_2Cl_2 at 20˚C (according to Scheme 3.17) monitored by ^{1}H NMR and UV/Vis spectroscopy. [Reagent] = [**220**] = [**223**]

NMR	10^4 [Reagent] / mol dm^{-3}		T / K	k_2 / dm^3 mol^{-1} s^{-1}		First $t_{½}$ / s
	1.75		293	4.14(3)		1380
UV/Vis	T / K	k_2 / dm^3 mol^{-1} s^{-1}	λ_{exp} / nm	ΔH^* / kJ mol^{-1}	ΔS^* / J K^{-1} mol^{-1}	ΔG^* / kJ mol^{-1}
	278	0.81 (3)	404	70493(3)	7(2)	68(4)
	293	4.32(6)				
	303	10.82 (2)				

For the ligand exchange of the mono-chelating alkoxy groups between **220** and **223**, it was found that the reaction goes under our conditions to completion. This is in contrast to what Fay and co-workers found for similar reactions.[20] However, Fay did not use ruthenocene-containing β-diketones, but acetyl acetone and the mono-chelating ligands were halides or ethanol. An interesting observation is that the ^{1}H NMR determined second order rate constant is equal to 4.14 dm^3 mol^{-1} s^{-1} at 293 K, which is close to the statistical value of 4 expected for

random scrambling of ligands.[20] This reaction was also studied by UV/Vis spectroscopy. UV/Vis overlay spectra of the reaction with time are shown in Figure 3.16. Absorbance values at 404 nm was collected and transformed to concentration values utilising Equation 3.8 for the reaction A + B → 2C.

$$[A]_t = [A]_0 - \frac{A_t - [A]_0\varepsilon_A - [A]_0\varepsilon_B}{2\varepsilon_C - \varepsilon_A - \varepsilon_B}$$

Equation 3.8.

Under second order conditions, [A] = [B] and in equation 3.8 $[A]_t$ = concentration of A at time t, $[A]_0$ = concentration of A at time 0, A_t = total absorption at time t, ε_x = extinction coefficient of compounds x = A, B or C at 404 nm, ε(**220**) = 866 $dm^3\ mol^{-1}\ cm^{-1}$, ε(**223**) = 965 $dm^3\ mol^{-1}\ cm^{-1}$ and ε(**232**) = 553 $dm^3\ mol^{-1}\ cm^{-1}$. Equation 3.8. was derived in section 4.7.2 (p 250). Insertion of the observed time-based concentration data into Equation 3.7 led to the linear plot of $1/C_t$ *vs* t (Figure 3.16) from which the second order rate constant k_2 could be obtained as the slope of the graph.

The UV/Vis rate constants (4.32 $dm^3\ mol^{-1}\ s^{-1}$ at 20ºC) are mutually constistant with that obtained by the ^1H NMR technique (4.14 $dm^3\ mol^{-1}\ s^{-1}$ at 20ºC) summarised in Table 3.11 .

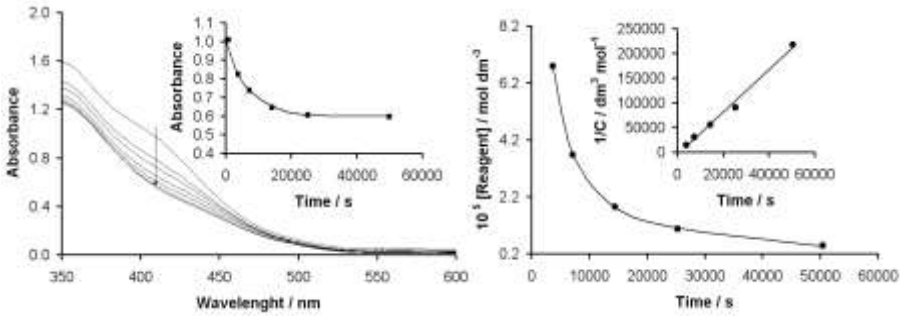

Figure 3.16. Left: Overlaid time scans of the ligand exchange reaction between **220** and **223**, [**220**] = [**223**]. Insert: Absorbance time trace at 404 nm. Right: Graph of concentration *vs* time of the ligand exchange reaction between **220** and **223**, Insert: Graph of 1/C *vs* time.

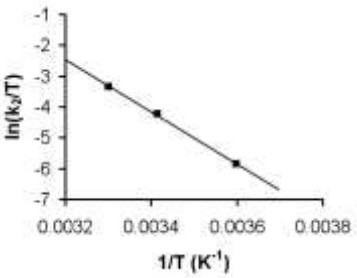

Figure 3.17. Eyring plot for the ligand exchange reaction between **220** and **223**. From these plots the activation parameters ΔH^* and ΔS^* (Table 3.11) could be obtained from the intercept of the plot with x-axis as well as the gradient of the graph.

The experimentally obtained second order rate law that applies to the reaction is thus:

$$\text{Rate} = -\frac{d[\text{reactants}]}{dt} = k_2[\mathbf{220}][\mathbf{223}]$$

where [**220**] = concentration of the titanium complex **220** and [**223**] = concentration of the titanium complex **223**.

The positive entropy of activation value implies that the mechanism of ligand exchange is dissociative of nature. Scheme 3.18 shows the proposed dissociative mechanism.

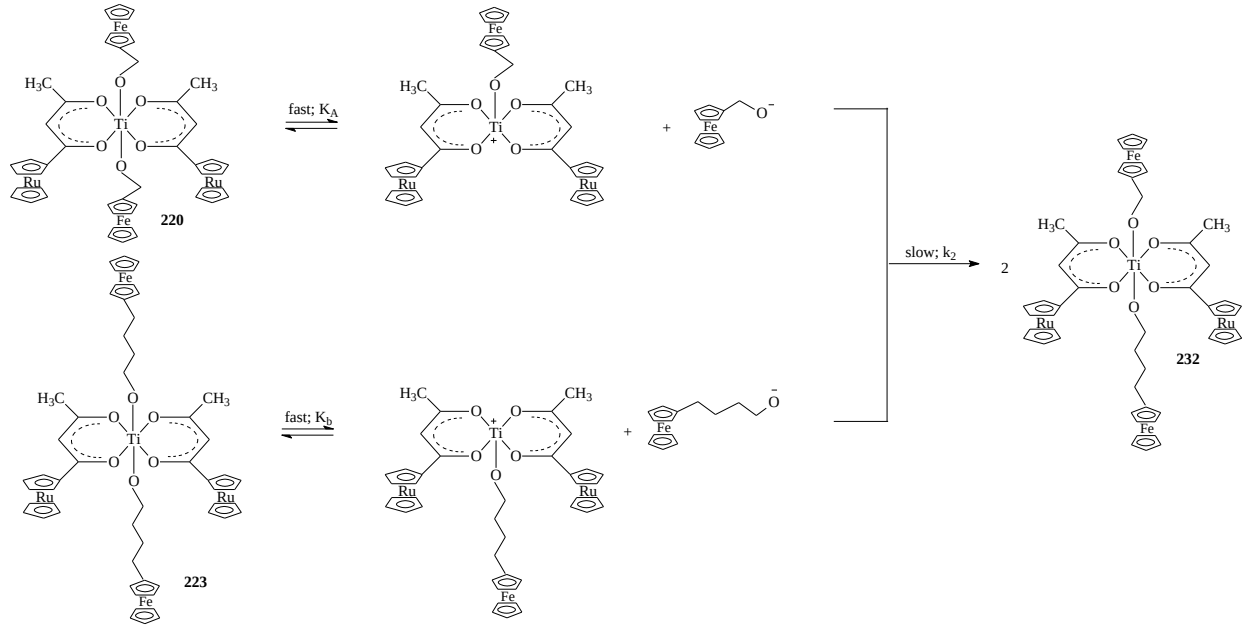

Scheme 3.18. Schematic representation of the proposed dissociative mechanism for the ligand exchange reaction between **220** and **223**.

3.5.3. Substitution kinetics

3.5.3.1. Introduction

Two types of substitution reactions were investigated in this part of the kinetic study. The first involves the substitution of the mono-chelating ferrocene-containing alkoxy groups of $[Ti(O(CH_2)_nFc)_2(RcCOCHCOCH_3)_2]$ {n = 1 (**220**), 2 (**221**), 3 (**222**)} with $HO(CH_2)_nFc$ {n = 2 (**171**), 3 (**172**), 4 (**173**)}. The second involves the substitution of the bi-chelating β-diketonato ligand of $[Ti(O(CH_2)_4Fc)_2(RcCOCHCOR)_2]$ {R = CH_3 (**223**), CF_3 (**225**)} with $RcCOCH_2COR$ {R = CH_3 (**151**), CF_3 (**152**)}.

3.5.3.2. UV/Vis Spectroscopic properties of reactants and products

Figure 3.18 shows the UV/Vis -spectra of $[Ti(O(CH_2)_nFc)_2(RcCOCHCOCH_3)_2]$ {n = 1 (**220**), 2 (**221**), 3 (**222**)}, $[Ti(O(CH_2)_4Fc)_2(RcCOCHCOR)_2]$ {R = CH_3 (**223**), CF_3 (**225**)}, $HO(CH_2)_nFc$ {n = 2 (**171**), 3 (**172**), 4 (**173**)} and $RcCOCH_2COR$ {R = CH_3 (**151**), CF_3 (**152**)}. Important spectral data are summarized in Table 3.12.

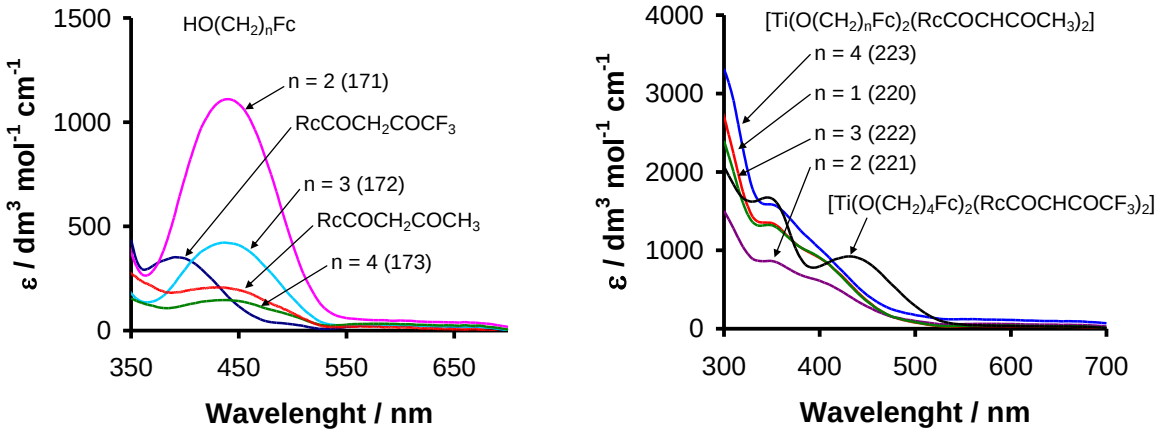

Figure 3.18. UV/Vis -spectra of **151** (orange, Left), **152** (dark blue, Left)**, 171** (pienk, Left)**, 172** (light blue, Left)**, 173** (green , Left)**, 220** (red, Right)**, 221** (purple Right)**, 222** (green, Right)**, 223** (blue, Right) and **225** (black, Right) at 20˚C in CH_2Cl_2.

Table 3.12. Molecular extinction coefficients of $[Ti(O(CH_2)_nFc)_2(RcCOCHCOCH_3)_2]$ {n = 1 (**220**), 2 (**221**), 3 (**222**)}, $[Ti(O(CH_2)_4Fc)_2(RcCOCHCOR)_2]$ {R = CH_3 (**223**), CF_3 (**225**)}, $HO(CH_2)_nFc$ {n = 2 (**171**), 3 (**172**), 4 (**173**)} and $RcCOCH_2COR$ {R = CH_3 (**151**), CF_3 (**152**)} at 20˚ in CH_2Cl_2.

Complex	λ_{max} / nm	ε_{max} / $dm^3\ mol^{-1}\ cm^{-1}$	λ_{exp} / nm	ε_{exp} / $dm^3\ mol^{-1}\ cm^{-1}$
220:$[Ti(O(CH_2)_1Fc)_2(RcCOCHCOCH_3)_2]$	345	1354	343	1397
221:$[Ti(O(CH_2)_2Fc)_2(RcCOCHCOCH_3)_2]$	345	860	345	860
222:$[Ti(O(CH_2)_3Fc)_2(RcCOCHCOCH_3)_2]$	345	1324	345	1324
223:$[Ti(O(CH_2)_4Fc)_2(RcCOCHCOCH_3)_2]$	345	1588	340	1662
225:$[Ti(O(CH_2)_4Fc)_2(RcCOCHCOCF_3)_2]$	345	1522	345	1522
171:$HO(CH_2)_2Fc$	435	1110	439	1110
172:$HO(CH_2)_3Fc$	440	420	435	420
173:$HO(CH_2)_4Fc$	435	146	436	146
151:$RcCOCH_2COCH_3$	424	200	424	200
152:$RcCOCH_2COCF_3$	389	350	392	350

The linear relationship (Figure 3.19) that exists between the absorbance values and different concentrations (from 0.0001 mol dm^{-3} to 0.005 mol dm^{-3}) of the complexes $Ti(O(CH_2)_nFc)_2(RcCOCHCOCH_3)_2]$ {n = 1 (**220**), 2 (**221**), 3 (**222**)}, $[Ti(O(CH_2)_4Fc)_2(RcCOCHCOR)_2]$ {R = CH_3 (**223**), CF_3 (**225**)}, $HO(CH_2)_nFc$ {n = 2 (**171**), 3 (**172**), 4 (**173**)} and $RcCOCH_2COR$ {R = CH_3 (**151**), CF_3 (**152**)} at 20˚C in CH_2Cl_2, illustrates that these complexes obey the Beer-Lambert law, $A = \varepsilon c\ell$ with A = absorbance, ε = extinction coefficient, c = concentration and ℓ = 1 cm path length.

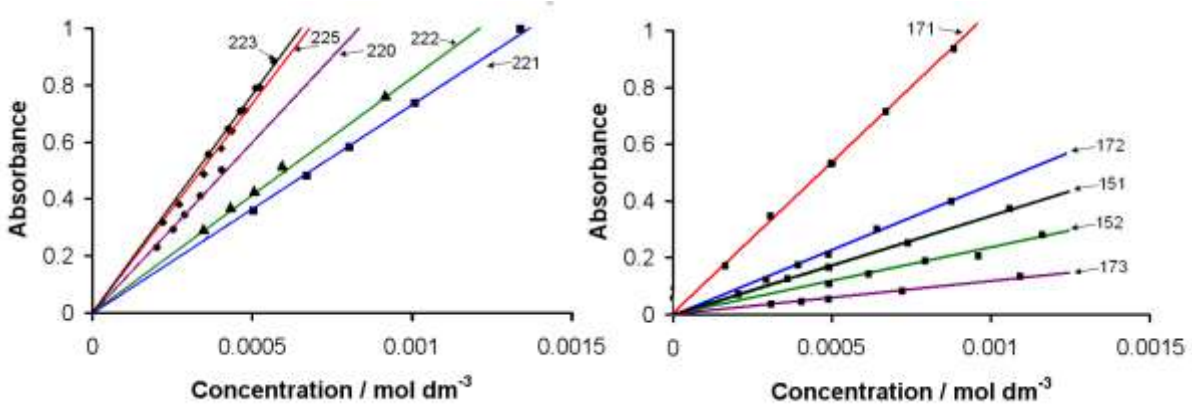

Figure 3.19. Graph of absorbance *vs* concentration of $Ti(O(CH_2)_nFc)_2(RcCOCHCOCH_3)_2]$ {n = 1 (**220,** red), 2 (**221,** purple), 3 (**222,** green)} and $[Ti(O(CH_2)_4Fc)_2(RcCOCHCOR)_2]$ {R = CH_3 (**223,** blue), CF_3 (**225,** black)} (Left), $HO(CH_2)_nFc$ {n = 2 (**171,** red), 3 (**172,** blue), 4 (**173**, purple)} and $RcCOCH_2COR$ {R = CH_3 (**151**, black), CF_3 (**152**, green)} (Right) at 20˚ in CH_2Cl_2. Absorbance measurements were made at λ_{exp} as indicated in Table 3.12.

3.5.3.3. Substitution kinetics of reaction between titanium complexes and ferrocene-containing alcohols

In this section the results of the substitution of the mono-chelating ferrocene-containing alkoxy ligands from $[Ti(O(CH_2)_nFc)_2(RcCOCHCOCH_3)_2]$ {n = 1 (**220**), 2 (**221**), 3 (**222**)} with $HO(CH_2)_nFc$ {n = 2 (**171**), 3 (**172**), 4 (**173**)} according to Scheme 3.19 is reported. The reaction takes place in two consecutive reaction steps A and B involving the substitution of one titanium bound ferrocenyl-alkoxy group at a time. All substitution reactions were carried out under pseudo first-order reaction conditions, with [ligand] = 10, 20, 40, 60, 80 and 100 times [Ti-complex]. The experimentally determined rate law was found to be

$$\frac{d}{dt}[\text{Products}] = k_A[\text{Ti-complex}][\text{incoming ligand}]$$

The data for these reactions was processed by the mathematical models shown in Equation 3.9.[21] In the case of the reaction shown in Scheme 3.19, the treatment of time-base data *via* the consecutive reaction models and the normal single stage treatment by utilising the first part of time-based absorption data for reaction A and the last part of the time based absorption

for reaction B gave very similar values for k_{1obs} and k_{3obs}. This is due to the fact that the rate of reaction A is much faster than the rate of reaction B.

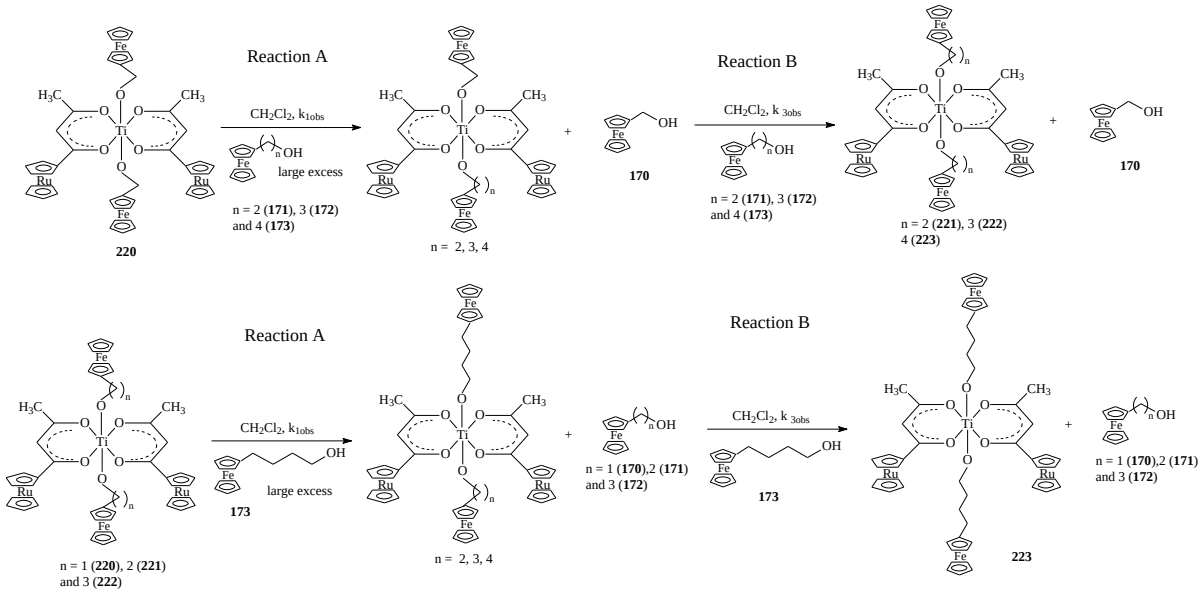

Scheme 3.19. Substitution reactions between $[Ti(O(CH_2)_nFc)_2(RcCOCHCOCH_3)_2]$ {n = 1 (**220**), 2 (**221**), 3 (**222**)} and $HO(CH_2)_nFc$ {n = 2 (**171**), 3 (**172**), 4 (**173**)}. $k_{1obs} = k_A[Fc(CH_2)_nOH]$, $k_{3obs} = k_B[Fc(CH_2)_nOH]$.

$$A \xrightarrow{k_{1obs}} B \xrightarrow{k_{3obs}} C$$

Normal single treatment

$$[A]_t = [A]_0 \exp(-k_{1obs}t)$$

$$[B]_t = [B]_0 \exp(-k_{3obs}t)$$

Consecutive reaction treatment

$$[B]_t = \frac{k_{1obs}[A]_0}{k_{3obs} - k_{1obs}} [\exp(-k_{1obs}t) - \exp(-k_{3obs}t)]$$

$$[C]_t = [A]_0 \left\{1 - \frac{1}{k_{3obs} - k_{1obs}} [k_{3obs} \exp(-k_{1obs}t) - k_{1obs} \exp(-k_{3obs}t)]\right\}$$

Equation 3.9.

In Equation 3.9 $k_{1obs} = k_A[Fc(CH_2)_nOH]$ (i.e. k_{1obs} is a pseudo first order rate constant, k_A is the second order rate constant associated with reaction A), A = **220**, B = intermediate, C = **221**, **222**, **223**. Also, $k_{3obs} = k_B[Fc(CH_2)_nOH]$ in Equation 3.9 for Scheme 3.19, top. Again, k_3 is a pseudo first order rate constant, while k_B is the second order rate constant associated with reaction B. Figure 3.20 shows the time traces with the different kinetic fits for the formation of **221**, **222** and **223** according to Scheme 3.19.

The pseudo first-order reaction rate constants k_{obs} were obtained by following the formation of **221, 222** or **223** at the indicated wavelength (Table 3.12). The product of the substitution had the same UV/Vis spectrum than authentic **221, 222** or **223**. ^{1}H NMR confirmed the formation of **221, 222** or **223** according to Scheme 3.19 as well.

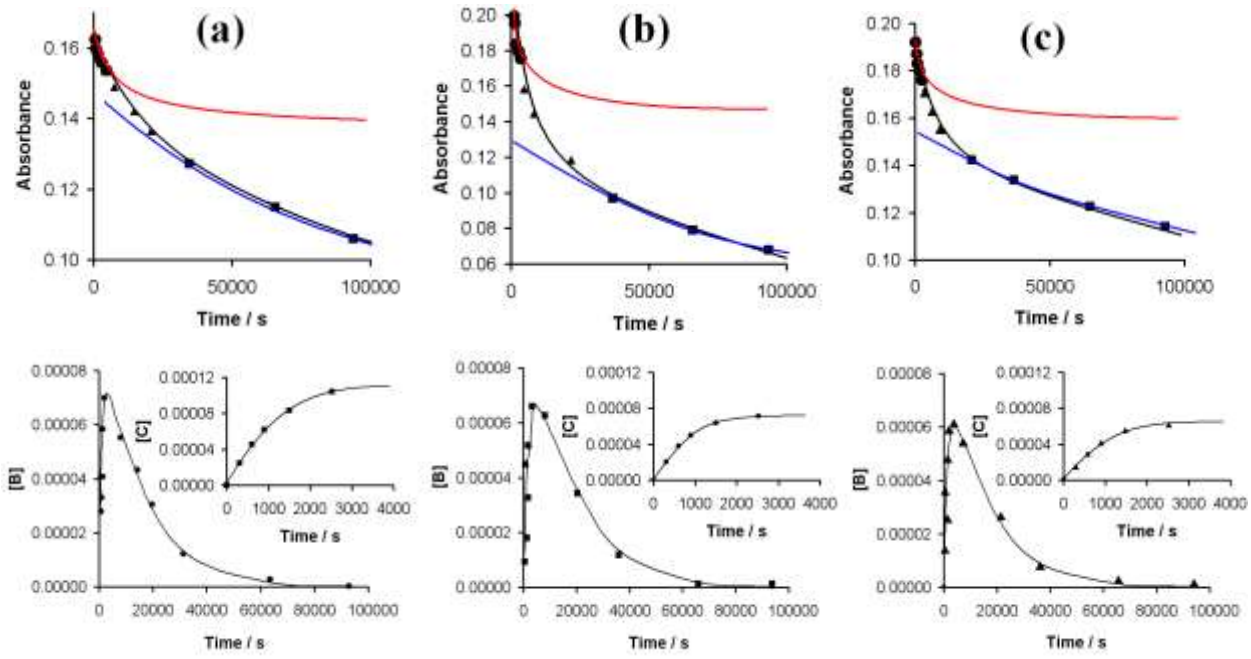

Figure 3.20. Top: Time trace (wavelength as per Table 3.12) showing kinetic fits of data for the formation of **221** (a), **222** (b) and **223** (c) according to Scheme 3.19. Single stage kinetic fits utilising Equation 3.9 was performed or data shown as (●), for reaction A (red) and data shown as (■) for reaction B (blue). The consectitive reaction treatment utilising Equation 3.9 was performed on all data marked as ●, ▲ and ■ (top) and results in the concentration profiles shown at the bottom for the formation and disappearance of B and the formation of C with time. Concentration is measured in units of mol dm^{-3}. The rate constant obtained by both methods were virtually identical and are summirised in Table 3.13. [**221**] = [**222**] = [**223**] = 7.74 x 10^{-5} mol dm^{-3}, [alcohol] = 1.55 x 10^{-5} mol dm^{-3} at 25°C.

All the graphs of k_{1obs} and k_{3obs} *vs* $[HO(CH_2)_nFc]$ for each titanium complex (Figure 3.21, shows as example the substitution in **220** with **173**) for reaction A and reaction B respectively are straight lines through the origin, which implies a first-order dependence on $[HO(CH_2)_nFc]$, with the second order rate constants (summarized in Table 3.13) given by the slope. Further, the zero intercept indicated, that the solvent does not contribute meaningful to the mechanism of substitution during reaction A or B.

A study of the dependence of k_{1obs} and k_{3obs} on temperature, Figure 3.21, resulted in the activation parameters listed in Table 3.13. ΔH^*, ΔS^* and ΔG^* were determined from Equation 3.11 and 3.12.

$$\ln \frac{k_i}{T} = -\frac{\Delta H^*}{RT} + \frac{\Delta S^*}{R} + \ln \frac{R}{Nh} \qquad \text{with i = A or B}$$

Equation 3.11.

$$\Delta G^* = \Delta H^* - T\,\Delta S^*$$

Equation 3.12.

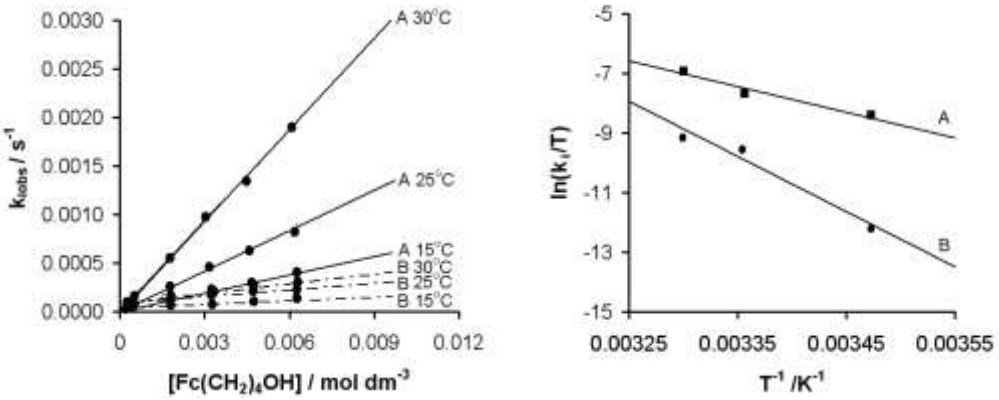

Figure 3.21. Left: Graph of k_{iobs} {with i = 1 (—, reaction A) or i = 3 (---, reaction B)} *vs* $[HO(CH_2)_4Fc]$ for the substitution of $(O(CH_2)Fc)^-$ from $[Ti(O(CH_2)_1Fc)_2(RcCOCHCOCH_3)_2]$ (**220**) with $HO(CH_2)_4Fc$ (**173**) at T = 15˚C, 25˚C and 30˚C, for $[Ti(O(CH_2)_1Fc)_2(RcCOCHCOCH_3)_2]$ = 7.74 x 10^{-5} mol dm^{-3}. The slopes are the second order rate constants k_A and k_B for reaction A and B, Scheme 3.19 respectively. Right: Graph of $ln(k_i/T)$ *vs* T^{-1} for i = A or B.

Table 3.13. The second order rate constants (k_A and k_B) and the activation parameters for substitution reactions of $[Ti(O(CH_2)_nFc)_2(RcCOCHCOCH_3)_2]$ {n = 1 (**220**), 2 (**221**), 3 (**222**)} with $HO(CH_2)_nFc$ {n = 2 (**171**), 3 (**172**), 4 (**173**)} at T = 25˚C for reaction steps A and B according to Scheme 3.19. Standard deviations are given in brackets. For the reaction between **220** and **171** the results obtained for the three different methods of data treatment are shown. As for the rest, only the consecutive treatment model on [B] are reported, but all three methods gave mutually consistent rate constants.

Titanium complex no; (n)	Incoming ligand no; (n)	Reaction A				Reaction B			
		$10^2 k_A$ / dm^3 mol^{-1} s^{-1}	ΔH_A^* / kJ mol^{-1}	ΔS_A^* / J K^{-1} mol^{-1}	ΔG_A^* / kJ mol^{-1}	$10^3 k_B$ / dm^3 mol^{-1} s^{-1}	ΔH_B^* / kJ mol^{-1}	ΔS_B^* / J K^{-1} mol^{-1}	ΔG_B^* / kJ mol^{-1}
220; (1)	**171;** (2)								
Single stage treatment		6.90(3)	117(2)	124(3)	80(4)	3.89(2)	91(2)	33(4)	81(2)
Consecutive treatment on [B]		6.94(1)	116(1)	123(3)	79(2)	3.87(4)	91(2)	33(3)	81(2)
Consecutive treatment on [C]		6.92(2)	116(2)	123(4)	79(3)	3.92(3)	90(1)	34(2)	79(2)
220; (1)	**172;** (3)	7.69(4)	115(2)	120(4)	79(3)	8.71(5)	130(3)	135(6)	90(5)
220; (1)	**173;** (4)	13.9(3)	112(3)	112(5)	78(4)	5.00(4)	239(2)	512(5)	86(2)
221; (2)	**173;** (4)	6.47(5)	111(2)	93(6)	83(2)	5.95(2)	248(2)	561(4)	81(3)
222; (3)	**173;** (4)	1.28(4)	105(1)	84(3)	80(2)	4.19(3)	271(2)	622(5)	86(2)

The activation parameters are all relatively large values. Typical expected values for single reactions are ΔH^{*} = 30 kJ mol^{-1} and ΔS^{*} < 10 J K^{-1} mol^{-1}.[22] The activation parameters listed in Table 3.18 are 1-2 orders of magnitude larger. This is consistent with more than one reaction occurring at the same time. Multiple reactions can easily be accounted for by recognising that the titanium complexes shown in Scheme 3.19 are not a single compound but a compound mixture of many isomers as shown in Figure 3.5 (p 94). It follows that the kinetic ΔH^{*} and ΔS^{*} values that are reported in Table 3.13 are actually the cummelative sum of all isomers reacting to produce a complex mixture of isomeric products.

Figures 3.22 and 3.24 show graphically the relationship between the second order rate constant as well as entropy of activation and alkyl chain length. For the first set of reactions studied (Scheme 3.19, Top), where the titanium complex is kept constant as $[Ti(O(CH_2)_1Fc)_2(RcCOCHCOCH_3)_2]$ (**220**) and the incoming ligand is varied as $HO(CH_2)_nFc$ {n = 2 (**171**), 3 (**172**), 4 (**173**)}, it was found that as the alkyl chain length of the incoming ligand increases the second order rate constant of reaction A (the first substitution) increases. This is consistent with the view that the longer alkyl chain lengths for the incoming ferrocene-containing alcohol makes the incoming alcohol a better nucleophile compared to the leaving alcohol. Electrochemical studies on the alcohols $Fc(CH_2)_nOH$ confirm this view.[1] It was also found that as the alkyl chain length of the incoming ligand increases the second order rate constant of the second substitution, reaction B, decreases. It may be that the longer alkoxy chain length of the intermediate product of reaction A imposes more steric hindrance on the titanium substrate thereby slowing down the attack of the second incoming alcohol, but a second explanation can also account for this observation. Once the original electrophilic substrate **220** has been converted *via* reaction A to the intermediate complex, the new intermediate should be less electrophylic (i.e. more nucleophylic than the original complex **220**). This should be more pronounced for longer alcohol chain lengths. It follows that the intermediate should became less reactive towards the incoming alcohol in reaction B as chain length increases. A consequence of this is slower substitution rates for reaction B with longer alcohol chain lengths. Further research is required to determine the relative contribution of each of these possible explanations.

The entropy of activation for reaction B also increases with an increase in alkyl chain length of the incoming ligand. This is consistent with longer chains introducing more disorder in the complexes. All entropy of activation values for both reaction A and reaction B is large positive values, implying that the mechanism of substitution for both reactions is dissociative of nature. This is expected, seeing as titanium is known for complexes which are five,[23, 24] and six coordinated.[25, 26] In contast, to our knowledge, no titanium complexes with coordination sphere of seven is known.

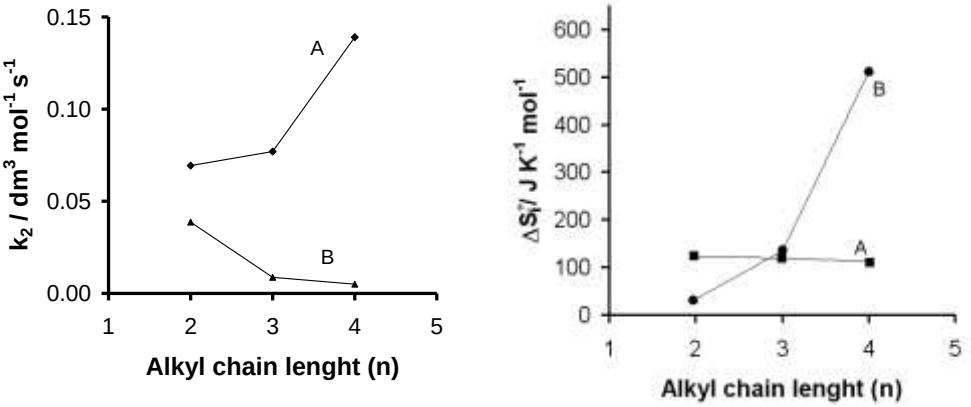

Figure 3.22. Left: Graph of second order rate constant ($k_i = k_A$ or k_B) *vs* alkyl chain length of the incoming ligand for the substitution of $(O(CH_2)Fc)^-$ from $[Ti(O(CH_2)_1Fc)_2(RcCOCHCOCH_3)_2]$ (**220**) with $HO(CH_2)_nFc$ {n = 2 (**171**), 3 (**172**), 4 (**173**)} at T = 25˚. Right: Entropy of activation *vs* alkyl chain lenght of the incoming ligand.

The second set of reactions in ferrocenylalkoxide substitution that was studied (Scheme 3.19, Bottom) is where the incoming ligand, the ferrocenyl-containing alcohol, $HO(CH_2)_4Fc$ (**173**) was kept constant and the titanium complex was varied as $[Ti(O(CH_2)_nFc)_2(RcCOCHCOCH_3)_2]$ with n = 1 (**220**), 2 (**221**), 3 (**222**). For this set of reactions, it was found that as the alkyl chain length of the alkoxy group on the titanium complexes was increased, the second order rate constant for reaction A decreased but for reaction B it increased. When applying the nucleophylic and electrophilic argumentation of the previous section, this is what is expected. With n = 1, **220** is the strongest electrophile and reaction A should be the fastest. As n increases through 2 to 3 for **222**, the elecrophilic nature of the complex decreases (because $OH(CH_2)_{3\text{ or }4}Fc$ is more electron-donating than $OH(CH_2)_{1\text{ or }2}Fc$ according to reference 1), and the rate of reaction becomes slower. The intermediate products of reaction A should become progressively weaker in electrophylic nature than the corresponding starting material with the result that the dissociative step to form a 5-coordinated intermediate capable of reacting with **173** becomes more favourable with the increase of n. This should account for the increase in rate of reaction B for longer n values of alkoxyferrocenyl ligands in **220**-**222**.

As for the first set of reactions, the entropy of activation also is slightly dependent on the alkyl chain length of the alkoxy group on the titanium complex. The entropy of activation values for both reaction A and reaction B are large positive values, which is consistent with a dissociative mechanism of substitution for both reaction steps. The enthalpy as well as the entropy of activation for reaction B is much larger than that found for reaction A. This is consistent with the view that the starting material **220**-**222** has less reacting isomers in solution than the intermediates which form **223**, simply because the alkoxy ligands in **220**-**222** are the same, but not in the intermediate which is formed, therefore the overall number of reactions taking place to generate **223** from the intermediate product during reaction B is much more than

for reaction A (which has less isomers reacting). The accumulative effect of these separate reactions leads to larger ΔS^* and ΔH^* values for reaction B compared to reaction A.

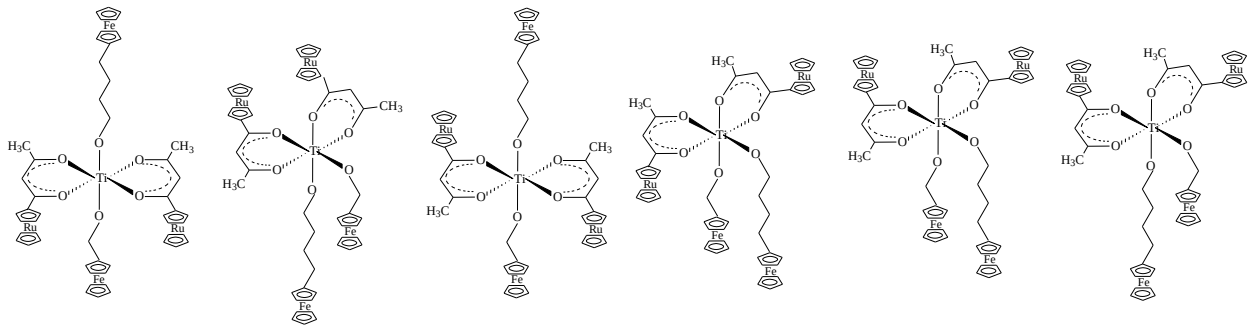

Figure 3.23. Six possible isomers of the intermediate that forms during the second reaction (bottom) of Scheme 3.18. Many other isomers may also exist, including isomers where the direction of ruthenocenyl protruding is reversed (i.e. up or down).

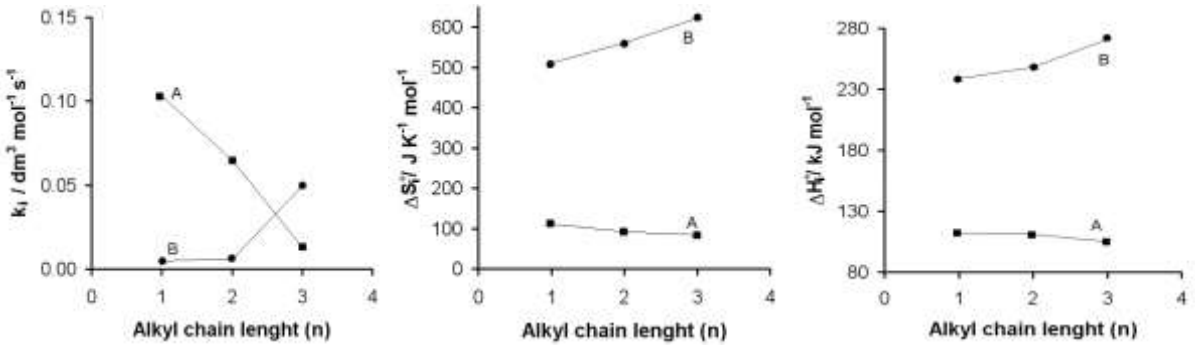

Figure 3.24. Left: Graph of second order rate constant ($k_i = k_A$ and k_B) *vs* alkyl chain length in substitution reactions for the substitution of $(O(CH_2)Fc)^-$ from $[Ti(O(CH_2)_nFc)_2(RcCOCHCOCH_3)_2]$ {n = 1 (**220**), 2 (**221**) and 3 (**222**)} with $HO(CH_2)_4Fc$ (**173**) at T = 25˚C for reaction A and B. Middel: Entropy of activation *vs* alkyl chain length of the titanium complexes. Right: Enthalpy of activation *vs* alkyl chain length of the titanium complex.

The schematic representation of the proposed dissociative mechanism in Scheme 3.20, shows two kinetically indistinguisable mechanism. For the first mechanism the rate determining step may be the dissociation of the ferrocenyl alkoxy group from the titanium complex (step i). Then step ii will be fast. This mechanism is, however kinetically indistinguishable from the one where step is a fast equilibrium and step ii is the rate determining step with rate constant k_2. This mechanism is proposed for both reaction A and B.

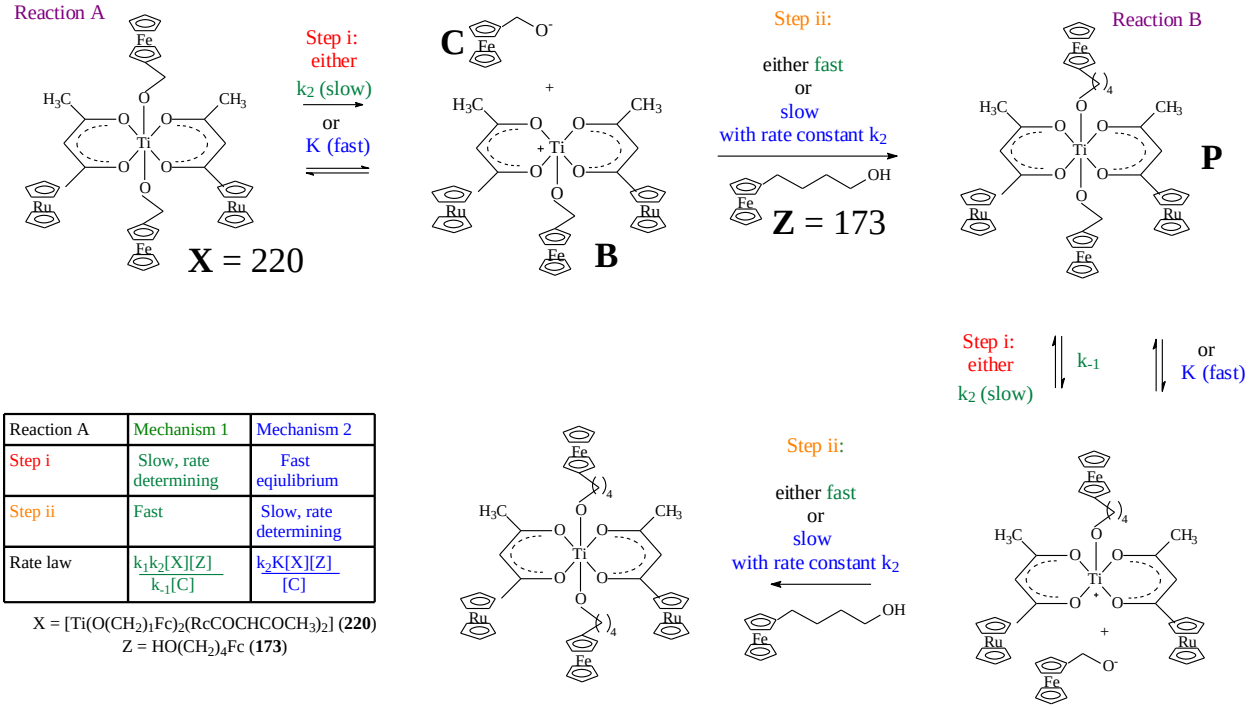

Reaction A	Mechanism 1	Mechanism 2
Step i	Slow, rate determining	Fast eqiulibrium
Step ii	Fast	Slow, rate determining
Rate law	$\frac{k_1 k_2[X][Z]}{k_{-1}[C]}$	$\frac{k_2 K[X][Z]}{[C]}$

X = $[Ti(O(CH_2)_1Fc)_2(RcCOCHCOCH_3)_2]$ (**220**)
Z = $HO(CH_2)_4Fc$ (**173**)

Scheme 3.20. Schematic representation of two proposed dissociative mechanisms for the substitution reaction between $[Ti(O(CH_2)_1Fc)_2(RcCOCHCOCH_3)_2]$ (**220**) with $HO(CH_2)_4Fc$ (**173**). The rectangle shows the two possible rate laws for reaction A. Reaction B follows the same rate laws, but then x = $\{Ti[O(CH_2)Fc][O(CH_2)_4Fc](RcCOCHCOCH_3)_2\}$. It is proposed that all the reactions summerised in Table 3.18 conform to the above reaction sequence.

To derive the rate laws shown in the rectangle in Scheme 3.20, it is convenient to consider the following equivalent mechanisms where the compounds have been substituted with symbols X, B, etc.:

$$X \underset{k_{-1}}{\overset{k_1}{\rightleftharpoons}} B + C$$

$$B + Z \xrightarrow{k_2} P$$

$$X + Z \longrightarrow C + P$$

Mechanism 1

$$X \overset{K}{\rightleftharpoons} B + C$$

$$B + Z \xrightarrow{k_2} P$$

$$X + Z \longrightarrow C + P$$

Mechanism 2

For Mechanism 1, the rate law is derived as follows:

$$\frac{d}{dt}[P] = k_2[B][Z] \qquad - - - (1)$$

By applying the principle of steady state to B it follows that:

$$\frac{d}{dt}[B] = 0 = k_1[X] - k_{-1}[B][C] - k_2[B][Z]$$

$$\therefore \quad [B] = \frac{k_1[X]}{k_{-1}[C] + k_2[Z]} \qquad - - - (2)$$

By substituting (2) into (1) it follows that:

$$\therefore \frac{d}{dt}[P] = \frac{k_2k_1[X][Z]}{k_{-1}[C] + k_2[Z]}$$

If $k_{-1}[C] >> k_2[Z]$; $\frac{d}{dt}[P] = \frac{k_2k_1[X][Z]}{k_{-1}[C]}$ which shows [C] will delay the reaction, first order

$$= k_A[X][Z]$$

Here k_A is the experimentally deterimined rate constants $k_A = \frac{k_2k_1}{k_{-1}[C]}$ for reaction A, Scheme 3.19. k_B has the same form.

If $k_2[Z] >> k_{-1}[C]$; $\frac{d}{dt}[P] = \frac{k_2k_1[X][Z]}{k_2[Z]}$

$$= k_1[X]$$

This shows that the reaction is independent of Z. This was not experimentally found to be so. The reaction was found to be first order in Z. Therefore kinetic results eliminate the second option $k_2[Z] >> k_{-1}[C]$ from mechanism 1.

For Mechanism 2 it follows that:

$$K = \frac{[B][C]}{[X]} \quad \text{thus} \quad B = \frac{K[X]}{[C]}$$

$$\frac{d}{dt}[P] = k_2[B][Z]$$

$$= \frac{k_2K[X][Z]}{[C]}$$ which theoretically shows [C] will delay the reaction

$= k_A[X][Z]$ or $k_B[X][Z]$ for the experimentally determined rate laws

It follows that k_A and k_B, the experimentally determined rate constants for reaction steps A and B in Scheme 3.19, has the form $(k_2K)/[C]$ if mechanism 2 holds.

Mechanism 1 and 2 above showed that the leaving ligand should delay the reaction. Thus, the influence of the leaving ligand was investigated. This study was preformed by reacting 7.74×10^{-5} mol dm^{-3} $[Ti(O(CH_2)_nFc)_2(RcCOCHCOCH_3)_2]$ {n = 1 (**220**), 2 (**221**), 3 (**222**)} with 7.74×10^{-3} mol dm^{-3} $HO(CH_2)_nFc$ {n = 2 (**171**), 3 (**172**), 4 (**173**)} in the presence of the leaving ligand $HO(CH_2)_nFc$ {n = 1 (**170**), 2 (**171**), 3 (**172**)} with concentrations ranging from 0, 7.74×10^{-4}, 1.55×10^{-3} and 3.10×10^{-3} mol dm^{-3} at 25°C. Table 3.14 summarises the results obtained.

Table 3.14. The observed rate constants (k_{obs}) for the reaction of the substitution reactions of $[Ti(O(CH_2)_nFc)_2(RcCOCHCOCH_3)_2]$ {n = 1 (**220**), 2 (**221**), 3 (**222**)} with $HO(CH_2)_nFc$ {n = 2 (**171**), 3 (**172**), 4 (**173**)} in the presence of the leaving ligand $HO(CH_2)_nFc$ {n = 1 (**170**), 2 (**171**), 3 (**172**)}at T = 25˚C for reaction steps A and B according to Scheme 3.20.

Leaving ligand (n); 10^4[ ]	10^5 k_{obsA} ; k_{obsB}	Leaving ligand (n); 10^4[ ]	10^5 k_{obsA} ; k_{obsB}	Leaving ligand (n); 10^4[ ]	10^5 k_{obsA} ; k_{obsB}
$[Ti(O(CH_2)Fc)_2(RcCOCHCOCH_3)_2]$, (**220**) + $HO(CH_2)_2Fc$, (**171**)		$[Ti(O(CH_2)Fc)_2(RcCOCHCOCH_3)_2]$, (**220**) + $HO(CH_2)_3Fc$, (**172**)		$[Ti(O(CH_2)Fc)_2(RcCOCHCOCH_3)_2]$, (**220**) + $HO(CH_2)_4Fc$, (**173**)	
(1); 0	83; 25	(1); 0	78; 12	(1); 0	68; 15
(1); 7.74	48; 13	(1); 7.74	46; 7.7	(1); 7.74	40; 8.6
(1); 15.5	32; 7.9	(1); 15.5	29; 5.5	(1); 15.5	17; 7.3
(1); 31.0	0.6; 5.9	(1); 31.0	0.6; 0.9	(1); 31.0	0.3; 4.7
$[Ti(O(CH_2)_2Fc)_2(RcCOCHCOCH_3)_2]$, (**221**) + $HO(CH_2)_4Fc$, (**173**)		$[Ti(O(CH_2)_3Fc)_2(RcCOCHCOCH_3)_2]$, (**222**) + $HO(CH_2)_4Fc$, (**173**)			
(2); 0	85; 15	(3); 0	100; 20		
(2); 7.74	50; 8.7	(3); 7.74	59; 12		
(2); 15.5	41; 5.1	(3); 15.5	51; 13		
(2); 31.0	13; 2.6	(3); 31.0	37; 17		

The study of the influence of the leaving group revealed that the leaving group does delay the reaction, providing more evidence to support proposed mechanism with $k_{-1}[C] >> k_2[Z]$ for these substitution reactions. Results were too eratic to pinpoint the delaying effect as first order delaying in C. In addition the same delaying effect was observed for the B part of the reaction (second substitution).

3.5.3.4. Substitution kinetics between titanium complexes and ruthenocene-containing β-diketones

In this next part of the kinetic study of this reseach program, the results of the substitution of the bi-chelating ruthenocene-containing β-diketonato ligands from $[Ti(O(CH_2)_4Fc)_2(RcCOCHCOR)_2]$ [R = CH_3 (**223**), CF_3 (**225**)} with $RcCOCH_2COR$ {R = CF_3 (**151**), CH_3 (**152**)} according to Scheme 3.21 are reported. The experimentally determined rate law was found to be

$$\frac{d}{dt}[\text{Products}] = k_A[\text{Ti-complex}][\text{incoming ligand}]$$

The reaction was studied by UV/Vis techniques under pseudo first order kinetics with concentrations of the incoming β-diketone ligand much larger than the concentration of the titanium complexes. This practice also forced the reaction to completion and made it impossible to isolate the intermediate mixed β-diketonato complex $[Ti(O(CH_2)_4Fc)_2(RcCOCHCOCH_3)(RcCOCHCOCF_3)]$ product.

That the titanium complexes **223** and **225** as well as the β-diketones **151** and **152** follows the Beer-Lambert law, was already demonstrated in Section 3.5.3.2, p 109-10. The wave length at which the study was conducted is 392 nm as per Table 3.12, p 109.

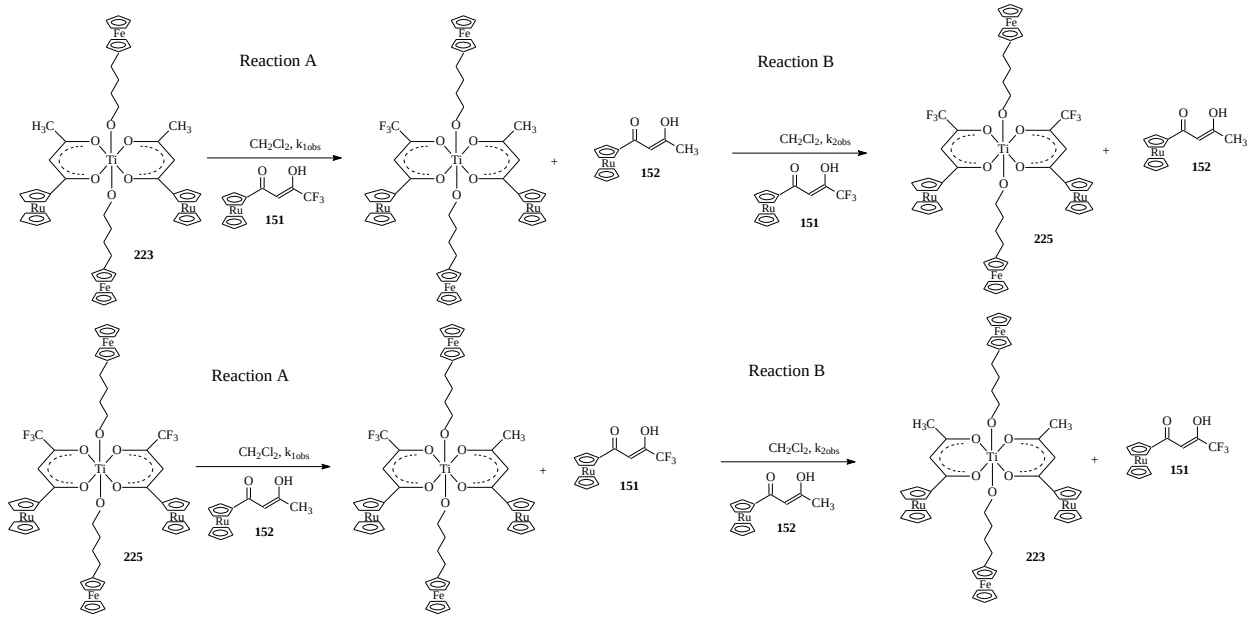

Scheme 3.21. Substitution reactions between $[Ti(O(CH_2)_4Fc)_2(RcCOCHCOR)_2]$ [R = CH_3 (**223**), CF_3 (**225**)} with $RcCOCH_2COR$ {R = CF_3 (**151**), CH_3 (**152**)}.

The reaction takes place in two consecutive reactions A and B involving the substitution of one bi-chelating β-diketonato ligand at a time. The obtained absorbance data was processed by Equation 3.9, for the treatment of consecutive reactions. Again, as was the case with the alkoxy replacement in section 3.5.3.3, results obtained from consecutive reaction treatment and normal single reaction treatment were mutually consistent, for the same reason as given in section 3.5.3.3. Figure 3.25 shows the graphs of the data fitted to Equation 3.9 for the treatment of consecutive reactions for the formation of **223** and **225** according to Scheme 3.21. Results are summarised in Table 3.15.

Table 3.15. The second order rate constants, k_A and k_B as well as the activation parameters for substitution reactions of $[Ti(O(CH_2)_4Fc)_2(RcCOCHCOR)_2]$ {R = CH_3 (**223**), CF_3 (**225**)} with $RcCOCH_2COR$ {R = CF_3 (**151**), CH_3 (**152**)} at T = 25˚C for reactions steps A and B according to Scheme 3.21. Standard deviations are given in brackets.

Titanium complex (R;χ_R)	Incoming ligand (R; χ_R)	Reaction A				Reaction B			
		$10^2 k_A$ / dm^3 mol^{-1} s^{-1}	ΔH_A^* / kJ mol^{-1}	ΔS_A^* / J K^{-1} mol^{-1}	ΔG_A^* / kJ mol^{-1}	$10^3 k_B$ / dm^3 mol^{-1} s^{-1}	ΔH_B^* / kJ mol^{-1}	ΔS_B^* / J K^{-1} mol^{-1}	ΔG_B^* / kJ mol^{-1}
CH_3; 2.34	CF_3; 3.01	31.0(4)	77(2)	5.4(5)	75(4)	16.9(5)	96(1)	44.9(3)	82(6)
CF_3; 3.01	CH_3; 2.34	49.7 (4)	78(1)	13.2(3)	75(3)	25.4(4)	98(2)	54.6(4)	82(3)

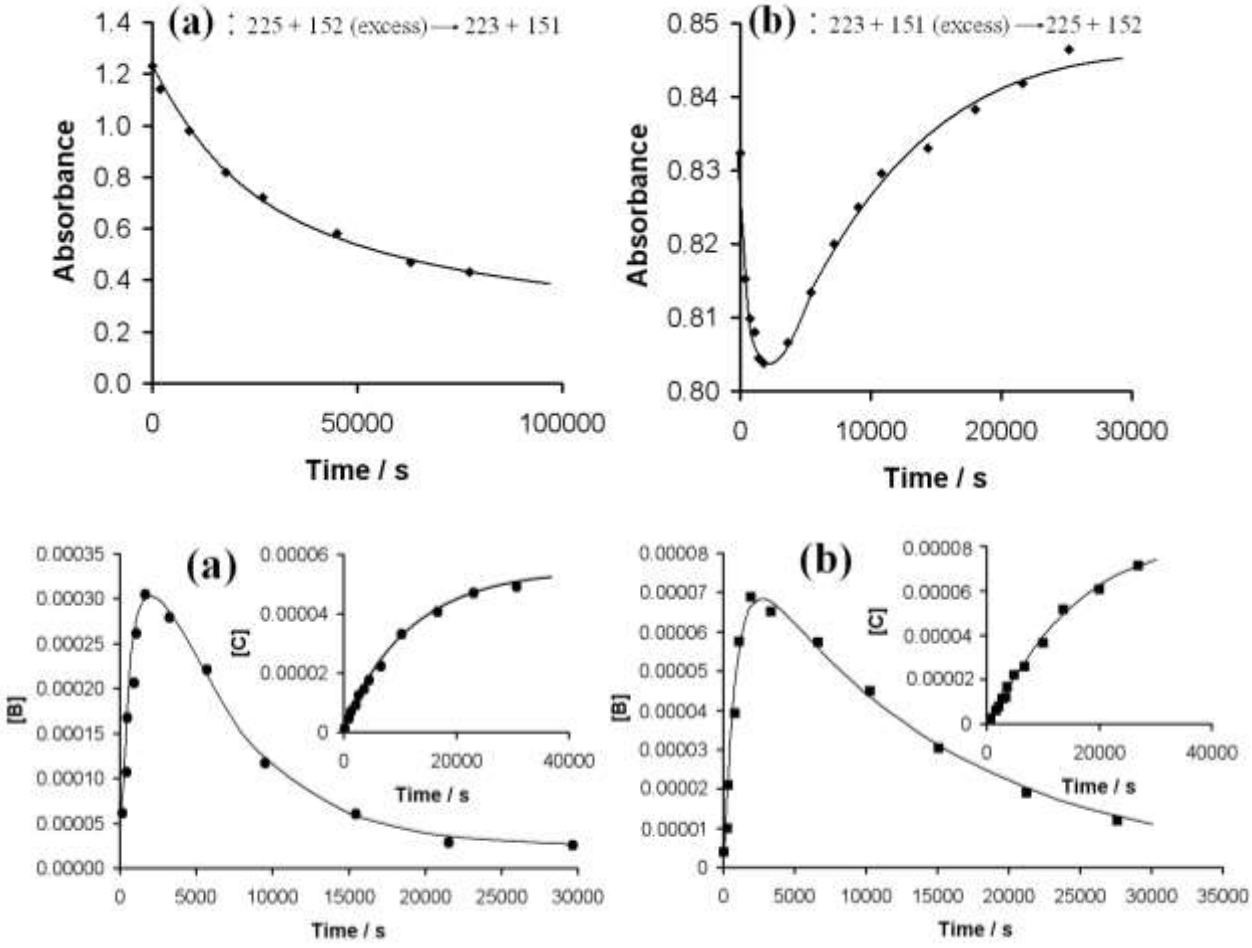

Figure 3.25. Top: Reaction profiles showing how absorbance changed with time for each reaction Bottom: Graphs of data fitted to consecutive reaction treatment utilising Equation 3.9 for the formation of **223** (a) and **225** (b) according to Scheme 3.20. [**223**] = [**225**] = 7.74 x 10^{-5} mol dm^{-3}, [**151**] = 1.55 x 10^{-3} mol dm^{-3} and [**152**] = 4.64 x 10^{-3} mol dm^{-3}.

All the graphs of k_{obs} *vs* [$RcCOCH_2COR$] for each titanium complex (Figure 3.26, shows the results of β-diketonato substitution in **223** with **152**) for reaction A and B are straight lines through the origin, which implies a first-order dependence on [$RcCOCH_2COR$]. The second order rate constants are given by the slope and results are summarised in Table 3.15. Further, the

zero intercept indicated that the solvent does not contribute meaningful to the mechanism of substitution during reaction A or B.

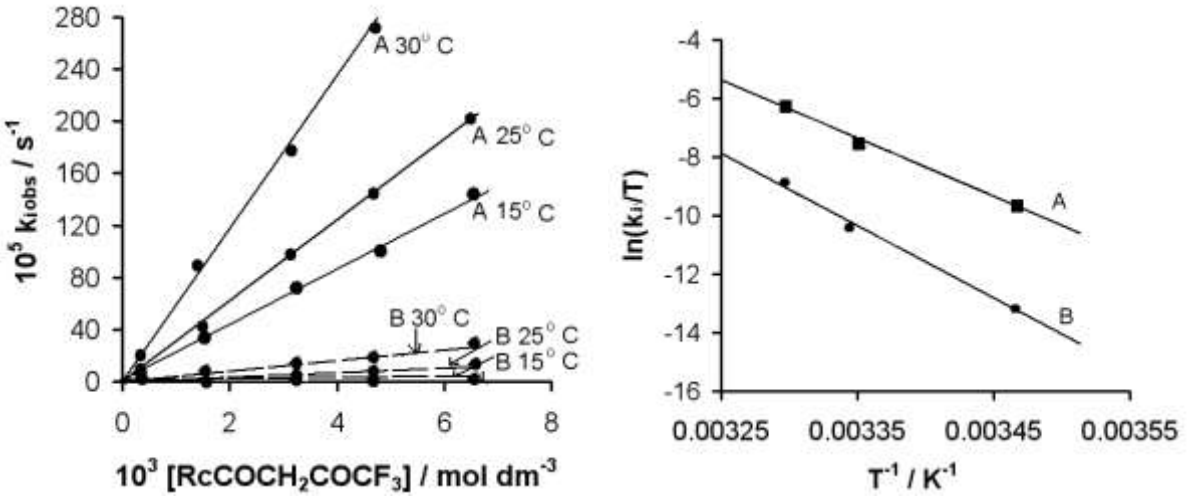

Figure 3.26. Left: Graph of k_{iobs} with i = 1 (—, reaction A) or i = 3 (---, reaction B) *vs* [$RcCOCH_2COR$] (Left) for the substitution of $(RcCOCHCOCH_3)^-$ from $[Ti(O(CH_2)_4Fc)_2(RcCOCHCOCH_3)_2]$ (**223**) with $RcCOCH_2COCF_3$ (**152**) at T = 0˚C, 25˚C and 30˚C. $[Ti(O(CH_2)_4Fc)_2(RcCOCHCOCH_3)_2] = 7.74 \times 10^{-5}$ mol dm^{-3}. The slopes are the second order rate constants k_A and k_B for reaction steps A and B, Scheme 3.21, respectively. Right: Graph of $\ln(k_i/T)$ *vs* T^{-1} for i = A or B.

The activation parameters are all relatively large values, due to the same argument given in section 3.5.3.3.

It can be seen from Table 3.15, that k_A and k_B for both reaction steps A and B are bigger (i.e. substitution is faster) if the incoming β-diketonato ligand is less electronegative (i.e. more electron rich) than the leaving β-diketonato ligand. Although the increase in second order rate constant is not kinetically significant, the trend is expected. Replacement of a strongly electron-withdrawing β-diketonato ligand from Ti^{IV} core with a relative electron-donating β-diketonato ligand will lessen the electrophilic nature of the electron starved Ti^{IV} core, thereby stabilizing it.

For both of reactions (**223-152, 225-151**) the entropy of activation were found to be large positive values, implying a dissociative mechanism of substitution. Scheme 3.22 shows two kinetically indistinguishable mechanisms that satisfy the observed rate law.

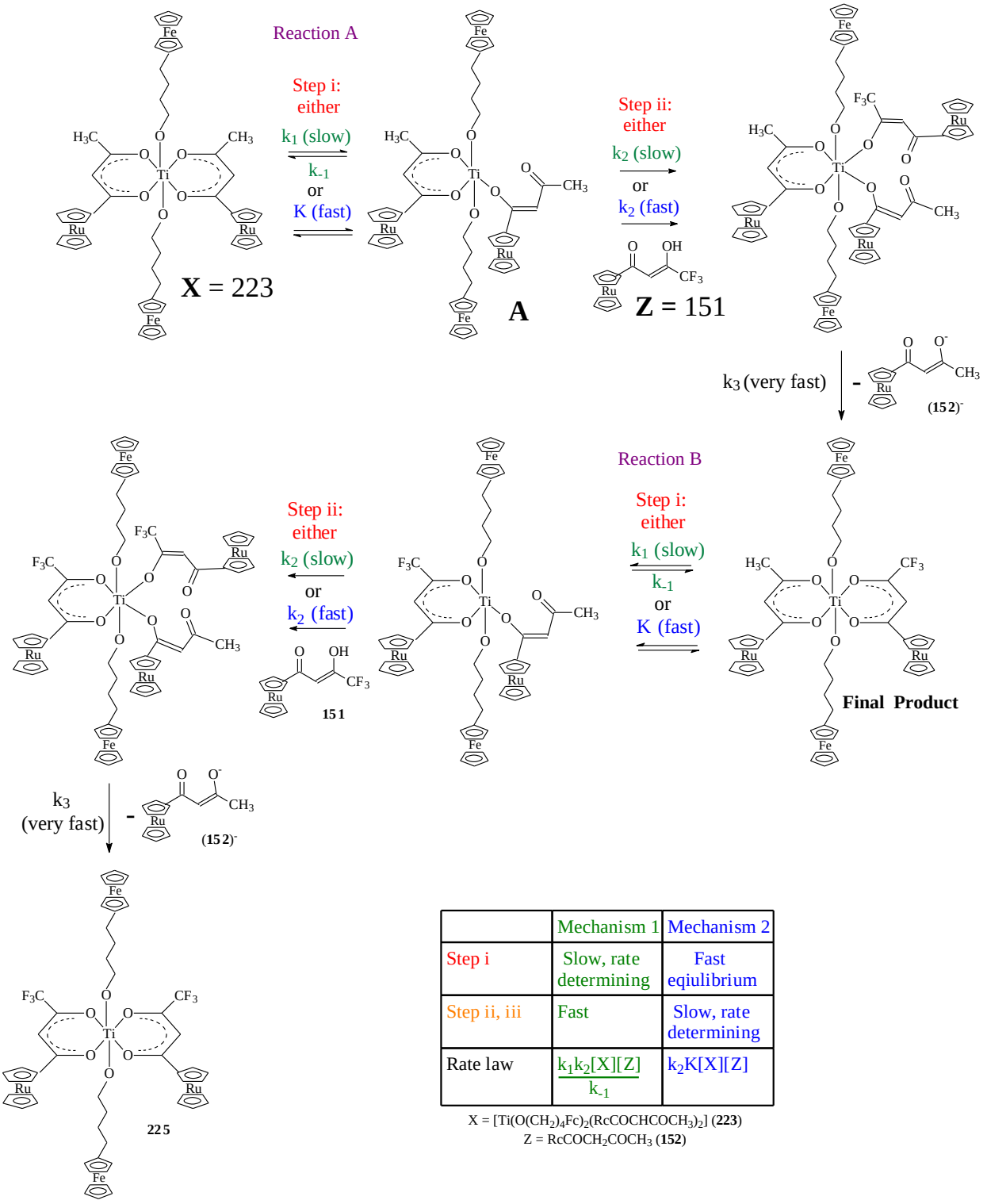

	Mechanism 1	Mechanism 2
Step i	Slow, rate determining	Fast eqiulibrium
Step ii, iii	Fast	Slow, rate determining
Rate law	$\frac{k_1 k_2[X][Z]}{k_{-1}}$	$k_2K[X][Z]$

X = $[Ti(O(CH_2)_4Fc)_2(RcCOCHCOCH_3)_2]$ (**223**)
Z = $RcCOCH_2COCH_3$ (**152**)

Scheme 3.22. Schematic representation of the proposed dissociative mechanism for the substitution reactions between $[Ti(O(CH_2)_4Fc)_2(RcCOCHCOCH_3)_2]$ (**223**) with $RcCOCH_2COCF_3$ (**151**) with the first substitution of $[Ti(O(CH_2)_4Fc)_2(RcCOCHCOCH_3)_2]$ (**223**) with $RcCOCH_2COCF_3$ (**152**), used as an example.

To derive the rate laws shown in the rectangle in Scheme 3.22, it is convient to consider the following equivalent mechanisms where the compounds have been substituted with symbols X, A and Z. The k_3 step is not considered, as it is so fast, it has no rate determining meaning.

$$X \underset{k_{-1}}{\overset{k_1}{\rightleftharpoons}} A \text{ (slow)} \qquad A + Z \xrightarrow{k_2} \text{products (fast)} \xrightarrow{k_3} \text{final products (very fast)}$$

Mechanism 1

or

$$X \underset{}{\overset{K}{\rightleftharpoons}} A \text{ (fast)} \qquad A + Z \xrightarrow{k_2} \text{products (slow)} \xrightarrow{k_3} \text{final products (very fast)}$$

Mechanism 2

For Mechanism 1, the rate law is derived as follows:

$$\frac{d}{dt}[\text{Products}] = k_2[A][Z] \qquad \text{- - - (1)}$$

By applying the principle of steady state to the intermediate A, it follows that:

$$\frac{d}{dt}[A] = 0 \text{ and } \quad k_1[X] = k_{-1}[A] + k_2[A][Z]$$

$$[A] = \frac{k_1[X]}{k_{-1} + k_2[Z]} \qquad \text{- - - (2)}$$

By substituting (2) into (1) it follows that:

$$\frac{d}{dt}[\text{Products}] = \frac{k_1k_2[X][Z]}{k_{-1} + k_2[Z]}$$

$$= \frac{k_1k_2}{k_{-1}}[X][Z] \qquad \text{provided that } k_{-1} >> k_2[Z] \quad \text{- - - (3)}$$

$$= k_A[X][Z]$$

Here k_A is the experimentally deterimined rate constants $k_A = \frac{k_2k_1}{k_{-1}}$ for reaction A, Scheme 3.22. k_B has the same form.

For Mechanism 2 the rate law is derived as follows:

$$K = \frac{[A]}{[X]} \qquad \text{thus } [A] = K[X]$$

$$\frac{d}{dt}[\text{Products}] = k_2[A][Z]$$

$$= k_2K[X][Z] \qquad \text{- - - (4)}$$

$$= k_A[X][Z] \qquad \text{with } k_A = k_2K$$

For both mechanisms it follows that k_A and k_B should be independent of the leaving β-diketonato. Kinetically equation (3) and (4) is equivalent, both confirming the experimentally determined rate law.

Another possible option for the mechanism is a type of interchange, where the presence of the incoming ligand cause the leaving ligand to dissociate completely before the incoming

ligand attacks the Ti-complex and the intermediate Ti-complex is a four coordinated specie. This is, however, very unlikely. Such a mechanism would also imply that the presence of free leaving β-diketonato would slow down the substitution reaction rate.

The mechanism derived for Scheme 3.22, showed that the leaving ligand does not delay the reaction. To confirm this, the kinetics describing the influence of the leaving ligand was investigated. This study was preformed by reacting 7.74 x 10^{-5} mol dm^{-3} $[Ti(O(CH_2)_4Fc)_2(RcCOCHCOR)_2]$ {R = CH_3 (**223**), CF_3 (**225**)}, with 7.74 x 10^{-3} mol dm^{-3} $RcCOCH_2COR$ {R = CF_3 (**151**), CH_3 (**152**)}in the presence of the leaving ligand $RcCOCH_2COR$ {R = CH_3 (**152**), CF_3 (**151**)} with concentrations ranging from 0, 7.74 x 10^{-4}, 1.55 x 10^{-3} and 3.10 x 10^{-3} mol dm^{-3} at 25˚C. Table 3.16 summarises the results obtained.

Table 3.16. The second order rate constants (k_2) for substitution reactions of $[Ti(O(CH_2)_4Fc)_2(RcCOCHCOR)_2]$ {R = CH_3 (**223**), CF_3 (**225**)}, with $RcCOCH_2COR$ {R = CF_3 (**151**), CH_3 (**152**)}in the presence of the leaving ligand $RcCOCH_2COR$ {R = CH_3 (**152**), CF_3 (**151**)} at T = 25˚C for reaction steps A and B according to Scheme 3.22. Standard deviations are given in brackets.

Leaving ligand (R); 10^4[ ]	10^5 k_{obsA} ; k_{obsB}	Leaving ligand (R); 10^4[ ]	10^5 k_{obsA} ; k_{obsB}
$[Ti(O(CH_2)_4Fc)_2(RcCOCHCOCH_3)_2]$, (**223**) + $RcCOCH_2COCF_3$ (**151**)		$[Ti(O(CH_2)_4Fc)_2(RcCOCHCOCF_3)_2]$, (**225**) + $RcCOCH_2COCH_3$ (**152**)	
(1); 0	240(5); 13(4)	(1); 0	385(1); 20(7)
(1); 7.74	232(2); 12(3)	(1); 7.74	381(6); 19(3)
(1); 15.5	229(5); 11(3)	(1); 15.5	377(9); 18(3)
(1); 31.0	224(3); 10(2)	(1); 31.0	374(6); 18(2)

Inspection of k_{obs} values in Table 3.16 revealed that the reaction rate in essence is independent of the leaving β-diketonato ligand.

3.5.3.5. Ligand exchange of ruthenocene-containing β-diketones

Under the pseudo first order conditions followed in section 3.5.3.4, the reaction can not be stopped at the transition state. However, when **223** and **225** are mixed in equimolar concentrations that is under second order conditions, the transition state should in principle be obtained. To explore this single stage process, the ligand exchange reactions of the bi-chelating ruthenocene-containing β-diketonato ligand between **223** and **225** were studied spectroscopically by ^{1}H NMR and UV/Vis (see Scheme 3.23 for the reaction), under second order conditions.

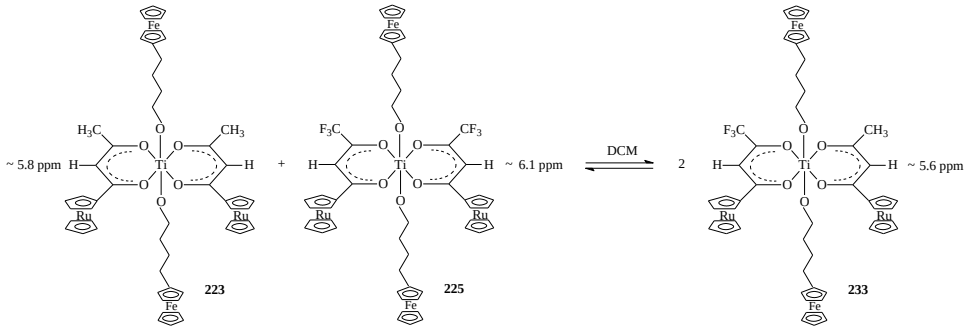

Scheme 3.23. Schematic representation of the ligand exchange reactions between **223** and **225**.

The reaction solution was made up as a solution containing equimolar amounts of **223** and **225** (i.e. [**223**] = [**225**]) in CD_2Cl_2 and the ^1H NMR was recorded with regular time intervals. It was found that the reaction between **223** and **225** yielding **233** is an equilibrium process, does not go to completion within 3 days. The partial ^1H NMR spectra (of the methine region around 6 ppm) obtained 120 s after dissolving **223** and **225** in CD_2Cl_2 and at $t = \infty$ (about 3 days) are shown in Figure 3.27.

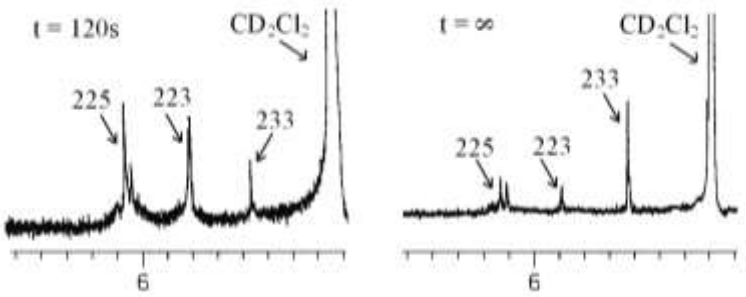

Figure 3.27. ^1H NMR of the ligand exchange reactions in CD_2Cl_2 at t = 120s and $t = \infty$ of **223** and **225**. [**223**] = [**225**] = 1.75 x 10^{-4} mol dm^{-3}.

Because the reaction between **223** and **225** was conducted with equal concentrations, a second order reaction was expected. However, the data obtained was found to fit the first order kinetic model according to Equation 3.6 (p 104). Results obtained for the ligand exchange reaction are given in Table 3.17 and comparative graphs are shown in Figure 3.28.

For the ligand exchange of the bi-chelating β-diketonato ligands between **223** and **225**, it was found that the reaction was an equilibrium, which is similar to what Fay and co-workers found for similar reactions.[20] The deviation of the equilibrium constant from the statistical value of 4 for the random scrambling of ligands can be rationalized in terms of an electrostatic model. It has been shown by Marcus and co-workers,[27] that electrostatic effects always stabilize mixed-ligand complexes relative to the parent complexes whenever the charges on the two exchanging ligands are unequal. This implies the average ligand-ligand repulsion energy is less for the mixed

complexes than for the starting materials. The effective charges on the donor oxygen atoms of the β-diketonate ligands which carry no and one CF_3 groups will differ because of the inductive effect of the fluorine atoms.

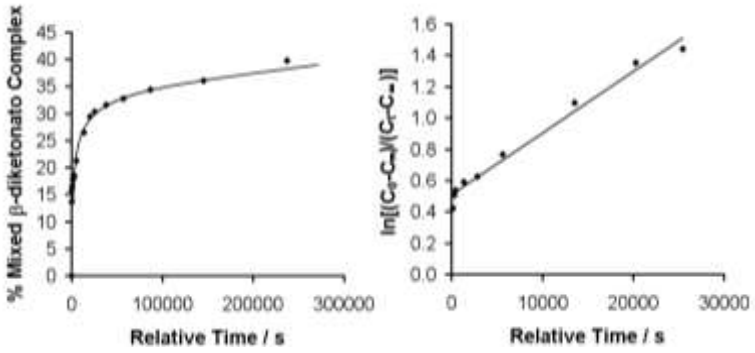

Figure 3.28. Graphs of the ligand exchange reaction between **223** and **225** in CD_2Cl_2 at 20˚C.

Table 3.17. Data for the ligand exchange reaction between **223** and **225** in CD_2Cl_2 at 20˚C, utilising ^1H NMR spectroscopy and in CH_2Cl_2 utilising UV/Vis spectroscopy.

^1H NMR	$10^5\ k_{obs}$ / s^{-1}	% product at equilibrium	K_c in CD_2Cl_2	ΔG / kJ mol^{-1}
	4.39(2)	39.8	1.51	-1008

	T / K	$10^5\ k_2$ / s^{-1}	λ_{exp} / nm	ΔH^* / kJ mol^{-1}	ΔS^* / J K^{-1} mol^{-1}	ΔG^* / kJ mol^{-1}
UV/Vis	278	0.12	359	99(2)	8(6)	96(3)
	293	4.21				
	303	12.1				

This reaction was also followed by UV/Vis spectroscopy. The rate constants obtained are summerised in Table 3.17 and the comparative graphs are shown in Figure 3.29.

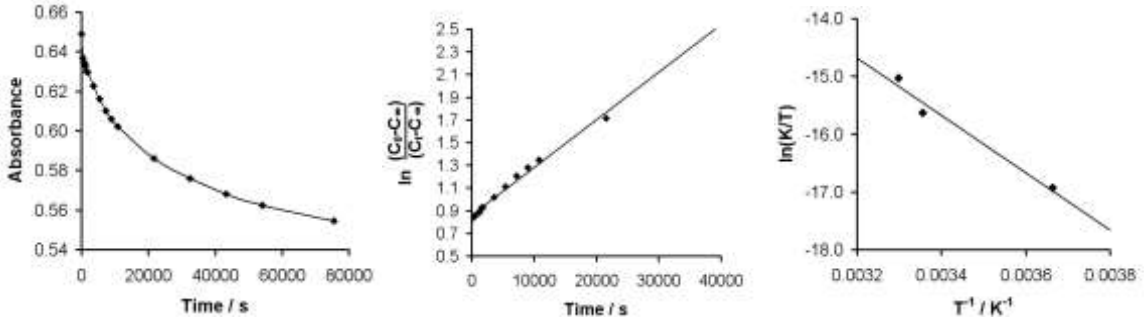

Figure 3.29. Left: Time trace at 358 nm of the ligand exchange reaction between **223** and **225**. Middel: A first order kinetic plot of data for this process that leads to the observed first order rate constant k_{obs}. Right: Eyring plot for the ligand exchange reaction between **223** and **225**. From these plots the activation parameters ΔH^* and ΔS^* (Table 3.17) could be obtained from the intercept of the plot with x-axis as well as the gradient of the graph.

The explanation for the first order behaviour of this reaction under second order conditions lies in the mechanism of the reaction. The positive entropy value implies that the mechanism of ligand exchange is dissociative of nature. A proposed mechanism is shown in Scheme 3.24.

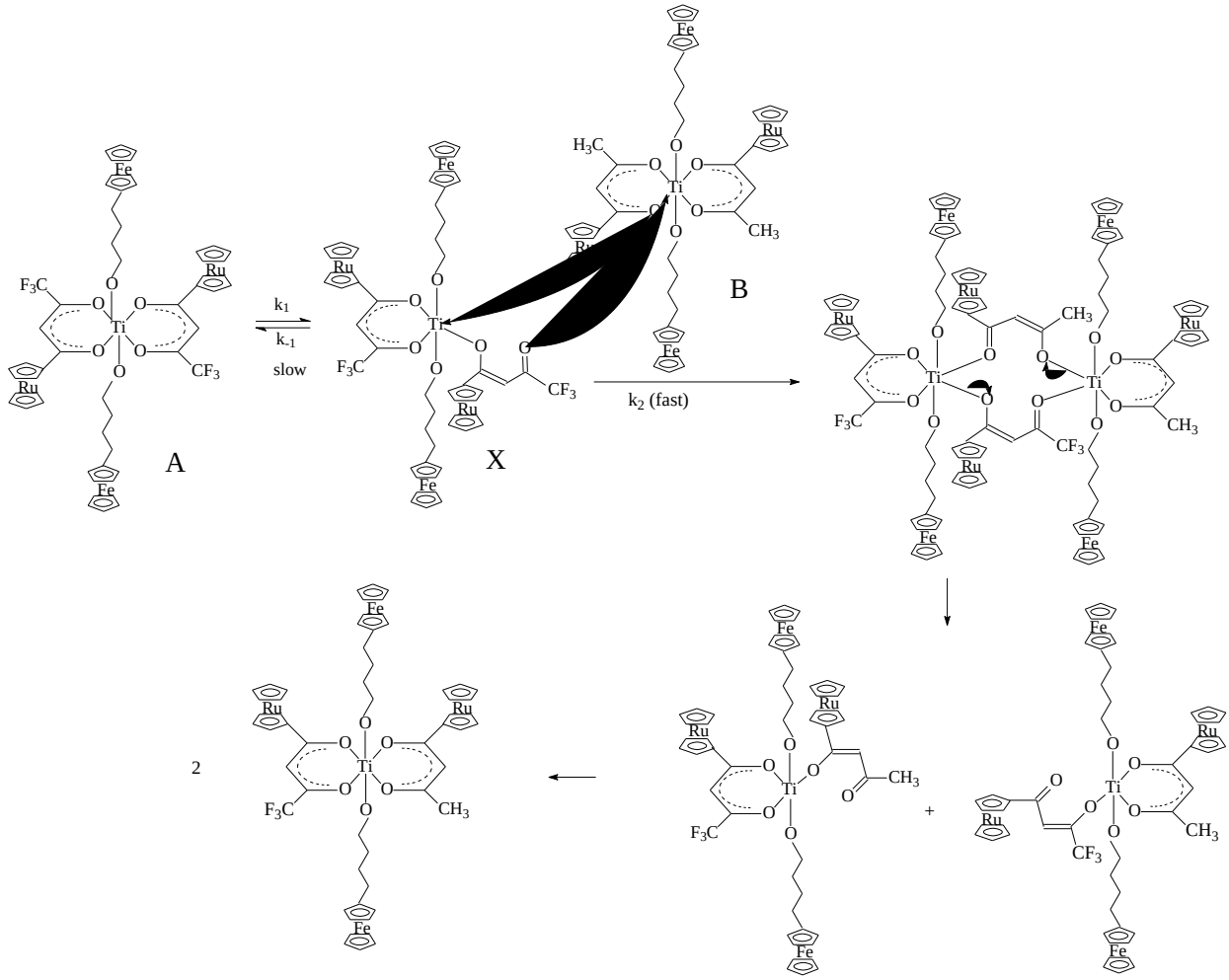

Scheme 3.24. Schematic representation of the proposed dissociative mechanism for the ligand exchange reaction between **223** and **225**.

The above mechanism in essence reduces to:

$$A \underset{k_{-1}}{\overset{\text{slow } k_1}{\rightleftharpoons}} X$$

$$X + B \xrightarrow[\text{fast}]{k_2} \text{prodcuts}$$

To derive a rate law for this mechanism,

$$\frac{d}{dt}\text{Products} = k_2[X][B] \qquad \text{- - - (1)}$$

By applying steady state conditions to X, it follows that $\frac{d[X]}{dt} = 0$ implying:

$$k_1[A] = k_{-1}[X] + k_2[X][B]$$

$$[X] = \frac{k_1[A]}{k_{-1} + k_2[B]} \qquad \text{- - - (2)}$$

By substituting (2) into (1) it follows that:

$$\frac{d}{dt}\text{Products} = \frac{k_2k_1[A][B]}{k_{-1} + k_2[B]} \qquad \text{- - - (3)}$$

On the assumption that $k_2[B] >> k_{-1}$, equation (3) reduces to:

$$\frac{d}{dt}\text{Products} = \frac{k_2k_1[A][B]}{k_2[B]} = k_1[A]^1$$

This theoretical first order rate law is applicable to the proposed mechanism and is consistent with the experimentally observed rate law of

$$\frac{d}{dt}[\mathbf{223}] = k_{obs}[\text{reactants}]^1$$

3.5.4. Aqueous stability and hydrolyses rates

3.5.4.1. Introduction

The titanium complexes of this study are all new and one of the reasons they were targeted for study, is to see if the presence of the ruthenocenyl moiety in its structure would not give it superior anti-cancer activity than the budotitane family of titanium complexes and titanocene dichloride, both compounds currently in phase II clinical trails. A severe drawback of the budotitane family of titanium complexes is the rate at which it hydrolysis in the presence of water according to the reaction in Scheme 3.25. Table 3.18 shows the times until precipitation starts of a few known complexes.

$$[Ti(\beta\text{-diketonato})_2X_2] \overset{H_2O}{\rightleftharpoons} [Ti(H_2O)(\beta\text{-diketonato})_2X]^+X^- \rightleftharpoons$$

$$[Ti(OH)(\beta\text{-diketonato})_2X] + HX \overset{H_2O}{\rightleftharpoons} [Ti(OH)(H_2O)(\beta\text{-diketonato})_2]^+X^- \rightleftharpoons$$

$$[Ti(OH)_2(\beta\text{-diketonato})_2] + HX \overset{-H_2O}{\rightleftharpoons} \text{polymers} \longrightarrow\!\!\!\!\!\!\rightarrow TiO_2$$

Scheme 3.25. Scheme of the hydrolysis of $[Ti(X)_2(PhCOCHCOCH_3)_2]$ with X = OEt or halogen.[28]

Table 3.18. The time from dissolving in water until presipitation sets in for different bis-β-diketonato titanium complexes.

Complex	Time until precipitation sets in[a]
$[Ti(OEt)_2(PhCOCHCOCH_3)_2]$	2.5 h
$[Ti(OEt)_2(CH_3COCHCOCH_3)_2]$	1.5 h
$[Ti(Cl)_2(PhCOCHCOCH_3)_2]$	10 s
$[Ti(Cl)_2(CH_3COCHCOCH_3)_2]$	5 s
$[Ti(Br)_2(PhCOCHCOCH_3)_2]$	5 s
$[Ti(Br)_2(CH_3COCHCOCH_3)_2]$	2 s

[a] 5µl H_2O added to a solution of 0.02 M of titanium complex in 30 ml ethanol.

3.5.4.2. Aqueous stability in H_2O/CH_3CN mixtures

In this section the kinetics of hydrolysis by way of analogy to Scheme 3.25 of $[Ti(O(CH_2)_4Fc)_2(RcCOCHCOR)_2]$ {CF_3 (**225**), C_6F_5 (**226**), CH_3 (**223**), Rc (**228**) and Fc (**229**)} is reported. The way the hydrolysis kinetics was studied, consists of dissolving the titanium complexes into solvent consisting of 2, 10 and 50g H_2O in CH_3CN made up to 100 ml solution. Figure 3.30 shows a typical time trace, graphs of k_{obs} *vs* $[H_2O]$ and the temperature dependence of these kinds of hydrolysis reactions utilising $[Ti(O(CH_2)_4Fc)_2(RcCOCHCOCH_3)_2]$ (**223**) as an example. Kinetic data are summarised in Table 3.19.

The dependence of the second order rate constant of the hydrolysis of the titanium complexes $[Ti(O(CH_2)_4Fc)_2(RcCOCHCOR)_2]$ with the group electronegativity of the R-group on the β-diketonato ligand as well as with the free β-diketone pK_a' are demonstrated in Figure 3.31. As the group electronegativity of the R-group increases, the second order rate constant also increased. In contrast, the second order hydrolysis rate constant decreased as the pK_a' of the free β-diketone increased (Figure 3.31). Both observations are consistent with the view that the more electron-withdrawing the R-group (such as CF_3), the more positive the titanium centre of the complex becomes and therefore the more susceptible towards the hydrolysis (nucleophilic attack of water) it becomes. The entropy of activation for all complexes is the same since in all cases water was the incoming ligand. The value of 55.5 J K^{-1} mol^{-1}, is a large positive value, and imply a dissociative hydrolysis mechanism.

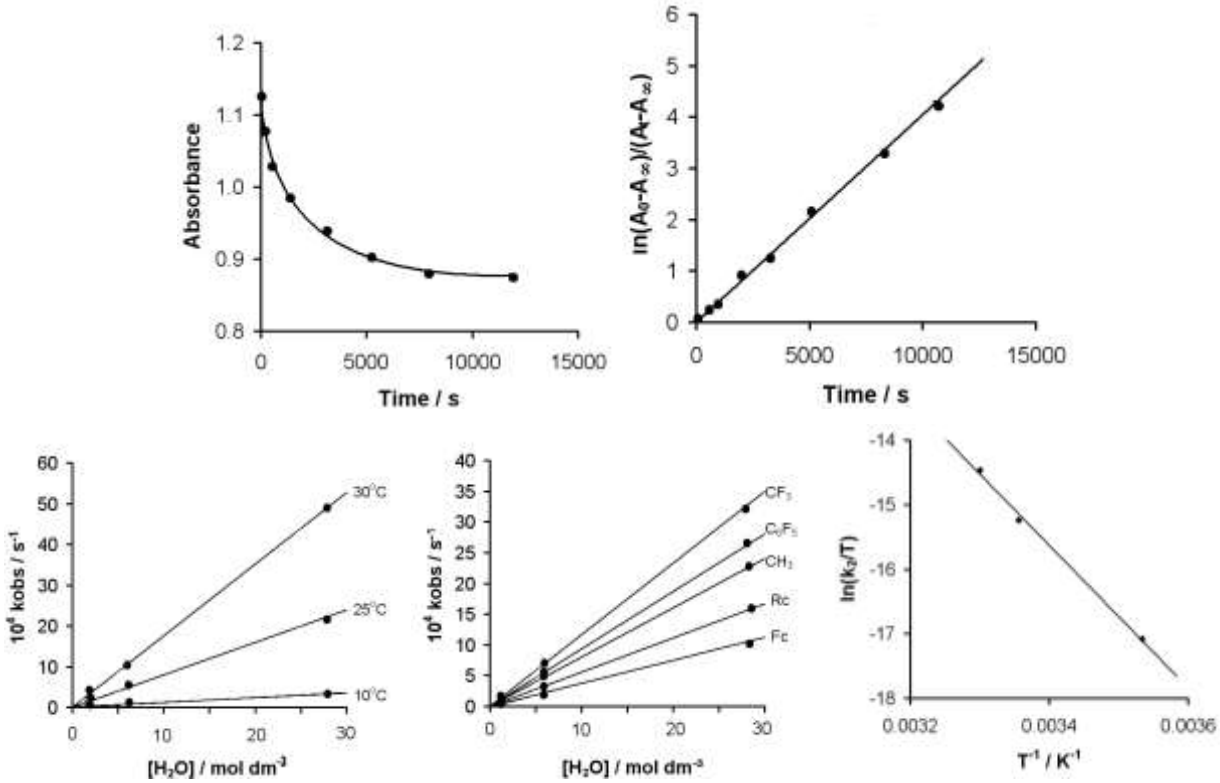

Figure 3.30. Top Left: Time trace at 350 nm of the hydrolysis of **223** at 25˚C and $[H_2O]$ = 5.56 mol dm^{-3} (10g) in CH_3CN. Top Right: A first order kinetic plot of data for this process that leads to the observed first order rate constant, k_{obs}. Bottom Left: Graph of k_{obs} *vs* $[H_2O]$ of **223** and graph of k_{obs} *vs* $[H_2O]$ of **223, 225, 226, 228** and **229** at 25˚C and $[H_2O]$ = 5.56 mol dm^{-3} (10g) (Bottom Middel). Bottom Right: The graph of *ln* (k_2/T) *vs* 1/T for the hydrolysis of $[Ti(O(CH_2)_4Fc)_2(RcCOCHCOCH_3)_2]$ (**223**) at T = 10˚C, 25˚C and 30˚C, for reaction A and B. [Ti-complex] = 0.0001 mol dm^{-3}.

Table 3.19. The second order rate constants (k_2) and the activation parameters for the hydrolysis of $[Ti(O(CH_2)_4Fc)_2(RcCOCHCOR)_2]$ {R = CF_3 (**225**), C_6F_5 (**226**), CH_3 (**223**), Rc (**228**) and Fc (**229**)} at T = 25˚C in H_2O/CH_3CN solvent mixtures. Apparent group electronegativities are also given. Standard deviations are given in brackets.

R-group	χ_R	$10^4 k_2$ / dm^3 mol^{-1} s^{-1}	ΔH^* / kJ mol^{-1}	ΔS^* / J K^{-1} mol^{-1}	ΔG^* / kJ mol^{-1}	$t_{½}$ [a] / s	t precipitation[b]
225: CF_3	3.01	5.82(2)	70(2)	55.5(3)	53(4)	309	4 h
226: C_6F_5	2.46	4.67(4)	30(6)	55.5(2)	13(4)	385	5.5 h
223: CH_3	2.34	4.00(1)	91(1)	55.5(2)	75(3)	450	7 h
228: Rc	1.99	2.78(3)	75(3)	55.5(1)	58(4)	647	9 h
229: Fc	1.87	1.87(4)	176(2)	55.5(3)	159(2)	962	10 h

a) Halflife for hydrolysis in 10g H_2O made up to 100 ml CH_3CN solution, [Ti-complex] = 0.0001 mol dm^{-3}.

b) Time until first precipitation was observed.

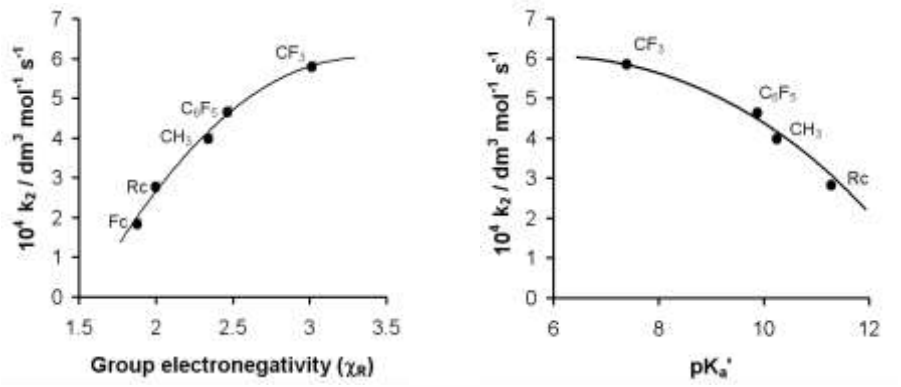

Figure 3.31. Left: Graph of group electronegativity of the R-group on the β-diketonato ligand *vs* second order rate constant of the hydrolysis of $[Ti(O(CH_2)_4Fc)_2(RcCOCHCOR)_2]$ {R = CF_3 (**225**), C_6F_5 (**226**), CH_3 (**223**), Rc (**228**) and Fc (**229**)} in CH_3CN. Right: Graph of pK_a' of the free β-diketone *vs* second order rate constant of the hydrolysis of $[Ti(O(CH_2)_4Fc)_2(RcCOCHCOR)_2]$ {R = CF_3 (**225**), C_6F_5 (**226**), CH_3 (**223**), Rc (**228**) and Fc (**229**)} in CH_3CN.

3.5.4.3. Aqueous stability in co-solvents

A drug intended for medical use in mammal must preferably be well soluble in water and relatively stable in terms of hydrolysis. If it is not soluble in water, a galenic formulation must be found to insure these properties. The titanium complexes of this study are much less susceptible to hydrolysis than previously known complexes, but for all practical purposes they are insoluble in water. Making use of a "co-solvent" system, which contains the titanium complex, Cremophor and propylene glycol (in mass ratio 1:9:1) produces micelles when dissolved in water. These micelles surround the titanium complexes, protecting it from hydrolysis and making it water-soluble. Utilizing this formulation 0.0001 mol dm^{-3} titanium complex concentration could be dissolved with ease in a solvent system containing 98% water. The other 2% is made up of the titanium complex, Cremophor and propylene glycol.

In this section the aqueous stability of $[Ti(O(CH_2)_nFc)_2(RcCOCHCOR)_2]$ { n = 1 (**220**), 2 (**221**), 3 (**222**), 4 (**223**), R = CH_3 and n = 4, R = $C_{10}F_{21}$ (**224**), CF_3 (**225**), C_6F_5 (**226**), $C_{10}H_{21}$ (**227**), CH_3 (**223**), Rc (**228**) and Fc (**229**)}in the described co-solvent system is reported. An overlay spectrum demonstrating the change in absorbance as hydrolysis takes place in the wavelength region 250-600 nm, of the thus micelle-protected complex is shown for $[Ti(O(CH_2)_4Fc)_2(RcCOCHCOCH_3)_2]$ (**223**) in Figure 3.32 and data for all complexes are summarized in Table 3.20. It can be seen that the stability is given here over several hours. Precipitation is only observed after several days and hence the requirements for good systematic activity in pharmacological and toxicological studies are complied with.

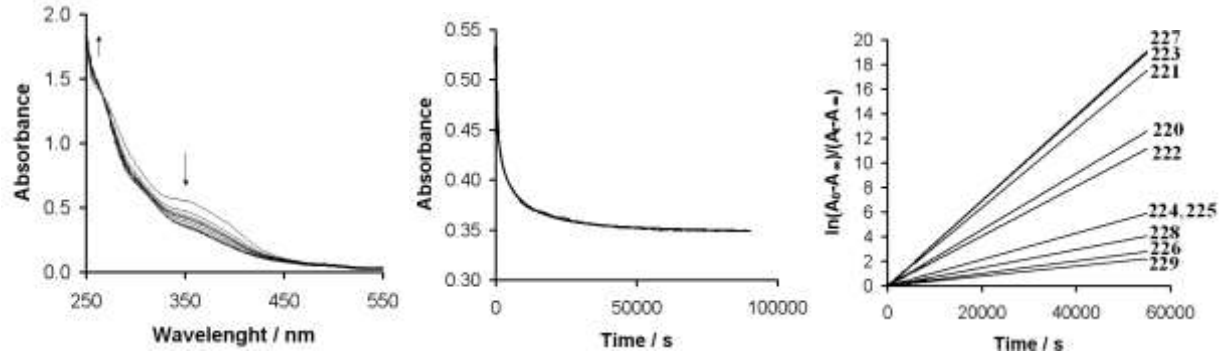

Figure 3.32. Left: Overlay spectra demonstrating change in absorbance as hydrolysis of the galenic form of $[Ti(O(CH_2)_4Fc)_2(RcCOCHCOCH_3)_2]$ (**223**) at T = 37˚C, 2% co-solvent (Ti-complex in galenic form) by weight in water at 351 nm takes place. Middel: Normal time tracefor the hydrolyses process of **223** at λ = 350 nm. Right: A kinetic plot of data for this process that leads to the observed first order rate constant k_{obs} of **220**-**229**.

Table 3.20. The observed rate constants (k_{obs}) and the experimental wavelength for the hydrolysis of $[Ti(O(CH_2)_nFc)_2(RcCOCHCOR)_2]$ {n = 1 (**220**), 2 (**221**), 3 (**222**), 4 (**223**), R = CH_3 and n = 4, R = $C_{10}F_{21}$ (**224**), CF_3 (**225**), C_6F_5 (**226**), $C_{10}H_{21}$ (**227**), CH_3 (**223**), Rc (**228**) and Fc (**229**)} at T = 37˚C .

Complex	λ_{exp} nm	10^5 k_{obs} / s^{-1}	$t_{½}$ / h	Time until precipitation sets in
224: $[Ti(O\{CH_2\}_4Fc)_2(RcCOCHCOC_{10}F_{21})_2]$	351	10.8(2)	1.78	5 days
225: $[Ti(O\{CH_2\}_4Fc)_2(RcCOCHCOCF_3)_2]$	344	10.7(5)	1.80	5 days
226: $[Ti(O\{CH_2\}_4Fc)_2(RcCOCHCOC_6F_5)_2]$	348	5.1(2)	3.78	> 7 days
227: $[Ti(O\{CH_2\}_4Fc)_2(RcCOCHCOC_{10}H_{21})_2]$	351	34.7(3)	0.55	3 days
223: $[Ti(O\{CH_2\}_4Fc)_2(RcCOCHCOCH_3)_2]$	350	34.4(4)	0.56	3 days
228: $[Ti(O\{CH_2\}_4Fc)_2(RcCOCHCORc)_2]$	328	7.1(4)	2.76	> 7 days
229: $[Ti(O\{CH_2\}_4Fc)_2(RcCOCHCOFc)_2]$	303	4.1(4)	4.70	> 7 days
220: $[Ti(O\{CH_2\}_1Fc)_2(RcCOCHCOCH_3)_2]$	379	22.9(3)	0.84	4 days
221: $[Ti(O\{CH_2\}_2Fc)_2(RcCOCHCOCH_3)_2]$	343	31.8(6)	0.61	4 days
222: $[Ti(O\{CH_2\}_3Fc)_2(RcCOCHCOCH_3)_2]$	350	20.3(3)	0.95	4 days

From Tabel 3.20 it is clear that the kinetic process that was followed in the described kinetic study does not lead to the product which ultimately precipitated because the time to precipitation is so much more than the half life of the studied kinetic process. Further research is required to prove exactly what product was first formed during hydrolysis and what precipitated. However, it is reasonable to assume that the charged species shown in Scheme 3.25 would not precipitate from water. It is expected that the precipitating species may be $[Ti(OH)_2(\beta\text{-diketonato})_2]$, polymers of it or more likely $[Ti(OH)_2(O(CH_2)_nFc)_2]$. From section 3.5.3.3, Table 3.13 (p 113) and section 3.5.3.4, Table 3.15 (p 121), it appears that β-diketonato substitution takes place one order of magnitude faster than alkoxide substitution.

3.6. Electrochemistry

3.6.1. Introduction

Cyclic voltammetry (CV), Oster Young square wave voltammerty (SW) and linear sweep voltammetry (LSV) were conducted on all complexes synthesised. The effect (if any) of the alkyl chain length (n) and the group electronegativity (χ_R) of substituents on the formal reduction potential of the redox active metallic nuclea of the complex were determined.

The metallic redox active centres studied in the synthesised complex are Ti^{4+}/Ti^{3+}, $2Rc/[2Rc^{+} \rightleftharpoons (Rc_2)^{2+}]$ and Fc/Fc^{+}. These redox active couples vary from being electrochemically reversible (theoretically this implies $\Delta E = 59$ mV but experimentally taken as $\Delta E < 90$ mV in this study), quasi-reversible (defined for the purpose of this study as 90 mV $< \Delta E <$ 150 mV) to irreversible (defined as $\Delta E >$ 150 mV). Formal redox potentials (E^{01}), peak cathodic potentials (E_{pc}) and peak anodic potentials (E_{pa}) are reported *vs* Fc/Fc^{+} as an internal standard, but were measured experimentally *vs* an in-house constructed Ag/AgCl reference electrode to minimise overpotentials and liquid junction potentials.

3.6.2. Ruthenocene

Since this study is focused on the use of ruthenocene- and ferrocene-containing ligands, the first step of an electrochemical study involving the present titanium complexes is a study of the parent metallocene ligands. The reversible electrochemistry of ferrocene according to the reaction $Fc \rightleftharpoons Fc^{+} + e^{-}$ is well known, but that of ruthenocene was only resently clarified by Geiger and co-workers,[29] which studied the electrochemistry of ruthenocene with cyclic voltammetry in $CH_2Cl_2/[NBu_4][B(C_6F_5)_4]$. They found that $Ru(C_5H_5)_2$ (**19**) can be oxidised to $[Ru(C_5H_5)_2]^{+}$, (**168**), and that the 17 electron ruthenocenium cation is in equilibrium with the dimeric cationic species $[Ru(C_5H_5)_2]_2^{2+}$, (**169**), under their experimental conditions (Figure 3.33).[29] The reduction of **169** is observed as an irreversible cathodic wave at -181 mV (Scan rate 200 mV s^{-1}) *vs* Fc/Fc^{+}. This cyclic voltammetry was repeated here and since our results were found to be mutually consistent with that found by Geiger (Figure 3.33 and Table 3.21), the results of all the new ruthenocene-containing complexes are reported with confidence.

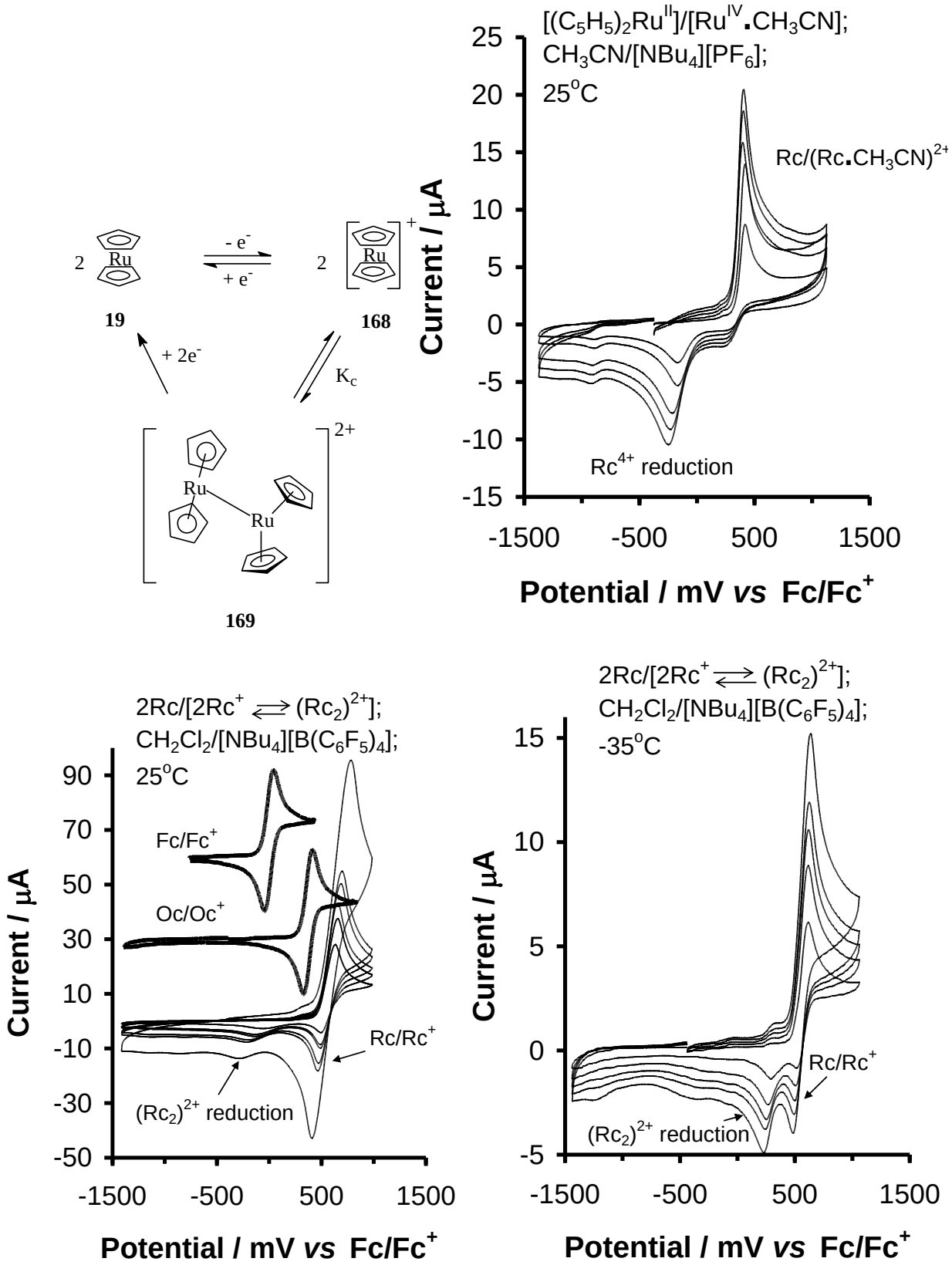

Figure 3.33. Top Left: Equilibrium between **19, 168** and **169**. Top Right: CV's of ruthenocene in CH_3CN/0.1 mol dm^{-3} $[NBu_4][PF_6]$, T = 25ºC. Bottom: CV's of ruthenocene (Rc), ferrocene (Fc at 300 mV s^{-1}) and osmocene (Oc at 300 mV s^{-1}) in CH_2Cl_2/0.1 mol dm^{-3} $[NBu_4][B(C_6F_5)_4]$, T = 25ºC (Left) and -35ºC (Right), v = 100, 200, 300, 400 and 500 mV s^{-1} (only at 25ºC).

Table 3.21. The cyclic voltammetry data obtained from voltammograms (potentials *vs* Fc/Fc^{+}) of (A) ferrocene, osmocene and ruthenocene measured in CH_2Cl_2/0.1 mol dm^{-3} $[NBu_4][B(C_6F_5)_4]$ with a glassy carbon working electrode at 25ºC and (B) at -35ºC, and (C) in CH_3CN/0.1 mol dm^{-3} $[NBu_4][PF_6]$ at 25ºC. Scan rates, E_{pa} (anodic peak potential), ΔE_p (difference between the anodic and cathodic peak potentials), E^{01} (formal reduction potentials), i_{pa} (anodic peak current) and i_{pa}/i_{pc} (anodic/cathodic peak current relationship) are shown. $E^{01} = (E_{pa} + E_{pc})/2$. The concentration of the metallocene was 2.0 mmol dm^{-3}.

v / mV s^{-1}	E_{pa} / mV	ΔE_p / mV	E^{01} / mV[a]	i_{pa} / μA	i_{pc}/i_{pa}	E_{pc} / mV	i_{pc} / μA
A:ferrocene at 300	45	90	0	35	1.00	-	-
A:osmocene at 300	427	104	375	36	0.98	-	-
	$[Ru(C_5H_5)_2]$, (**19**)/$[Ru(C_5H_5)_2]^+$, (**169**)					$[(Ru(C_5H_5)_2)_2]^{2+}$, (**169**)	
A: 25˚C; 50	687	78	648	33.6	0.44	-63	2.8
A: 25˚C; 100	701	87	658	42.5	0.48	-88	3.9
A: 25˚C; 200	718	100	668	51.4	0.52	-113	5.1
A: 25˚C; 300	728	119	668	60.3	0.55	-137	6.1
A: 25˚C; 400	736	131	671	69.2	0.59	-162	7.3
A: 25˚C; 500	746	143	675	78.2	0.63	-188	8.4
B: -35˚C; 50	646	100	596	5.7	0.57	325	2.7
B: -35˚C; 100	647	105	595	7.2	0.57	318	2.9
B: -35˚C; 200	647	114	590	8.8	0.58	293	3.2
B: -35˚C; 300	650	124	588	10.3	0.58	280	3.4
B: -35˚C; 400	658	136	590	11.9	0.59	270	3.7
B: -35˚C; 500	667	155	590	13.3	0.60	256	4.0
C: 25˚C; 50	470	-	-	6.9	-	-115[a]	3.1[a]
C: 25˚C; 100	472	-	-	9.1	-	-123[a]	4.2[a]
C: 25˚C; 200	476	-	-	11.3	-	-131[a]	5.3[a]
C: 25˚C; 300	477	-	-	13.5	-	-139[a]	6.5[a]
C: 25˚C; 400	482	-	-	15.7	-	-154[a]	7.6[a]
C: 25˚C; 500	485	-	-	17.9	-	-171[a]	8.8[a]

a) In CH_3CN $(Ru(C_5H_5))_2^{2+}$ does not exist. Since $((C_5H_5)_2Ru^{IV}CH_3CN)^{2+}$ is known to exist, this peak is tentatively assigned to the reduction of this Ru^{IV} species.

As can be seen from Table 3.21 and Figure 3.33 (Top, Right), the CV of ruthenocene in CH_3CN/0.1 mol dm^{-3} $[NBu_4][PF_6]$ system is complex and electrochemically irrevesible. The Rc oxidation wave is considered to generate a Ru^{IV} species at ± 470 mV.[30] The reduction wave at -200 mV is associated with the reduction of $[(C_5H_5)_2Ru^{IV}(CH_3CN)]^{2+}$ in analogy with osmocene.[31] However, in $CH_2Cl_2/[NBu_4][B(C_6F_5)_4]$ at 25ºC and scan rate 50 mV s^{-1}, ruthenocene

are electrochemically reversibly oxidised to Rc^+ and reduced back to Rc (Figure 3.33, Left). Since ΔE_p = 78 mV full electrochemical reversibility is implied. The Rc^+ species dimerise to $(Rc_2)^{2+}$ and reduction of this dimeric species is observed as a weak broadened peak at -63 to -188 mV *vs* Fc/Fc^+ depending on scan rate. At -35˚C (Figure 3.33, bottom Right) ruthenocene oxidation is quasi-reversible with ΔE_p = 100 mV, and is the result of the slower rate of electron transfer between electrode and Rc substrate at lower temperature. Strikingly evident is that at lower temperatures, the equilibrium $2Rc^+ \rightleftharpoons (Rc_2)^{2+}$ lies further in favour of the dimer. E_{pc} for the dimer is also shifted with ≈ 380 mV (at 50 mV s^{-1}) to more positive potentials and is attributed to slow electrode kinetics. It is important to note that Geiger under their conditions did not observe the $(Rc_2)^{2+}$ cathodic reduction at 25˚C. Seeing that ruthenocene in CH_2Cl_2/0.1 mol dm^{-3} $[NBu_4][B(C_6F_5)_4]$ at 25˚C and at -35˚C gave results that were well interpretable, this solvent system was used in further studies. The CH_2Cl_2/0.1 mol dm^{-3} $[NBu_4][B(C_6F_5)_4]$ system gave better interpretable results than $CH_3CN/[NBu_4][PF_6]$ because CH_2Cl_2 is less coordinating than CH_3CN and the $[B(C_6F_5)_4]^-$ anion is hyper uncoordinating while $[PF_6]^-$ is weakly coordinating.

3.6.3. Ruthenocene-containing β-Diketones

The electrochemistry of the ruthenocene-containing β-diketones $RcCOCH_2COR$ [where R = CF_3 (**152**), CH_3 (**151**), Rc (**155**) and Fc (**154**)], in $CH_3CN/[NBu_4][PF_6]$ were reported before.[17] In this study, the electrochemistry of all synthesised ruthenocene-containing β-diketones, $RcCOCH_2COR$ [where R = $C_{10}F_{21}$ (**177**), CF_3 (**152**), C_6F_5 (**178**), $C_{10}H_{21}$ (**179**), CH_3 (**151**), Rc (**155**) and Fc (**154**)], were studied in $CH_2Cl_2/[NBu_4][B(C_6F_5)_4]$. Analysis of the cyclic voltammetry data of the ruthenocene-containing β-diketones were very complex and quasi-reversible to irreversible electrochemistry was found for the $2Rc/[2Rc^+ \rightleftharpoons (Rc_2)^{2+}]$ fragment.

The first thing to decide was at what temperature should the β-diketones be studied. This was decided upon utilising [Rc-CO-CH_2-CO-CH_3 ⇌ Rc-CO-CH=C(OH)-CH_3], **151**.

Figure 3.34, left, shows the CV's of **151** at 25, -5, -35˚C. Utilising the 25˚C voltammograms, two clear ruthenocene-based oxidation peaks 1 and 2 were observed. Based on results that will be discussed shortly, these are assigned to the one-electron oxidation of the ruthenocenyl fragment of the enol (peak 1) and keto (peak 2) isomers of **151** respectively to the ruthenocenium, Rc^+, fragment. The cathodic reduction of waves of $\mathbf{151}^+$, peak 3, are only observed at fast scan rates (2000 mV s^{-1}). In analogy with the parent metallocene, ruthenocene, see Figure 3.33, this is regarded as the reduction of the Rc^+ fragment. However, in analogy to ruthenocene itself, it is expected that $\mathbf{151}^+$ must dimerise to form $(\mathbf{151})_2^{2+}$ according to Scheme

3.26. If the equilibrium between these oxidized monomers and dimers are slow, one would expect two peaks for the reduction of the dimer, one corresponding to keto $(\mathbf{151})_2^{2+}$ reduction and one to enol $(\mathbf{151})_2^{2+}$ reduction. At fast scan rates two very broad peaks X and Y are observed (Figure 3.34). In analogy to ruthenocene itself, peaks X and Y are considered as consistent with the separate reduction of keto $(\mathbf{151})_2^{2+}$ and enol $(\mathbf{151})_2^{2+}$ respectively. The reduction waves X and Y are poorly observable due to the broadness of each peak. This is consistent with many different keto and enol isomers of $(\mathbf{151})_2^{2+}$ existing simultaneously and in equilibrium with each other as explained in Scheme 3.26.

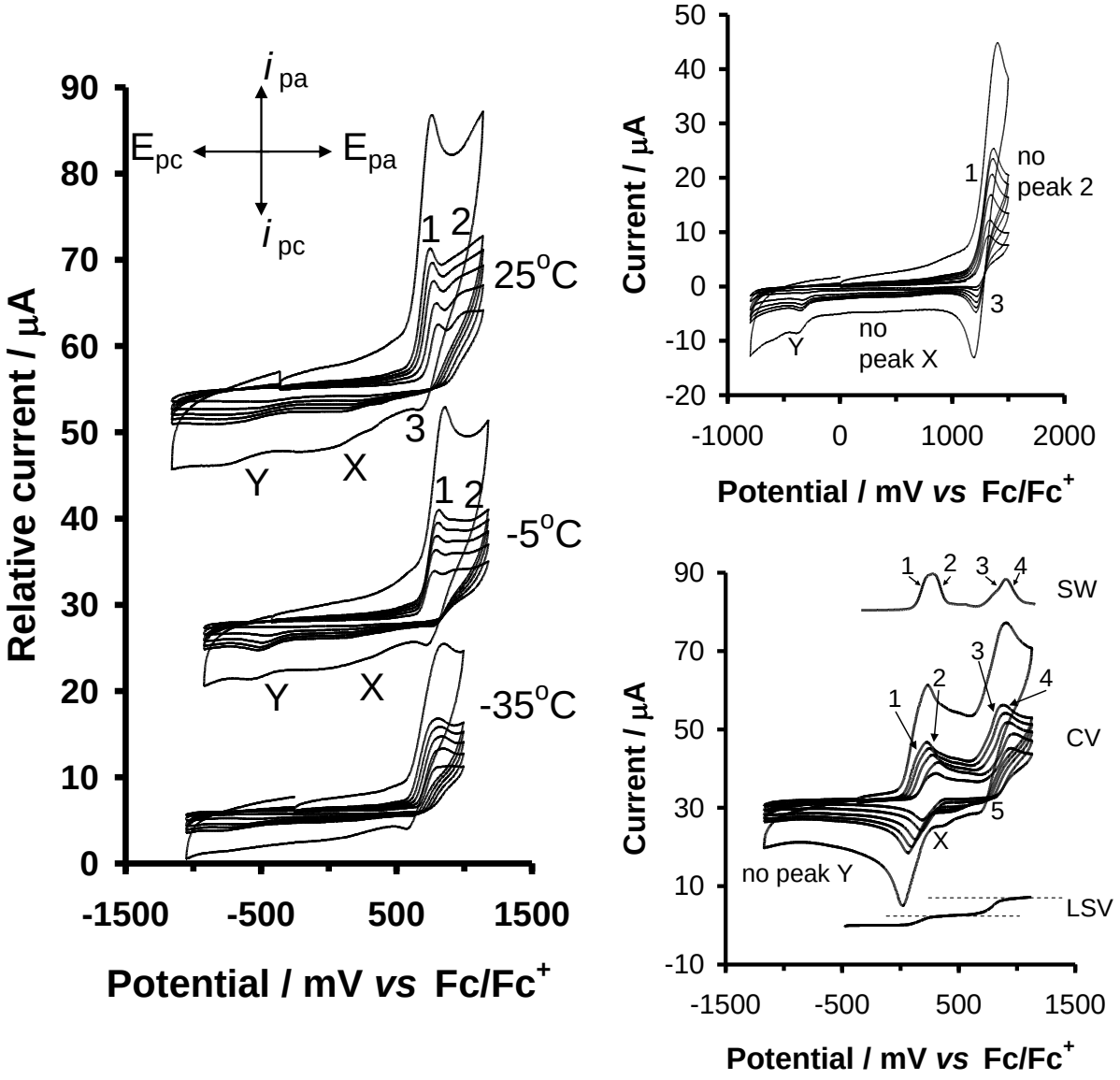

Figure 3.34. Left: Comparative cyclic voltammograms of 2.0 mmol dm^{-3} $RcCOCH_2COCH_3$ (**151**) solutions in CH_2Cl_2/0.1 mol dm^{-3} $[NBu_4][B(C_6F_5)_4]$ on a glassy carbon-working electrode at scan rates of 50, 100, 200, 300, 400, 500 and 2000 mV s^{-1} and temperatures of 25ºC, -5ºC and -35ºC. Right Top: Cyclic voltammograms of 2.0 mmol dm^{-3} solutions of $RcCOCH_2COC_{10}F_{21}$ (**177**) at 25ºC. Right Bottom: Cyclic voltammograms (CV), Oster Young square wave voltammograms (SW) at 10 Hz and linear sweep voltammetry at 2 mV s^{-1} of 2.0 mmol dm^{-3} solutions of $RcCOCH_2COFc$ (**154**) at 25ºC.

From Figure 3.34 it is notable that the peak anodic currents decrease as the temperature decreases. This is due to the fact that the electron transfer between β-diketone and electrode are more sluggish (slower) when the temperature is low. Also, the reduction peaks labelled X and Y in the negative region becomes smaller with decrease in temperature. Since there was no new features observed at -35ºC that could not also be identified by performing CV studies 25ºC, it was decided to report results for the other β-diketones just at 25ºC.

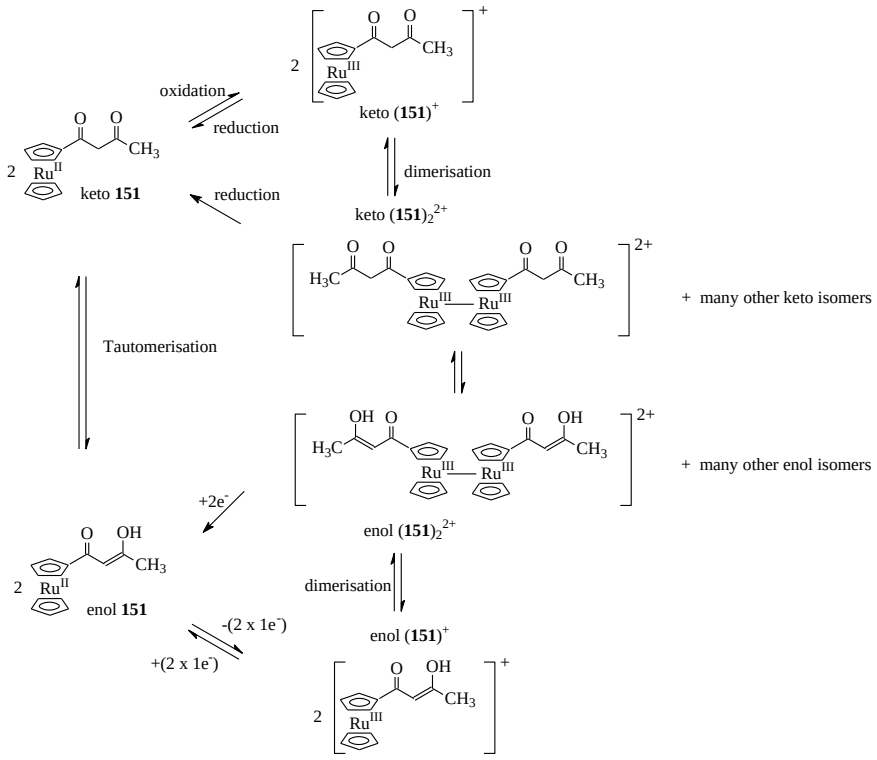

Scheme 3.26. The oxidation of keto and enol isomers of **151** to give $RcCOCH_2COCH_3^+$ $(\mathbf{151})^+$ and the proposed formation of dimeric cationic species. Similar reactions can be written for the other enol isomer. Mixed dimer with substituted C_5H_4 ring "*trans*" and not "*cis*" to each other as well as dimers having mixtures of enol and keto subtituents may also exist.

If the assignment that peaks X and 2 belongs to keto and peaks Y and 1 belongs to the enol isomers of $(\mathbf{151})_2^{2+}$ and $\mathbf{151}^+$ are correct, then a compound that exists almost exclusively in the enol form should show only one oxidation peak in its CV, and only one of the two waves X and Y in the cathodic side of its CV. Such a compound is $RcCOCH_2CO(C_{10}F_{21})$, **177**. The CV's of **177** at 25ºC is shown in Figure 3.34 top right. Only one oxidation peak, namely peak 1, is observed, and peak X is gone. Only peak Y remains, which implies that enol dimeric ruthenocenium cations are reduced at lower potentials than the keto counterpart. It is also striking that peak 3 which corresponds to the reduction of monomeric $(\mathbf{177})^+$ is much more

prominent than that for (**151**)$^{+}$. It implies that the equilibrium $2[Rc_{Beta}]^{+} \rightleftharpoons [Rc_{Beta}\text{-}Rc_{Beta}]^{2+}$ lies more to the side of the monomer for β-diketones having electron withdrawing substituents.

The multiple oxidation peaks observed for the complexes with R = $C_{10}H_{21}$, CH_3, Rc and Fc are not attributed to adhesion of ruthenocene-containing β-diketones to the glassy carbon working electrode surface even though electrode deposition has been found to occur with cobaltocenium salts.[32] This conclusion was reached based on the shape of the cyclic voltammograms obtained. If electrode deposition occurred, a very large, sharp peak indicating large current flows (> 100 μA) would be obtained (see for example referance 32). The CV's in Figure 3.34, showed no such sharp peaks and large currents.

Figure 3.34 (bottom right) shows the cyclic voltammograms of **154**. A few interesting observation can be made from these cyclic voltammograms. Firstly peaks 1,2 and 3,4 are shoulders that are unresolved. The Oster Young square wave voltammetry (SW) differentiated better between peaks 1 and 2. The difference between SW peak potentials were found to be ca. 50 mV at a frequency of 10 Hz. Peaks 1 and 2 is associated with the ferrocenyl group of **154** and belong to the enol and keto isomers of this β-diketone. Peaks 3 and 4 belong to the enol and keto signal of the ruthenocenyl fragment of **154**. These peak pairs are identifiable because slow isomerisation kinetic (section 3.5.1, p 100) freeze each isomer on the CV time scale. At equilibrium in CD_2Cl_2 **154** exists as ~50% enol and ~50% keto (Table 3.9, p 103) according to Scheme 3.16 (p 101).

The very weak reduction peak of monomeric ($Fc^{+}COCH_2CORc^{+}$), **154**$^{2+}$, at 810 mV, peak 5, that can be seen at the scan rate 2000 mV s^{-1} is assigned to the reduction of the ruthenocenyl fragment of monomeric (**154**)$^{2+}$. As the scan rate increases a drifting reduction peak labelled X appears at 450-550 mV in the cyclic voltammogram (just before Fc^{+} reduction). This is assigned to reduction of the dimeric species keto (**154**)$_2^{4+}$. No peak that, in analogy with the CV of free ruthenocene could be attributed to the reduction of enol (**154**)$_2^{4+}$, could be identified for **154**.

Figure 3.35 shows the comparative cyclic voltammograms of the ruthenocene-containing β-diketones at scan rate = 200 mV s^{-1} and 25ºC. The comparative electrochemical data resulting from these voltammograms are summarised in Table 3.22.

The Rc/Rc^{+} couple for all the β-diketones were found to be for all practical purposes electrochemically quasi-reversible (90 mV < ΔE < 150 mV) and chemically irreversible ($i_{pc}/i_{pa} \neq 1$) at slow scan rates. Rc^{+} reduction was best observed for the fluorine containing β-diketones **177, 152** and **178**, the Rc^{+} reduction for the other β-diketones was only detected at high scan rates. See for example Figure 3.34 for **151**.

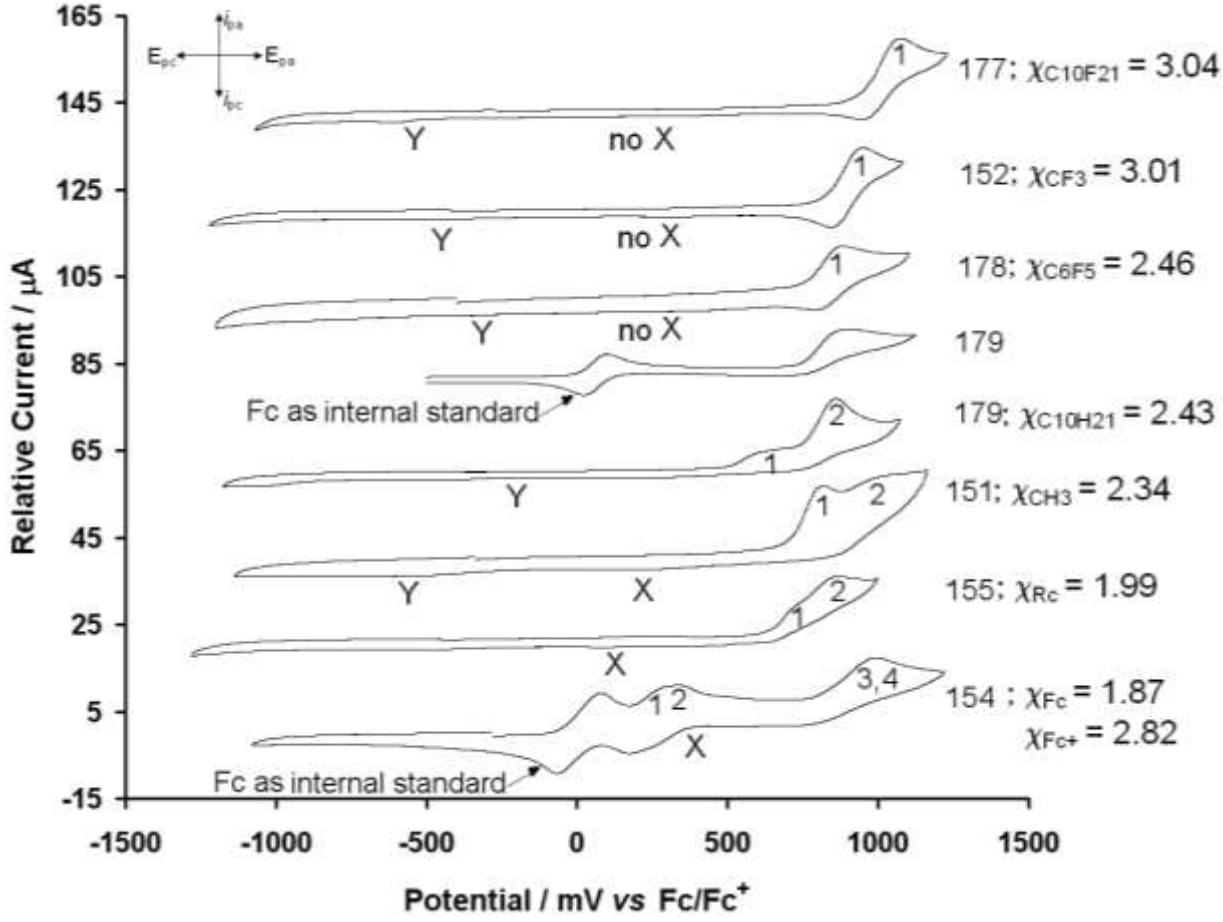

Figure 3.35. Cyclic voltammograms of 2.0 mmol dm^{-3} ruthenocene-containing β-diketone solutions, $RcCOCH_2COR$ [where R = $C_{10}F_{21}$ (**177**), CF_3 (**152**), C_6F_5 (**178**), $C_{10}H_{21}$ (**179**), CH_3 (**151**), Rc (**155**) and Fc (**154**)] in CH_2Cl_2/0.1 mol dm^{-3} $[NBu_4][B(C_6F_5)_4]$ on a glassy carbon-working electrode at 25ºC and a scan rate of 200 mV s^{-1}. χ_R = group electronegativity of the indicated R groups.

The general trend for the peak anodic potentials 1 and 2 is to increase as the group electronegativity of the R group increases. This is expected, because the more electron-withdrawing the R group becomes, the more electron density will be removed for the ruthenocenyl group, making it relatively more positive and more difficult to oxidize according to the reaction Ru(II) → Ru(III) + e^-. At first glance it appears as if **154** (R = Fc) does not fit into this trend. It would be expected that E_{pa} of the Rc group should be at less positive potentials. However, during the electrochemical experiment the ferrocenyl group is first converted to ferrocenium, Fc^+, with χ_{Fc+} = 2.82, before the ruthenocenyl group is oxidised. Therefore, when the Rc group of $FcCOCH_2CORc$, **154**, is oxidised, the redox active species is actually the compound Fc^+COCH_2CORc. Since the Rc group now experience the electron-withdrawing power of Fc^+, the oxidation of Rc should occur at potentials more positive for **178** with R = C_6F_5 and χ_{C6F5} = 2.46, but less positive than for **152** with R = CF_3 and χ_{CF3} = 3.01. This was actually observed, see Table 3.22.

Table 3.22. Data of $RcCOCH_2COR$, group electronegativity of the R group, temperature, peak anodic potentials, E_{pa} (*vs* Fc/Fc^+ couple as an internal standard) of the first oxidation peak of the ruthenocenyl moiety; difference in peak anodic and peak cathodic potentials, ΔE_p; formal reduction potentials, E^{01}; peak anodic currents, i_{pa}; and peak anodic/peak cathodic current ratios, i_{pa}/i_{pc}, for indicated compounds (concentration 2.0 mmol dm^{-3}) in CH_2Cl_2/0.1 mol dm^{-3} $[NBu_4][B(C_6F_5)_4]$ at T = 25ºC.

v / mV s^{-1}	E_{pa1} / mV	ΔE_{p1} / mV	$E^{01}{}_1$ / mV	i_{pa1} / μA	i_{pc}/i_{pa}	E_{pa2} / mV	i_{pa2} / μA	E_{pcX} / mV	E_{pcY} / mV
177, $RcCOCH_2COC_{10}F_{21}$, T = 25ºC; χ_{C10F21} = 3.04									
50	1066	-	-	4.9	-	-[a]	-[a]	-[a]	-
100	1072	119	1013	10.3	0.4	-[a]	-[a]	-[a]	-604
200	1082	138	1013	16.2	0.4	-[a]	-[a]	-[a]	-608
300	1092	147	1019	22.3	0.5	-[a]	-[a]	-[a]	-614
400	1101	156	1023	28.4	0.5	-[a]	-[a]	-[a]	-622
500	1135	217	1027	34.2	0.5	-[a]	-[a]	-[a]	-627
152 ,$RcCOCH_2COCF_3$, T = 25ºC; χ_{CF3} = 3.01									
50	952	110	897	5.7	0.4	-[a]	-[a]	-[a]	-
100	950	113	894	7.3	0.5	-[a]	-[a]	-[a]	-386
200	951	118	892	8.9	0.5	-[a]	-[a]	-[a]	-452
300	954	116	896	10.5	0.5	-[a]	-[a]	-[a]	-471
400	958	122	897	12.1	0.5	-[a]	-[a]	-[a]	-486
500	961	128	897	13.9	0.5	-[a]	-[a]	-[a]	-501
178 ,$RcCOCH_2COC_6F_5$, T = 25ºC; χ_{C6F5} = 2.46									
50	845	-	-	2.2	-	-[a]	-[a]	-[a]	-
100	848	113	792	2.3	0.2	-[a]	-[a]	-[a]	-527
200	846	100	796	2.8	0.3	-[a]	-[a]	-[a]	-551
300	845	102	794	3.6	0.4	-[a]	-[a]	-[a]	-513
400	844	103	793	4.0	0.4	-[a]	-[a]	-[a]	-540
500	844	103	793	4.5	0.5	-[a]	-[a]	-[a]	-605
179 ,$RcCOCH_2COC_{10}H_{21}$, T = 25ºC; χ_{C10H21} = 2.43									
50	537[b]	-[a]	-[a]	2.1	-[a]	771	7.7	-	-
100	540[b]	-[a]	-[a]	2.5	-[a]	781	10.1	178	-396
200	548[b]	-[a]	-[a]	3.0	-[a]	800	12.5	166	-483
300	563[b]	-[a]	-[a]	3.6	-[a]	810	14.9	128	-524
400	581[b]	-[a]	-[a]	3.2	-[a]	818	17.3	111	-554
500	591[b]	-[a]	-[a]	4.8	-[a]	825	19.8	84	-579

Table 3.22. (continued) Data of $RcCOCH_2COR$, group electronegativity of the R group, temperature, peak anodic potentials, E_{pa} (*vs* Fc/Fc^+ couple as an internal standard) of the first oxidation peak of the ruthenocenyl moiety; difference in peak anodic and peak cathodic potentials, ΔE_p; formal reduction potentials, E^{01}; peak anodic currents, i_{pa}; and peak anodic/peak cathodic current ratios, i_{pa}/i_{pc}, for indicated compounds (concentration 2.0 mmol dm^{-3}) in CH_2Cl_2/0.1 mol dm^{-3} $[NBu_4][B(C_6F_5)_4]$ at T = 25ºC.

v / mV s^{-1}	E_{pa1} / mV	ΔE_{p1} / mV	$E^{01}{}_1$ / mV	i_{pa1} / μA	i_{pc}/i_{pa}	E_{pa2} / mV	i_{pa2} / μA	E_{pcX} / mV	E_{pcY} / mV
151 ,$RcCOCH_2COCH_3$, T = 25ºC; χ_{CH3} = 2.34									
50	836	-[a]	-[a]	4.6	-[a]	1050	5.4	-	-355
100	811	-[a]	-[a]	6.3	-[a]	1078	9.0	229	-525
200	795	-[a]	-[a]	8.1	-[a]	-	-	194	-754
300	776	-[a]	-[a]	9.7	-[a]	-	-	184	-776
400	765	-[a]	-[a]	11.4	-[a]	-	-	156	-818
500	751	-[a]	-[a]	13.1	-[a]	-	-	42	-856
151 ,$RcCOCH_2COCH_3$, T = -5ºC; χ_{CH3} = 2.34									
50	774	-[a]	-[a]	3.7	-[a]	975	3.6	-	-
100	783	-[a]	-[a]	4.9	-[a]	949	3.8	-	-
200	792	-[a]	-[a]	6.1	-[a]	945	4.1	-	-463
300	809	-[a]	-[a]	7.3	-[a]	941	4.3	-	-493
400	809	-[a]	-[a]	8.6	-[a]	929	4.5	-	-515
500	815	-[a]	-[a]	9.9	-[a]	-	-	-	-527
151 ,$RcCOCH_2COCH_3$, T = -35ºC; χ_{CH3} = 2.34									
50	826[b]	-[a]	-[a]	3.4	-[a]	889	-[a]	-	-
100	817[b]	-[a]	-[a]	4.5	-[a]	885	-[a]	-	-
200	803[b]	-[a]	-[a]	5.4	-[a]	845	-[a]	-	-552
300	797[b]	-[a]	-[a]	6.5	-[a]	835	-[a]	-	-678
400	792[b]	-[a]	-[a]	7.6	-[a]	823	-[a]	-	-766
500	777[b]	-[a]	-[a]	8.6	-[a]	805	-[a]	-	-852
155 ,$RcCOCH_2CORc$, T = 25ºC; χ_{Rc} = 1.99									
50	738[b]	-[a]	-[a]	-[c]	-[a]	840	-[c]	247	-
100	744[b]	-[a]	-[a]	-[c]	-[a]	858	-[c]	205	-
200	750[b]	-[a]	-[a]	-[c]	-[a]	880	-[c]	178	-
300	756[b]	-[a]	-[a]	-[c]	-[a]	899	-[c]	133	-
400	762[b]	-[a]	-[a]	-[c]	-[a]	915	-[c]	87	-
500	771[b]	-[a]	-[a]	-[c]	-[a]	924	-[c]	35	-

Table 3.22. (continued) Data of $RcCOCH_2COR$, group electronegativity of the R group, temperature, peak anodic potentials, E_{pa} (*vs* Fc/Fc^+ couple as an internal standard) of the first oxidation peak of the ruthenocenyl moiety; difference in peak anodic and peak cathodic potentials, ΔE_p; formal reduction potentials, E^{01}; peak anodic currents, i_{pa}; and peak anodic/peak cathodic current ratios, i_{pa}/i_{pc}, for indicated compounds (concentration 2.0 mmol dm^{-3}) in CH_2Cl_2/0.1 mol dm^{-3} $[NBu_4][B(C_6F_5)_4]$ at T = 25ºC.

v / mV s^{-1}	E_{pa1}[b] / mV	E_{pa2} / mV	ΔE_{p2} / mV	$E^{01}{}_2$ / mV	i_{pa2} / μA	i_{pa}/i_{pa}	E_{pa3+4}[a] / V	i_{pa3+4} / μA	E_{pcX} / mV
154 ,$RcCOCH_2COFc$, T = 25ºC; χ_{Fc} = 1.87									
50	237	307	122	246	5.6	1.0	947	8.4	490
100	256	325	146	252	6.7	1.0	973	9.6	472
200	188	275	156	197	7.8	1.0	927	10.7	460
300	173	249	162	168	8.9	1.0	902	11.9	421
400	16	227	167	144	10.0	1.0	884	12.6	365
500	150	236	222	125	11.2	1.0	907	14.7	339

(a) Not possible to determine with confidence due to small intensity, poor resolution or absence of peaks.

(b) Not an exact E_{pa} due to poor resolution between peaks 1 and 2. Values are estimates only.

(c) Peaks overlap to the extent that they could not be separated. Hence no peak current is provided for these peak.

Figure 3.36 (Left) shows the Oster Young square wave (SW) of $RcCOCH_2COCH_3$ (2.0 mmol dm^{-3}) at 25˚C (Top) and -35˚C (Bottom), at different frequencies (10-100 Hz). From the SW diagrams at 25˚C, it can be seen that at the lowest frequencies, the two oxidation peaks at 720 mV (1_A) and 870 mV (1_B) are very well separated and well defined. As the frequency increases, the peak 1_B (870 mV) becomes a shoulder of peak 1_A, and the two eventually overlap. A peak at 1100 mV (labelled 2) becomes more prominent as the frequency increases. This result would be consistent with the CV of **151** (Figure 3.34, left) if SW peaks $1_{A,\,B}$ are assigned to the two possible enol isomers and peak 2 to the keto isomer. Under low frequency square wave conditions, apparently, both enol isomers of **151** can be observed. The poor observability of peak 2 at small frequencies can also be rationalized. At small frequencies the keto form has time to convert to the enol form during the SW scan as the enol form is oxidised. By the time the potential is reached where the keto should be oxidised, no more (or at best limited amounts) of keto (**151**) is available. However, at fast frequencies, not all the keto isomer content had time to convert to enol isomer prior to reaching the potential at which keto oxidation takes place. Hence the peak labelled 2 (which is the oxidation of the keto form of **151**) can be observed. The fact that 1_A and 1_B can be observed shows that equilibrium $enol_A \rightleftharpoons enol_B$ is not fast under these conditions (see Scheme 3.16, p 101 for the isomerisation). At -35˚C the current drawn is dramatically smaller than at 25˚C. There is a broad peak at 670 mV (peak $1_{A,\,B}$ overlapping) that is assigned to Rc-oxidation of the two enol isomers of **151**. The peak at 1120 mV peak 2, is again assigned to the keto isomer of **151**.

Figure 3.36 (Right) shows the linear sweep voltammograms of 2.0 mmol dm^{-3} $RcCOCH_2COCH_3$ at 25˚C (Top) and -35˚C (Bottom), at scan rate 2 mV s^{-1}. From the linear sweep voltammogram taken at 25˚C it can be seen that three oxidation processes takes place. As was done for the SW voltammogram, these oxidation processes are assigned to the oxidation of the two enol tautomers (peaks 1_A and 1_B) and keto isomer (peak 2). The voltammogram taken at -35˚C shows only poorly resolved processes in which the current gradually increases. This implies that at low temperatures the rate of electron transfer become so slow that it rendered LSV as a useless diagnositic tool.

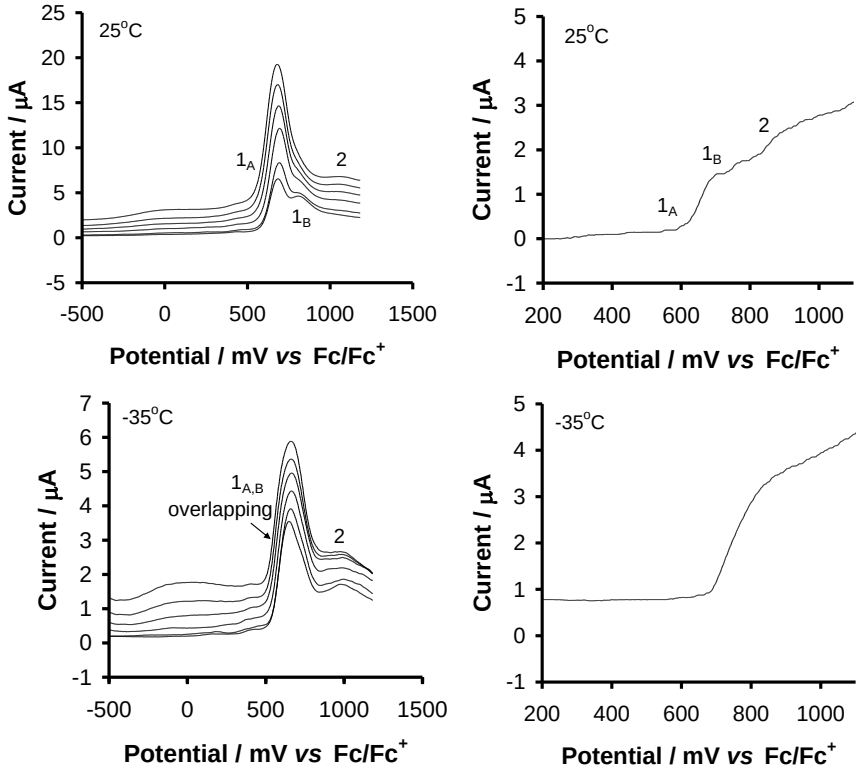

Figure 3.36. Left: Oster Young square wave voltammetry of 2.0 mmol dm^{-3} solutions of $RcCOCH_2COCH_3$ at 25˚C (Top), -35˚C (Bottom) at frequencies 10, 20, 40, 60, 80 and 100 Hz in CH_2Cl_2/0.1 mol dm^{-3} $[NBu_4][B(C_6F_5)_4]$ on a glassy carbon working electrode. Right: Linear sweep voltammogram of 2.0 mmol dm^{-3} solutions of $RcCOCH_2COCH_3$ at 25˚C (Top), -35˚C (Bottom), at scan rate 2 mV s^{-1}.

3.6.4. Electrochemical isomerisation kinetics

In the previous section, the hypothesis was put forward that peak 1 of the CV of $FcCOCH_2CORc$, (**154**) (Figure 3.34, right bottom, p138), corresponds to the enol signal of the ferrocenyl group of **154** while peak 2 corresponds to the keto signal of the ferrocenyl group of **154**. Upon assuming that this is the case, an attempt was made to follow the kinetics of enol to keto conversion according to the equilibrium $Fc\text{-}CO\text{-}CH{=}C(OH)\text{-}Rc \underset{k_{-1}}{\overset{k_1}{\rightleftharpoons}} Fc\text{-}CO\text{-}CH_2\text{-}CO\text{-}Rc$

utilising cyclic voltammetry and Oster Young square wave voltammetry measurements. A 2.0 mmol dm^{-3} enol-enriched FcCOCHC(OH)Rc (**154**) solution in CH_2Cl_2/0.1 M [NBu][$B(C_6F_5)_4$] at a glassy carbon working electrode at 25ºC and scan rate 250 mV s^{-1} (for the CV) and 10 Hz (for the SW) was used for this study. Figure 3.37 shows how peak 1 decreased with time while peak 2 increased with time as the equilibrium shifted to the keto side. Some of the data that were collected with time are shown in Tables 3.23 and 3.24.

Tabel 3.23. Cyclic voltammetry data collected with time of the conversion of enol to keto isomers of $RcCOCH_2COFc$ in CH_2Cl_2 at 25˚C.

Relative time / s	$i_{pa,\ enol}$ / μA	$i_{pa,\ keto}$ / μA	% keto[a]	$\ln \frac{(\%keto)_0 - (\%keto)_\infty}{(\%keto)_t - (\%keto)_\infty}$
0	14.67	5.67	27.9	0
120	11.39	7.37	39.2	0.5073
300	10.05	8.71	46.4	1.0503
540	9.67	10.31	51.6	1.795
t = ∞	9.99	12.88	56.3	-

a) $\%keto = \frac{i_{pa},\ keto}{i_{pa},\ keto + i_{pa},\ enol} \times 100$

Tabel 3.24. Oster Young square wave voltammetry data collected with time of the equilibrium between enol and keto isomers of $RcCOCH_2COFc$ in CH_2Cl_2 at 25˚C.

Relative time / s	$i_{pa,\ enol}$ / μA	$i_{pa,\ keto}$ / μA	% keto[a]	$\ln \frac{(\%keto)_0 - (\%keto)_\infty}{(\%keto)_t - (\%keto)_\infty}$
0	8.02	7.28	47.6	0
120	7.98	7.38	48.0	0.0917
600	7.67	7.53	49.5	0.4785
660	7.62	7.63	50.0	0.6482
1260	6.06	6.45	51.6	1.4971
t = ∞	6.30	7.01	52.7	-

a) $\%keto = \frac{i_{pa},\ keto}{i_{pa},\ keto + i_{pa},\ enol} \times 100$

K_c can be calculated from Equation 3.3 (p 102). The graphs of percentage keto content *vs* time is shown Figure 3.38 for **154**. From this graph the first order rate constant, k_{obs}, can be determined by application of Equation 3.5 (p 102).

By simultaneously solving of equations $k_{obs} = k_1 + k_{-1}$ (Equation 3.5) and $K_c = k_1/k_{-1}$ (Equation 3.3), rate constants k_1 and k_{-1} can be separated. The kinetic data obtained for the β-

diketone in CD_2Cl_2 (obtained by ^1H NMR) and CH_2Cl_2 (obtained for electrochemical data) is summarised in Table 3.25.

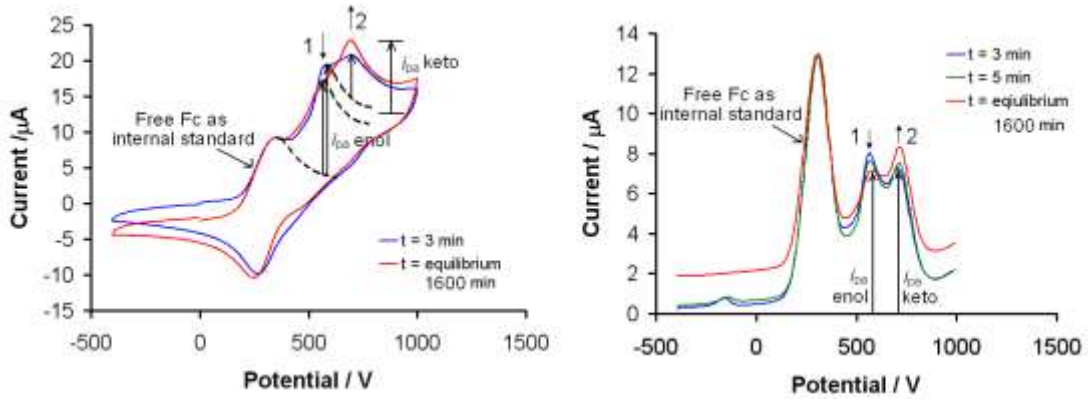

Figure 3.37. Sample cyclic voltammograms (Left) and square wave voltammograms (Right) showing the isomerization according to equation Fc-CO-CH=C(OH)-Rc ⇌ Fc-CO-CH_2-CO-Rc. Peak 1 shows how the enol form becomes less prominant while peak 2 shows how the keto form becomes more prominent.

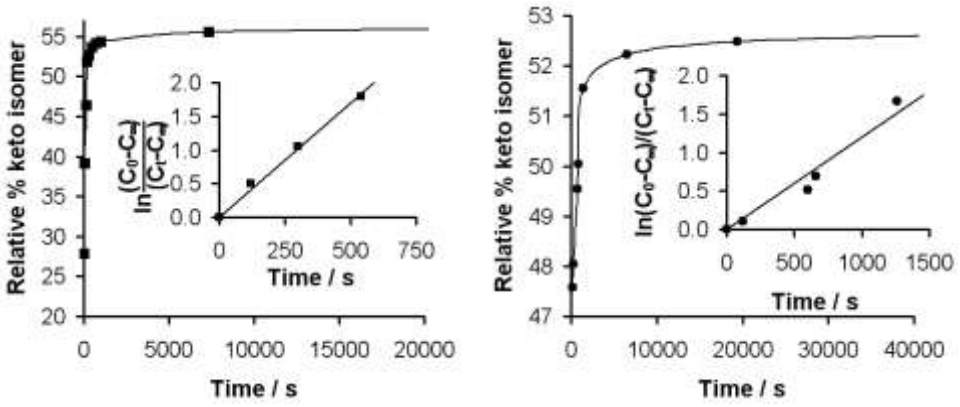

Figure 3.38. Time trace showing of the CV (Left) and SW (Right) the conversion from keto- to enol isomer for **154** at 25˚C in CH_2Cl_2. Insert: a kinetic plot of data for this process that leads to the first order rate constant k_1 (C = % keto).

Table 3.25. Equilibrium constants, K_c, for the keto-enol equilibrium of $RcCOCH_2COFc$ in CH_2Cl_2 at 25˚C. The first order rate constant, k_{obs}, first order rate constant for the keto to enol half reaction, k_1, and first order rate constant for the enol to keto half reaction, k_{-1}, are also listed.

Experiment	$10^4\ k_{obs}$ / s^{-1}	$10^4\ k_1$ / s^{-1}	$10^{-4}\ k_{-1}$ / s^{-1}	Relative % enol at equilibrium	K_c in CH_2Cl_2
CV	34.1 (4)	14.9	19.2	56.3	0.776
SW	18.1 (6)	5.75	6.35	52.5	0.905
^1H NMR[a]	14.7(4)	7.33	7.36	50.1	0.996
^1H NMR[a, b]	12.8(3)	6.38	6.43	50.2	0.992

a) Determined in CD_2Cl_2, discussed in section 3.5.5. (p 100)

b) In the presence of 8.75 x 10^{-2} mol dm^{-3}, $[NBu_4][B(C_6F_5)_4]$

As can be seen from Table 3.25, the first order rate constants (k_{obs}, k_1 and k_{-1}) and equilibrium constant (K_c) obtained by ^{1}H NMR and SW are mutually consistent. The k_{obs} for CV is twice that which was found by ^{1}H NMR, due to the inaccuracy of obtaining i_{pa} values, but can still be regarded as kinetically equivalent. This particular gratifying result implies that the interpretation of the previous section that the enol isomer is easier to oxidize than the keto isomer, that peak 1 is associated with the enol isomer and peak 2 (Figure 3.34) is associated with the keto isomer of β-diketones, and that these peaks could be separated on a CV time scale, were all correct.

3.6.5. Titanium complexes

3.6.5.1. Bis(η^5-cyclopentadienyl)dimetallocenyl titanium(IV) complexes

The cyclic voltammetric behaviour of the di(cyclopentadienyl)dimetallocenyl titanium(IV) complexes $[(C_5H_5)_2Ti\{(C_5H_4)M(C_5H_5)\}_2]$ (M = Fe (**100**), Ru (**188**) and Os (**189**)) were studied in CH_2Cl_2/0.1 mol dm^{-3} $[NBu_4][B(C_6F_5)_4]$. Analysis of the CV data revealed quasi-reversible to irreversible electrochemistry for the Ti^{4+}/Ti^{3+} couples and quasi-reversible electrochemistry for the Fc/Fc^+,Oc/Oc^+ and $2Rc/[2Rc^+ \rightleftharpoons (Rc_2)^{2+}]$ couples. The CV data is summerised in Table 3.26.

The CV of **100** (Figure 3.39, Left) is simple and easy to interpret. The peak labelled 1 is associated with the Ti^{4+}/Ti^{3+} couple. This reduction wave is quasi-reversible (ΔE = 90-110 mV) and chemically reversible with $i_{pa}/i_{pc} \approx 1$. The almost overlapping peaks labelled 4, 5 are assigned to the two ferrocenyl fragments that are reversible at slow scan rates (50-200 mV s^{-1}) and quasi-reversible at higher scan rates with ΔE = 72-102 mV. Peak 5 is observed as a small shoulder of peak 4. The existence of the two peaks 4 and 5 is explained by the two ferrocenyl moieties, which are not oxidised at exactly the same potential. From the LSV of **100** (Figure 3.39, Left), it can be seen that the i_p of ferrocenyl oxidation is twice that of Ti^{4+} reduction. This proves that the two ferrocenyl moieties transfers twice as much electrons as the titanium center, and it is consistent with Ti^{4+} being reduced to Ti^{3+} in a one-electron process.

The CV of **189** (Figure 3.39, Left) is similar to that observed for **100**. Peak 1 belongs to the Ti^{4+}/Ti^{3+} couple which was found to be electrochemically reversible at scan rates 50 and 100 mV s^{-1}, but electrochemical and chemically irreversible with ΔE > 150 mV at higher scan rates. Overlapping peaks 4, 5 are assigned to the reversible oxidation of the two osmocenyl moieties.

The two osmocenyl moieties are for all practical purposes oxidised at the same potential. This oxidation wave was found to be electrochemically reversible with ΔE = 79-89 mV.

The CV of **188** (Figure 3.39, Left) was much more complex than that of **100** and **189**. Peaks 3, 4 and 5 are assigned to the ruthenocenyl groups. Peaks 4 and 5 are well resolved without shoulders, unlike what was found with **100** and **189**. A possible explanation why the ruthenocenyl moieties are oxidised at different potentials may center in the fact that the distance between the two C_5H_5 rings are larger for ruthenocene than for the other two metallocenes. The distance between the parallel cyclopentadienyl planes are 3.68 Å for ruthenocene, 3.32 Å for ferrocene and 3.64 Å for osmocene.[33] Thus free rotation for the ruthenocene moieties around the bond connecting them to the titanium(IV) metal centre may be more impaired than for the other two metallocenes. It may be possible to lock the two ruthenocenyl ligands in different positions making their electronic surroundings different.

The more detailed CV traces of the ruthenocene-derivative (**188**) at 25ºC (Figure 3.39 Right bottom) shows 5 reduction waves, three of which are associated with the ruthenocenyl group (peaks 3-5) and two reduction waves for Ti (peaks 1 and 2). Seeing as Rc^+ has generally a very short existence time, peak 3 could be associated, in analogy with free ruthenocene, with a dimerised cationic species. Peak 5 has a clear reduction half wave associated with it. However the intensity of the reduction half wave of peak 4 becomes more and more prominent as scan rate increases. Concomitantly with this, the reduction wave 3 decreases in current intensity as wave 4 reduction intensity increases with increased scan rate. This result is consistent with dimerisation taking place predominantly with the mixed valent ruthenocene species, *but at a slow rate*. Peak 3 is associated with dimer reduction. Hence, at fast scan rates, Rc^+ reduction occurs mostly before dimerisation takes place as indicated by large i_{4red} currents. However, at slow scan rates, before potentials are reached during the reduction cycle, the Rc^+ species dimerised to Rc_2^{2+}. This then accounts for the relatively more intense reduction half wave of peak 3 that is observed at slow scan rates. The two peaks labelled 1 and 2 in the CV of **188**, (Figure 3.39, Right bottom) are also mutually consistent with two unequal Ti centres which should arise if the ruthenocenyl groups cannot rotate freely about the bond binding them to the titanium center. The lack of free rotation argument is further supported when the temperature study for **188** is considered. At -35ºC, the Ti reduction wave does not have a clearly resolved second peak. It is, however, much broadened. This poorer resolution is expected due to slower electron transfer rates at lower temperatures. However, peaks 4 and 5 at -35ºC becomes much more ideal, which would be consistent with two preferred rotational conformations for the ruthenocenyl groups being frozen on the CV time scale.

The CV of the ruthenocenyl complex showed at -35ºC that both oxidation waves have pronounced reduction peaks, with $\Delta E \approx 150$ mV. This makes both peaks 1 and 2 quasi-reversible. Interesting to note is that at -35˚C, both ruthenocene peaks 1 and 2 have $i_{pc}/i_{pa} \approx 0.9$, implying almost all Ru^{III} formed during oxidation are reduced back to Ru^{II}. Therefore no cationic dimer could have formed. Peak 3 was also not observed at low temperatures. Thus for **188** at low temperatures, the formation of cationic ruthenocene dimers is severely impaired. The LSV of **188** and **189** showed unexpected large current flows for the Ti^{4+}/Ti^{3+} couple. This is rationalised in terms of **188** and **189** becoming deposited on the electrode surface during Ti^{4+} reduction. The shape of peak 1 for **189** and peak 1 and 2 for **188** is also consistent with electrode deposition of the analyte. It is not expected that the large currents associated with the LSV of peaks 1 and 2 of **188** is indicative of Ti^{2+} which is normally only formed at ca. -2500 mV *vs* Fc/Fc^{+}.[34] The above described results are consistent with the following electrochemical scheme (Scheme 3.27) describing the redox behaviour of $(C_5H_4)_2TiRc_2$.

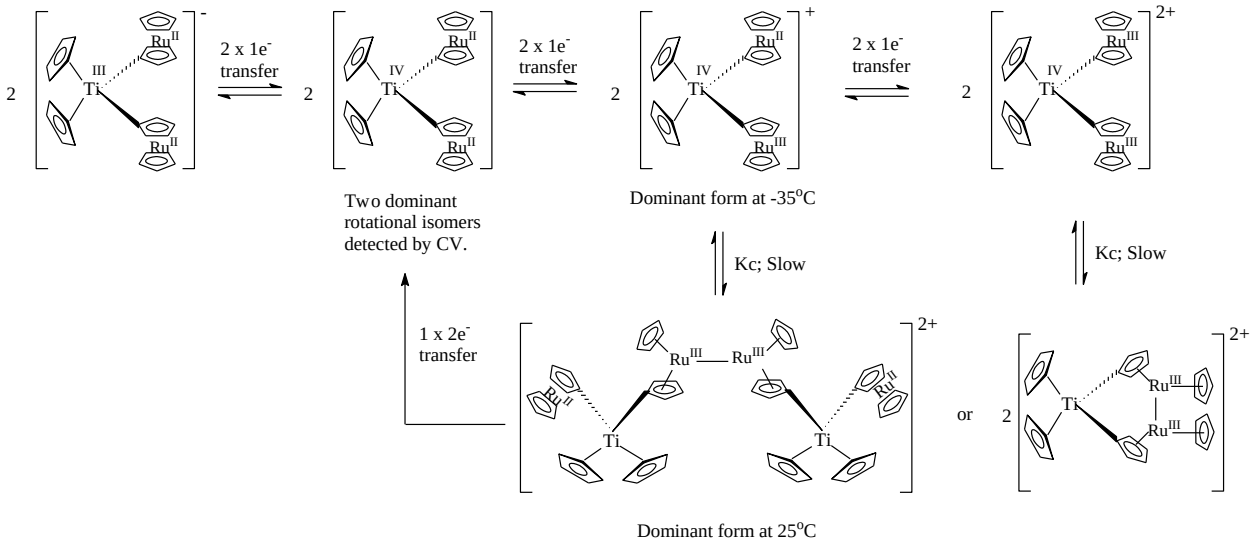

Scheme 3.27. Electrochemical scheme which is consistent with the observed electrochemical behaviour of $[(C_5H_5)_2Ti\{(C_5H_4)Ru(C_5H_5)\}_2]$, **188**.

The E^{01} of $(C_5H_4)M(C_5H_5)$ (M = Fe, Ru and Os) is dependent on the atomic electronegativity of the metal [Fe (χ_{Fe} = 1.64), Os (χ_{Os} = 1.52) and Ru (χ_{Ru} = 1.42)]. As the atomic electronegativity increases the E^{01} of the Ru-, Os- and Fe-based metallocene decreases. This is expected. Stronger electronegative metals imply that the metal centre is more electron deficient. It therefore will accept an electron from an external source (such as an electrode) with greater ease. Therefore metals in complexes which are stronger electronegative will be easier to be oxidised. The "E^{01}" of the titanium is also dependent on the atomic electronegativity of the

metal [Fe (χ_{Fe} = 1.64), Os (χ_{Os} = 1.52) and Ru (χ_{Ru} = 1.42)]. As the metal atomic electronegativity of the organometallic substituent increases, the substituent metallocene withdraws more electron density from the titanium center, which implies E^{01} of the Ti^{4+}/Ti^{3+} couple will become more positive.

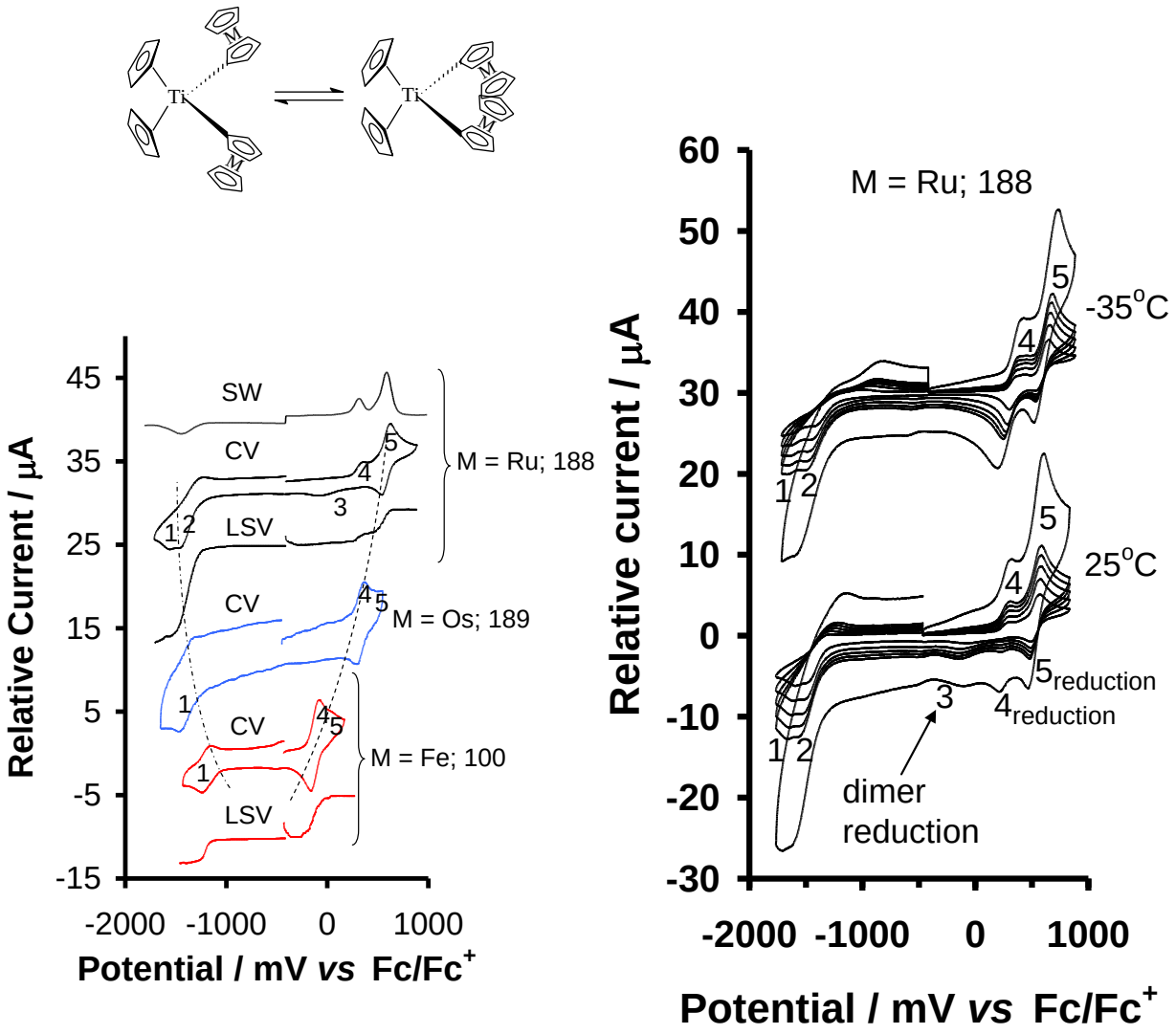

Figure 3.39. Left: Cyclic voltammograms of a 2.0 mM solution of $[(C_5H_5)_2Ti\{(C_5H_4)M(C_5H_5)\}_2]$ with M = Fe (**100**), Ru (**188**) and Os (**189**) measured in CH_2Cl_2/0.1 mol dm^{-3} $[NBu_4][B(C_6F_5)_4]$ at a glassy carbon working electrode at 25ºC and a scan rate of 200 mV s^{-1}. The SW voltammogram of **188** is also shown. Right: The cyclic voltammograms of $[(C_5H_5)_2Ti\{(C_5H_4)Ru(C_5H_5)\}_2]$ at 25ºC (Bottom) and at -35ºC (Top) at a scan rate of 100, 200, 300, 400, 500 and 2000 mV s^{-1}.

Table 3.26. Cyclic voltammetry data obtained from voltammograms (*vs* Fc/Fc^{+}) of $[Cp_2Ti(Mc)_2]$ with Mc = Fc ($(C_5H_4)Fe(C_5H_5)$), Oc ($(C_5H_4)Os(C_5H_5)$) and Rc ($(C_5H_4)Ru(C_5H_5)$), measured CH_2Cl_2/0.1 mol dm^{-3} $[NBu_4][B(C_6F_5)_4]$ at a glassy carbon working electrode at 25ºC. The concentration of the metallocene dichloride complexes was 2.0 mmol dm^{-3}. Atomic electronegativity of the metals, χ_M, is also shown.

v / mV s^{-1}	E_{pc1} / mV	ΔE_{p1} / mV	$E^{01}{}_1$ / mV	i_{pa1} / μA	i_{pa}/i_{pc}	E_{pa2} / mV	ΔE_{p2} / mV	$E^{01}{}_2$ / mV	i_{pa2} / μA	i_{pc}/i_{pa}	E_{pa3} / mV	ΔE_{p3} / mV	$E^{01}{}_3$ / mV	i_{pa3} / μA	i_{pc}/i_{pa}	E_{pa4} / mV	ΔE_{p4} / mV	$E^{01}{}_4$ / mV	i_{pa4} / μA	i_{pc}/i_{pa}	E_{pa5} / mV	ΔE_{p5} / mV	$E^{01}{}_5$ / mV	i_{pa5} / μA	i_{pc}/i_{pa}
$[Cp_2Ti(Fc)_2]$; χ_{Fe} = 1.64																									
50	-1236	90	-1191	1.5	0.6	-	-	-	-	-	-	-	-	-	-	-85	72	-121	3.8	1.0	26[a]	-	-	-[b]	-
100	-1241	92	-1195	1.4	0.5	-	-	-	-	-	-	-	-	-	-	-83	79	-123	4.6	1.0	28[a]	-	-	-[b]	-
200	-1247	96	-1199	2.3	0.4	-	-	-	-	-	-	-	-	-	-	-79	85	-122	5.4	1.0	30[a]	-	-	-[b]	-
300	-1241	99	-1192	3.1	0.4	-	-	-	-	-	-	-	-	-	-	-77	91	-123	6.2	1.0	30[a]	-	-	-[b]	-
400	-1256	102	-1205	3.9	0.3	-	-	-	-	-	-	-	-	-	-	-74	98	-123	7.1	1.0	32[a]	-	-	-[b]	-
500	-1260	110	-1205	4.8	0.3	-	-	-	-	-	-	-	-	-	-	-72	102	-123	8.0	1.0	34[a]	-	-	-[b]	-
$[Cp_2Ti(Oc)_2]$; χ_{Os} = 1.52																									
50	-1389	104	-1337	1.2	0.6	-	-	-	-	-	-	-	-	-	-	400	79	360	0.4	0.6	465[a]	-	-	-[b]	-
100	-1395	130	-1330	1.8	0.5	-	-	-	-	-	-	-	-	-	-	409	81	369	0.5	0.6	470[a]	-	-	-[b]	-
200	-1414	155	-1337	2.7	0.4	-	-	-	-	-	-	-	-	-	-	404	82	364	0.7	0.7	474[a]	-	-	-[b]	-
300	-1434	180	-1344	3.3	0.3	-	-	-	-	-	-	-	-	-	-	410	82	369	0.8	0.7	488[a]	-	-	-[b]	-
400	-1440	205	-1337	3.9	0.2	-	-	-	-	-	-	-	-	-	-	411	81	371	1.0	0.8	498[a]	-	-	-[b]	-
500	-1456	233	-1339	4.8	0.2	-	-	-	-	-	-	-	-	-	-	413	89	369	1.2	0.8	512[a]	-	-	-[b]	-
$[Cp_2Ti(Rc)_2]$ at 25ºC; χ_{Ru} = 1.42																									
50	-1590	-	-	-[b]	-	-1521	-	-	4.9	-	-80	-	-	0.7	-	311	-	-	0.8	-	580	91	534	3.2	0.3
100	-1599	-	-	-[b]	-	-1523	-	-	5.8	-	-87	-	-	0.9	-	311	-	-	1.4	-	585	104	533	4.6	0.3
200	-1615	-	-	-[b]	-	-1528	-	-	6.7	-	-138	-	-	1.2	-	317	-	-	1.9	-	585	104	533	6.0	0.4
300	-1630	-	-	-[b]	-	-1552	-	-	7.6	-	-156	-	-	1.6	-	317	-	-	2.3	-	588	110	533	7.8	0.4
400	-1652	-	-	-[b]	-	-1580	-	-	8.5	-	-158	-	-	1.9	-	319	87	276	2.7	1.0	591	113	535	8.1	0.5
500	-1667	-	-	-[b]	-	-1595	-	-	9.5	-	-159	-	-	2.1	-	319	92	273	3.1	0.9	594	120	534	10.3	0.5
$[Cp_2Ti(Rc)_2]$ at -35ºC; χ_{Ru} = 1.42																									
50	-1601	-	-	2.8	-	-1445	-	-	4.9	-	-	-	-	-	-	373	78	334	2.1	1.0	637	110	582	7.0	0.3
100	-1615	-	-	3.1	-	-1454	-	-	5.7	-	-	-	-	-	-	376	79	337	2.4	1.0	649	117	591	7.9	0.3
200	-1639	-	-	3.4	-	-1469	-	-	6.5	-	-	-	-	-	-	378	99	329	2.7	1.0	660	131	595	8.8	0.4
300	-1652	-	-	3.7	-	-	-	-	7.3	-	-	-	-	-	-	388	120	328	3.1	0.9	668	136	600	9.7	0.5

						1491																		
400	-1661	-	-	4.0	-	-1505	-	-	8.1	-	-	-	-	-	-	391	136	323	3.3	0.9	675	145	603	10.6	0.5
500	-1671	-	-	4.2	-	-1515	-	-	9.1	-	-	-	-	-	-	398	155	321	3.6	0.9	684	157	606	11.9	0.6

a) Estimate, real value could not be determined due to overlapping of peaks.

b) Peaks overlap to the extent that they could not be separated. Hence no peak current are provided for these peak.

3.6.5.2. β-Diketonatobis(η^5-cyclopentadienyl)titanium(IV) perchlorate

The cyclic voltammetric behaviour of the new mono-β-diketonato titanocenyl complexes $[(C_5H_5)_2Ti(RcCOCHCOR)]^+ClO_4^-$ [R = $C_{10}F_{21}$ (**195**), CF_3 (**196**), C_6F_5 (**197**), $C_{10}H_{21}$ (**198**), CH_3 (**194**), Rc (**199**) and Fc (**200**)] were studied in CH_2Cl_2/0.1 mol dm^{-3} $[NBu_4][B(C_6F_5)_4]$. Selected cyclic voltammograms are shown in Figure 3.40. The electrochemical results extracted from this study are summerised in Table 3.27.

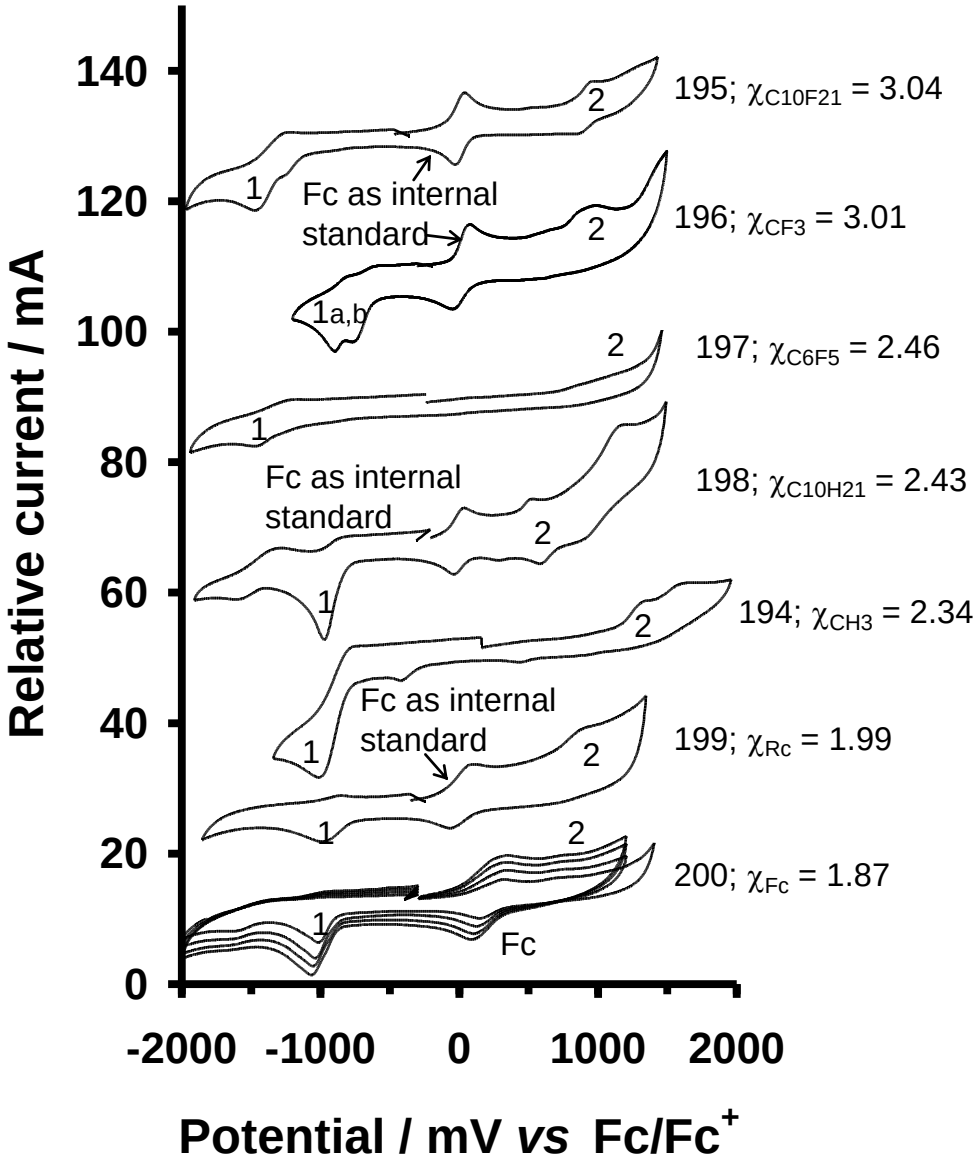

Figure 3.40. Cyclic voltammgrams of the indicated 2.0 mmol dm^{-3} mono-β-diketonato titanocenyl complexes $[(C_5H_5)_2Ti(RcCOCHCOR)]^+ClO_4^-$ recorded in CH_2Cl_2/0.1 mol dm^{-3} $[NBu_4][B(C_6F_5)_4]$ at a glassy carbon-working electrode at 25ºC and a scan rate of 200 mV s^{-1}. Cyclic voltammograms for $[(C_5H_5)_2Ti(RcCOCH_2COFc)]^+ClO_4^-$ (**200**) are shown at scan rates of 100, 200, 300 and 400 mV s^{-1}.

All the $[(C_5H_5)_2Ti(RcCOCHCOR)]^+ClO_4^-$ complexes, except the $C_{10}H_{21}$ compound were found to exhibit an electrochemical irreversible Ti^{4+}/Ti^{3+} couple with $\Delta E > 150$ mV. Only the $C_{10}F_{21}$ complex (Figure 3.40) showed $i_{pc}/i_{pa} \approx 1$ for the Ti^{4+}/Ti^{3+} couple, the others show very poor oxidation with $i_{pc}/i_{pa} < 0.4$. Execpt for $C_{10}F_{21}$, all complexes showed an electrochemical irreversible Rc/Rc^+ couple with $\Delta E > 150$ mV. The ruthenocenyl reduction half wave was very weak with $i_{pc}/i_{pa} < 0.3$. The $C_{10}F_{21}$ complex showed quasi-reversible electrochemistry for Rc/Rc^+ couple with $\Delta E = 132$-140 mV and $i_{pc}/i_{pa} \approx 1$ depending on scan rate.

In the comparative voltammograms of **194**-**200**, it can be seen that the peak cathodic currents of the Ti^{4+}/Ti^{3+} couple wave 1 are not of equal size, the same was found with Rc/Rc^+ couple. The shape of wave 1 is typical of substate adsorption onto the working electrode, and the observed current fluctuations is attributed to this.

The $[(C_5H_5)_2Ti(RcCOCHCOCF_3)]^+ClO_4^-$ (**195**) exhibits two reduction peaks (1_a and 1_b), but no significance is attributed to this again because of substrate deposition on the working electrode. The $[(C_5H_5)_2Ti(RcCOCHCOFc)]^+ClO_4^-$ (**200**) exhibits a very broadend oxidation wave for the ferrocenyl group at the peak labelled Fc (ca. 330 mV *vs* Fc/Fc^+). Allthough this may be indicative of mix valent intra-molecular communication between metal centers, the extensive electrode deposition observed prohibits a confident unique explanation for this observation. The Rc/Rc^+ couple did not display this excessive broadening in peak 2.

Probably because of electrode deposition, no meaningful relationship could be found between the E_{pc} of Ti^{4+}/Ti^{3+} couple, E^{01} of Rc/Rc^+ couple and χ_R.

Table 3.27. Cyclic voltammetry data of $[(C_5H_5)_2Ti(RcCOCHCOR)]^+ClO_4^-$ group electronegativity of the R group, peak anodic potentials, E_{pa} or E_{pc} (*vs* Fc/Fc^+ couple as an internal standard); difference in peak anodic and peak cathodic potentials, ΔE_p; formal reduction potentials, E^{01}; peak anodic currents, i_{pa}; and peak anodic/peak cathodic current ratios, i_{pa}/i_{pc}, for indicated compounds (concentration 2.0 mmol dm^{-3}) in CH_2Cl_2/0.1 mol dm^{-3} $[NBu_4][B(C_6F_5)_4]$.

v / mV s^{-1}	E_{pc1} / mV	ΔE_{p1} / mV	$E^{01}{}_1$ / mV	i_{pa1} / μA	i_{pa}/i_{pc}	E_{pa2} / mV	ΔE_{p2} / mV	$E^{01}{}_2$ / mV	i_{pa2} / μA	i_{pc}/i_{pa}
$[(C_5H_5)_2Ti(RcCOCHCOC_{10}F_{21})]^+ClO_4^-$ (**195**); $\chi_{C10F21} = 3.04$										
50	-1386	-	-	3.5	-	973	-	-	2.7	-
100	-1381	-	-	5.7	-	974	-	-	3.7	-
200	-1399	302	-1248	6.9	0.9	975	-	-	4.6	-
300	-1405	305	-1253	7.5	0.9	977	132	911	5.8	0.9
400	-1421	310	-1266	9.9	1.0	977	136	909	6.4	1.0
500	-1465	312	-1309	11.8	1.0	979	140	909	7.2	1.0

Table 3.27. (continued) Cyclic voltammetry data of $[(C_5H_5)_2Ti(RcCOCHCOR)]^+ClO_4^-$ group electronegativity of the R group, peak anodic potentials, E_{pa} or E_{pc} (*vs* Fc/Fc^+ couple as an internal standard); difference in peak anodic and peak cathodic potentials, ΔE_p; formal reduction potentials, E^{01}; peak anodic currents, i_{pa}; and peak anodic/peak cathodic current ratios, i_{pa}/i_{pc}, for indicated compounds (concentration 2.0 mmol dm^{-3}) in CH_2Cl_2/0.1 mol dm^{-3} $[NBu_4][B(C_6F_5)_4]$.

v / mV s^{-1}	E_{pc1} / mV	ΔE_{p1} / mV	$E^{01}{}_1$ / mV	i_{pa1} / μA	i_{pa}/i_{pc}	E_{pa2} / mV	ΔE_{p2} / mV	$E^{01}{}_2$ / mV	i_{pa2} / μA	i_{pc}/i_{pa}
$[(C_5H_5)_2Ti(RcCOCHCOCF_3)]^+ClO_4^-$ (**196**); χ_{CF3} = 3.01										
50	-699[a] -875[a]	-	-	3.1[a] 4.1[a]	-	961	-	-	2.4	-
100	-696[a] -875[a]	-	-	4.4[a] 4.8[a]	-	977	-	-	2.8	-
200	-691[a] -875[a]	-	-	5.7[a] 5.5[a]	-	1003	-	-	3.2	-
300	-706[a] -891[a]	-	-	7.0[a] 6.2[a]	-	1003	-	-	3.6	-
400	-736[a] -913[a]	-	-	8.3[a] 6.9[a]	-	1015	-	-	3.9	-
500	-793[a] -936[a]	-	-	9.7[a] 7.8[a]	-	1036	-	-	4.3	-
$[(C_5H_5)_2Ti(RcCOCHCOC_6F_5)]^+ClO_4^-$ (**197**); χ_{C5F5} = 2.46										
50	-1461	300	-1311	1.6	0.3	845[b]	-	-	0.8	-
100	-1469	307	-1316	1.9	0.3	889[b]	-	-	0.9	-
200	-1479	316	-1321	2.2	0.2	890[b]	-	-	1.1	-
300	-1489	328	-1325	2.5	0.2	895[b]	-	-	1.3	-
400	-1493	351	-1318	2.9	0.1	911[b]	-	-	1.4	-
500	-1497	357	-1319	3.3	0.1	915[b]	-	-	1.6	-
$[(C_5H_5)_2Ti(RcCOCHCOC_{10}H_{21})]^+ClO_4^-$ (**198**); χ_{C10H21} = 2.43										
50	-953	-	-	4.2	-	491	152	415	1.5	0.9
100	-969	-	-	6.3	-	513	218	404	1.7	0.8
200	-981	-	-	8.4	-	535	252	409	1.9	0.8
300	-993	100	-943	10.5	0.5	559	294	412	2.1	0.8
400	-1001	100	-951	12.7	0.5	595	346	422	2.3	0.8
500	-1003	104	-951	14.9	0.5	621	394	424	2.5	0.8
$[(C_5H_5)_2Ti(RcCOCHCOCH_3)]^+ClO_4^-$ (**194**); χ_{CH3} = 2.34										
50	-1082	-	-	9.6	-	1322	-	-	2.0	-
100	-1074	-	-	11.8	-	1340	-	-	2.3	-
200	-1016	-	-	13.0	-	1356	-	-	2.7	-
300	-1096	354	-919	15.2	<0.1	1354	-	-	3.1	-
400	-1134	404	-932	17.5	<0.1	1356	-	-	3.5	-
500	-1166	424	-954	20.7	<0.1	1366	-	-	4.1	-

Table 3.27. (continued) Cyclic voltammetry data of $[(C_5H_5)_2Ti(RcCOCHCOR)]^+ClO_4^-$ group electronegativity of the R group, peak anodic potentials, E_{pa} or E_{pc} (*vs* Fc/Fc^+ couple as an internal standard); difference in peak anodic and peak cathodic potentials, ΔE_p; formal reduction potentials, E^{01}; peak anodic currents, i_{pa}; and peak anodic/peak cathodic current ratios, i_{pa}/i_{pc}, for indicated compounds (concentration 2.0 mmol dm^{-3}) in CH_2Cl_2/0.1 mol dm^{-3} $[NBu_4][B(C_6F_5)_4]$.

v / mV s^{-1}	E_{pc1} / mV	ΔE_{p1} / mV	$E^{01}{}_1$ / mV	i_{pa1} / μA	i_{pa}/i_{pc}	E_{pa2} / mV	ΔE_{p2} / mV	$E^{01}{}_2$ / mV	i_{pa2} / μA	i_{pc}/i_{pa}
$[(C_5H_5)_2Ti(RcCOCHCORc)]^+ClO_4^-$ (**199**); χ_{Rc} = 1.99										
50	-1015	-	-	3.2	-	902 [b]	-	-	2.7	-
100	-1015	-	-	3.6	-	913 [b]	-	-	2.8	-
200	-1015	-	-	3.9	-	933 [b]	-	-	2.9	-
300	-1035	-	-	4.3	-	943 [b]	-	-	3.0	-
400	-1049	262	-1180	4.7	<0.1	957 [b]	-	-	3.1	-
500	-1055	256	-927	5.1	<0.1	965 [b]	-	-	3.3	-

v / mV s^{-1}	E_{pc1} / mV	ΔE_{p1} / mV	$E^{01}{}_1$ / mV	i_{pa1} / μA	i_{pa}/i_{pc}	E_{paFc} / mV	ΔE_{pFc} / mV	$E^{01}{}_{Fc}$ / mV	i_{paFc} / μA	i_{pc}/i_{pa}	E_{pa2} / mV	i_{pa2} / μA
$[(C_5H_5)_2Ti(RcCOCHCOFc)]^+ClO_4^-$ (**200**); χ_{Fc} = 1.87; χ_{Fc+} = 2.82												
50	-893	-	-	3.0	-	409	134	342	1.1	1.0	811 [b]	1.2
100	-92-	-	-	3.6	-	415	186	322	1.9	1.0	823 [b]	1.4
200	-953	-	-	4.3	-	435	214	328	2.7	1.0	833 [b]	1.6
300	-969	-	-	4.9	-	439	242	318	3.7	1.0	835 [b]	1.8
400	-981	-	-	5.6	-	439	270	304	4.8	1.0	837 [b]	2.1
500	-933	-	-	18.0	-	465	298	316	5.6	1.0	861 [b]	2.4

a) The data for peak 1 a (top) and b (bottom).

b) Not an exact value, but an estimate due to poor resolution of peak.

3.6.5.3. Bis(cyclopentadienyl)di(ferrocenylalkoxy) titanium(IV)

The cyclic voltammetric behaviour of the series of bis(cyclopentadienyl)di(ferrocenylalkoxy)titanium(IV) complexes $[(C_5H_5)_2Ti(O(CH_2)_nFc)_2$, n = 1 (**201**), 2 (**202**), 3 (**203**), 4 (**204**)] were studied in CH_2Cl_2/0.1 mol dm^{-3} $[NBu_4][B(C_6F_5)_4]$. Selected cyclic voltammograms are shown in Figure 3.41. The electrochemical wave associated with the Ti^{4+}/Ti^{3+} couple is labelled 1 and those associated with the ferrocenyl groups are labelled 2 and 3. Electrochemical data are summerised in Table 3.28.

The LSV trace (Figure 3.41, Right below) revealed half the amount of electrons are transferred at wave 1, compared to the amount of electrons that are transferred for the ferrocenyl groups (waves 2 and 3). Since the latter involves two one-electron transfer processes the assumption that wave 1 involves the generation of Ti^{3+} in a one electron transfer process is valid.

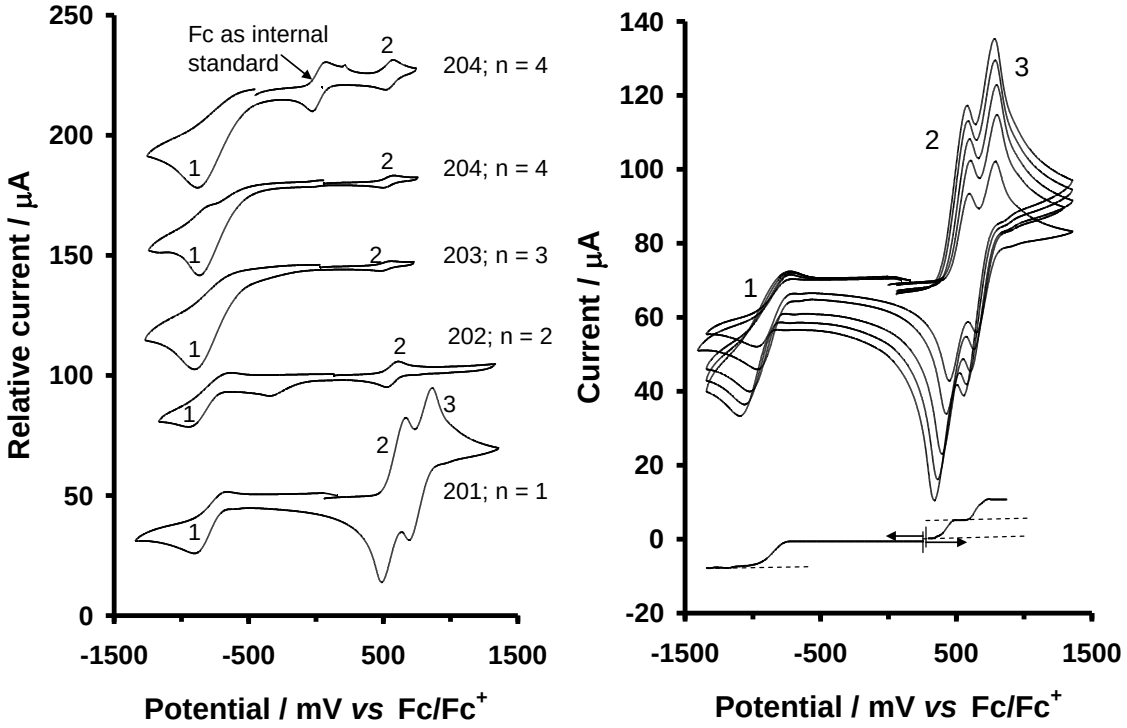

Figure 3.41. Left: Cyclic voltammograms of the various solutions of 2.0 mmol dm^{-3} $[(C_5H_5)_2Ti(O(CH_2)_nFc)_2]$ measured in CH_2Cl_2/0.1 mol dm^{-3} $[NBu_4][B(C_6F_5)_4]$ at glassy carbon-working electrode and a scan rate of 200 mV s^{-1}. Right above: The cyclic voltammogram of $[(C_5H_5)_2Ti(O(CH_2)_3Fc)_2]$ (**201**), at scan rates of 100, 200, 300, 400 and 500 mV s^{-1}. Right below: The linear sweep voltammogram of $[(C_5H_5)_2Ti(O(CH_2)_3Fc)_2]$ (**201**), at scan rate 2 mV s^{-1}. T = 25ºC.

The Ti^{4+}/Ti^{3+} couple was found to be electrochemically and chemically irreversible with $\Delta E > 150$ mV and $i_{pa}/i_{pc} = 0.2\text{-}0.5$. At 50 mV s^{-1} scan rate the $(CH_2)_nFc/(CH_2)_nFc^+$ couple were found to be quasi-reversible for all compounds except **204** which showed reversible electrochemical behaviour. Chemically reversiblity with $i_{pa}/i_{pc} = 1.0$ were observed at all scan rates.

In the comparative cyclic voltammograms of **201-204** (Figure 3.41, Left), even though the concentration of all the complexes are the same, the peak current of the ferrocene and titanium fragments of the different complexes are not comparable. As the alkyl chain length between the ferrocene and the oxygen increases, peak anodic current of the $(CH_2)_nFc/(CH_2)_nFc^+$ couple decreases and the peak cathodic current of the Ti^{4+}/Ti^{3+} couple increases. The current fluctuations are possibly attributed to different degrees of substrate deposition on the electrode.

The two expected ferrocenyl waves of the two ferrocenyl groups of **202-204** (wave 2) were overlapping indicating that the ferrocenyl centres exist for all practical purposes independent of each other in these three complexes. For these three complexes, the side chain lengths appear to be long enough to prohibit through-space intra molecular electrostatic communication between electrochemically generated intermediate mixed-valent centres of the

type $[(C_5H_5)_2Ti(O(CH_2)_nFc)(O(CH_2)_nFc^+)]$. Oster Young square wave voltammetry also failed to demonstrate meaningful communication between ferrocenyl and ferrocenium fragments of mixed-valent intermediates for these three complexes. However, complex **201**, $[(C_5H_5)_2Ti(O(CH_2)Fc)_2]$, show two well resolved ferrocenyl peaks labelled 2 and 3 (Figure 3.41). These peaks are typical of multi-nuclear mixed-valent intermediates that are experiencing an electrostatic influence between each other.[1] Because it is only the n = 1 complex **201** that exhibit this behaviour, it is anticipated that through-space intramolecular communication (as opposed to intermolecular communication) of the iron metal centers give rise to the observed peaks 2 and 3 for this complex.

Table 3.28. Cyclic voltammetry data of bis(cyclopentadienyl)di(ferrocenylalkoxy)titanium(IV) complexes, showing peak anodic or cathodic potentials, E_{pa} or E_{pc} (*vs* Fc/Fc^+ couple as an internal standard); difference in peak anodic and peak cathodic potentials, ΔE_p; formal reduction potentials, E^{01}; peak anodic or cathodic currents, i_{pa} or i_{pc}; and peak anodic/peak cathodic current ratios, i_{pa}/i_{pc}, for indicated compounds (concentration 2.0 mmol dm^{-3}) in CH_2Cl_2/0.1 mol dm^{-3} $[NBu_4][B(C_6F_5)_4]$ at T = 25ºC.

v / mV s^{-1}	E_{pc1} / mV	ΔE_{p1} / mV	$E^{01}{}_1$ / mV	i_{pc1} / μA	i_{pa}/i_{pc}	E_{pa2} / mV	ΔE_{p2} / mV	$E^{01}{}_2$ / mV	i_{pa2} / μA	i_{pc}/i_{pa}
$(C_5H_5)_2Ti(O(CH_2)Fc)_2$, **201**										
50	-941	-	-	12.8	-	619[a] 812[b]	142[a] 143[b]	548[a] 741[b]	10.6[a] 11.2[b]	1.0[a] 1.0[b]
100	-980	236	-862	15.6	0.4	604[a] 791[b]	168[a] 160[b]	520[a] 711[b]	23.7[a] 22.9[b]	0.97[a] 0.9[b]
200	-921	272	-785	19.9	0.5	677[a] 871[b]	199[a] 174[b]	578[a] 784[b]	31.9[a] 32.8[b]	1.0[a] 1.0[b]
200[Fc]	-930	249	-806	19.2	0.5	682[a] 873[b]	209[a] 169[b]	578[a] 789[b]	34.6[a] 34.2[b]	1.02[a] 0.98[b]
300	-1032	476	-794	22.7	0.4	610[a] 806[b]	224[a] 211[b]	498[a] 701[b]	38.5[a] 37.7[b]	1.0[a] 0.94[b]
400	-1070	514	-813	24.9	0.3	595[a] 797[b]	241[a] 219[b]	475[a] 688[b]	43.4[a] 43.4[b]	1.0[a] 0.97[b]
500	-1106	536	-838	26.3	0.3	590[a] 794[b]	263[a] 250[b]	459[a] 669[b]	46.7[a] 45.9[b]	1.0[a] 1.0[b]
$(C_5H_5)_2Ti(O(CH_2)_2Fc)_2$, **202**										
50	-925	-	-	10.6	-	620	101	564	0.5	1.0
100	-919	269	-784	12.9	0.2	613	96	565	1.1	1.0
200	-933	283	-791	15.8	0.2	604	92	566	2.3	1.0
200[Fc]	-1009	402	-808	15.5	0.2	620	109	566	2.1	1.0
300	-947	322	-786	18.8	0.2	618	99	568	4.5	1.0
400	-955	341	-785	21.6	0.2	618	114	561	5.7	1.0
500	-968	362	-787	22.6	0.2	618	122	557	6.6	1.0
$(C_5H_5)_2Ti(O(CH_2)_3Fc)_2$, **203**										
50	-855	-	-	19.1	-	570	97	522	0.6	1.0
100	-871	-	-	23.4	-	564	91	518	0.9	1.0
200	-916	-	-	32.6	-	563	94	516	1.2	1.0
200[Fc]	-1038	-	-	30.2	-	573	114	516	1.0	1.0
300	-947	-	-	36.3	-	564	98	515	1.8	1.0
400	-991	-	-	44.7	-	567	103	515	2.1	1.0
500	-1021	-	-	53.2	-	567	105	514	2.4	1.0

Table 3.28. (continued) Cyclic voltammetry data of bis(cyclopentadienyl)di(ferrocenylalkoxy)titanium(IV) complexes, showing peak anodic or cathodic potentials, E_{pa} or E_{pc} (*vs* Fc/Fc^+ couple as an internal standard); difference in peak anodic and peak cathodic potentials, ΔE_p; formal reduction potentials, E^{01}; peak anodic or cathodic currents, i_{pa} or i_{pc}; and peak anodic/peak cathodic current ratios, i_{pa}/i_{pc}, for indicated compounds (concentration 2.0 mmol dm^{-3}) in CH_2Cl_2/0.1 mol dm^{-3} $[NBu_4][B(C_6F_5)_4]$ at T = 25ºC.

v / mV s^{-1}	E_{pc1} / mV	ΔE_{p1} / mV	$E^{01}{}_1$ / mV	i_{pc1} / μA	i_{pa}/i_{pc}	E_{pa2} / mV	ΔE_{p2} / mV	$E^{01}{}_2$ / mV	i_{pa2} / μA	i_{pc}/i_{pa}
$(C_5H_5)_2Ti(O(CH_2)_4Fc)_2$, **204**										
50	-836	-	-	20.4	-	590	88	546	0.8	1.0
100	-856	-	-	26.3	-	595	87	551	1.6	1.0
200	-875	-	-	34.8	-	590	92	544	1.9	1.0
200[Fc]	-897			32.2		581	74	544	1.7	1.0
300	-916	-	-	43.1	-	600	94	553	3.9	1.0
400	-935	-	-	49.3	-	603	101	553	4.2	1.0
500	-951	-	-	56.2	-	605	103	554	5.1	1.0

Fc: The cyclic voltammogram with ferrocene as internal standard at scan rate 200 mV s^{-1}.

a) Data is associated with wave 2.

b) Data is associated with wave 3.

Comparison of the formal reduction potential (E^{01}) of the ferrocenyl groups *vs* the alkyl chain length (Figure 3.42, Left) showed no direct relationship, however the general trend appears to be that as the alkyl chain length increased, E^{01} decreased. This is because as the alkyl chain length increased; the ferrocenyl moiety is less under the influence of the electron-withdrawing effect of the oxygen and titanium, making the ferrocenyl group easier to oxidize.

Comparison of the peak cathodic potential of the Ti^{4+}/Ti^{3+} couple showed that for complexes with n > 1 that as the alkyl chain length increased (Figure 3.42, Right), E_{pc} increased. This result is consistent with the Ti complex becoming easier to reduce as it becomes more under the influence of the electrondonating ferrocenyl group with shorter chain lengths.

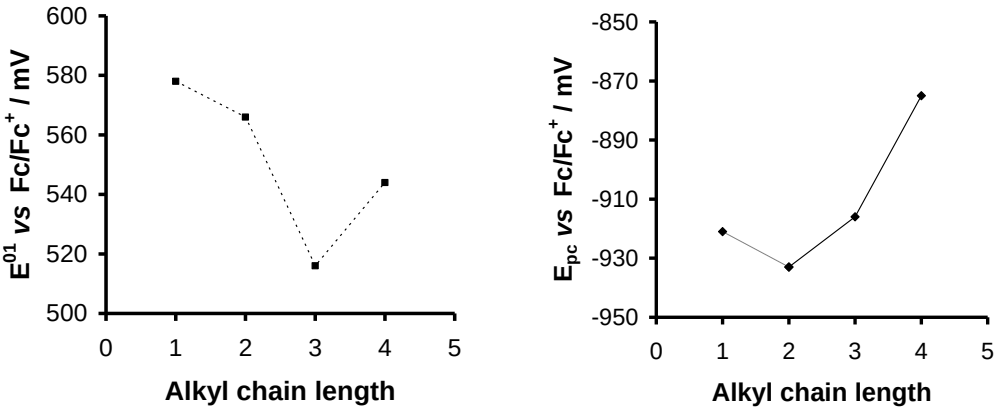

Figure 3.42. Left: Graph of the comparison of E^{01} of the $(CH_2)_nFc/(CH_2)_nFc^+$ couple *vs* the alkyl chain length of **201-204** at *v* = 200 mV s^{-1}. Right: Graph of the comparison of E_{pc} of the Ti^{4+}/Ti^{3+} couple *vs* the alkyl chain length of **201-204** at *v* = 200 mV s^{-1}.

3.6.5.4. Cyclopentadienyltri(ferrocenylalkoxy)titanium(IV)

The cyclic voltammetric behaviour of the series of cyclopentadienyltri(ferrocenylalkoxy)titanium(IV) complexes $[(C_5H_5)Ti(O(CH_2)_nFc)_3$, n = 1 (**205**), (**206**), (**207**), 4 (**208**)] were studied in CH_2Cl_2/0.1 mol dm^{-3} $[NBu_4][B(C_6F_5)_4]$. Selected cyclic voltammograms are shown in Figure 3.43. The electrochemical wave associated with the Ti^{4+}/Ti^{3+} couple is labelled 1 and those associated with $(CH_2)_nFc/(CH_2)_nFc^+$ are labelled 2 and 3. Electrochemical data are summerised in Table 3.29.

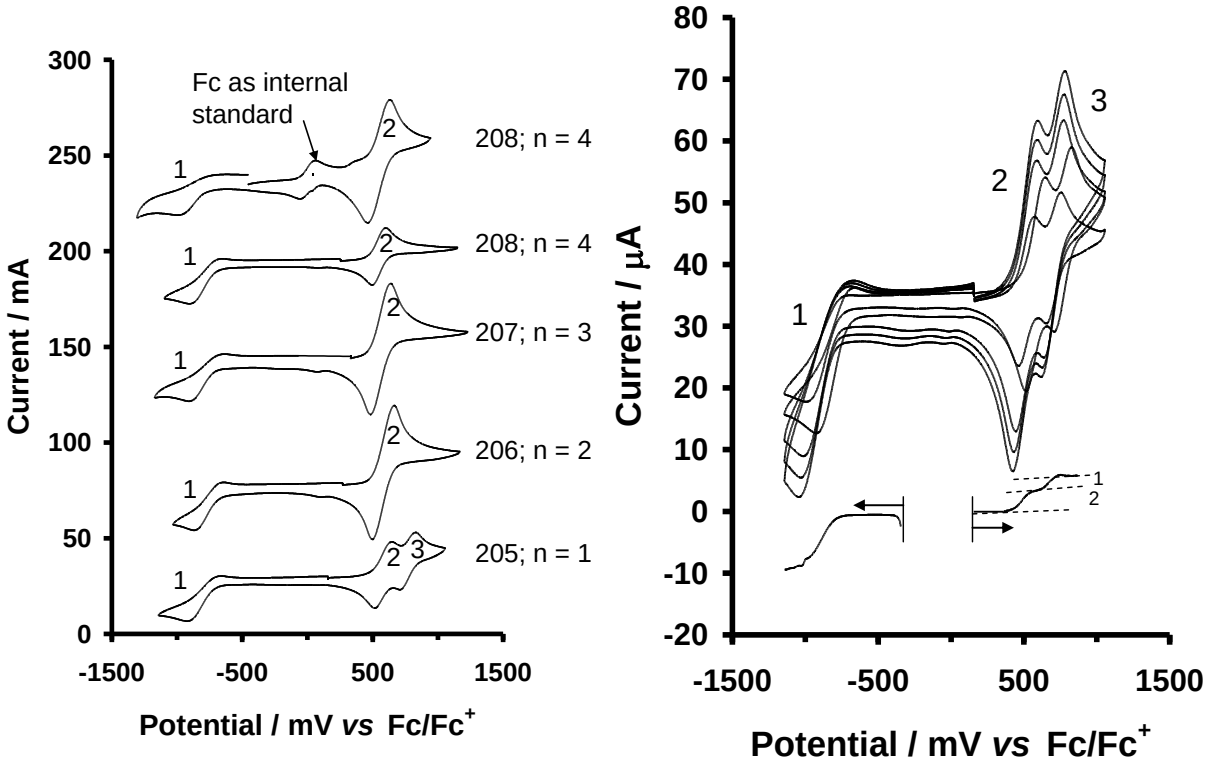

Figure 3.43. Left: Cyclic voltammograms of the various solutions of 2.0 mmol dm^{-3} $[(C_5H_5)Ti(O(CH_2)_nFc)_3]$ measured in CH_2Cl_2/0.1 mol dm^{-3} $[NBu_4][B(C_6F_5)_4]$ at glassy carbon-working electrode and a scan rate of 200 mV s^{-1}. Right: The cyclic voltammogram of $[(C_5H_5)Ti(O(CH_2)_3Fc)_3]$ (**207**), at scan rates of 100, 200, 300, 400 and 500 mV s^{-1}. Right below: The linear sweep voltammogram of $[(C_5H_5)Ti(O(CH_2)_3Fc)_3]$ (**207**), at scan rate 2 mV s^{-1}. T = 25ºC. T = 25ºC.

Despite the LSV traces showing ca. 4 electrons being transferred at wave 1, in comparison with three one-electron transfer processes of the ferrocenyl groups (Figure 3.45 right, below), it is assumed that the titanium(IV) centre is reduced to titanium(III) at wave 1. This assumption is made because Ti^{4+}/Ti^{3+} couples are typically around -0.9 V *vs* Fc/Fc^+.[36] In contrast titanium(II) is formed at *ca.* -2.5 V *vs* Fc/Fc^+. The larger than expected current flows observed in the LSV traces of wave 1 of **205-208** is considered to be the result of substrate deposition on the electrode during LSV scans.

Table 3.29. Cyclic voltammogram data of cyclopentadienyltri(ferrocenylalkoxy)titanium(IV) complexes, showing peak anodic or cathodic potentials, E_{pa} or E_{pc} (*vs* Fc/Fc^+ couple as an internal standard); difference in peak anodic and peak cathodic potentials, ΔE_p; formal reduction potentials, E^{01}; peak anodic or cathodic currents, i_{pa} or i_{pc}; and peak anodic/peak cathodic current ratios, i_{pa}/i_{pc}, for indicated compounds (concentration 2.0 mmol dm^{-3}) in CH_2Cl_2/0.1 mol dm^{-3} $[NBu_4][B(C_6F_5)_4]$ at T = 25ºC.

v / mV s^{-1}	E_{pc1} / mV	ΔE_{p1} / mV	$E^{01}{}_1$ / mV	i_{pc1} / μA	i_{pa}/i_{pc}	E_{pa2} / mV	ΔE_{p2} / mV	$E^{01}{}_2$ / mV	i_{pa2} / μA	i_{pc}/i_{pa}
$(C_5H_5)TiO(CH_2)Fc)_3$, **205**										
50	-978	-	-	12.0	-	601[a] 784[b]	120[a] 110[b]	541[a] 729[b]	9.9[a] 7.6[b]	1.0[a] 1.0[b]
100	-1009	298	-860	13.9	0.1	574[a] 744[b]	124[a] 118[b]	512[a] 685[b]	12.0[a] 8.7[b]	1.0[a] 1.0[b]
200	-943	291	-798	15.4	0.1	653[a] 836[b]	149[a] 133[b]	579[a] 770[b]	14.7[a] 9.1[b]	1.0[a] 1.0[b]
200[Fc]	-973	352	-797	15.2	0.1	654[a] 840[b]	151[a] 147[b]	579[a] 767[b]	17.4[a] 11.4[b]	1.0[a] 1.0[b]
300	-1025	340	-855	18.9	0.1	595[a] 779[b]	160[a] 140[b]	515[a] 709[b]	20.3[a] 12.8[b]	1.0[a] 1.0[b]
400	-1042	371	-857	22.7	0.1	597[a] 783[b]	176[a] 168[b]	509[a] 699[b]	23.2[a] 14.5[b]	1.0[a] 1.0[b]
500	-1053	395	-855	25.2	0.1	601[a] 787[b]	182[a] 179[b]	510[a] 698[b]	25.2[a] 16.6[b]	1.0[a] 1.0[b]
$(C_5H_5)Ti(O(CH_2)_2Fc)_3$, **206**										
50	-924	-	-	10.1	-	623	146	550	10.0	1.0
100	-937	-	-	12.6	-	623	162	542	19.1	1.0
200	-881	248	-757	14.2	<0.1	674	184	582	24.6	1.0
200[Fc]	-1025	431	-809	13.8	<0.1	693	222	582	24.1	1.0
300	-988	332	-822	17.0	<0.1	649	222	538	31.2	1.0
400	-1007	354	-830	21.4	<0.1	651	248	527	32.4	1.0
500	-1029	395	-831	22.7	0.1	661	264	529	35.6	1.0
$(C_5H_5)Ti(O(CH_2)_3Fc)_3$, **207**										
50	-925	-	-	10.1	-	654	136	586	16.0	1.0
100	-930	297	-781	12.3	0.4	634	145	562	24.2	1.0
200	-930	313	-774	16.8	0.3	645	172	559	33.6	1.0
200[Fc]	-975	406	-772	16.2	0.3	652	186	559	33.4	1.0
300	-949	338	-780	19.6	0.2	651	191	556	36.8	1.0
400	-964	362	-783	21.8	0.1	659	209	555	43.2	1.0
500	-984	391	-789	23.5	<0.1	661	228	547	46.4	1.0
$(C_5H_5)Ti(O(CH_2)_4Fc)_3$, **208**										
50	-944	-	-	11.8	-	587	112	531	9.5	1.0
100	-971	-	-	14.1	-	578	118	519	17.8	1.0
200	-922	279	-763	16.5	<0.1	604	119	545	24.1	1.0
200[Fc]	-1012	408	-808	16.1	<0.1	637	184	545	23.4	1.0
300	-994	354	-817	18.8	<0.1	599	164	517	30.4	1.0
400	-1011	371	-826	21.2	<0.1	605	178	516	35.7	1.0
500	-1031	391	-836	23.5	<0.1	616	195	518	38.8	1.0

Fc: The cyclic voltammogram with ferrocene as internal standard at scan rate 200 mV s^{-1}.
a) Data is associated with wave 2.
b) Data is associated with wave 3.

The Ti^{4+}/Ti^{3+} couple was found to be electrochemically and chemically irreversible with ΔE > 150 mV and i_{pa}/i_{pc} = <0.4. The $(CH_2)_nFc/(CH_2)_nFc^+$ couple were found to be

electrochemically quasi-reversible with $110 < \Delta E < 146$ m V at a scan rate of 50 mV s^{-1} and chemically reversible with $i_{pa}/i_{pc} = 1.0$.

In the comparative voltammograms of **205-208** (Figure 3.43, Left), it can be seen that the peak cathodic currents of the Ti^{4+}/Ti^{3+} couples (wave 1) are almost the same for all four complexes and about 14–17 μA at scan rate of 200 mV s^{-1}. However, the peak anodic current for ferrocenyl groups of the different complexes are not comparable; they vary between 10-34 μA at scan rate of 200 mV s^{-1}. It is thought that different degrees of substrate deposition on the working electrode caused the observed current fluctuations.

The three ferrocenyl waves of each of the compounds **206-208** (wave 2) were all overlapping. This indicated that the three ferrocenyl centres exist for all practical purposes independent of each other in these three complexes. However, complex **205**, $[(C_5H_5)TiO(CH_2)Fc)_3]$, shows two well resolved ferrocenyl peaks labelled 2 and 3 (Figure 3.41). Currents for peak 2 were measured 1.4 to 1.6 times larger than for peak 3. The LSV shows peak 2 to be involved in 1.9 times the amount of electrons compaired to peak 3. It is thus concluded that the broadened peak 2 is associated with 2 of the OCH_2Fc groups while peak 3 represents the third OCH_2Fc/OCH_2Fc^+ couple.

Comparison of the formal reduction potential (E^{01}) of the ferrocenyl groups *vs* the alkyl chain length for these complexes with $n \geq 2$ (Figure 3.44, Left), revealed that as the alkyl chain length increased, E^{01} decreased. This is because as the alkyl chain length increased; the ferrocenyl moiety is less under the influence of the electron-withdrawing effects of the oxygen and titanium centres, making the ferrocenyl group easier to oxidize.

Comparison of the peak cathodic potentials or E^{01} values of the Ti^{4+}/Ti^{3+} couple revealed no general trend as the alkyl chain length increased (Figure 3.44, Right). No significance is, however, attributed to this observation because the Ti^{4+}/Ti^{3+} couple is not chemically or electrochemically reversible in the compound series **205-208**.

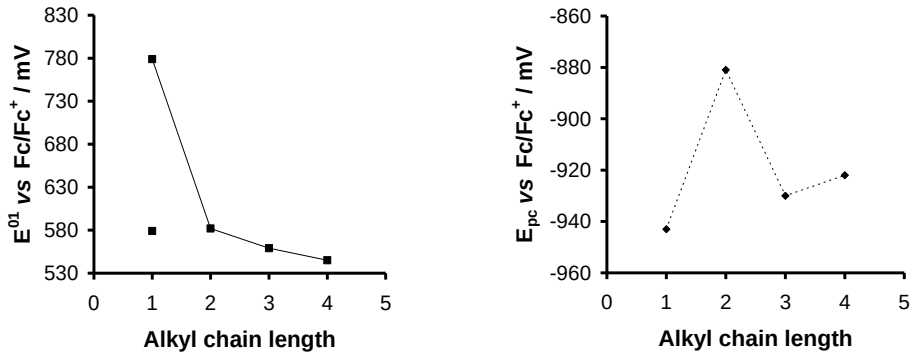

Figure 3.44. Left: Graph of the comparison of E^{01} of the $(CH_2)_nFc/(CH_2)_nFc^+$ couple *vs* the alkyl chain length of **205-208** at v = 200 mV s^{-1}. Right: Graph of the comparison of E_{pc} of the Ti^{4+}/Ti^{3+} couple *vs* the alkyl chain length of **205-208** at v = 200 mV s^{-1}.

3.6.5.5. Tetra(ferrocenylalkoxide)titanium(IV)

The cyclic voltammetric behaviour of the series of tetra(ferrocenylalkoxy)titanium(IV) complexes [Ti(O(CH$_2$)$_n$Fc)$_4$, n = 1 (**209**), 2 (**210**), 3 (**211**), 4 (**212**)] were studied in CH$_2$Cl$_2$/0.1 mol dm^{-3} [NBu$_4$][B(C$_6$F$_5$)$_4$]. Selected cyclic voltammograms are shown in Figure 3.45. The electrochemical wave associated with the Ti^{4+}/Ti^{3+} couple is labelled 1 and those associated with $(CH_2)_nFc/(CH_2)_nFc^+$ are labelled 2 and 3. Electrochemical data is summerised in Table 3.30.

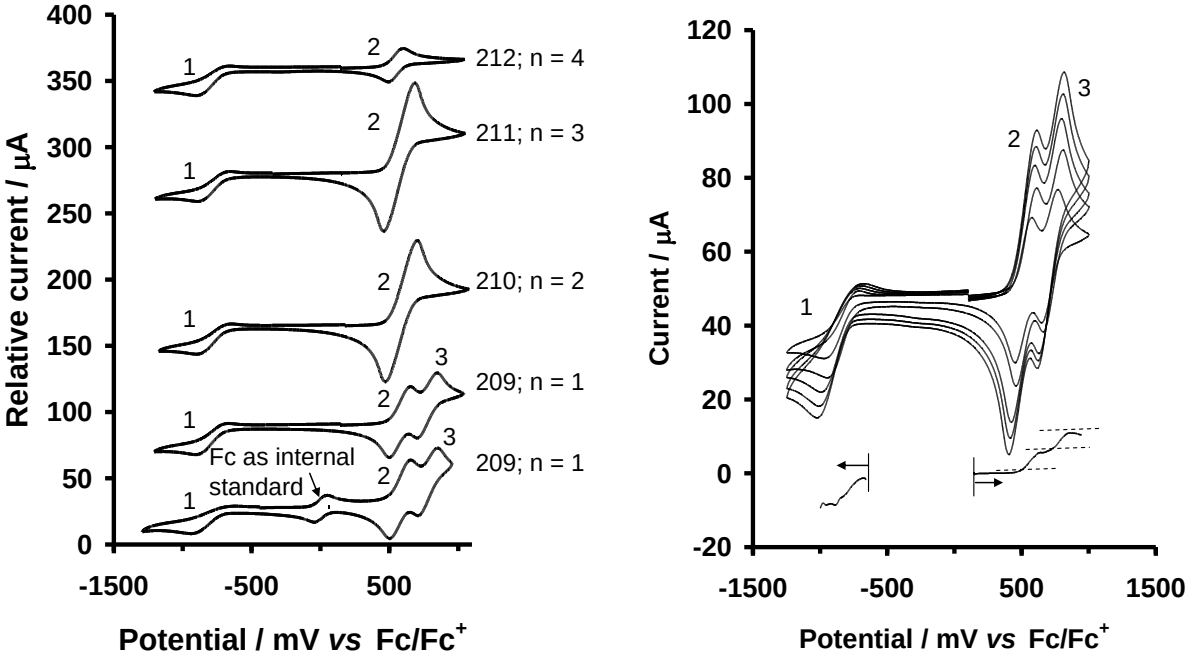

Figure 3.45. Left: Cyclic voltammograms of the various 2.0 mmol dm^{-3} solutions of [Ti(O(CH$_2$)$_n$Fc)$_4$] measured in CH$_2$Cl$_2$/0.1 mol dm^{-3} [NBu$_4$][B(C$_6$F$_5$)$_4$] at a glassy carbon-working electrode and a scan rate of 200 mV s^{-1}. Right above: Cyclic voltammograms of [Ti(O(CH$_2$)Fc)$_4$], (**209**) at scan rates of 100, 200, 300, 400 and 500 mV s^{-1}. Right below: Linear sweep voltammogram of **209** at a scan rate of 2 mV s^{-1}. T = 25ºC.

Ferrocene is known to be involved in a one electron transfer. Thus, in these complexes the ferrocenyl waves labelled 2 and 3 will be a four-fold one-electron transfer process. From the LSV (Figure 3.45, Right below) in comparison with the ferrocenyl waves, the titanium wave (labelled 1) is calculated to indicate transfer of 2 electrons. This would imply that wave 1 will be the Ti^{4+}/Ti^{2+} couple. This is assumed to be incorrect, seeing as Ti^{2+} generation takes place at potentials lower than -2500 mV *vs* Fc/Fc^+.[34] It is assumed that wave 1 is a Ti^{4+}/Ti^{3+} couple, seeing as this couple is typically found around -900 mV.[36] The larger than expected current flows observed in the LSV of wave 1 of **209-212** is considered to be deposition of the substrate on the electrode during the LSV scans.

The Ti^{4+}/Ti^{3+} couple was found to be electrochemically and chemically irreversible with ΔE > 150 mV and i_{pa}/i_{pc} = 0.2-0.5, whereas the ferrocenyl group were found to exhibit

electrochemically quasi-reversible (except for **211**) and chemically reversible with 150 mV > ΔE > 90 mV and i_{pa}/i_{pc} = 1.0.

Table 3.30. Cyclic voltammogram data of $[Ti(O(CH_2)_nFc)_4]$, peak anodic or cathodic potentials, E_{pa} or E_{pc} (*vs* Fc/Fc^+ couple as an internal standard); difference in peak anodic and peak cathodic potentials, ΔE_p; formal reduction potentials, E^{01}; peak anodic or cathodic currents, i_{pa} or i_{pc}; and peak anodic/peak cathodic current ratios, i_{pa}/i_{pc}, for indicated compounds (concentration 2.0 mmol dm^{-3}) in CH_2Cl_2/0.1 mol dm^{-3} $[NBu_4][B(C_6F_5)_4]$ at T = 25ºC.

v / mV s^{-1}	E_{pc1} / mV	ΔE_{p1} / mV	$E^{01}{}_1$ / mV	i_{pc1} / μA	i_{pa}/i_{pc}	E_{pa2} / mV	ΔE_{p2} / mV	$E^{01}{}_2$ / mV	i_{pa2} / μA	i_{pc}/i_{pa}
$Ti(O(CH_2)Fc)_4$, **209**										
50	-950	-	-	13.0	-	617[a] 817[b]	131[a] 130[b]	551[a] 752[b]	16.7[a] 15.4[b]	1.0[a] 1.0[b]
100	-948	-	-	14.6	-	615[a] 820[b]	135[a] 139[b]	548[a] 751[b]	19.2[a] 17.5[b]	1.0[a] 1.0[b]
200	-923	258	-794	17.4	0.2	661[a] 852[b]	175[a] 141[b]	574[a] 781[b]	27.3[a] 25.7[b]	0.90[a] 0.85[b]
200[Fc]	-954	348	-780	16.9	0.2	700[a] 896[b]	169[a] 163[b]	575[a] 774[b]	30.2[a] 28.4[b]	1.0[a] 1.0[b]
300	-964	301	-814	20.6	0.2	648[a] 849[b]	196[a] 174[b]	560[a] 762[b]	33.4[a] 31.2[b]	0.95[a] 0.89[b]
400	-980	339	-811	23.2	0.2	661[a] 861[b]	215[a] 209[b]	553[a] 756[b]	38.3[a] 34.6[b]	0.90[a] 0.85[b]
500	-996	368	-812	25.8	0.2	661[a] 867[b]	228[a] 221[b]	547[a] 756[b]	42.2[a] 40.0[b]	0.90[a] 0.85[b]
$Ti(O(CH_2)_2Fc)_4$, **210**										
50	-924	-	-	13.4	-	668	170	583	30.1	1.0
100	-934	287	-791	15.7	0.5	677	203	576	44.2	1.0
200	-940	291	-795	19.6	0.4	706	241	585	60.5	1.0
200[Fc]	-978	372	-792	19.0	0.4	718	267	585	58.7	1.0
300	-952	310	-797	21.3	0.4	704	281	564	71.2	1.0
400	-980	329	-816	23.5	0.2	711	309	557	79.8	1.0
500	-1009	352	-833	25.7	0.2	717	331	552	88.4	1.0
$Ti(O(CH_2)_3Fc)_4$, **211**										
50	-939	-	-	11.7	-	627	210	522	26.3	1.0
100	-946	-	-	14.3	-	623	186	530	41.6	1.0
200	-908	282	-767	17.5	0.5	681	232	565	59.8	1.0
200[Fc]	-958	376	-770	17.2	0.4	674	219	565	58.3	1.0
300	-955	290	-810	19.6	0.4	681	282	540	65.0	1.0
400	-974	298	-825	22.3	0.3	693	305	541	78.0	1.0
500	-993	349	-819	24.4	0.2	703	328	539	88.4	1.0
$Ti(O(CH_2)_4Fc)_4$, **212**										
50	-907	-	-	13.3	-	599	104	547	5.5	1.0
100	-910	-	-	15.6	-	601	110	546	10.1	1.0
200	-922	270	-787	18.7	0.3	606	122	545	13.3	1.0
200[Fc]	-973	349	-799	18.4	0.3	612	135	545	13.0	1.0
300	-937	290	-792	21.8	0.3	608	133	541	15.6	1.0
400	-950	322	-789	23.4	0.3	615	146	542	18.7	1.0
500	-967	348	-793	25.0	0.3	617	151	541	21.1	1.0

Fc: The cyclic voltammogram with ferrocene as internal standard at scan rate 200 mV s^{-1}.

a) Data is associated with wave 2.

b) Data is associated with wave 3.

In the comparative cyclic voltammograms of **209-212** (Figure 3.45, Left), it can be seen that the peak cathodic current of the Ti^{4+}/Ti^{3+} couples (wave 1) are almost the same and about 18-20 μA at scan rate of 200 mV s^{-1} for all four complexes. However, the peak anodic current for ferrocenyl groups of the different complexes are not comparable, they vary between 13-60 μA at scan rate of 200 mV s^{-1}. The observed current fluctuations are attributed to different degrees of substrate deposition on the working electrode.

For the complexes **210-212** it was found that the four expected ferrocenyl-based waves are all overlapping. This implies that for all practical purposes they exist independent of each other in these complexes. It appears that in these complexes the side chain is long enough to prohibit through-space intra molecular electrostatic communication between electrochemically generated intermediate mixed-valent centres. Oster Young square wave voltammetry also failed to demonstrate meaningful communication between ferrocenyl and ferrocenium fragments of the mixed valent intermediates for these three complexes. However, the CV of **209**, $[Ti(O(CH_2)Fc)_4]$, showed two well resolved ferrocenyl peaks labelled 2 and 3 (Figure 3.45). These peaks are typical of multinuclear mixed-valent intermediates that are experiencing an electrostatic influence from each other.[1] Seeing as this was only observed for the n = 1 complex **209**, it is anticipated that the through-space intramolecular communication (i.e. not intermolecular communication) of the iron metal centres as shown in Scheme 3.28 give rise to the observed peaks 2 and 3 for this complex. Both the LSV and the CV i_{pa} currents indicate that peak 2 and peak 3 draw approximately the same amount of current. This implies peak 2 is associated with the oxidation and reduction of the first two OCH_2Fc groups, while peak 3 is associated with two simultaneous one-electron processes for the third and fourth OCH_2Fc groups.

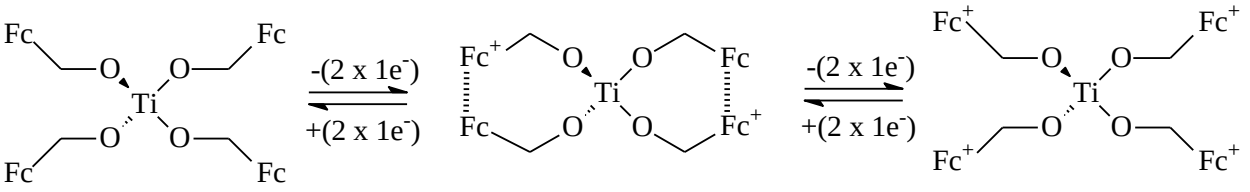

Scheme 3.28. Proposed intramolecular communication between mixed valent Fc and Fc^+ centres in **209**, $[Ti(O(CH_2)Fc)_4]$, that is generated during cyclic voltammetry, LSV and SW voltammetry.

Comparison of the formal reduction potential (E^{01}) of the ferrocenyl groups *vs* the alkyl chain length with n ≥ 2 (Figure 3.46, Left), revealed that as the alkyl chain length increased, E^{01} decreased. This is because as the alkyl chain length increased, the ferrocenyl moiety is less under

the influence of the electron-withdrawing effect of the oxygen and titanium centres, making the ferrocene easier to oxidize.

Comparison of the peak cathodic potential or E^{01} of the Ti^{4+}/Ti^{3+} couple revealed no general trend as the alkyl chain length increased (Figure 3.46, Right). No significant meaning is, however, attributed to this observation because the Ti^{4+}/Ti^{3+} couple is chemically and electrochemically irreversible in this compound series **209-212**.

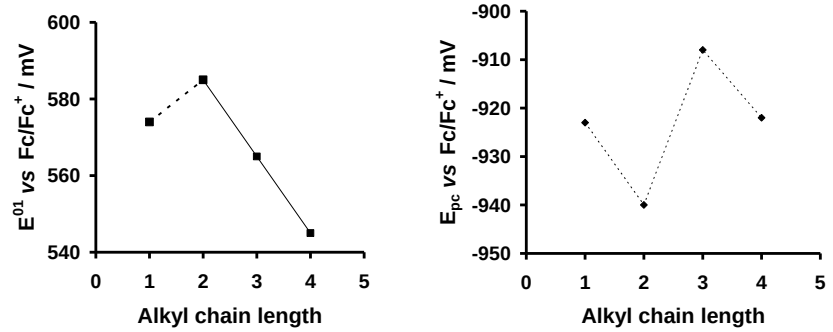

Figure 3.46. Left: Graph of the comparison of E^{01} of the $(CH_2)_nFc/(CH_2)_nFc^+$ couple *vs* the alkyl chain length of **209-212** v = 200 mV s^{-1}. Right: Graph of the comparison of E_{pc} of the Ti^{4+}/Ti^{3+} couple *vs* the alkyl chain length of **209-212** v = 200 mV s^{-1}.

3.6.5.6. Dichlorobis(β-diketonato)titanium(IV)

The cyclic voltammetric behaviour of the series of dichlorobis(β-diketonato)titanium(IV) complexes [$TiCl_2$(RcCOCHCOR)$_2$, R = $C_{10}F_{21}$ (**213**), CF_3 (**214**), C_6F_5 (**215**), $C_{10}H_{21}$ (**216**), CH_3 (**217**), Rc (**218**) and Fc (**219**)] were studied in CH_2Cl_2/0.1 mol dm^{-3} [NBu_4][$B(C_6F_5)_4$]. Selected cyclic voltammograms are shown in Figure 3.47. Electrochemical data are summerised in Table 3.31.

Figure 3.47 (Left) shows the comparative cyclic voltammograms of [$TiCl_2$(RcCOCHCOR)$_2$, R = $C_{10}F_{21}$ (**213**), CF_3 (**214**), C_6F_5 (**215**), $C_{10}H_{21}$ (**216**), CH_3 (**217**), Rc (**218**) and Fc (**219**)]. A blow up CV of **217**, **218** (Figure 3.47), **214** and **216** (Figure 3.48) is also shown.

Peak 1 (Figure 3.47 and 3.48) shows electrochemically irreversible Ti^{4+} reduction to Ti^{3+} with ΔE > 150 mV. Peak 2 represents a multitude of signals that is associated with the irreversible one-electron oxidation of the ruthenocenyl groups to ruthenocenium groups. However, the product fragment Rc^+ species is in equilibrium with the dimeric species $(Rc_{fragment})_2^{2+}$ as shown in the following equation:

$$2(Rc_{fragment}) \xrightarrow{2(-e^-)} 2(Rc^+_{fragment}) \rightleftharpoons (Rc_{fragment} - Rc_{fragment})_2^{2+}$$

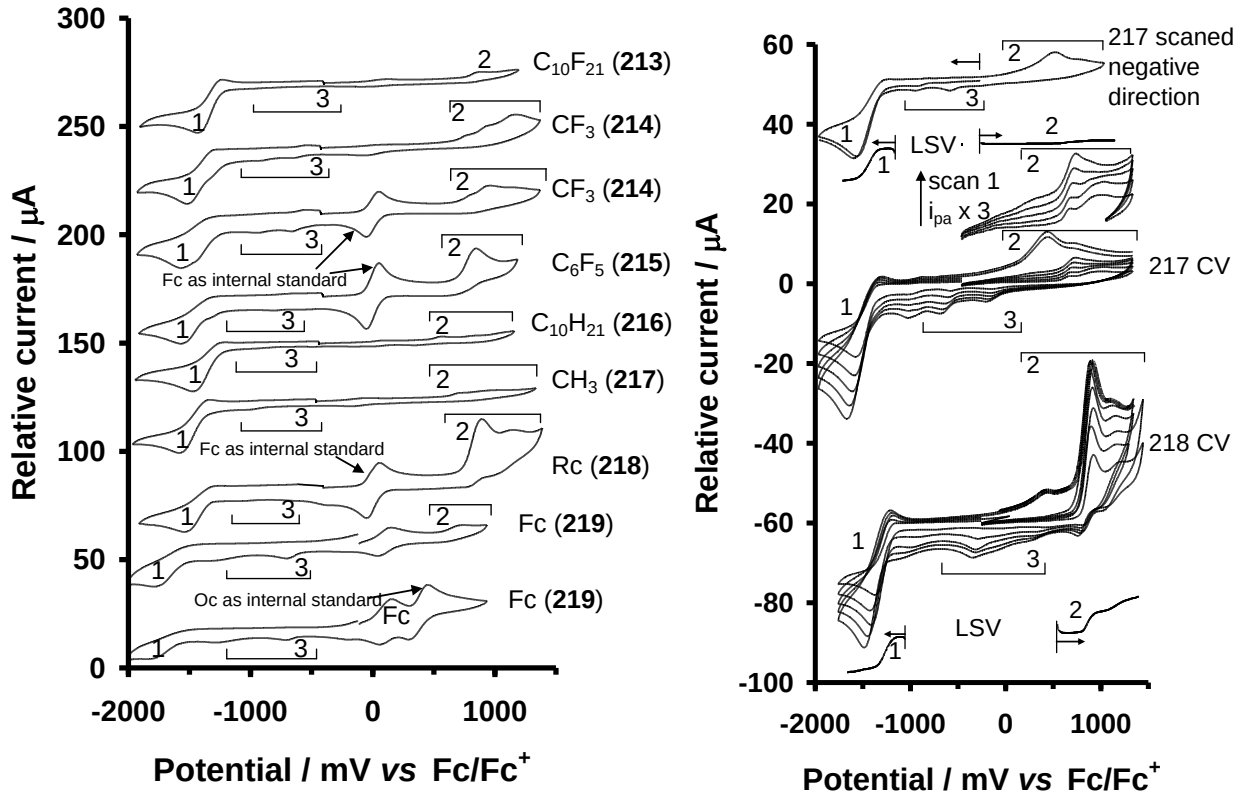

Figure 3.47. Left: Cyclic voltammograms (CV) of the 2.0 mmol dm^{-3} solutions of $[TiCl_2(RcCOCHCOR)_2]$ measured in CH_2Cl_2/0.1 mol dm^{-3} $[NBu_4][B(C_6F_5)_4]$ at a glassy carbon-working electrode and a scan rate of 200 mV s^{-1}. T = 25ºC. Peak 1 is associated with the Ti^{4+}/Ti^{3+} couple, peak 2 with the Rc/Rc^+ couple and peak 3 with reduction of $(Rc^+\text{-}Rc^+)$. Fc = ferrocenyl/ferrocenium, Oc = osmocenyl/osmocenium and Rc = ruthenocyl. Right top and middel: CV's and LSV of $[TiCl_2(RcCOCHCOCH_3)_2]$ at scan rates 100, 200, 300 400 and 500 mV s^{-1}. The CV at the top was scanned in the negative direction at scan rate 200 mV s^{-1}. Note peak 3 is absent during the first cycle, it only appears during cycle 2, after the Rc fragment oxidation took place. The insert peak extrapolation is peak 2 with current blown up 3 times, the LSV trace shows that extensive electrode deposition during the reduction cycle of wave 1 occurs. Right Bottom: CV's and LSV of $[TiCl_2(RcCOCHCORc)_2]$ at scan rates 100, 200, 300 400 and 500 mV s^{-1}.

Only the complex $[TiCl_2(RcCOCHCORc)_2]$, 218, showed any sign of $(Rc_{fragment})^+$ reduction with a very weak reduction peak at wave 2 that could only be clearly identified at fast scan rates. Proof of the existence of the dimeric $(Rc_{fragment}—Rc_{fragment})_2^{2+}$ species, in analogy with free ruthenocene, is proposed to be the set of peaks labelled 3 in each cyclic voltammogram. Peak 3 and peak 2 are both multiple peaks and clearly linked to each other because if the scan direction is chosen to first be in the negative direction, then peak 3 was never observed during the first cycle (Figure 3.47, Top). However, unambiguous proof that the complex series $[TiCl_2(RcCOCHCOR)_2]$ exists as a dimer upon ruthenocene oxidation is still not available. It is hoped that isolation of the product formed at peak 2 during a bulk electrolyses experiment may lead to a crystal structure in future research. Only then will the hypotheses that Rc^+ fragments in

these complexes dimerise be proved. The multiple peaks observed for wave 2 and 3 are consistent with the view that more than one isomer of each complex exists. This was also observed in the ^{1}H NMR spectra of these complexes (see section 3.2.4.6, p 92). In contrast to the irreversible nature of waves 1, 2 and 3 the the Fc/Fc^+ couple of $[TiCl_2(RcCOCHCOFc)_2]$ were found to be electrochemically quasi-reversible and chemically reversible with ΔE = 112-136 mV and i_{pc}/i_{pa} = 1.0 (Figure 3.47 and Table 3.31).

There are no direct relationships between the apparent group electronegativity of the R-group and the peak cathodic potential of Ti^{4+}/Ti^{3+} couple and the peak anodic potential of the Rc/Rc^+ couple, but the general trend appears to be as χ_R increases the E_{pc} of Ti^{4+}/Ti^{3+} couple decreases and E_{pa} of the Rc/Rc^+ couple increases. This is what was expected, because as χ_R increases, a relatively larger positive charge is induced on the Ti^{4+} of titanium(IV) and ruthenocenyl centres, this makes the Ti^{4+} easier to reduce and Rc more difficult to oxidise.

From the cyclic voltammograms in Figure 3.47 and 3.48 it can be seen that as the scan rate increases, the oxidation peak of the Ti^{4+}/Ti^{3+} couple (of **216, 217** and **218**) and the reduction peak of Rc/Rc^+ couple (of **216**) increases slightly which is a consequence of the electrochemical irreversible nature of these couples. Another interesting point that can be seen from Figures 3.47 and 3.48 is that i_{pc} for peak 1 is always very large. The shape of this reduction wave is typical of excessive electrode deposition taking place. Sometimes the reduction half wave of peak 1 is preceded by a small peak adjacent to it. This peak is not regarded as part of wave 3, but is rather interpreted as an electrode deposition artefact of the Ti^{4+} reduction wave. This is especially well demonstrated for the CV that was initiated in the negative direction for $[TiCl_2(RcCOCHCOCH_3)_2]$ (Figure 3.47, Top right). The consequence of this electrode deposition at wave 1 is clearly seen in wave 2 during the second CV cycle. In each case peak 2 became much larger with an intense peak observed at the onset of wave 2. The complex $[TiCl_2(RcCOCHCORc)_2]$ suffered the least from electrode deposition as peak 2 is the least distorted for this complex during the second CV cycle (Figure 3.47, bold line). The LSV curves for **217** and **218** also shows large electrode poisoning (deposition) at peak 1 compared to peak 2. For $[TiCl_2(RcCOCHCOCH_3)_2]$, (**217**), as the scan rate increases, one of the sub peaks of wave 2 (first cycle) becomes more dominant (Figure 3.47, insert section top, right). This is possibly because as the time passed during the recording of the consecutive cyclic voltammograms, one of the possible isomers of $[TiCl_2(RcCOCHCOCH_3)_2]$ is more stable and its peak becomes more dominant as the equilibrium between isomers sets in. This was actually found by other researchers when it was found that isomers having the b-diketonato ligands in the *cis* conformation are actually preferred over isomers having the b-diketonato ligands in the *trans* conformation. (Representative different isomers are shown in Figure 3.23, p 116).

Table 3.31. Cyclic voltammetric data of dichlorobis(β-diketonato)titanium(IV) complexes showing peak anodic or cathodic potentials, E_{pa} or E_{pc} (*vs* Fc/Fc^{+} couple as an internal standard); difference in peak anodic and peak cathodic potentials, ΔE_p; formal reduction potentials, E^{01}; peak anodic or cathodic currents, i_{pa} or i_{pc}; and peak anodic/peak cathodic current ratios, i_{pa}/i_{pc}, for indicated compounds (concentration 2.0 mmol dm^{-3}) in CH_2Cl_2/0.1 mol dm^{-3} $[NBu_4][B(C_6F_5)_4]$ at 25ºC.

v / mV s^{-1}	E_{pc1} / mV	ΔE_{p1} / mV	$E^{01}{}_1$ / mV	i_{pc1} / μA	i_{pa}/i_{pc}	E_{pa2} / mV[a]	i_{pc2} / μA[b]	E_{pa3} / mV	i_{pc3} / μA
$TiCl_2(RcCOCHCOC_{10}F_{21})_2$ (**213**); χ_{C10F21} = 3.04									
50	-1471	-	-	10.8	-	849	0.8	-79	1.7
100	-1493	232	-1377	14.3	0.6	805	1.1	-85	2.0
200	-1533	294	-1386	17.9	0.6	839	1.7	-97	2.3
300	-1527	220	-1417	21.4	0.5	787	2.4	-109	2.6
400	-1569	242	-1448	25.0	0.5	757	3.6	-129	3.0
500	-1605	266	-1472	28.6	0.4	735	4.9	-151	3.4
$TiCl_2(RcCOCHCOCF_3)_2$ (**214**); χ_{CF3} = 3.01									
50	-1525	-	-	21.1	-	737; 913; 1103	7.9; 7.0; 3.9	-75; -373; -665	1.3; 0.8; 2.6
100	-1533	-	-	24.9	-	745; 921; 1077	8.4; 8.4; 4.8	-85; -387; -671	2.4; 1.2; 3.6
200	-1551	-	-	28.7	-	761; 933; 1115	9.0; 9.8; 5.7	-71; -397; -679	3.5; 1.6; 4.6
300	-1585	-	-	32.5	-	767; 965; 1117	9.5; 11.2; 6.6	-81; -433; -689	4.7; 2.1; 5.7
400	-1605	-	-	36.3	-	771; 967; 1129	9.9; 12.6; 7.5	-89; -443; -689	5.9; 2.5; 6.7
500	-1631	-	-	40.1		779; 969; 1125	10.5; 14.1; 8.6	-105; -451; -697	7.0; 3.1; 7.9
$TiCl_2(RcCOCHCOC_6F_5)_2$ (**215**); χ_{C6F5} = 2.46									
50	-1550	-	-	11.4	-	758; 1088	7.4;5.8	-90; -590	0.1; 3.1
100	-1558	-	-	13.5	-	782; 1112	7.5; 8.7	-94; -590	1.2; 2.9
200	-1570	276	-1432	15.6	0.5	799; 1126	7.6; 11.6	-96; -614	2.5; 2.6
300	-1572	288	-1428	17.7	0.4	816; 1140	7.7; 14.5	-98; -626	3.8; 2.3
400	-1596	312	-1440	19.8	0.4	808; 1194	7.9; 17.4	-116; -638	4.1; 2.0
500	-1614	334	-1447	22.0	0.3	812; 1214	8.1; 20.3	-130; -642	6.4; 1.7
$TiCl_2(RcCOCHCOC_{10}H_{21})_2$ (**216**); χ_{C10H21} = 2.43									
50	-1688	-	-	11.6	-	-108; 336; 652	0.5; 1.0; 1.5	-228; -328; -658	0.5; 0.8; 0.5
100	-1686	-	-	15.1	-	-102; 336; 658	0.6; 1.1; 1.7	-230; -348; -676	0.5; 0.8; 0.7
200	-1698	270	-1563	18.7	0.6	-100; 344; 654	0.7; 1.2; 1.9	-216; -382; -720	0.6; 0.9; 0.9
300	-1720	286	-1577	22.3	0.5	-86; 350; 667	0.9; 1.4; 2.1	-228; -438; -724	0.6; 1.0; 1.1
400	-1736	306	-1583	25.9	0.4	-84; 354; 680	1.1; 1.6; 2.3	-230; -458; -734	0.7; 1.1; 1.3
500	-1756	340	-1586	29.3	0.3	-82; 358; 686	1.3; 1.8; 2.5	-232; -482; -738	0.7; 1.2; 1.5

Table 3.31. (continued) Cyclic voltammetric data of dichlorobis(β-diketonato)titanium(IV) complexes showing peak anodic or cathodic potentials, E_{pa} or E_{pc} (*vs* Fc/Fc^{+} couple as an internal standard); difference in peak anodic and peak cathodic potentials, ΔE_p; formal reduction potentials, E^{01}; peak anodic or cathodic currents, i_{pa} or i_{pc}; and peak anodic/peak cathodic current ratios, i_{pa}/i_{pc}, for indicated compounds (concentration 2.0 mmol dm^{-3}) in CH_2Cl_2/0.1 mol dm^{-3} $[NBu_4][B(C_6F_5)_4]$ at 25ºC.

v / mV s^{-1}	E_{pc1} / mV	ΔE_{p1} / mV	$E^{01}{}_1$ / mV	i_{pc1} / μA	i_{pa}/i_{pc}	E_{pa2} / mV[a]	i_{pc2} / μA[b]	E_{pa3} / mV	i_{pc3} / μA
$TiCl_2(RcCOCHCOCH_3)_2$ (**217**); χ_{CH3} = 2.34									
50	-1559	-	-	13.2	-	657; 1021	0.9; 2.6	-211; -605	0.4; 2.0
100	-1577	-	-	15.9	-	689; 1023	1.3; 2.3	-161; -587	0.4; 2.3
200	-1591	278	-1452	18.6	0.5	699; 1043	1.7; 1.8	-169; -611	0.4; 2.6
300	-1615	302	-1464	21.3	0.4	717; -	2.1; -	-169; -649	0.3; 2.9
400	-1643	338	-1474	24.1	0.4	729; -	2.4; -	-191; -669	0.3; 3.2
500	-1669	376	-1481	26.8	0.4	741; -	2.9; -	-215; -695	0.3; 3.5
$TiCl_2(RcCOCHCORc)_2$ (**218**); χ_{Rc} = 1.99									
50	-1364	-	-	14.1	-	956; 1272	11.0; 9.8	-	-
100	-1374	-	-	15.2	-	926; 1250	15.4; 9.7	-72	0.7
200	-1426	202	-1316	16.2	0.6	902; 1184	19.9; 9.3	-292	1.0
300	-1416	214	-1309	17.2	0.5	924; 1184	23.4; 8.9	-318	1.4
400	-1450	252	-1324	18.3	0.5	916; 1164	27.8; 8.5	-318	1.8
500	-1486	272	-1350	19.3	0.5	892; 1128	33.5; 8.2	-348	2.1

v / mV s^{-1}	E_{pc1} / mV	i_{pc1} / μA	$E_{pa\,Fc}$ / mV	$\Delta E_{p\,Fc}$ / mV	$E^{01}{}_{Fc}$ / mV	$i_{pc\,Fc}$ / μA	i_{pc}/i_{pa}	E_{pa2} / mV[a]	i_{pc2} / μA[b]	E_{pa3} / mV	i_{pc3} / μA
$TiCl_2(RcCOCHCOFc)_2$ (**219**); χ_{Fc} = 1.87											
50	-1739	8.2	163	112	107	2.7	1.0	704	0.5	-679	0.1
100	-1753	9.2	160	113	104	4.8	1.0	728	0.6	-713	0.2
200	-1791	10.3	159	114	102	6.9	1.0	751	0.6	-699	0.2
300	-1821	11.3	157	120	97	9.0	1.0	781	0.6	-725	0.3
400	-1845	12.4	161	130	96	11.2	1.0	817	0.7	-747	0.4
500	-1867	13.4	161	136	93	13.4	1.0	829	0.7	-767	0.5

a) Most prominent potentials for peak 2 (Rc oxidation) are listed in a sequencial manner, values for the first cycle

b) Currents corresponding to potentials shown in E_p column.

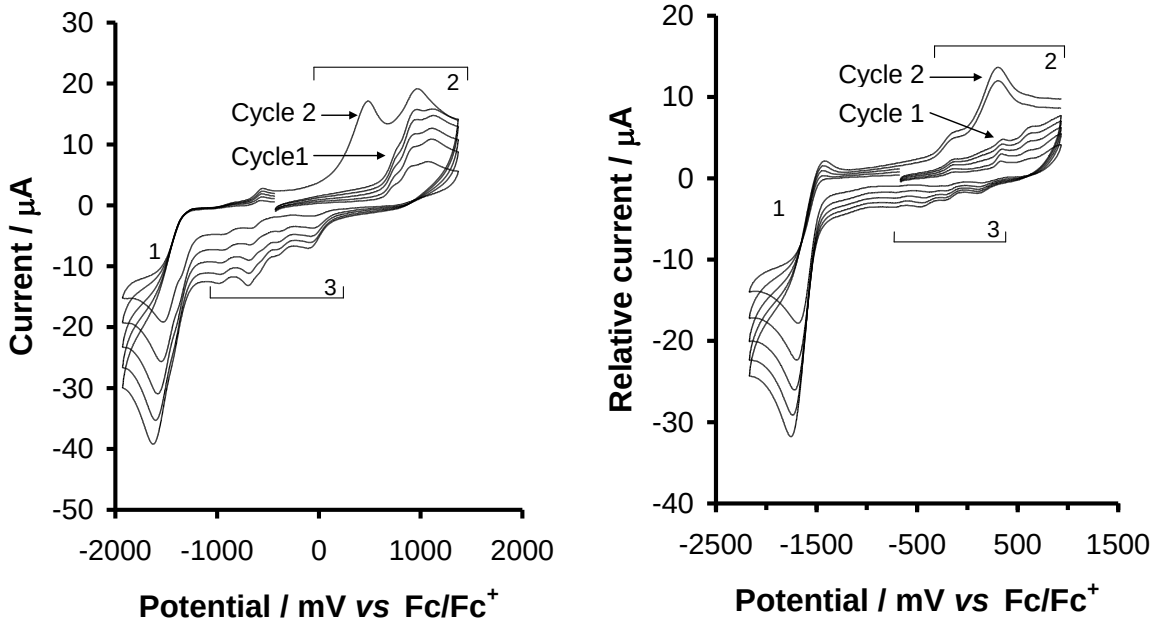

Figure 3.48. Cyclic voltammograms of $[TiCl_2(RcCOCHCOCF_3)_2]$ **214** (Left) and $[TiCl_2(RcCOCHCOC_{10}H_{21})_2]$ **216** (Right) measured in CH_2Cl_2/0.1 mol dm^{-3} $[NBu_4][B(C_6F_5)_4]$ at a glassy carbon-working electrode and scan rates of 100, 200, 300, 400 and 500 mV s^{-1} T = 25ºC.

3.6.5.7. Di(ferrocenylalkoxy)bis(1-ruthenocenoylbutane-1,3-dionato) titanium(IV)

The cyclic voltammetric behaviour of the series of di(ferrocenylalkoxy)bis(1-ruthenocenoylbutane-1,3-dionato)titanium(IV) complexes $[Ti(O(CH_2)_nFc)_2(RcCOCHCOCH_3)_2$, n = 1 (**220**), 2 (**221**), 3 (**222**), 4 (**223**), were studied in CH_2Cl_2/0.1 mol dm^{-3} $[NBu_4][B(C_6F_5)_4]$. Selected cyclic voltammograms are shown in Figure 3.49. Electrochemical data are summerised in Table 3.32. In these complexes there are three redox active centres, namely: the Ti^{4+}/Ti^{3+} couple (which is an electrochemically irreversible process, seeing as the coordination sphere of these particular complexes is not the same for Ti^{IV} and Ti^{III}), the $O(CH_2)_nFc/O(CH_2)_nFc^+$ couple (which is an electrochemically reversible to quasi-reversible and chemically reversible) and $2Rc/[2Rc^+ \rightleftharpoons (Rc_2)^{2+}]$ couple (which is electrochemically irreversible).

Figure 3.49 (Left) shows the comparative cyclic voltammograms of $[Ti(O(CH_2)_nFc)_2(RcCOCHCOCH_3)_2]$, n = 1 (**220**), 2 (**221**), 3 (**222**), 4 (**223**). Peak 1 is associated with the electrochemical irreversible reduction of Ti^{4+} to Ti^{3+} with ΔE > 150 mV. It is not expected that Ti^{2+} forms because the Ti^{3+}/Ti^{2+} couple typically lies at -2500 mV *vs* Fc/Fc^+.[34] Peak 2 represents the quasi-reversible (reversible for **223** at slow scan rates) electrochemical and chemical reversible oxidation wave of the ferrocenyl group of the alkoxy moiety with 90 mV <

$\Delta E < 150$ mV and $i_{pc}/i_{pa} \approx 1$. Lastly peak 3 is assigned to the irreversible oxidation of the ruthenocenyl moiety.

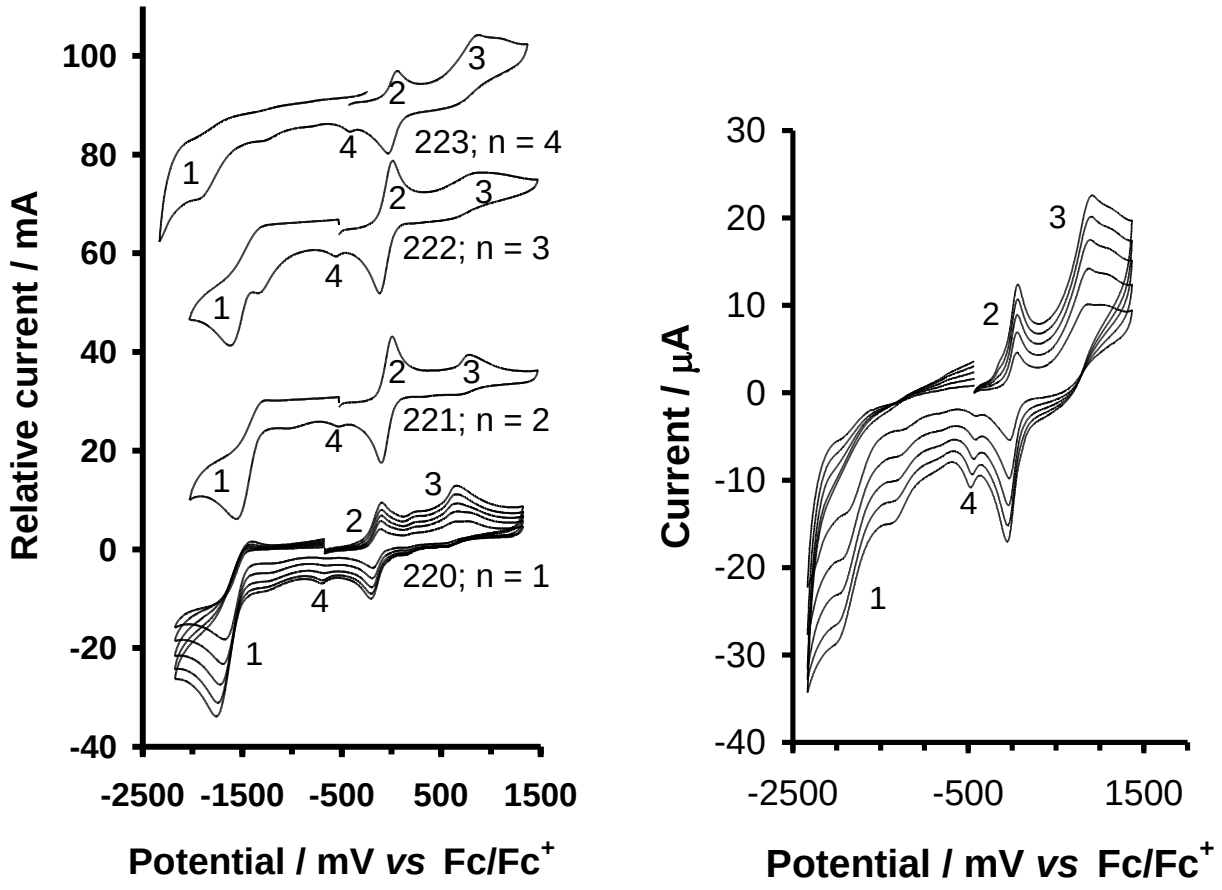

Figure 3.49. Left: Cyclic voltammograms of the 2.0 mmol dm^{-3} solutions of $[Ti(O(CH_2)_nFc)_2(RcCOCHCOCH_3)_2]$ measured in CH_2Cl_2/0.1 mol dm^{-3} $[NBu_4][B(C_6F_5)_4]$ at a glassy carbon-working electrode at 25ºC and a scan rate of 200 mV s^{-1}. Right: Cyclic voltammogram of **223** at scan rates 100, 200, 300, 400 and 500 mV s^{-1}.

This series of complexes showed oxidation peaks for the ruthenocenyl moiety which could be clearly indentified. As was the case with $[TiCl_2(RcCOCHCOR)_2]$ complexes, many isomers exist for each of these $[Ti(O(CH_2)_nFc)_2(RcCOCHCOCH_3)_2]$ complexes, which account for the broadness of peak 3. Unlike the dichlorobis(β-diketonato)titanium complexes (section 3.6.5.6.), these complexes revealed very little formation of the $(Rc_{fragment}—Rc_{fragment})_2^{2+}$ ionic dimer, because of the low intensity reduction peak number 4 in the -500 till -700 mV range. This is possibly because the ferrocenyl alkoxy side chains hamper the formation of the dimer.

Table 3.32. Cyclic voltammogram data of di(ferrocenylalkoxy)bis(1-ruthenocenoylbut-1,3-dionato)titanium(IV) complexes $[Ti(O(CH_2)_nFc)_2(RcCOCHCOCH_3)_2$, peak anodic or cathodic potentials, E_{pa} or E_{pc} (*vs* Fc/Fc^+ couple as an internal standard); difference in peak anodic and peak cathodic potentials, ΔE_p; formal reduction potentials, E^{01}; peak anodic or cathodic currents, i_{pa} or i_{pc}; and peak anodic/peak cathodic current ratios, i_{pa}/i_{pc}, for indicated compounds (concentration 2.0 mmol dm^{-3}) in CH_2Cl_2/0.1 mol dm^{-3} $[NBu_4][B(C_6F_5)_4]$ at T = 25ºC.

v / mV s^{-1}	E_{pc1} / mV	ΔE_{p1} / mV	$E^{01}{}_1$ / mV	i_{pc1} / μA	i_{pc}/i_{pa}	E_{pa2} / mV	ΔE_{p2} / mV	$E^{01}{}_2$ / mV	i_{pc2} / μA	i_{pc}/i_{pa}	E_{pa3} / mV	i_{pc3} / μA
$Ti(O(CH_2)Fc)_2(RcCOCHCOCH_3)_2$ (**220**); n = 1												
50	-1678	-	-	20.1	-	-108	92	-62	2.8	1.0	665	5.7
100	-1682	-	-	25.9	-	-108	84	-66	5.6	1.0	667	7.9
200	-1698	286	-1555	31.8	0.6	-102	94	-55	8.2	1.0	668	9.1
300	-1726	308	-1572	37.7	0.5	-102	98	-53	10.8	1.0	667	10.3
400	-1748	340	-1578	43.6	0.4	-100	106	-47	13.4	1.0	654	12.5
500	-1764	366	-1581	49.6	0.3	-96	112	-40	16.0	1.0	656	16.8
$Ti(O(CH_2)_2Fc)_2(RcCOCHCOCH_3)_2$ (**221**); n = 2												
50	-1538	-	-	12.2	-	-4	102	-55	6.9	1.0	792	1.6
100	-1544	-	-	14.7	-	4	100	-46	9.3	1.0	772	2.2
200	-1568	320	-1408	17.2	0.5	10	112	-46	11.7	1.0	790	2.8
300	-1590	324	-1419	19.7	0.5	14	126	-49	14.1	1.0	804	3.4
400	-1612	376	-1424	22.3	0.4	18	136	-50	16.6	1.0	818	4.0
500	-1634	408	-1430	24.9	0.3	22	146	-51	19.1	1.0	830	4.6
$Ti(O(CH_2)_3Fc)_2(RcCOCHCOCH_3)_2$ (**222**); n = 1												
50	-1546	-	-	9.8	-	2	106	-51	7.2	1.0	830	2.3
100	-1576	-	-	11.6	-	6	114	-51	9.7	1.0	852	3.5
200	-1624	-	-	13.4	-	14	136	-54	12.2	1.0	918	4.4
300	-1662	-	-	15.2	-	18	150	-57	14.7	1.0	934	5.5
400	-1690	-	-	16.9	-	26	164	-56	17.2	1.0	948	6.7
500	-1718	-	-	18.6	-	32	178	-57	19.7	1.0	966	7.5
$Ti(O(CH_2)_4Fc)_2(RcCOCHCOCH_3)_2$ (**223**); n = 4												
50	-1889	-	-	5.5	-	54	84	12	3.5	1.0	868	7.0
100	-1921	-	-	7.1	-	55	86	12	4.6	1.0	871	9.2
200	-1977	-	-	8.5	-	57	92	11	5.7	1.0	877	11.4
300	-1991	-	-	10.1	-	59	104	7	6.8	1.0	891	13.6
400	-1997	-	-	11.6	-	63	114	6	7.9	1.0	903	15.7
500	-2015	-	-	13.0	-	65	122	4	9.0	1.0	915	18.0

Comparison of the E^{01} of Fc/Fc^+ couple *vs* the alkyl chain length of the ferrocenyl-containing alkoxy group revealed no direct relationship exists, however, the general trend indicates as the alkyl chain length increased, E^{01} increased (Figure 3.50). This is contrary to what was expected. Figure 3.50 also indicates how the ferrocenyl group reduction potential of the free alcohol change with chain length.[1] Also, complex $[Ti(O(CH_2)Fc)_2(RcCOCHCOCH_3)_2]$ showed no splitting of the ferrocenyl group into two peaks as did the $[Ti(O(CH_2)Fc)_4]$ (**201**), $[(C_5H_5)Ti(O(CH_2)Fc)_3]$ (**205**) and $[(C_5H_5)_2Ti(O(CH_2)Fc)_2]$ (**209**) complexes (section 3.6.5.3, 3.6.5.4 and 3.6.5.5 respectively).

No direct relationship exists between E_{pa} of Rc/Rc^+ couple and the alkyl chain length of the ferrocenyl-containing alkoxy group. However, the general trend is as the alkyl chain length increased, E_{pa} increased. Again this trend is contrary to what was expected. A few possible explanations could be given. The first could be that the electrochemical irreversible ruthenocene couple (peak 3) is not a true thermodynamic equilibrium. Consequently, no thermodynamic meaning should necessary be attached to the observed relationship between the reduction potentials and chain length. While this could be true for the ruthenocene couple, it does not explain the observed ferrocenyl trend. The more likely explanation, however, is that the through-space interaction between the already oxidised ferrocenyl and ruthenocenyl group is the cause of this behaviour. As the chain length increases the ruthenocenyl group could get into closer proximity to the already oxidised and electron withdrawing ferricenium group when the potentials are reached where the ruthenocenyl group is oxidized. The through-space electron withdrawing effect of the ferricenium on the ruthenocenyl fragment may then be responsible for the increase in ruthenocenyl oxidation potential as ferrocenyl alkoxy chain length increases; the positive charge on the oxidized ferrocenium species induces a more positive charge on the ruthenium, making it more difficult to oxidize. Figure 3.50 shows this diagrammatically. The same argument is applied for the ferrocenyl oxidation but this time the ferrocenyl group is exposed to the electron withdrawing power of the Ti^{4+} moiety.

The absence of a direct relationship between the E_{pc} of Ti^{4+}/Ti^{3+} couple and the alkyl chain length of the ferrocenyl-containing alkoxy group is attributed to the intense electrode deposition of the complex during reduction of Ti^{4+}.

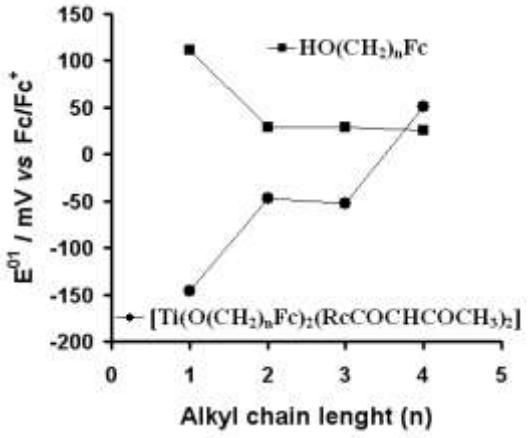

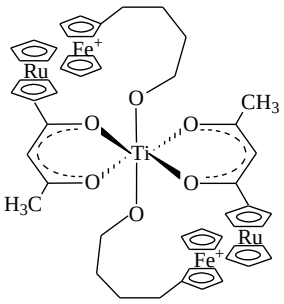

Good through-space interaction between metallocenenyl groups are possibly because close proximity of metallocene can be achieved for long chain alkoxy substituents.

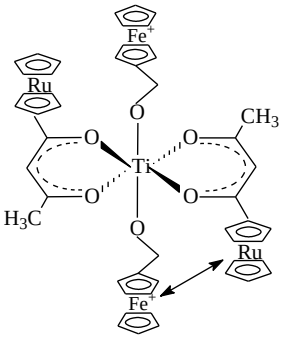

Large seperation implies poor through-space commenucation between metallocenyl group.

Figure 3.50. Left: The comparative graphs of alkyl chain length of either the free ferrocene-containing alcohol (■) or $[Ti(O(CH_2)Fc)_2(RcCOCHCOCH_3)_2]$ (●) *vs* E^{01} of the Fc/Fc^+ couple of the ferrocene-containing alcohol or alkoxy group. Right: A schematic representation of the possible interaction between the ferrocenium moeity and the ruthenocenyl group of the $[Ti(O(CH_2)Fc)_2(RcCOCHCOCH_3)_2]$ complexes.

3.6.5.8. Di(4-ferrocenylbutoxy)bis(β-diketonato)titanium(IV)

The cyclic voltammetric behaviour of the series of di(4-ferrocenylbutoxy)bis(β-diketonato)titanium(IV) complexes $[Ti(O(CH_2)_4Fc)_2(RcCOCHCOR)_2$, R = $C_{10}F_{21}$ (**224**), CF_3 (**225**), C_6F_5 (**226**), $C_{10}H_{21}$ (**227**), CH_3 (**223**), Rc (**228**) and Fc (**229**)] were studied in CH_2Cl_2/0.1 mol dm^{-3} $[NBu_4][B(C_6F_5)_4]$. Selected cyclic voltammograms are shown in Figure 3.51. Electrochemical data are summerised in Table 3.33. As was the case for the diferrocenylalkoxybis(1-ruthenocenoylbutane-1,3-dionato)titanium(IV) complexes (section 3.6.5.7.), these complexes have three redox active centres, namely the Ti^{4+}/Ti^{3+} couple, the $O(CH_2)_nFc/ O(CH_2)_nFc^+$ couple and $2Rc/[2Rc^+ \rightleftharpoons (Rc_2)^{2+}]$ couple.

Peak 1 shows the electrochemical irreversible reduction of Ti^{4+} to Ti^{3+} with $\Delta E > 150$ mV. Peak 2 represents the reversible to quasi-reversible and chemical reversible oxidation wave of the ferrocenyl group of the alkoxy moiety with ΔE = 80-118 mV and $i_{pc}/i_{pa} \approx 1$. Peak 3 is assigned to the irreversible oxidation of the ruthenocenyl moiety. This peak is again broadened due to the presence of many different isomers in solution. The peak labelled 'Fc' belongs to the ferrocenyl moiety of the β-diketonato ligand of **229**. It is evident that the ferrocenyl moiety of the alkoxy group of **229** is oxidized at a lower potential than the ferrocenyl moiety of the β-diketonato ligand. This is rationalised upon recognising that the β-diketone is strongly under the influence of the electronwithdrawing power of the Ti^{4+} centre *via* conjugation in the pseudo-aromatic β-diketonato core. In contrast the ferrocenyl group on the alkoxy chain is isolated from the Ti^{4+} centre by the C_4 linear alkoxy chain.

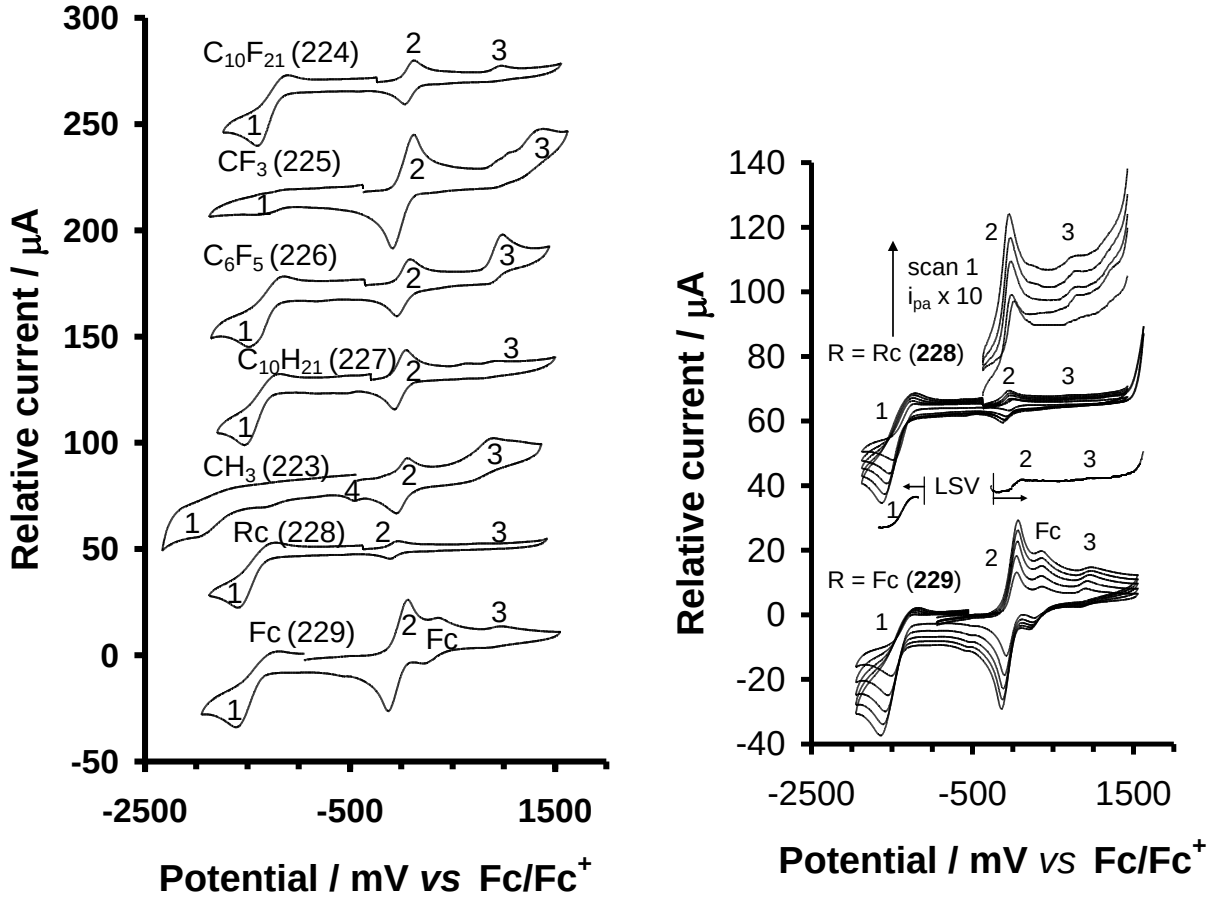

Figure 3.51. Left: Cyclic voltammograms of 2.0 mmol dm^{-3} solutions of $[Ti(O(CH_2)_4Fc)_2(RcCOCHCOR)_2]$ measured in CH_2Cl_2/0.1 mol dm^{-3} $[NBu_4][B(C_6F_5)_4]$ at a glassy carbon-working electrode at 25ºC and a scan rate of 200 mV s^{-1}. Right: Cyclic voltammograms of **228** and **229** (bottom) at scan rates of 100, 200 ,300, 400 and 500 mV s^{-1}. The LSV of **228**, currents are blown up 10 times, is also shown. The insert at the top is peaks 2 and 3 blown up 10 times for **228**.

Again, like the di(ferrocenylalkoxy)bis(1-ruthenocenoylbutane-1,3-dionato)titanium(IV) complexes (section 3.6.5.7.), these complexes show small to no formation of the $(Rc_{fragment}—Rc_{fragment})_2^{2+}$ ionic dimer. The strongest indication of dimer formation in this coumpound series was observed for the R = CH_3 complexes (peak 4).

No direct relationship between the apparent group electronegativity of the R-group and the peak cathodic potential of Ti^{4+}/Ti^{3+} couple and the peak anodic potential of the Rc/Rc^+ couple exists. However, the general trend appears to be as χ_R increases the E_{pc} of Ti^{4+}/Ti^{3+} couple, E^{01} of the $O(CH_2)_nFc/O(CH_2)_nFc^+$ couple and E_{pa} of the Rc/Rc^+ couple increases. This trend is graphically illustatred in Figure 3.52. This is what was expected for the $O(CH_2)_nFc/O(CH_2)_nFc^+$ and Rc/Rc^+ couples, because as χ_R increases, a relatively more positive charge is induced on Fc, Rc and Ti, this makes the Ti easier to reduce and, Fc and Rc more difficult to oxidise.

Table 3.33. Cyclic voltammogram data of di(4-ferrocenylbutoxy)bis(β-diketonato)titanium(IV) complexes $[Ti(O(CH_2)_4Fc)_2(RcCOCHCOR)_2$, peak anodic or cathodic potentials, E_{pa} or E_{pc} (*vs* Fc/Fc^+ couple as an internal standard); difference in peak anodic and peak cathodic potentials, ΔE_p; formal reduction potentials, E^{01}; peak anodic or cathodic currents, i_{pa} or i_{pc}; and peak anodic/peak cathodic current ratios, i_{pa}/i_{pc}, for indicated compounds (concentration 2.0 mmol dm^{-3}) in CH_2Cl_2/0.1 mol dm^{-3} $[NBu_4][B(C_6F_5)_4]$ at T = 25ºC.

v / mV s^{-1}	E_{pc1} / mV	ΔE_{p1} / mV	$E^{01}{}_1$ / mV	i_{pc1} / μA	i_{pc}/i_{pa}	E_{pa2} / mV	ΔE_{p2} / mV	$E^{01}{}_2$ / mV	i_{pc2} / μA	i_{pc}/i_{pa}	E_{pa3} / mV	i_{pc3} / μA
$Ti(O(CH_2)_4Fc)_2(RcCOCHCOC_{10}F_{21})_2$ (**224**); χ_{C10F21} = 3.04												
50	-1341	-	-	11.0	-	137	80	97	2.9	1.0	1011	1.7
100	-1353	248	-1229	14.1	0.6	109	64	77	4.3	1.0	973	2.1
200	-1307	214	-1200	17.2	0.6	191	106	138	5.7	1.0	1021	2.5
300	-1357	266	-1224	20.3	0.5	171	100	121	7.1	1.0	1091	2.9
400	-1407	302	-1256	23.4	0.4	127	96	79	8.5	1.0	977	3.1
500	-1447	330	-1282	26.5	0.3	100	101	50	10.1	1.0	951	3.7
$Ti(O(CH_2)_4Fc)_2(RcCOCHCOCF_3)_2$ (**225**); χ_{CF3} = 3.01												
50	-1443	106	-1390	2.2	0.2	81	111	26	10.7	1.0	1319	11.7
100	-1441	104	-1389	2.9	0.1	97	136	29	13.9	1.0	1323	13.9
200	-1479	-	-	3.6	-	103	160	23	17.1	1.0	1357	16.1
300	-1465	-	-	4.3	-	117	190	22	20.3	1.0	1373	18.3
400	-1437	-	-	5.0	-	123	208	19	23.6	1.0	1395	20.5
500	-1415	-	-	5.8	-	133	226	20	26.7	1.0	1411	22.6
$Ti(O(CH_2)_4Fc)_2(RcCOCHCOC_6F_5)_2$ (**226**); χ_{C6F5} = 2.46												
50	-1427	-	-	10.7	-	33	82	-8	1.4	1.0	887	2.4
100	-1447	228	-1333	13.3	0.5	11	74	-26	2.9	1.0	867	4.6
200	-1435	264	-1303	15.6	0.5	71	112	15	5.3	1.0	917	7.9
300	-1461	310	-1306	18.2	0.4	81	124	19	7.8	1.0	975	11.2
400	-1491	350	-1316	20.8	0.4	95	140	25	10.3	1.0	987	14.5
500	-1515	388	-1321	23.8	0.3	95	146	22	12.8	1.0	997	18.0
$Ti(O(CH_2)_4Fc)_2(RcCOCHCOC_{10}H_{21})_2$ (**227**); χ_{C10H21} = 2.43												
50	-1415	-	-	14.8	-	105	108	51	4.5	1.0	945	1.6
100	-1441	-	-	17.1	-	61	88	17	6.1	1.0	946	2.0
200	-1460	228	-1346	19.7	0.5	62	120	2	7.7	1.0	947	2.3
300	-1491	306	-1338	22.3	0.4	59	106	6	9.3	1.0	943	2.7
400	-1531	344	-1359	24.9	0.4	47	116	-11	10.9	1.0	943	3.1
500	-1557	382	-1366	27.3	0.2	45	126	-18	12.5	1.0	943	3.5

Table 3.33. (continued) Cyclic voltammogram data of di(4-ferrocenylbutoxy)bis(β-diketonato)titanium(IV) complexes $[Ti(O(CH_2)_4Fc)_2(RcCOCHCOR)_2$, peak anodic or cathodic potentials, E_{pa} or E_{pc} (*vs* Fc/Fc^+ couple as an internal standard); difference in peak anodic and peak cathodic potentials, ΔE_p; formal reduction potentials, E^{01}; peak anodic or cathodic currents, i_{pa} or i_{pc}; and peak anodic/peak cathodic current ratios, i_{pa}/i_{pc}, for indicated compounds (concentration 2.0 mmol dm^{-3}) in CH_2Cl_2/0.1 mol dm^{-3} $[NBu_4][B(C_6F_5)_4]$ at T = 25ºC.

v / mV s^{-1}	E_{pc1} / mV	ΔE_{p1} / mV	$E^{01}{}_1$ / mV	i_{pc1} / μA	i_{pc}/i_{pa}	E_{pa2} / mV	ΔE_{p2} / mV	$E^{01}{}_2$ / mV	i_{pc2} / μA	i_{pc}/i_{pa}	E_{pa3} / mV	i_{pc3} / μA
$Ti(O(CH_2)_4Fc)_2(RcCOCHCOCH_3)_2$ (**223**); χ_{CH3} = 2.34												
50	-1889	-	-	5.5	-	54	84	12	3.5	1.0	-1889	7.0
100	-1921	-	-	7.1	-	55	86	12	4.6	1.0	-1921	9.2
200	-1977	-	-	8.5	-	57	92	11	5.7	1.0	-1977	11.4
300	-1991	-	-	10.1	-	59	104	7	6.8	1.0	-1991	13.6
400	-1997	-	-	11.6	-	63	114	6	7.9	1.0	-1997	15.7
500	-2015	-	-	13.0	-	65	122	4	9.0	1.0	-2015	18.0
$Ti(O(CH_2)_4Fc)_2(RcCOCHCORc)_2$ (**228**); χ_{Rc} = 1.99												
50	-1463	-	-	12.5	-	49	80	9	1.3	1.0	871	0.2
100	-1491	274	-1354	15.1	0.8	19	68	4	1.5	1.0	869	0.3
200	-1539	322	-1378	17.7	0.7	-11	98	-60	1.7	1.0	833	0.4
300	-1573	338	-1404	20.3	0.5	-23	122	-84	1.9	1.0	813	0.5
400	-1597	372	-1411	23.0	0.4	-29	142	-100	2.1	1.0	805	0.6
500	-1631	420	-1421	25.7	0.3	-47	176	-135	2.3	1.0	785	0.7

$Ti(O(CH_2)_4Fc)_2(RcCOCHCOFc)_2$ (**229**); χ_{Fc} = 1.87																			
v / mV s^{-1}	E_{pc1} / mV	ΔE_{p1} / mV	$E^{01}{}_1$ / mV	i_{pc1} / μA	i_{pc}/i_{pa}	E_{pa2} / mV	ΔE_{p2} / mV	$E^{01}{}_2$ / mV	i_{pc2} / μA	i_{pc}/i_{pa}	$E_{pa\,Fc}$ / mV	$\Delta E_{p\,Fc}$ / mV	$E^{01}{}_{Fc}$ / mV	$i_{pc\,Fc}$ / μA	i_{pc}/i_{pa}	E_{pa3} / mV	ΔE_{p3} / mV	$E^{01}{}_3$ / mV	i_{pc3} / μA	i_{pc}/i_{pa}
50	-1505	-	-	13.3	-	33	116	-25	9.3	1.0	347	84	305	6.6	1.0	879	-	-	3.9	-
100	-1515	298	-1366	16.5	0.8	49	120	-16	13.0	1.0	349	88	305	7.9	1.0	903	-	-	4.5	-
200	-1555	330	-1390	19.8	0.6	45	160	-35	16.7	1.0	355	114	298	9.2	1.0	923	-	-	5.1	-
300	-1587	376	-1399	23.1	0.4	59	178	-30	20.4	1.0	357	128	293	10.5	1.0	957	-	-	5.7	-
400	-1615	424	-1403	26.4	0.3	63	192	-33	24.1	1.0	357	140	287	11.9	1.0	971	158	892	6.4	0.2
500	-1643	466	-1410	29.2	0.1	67	208	-37	27.9	1.0	355	156	277	13.3	1.0	971	166	888	7.0	0.2

From the cyclic voltammograms in Figure 3.51 and 3.52 it can be seen that the oxidation peak of the Ti^{4+}/Ti^{3+} couple (of **224, 226, 228** and **229**) are more intense than for most other complexes. The LSV's of all complexes showed exessive electrode deposition took place at peak 1 (the Ti^{4+}/Ti^{3+} couple). However, the LSV's also showed that in general the same amount of electrons (2 x 1 e^-) are transferred at peaks 2 and 3. This expected result confirms that electrode deposition at peak 1 does not have an influence on peaks 2 and 3. This is demonstrated in Figure 3.52 for complexes **225** and **226**.

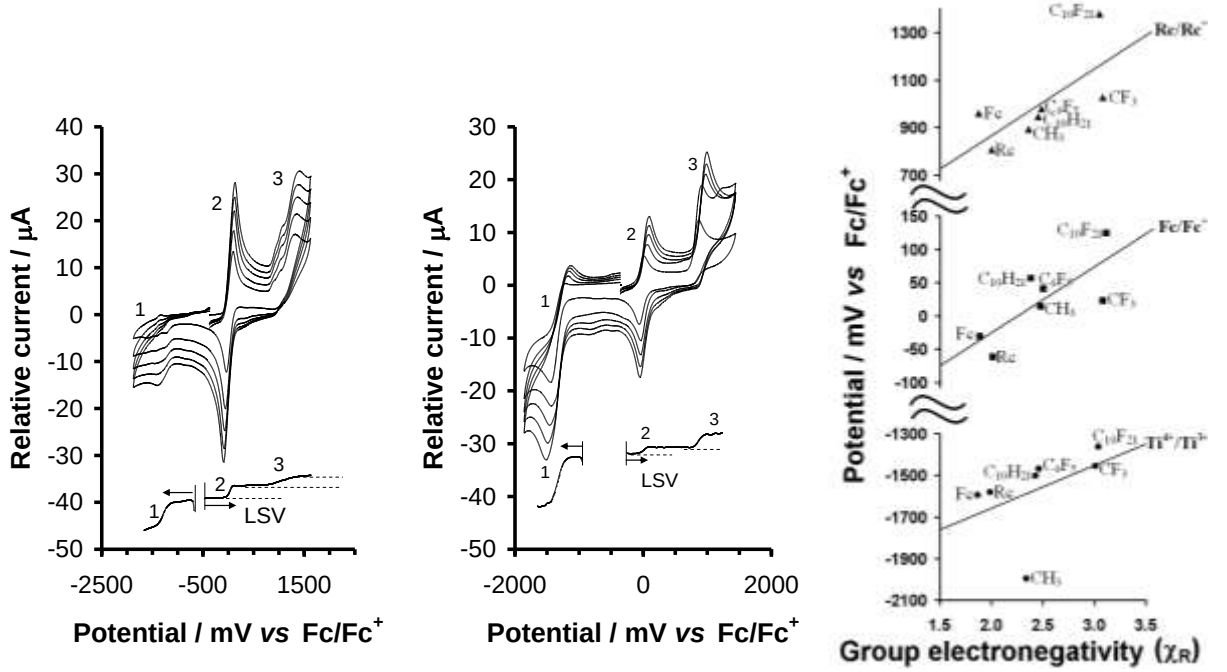

Figure 3.52. Cyclic voltammogram and LSV's of 2.0 mmol dm^{-3} solutions of $[Ti(O(CH_2)_4Fc)_2(RcCOCHCOCF_3)_2]$ **225** (Left) and $[Ti(O(CH_2)_4Fc)_2(RcCOCHCOC_6F_5)_2]$ **226**, (Middel) measured in CH_2Cl_2/0.1 mol dm^{-3} $[NBu_4][B(C_6F_5)_4]$ at a glassy carbon-working electrode at 25ºC and scan rates of 100, 200, 300, 400 and 500 mV s^{-1} at 25ºC. Right: Graph of E_{pc} or E_{pa} of the Ti^{4+}/Ti^{3+}, Fc/Fc^+ and Rc/Rc^+ couples of **223-229** *vs* group electrongativity of the R group.

3.6.5.9. Cyclopentadienyl(4-ferrocenylbutoxy)bis(1-ruthenocenoylbutane-1,3-dionato)titanium(IV)

The cyclic voltammetric behaviour of cyclopentadienyl(4-ferrocenylbutoxy)bis(1-ruthenocenoylbutane-1,3-dionato)titanium(IV) (**231**) was studied in CH_2Cl_2/0.1 mol dm^{-3} $[NBu_4][B(C_6F_5)_4]$. Cyclic voltammograms are shown in Figure 3.53 and the electrochemical data are summerised in Table 3.34.

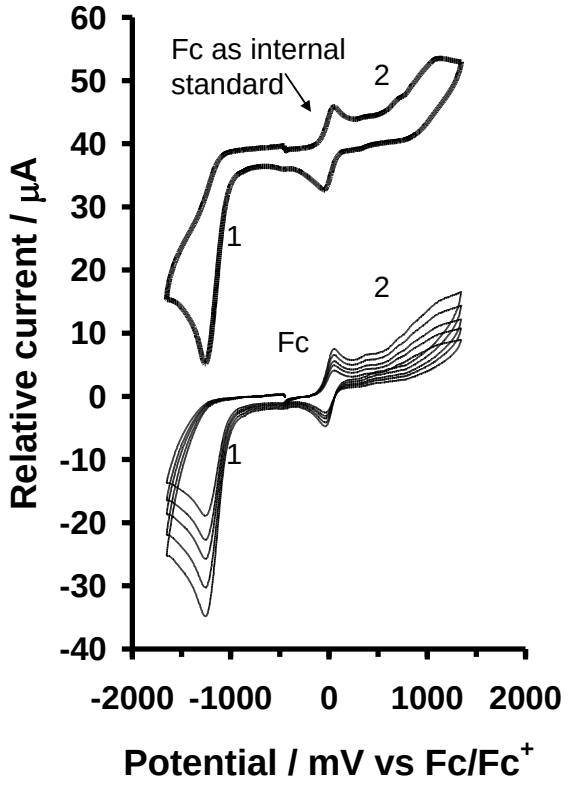

Figure 3.53. Cyclic voltammograms of a 2.0 mmol dm^{-3} cyclopentadienyl(4-ferrocenylbutoxy)bis(1-ruthenocenoylbutane-1,3-dionato)titanium(IV) (**231**) solution at scan rates of 100, 200, 300, 400 and 500 mV s^{-1}, measured in CH_2Cl_2/0.1 mol dm^{-3} $[NBu_4][B(C_6F_5)_4]$ at a glassy carbon-working electrode at 25ºC. The CV in bold (top CV) is where ferrocene is added as an internal standard at scan rate 200 mV s^{-1}.

Table 3.34. Cyclic voltammetry data of cyclopentadienyl(4-ferrocenylbutoxy)bis(1-ruthenocenoylbutane-1,3-dionato)titanium(IV) (**231**), peak anodic or cathodic potentials, E_{pa} or E_{pc} (*vs* Fc/Fc^+ couple as an internal standard); difference in peak anodic and peak cathodic potentials, ΔE_p; formal reduction potentials, E^{01}; peak anodic or cathodic currents, i_{pa} or i_{pc}; and peak anodic/peak cathodic current ratios, i_{pa}/i_{pc}, for indicated compounds (concentration 2.0 mmol dm^{-3}) in CH_2Cl_2/0.1 mol dm^{-3} $[NBu_4][B(C_6F_5)_4]$.

v / mV s^{-1}	E_{pc1} / mV	i_{pc1} / μA	E_{paFc} / mV	$E^{01}{}_{Fc}$ / mV	ΔE_{pFc} / mV	i_{pcFc} / μA	i_{pc}/i_{pa}	E_{pa2} / mV	i_{pc2} / μA
50	-1259	17.1	55	8	94	3.3	1.0	-[a]	-[a]
100	-1259	20.0	55	8	95	4.0	1.0	-[a]	-[a]
200	-1260	22.9	55	7	97	4.6	1.0	-[a]	-[a]
300	-1261	25.8	57	8	99	5.3	1.0	-[a]	-[a]
400	-1262	28.7	57	7	100	6.0	1.0	-[a]	-[a]
500	-1263	31.6	57	6	102	6.6	1.0	-[a]	-[a]

a) E_{pa} and i_{pa} could not be determined due to extreme peak broadening.

In Figure 3.53, peaks 1 and 2 are the chemically irreversible Ti^{4+}/Ti^{3+} and Rc/Rc^+ couples respectively. The peak labelled 'Fc' is assigned to the electrochemically quasi-reversible and

chemically reversible $O(CH_2)_4Fc/O(CH_2)_4Fc^+$ couple for **231** with ΔE_p = 94 mV at 50 mV s^{-1} and $i_{pc}/i_{pa} \approx 1.0$. The Ti i_{pc} current was greatly inhanced due to electrode deposition. The oxidation peak of the Rc/Rc^+ couple in **231** is broadend due to the presence of many different isomers. Addition of free ferrocene as an internal standard, caused the ruthenocene peak anodic half waves to be more pronounced (Figure 3.53, CV in bold).

3.6.6. Enaminones

The cyclic voltammetric behaviour of 1-ferrocenylbutan-3-one-4-aniline (**184**) and 1-ruthenocenyl-3-ferrocenylpropan-1-one-3-N-cobalticiniumenamine hexafluorophosphate (**187**) were studied in CH_2Cl_2/0.1 mol dm^{-3} $[NBu_4][B(C_6F_5)_4]$. Cyclic voltammograms are shown in Figure 3.54 and the electrochemical results are summerised in Table 3.35.

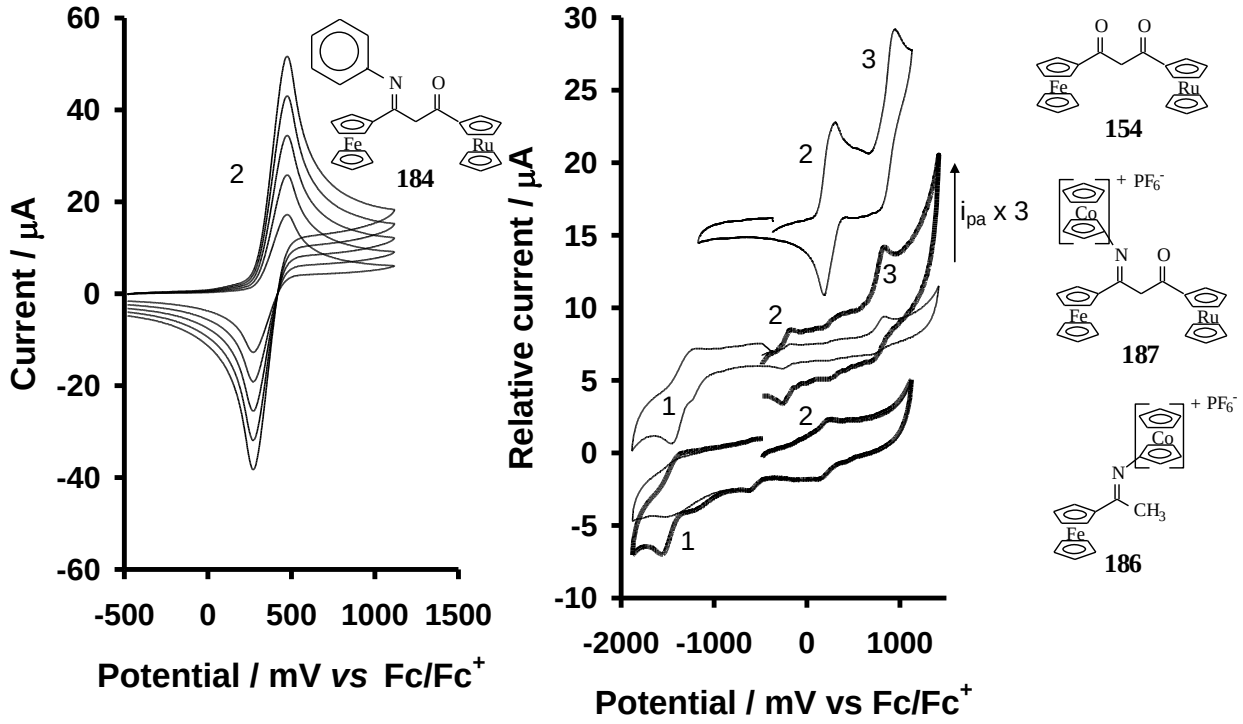

Figure 3.54. Left: Cyclic voltammograms of a 2.0 mmol dm^{-3} solution of ferrocenylbutan-3-one-4-aniline (**184**) measured in CH_2Cl_2/0.1 mol dm^{-3} $[NBu_4][B(C_6F_5)_4]$ at a glassy carbon-working electrode at 25ºC and scan rates of 50, 100, 200, 300, 400 and 500 mV s^{-1}. Right: Cyclic voltammograms of (Top) $RcCOCH_2COFc$ (**154**), (Middle) the ruthenocenyl-3-ferrocenylpropan-1-one-3-N-cobalticiniumenamine cation (**187**), and (Bottom) *N*-cobalticinium-*N*-(ferrocenylethylidene)amine hexafluorophosphate (**186**) at scan rate 100 mV s^{-1}. Right bottom, 100 mV s^{-1} bold second successive cycle, right middle bold scan has currents enlarged 3 times.

Table 3.35. Cyclic voltammetry data of 1-ferrocenylbutan-3-one-4-aniline (**184**) and 1-ruthenocenyl-3-ferrocenylpropan-1-one-3-N-cobalticiniumamine salt (**187**), peak anodic or cathodic potentials, E_{pa} or E_{pc} (*vs* Fc/Fc^+ couple as an internal standard); difference in peak anodic and peak cathodic potentials, ΔE_p; formal reduction potentials, E^{01}; peak anodic or cathodic currents, i_{pa} or i_{pc}; and peak anodic/peak cathodic current ratios, i_{pa}/i_{pc}, for indicated compounds (concentration 2.0 mmol dm^{-3}) in CH_2Cl_2/0.1 mol dm^{-3} $[NBu_4][B(C_6F_5)_4]$.

v / mV s^{-1}	E_{pa2} / mV	$E^{01}{}_2$ / mV	ΔE_{p2} / mV	i_{pa2} / μA	i_{pc}/i_{pa}
1-ferrocenylbutan-3-one-4-aniline (**184**)					
50	479	374	212	20.1	1.0
100	483	377	212	24.4	1.0
200	484	378	213	27.9	1.0
300	486	378	216	31.6	1.0
400	487	379	217	37.1	1.0
500	489	380	219	42.0	1.0

v / mV s^{-1}	E_{pc1} / mV	i_{pc1} / μA	E_{pa2} / mV	$E^{01}{}_2$ / mV	ΔE_{p2} / mV	i_{pa2} / μA	i_{pc}/i_{pa}	E_{pa3} / mV	i_{pa3} / μA
1-ruthenocenyl-3-ferrocenylpropan-1-one-3-N-cobalticiniumamine salt (**187**)									
50	-1402	1.0	-230	-181	98	0.4	1.0	847	0.5
100	-1457	1.4	-231	-178	106	0.6	1.0	843	1.0
200	-1422	1.6	-234	-179	110	0.7	1.0	841	1.6
300	-1443	2.1	-238	-171	134	1.0	1.0	823	1.9
400	-1473	2.6	-242	-170	144	1.2	1.0	805	2.1
500	-1498	3.1	-249	-173	152	1.6	1.0	800	2.4

The ferrocenyl couple (labelled 2) for **184** were found to be electrochemically irreversible and chemically reversible with ΔE_p < 150 mV and i_{pc}/i_{pa} = 1. No other peaks could be detected in the CV between -1200 and 1500 mV.

The ferrocenyl couple (labelled 2) for **187** was electrochemically quasi-reversible and chemically reversible with 90 m V < ΔE_p < 150 mV and i_{pc}/i_{pa} = 1. The Cc/Cc^+ couple (Cc = cobalticenyl) (peak labelled 1) and Rc/Rc^+ couple (peak labelled 3 in Figure 3.54) for **187** are electrochemically irreversible. An oxidation peak for Cc and reduction peak for Rc was also observed for the very first scan. During this first scan so much electrode deposition took place at peak 1 that further scans were clearly distorted. The same applied to precursor **186** (Figure 3.54, Bottom right). Interesting, for **187** $i_{pa,Fc} < i_{pa,\,Rc} < i_{pc,Cc}$. This clearly shows enamine **187** does not exist in the conjugated enol form but rather the keto form as shown below. Free rotation around the methylene carbon is allowed.

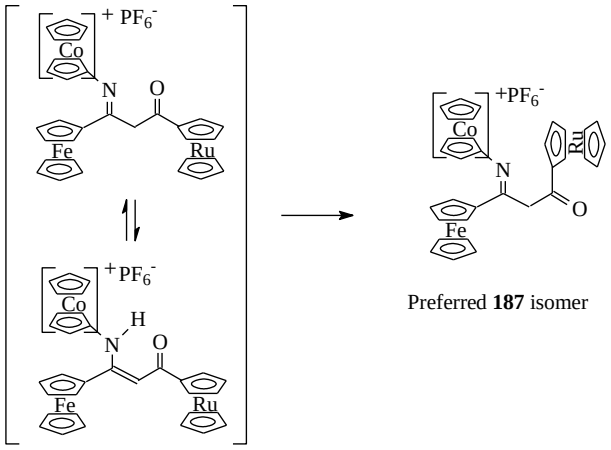

Preferred **187** isomer

The observed current ratios $i_{pa,Fc} < i_{pa,\ Rc} < i_{pc,Cc}$ is also consistent with keto **187** aligning preferentially with the cobalticenium group in closest contact with the electrode surface and ferrocenyl group the furthest.

Comparison of the enaminone **187**, with the β-diketone $RcCOCH_2COFc$, **154**, (section 3.6.3, p 137) reveal that the E^{01} of the Fc/Fc^+ couple shifted ~ 469 mV and the E_{pa} of the Rc/Rc^+ couple shifted ~ 136 mV towards a more negative potential with the replacement of the oxygen on the ferrocenyl side of the β-diketone with a cobalticenium-containing imine. It can thus be concluded that the cobalticenium-containing imine has a larger influence on the Fc/Fc^+ couple than on the Rc/Rc^+ couple. This is also consistent with **187** existing in the keto form, thereby isolating the ruthenocenyl group from through-bond functional group communication. This is expected seeing as the cobalticenium moiety is closer to the ferrocenyl moiety than the ruthenocenyl moiety. The movement of the E^{01} and E_{pc} was in the opposite direction from what was expected, seeing as the cobalticenium-containing amine is a positively charged specie. With the positive charge on the enaminone, it was expected that the Fc/Fc^+ couple and Rc/Rc^+ couple would be more difficult to oxidize, moving E^{01} and E_{pc} to higher potential, rather than the observed lower potentials. In contrast, for the enamine **184**, the ferrocenyl group is oxidized at a potential ≈ 400 mV more positive than in **187**.

3.7. Crystallography

The single crystal structure of $[(C_5H_5)_2Ti(RcCOCHCOCH_3)]^+ClO_4^-$ (**194**) was determined. Dr. A.J. Muller from the Department of Chemistry at the University of the Free State is acknowledged for determining and solving the crystal structure.

A perspective view of **194** showing atom labelling is presented in Figure 3.55. Crystal data of **194** are summirized in Table 3.36, selected bond lengths and angles can be found in Table 3.37.

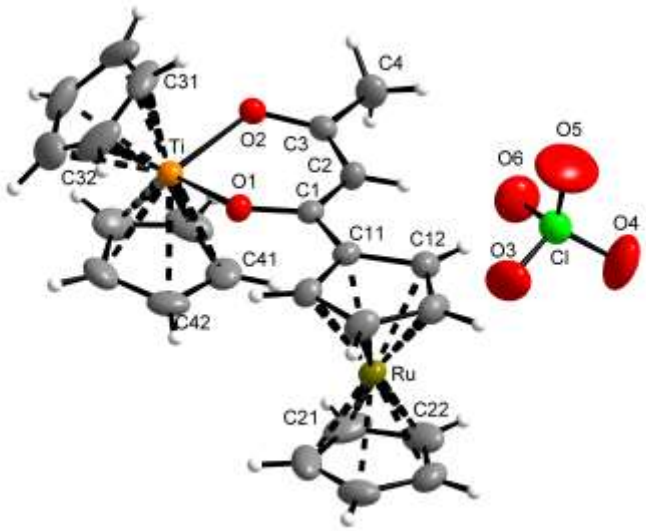

Figure 3.55. A perspective view of **194**.

The titanium atom displays a distorted tetrahedral geometry. The bond angles around Ti [O(1)-Ti-O(2) = 86.86º, C*(31-35)-Ti-C*(41-45) = 133.37º, O(1)-Ti-C*(31-35) = 104.84º, O(1)-Ti-C*(41-45) = 105.75º, O(2)-Ti-C*(31-35) = 106.41º and O(1)-Ti-C*(41-45) = 105.42º] differ the most with 23.9º from 109.47º, the angle for a regular tetrahedron. It is predicted that complexes of this type has a O-Ti-O angle between 85-88º, [35] which is in agreement with the 86.86º that was observed here.

The bond length C(3)-C(2) [1.372(4) Å] is not significantly shorter than that of C(1)-C(2) [1.407(4) Å]. This shows that the β-diketonato ligand is for all practial purposes almost symmetrically bound to Ti. The angles O(1)-C(1)-C(2) [122.3(3)º], C(3)-C(2)-C(1) [124.3(3)º] and O(2)-C(3)-C(2) [123.7(3)º] are none near to the theoretical value of 120º expected for the sp^2 hybridization. This means that the pseudo-aromatic ring is distorted, implying that the through bond electronic communication between the Ti centre, the R-group and the ruthenocenyl group should not to be optimum. This observation explains the non-linear relationship observed between E_{pa} for the Rc group and the group electronegativity of the R-group of the β-diketonato ligand, χ_R, and between E^{01} for the Ti^{4+}/Ti^{3+} couple and χ_R (see Section 3.6.5.2, p 153). From Figure 3.56 (Left) it can be seen that the cyclopentadienyl rings of the ruthenocenyl group are in the eclipsed conformation. Figure 3.56 (Right) shows that the ruthenocenyl cyclopentadienyl rings are orientated parallel to one another and that the β-diketonato plane is almost parallel to

* Centroid of cyclopentadienyl ring of the given numbers.

the cyclopentadienyl planes. The torsion angle of 3.2(4) between the plane formed by O(1)-C(1)-C(11)-C(15) and the plane formed by the C(11-15) cyclopentadienyl carbon atoms, emphizise effective conjugation of the ruthenocenyl group into the pseudo-aromatic ring of the β-diketonato side chain.

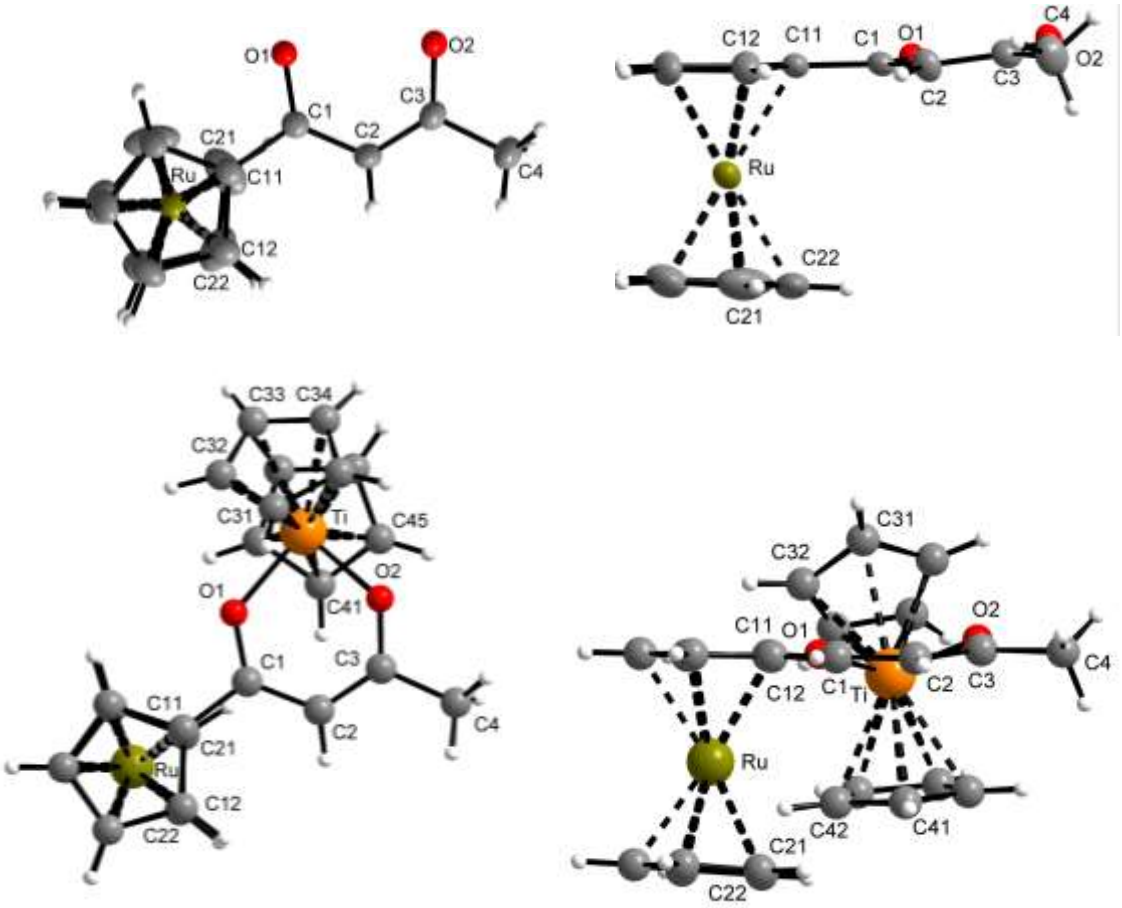

Figure 3.56. Top Left: A partial view of **194**, highlighting the eclipsed formation of the two cyclopentadienyl rings of the Ru. Top Right: The plane formed by the cyclopentadienyl ring consisting of C(11)-C(12)-C(13)-C(14)-C(15) by the β-diketonato ligand are parallel to the plane formed by the cyclopentadienyl ring consisting of C(21)-C(22)-C(23)-C(24)-C(25). Bottom: Two perspective views showing the titanium centre is displaced out of the β-diketonato plain. This results in a non-symmetric cyclopentadienyl position around the β-diketonato plain.

Bond Ti-O(1) [1.964(2) Å] is not significantlty longer than Ti-O(2) [1.957(2) Å] implying the stronger electron donating property of the ruthenocenyl group (χ_{Rc} = 1.99), compared to that of the CH_3 group (χ_{CH3} = 2.34) on the pseudo-aromatic β-diketonato ligand does not transmit through through-bond communication to the titanium centre.

The average Ti-C bond length for the C_5H_5 ring defined by carbon atoms C(31)-C(35) is 2.368(4) Å, while that of the cyclopentadienyl ring formed by C(41)-C(45) is 2.349(4) Å. This compares well with the corresponding length of titanocene dichloride itself which has an average

Ti-C bond length of 2.317(7) Å. The average Ru-C bond lengths are however, at least 0.18 Å shorter. The average Ru-C bond lengths being 2.162(4) Å for the cyclopentadienyl ring defined by C(21)-C(25) and 2.172(3) for the cyclopentadienyl ring defined by C(11)-C(15) respectively.

The reported $(C_5H_5)_2Ti^{III}(CH_3COCHCOCH_3)$ complex,[36] revealed a O-Ti-O angle of 84.3º, which is smaller than what was found for the titanium(IV) species, **194** [86.86(9)º]. For **194**, the average distance between the Ti^{IV} and oxygen atoms, 1.961(2) Å, is shorter than the Ti^{III}-O distance [2.068(5) Å] found for the reported $(C_5H_5)_2Ti^{III}(CH_3COCHCOCH_3)$ complex.[36] $(C_5H_5)_2Ti^{III}(CH_3COCHCOCH_3)$ has an average Ti-C distance of 2.375(8) Å. This clearly demonstrates that the Ti^{IV} centre is noticeably more electrophylic than the Ti^{III} centre. This value is similar to values found for other titanocene(III)[37] and titanocene(IV) derivatives.[38] The average Ti-C bond distance for **194**, are 2.368 Å and 2.348 Å for the two rings respectively.

Table 3.36. Crystal data and structure refinement for **194**.

Empirical formula	$C_{24}H_{23}O_6ClTiRu$	Theta range for data collection	2.02 to 28.30°.
Formula weight	646.097	Index ranges	-8<=h<=13, -26<=k<=26, -14<=l<=15
Temperature	293(2)	Reflections collected	15804
Crystal size	0.34 x 0.18 x 0.03 mm^3	Independent reflections	5656 [R(int) = 0.0396]
Crystal system	Monoclinic	Completeness to theta = 28.30°	99.2 %
Space group	$P2_1/n$	Absorption correction	Semi-empirical from equivalents
Unit cell dimensions	a = 9.973(2) Å b = 20.176(4) Å c = 11.509(2) Å α= 90° β= 97.32(3)° γ = 90°.	Max. and min. transmission	0.9660 and 0.6937
		Refinement method	Full-matrix least-squares on F^2
Volume	2296.9(8) $Å^3$	Data / restraints / parameters	5656 / 0 / 299
Density (calculated)	1.711 Mg/m^3	Goodness-of-fit on F^2	1.016
Z	4	Final R indices [I>2sigma(I)]	R1 = 0.0380, wR2 = 0.0759
Absorption coefficient	1.160 mm^{-1}	R indices (all data)	R1 = 0.0776, wR2 = 0.0889
F(000)	1192	Largest diff. peak and hole	0.387 and -0.346 e.$Å^{-3}$

Table 3.37. Bond lengths (Å) and angles (º) for **194**. The standard deviation of the last decimal is given in parentheses.

Atoms	Bond	Atoms	Bond	Atoms	Bond
Ti-O(2)	1.957(2)	C(1)-C(11)	1.458(4)	C(25)-H(25)	0.9300
Ti-O(1)	1.964(2)	C(2)-C(3)	1.372(4)	C(31)-C(32)	1.377(6)
Ti-C(31)	2.355(4)	C(2)-H(2)	0.9300	C(31)-C(35)	1.393(7)
Ti-C(32)	2.344(4)	C(3)-C(4)	1.497(4)	C(31)-H(31)	0.9300
Ti-C(33)	2.345(4)	C(4)-H(4A)	0.9600	C(32)-C(33)	1.339(6)
Ti-C(34)	2.344(4)	C(4)-H(4B)	0.9600	C(32)-H(32)	0.9300
Ti-C(35)	2.351(4)	C(4)-H(4C)	0.9600	C(33)-C(34)	1.342(6)
Ti-C(41)	2.402(4	C(11)-C(15)	1.429(4)	C(33)-H(33)	0.9300
Ti-C(42)	2.373(4)	C(11)-C(12)	1.433(4)	C(34)-C(35)	1.365(6)
Ti-C(43)	2.341(4)	C(12)-C(13)	1.409(5)	C(34)-H(34)	0.9300
Ti-C(44)	2.345(4)	C(12)-H(12)	0.9300	C(35)-H(35)	0.9300
Ti-C(45)	2.381(4)	C(13)-C(14)	1.408(5)	C(41)-C(42)	1.380(6)
Ru-C(25)	2.157(4)	C(13)-H(13)	0.9300	C(41)-C(45)	1.384(6)
Ru -C(24)	2.161(4)	C(14)-C(15)	1.418(5)	C(41)-H(41)	0.9300
Ru-C(23)	2.169(4)	C(14)-H(14)	0.9300	C(42)-C(43)	1.375(6)
Ru-C(22)	2.161(4)	C(15)-H(15)	0.9300	C(42)-H(42)	0.9300
Ru-C(21)	2.162(4)	C(21)-C(22)	1.388(6)	C(43)-C(44)	1.378(6)
Ru-C(13)	2.164(3)	C(21)-C(25)	1.415(7)	C(43)-H(43)	0.9300
Ru-C(12)	2.166(3)	C(21)-H(21)	0.9300	C(44)-C(45)	1.376(6)
Ru-C(15)	2.174(3)	C(22)-C(23)	1.358(6)	C(44)-H(44)	0.9300
Ru-C(14)	2.177(3)	C(22)-H(22)	0.9300	C(45)-H(45)	0.9300
Ru-C(11)	2.178(3)	C(23)-C(24)	1.374(6)	Cl-O(5)	1.377(4)
O(1)-C(1)	1.285(3)	C(23)-H(23)	0.9300	Cl-O(4)	1.391(3)
O(2)-C(3)	1.297(4)	C(24)-C(25)	1.395(6)	Cl-O(3)	1.406(3)
C(1)-C(2)	1.407(4)	C(24)-H(24)	0.9300	Cl-O(6)	1.410(3)
Atoms	Angle	Atoms	Angle	Atoms	Angle
O(2)-Ti-O(1)	86.86(9)	C(14)-C(13)-H(13)	125.4	C(32)-C(33)-H(33)	125.5
C(1)-O(1)-Ti	127.86(19)	C(12)-C(13)-H(13)	125.4	C(34)-C(33)-H(33)	125.5
C(3)-O(2)-Ti	125.36(19)	C(13)-C(14)-C(15)	108.3(3)	C(33)-C(34)-C(35)	108.8(4)
O(1)-C(1)-C(2)	122.3(3)	C(13)-C(14)-H(14)	125.9	C(33)-C(34)-H(34)	125.6
O(1)-C(1)-C(11)	116.2(3)	C(15)-C(14)-H(14)	125.9	C(35)-C(34)-H(34)	125.6
C(2)-C(1)-C(11)	121.5(3)	C(14)-C(15)-C(11)	107.3(3)	C(34)-C(35)-C(31)	107.0(4)
C(3)-C(2)-C(1)	124.3(3)	C(14)-C(15)-H(15)	126.4	C(34)-C(35)-H(35)	125.6
C(3)-C(2)-H(2)	117.9	C(11)-C(15)-H(15)	126.4	C(31)-C(35)-H(35)	125.6
C(1)-C(2)-H(2)	117.9	C(22)-C(21)-C(25)	107.1(4)	C(42)-C(41)-C(45)	107.0(4)
O(2)-C(3)-C(2)	123.7(3)	C(22)-C(21)-H(21)	126.4	C(42)-C(41)-H(41)	126.2
O(2)-C(3)-C(4)	114.9(3)	C(25)-C(21)-H(21)	126.4	C(45)-C(41)-H(41)	126.2
C(2)-C(3)-C(4)	121.3(3)	C(23)-C(22)-C(21)	108.9(4)	C(43)-C(42)-C(41)	107.6(4)
C*(31-35)-Ti-C*(41-45)	133.37º	C(23)-C(22)-H(22)	125.6	C(43)-C(42)-H(42)	126.2
O(1)-Ti-C*(31-35)	104.84º	C(21)-C(22)-H(22)	125.6	C(41)-C(42)-H(42)	126.2
O(1)-Ti-C*(41-45)	105.75º	C(22)-C(23)-C(24)	109.0(4)	C(42)-C(43)-C(44)	109.1(4)
O(2)-Ti-C*(31-35)	106.41º	C(22)-C(23)-H(23)	125.5	C(42)-C(43)-H(43)	125.4
O(1)-Ti-C*(41-45)	105.42º	C(24)-C(23)-H(23)	125.5	C(44)-C(43)-H(43)	125.4
C(3)-C(4)-H(4A)	109.5	C(23)-C(24)-C(25)	108.3(4)	C(45)-C(44)-C(43)	106.9(4)
C(3)-C(4)-H(4B)	109.5	C(23)-C(24)-H(24)	125.9	C(45)-C(44)-H(44)	126.5
H(4A)-C(4)-H(4B)	109.5	C(25)-C(24)-H(24)	125.9	C(43)-C(44)-H(44)	126.5
C(3)-C(4)-H(4C)	109.5	C(24)-C(25)-C(21)	106.7(4)	C(44)-C(45)-C(41)	108.8(4)
H(4A)-C(4)-H(4C)	109.5	C(24)-C(25)-H(25)	126.6	C(44)-C(45)-H(45)	125.6
H(4B)-C(4)-H(4C)	109.5	C(21)-C(25)-H(25)	126.6	C(41)-C(45)-H(45)	125.6
C(15)-C(11)-C(12)	108.1(3)	C(32)-C(31)-C(35)	106.5(4)	O(5)-Cl-O(4)	113.5(3)
C(15)-C(11)-C(1)	124.4(3)	C(32)-C(31)-H(31)	126.7	O(5)-Cl-O(3)	109.6(3)
C(12)-C(11)-C(1)	127.4(3)	C(35)-C(31)-H(31)	126.7	O(4)-Cl-O(3)	108.9(2)
C(13)-C(12)-C(11)	107.0(3)	C(33)-C(32)-C(31)	108.6(4)	O(5)-Cl-O(6)	107.7(3)
C(13)-C(12)-H(12)	126.5	C(33)-C(32)-H(32)	125.7	O(4)-Cl-O(6)	110.0(2)
C(11)-C(12)-H(12)	126.5	C(31)-C(32)-H(32)	125.7	O(3)-Cl-O(6)	107.0(2)
C(14)-C(13)-C(12)	109.2(3)	C(32)-C(33)-C(34)	109.1(5)	-	-

* Centroid of cyclopentadienyl ring of the given numbers.

3.8. Phase studies

Seeing as long alkyl chains are known to be amorph, the phase studies of the complexes containing the β-diketones with the long alkyl chain length were studied utilising differential scanning calorimetry. The four complexes $RcCOCH_2COR$ [where R = $C_{10}F_{21}$ (**177**), $C_{10}H_{21}$ (**179**)], $TiCl_2(RcCOCHCOC_{10}H_{21})_2$ (**216**) and $Ti(O(CH_2)_4Fc)_2(RcCOCHCOC_{10}H_{21})_2$ (**227**) were expected to show interesting phase behaviour due to the long chain substituents they possess. These were studied using differential scanning calorimetry (DSC) and polarised light optical microscopy. Prof. M.J. Cook from the Department of Chemistry at the University of East Anglia, England, is acknowledged for access to this equipment, and Prof. J.C. Swarts from the Department of Chemistry at the University of the Free State (supervisor) for performing these tests. Unexpectedly no thermotropic liquid crystal properties were found for the complexes. They all only exhibited different solid state crystal phases. The DSC traces of **177**, **179** and **227** are shown in Figure 3.57.

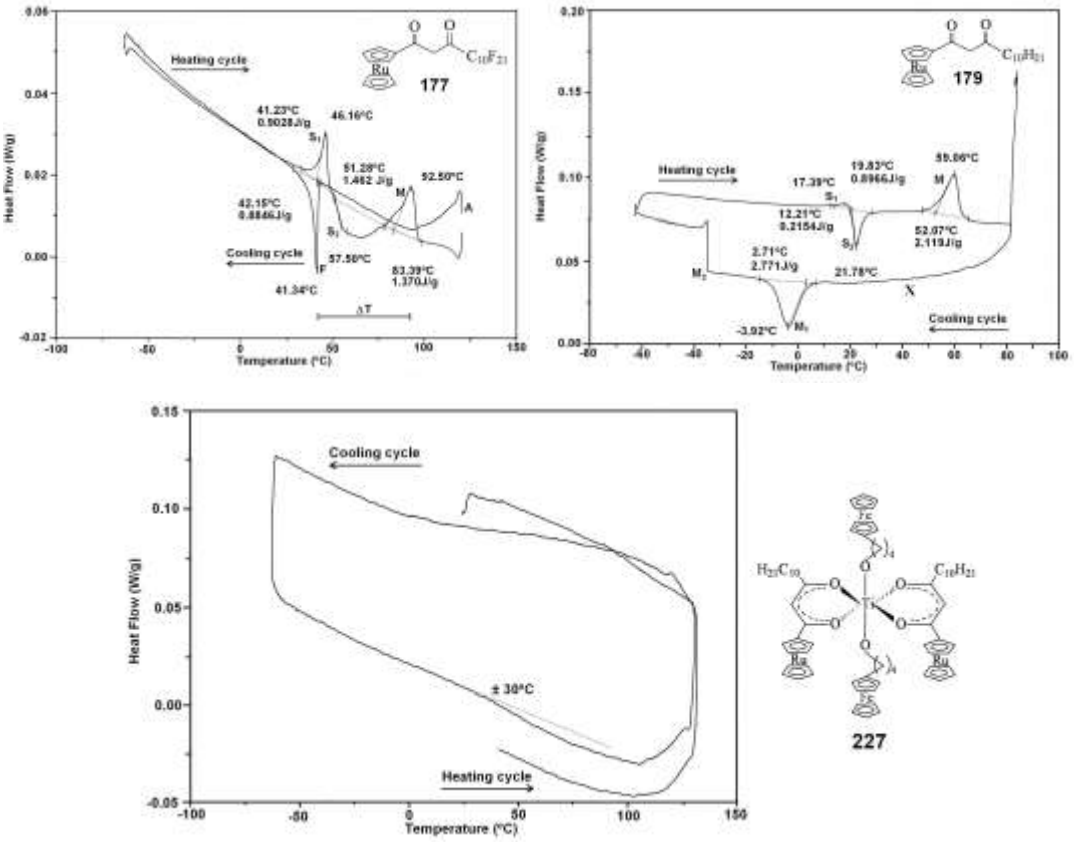

Figure 3.57. Differential scanning calorimetry thermogram of heat flow *vs* temperature of $RcCOCH_2COR$ [where R = $C_{10}F_{21}$ (**177**), $C_{10}H_{21}$ (**179**)] and $Ti(O(CH_2)_4Fc)_2(RcCOCHCOC_{10}H_{21})_2$ (**227**) respectively. A heating and cooling rate of 10°C min^{-1} was used. Three successive heating and cooling cycles were employed. The thermograms shown are from the second cycle.

From the DSC scan for **177** in the melted phase (Figure 2.57, top left), peak A shows an apparent instability (compound decomposition). It was found that the complex starts to freeze at 41ºC (peak F) during the cooling cycle. During the rest of the cooling cycle, apart from the liquid to solid phase change at the peak labelled F, no other noticeable phase change was observed. During the heating cycle at 46 ºC (peak S_1) an exothermic solid state phase change occurs. This is ascribed to the long -$C_{10}F_{21}$ side chain that settles into a different conformation (the exact conformation is unknown). Following this exothermic solid phase change is an endothermic solid phase change (peak S_2) at 57 ºC. The broadness of this peak is an indication of slow kinetics of conformational changes, due to the "low" flexibility of the long $C_{10}F_{21}$ side chain. Eventually melting sets in at 83ºC (peak M). The peak M at 83ºC was the true melting point of this β-diketone and was confirmed by polarized light optical microscopy. The temperature range between the melting- and freezing peak $\Delta T = 83.39 - 41.34 = 42.05$ºC. The observed phase changes are not attributed to the formation of a liquid crystal phase. The typical temperature difference of liquid crystal going to an isotropic liquid, defining a liquid crystal phase, is 5ºC.[39] Also, phase transitation energies between liquid crystal and isotropic liquid phases are normally very small compared to heats of melting or crystallisation. Here, all phase changes had heats of conversion 0.88-1.46 J g^{-1}, (Mr **177** = 819.5701 g mol^{-1}) which is very similar. A mesophase conversion would be expected to have ΔH values of 0.05 J g^{-1} or less.

The cooling cycle of **179** (DSC scan in Figure 3.57, top right) shows slow melting kinetics sets in at 21.78ºC (peak M_1). A further solid state reorginasation appears to take place at -36ºC (peak labelled M_2). On the heating cycle an exothermic solid phase rearrangement (S_1) is observed at 17.39ºC, followed immediately by an endothermic solid phase change (S_2) at 19.88ºC, which absorbed packing energy. True melting sets in at 52.07ºC (peak M). This transition was confirmed as a melting point by polarized light optical microscopy. The absence of a low energy transition peak at the position labelled X at *ca*. 50ºC, shows that **179** also does not posses liquid crystal properties. It is concluded that the attractive forces between the β-diketone molecules are not strong enough to support a liquid crystal phase, thus no mesophase is observed.

For **227** no interpretable phase changes (like melting point, see Figure 3.56 bottom), could be observed utilising the DSC technique. However, when compound **227** was investigated with a polarised light optical microscope, from ± 30ºC, intra and intermolecular oxygen-titanium interactions appear to take place. The oxygen originates from the alkoxy and β-diketonato ligands. This conclusion was reached because the same effect was observed regardless of whether the experiment was preformed under an inert nitrogen atmosphere or in a normal atmospheric oxygen atmosphere. Melting never was observed, even up to 300ºC. The change

that sets in at ± 30ºC, therefore, does not represent a phase change, but a chemical reaction. From the DSC scan it can be seen that repeat scans are not following the superimposable when the experiment is repeated over 2, 3 or more consecutive cycles. This is consistent with energy being released from the system due to the oxygen bridges that form. It is expected that eventually TiO_2 will be the sole product.

216 was also investigated and the same resultend trend was observed as with **227**. The oxygen bridge formation was just observed in a more severe degree. This shows that the Cl^- group is more labile towards oxygen than the alkoxy group in **227**. This result is therefore consistent with what was reported for the hydrolysis of $Ti(bzac)_2Cl_2$ and $Ti(bzac)_2(OEt)_2$, where these complexes were hydrolysed after 10 s and 2.5 h respectively.[28]

3.9. Cytotoxicity evaluation

3.9.1. Introduction

The purpose of the synthesis of all the described complexes of this study was to investigate their physical properties, and also to investigate their application possibilities in terms of cancer treatment. The latter was probed by determining the cytotoxicity of selected compounds against cancer cells. The types of cancer cells that were used in this investigation were CoLo (a human colorectral cell line) and HeLa (a human cervix epitheloid cancer cell line). Prof. C.E.J. Medlen from the Department of Pharmacology at the University of Pretoria is acknowledged for performing these tests and for constructing the survival curves of the obtained results. Survival curves indicate percentage cell survival, plotted as a function of drug dose with concentration expressed in μmol dm^{-3}. IC_{50} values (drug dose required for 50% cell death) were estimated by extrapolation.

3.9.2. Complexes of the type $[(C_5H_5)_2Ti(RcCOCHCOR)]^+ClO_4^-$

The cytotoxicity data of mono-β-diketonato titanocenyl complexes $[(C_5H_5)_2Ti(RcCOCHCOR)]^+ClO_4^-$ with R = $C_{10}F_{21}$ (**195**), CF_3 (**196**), C_6F_5 (**197**), $C_{10}H_{21}$ (**198**), CH_3 (**194**), Rc (**199**) and Fc (**200**) are shown in Table 3.38. and the survival curves of the complex that gave the best result *vs* CoLo and HeLa cancer cells, namely **196** with R = CF_3, are shown in Figure 3.58.

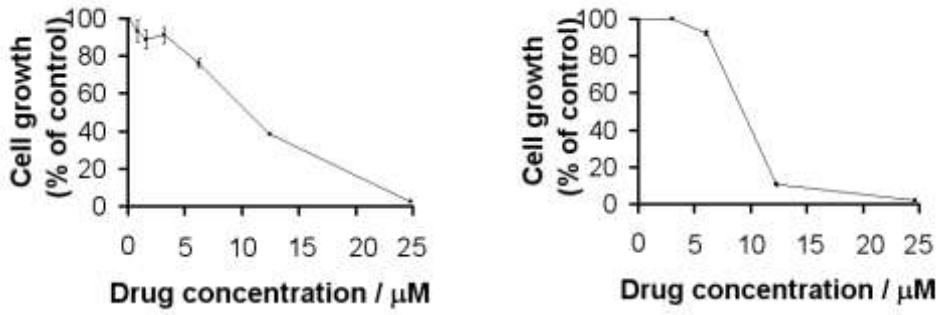

Figure 3.58. Plots of percentage CoLo cell survival (left) and HeLa cell survival (right) against concentration (μmol dm^{-3}) of $[(C_5H_5)_2Ti(RcCOCHCOCF_3)]^+ClO_4^-$, (**196**).

Table 3.38. IC_{50} values for CoLo and HeLa cell lines after treatment with $[(C_5H_5)_2Ti(RcCOCHCOR)]^+ClO_4^-$ [R = $C_{10}F_{21}$ (**195**), CF_3 (**196**), C_6F_5 (**197**), $C_{10}H_{21}$ (**198**), CH_3 (**194**), Rc (**199**) and Fc (**200**)]. Group electronegativities (χ_R) of the R-groups on the β-diketonato ligand and the peak anodic potential of the Rc/Rc^+ couple and the peak cathodic potentials of the Ti^{4+}/Ti^{3+} couple *vs* Fc/Fc^+ at 200 mV s^{-1} are also shown.

R	χ_R	Rc/Rc^+ E_{pa} / mV	Ti^{4+}/Ti^{3+} E_{pc} / mV	IC_{50} value for CoLo cell line / μmol dm^{-3}	IC_{50} value for HeLa cell line / μmol dm^{-3}
195: $C_{10}F_{21}$	3.04	975	-1399	-[a]	-[a]
196: CF_3	3.01	1003	-691; -875	10.21	9.69
197: C_6F_5	2.46	890	-1475	10.90	11.01
198: $C_{10}H_{21}$	2.43	535	-981	18.42	39.47
194: CH_3	2.34	1356	-1016	14.78	20.26
199: Rc	1.99	933	-1015	22.07	20.14
200: Fc	1.87	833	-953	16.23	38.44
cisplatin		-	-	1.84	1.33
$(C_5H_5)_2TiCl_2$		-	-	39.37	84.51

a) not soluble in test medium to perform experiments.

The complex where R = $C_{10}F_{21}$ could not be used in the survey due to difficulties in dissolving it in appropriate concentrations. For the other complexes the general trend appears to be as the group electronegativity of the R-group on the β-diketonato ligand increases, the IC_{50} values decreases. Comparison of the electrochemical data with the IC_{50} values revealed no direct relationship but the general trend for non fluorine containing complexes appear to be that as the potential (E_{pa} of the Rc/Rc^+ couple and E_{pc} of Ti^{4+}/Ti^{3+} couple) increases the IC_{50} decreases. The fluorine-containing complexes show the best overall results (i.e. lowest IC_{50} values). These IC_{50} values of the F-complexes were also independent of E_p values. It implies that the redox inactive F is a cytotoxic active fragment on its own and that it is so powerful, it is the dominant drug fragment in **196-197**.

None of the complexes were as effective as cisplatin in killing cancer cells. However, cisplatin has many side effects including extreme nephrotoxicity. Known titanium complexes like titanocene dichloride exhibit much less side effects. The present class of compounds may therefore also have less toxic side effects. This is currently under investigation. In comparison with titanocene dichloride, $(C_5H_5)_2TiCl_2$, all the complexes of Table 3.38 showed enhanced cytotoxic activity. This clearly shows that by combining more than one type of anti-cancer active moiety in the same molecule, here titanium and ruthenium, enhanced anti-cancer activity may be obtained. Another benefit that is envisaged is that the present series of drugs may all be less prone to cancer cell lines developing a resistance against them. This is envisaged because the mechanism of action of each drug fragment is not expected to be the same. Further research is required to clarify the exact mechanism by which each drug fragment kills cancer cells. All the complexes proved to be more effective in killing cancer cells than the parent titanocene dichloride drug. Titianocene dichloride is currently in phase II clinical trails.

3.9.3. $(C_5H_5)_2Ti(O(CH_2)_nFc)_2$, $(C_5H_5)Ti(O(CH_2)_nFc)_3$ and $Ti(O(CH_2)_nFc)_4$ complexes

The cytotoxicity data of bis(cyclopentadienyl)di(ferrocenylalkoxy)titanium(IV) complexes [$(C_5H_5)_2Ti(O(CH_2)_nFc)_2$, n = 1 (**201**), 2 (**202**), 3 (**203**), 4 (**204**)], cyclopentadienyltri(ferrocenylalkoxy)titanium(IV) complexes [$(C_5H_5)Ti(O(CH_2)_nFc)_3$, n = 1 (**205**), 2 (**206**), 3 (**207**), 4 (**208**)] and tetra(ferrocenylalkoxy)titanium(IV) [$Ti(O(CH_2)_nFc)_4$, n = 1 (**209**), 2 (**210**), 3 (**211**), 4 (**212**)] are shown in Table 3.39 and the survival curves of the complexes of each series that gave the best result *vs* CoLo and HeLa are shown in Figure 3.59.

For the complexes of the form $(C_5H_5)_2Ti(O(CH_2)_nFc)_2$, it can be seen from Table 3.39 that the complexes with even amounts of C-atoms in the complexes with alkyl spacer between the oxygen and the ferrocenyl group, show better cytotoxic properties than complexes with uneven numbers of C-atoms. Complex **204** with n = 4 gave the best results (i.e. lowest IC_{50} value) for both cell lines. As for the complexes with the form $(C_5H_5)Ti(O(CH_2)_nFc)_3$, the general structural influence for both cell lines appear to be as the alkyl chain length increases, cytotoxicity also increases. Again the complex with n = 4 had the lowest IC_{50} value. In contrast, complexes with the form $Ti(O(CH_2)_nFc)_4$, revealed no direct trend between alkyl chain length and cytotoxicity. The complex **211** where n = 3 gave the best overall results. None of the complexes **201-212** revealed enhanced cytotoxic activity over cisplatin, but could have less negative side effects. However, all complexes except **203** (*vs* CoLo) proved to be more effective

in killing cancer cells than titanocene dichloride. From these complexes, $[(C_5H_5)_2Ti(O(CH_2)_nFc)_2$, $(C_5H_5)Ti(O(CH_2)_nFc)_3$ and $Ti(O(CH_2)_nFc)_4]$, it was found that the complex with the most ferrocenyl alkoxy groups displays the best cytotoxic properties, $Ti(O(CH_2)_nFc)_4$.

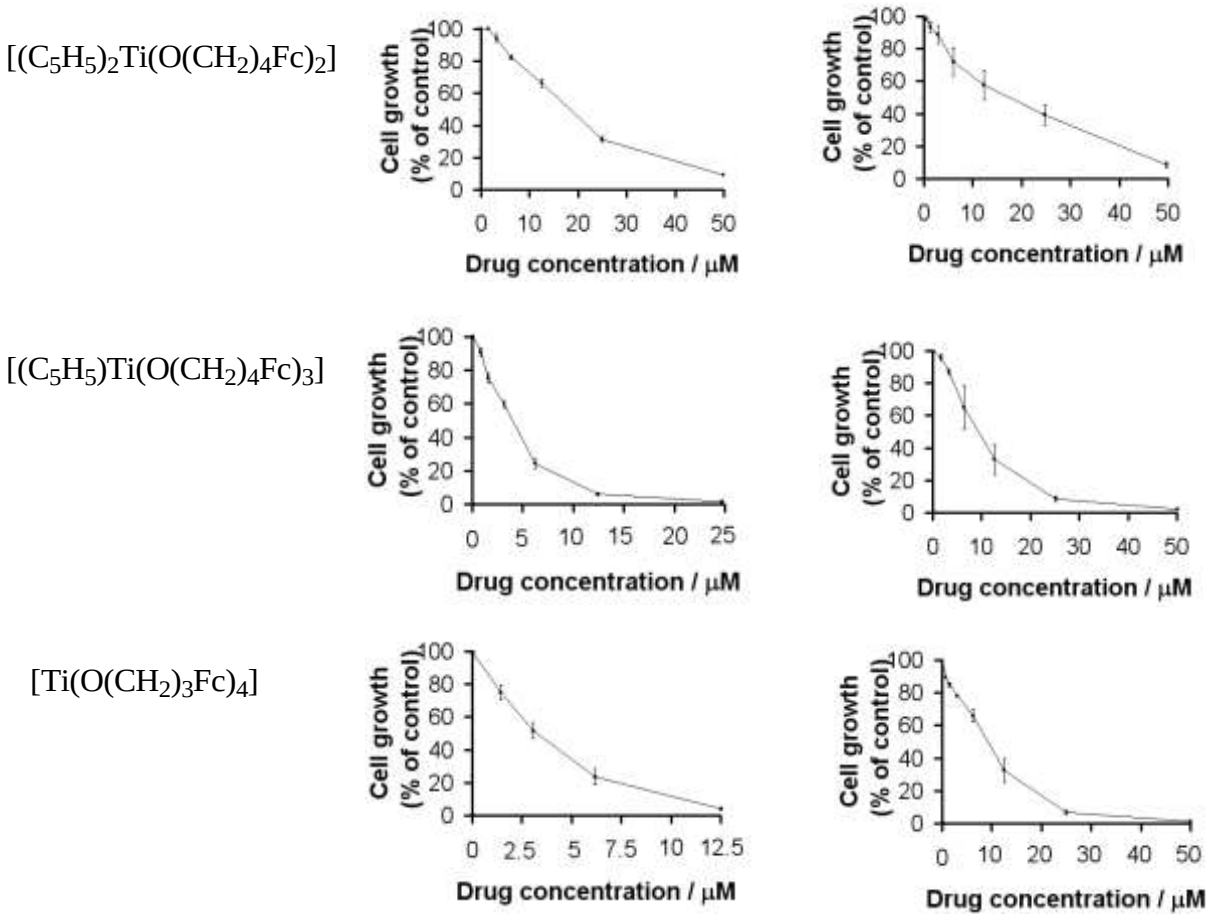

Figure 3.59. Plots of percentage survival CoLo (left) and HeLa cells (right) against concentration (μmol dm^{-3}) of $(C_5H_5)_2Ti(O(CH_2)_4Fc)_2$ (**204**) (Top), $(C_5H_5)Ti(O(CH_2)_4Fc)_3$ (**208**) (Middle) and $Ti(O(CH_2)_3Fc)_4$ (**211**) (Bottom).

As can be seen from Figure 3.60 (Top), the general trend for both CoLo and HeLa cell lines is as the formal reduction potential of the $O(CH_2)_nFc/O(CH_2)_nFc^+$ couple decreases, the IC_{50} values also decreases for all three types of complexes $[(C_5H_5)_2Ti(O(CH_2)_nFc)_2$, $(C_5H_5)Ti(O(CH_2)_nFc)_3$ and $Ti(O(CH_2)_nFc)_4]$. Comparison of the Ti^{4+}/Ti^{3+} couple's E_{pc} against IC_{50} values did not reveal a general trend for both CoLo and HeLa cell lines. From the ferrocenyl E^{01}/IC_{50} relationship it can be concluded that for these types of complexes $[(C_5H_5)_2Ti(O(CH_2)_nFc)_2$, $(C_5H_5)Ti(O(CH_2)_nFc)_3$ and $Ti(O(CH_2)_nFc)_4]$, an electron transfer mechanism is propably the cause of cell death for both anti-cancer fragments.

Table 3.39. IC_{50} values for CoLo and HeLa cell lines after treatment with bis(cyclopentadienyl)di(ferrocenylalkoxy)titanium(IV) complexes $(C_5H_5)_2Ti(O(CH_2)_nFc)_2$, cyclopentadienyl-tri(ferrocenylalkoxy)titanium(IV) complexes $(C_5H_5)Ti(O(CH_2)_nFc)_3$, and tetra(ferrocenylalkoxy)titanium(IV) $Ti(O(CH_2)_nFc)_4$. Peak cathodic potentials of the Ti^{4+}/Ti^{3+} couple and the formal reduction potentials of the Fc/Fc^+ couple *vs* Fc/Fc^+ at v = 200mV s^{-1} are also shown.

Alkyl chain length	Ti^{4+}/Ti^{3+} E_{pc} / mV	Fc/Fc^+ E^{01} / mV	IC_{50} value for CoLo cell line / μmol dm^{-3}	IC_{50} value for HeLa cell line / μmol dm^{-3}
$(C_5H_5)_2Ti(O(CH_2)_nFc)_2$				
201: 1	-921	578; 784	>50	>50
202: 2	-933	566	24.99	25.32
203: 3	-916	516	43.95	32.71
204: 4	-875	544	18.27	19.00
$(C_5H_5)Ti(O(CH_2)_nFc)_3$				
205: 1	-943	579; 770	16.75	28.79
206: 2	-881	582	14.48	14.15
207: 3	-930	559	8.27	14.58
208: 4	-922	545	4.09	8.81
$Ti(O(CH_2)_nFc)_4$				
209: 1	-923	574; 575	11.12	8.67
210: 2	-940	585	6.89	15.57
211: 3	-908	565	3.20	9.25
212: 4	-922	545	6.20	11.75
cisplatin	-	-	1.84	1.33
$(C_5H_5)_2TiCl_2$	-	-	39.37	84.51

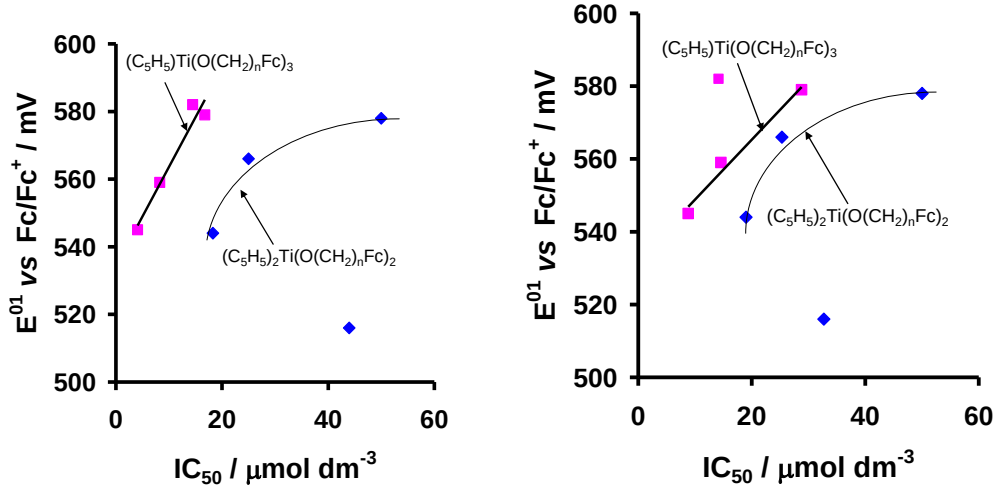

Figure 3.60. Top: Plots of E^{01} of the Fc/Fc^+ couple against IC_{50} values of CoLo (left) and HeLa cells (right) for $(C_5H_5)_2Ti(O(CH_2)_4Fc)_2$, $(C_5H_5)Ti(O(CH_2)_4Fc)_3$ and $Ti(O(CH_2)_3Fc)_4$.

3.9.4. Complexes of the type $TiCl_2(RcCOCHCOR)_2$

Seeing as some of the mono-ruthenocene-containing-β-diketonato titanium complexes of section 3.9.2 did not display anti-cancer activity at the same level as the multiple ferrocenyl alkoxy series of titanium complexes in section 3.9.3, it was thought that the coordination of two β-diketonate ligands onto a titanium core might increase the complexes' cytotoxicity of β-diketonato titanium(IV) complexes more efficiently. The cytotoxicity data of dichlorobis(β-diketonato)titanium(IV) complexes [$TiCl_2(RcCOCHCOR)_2$, R = $C_{10}F_{21}$ (**213**), CF_3 (**214**), C_6F_5 (**215**), $C_{10}H_{21}$ (**216**), CH_3 (**217**), Rc (**218**) and Fc (**219**)] are shown in Table 3.40, and the survival curves of the complex that gave the best result *vs* CoLo and HeLa cells are shown in Figure 3.61.

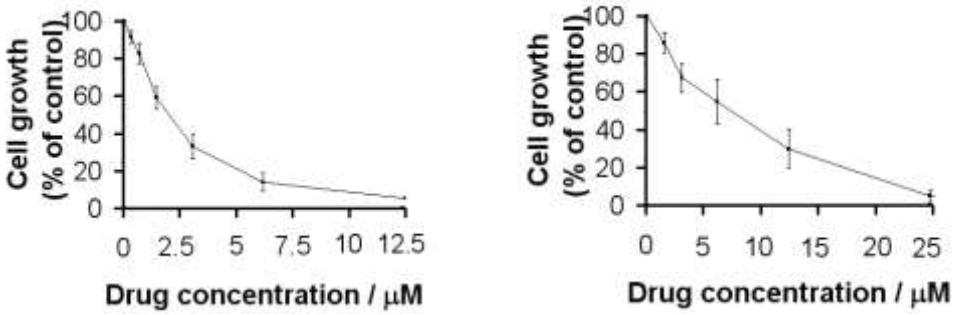

Figure 3.61. Plots of percentage survival CoLo (left) and HeLa cells (right) against concentration (μmol dm^{-3}) of [$TiCl_2(RcCOCHCOC_{10}F_{21})_2$] (**213**).

The complexes of the form $TiCl_2(RcCOCHCOR)_2$, all revealed very good cytotoxic properties against both cell lines. The fluorine containing complexes were most reactive. If one considers the F-containing compounds and the other compounds as two separate classes a general trend between group electronegativity and IC_{50} values can be identified. Non-F containing compounds seem to be more cytotoxic when group electronegativity decreases. In contrast, for the F-containing compounds, the opposite seems to be valid for CoLo cells. Comparison of the IC_{50} values with the electrochemical data again revealed no direct relationship.

The complexes that are most suited to cancer treatment were those containing either fluorine or a ferrocenyl groups. This is propably due to a synergistic effect that exists between the fluorine (or ferrocenyl group), and the ruthenocenyl and titanium(IV) anti-cancer fragments. Complex **213** [IC_{50} 1.85 mmol dm^{-3}] showed cytotoxicity comparable with what was found for cisplatin [IC_{50} 1.84 mmol dm^{-3}] against the CoLo cell line. As for the other complexes, non are

as effective as cisplatin in killing cancer cells. All complexes showed enhanced cytotoxic activity in comparison with titanocene dichloride.

Table 3.40. IC_{50} values for CoLo and HeLa cell lines after treatment with dichlorobis(β-diketonato)titanium(IV) complexes [$TiCl_2(RcCOCHCOR)_2$, R = $C_{10}F_{21}$ (**213**), CF_3 (**214**), C_6F_5 (**215**), $C_{10}H_{21}$ (**216**), CH_3 (**217**), Rc (**218**) and Fc (**219**)]. Group electronegativity (χ_R) of the R-groups on the β-diketonate, the peak anodic potential of the Rc/Rc^+ couple and the peak cathodic potentials of the Ti^{4+}/Ti^{3+} couple *vs* Fc/Fc^+ at v = 200 mV s^{-1} are also shown.

R	χ_R	Rc/Rc^+ E_{pa} / mV	Ti^{4+}/Ti^{3+} E_{pc} / mV	IC_{50} value for CoLo cell line / μmol dm^{-3}	IC_{50} value for HeLa cell line / μmol dm^{-3}
213: $C_{10}F_{21}$	3.04	839	-1533	1.85	7.48
214: CF_3	3.01	761; 933; 115	-1551	3.46	4.41
215: C_6F_5	2.46	799; 1126	-1570	3.09	3.79
216: $C_{10}H_{21}$	2.43	-100; 344; 650	-1698	16.42	23.15
217: CH_3	2.34	699; 1043	-1591	16.06	25.73
218: Rc	1.99	902; 1184	-1426	14.78	21.37
219: Fc	1.87	751	-1791	10.29	9.11
cisplatin		-	-	1.84	1.33
$(C_5H_5)_2TiCl_2$		-	-	39.37	84.51

3.9.5. Complexes of the type $Ti(O(CH_2)_nFc)_2(RcCOCHCOR)_2$

Seeing as the $TiCl_2(RcCOCHCOR)_2$ and the titanium complexes containing ferrocenyl alkoxy groups display such good reactivity, it was decided to investigate the effect that the combination of two β-diketonate ligands and two ferrocenyl-containing alkoxy groups coordinated to the titanium core might have on the complexes' anti-cancer properties. The cytotoxicity data of [$Ti(O(CH_2)_nFc)_2(RcCOCHCOR)_2$, n = 1 (**220**), 2 (**221**), 3 (**222**), 4 (**223**), R = CH_3 and n = 4, R = $C_{10}F_{21}$ (**224**), CF_3 (**225**), C_6F_5 (**226**), $C_{10}H_{21}$ (**227**), CH_3 (**223**), Rc (**228**) and Fc (**229**)] are shown in Table 3.41 and the survival curves of the complex that gave the best result *vs* CoLo and HeLa are shown in Figure 3.62.

The series of complexes with the form $Ti(O(CH_2)_nFc)_2(RcCOCHCOCH_3)_2$, was tested in two different ways: firstly in 0.5% DMSO and then in a "co-solvent" system consisting of titanium complex, Cremophor and propylene glycol (in ratio 1:9:1) which produces micelles when dissolved in water.[28] It was found that the "co-solvent" improved results especially for complex **221**. Since the "co-solvent" system also had less chance of substituting ligands on the titanium complex than the DMSO, it was decided to perform all further experiments utilising the "co-solvent" system.

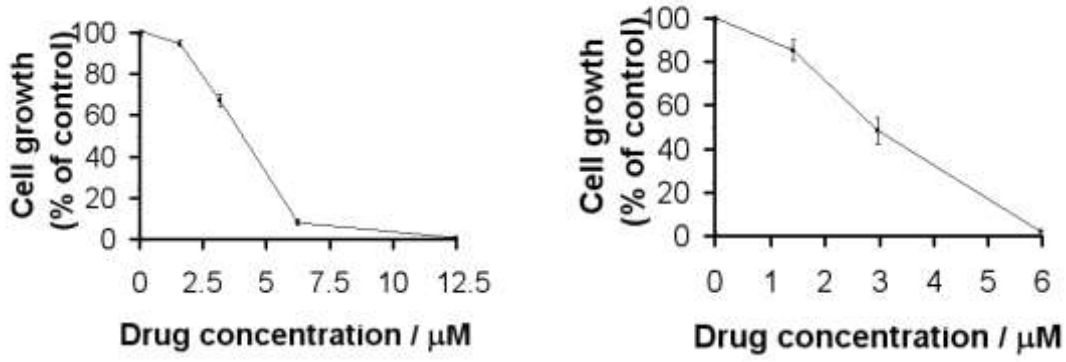

Figure 3.62. Plots of percentage survival CoLo (left) and HeLa cells (right) against concentration (μmol dm^{-3}) of $[Ti(O(CH_2)_4Fc)_2(RcCOCHCOC_{10}F_{21})_2$, (**224**).

Table 3.41. IC_{50} values for CoLo and HeLa cell lines after treatment with $Ti(O(CH_2)_nFc)_2(RcCOCHCOR)_2$ complexes. Group electronegativities (χ_R) of the R-groups on the β-diketonate and the peak anodic potential of the Rc/Rc^+ couple, formal reduction potential of the $O(CH_2)_nFc/O(CH_2)_nFc^+$ couple and the peak cathodic potentials of the Ti^{4+}/Ti^{3+} couple *vs* Fc/Fc^+ at v = 200 mV s^{-1} are also shown.

	χ_R	Rc/Rc^+ E_{pa} / mV	Fc/Fc^+ E^{01} / mV	Ti^{4+}/Ti^{3+} E_{pc} / mV	IC_{50} / CoLo[a]	IC_{50} / HeLa[a]	IC_{50} / CoLo[b]	IC_{50} / HeLa[b]
220: 1	2.34	668	-55	-1698	9.70	9.45	9.87	8.49
221: 2	2.34	790	-46	-1568	20.83	22.89	>50	>50
222: 3	2.34	918	-54	-1624	10.26	12.28	11.92	7.91
223: 4	2.34	877	11	-1977	5.40	12.08	5.82	7.70
224: $C_{10}F_{21}$	3.04	1021	138	-1307	3.85	3.03	-	-
225: CF_3	3.01	1357	23	-1479	8.76	8.10	-	-
226: C_6F_5	2.46	917	15	-1435	5.45	5.02	-	-
227: $C_{10}H_{21}$	2.43	947	2	-1460	13.25	20.18	-	-
223: CH_3	2.34	877	11	-1977	5.40	12.08	-	-
228: Rc	1.99	833	-60	-1539	8.45	16.20	-	-
229: Fc	1.87	923	-35	-1555	9.42	9.29	-	-

a) IC_{50} measure in μmol dm^{-3}, drug introduced as "co-solvent" system to cancer cells.

b) IC_{50} measure in μmol dm^{-3}, drug introduced to cancer cells as 0.5% DMSO solution in H_2O.

The series of complexes with the form $Ti(O(CH_2)_nFc)_2(RcCOCHCOCH_3)_2$, revealed that there is no relationship between the alkyl chain length and the IC_{50} values. The complexes with n = 4 had the lowest IC_{50} value.

It was than decided to keep n = 4 while the β-diketonato ligand was varied to see if the IC_{50} value could be lowered even more for better anti-cancer treatment.

No direct relationship could be found between the apparent group electronegativities of the R-group on the β-diketonato ligand, or metal centre redox potentials and the IC_{50} values. However, excluding especially **227** containing a long chain alkyl substituent the general trend for both cell lines appears to be that as these parameters increase, the cytotoxic property of these complexes increases.

3.9.6. Complexes of the type $(C_5H_5)TiCl(RcCOCHCOCH_3)_2$ and $(C_5H_5)Ti(O(CH_2)_4Fc)(RcCOCHCOCH_3)_2$

The cytotoxicity data of chloro(cyclopentadienyl)bis(1-ruthenocenoylbutane-1,3-dionato)titanium(IV) (**230**) and cyclopentadienyl(4-ferrocenylbutoxy)bis(1-ruthenocenoylbutane-1,3-dionato)titanium(IV) (**231**) are shown in Table 3.42 and the survival curves of the complex (**231**) that gave the best result *vs* CoLo and HeLa are shown in Figure 3.63.

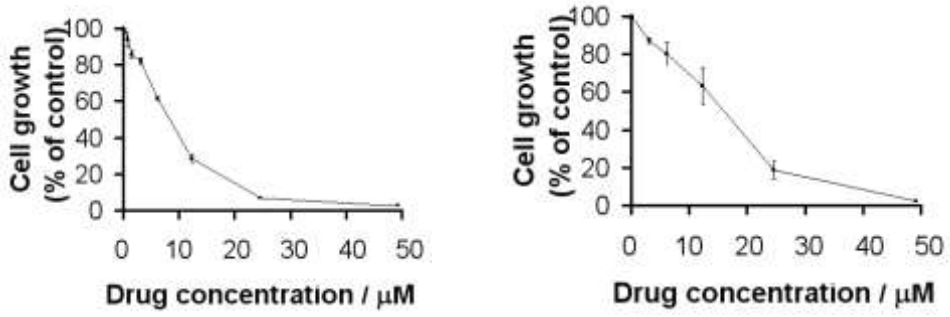

Figure 3.63. Plots of percentage survival CoLo (left) and HeLa cells (right) against concentration (μmol dm^{-3}) of cyclopentadienyl(4-ferrocenylbutoxy)bis(1-ruthenocenoylbutane-1,3-dionato)titanium(IV) (**231**).

From these two complexes the enhanced cytotoxic activity of the ferrocene-containing complex **231** over the chloro complex **230** is apparent. The enhanced activity is due to a synergistic effect between the titanium and ferrocenyl moiety in complex **231**.

Table 3.42. IC_{50} values for CoLo and HeLa cell lines after treatment with chloro(cyclopentadienyl)bis(1-ruthenocenoylbutane-1,3-dionato)titanium(IV) (**230**) and cyclopentadienyl(4-ferrocenylbutoxy)bis(1-ruthenocenoylbutane-1,3-dionato)titanium(IV) (**231**), group electronegativity (χ_R) of the R-groups on the β-diketonate and e, formal reduction potential of the Fc/Fc^+ couple and the peak cathodic potentials of the Ti^{4+}/Ti^{3+} couple *vs* Fc/Fc^+ at v = 200 mV s^{-1} are also shown.

no	Fc/Fc^+ E^{01} / mV	Ti^{4+}/Ti^{3+} E_{pc} / mV	IC_{50} value for CoLo cell line / μmol dm^{-3}	IC_{50} value for HeLa cell line / μmol dm^{-3}
230	-	-	45.42	12.36
231	8	-1260	7.49	16.24

3.9.7. Conclusion

Some of the newly synthesised titanium complexes, such as $[(C_5H_5)_2Ti(RcCOCHCOR)]^+ClO_4^-$ and $TiCl_2(RcCOCHCOR)_2$, showed enchanced anti-cancer activity over its free components (starting materials), $(C_5H_5)_2TiCl_2$ and $RcCOCH_2COR$. Other titanium complexes such as $[(C_5H_5)_2Ti(O(CH_2)_nFc)_2$, $(C_5H_5)Ti(O(CH_2)_nFc)_3$ and $Ti(O(CH_2)_nFc)_4]$ did not show enhanced activity over the free ferrocene-containing alcohols.

The enhanced anti-cancer activity of some the synthesised titanium complexes over pure titanocene dichloride was thought to be due to a synergistic effect. This is proven to be the case for **194, 200, 217** and **219**. In these complexes, for **194** and **200** the two Cl^- groups were replaced with the β-diketonato ligand RcCOCHCOR (R = CH_3 and Fc) and for **217** and **219** the two C_5H_5 ligands were relaced with two β-diketonato ligands RcCOCHCOR (R = CH_3 and Fc) (see Figure 3.64, Top). The synergistic effects that are created for these four compounds are shown in Figure 3.64 (Middel and Bottom).

From Figure 3.64 (Middel), it can be seen that the activity for **217** against CoLo and HeLa cell lines has increased 92% and 43% respectively in comparison with the accumulative activity of **89** and **151**. The ferrocenyl derivative (**219**) showed enchanced activity of 100% and 92% against CoLo and HeLa cell lines respectively in comparison with the accumulative activity of **89** and **154**. This result implies that a good synergistic effect is created when the two anti-cancer drugs **89** and **151** (or **154**) are combined in one complex namely **217** (or **219**). **219** show a slightly better synergistic effect than **217**, probably due to the ferrocenyl moiety included in the structure.

194 showed (Figure 3.64, Bottom) excellent synergistic effects where the activity against CoLo and HeLa cell lines has increased 285% and 117% respectively in comparison with the accumulative activity of **89** and **151**. The synergistic effect of the ferrocenyl derivative (**200)** was not as impressive as **194**, with enchanced activity of 72% and 39% against CoLo and HeLa cell lines respectively in comparison with the accumulative activity of **89** and **154**.

It has been shown that the combination of two anti-cancer drugs (i.e. *cis*-platin with cytoxin and/or 5-fluorouracil) on a L1210-cancertumor in BDF_1-mice has a synergistic effect that increases the lifespan of the mice ~100% over the accumulative lifespan of the two drugs.[40, 41] **194**'s activity increased with 285%, which shows that this complex created a much better synergistic effect than the *cis*-platin in combination with cytoxin and/or 5-fluorouracil. As for the other complexes, they may not have better synergism than the *cis*-platin combinations, but may have less toxic side effects and can be used against platinum resistant cell lines.

In conclusion it was found that complexes with more than one anti-cancer moiety, showed enhanced antineoplatic activity over pure titanocene dichloride (IC_{50} = 84.51), which is due to synergistic effects. The complexes containing F had the best results in each type of compound. The complex $TiCl_2(RcCOCHCOC_{10}F_{21})_2$ matched the IC_{50} values of cisplatin against CoLo cell lines. The family of complexes having the general structure $TiCl_2(RcCOCHCOR)_2$ gave the best overall results (lowest IC_{50} values) against both CoLo and HeLa cell lines.

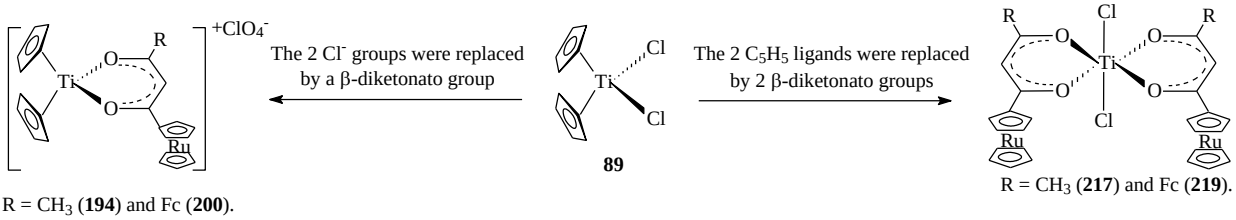

R = CH_3 (**194**) and Fc (**200**).

R = CH_3 (**217**) and Fc (**219**).

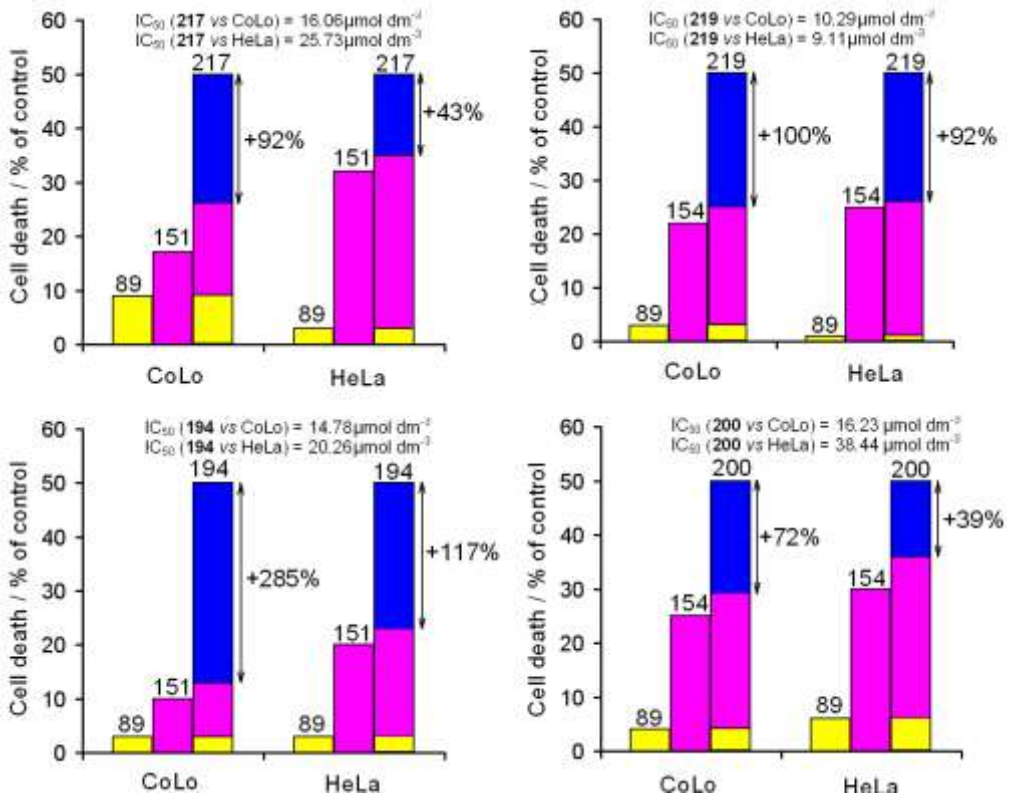

Figure 3.64. Top: Scheme showing how the complexes (**194, 200, 217** and **219**) differ from pure titanocene dichloride (**89**). Middle: The graphs showing the synergistic effect (activity gain) of **217** (Left) and **219** (Right) against CoLo and HeLa cell lines. Bottom: The graphs showing the synergistic effect of **194** (Left) and **200** (Right) against CoLo and HeLa cell lines. As benchmark concentrations was taken IC_{50} (i.e. drug concentration inducing 50% cell death) values of **217, 219, 194** and **200**. The % cell death that **89** (yellow) and the free β-diketone ligands (pink) induced at the IC_{50} concentration of the multi component drug was then determined (J.C. Swarts, unpublished results). However, for **217** and **219**, the β-diketone concentration used was 2 x IC_{50} of **217** or **219** because the multi component drug has 2 β-diketonato ligands in its structure. Adding the yellow and pink bars, result in the expected efficiency of **194, 200, 217** and **219** in killing CoLo and HeLa cancer cells. The gain in efficiency of the combined drug (due to synergism) is shown with the blue bar, % efficiency increase is indicated next to the blue bar.

[1] W.L. Davis, R.F. Shago, E.H.G. Langer and J.C. Swarts, *Polyhedron*, 2005, **24**, 1611.

[2] J. Kotz and D. Pedrotty, *Organomet. Chem. Rev. A*, 1969, **4**, 479.

[3] M.D. Rausch, E.O. Fischer and H. Gurbert, *J. Am. Chem. Soc.*, 1960, **82**, 76.

[4] A.R. Katritzky and A. Pastor, *J. Org. Chem.*, 2000, **65**, 3679.

[5] A.R. Katritzky, Y. Zhang and S.K. Singh, *Synthesis*, 2003, **18**, 2795.

[6] A.R. Katritzky, Y. Fang, A. Donkor and J. Xu, *Synthesis*, 2000, **14**, 2029.

[7] J.E. Sheats and M.D. Rausch, *J. Org. Chem.*, 1970, **35**, 3245.

[8] N. Rabjohn, Ed., *Organic Syntheses*, vol IV, Wiley, New York, 1963, 476.

[9] G. Doyle and R.S. Tobias, *Inorg. Chem.*, 1967, **6**, 1111.

[10] R.E. Kagarise, *J. Am. Chem. Soc.*, 1955, **77**, 1377.

[11] W.C. du Plessis, T.G. Vosloo and J.C. Swarts, *J. Chem. Soc., Dalton Trans.*, 1998, 2507.

[12] G.A Olah, M. Stephenson, J.G. Shih, V.V. Krishnamurthy and G.K. Surya Prakash, *J. Fluorine Chem.*, 1988, **40**, 319.

[13] P.J. Dickens, H.P. Gilday, J.T. Negri and D.A. Widdowson, *Pure & Appl. Chem.*, 1990, **62**, 575.

[14] R. Fandos, C. Hernandez, A. Otero, A. Rodriguez, M. Jose Ruiz and P. Terreros, *J. Organomet. Chem.*, 2000, **606**, 156.

[15] R.D. Shannon, *Acta Cryst.*, 1976, **5**, 751.

[16] K. Ito, T. Tomino, M. Ohisma, H. Kurokawa, K. Suugiyama ans H. Miura, *App. Catal. A: Gen.*, 2003, **249**, 19.

[17] K.C. Kemp, M.Sc. Study, *Synthesis, electrochemical, kinetic and thermodynamic studies of new ruthenocene-containing betadiketonato rhodium(I) complexes with biomedical applications,* University of the Orange Free State, R.S.A., 2004.

[18] R.G. Wilkins, *The study of kinetics and mechanism of reactions of transitionmetal complexes,* Allyn and Bacon, Boston, 1974, 44-45.

[19] W.C. du Plessis, W.L. Davis, S.J. Cronje and J.C. Swarts, *Inorg. Chim. Acta*, 2001, **314**, 97.

[20] R.C. Fay and R.N. Lowry, *Inorg. Chem.*, 1974, **13**, 1309.

[21] J. Conradie, Ph.D. Study, *Chemical kinetics, electrochemistry and structural aspects of ferrocene-containing β-diketoeato complexes of rhodium(I) and iridium(I)*, University of the Orange Free State, R.S.A., 2001.

[22] T.G. Vosloo, W.C. du Plessis and J.C. Swarts, *Inorg. Chim. Acta*, 2002, **331**, 188.

[23] F. Marchetti, C. Pettinari and R. Pettinari, *Coord. Chem. Rev.*,2005, in press.

[24] V. Reimer, T.P. Spaniol, J. Okuda, H. Ebeling, A. Tuchbreiter and R. Mulhaupt, *Inorg. Chim. Acta*, 2003, 345, 221.

[25] M.J. Frazer and W.E. Newton, *Inorg. Chem.*, 1971, **10**, 2137.

[26] R.C. Fay and R.N. Lowry, *Inorg. Chem.*, 1967, **6**, 1512.

[27] Y. Marcus and I. Eliezer, *J. Phys. Chem.*, 1962, **66**, 1661.

[28] B.K. Keppler and M.E. Heim, *Drugs of Future.* 1988, **13**, 637.

[29] S. Trupia, A. Nafady and W.E. Geiger, *Inorg. Chem. Comm.*, 2003, **42**, 5480.

[30] M.G. Hill, W.M. Lamanna and K.R. Mann, *Inorg. Chem.*, 1991, **30**, 4690.

[31] M.W. Droege, W.D. Harman and H. Taube, *Inorg. Chem.*, 1987, **26**, 1309.

[32] J. C. Swarts, D. Laws and W. E. Geiger, *Organomet.*, 2005, **24**, 341.

[33] Z.S. Ambrose, M.Sc. Study, unpublished results.

[34] R.C. Weast, Editor, *Handbook of Chemistry and Physics*, 51st Edition, The Chemical Rubber Co., Cleveland, 1970, p. D111.

[35] K. Prout, T.S. Cameron, R.A. Forder, S.R. Critchley, B. Denton and G.V. Rees, *Acta Crystllogr., Sect B*, 1974, **30**, 2290.

[36] A.M. Bond, R. Colton, U. Englert, H. Hugel and F. Marken, *Inorg. Chim. Acta*, 1995, **235**, 117.

[37] F. Bottomley, I.J.B. Lin and P.S. White, *J. Organomet. Chem.*, 1981, **212**, 341.

[38] U. Thewalt and H.P. Klein, *J. Organomet. Chem.*, 1980, **194**, 297, and references therein.

[39] J.C. Swarts, E.H.G. Langner, N. Krokeide-Hove, M.J. Cook, *J. Materchem*., 2001, **11**, 434.

[40] R.J. Speer, S. Lapis and H. Ridgway, *Advances in Antimicrobial and Antineoplatis Chemotherapy*, Univ. Park Press, Baltimore, 1972, 254.

[41] L.van Camp and B. Rosenberg, *Advances in Antimicrobial and Antineoplatis Chemotherapy*, Univ. Park Press, Baltimore, 1972, 239.

Chapter 5

Summary, Conclusions and Future Perspectives

In this study, 4 ferrocene-containing alcohols, 7 ruthenocene-containing β-diketones (3 of which are new), 2 new ruthenocene- and ferrocene-containing enaminones as well as 42 new ruthenocene- and/or ferrocene-containing titanium(IV) complexes were synthesised in multistep reactions. In some cases, new synthetic protocols had to be designed to achieve synthetic success. Key compounds are shown in Figure 5.1. These complexes were all characterised spectroscopically with UV/Vis, IR and ^{1}H NMR. Their physical properties were investigated with electrochemical, thermodynamic and kinetic techniques. Most of the new compounds were also evaluated as potentially new anti-cancer drugs by determining IC_{50} values on CoLo and HeLa human cancer cell lines.

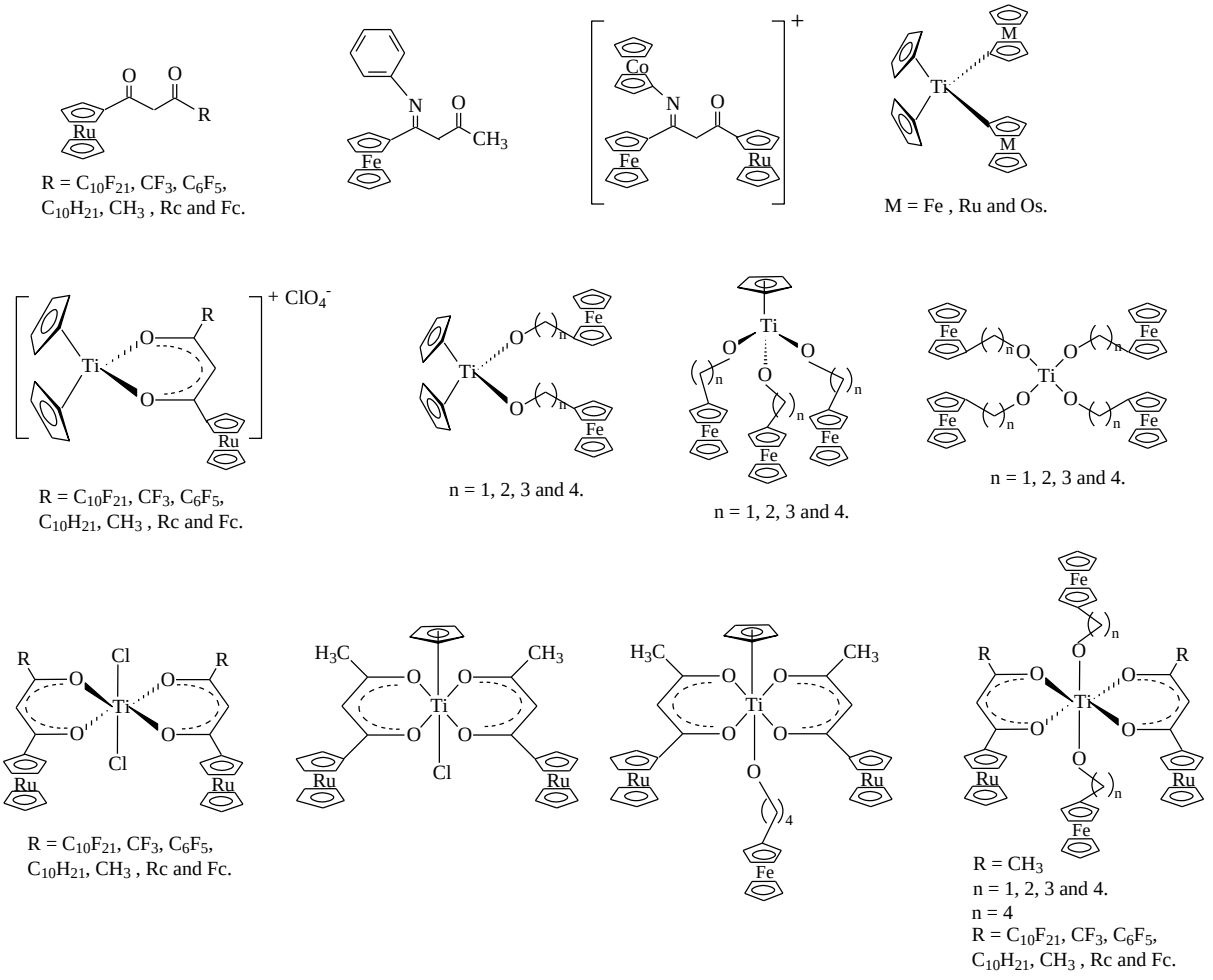

Figure 5.1. Structures of the series of key compounds synthesized in this study. Fc = ferrocenyl and Rc = ruthenocenyl.

A variety of new tetrahedral mono-β-diketonato titanocenyl(IV) complexes of the form $[(C_5H_5)_2Ti(RcCOCHCOR)]^+ClO_4^-$ (see Figure 5.1, 2nd row left) were obtained *via* two different routes; the known route which used titanocene dichloride as reactant and a new route developed here which involves the substitution of $CH_3COCHCOCH_3^-$ with the desired β-diketone from $[(C_5H_5)_2Ti(CH_3COCHCOCH_3)]^+ClO_4^-$. The latter substitution route is the higher yielding route. Yields were found to be dependent on the group electronegativity of the R-group of the incoming β-diketone as well as on the bulkiness of the R-group.

The titanium series bis(cyclopentadienyl)dimetallocenyl titanium(IV) complexes of the form $[(C_5H_5)_2Ti\{(C_5H_4)M(C_5H_5)\}_2]$ (M = Fe, Ru, and Os) (see Figure 5.1, first row right), was synthesized by the treatment of the appropriate lithiated metallocene (FcLi, RcLi or OcLi) with titanocene(IV) dichloride in THF.

Various kinds of new ferrocene-containing alkoxy titanium(IV) complexes of the form: $(C_5H_5)_2Ti(O(CH_2)_nFc)_2$, $(C_5H_5)Ti(O(CH_2)_nFc)_3$ and $Ti(O(CH_2)_nFc)_4$ with n = 1, 2, 3 and 4 were synthesized (Figure 5.1, middle row). Bis(cyclopentadienyl)di(ferrocenylalkoxy)titanium(IV), cyclopentadienyltri(ferrocenylalkoxy)titanium(IV) and tetra(ferrocenylalkoxy)titanium(IV)) were prepared by reacting the appropriated ferrocene-containing alcohol with the appropriate titanium complex, which was either $(C_5H_5)_2TiCl_2$, $(C_5H_5)TiCl_3$ or $TiCl_4$. The yield of all these complexes increased as the alkyl chain length of the ferrocenyl containing alcohol increased.

A series of 7 new octahedral bis-β-diketonato titanium(IV) complexes, of the form $[TiCl_2(RcCOCHCOR)_2]$, $[Ti(O(CH_2)_nFc)_2(RcCOCHCOR)_2]$, $[(C_5H_5)TiCl(RcCOCHCOCH_3)_2]$ and $[(C_5H_5)Ti(O(CH_2)_4Fc)(RcCOCHCOCH_3)_2]$ (Figure 5.1), were also prepared. From ^1H NMR studies on the bis-β-diketonato complexes it was established that these compounds exist as more than one isomer in solution.

These alkoxide bis-β-diketonato titanium complexes could be synthesized by two different routes starting with either tetra(ferrocenylalkoxy)titanium(IV) and reacting it with the appropriate ruthenocene-containing β-diketone or by reacting dichlorobis(βdiketonato)titanium(IV) with the appropriate ferrocene-containing alcohol. Yields were dependent on the alkyl chain length of the ferrocene-containing alcohol or the group electronegativity of the R-group on the β-diketone.

Chloro(cyclopentadienyl)bis(1-ruthenocenoylbutane-1,3-dionato)titanium(IV) and cyclopentadienyl(4-ferrocenylbutoxy)bis(1-ruthenocenoylbutane-1,3-dionato)titanium(IV) on the other hand are two octahedral titanium(IV) complexes which were synthesised from titanocene dichloride.

The group electronegativities of C_6F_5 (2.46), $C_{10}H_{21}$ (2.43) and $C_{10}F_{21}$ (3.04) were obtained by inserting the value of the carbonyl stretching frequency for the methyl ester of

C_6F_5COOMe, $C_{10}H_{21}COOMe$ and $C_{10}F_{21}COOMe$ into the plot of known carbonyl stretching frequencies of RCOOMe compounds *vs* Gordy scale group electronegativities, χ_R, of appropriate R-groups. The pK_a' values for the new β-diketone with R = $C_{10}F_{21}$ (7.14(4)), C_6F_5 (9.92(3)) and $C_{10}H_{21}$ (10.06(2)) were determined spectroscopically in water containing 10% acetonitrile.

The isomerization kinetics of the new β-diketones $RCCOCH_2COR$ with R = $C_{10}F_{21}$, C_6F_5 and $C_{10}H_{21}$ were studied in $CDCl_3$ while β-diketones with R = $C_{10}F_{21}$, CF_3, C_6F_5, $C_{10}H_{21}$, CH_3, Rc and Fc were studied in CD_3CN by ^1H NMR spectroscopy. Observed rates of keto-enol conversion become slower as the group electronegativity of the R-group becomes smaller.

Ligand exchange processes for the reaction between $[Ti(O(CH_2)Fc)_2(RcCOCHCOCH_3)_2$ + $[Ti(O(CH_2)_4Fc)_2(RcCOCHCOCH_3)_2]$ and $[Ti(O(CH_2)_4Fc)_2(RcCOCHCOCH_3)_2]$ + $[Ti(O(CH_2)_4Fc)_2(RcCOCHCOCF_3)_2]$ were followed by ^1H NMR spectroscopy. It was shown that alkoxy exchange goes to completion in a second order process whereas bidentate β-diketonato exchange is a first order equilibrium process. Rate constants for these reactions were determined.

Substitution reactions investigated in this kinetic study involved the substitution of the mono-dentate ferrocene-containing alkoxy groups of $[Ti(O(CH_2)_nFc)_2(RcCOCHCOCH_3)_2]$ {n = 1, 2, 3} with $HO(CH_2)_nFc$ {n = 2, 3, 4} and the substitution of the bi-dentate β-diketonato ligand of $[Ti(O(CH_2)_4Fc)_2(RcCOCHCOR)_2]$ {R = CH_3, CF_3} with other β-diketones. The substitution of two mono-dentate alkoxy ligands take place in two consecutive reactions. For both reactions, the entropy of activation was found to have a large positive value. This implied a dissociative mechanism of substitution. Rate constants for the overall second order alkoxy substitution reactions could be determined, and substitution reactions were slowed down by the presence of free leaving ligand in solution. A theoretical derived rate law from a proposed reaction mechanism was found to be mutually consistent with the experimentally determined rate law.

Two kinds of hydrolysis reactions were studied kinetically. The first is where the titanium complexes $[Ti(O(CH_2)_4Fc)_2(RcCOCHCOR)_2]$ with R = CF_3, C_6F_5, CH_3, Rc and Fc, were dissolved in solvent mixtures consisting of 2, 10 and 50% H_2O in acetonitrile by mass. The second type is where the same compounds were dissolved in a "co-solvent" system containing titanium complex, Cremophor and propylene glycol (in ratio 1:9:1). When 2% of this mixture is mixed with water (98%) by mass), micelles are produced[1] The second order rate constants that was determined for the hydrolysis of the titanium compounds in both these media were dependent on the group electronegativity of the R-group on the β-diketonato ligand. Especially gratifying was the observation that the new titanium/ruthenium/iron conjugates which were designed for use as anti-cancer drugs, were stable in water for periods up to 10 h (in 10% H_2O in acetonitrile mixture) and more than 7 days in the "co-solvent system".

Electrochemical studies in dichloromethane utilising cyclic voltammetry, linear sweep voltammetry and Oster Young square wave voltammetry were preformed on all synthesised complexes. In general all Ti^{4+}/Ti^{3+}, Ru^{3+}/Ru^{2+} and Co^{3+}/Co^{2+} couples were found to be chemically and electrochemically irreversible while the Fc/Fc^{+} couple were mostly found to be chemically reversible but electrochemically quasi-reversible. In addition, for the ferrocene-containing β-diketones, the multiple oxidation and reduction peaks that were observed could be contributed to mixtures of keto and enol isomers in solution. Evidence for the exsistance of isomers in solution for all octahedral complexes were found during electrochemical studies. Almost all ruthenocene-containing complexes also exhibited multiple cathodic (reduction) waves due to the formation of dimerized ruthenicium species such as $(Rc^{III}\text{-}Rc^{III})^{2+}$.

The electrochemistry of $[(C_5H_5)_2Ti\{(C_5H_4)M(C_5H_5)\}_2]$ (M = Fe, Ru and Os) revealed that the electrochemistry of the ferrocenyl, ruthenocenyl and osmocenyl groups are quasi-reversible. The titanium reduction wave for all three complexes showed both oxidation and reduction peaks with $\Delta E \approx 146$ mV (at scan rate 50 mV s^{-1}) for the ferrocene complex and $\Delta E >$ 200 mV for the osmocene and ruthenocene complexes. The formal reduction potentials of all the reversible redox active centres of these complexes are dependent on the atomic electronegativity of the metal [Fe ($\chi_{Fe} = 1.64$), Ru ($\chi_{Ru} = 1.42$) and Os ($\chi_{Os} = 1.52$)].

The redox active centres' of all the tetra-coordinated titanium alkoxide complexes exhibited E^{01} and E_{pc} values that are dependent on the alkyl chain length of the ferrocenyl containing alkoxy group. For the Fc/Fc^{+} couples of two of the three series of complexes, it was found that, E^{01} decreased as the alkyl chain length increased. This is because as the alkyl chain length increased its electrondonating properties increased, making the ferrocenyl group easier to oxidize.

For $[Ti(O(CH_2)_nFc)_2(RcCOCHCOR)_2]$ no direct relationship exists between E_{pc} and the alkyl chain length of the ferrocenyl alkoxy group. This is attributed to intense electrode deposition. The E^{01} for Fc/Fc^{+} and the peak anodic potential of the Rc/Rc^{+} couple increased as the alkyl chain length of the $Fc(CH_2)_nO$ fragment increased. The behaviour of the Fc/Fc^{+} couple can not be explained at this time, however, for the Rc/Rc^{+} couple it is thought that intra molecular through-space interactions between Rc and oxidised Fc^{+} fragment on the same molecule is the cause of this behaviour. To rationalise this, one should realise that as the chain length of $Fc(CH_2)_nO$ fragment increases, the oxidised Fc^{+} group could get into closer proximity of the Rc group by simple folding/rotation of the $Fc(CH_2)_nO$ chain. Better through-space interaction between these metallocenyl groups is then possible with the result that the positive charge on the oxidized ferrocenium may exert an electron-withdrawing effect on the ruthenyl group, making it more difficult to oxidize.

The cytotoxic properties with the view to probe potential anti-cancer treatment applications of the new titanium(IV) complexes were studied. Human colorectral (CoLo) and human cervix epitheloid cancer cell line (HeLa) cell lines were utilised to determine the cytotoxicity of the complexes.

For $(C_5H_5)_2Ti(O(CH_2)_nFc)_2$, $(C_5H_5)Ti(O(CH_2)_nFc)_3$, $Ti(O(CH_2)_nFc)_4$ and $[Ti(O(CH_2)_nFc)_2(RcCOCHCOCH_3)_2]$ complexes, the IC_{50} values decreased as the alkyl chain length of the ferrocenyl containing alkoxy groups increased from 1 through 4. As for the β-diketonato-containing titanium(IV) complexes $[(C_5H_5)_2Ti(RcCOCHCOR)]^+ClO_4^-$, $TiCl_2(RcCOCHCOR)_2$ and $Ti(O(CH_2)_4Fc)_2(RcCOCHCOR)_2$, it was found that R = $C_{10}F_{21}$, CF_3, C_6F_5 or Fc are the most cytotoxic. This is rationalized in terms of a synergistic effect between the anti-cancer active Ti(IV) ruthenocenyl and fluorine fragments. $[Ti(O(CH_2)_4Fc)_2(RcCOCHCOC_{10}F_{21})_2]$ are the most cytotoxic of all the titanium(IV) complexes synthesised in this study against both CoLo and HeLa cell lines, with IC_{50} = 3.85 and 3.03 μmol dm^{-3} respectively. $TiCl_2(RcCOCHCOC_{10}F_{21})_2$'s IC_{50} values of 1.85 μmol dm^{-3} matched that of cisplatin (IC_{50} = 1.84 μmol dm^{-3}). All the drugs that were investigated in this study had a lower IC_{50} value than titanocene dichloride (IC_{50} = 84.51 μmol dm^{-3}) making them all potentially more effective anti-cancer drugs than titanocene dichloride.

Phase studies revealed that neither of the β-diketones ($RcCOCH_2COCR$) with R = $C_{10}H_{21}$ and $C_{10}F_{21}$, or the titanium complexes $[TiCl_2(RcCOCHCOC_{10}H_{21})_2]$ and $[Ti(O(CH_2)_4Fc)_2(RcCOCHCOC_{10}H_{21})_2]$ exhibits liquid-crystal properties. The free β-diketones exhibited complex solid state phase behaviour while the titanium bis-β-diketonato complexes underwent intramolecular oxygen bridge formation *via* chemical reactions upon heating.

The crystal structure of $[(C_5H_5)_2Ti(RcCOCHCOCH_3)]^+ClO_4^-$ is also reported.

Future study possibilities from this study are vast. In this study, a series of ruthenocene-containing mono-β-diketonato, bis-β-diketonato and bi-, tri and tetraferocene-containing alkoxy titanium(IV) complexes were synthesised and subjected to electrochemistry and ligand exchange, substitution kinetics and hydrolysis kinetics studies. Similar studies could be extended towards Zr, Hf, V, Nb and Mo complexes. Quantification of trends within a group (Ti, Zr and Hf) or a certain period (Ti and V; Zr, Nb and Mo complexes) of the periodic table must be made. Application of these complexes synthesised in this study in terms of catalysis and anti-cancer activity should be addressed.

The study could also be extended to the use of either ferrocene-, osmocene- or cobalticenium-containing β-diketones instead of ruthenocene-containing β-diketones. These β-diketones can be modified to be enaminones, thio-β-diketones, dithio-β-diketones or even β-

enaminothiones. The study of the ferrocene-containing alcohols could be extended toward the thio- and amine-derivatives. New ruthenocene- and osmocene-containing alcohols can also be designed and complexed with Ti, Zr, Hf, V, Nb and Mo.

A clarification study as to what mode of action the present complexes has in killing cancer cells needs to be performed. The cytotoxic properties with respect to HeLa and CoLo cancer cell lines were reported in this study, the toxicity on healthy cells in comparison with the cancer cells should still be investigated. The next step of testing some of the titanium complexes, which showed low IC_{50} values, i.e. $TiCl_2(RcCOCHCOC_{10}F_{21})_2$, should be initiated. These include tests on rats and possibly upgraded to phases I, II and III clinical trials.

The $C_{10}H_{21}$ and $C_{10}F_{21}$ β-diketones' complexes of the present study was aimed at introducing liquid crystalline properties into the complexes. It failed because the β-diketonato aromatic core did not stabilize columnar mesophases enough to introduce liquid crystal properties. By extending conjugated aromatic patterns, as described by Deschenaux (e.g. see Figure 5.2),[2, 3] new material with liquid crystal properties may be obtained.

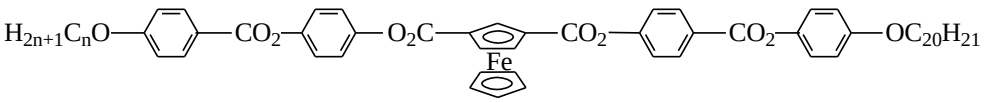

n = 10, 11, 12, 13, 14, 16, 18

Figure 5.2. Structure of liquid crystal ferrocene derivative reported by Deschenaux.

A series of new cobalticenium-containing β-diketones, ferrocene and/or ruthenocene-containing enaminones as well as a new series of titanocene-containing β-diketones and ruthenocene-containing β-ketoesters may be designed. A study involving the effect of R group substituents on these complexes, including pK_a', electronegativity, electrochemistry and keto-enol kinetics will characterise these new materials. These complexes can also be complexed to transition metals such as rhodium, iridium and platinum to find possible synergistic antineoplastic effects as well as catalytic properties.

In conclusion, metallocene complexes represent a class of organometallic compounds with extra-ordinary behaviour and application possibilities. An interested, motivated researcher will be richly rewarded in exploring and researching new complexes and new applications of this type.

[1] B.K. Keppler and M.E. Heim, *Drugs of Future.* 1988, **13**, 637.

[2] R. Deschenaux, M. Rama and J. Santiago, *Tet. Lett.,* 1993, **34**, 3293.

[3] R. Deschenaux and J. Santiago, *Tet. Lett.,*1994, **35**, 2169.

Appendix

^{1}H NMR Spectra

Ferrocene complexes

Spectrum 1: Ferrocenecarboxaldehyde, 23

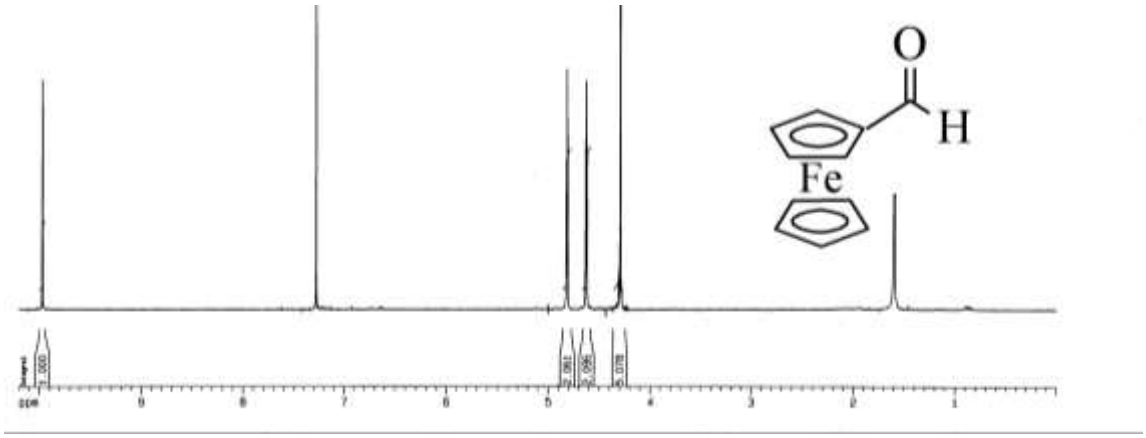

Spectrum 2: Ferrocenylmethanol, 170

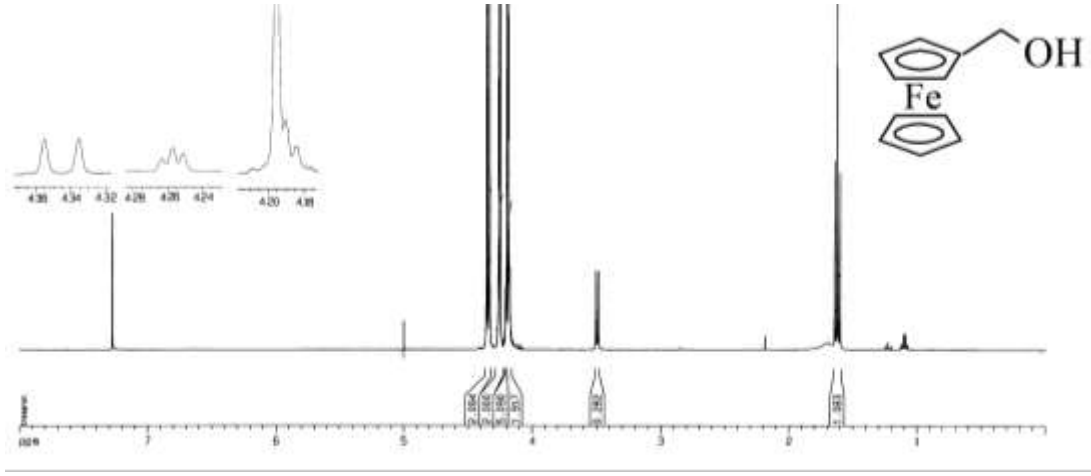

Spectrum 3: *N*,*N*-Dimethylaminomethylferrocene, 20

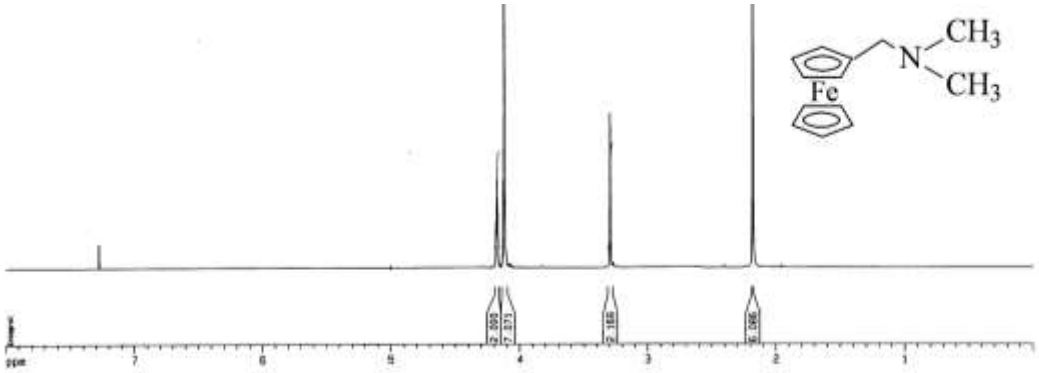

Spectrum 4: *N,N*-dimethylaminomethylferrocene methiodide, 22

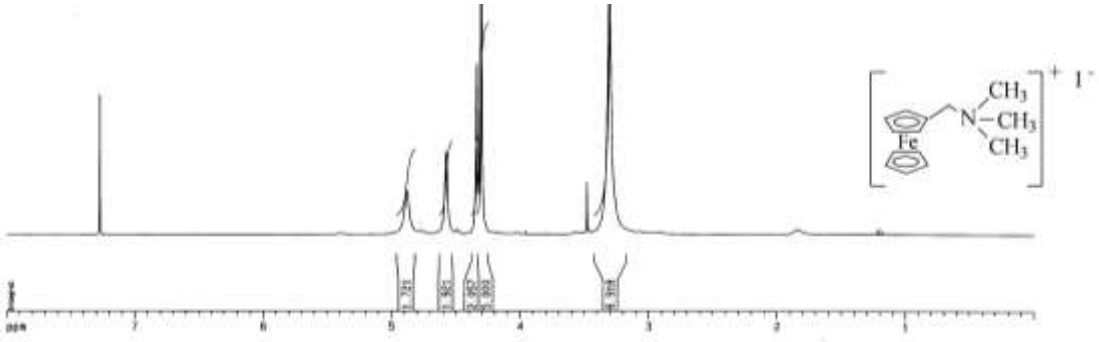

Spectrum 5: Ferroceneacetonitrile, 174

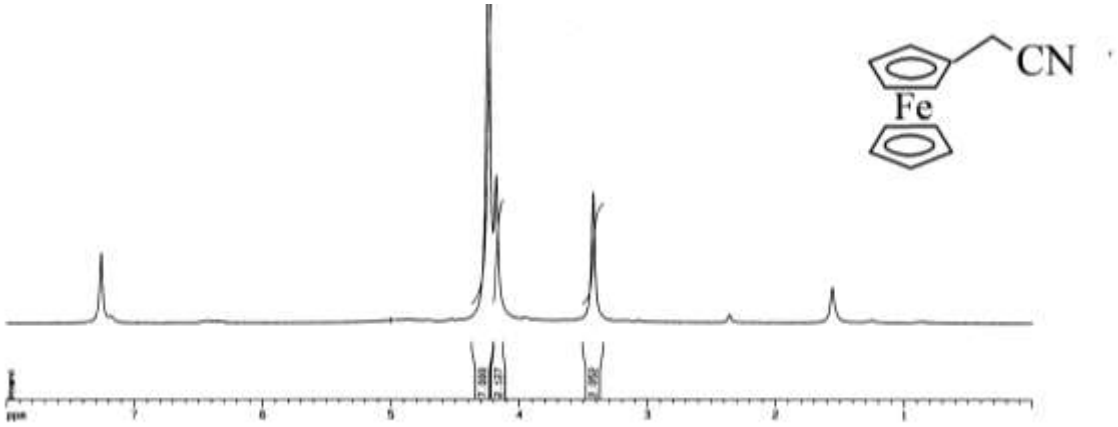

Spectrum 6: Ferroceneacetic acid, 30

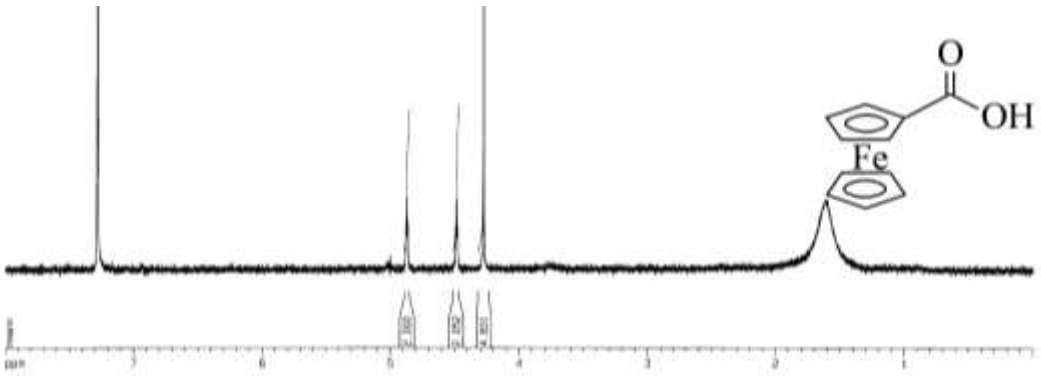

Spectrum 7: 2-Ferrocenylethanol, 171

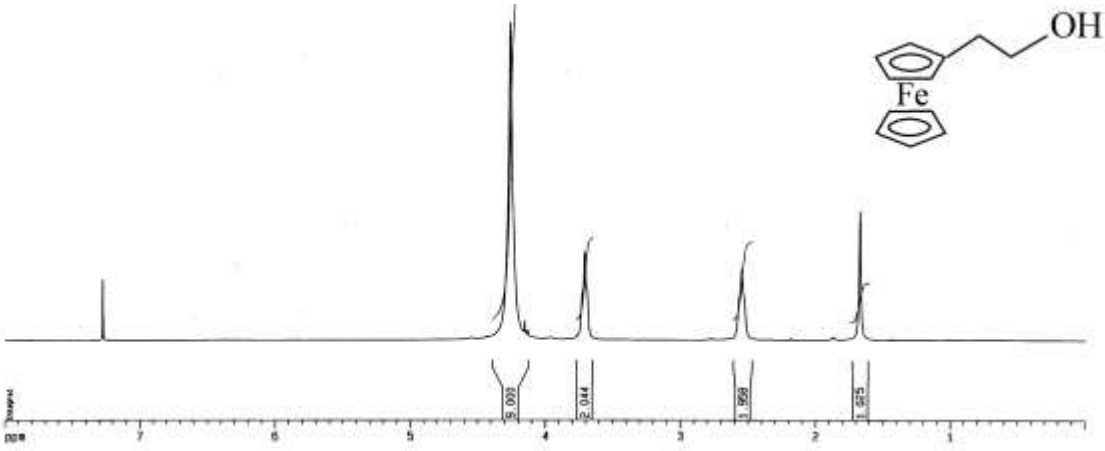

Spectrum 8: 3-Ferrocenylacrylic acid, 176

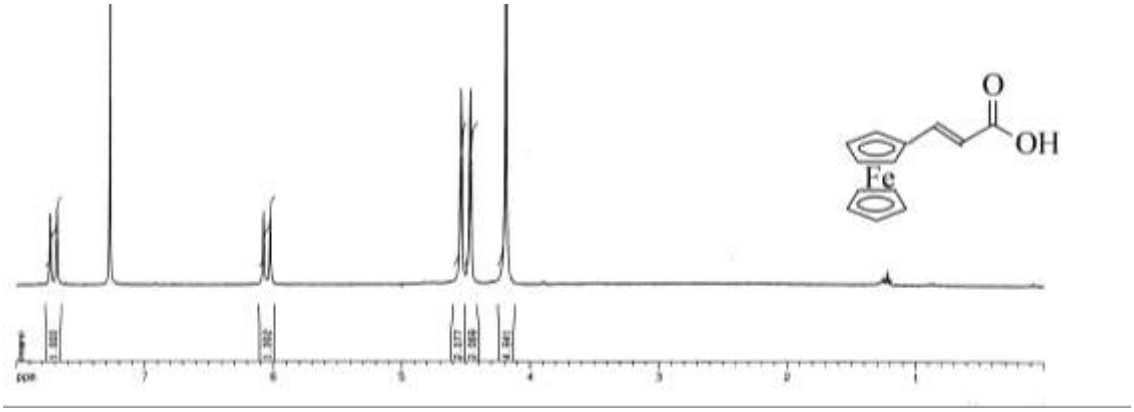

Spectrum 9: 3-Ferrocenylpropanoic acid, 31

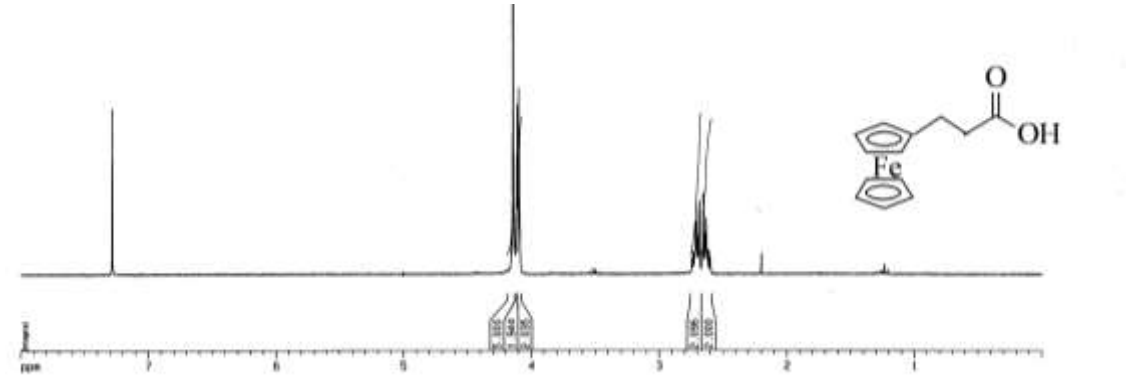

Spectrum 10: 3-Ferrocenylpropanol, 172

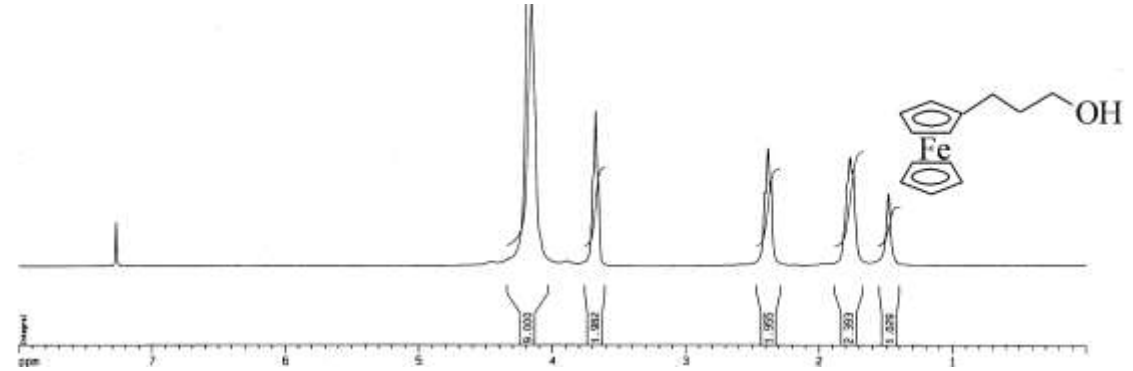

Spectrum 11: 3-Ferrocenoylpropionoic acid, 175

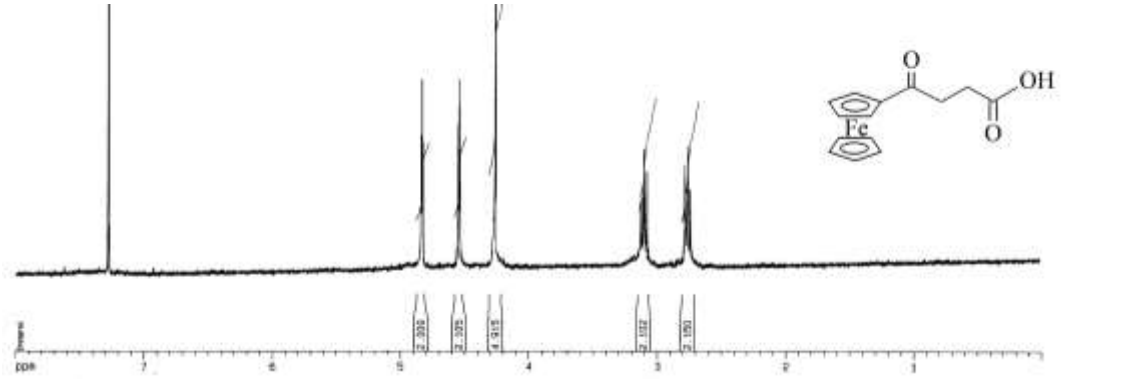

Spectrum 12: 4-Ferrocenylbutanol, 173

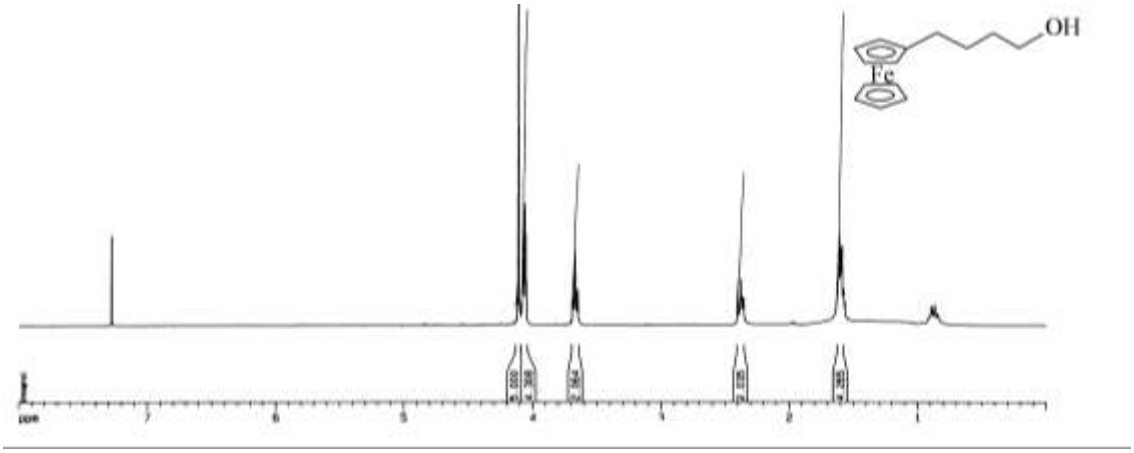

Spectrum 13: 2-Chlorobenzoylferrocene, 26

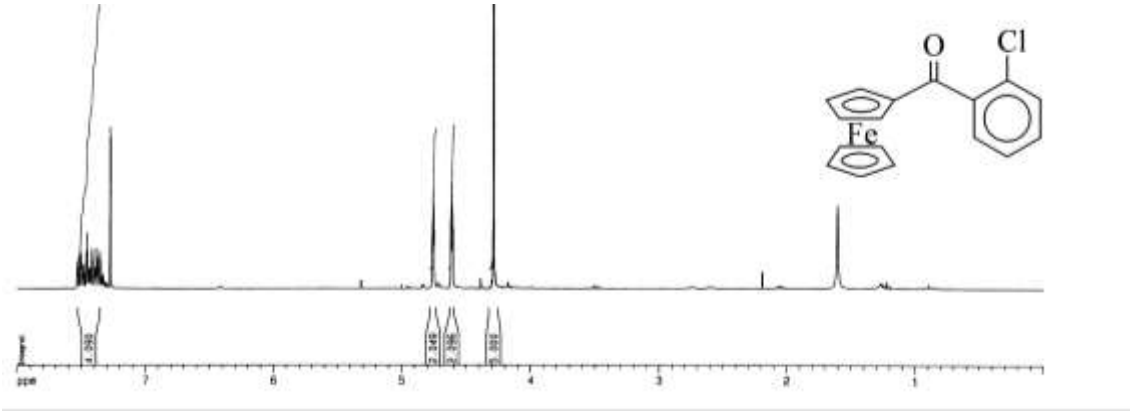

Spectrum 14: Ferrocenecarboxylic acid, 27

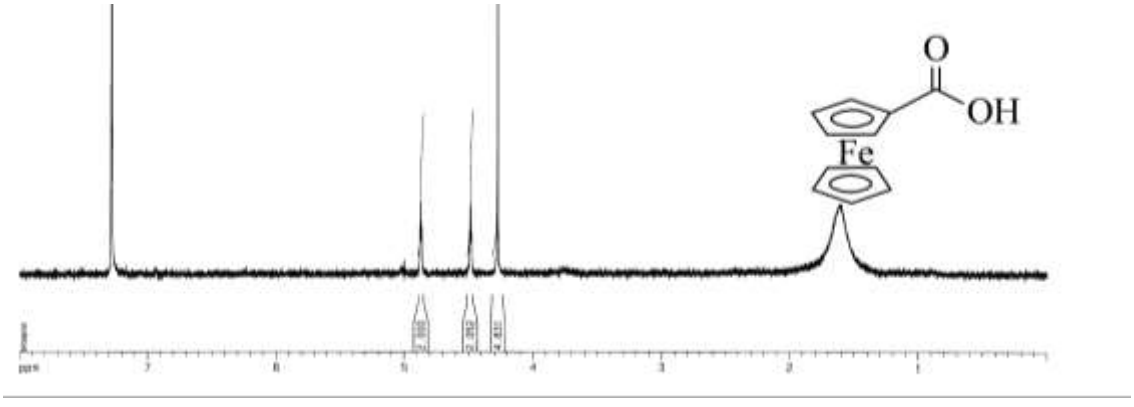

Spectrum 15: Methylferrocenoate, 28

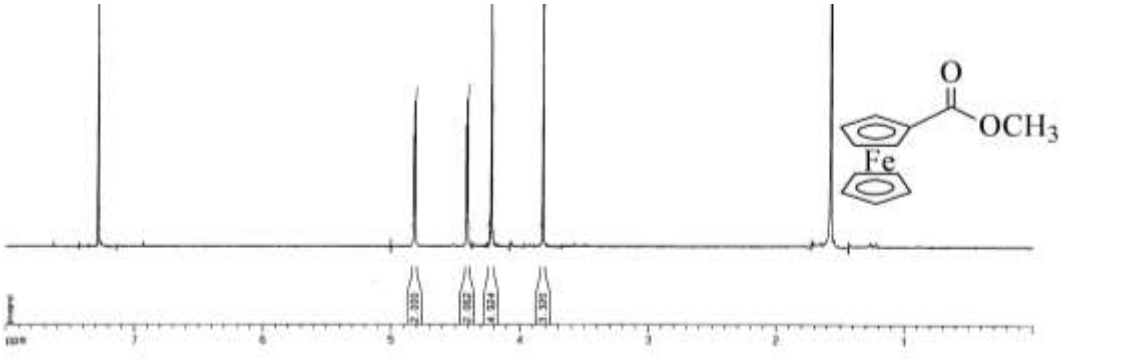

Spectrum 16: *N*-Phenyl-*N*-(ferrocenylethylidene)amine, 183

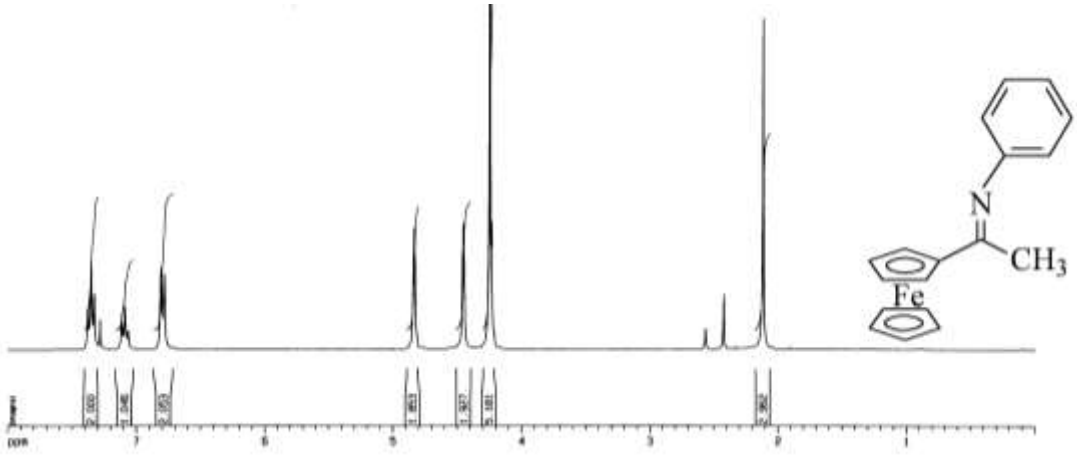

Ruthenocene complexes

Spectrum 17: Acetylruthenocene, 42

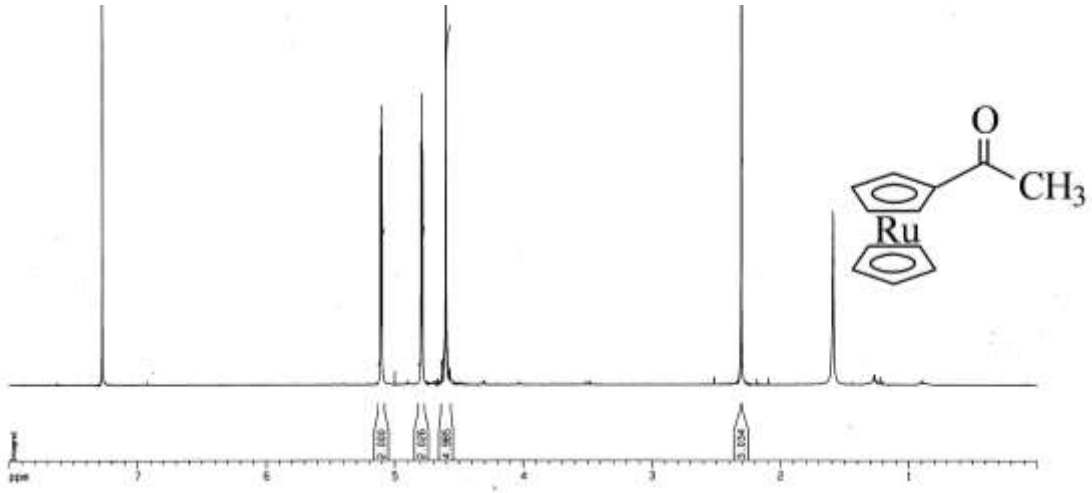

Spectrum 18: 2-Chlorobenzoylruthenocene, 234

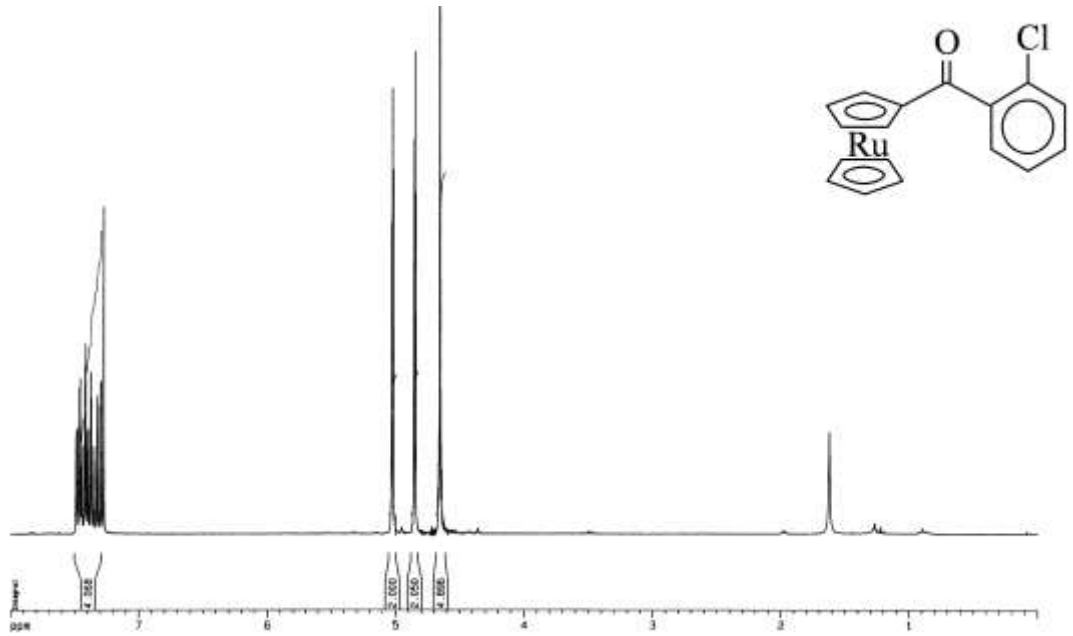

Spectrum 19: Ruthenocenecarboxilic acid, 65

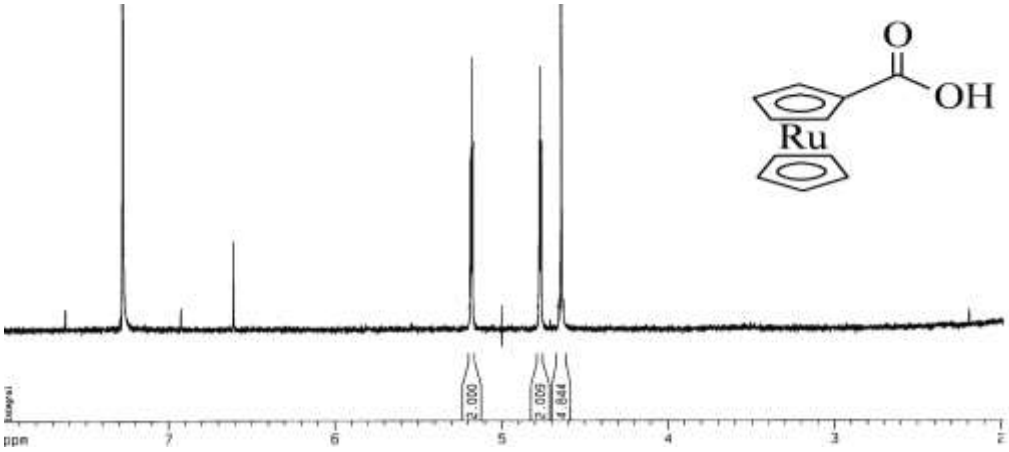

Spectrum 20: Methylruthenocenoate, 235

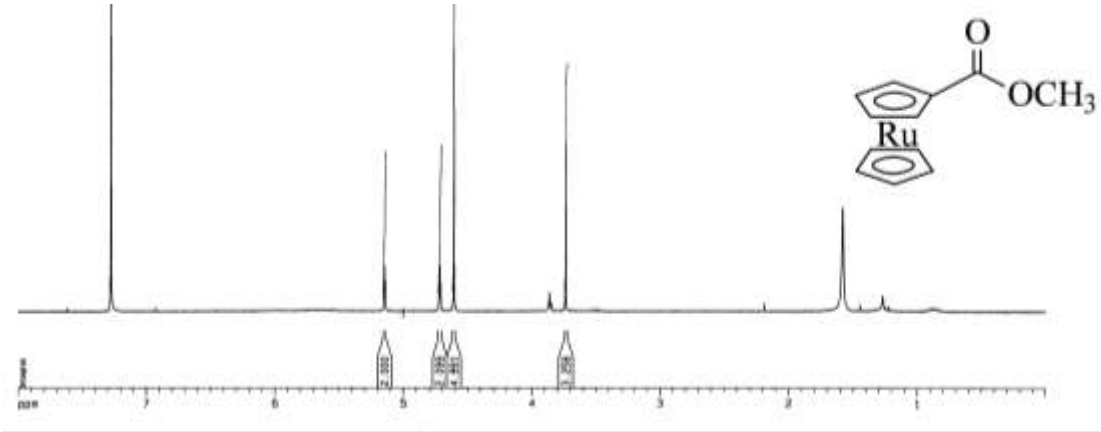

Spectrum 21: Ruthenocenoyl chloride, 180

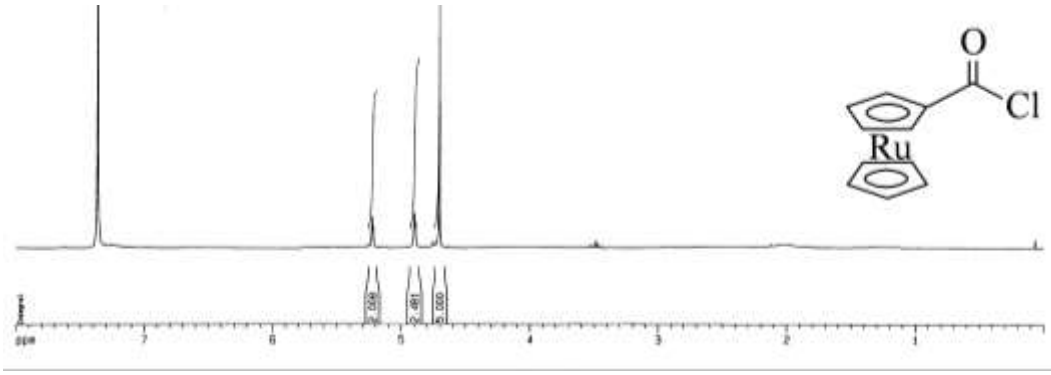

Spectrum 22: 1-H-1,2,3-Benzotriazol-1-yl(ruthenocenyl)methanone, 182

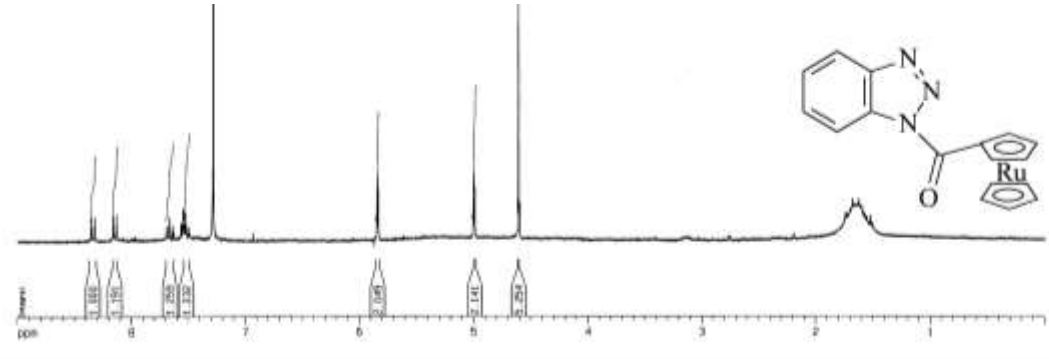

β-Diketones

Spectrum 23: 1-Ruthenocenyl-4,4,4-trifluorobutan-1,3-dione, Hrctfa, 152

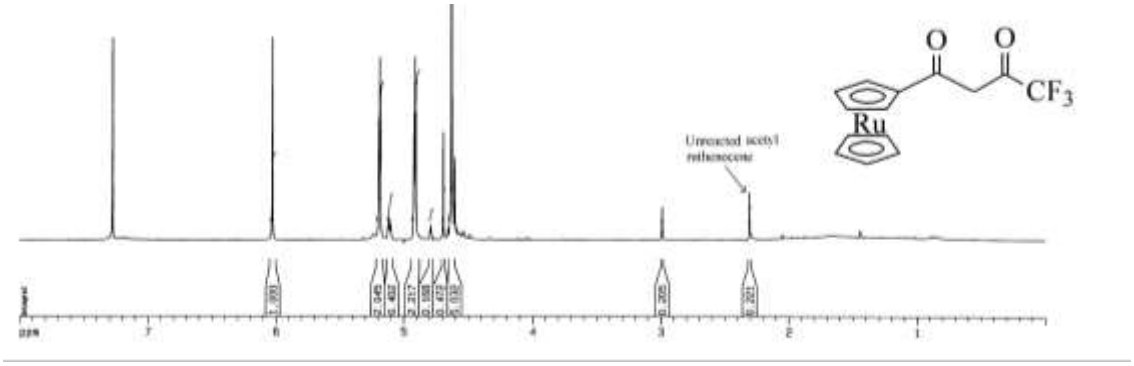

Spectrum 24: 1-Ruthenocenyl-4-methylprop-1,3-dione, Hrca, 151

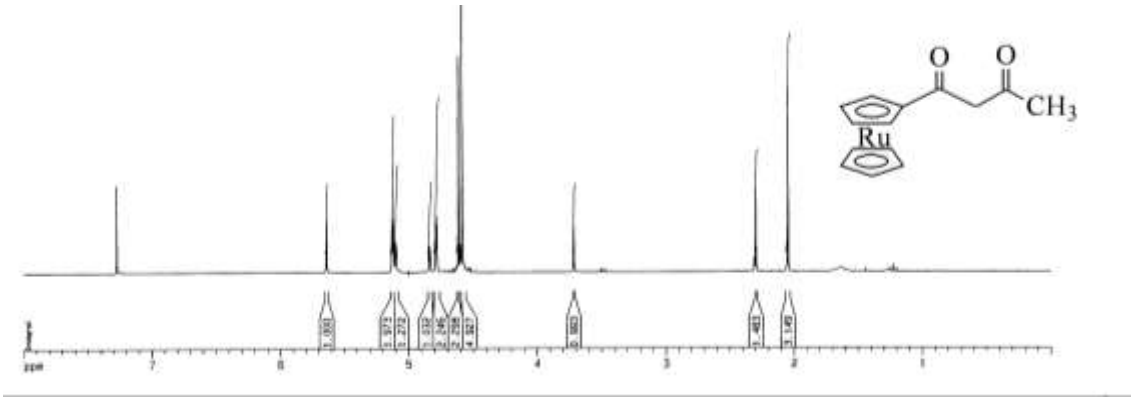

Spectrum 25: 1-Ferrocenyl-3-ruthenocenylpropan-1,3-dione, 154 in acetone d_6

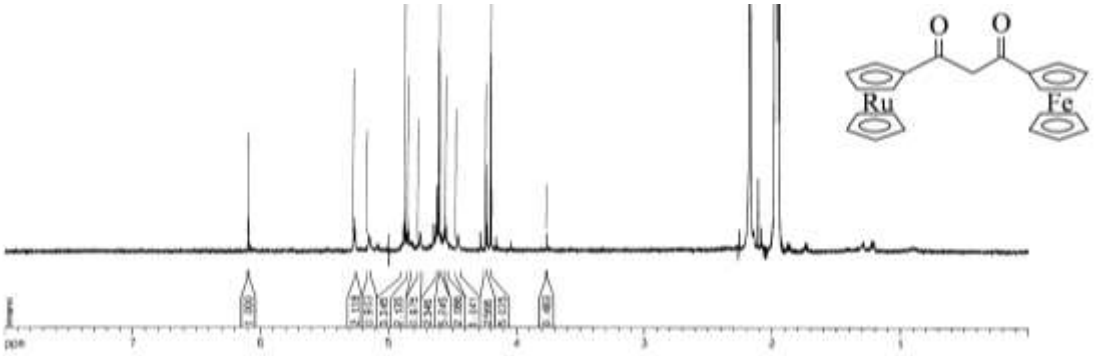

Spectrum 25(a): 1-Ferrocenyl-3-ruthenocenylpropan-1,3-dione, 154 in CD_2Cl_2

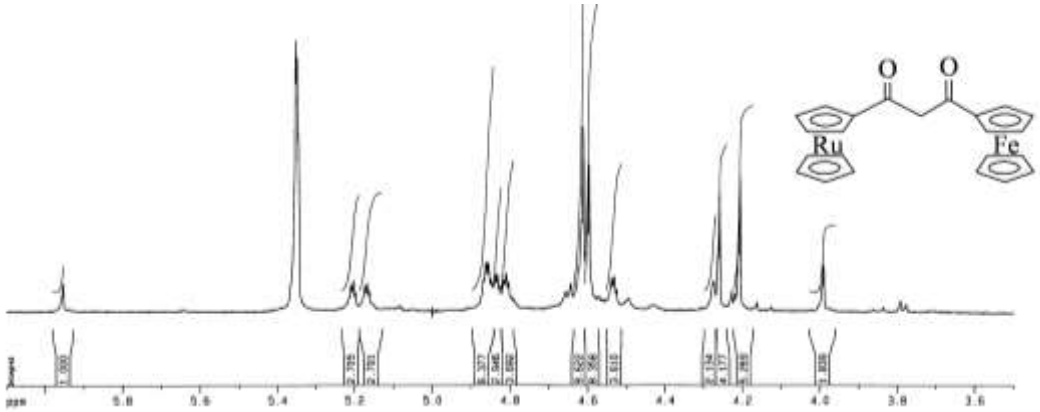

Spectrum 26: 1,3-Diruthenocenylpropan-1,3-dione, 155 in acetone d_6

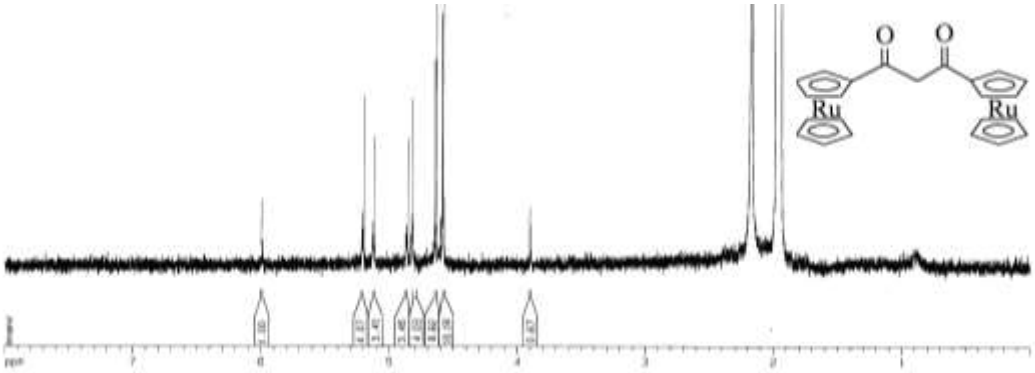

Spectrum 27: 1-Ruthenocenyl-4-(2,3,4,5,6-pentafluorophenyl)prop-1,3-dione, 178

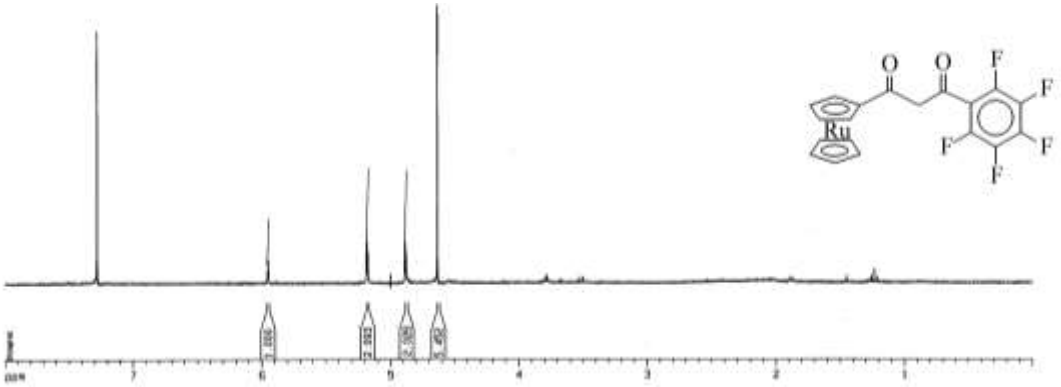

Spectrum 28: 1-Ruthenocenyl-4-undecylprop-1,3-dione, 179

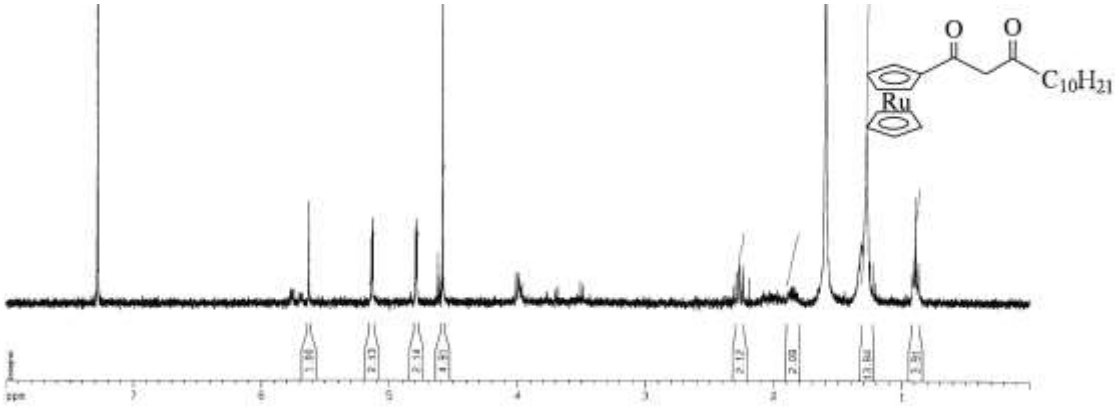

Spectrum 29: 1-Ruthenocenyl-4-perfluoroundecylprop-1,3-dione, 177

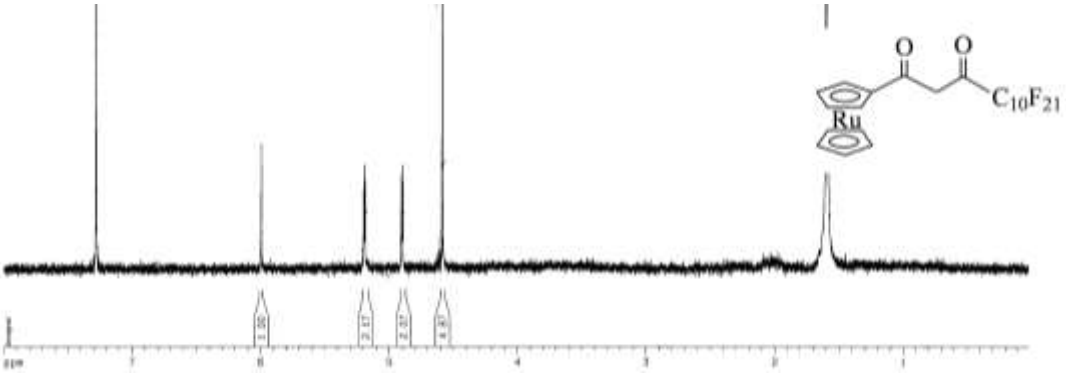

Enaminones

Spectrum 30: 1-Ferrocenylbutan-3-one-4-aniline, 184

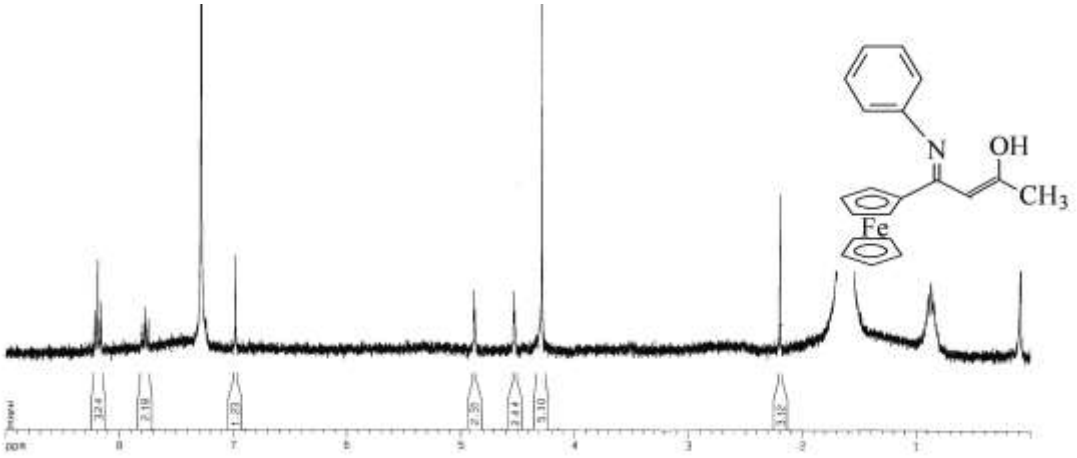

Spectrum 31: 1-Ruthenocenyl-3-ferrocenylpropan-1-one-3-N-cobalticinium amine salt, 187

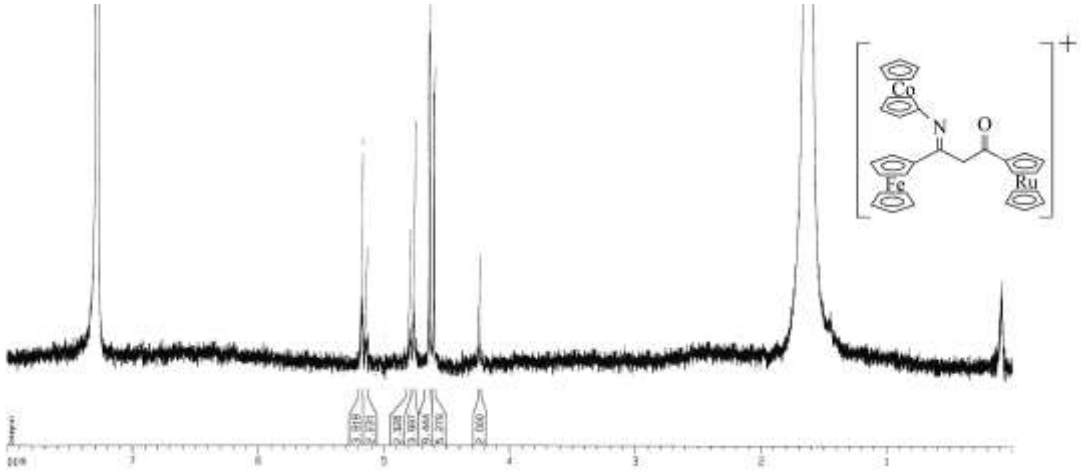

Cobalt complexes

Spectrum 32: Crude Cobalticinium, methylcobalticinium and 1,1'-dimethylcobalticinium hexafluorophosphate mixture, 239

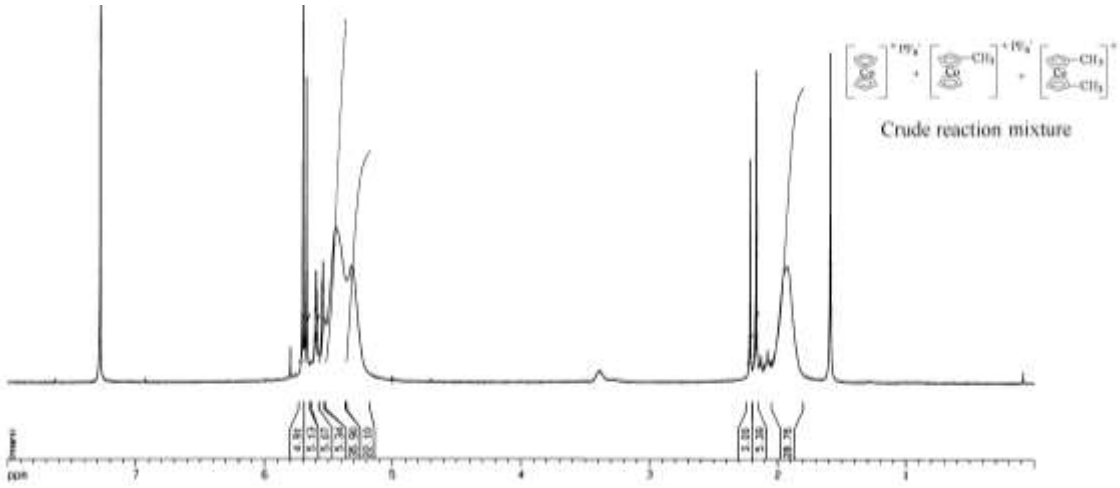

Spectrum 33: Carboxycobalticinium, 240

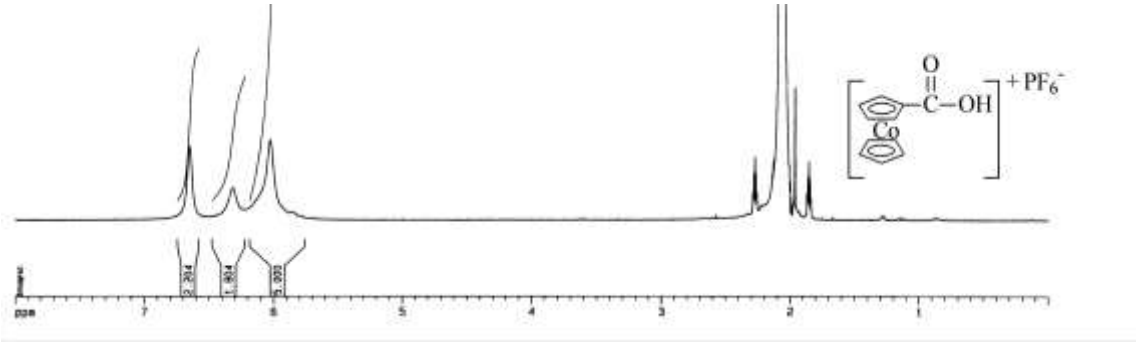

Spectrum 34: Chlorocarbonylcobalticinium salt, 241

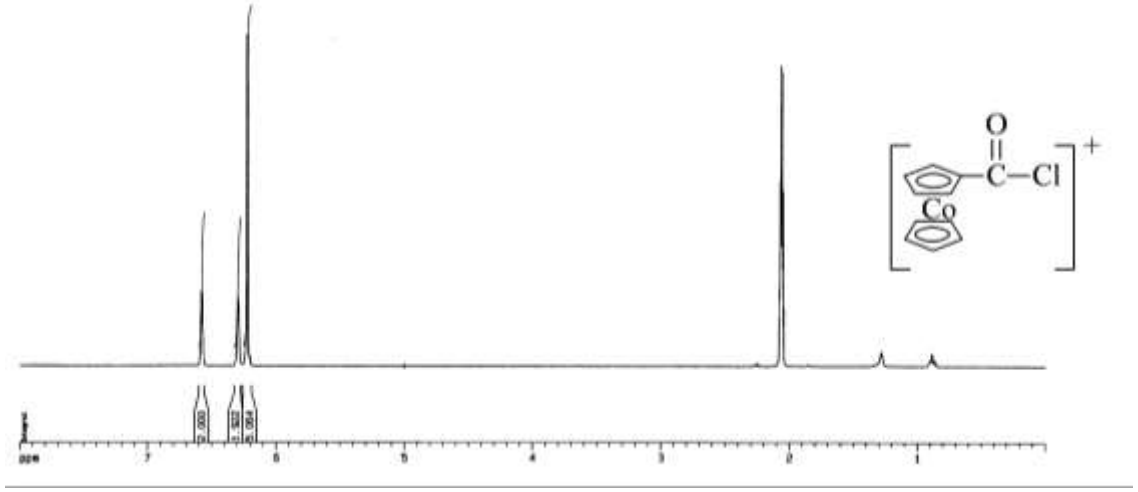

Spectrum 35: Carbonylazidocobalticinium salt, 242

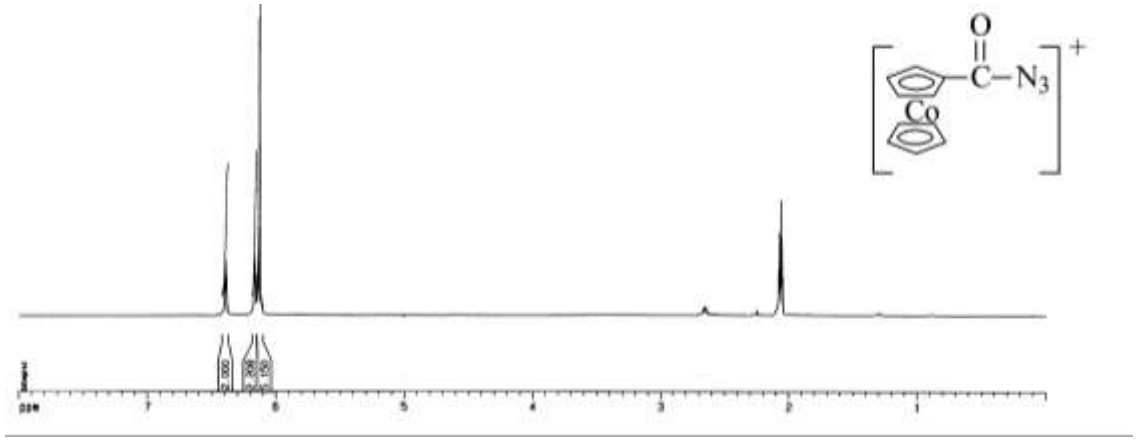

Spectrum 36: Aminocobalticinium salt, 185

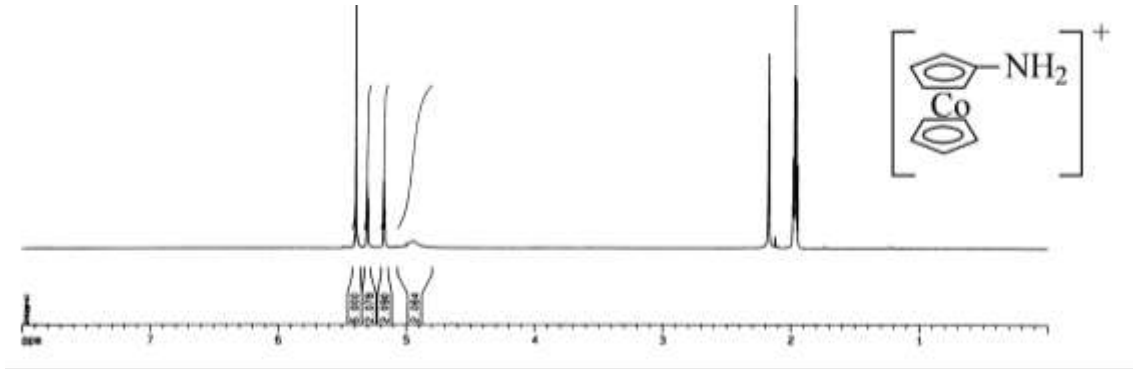

Spectrum 37: *N*-Cobalticinium-*N*-(ferrocenylethylidene)amine salt, 186

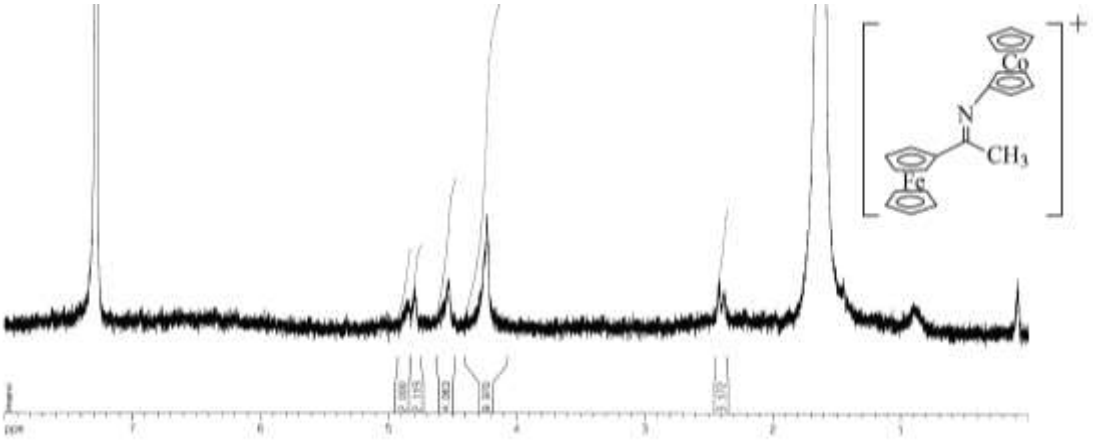

Titanium(IV) complexes

Spectrum 38: Tetra(ferrocenylmethoxide)titanium(IV), 209

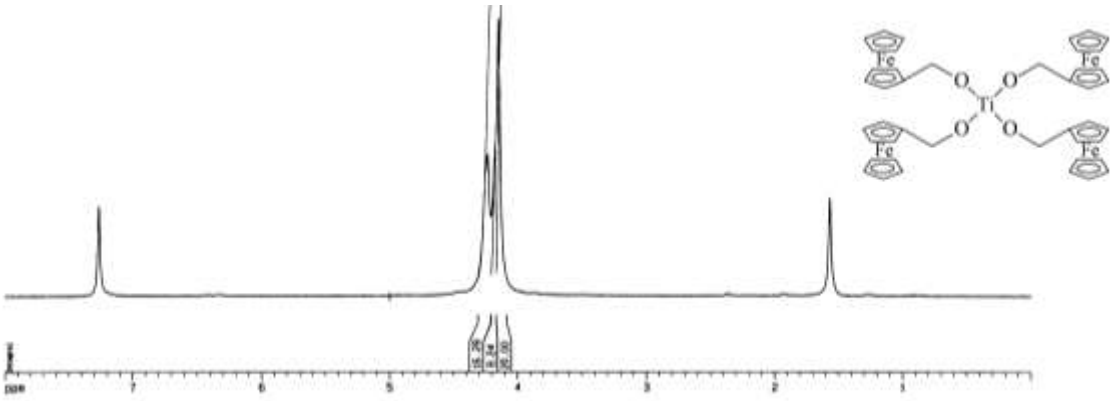

Spectrum 39: Tetra(ferrocenylethoxide)titanium(IV), 210

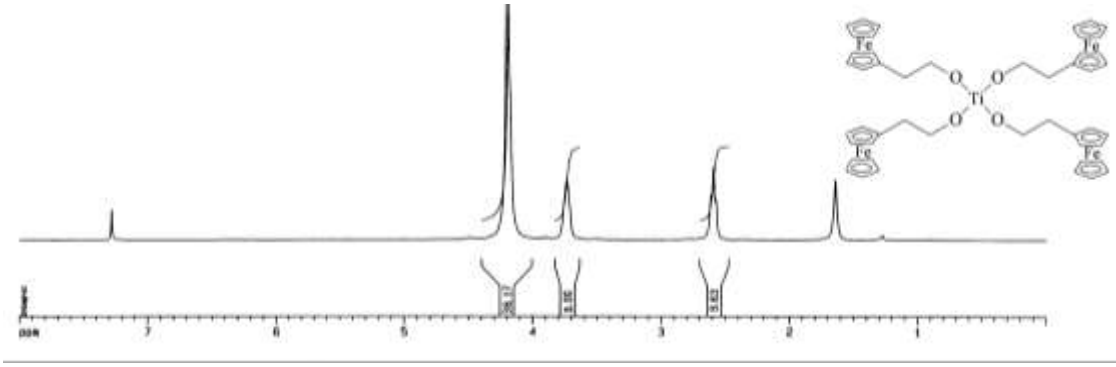

Spectrum 40: Tetra(ferrocenylpropoxide)titanium(IV), 211

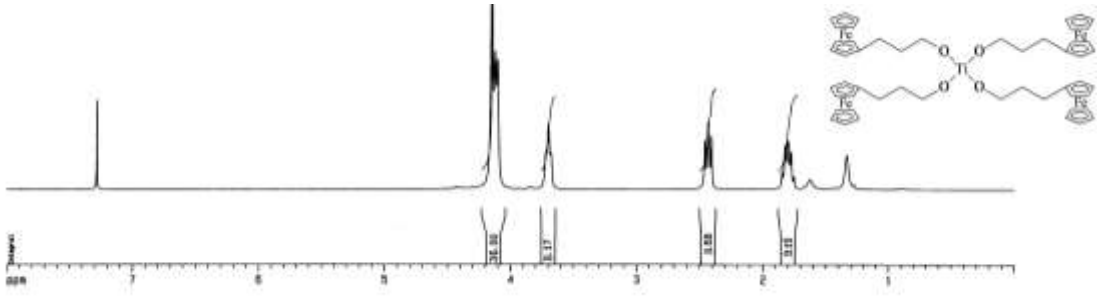

Spectrum 41: Tetra(ferrocenylbutoxide)titanium(IV), 212

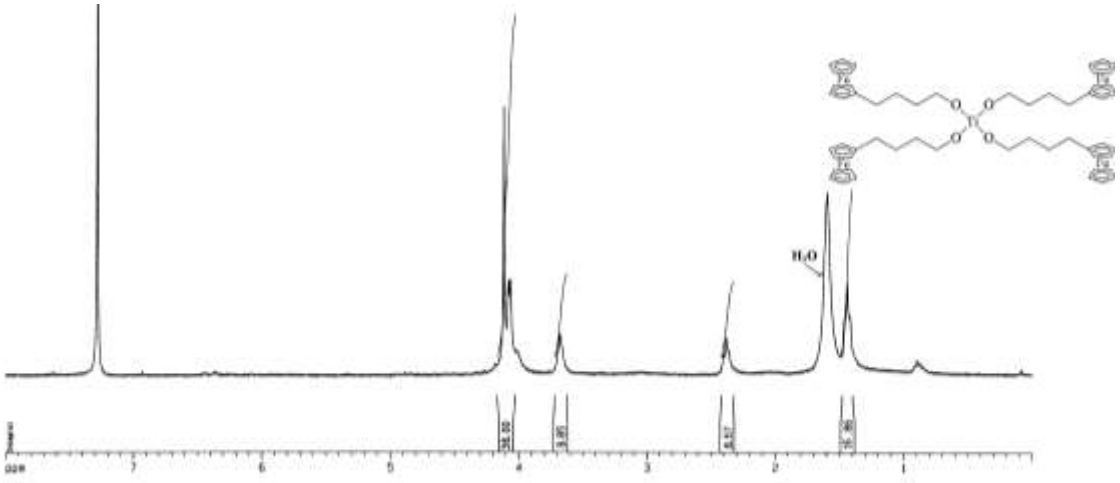

Spectrum 42: Dichlorobis(1-ruthenocenyl-4,4,4-trifluoroprop-1,3-dionato-κ^2O,O')titanium(IV), 214

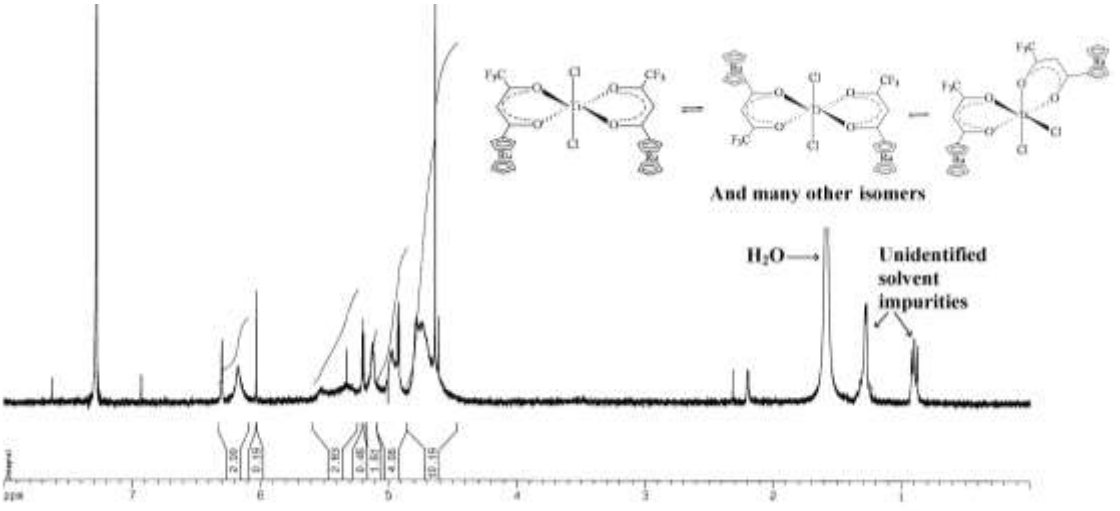

Spectrum 43: Dichlorobis(1-ruthenocenyl-4-methylprop-1,3-dionato-κ^2O,O') titanium(IV), 217

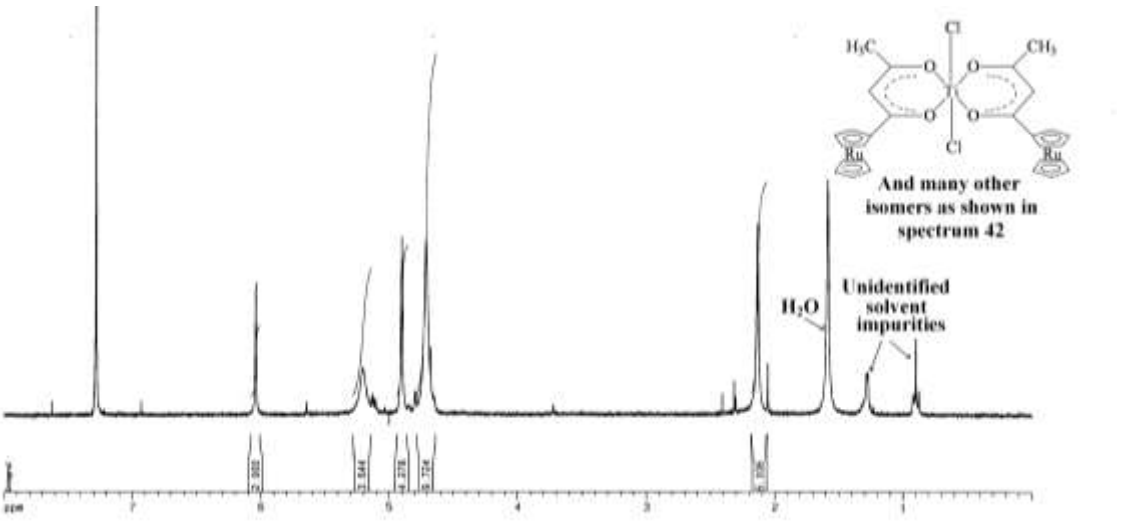

Spectrum 44: Dichlorobis(1-ferrocenyl-4-ruthenocenylprop-1,3-dionato-κ^2O,O')titanium(IV), 219

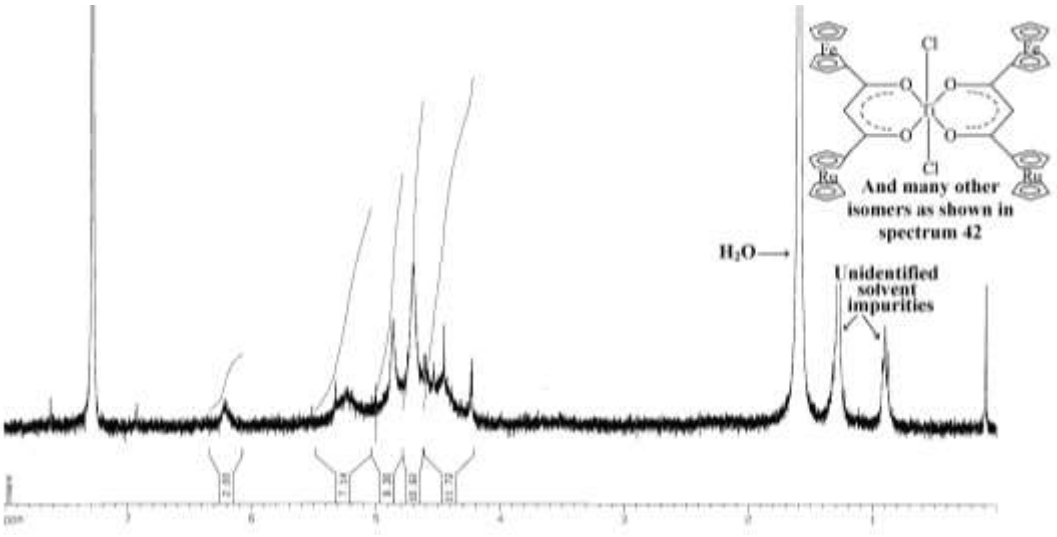

Spectrum 45: Dichlorobis(1,4-diruthenocenylprop-1,3-dionato-κ^2O,O') titanium(IV), 218

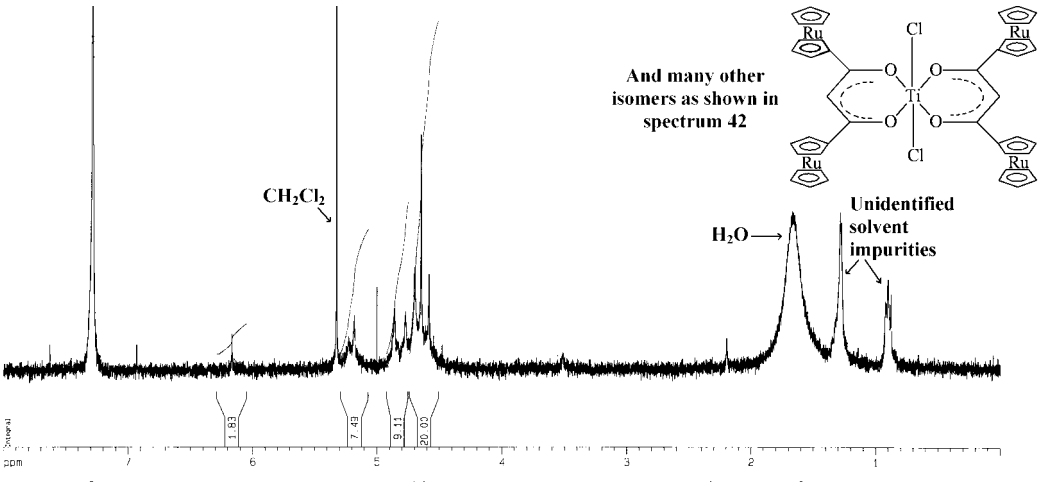

Spectrum 46: Dichlorobis(1-ruthenocenyl-4-2,3,4,5,6-pentafluorobenzylprop-1,3-dionato-κ^2O,O')titanium(IV), 215

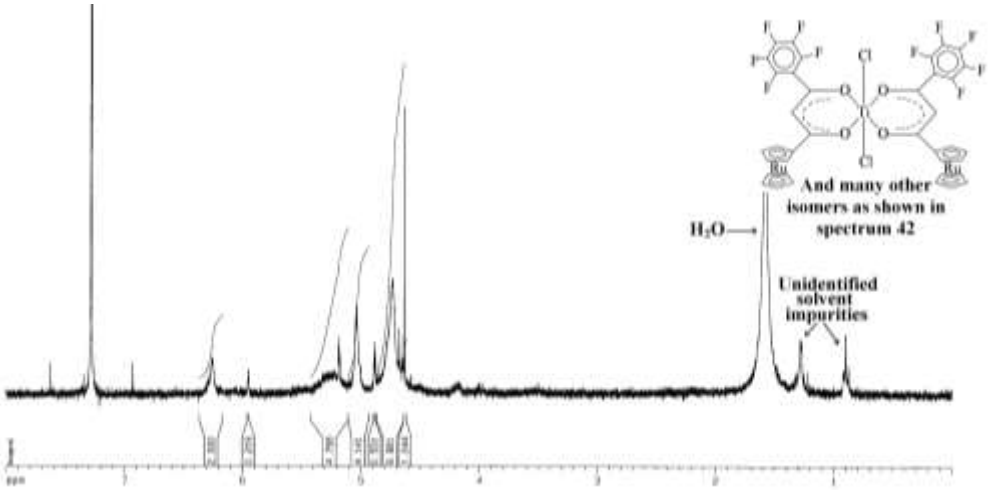

Spectrum 47: Dichlorobis(1-ruthenocenyl-4-undecylprop-1,3-dionato-κ^2O,O')titanium(IV), 216

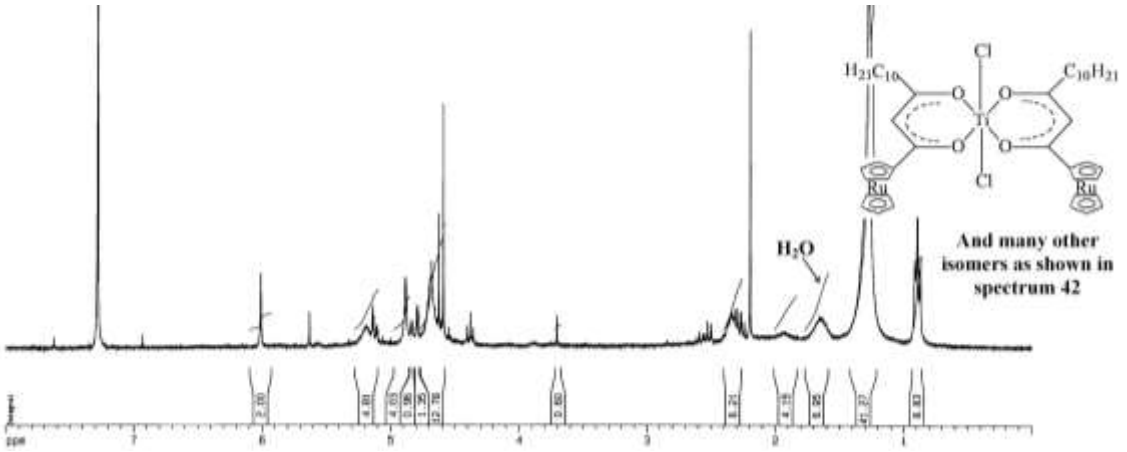

Spectrum 48: Dichlorobis(1-ruthenocenyl-4-perfluoroundecylprop-1,3-dionato-κ^2O,O')titanium(IV), 213

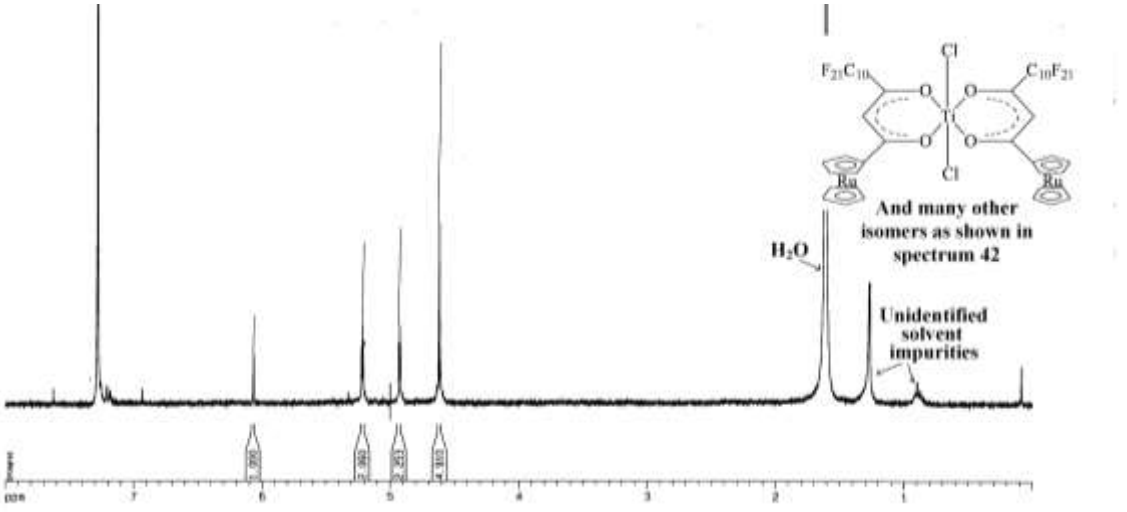

Spectrum 49: Di(ferrocenylmethoxy)bis(1-ruthenocenyl-3-methylprop-1,3-dionato-κ^2O,O')titanium(IV), 220

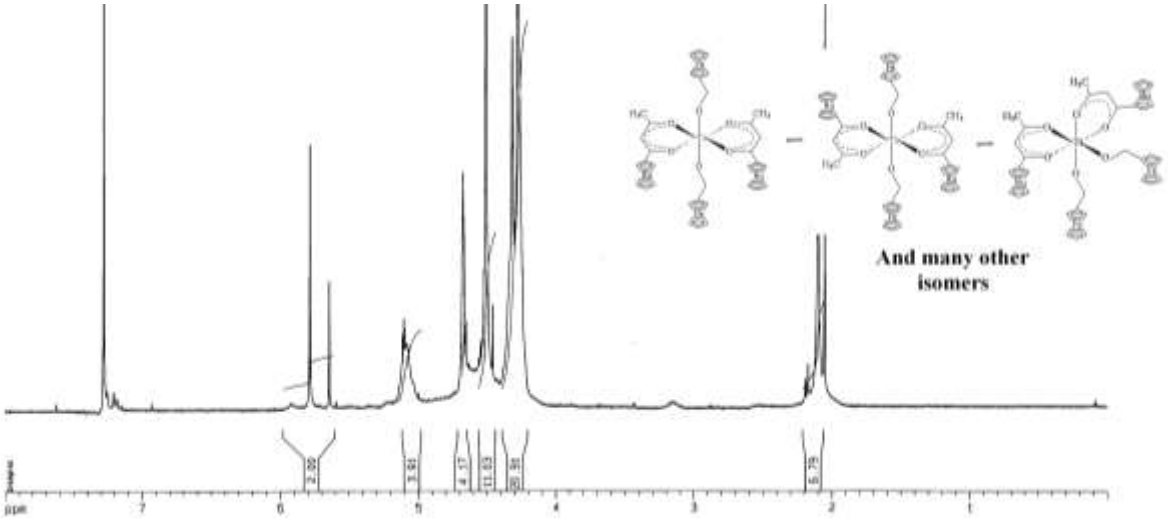

Spectrum 50: Di(ferrocenylethoxy)bis(1-ruthenocenyl-3-methylprop-1,3-dionato-κ^2O,O')titanium(IV), 221

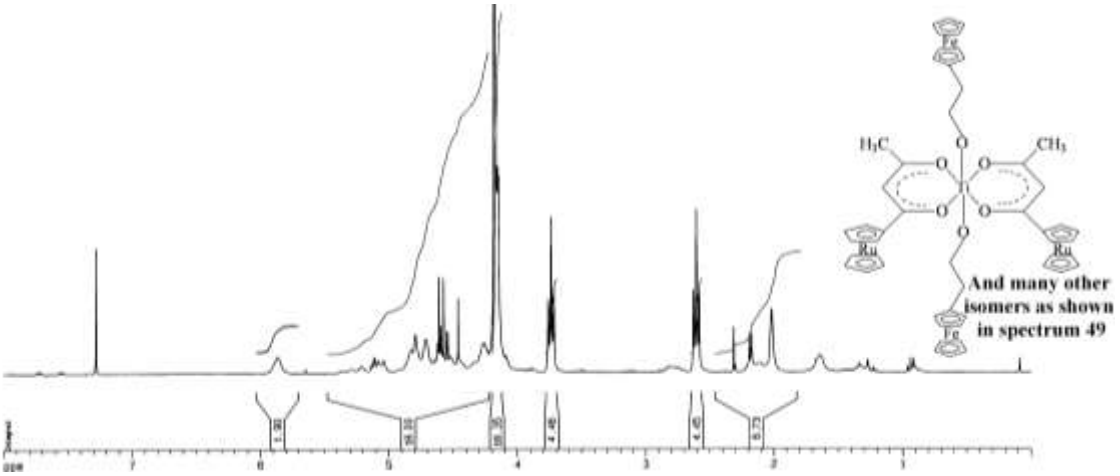

Spectrum 51: Diferrocenylpropoxybis(1-ruthenocenyl-3-methylprop-1,3-dionato-κ^2O,O')titanium(IV), 222

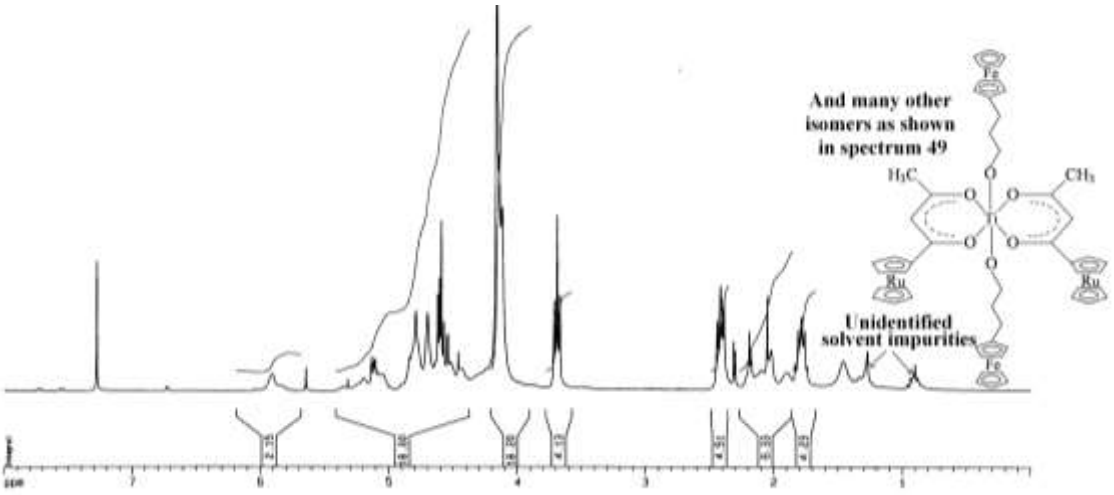

Spectrum 52: Di(ferrocenylbutoxy)bis(1-ruthenocenyl-3-methylprop-1,3-dionato-κ^2O,O')titanium(IV), 223

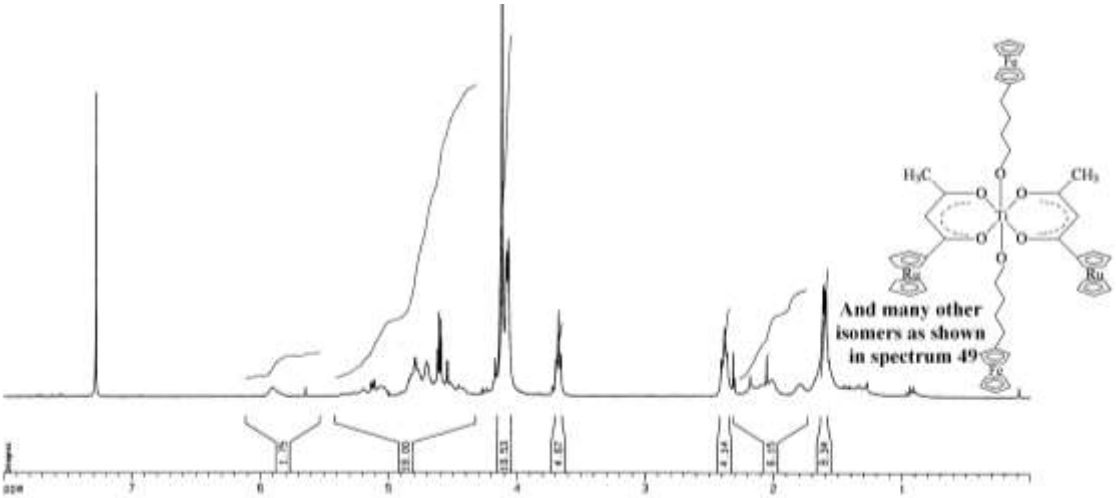

Spectrum 53: Di(ferrocenylbutoxy)bis(1-ruthenocenyl-4,4,4-trifluorobutane-1,3-dionato-κ^2O,O')titanium(IV), 225

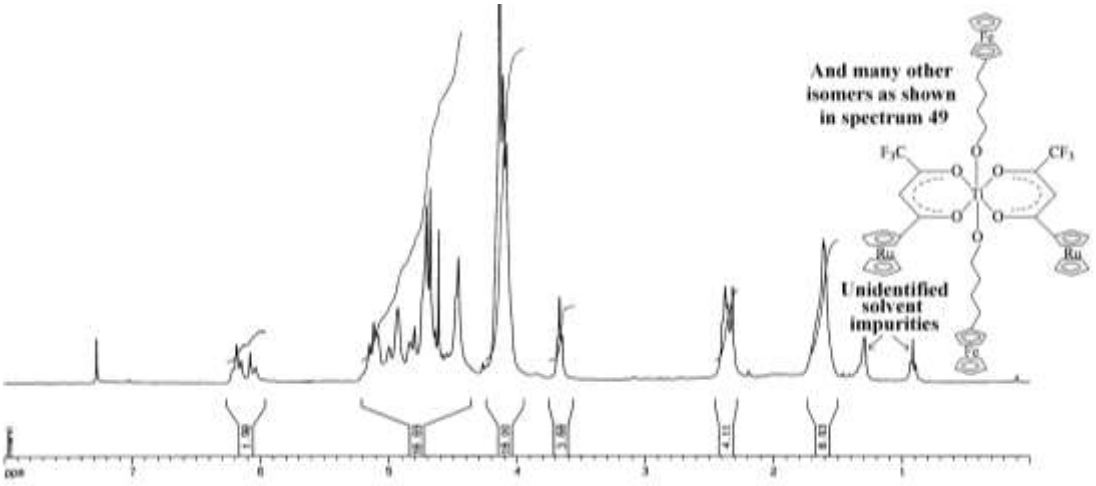

Spectrum 54: Di(ferrocenylbutoxy)bis(1-ferrocenyl-3-ruthenocenylprop-1,3-dionato-κ^2O,O')titanium(IV), 229

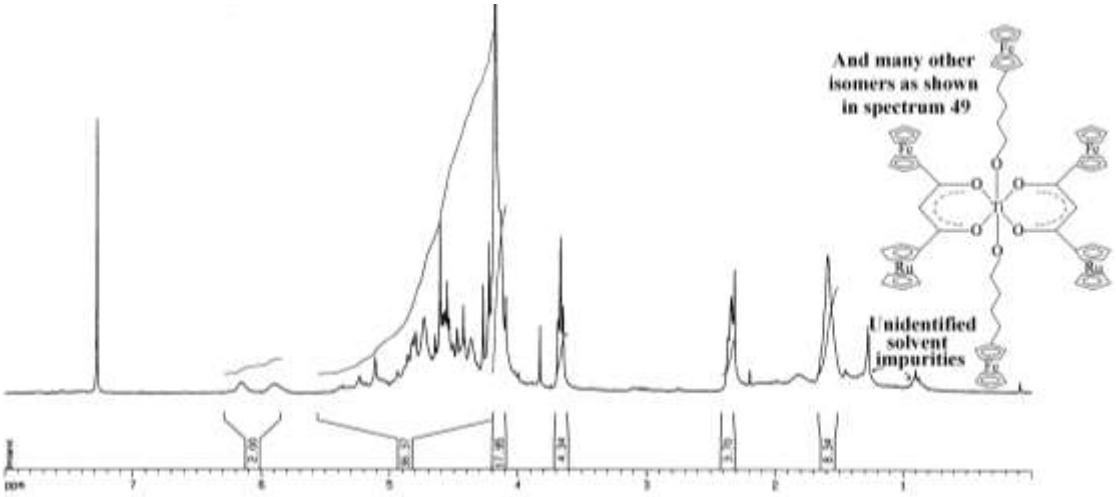

Spectrum 55: Di(ferrocenylbutoxy)bis(1,3-diruthenocenylprop-1,3-dionato-κ^2O,O')titanium(IV), 228

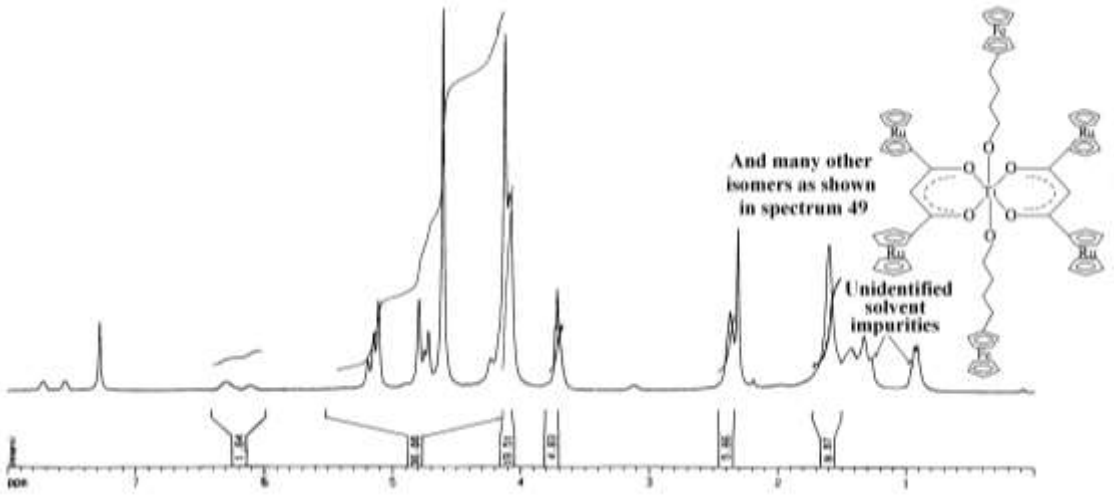

Spectrum 56: Di(ferrocenylbutoxy)bis(1-ruthenocenyl-3-2,3,4,5,6-penta fluorobenzyl prop-1,3-dionato-κ^2O,O')titanium(IV), 226

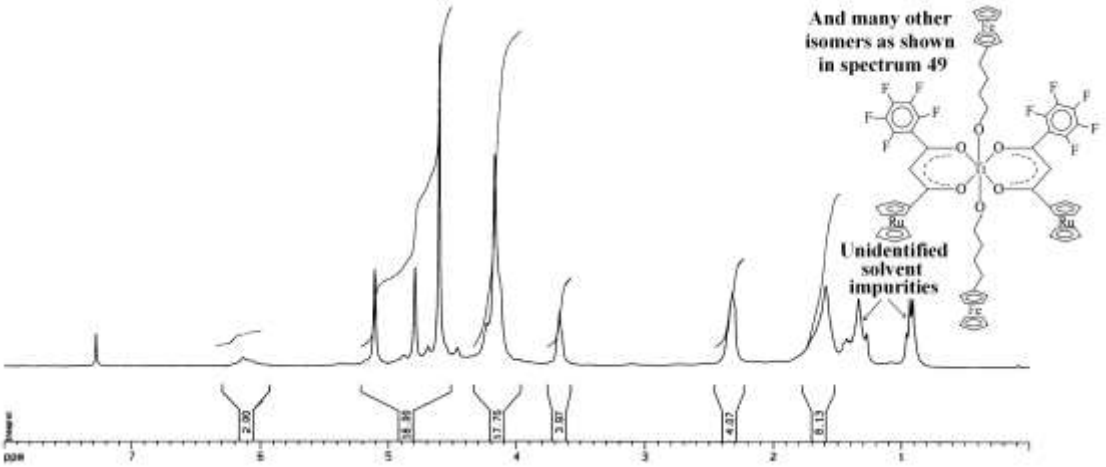

Spectrum 57: Di(ferrocenylbutoxy)bis(1-ruthenocenyl-3-undecylprop-1,3-dionato-κ^2O,O')titanium(IV), 227

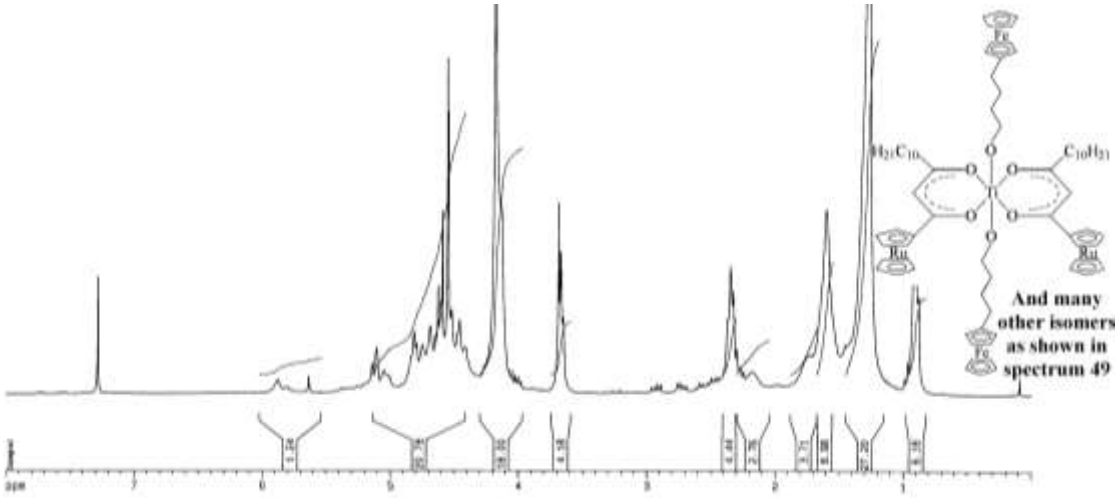

Spectrum 58: Di(ferrocenylbutoxy)bis(1-ruthenocenyl-3-perfluorodecylprop-1,3-dionato-κ^2O,O')titanium(IV), 224

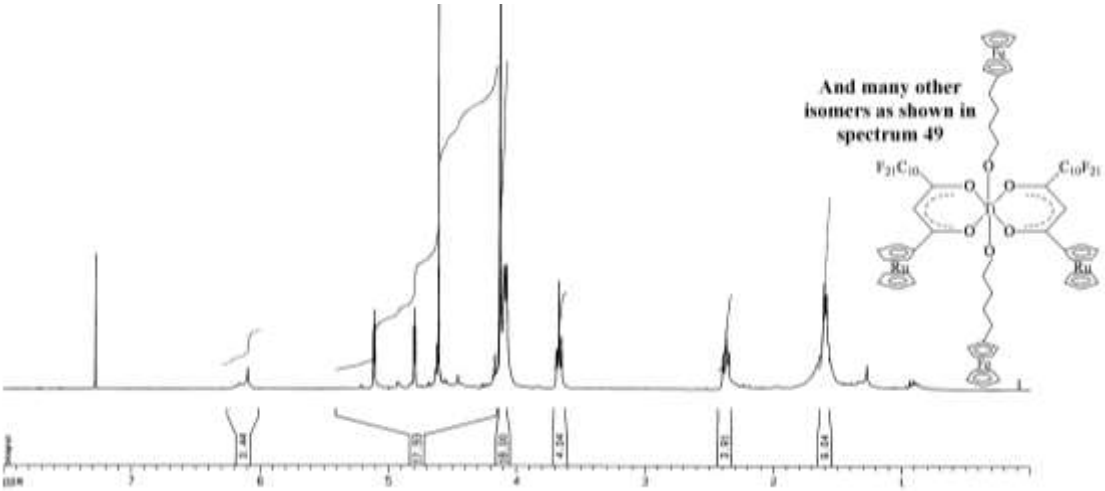

Spectrum 59: Bis(cyclopentadienyl)di(ferrocenylmethoxy)titanium(IV), 201

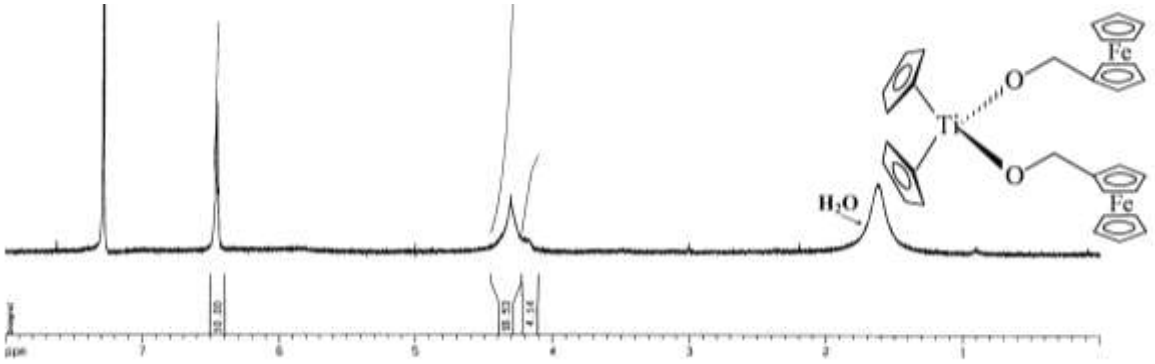

Spectrum 60: Bis(cyclopentadienyl)di(2-ferrocenylethoxy)titanium(IV), 202

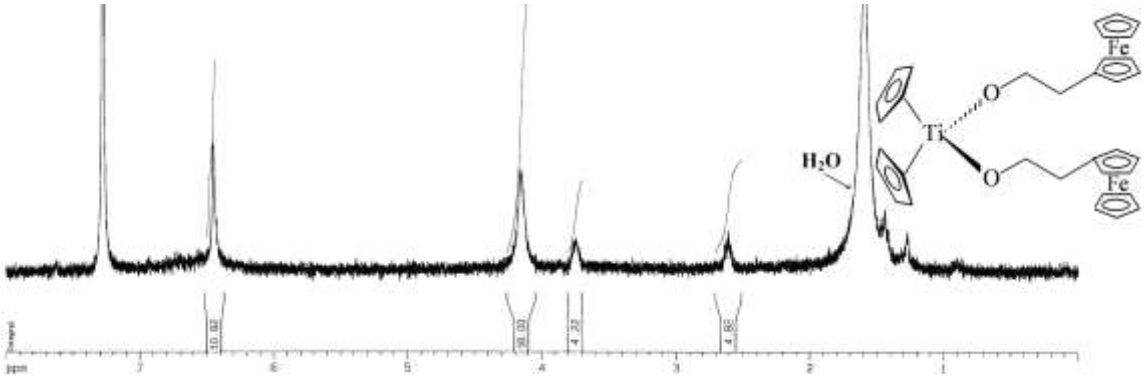

Spectrum 61: Bis(cyclopentadienyl)di(3-ferrocenylpropoxy)titanium(IV), 203

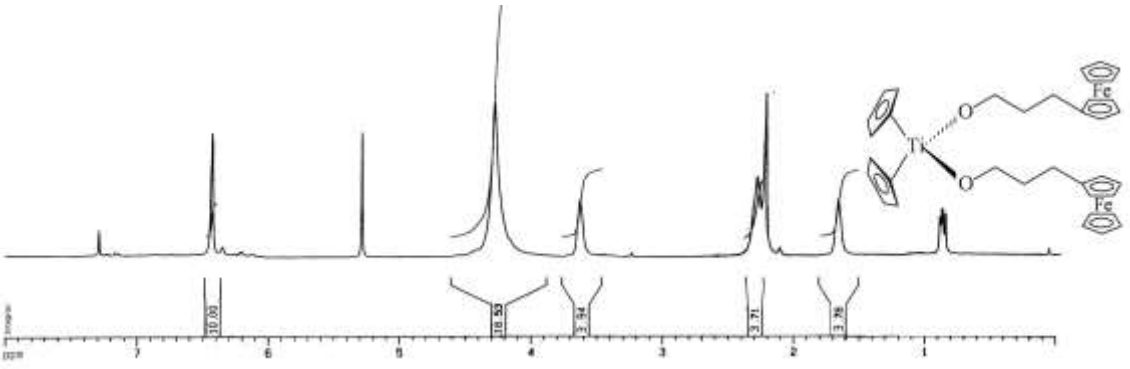

Spectrum 62: Bis(cyclopentadienyl)di(4-ferrocenylbutoxy)titanium(IV), 204

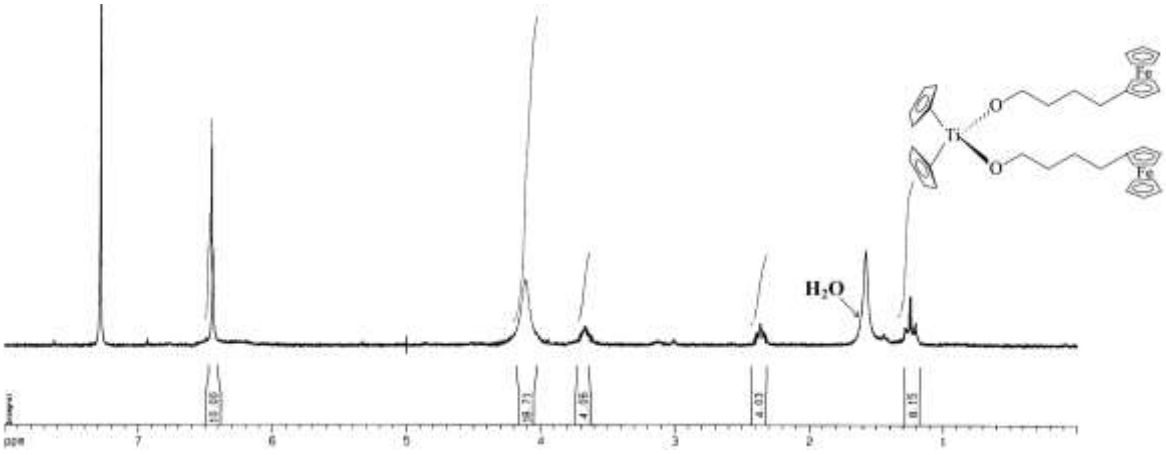

Spectrum 63: Cyclopentadienyltri(ferrocenylmethoxy)titanium(IV), 205

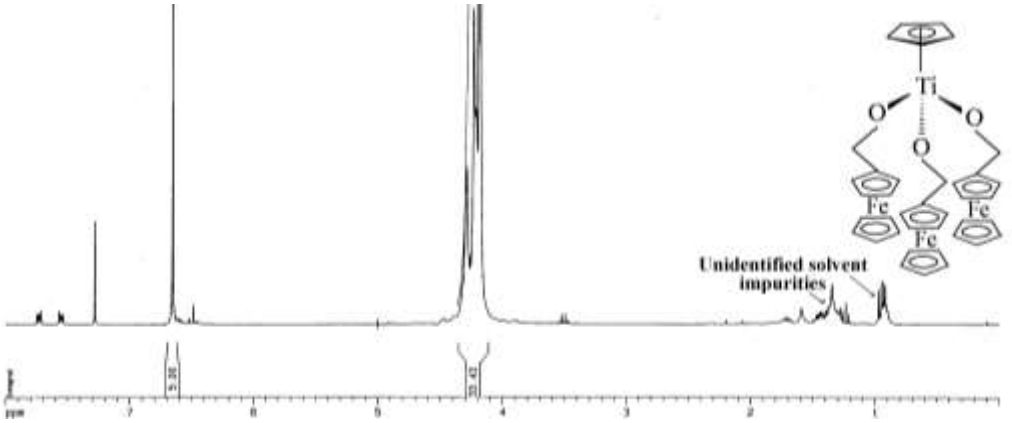

Spectrum 64: Cyclopentadienyltri(2-ferrocenylethoxy)titanium(IV), 206

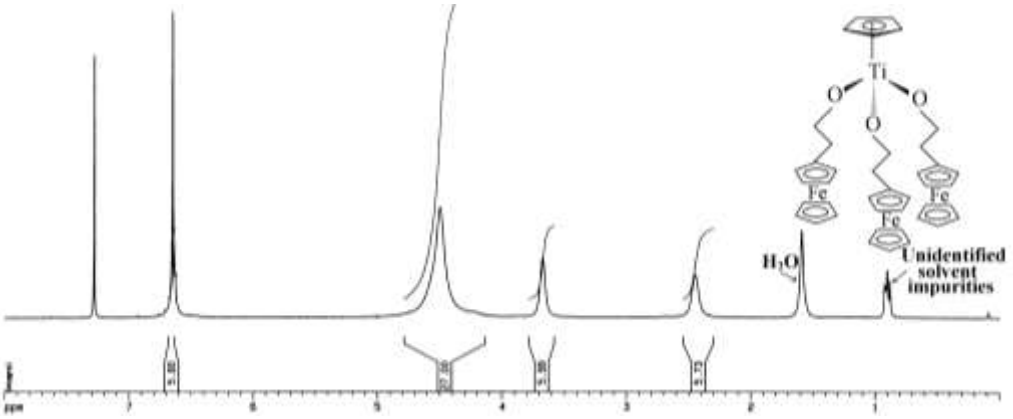

Spectrum 65: Cyclopentadienyltri(3-ferrocenylpropoxy)titanium(IV), 207

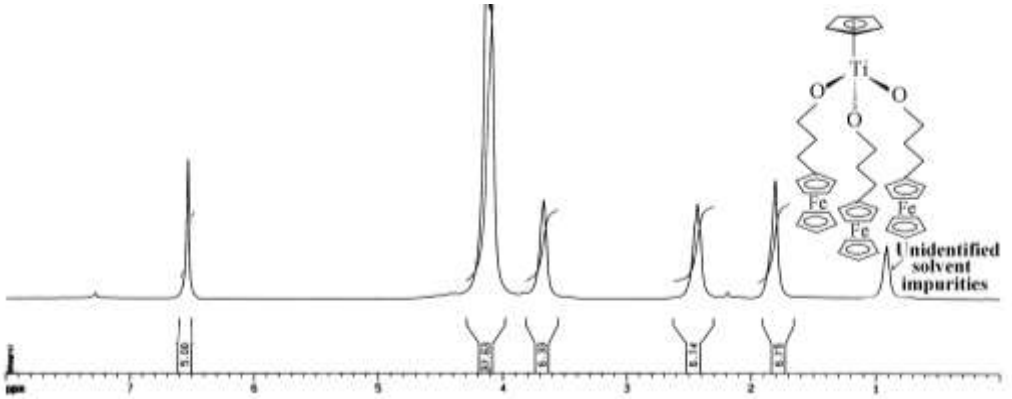

Spectrum 66: Cyclopentadienyltri(4-ferrocenylbutoxy)titanium(IV), 208

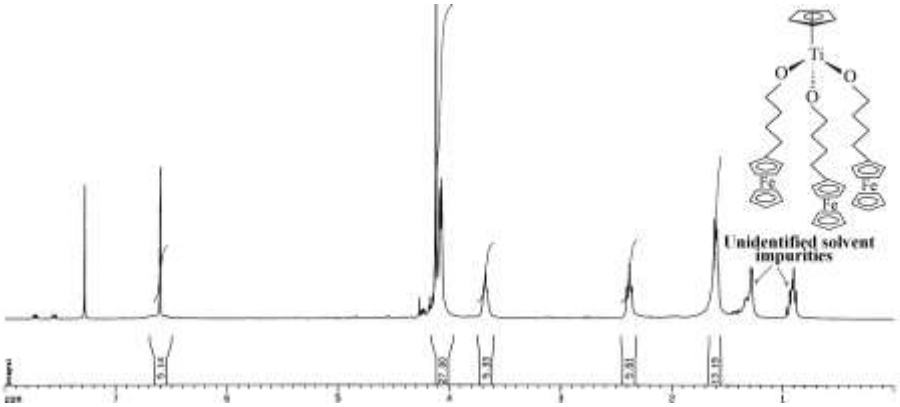

Spectrum 67: Chloro(η^5-cyclopentadienyl)bis(1-ruthenocenoylbutane-1,3-dionato-κ^2O,O')titanium(IV), 230

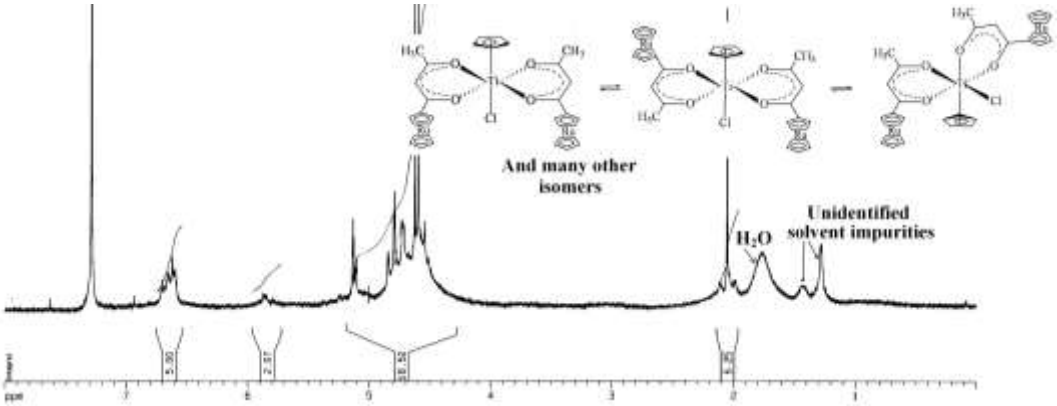

Spectrum 68: (η^5-Cyclopentadienyl)ferrocenylbutoxybis(1-ruthenocenoylbutane-1,3-dionato-κ^2O,O')titanium(IV), 231

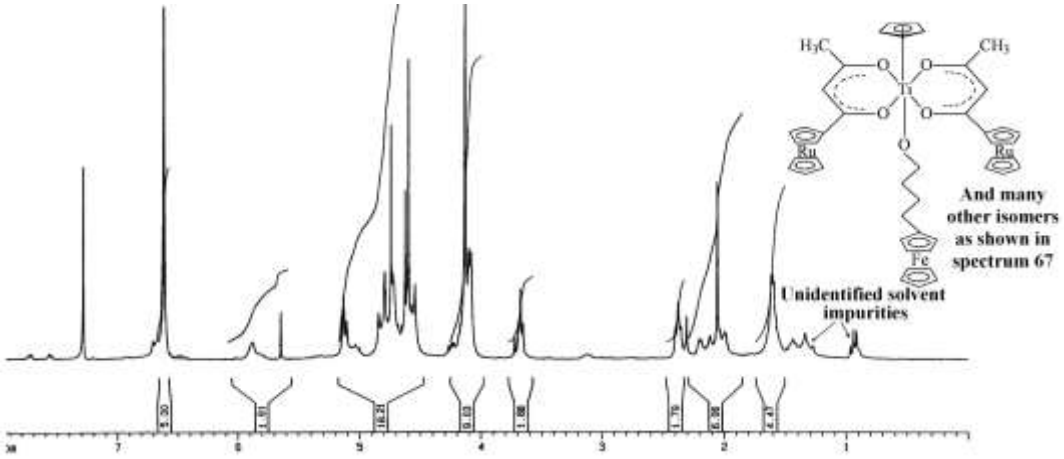

Spectrum 69: Bis(η^5-cyclopentadienyl)diferrocenyl titanium(IV), 100

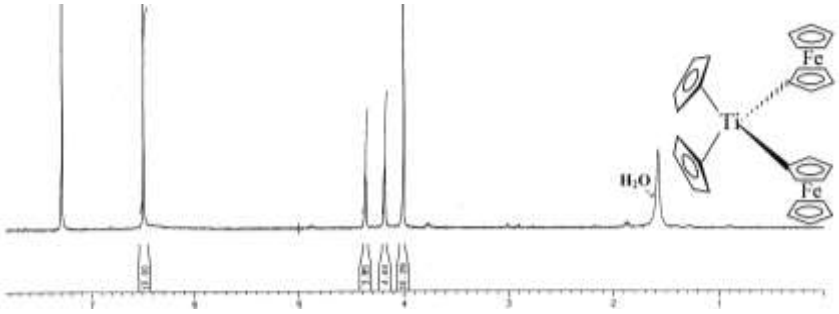

Spectrum 70: Bis(η^5-cyclopentadienyl)diruthenocenyl titanium(IV), 188

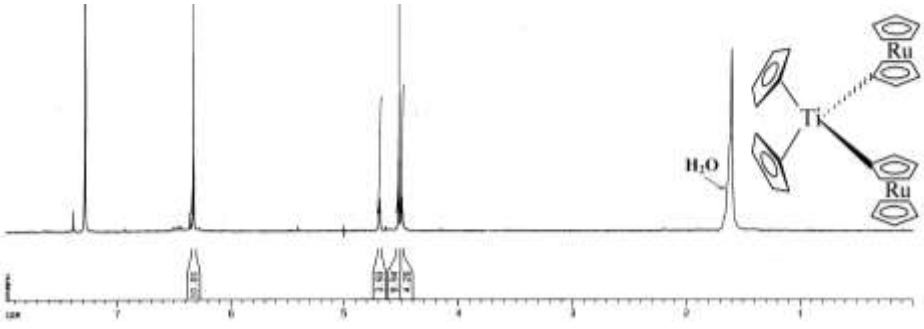

Spectrum 71: Bis(η^5-cyclopentadienyl)diosmocenyl titanium(IV), 189

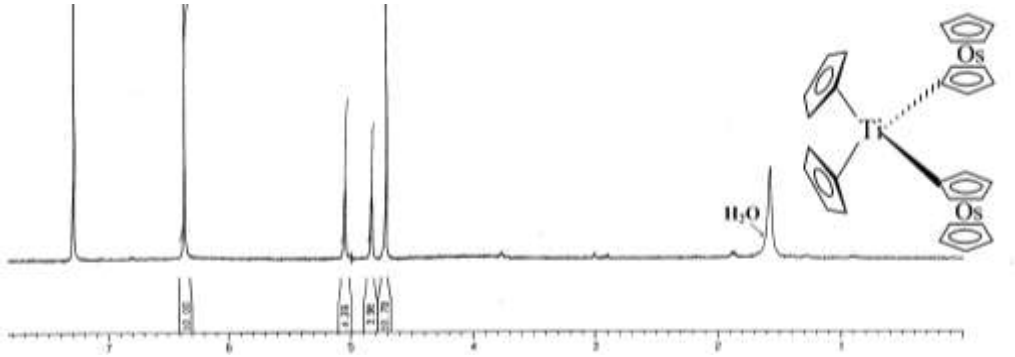

Spectrum 72: 2,4-Pentanedionato-κ^2O,O'-bis(η^5-cyclopentadienyl) titanium(IV) perchlorate, 193 in $CDCl_3$

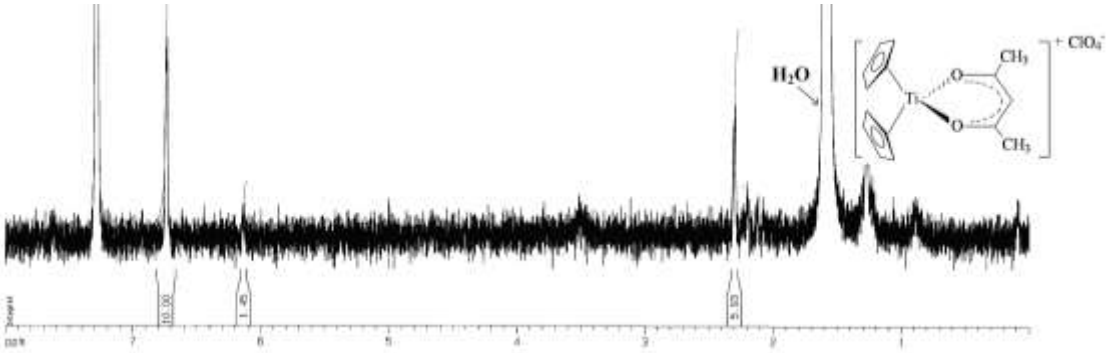

Spectrum 72 (a): 2,4-Pentanedionato-κ^2O,O'-bis(η^5-cyclopentadienyl) titanium(IV) perchlorate, 193 in acetone *d_6*

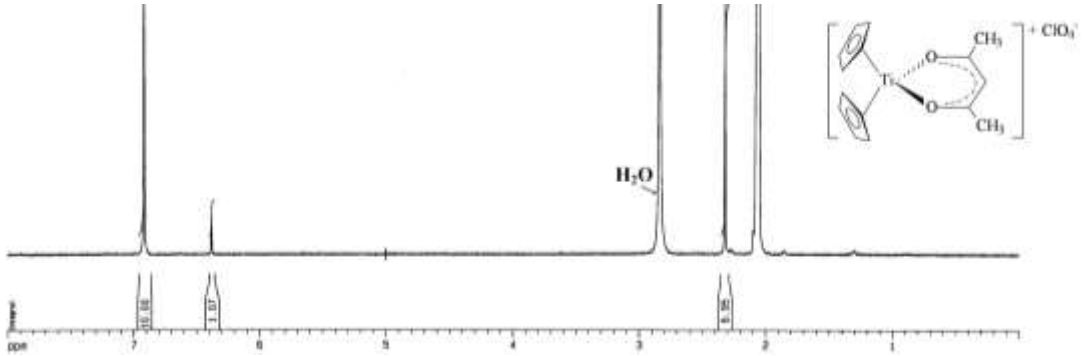

Spectrum 73: 1-Rutnenocenyl-3-methylprop-1,3-dionato-κ^2O,O'-bis(η^5-cyclo pentadienyl)titanium(IV) perchlorate, 194 in $CDCl_3$

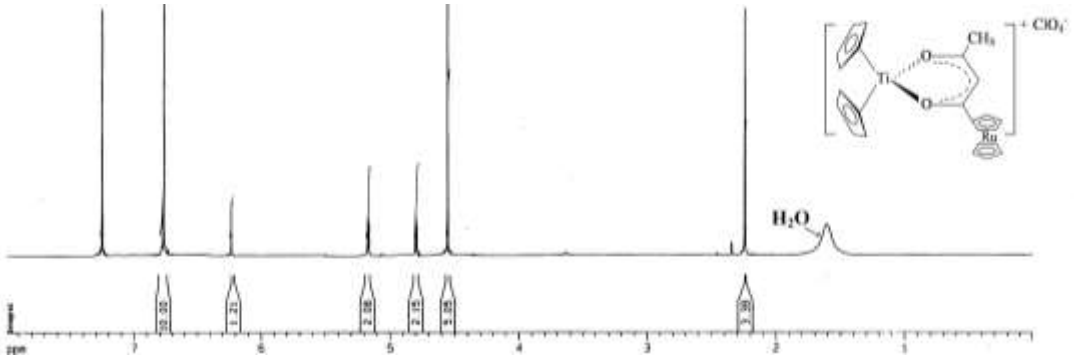

Spectrum 73 (a): 1-Rutnenocenyl-3-methylprop-1,3-dionato-κ^{2}O,O'-bis(η^5-cyclopentadienyl)titanium(IV) perchlorate, 194 in acetone *d*$_6$

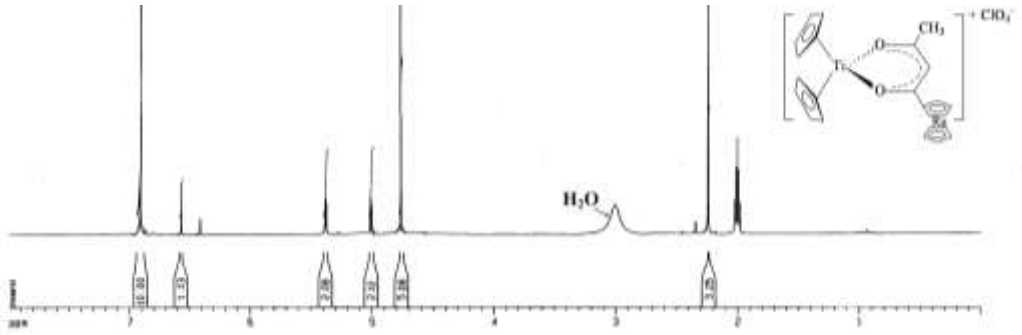

Spectrum 74: 1-Ruthenocenyl-3,3,3-trifluorobutane-1,3-dionato-κ^{2}O,O'-bis(η^5-cyclopentadienyl)titanium(IV) perchlorate, 196

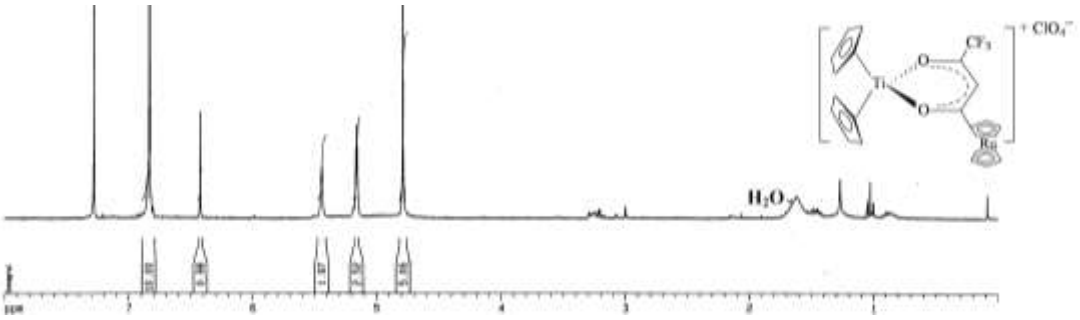

Spectrum 75: 1-Ruthenocenyl-3-ferrocenylprop-1,3-dionato-κ^{2}O,O'-bis(η^5-cyclopentadienyl)titanium(IV) perchlorate, 200 in CDCl$_3$

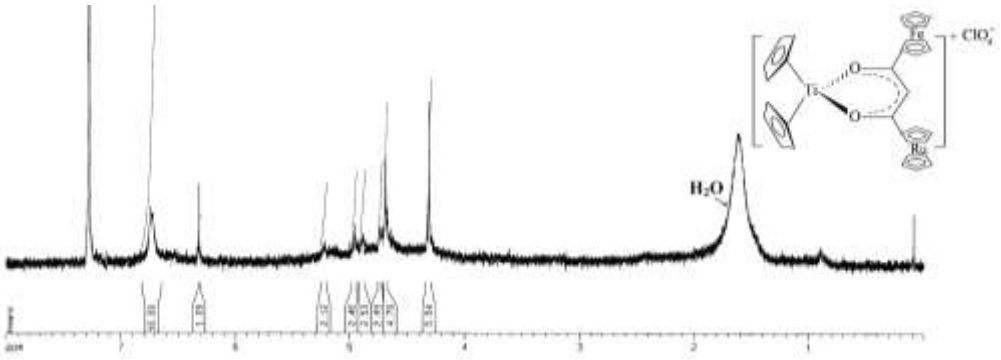

Spectrum 75 (a): 1-Ruthenocenyl-3-ferrocenylprop-1,3-dionato-κ^{2}O,O'-bis(η^5-cyclopentadienyl)titanium(IV) perchlorate, 200 in acetone *d*$_6$

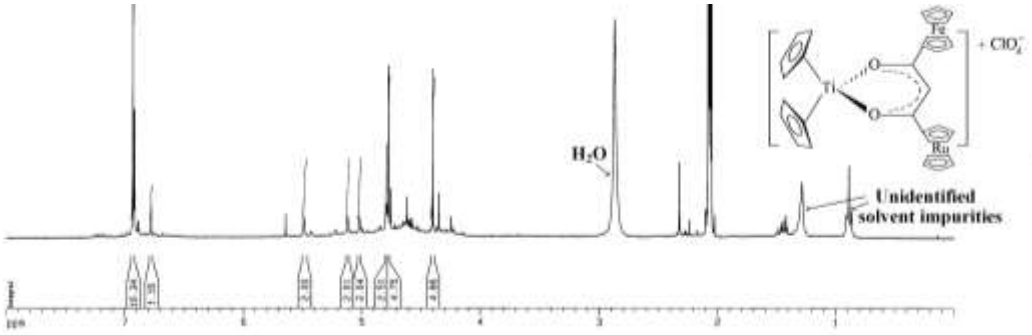

Spectrum 76: 1,3-Diruthenocenylprop-1,3-dionato-κ^2O,O'-bis(η^5-cyclo pentadienyl)titanium(IV) perchlorate, 199

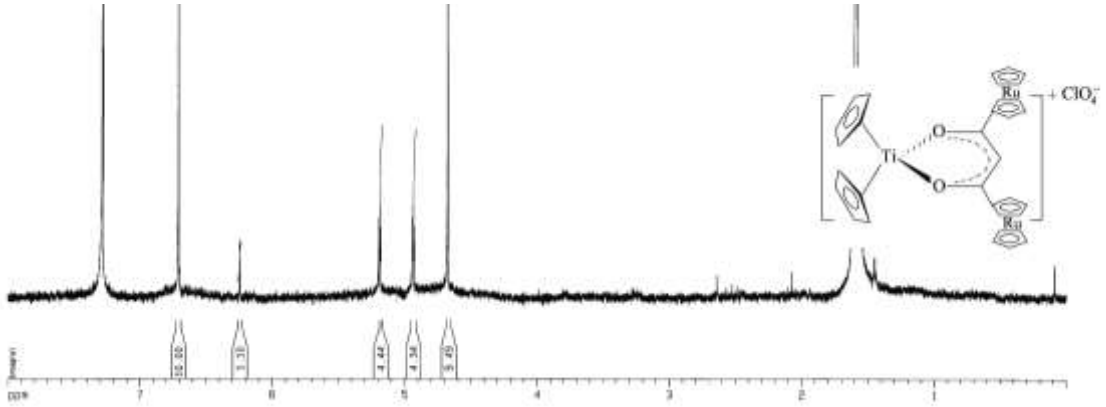

Spectrum 77: 1-Ruthenocenyl-3-(2,3,4,5,6-perfluorbenzyl)prop-1,3-dionato-κ^2O,O'-bis(η^5-cyclopentadienyl)titanium(IV) perchlorate, 197

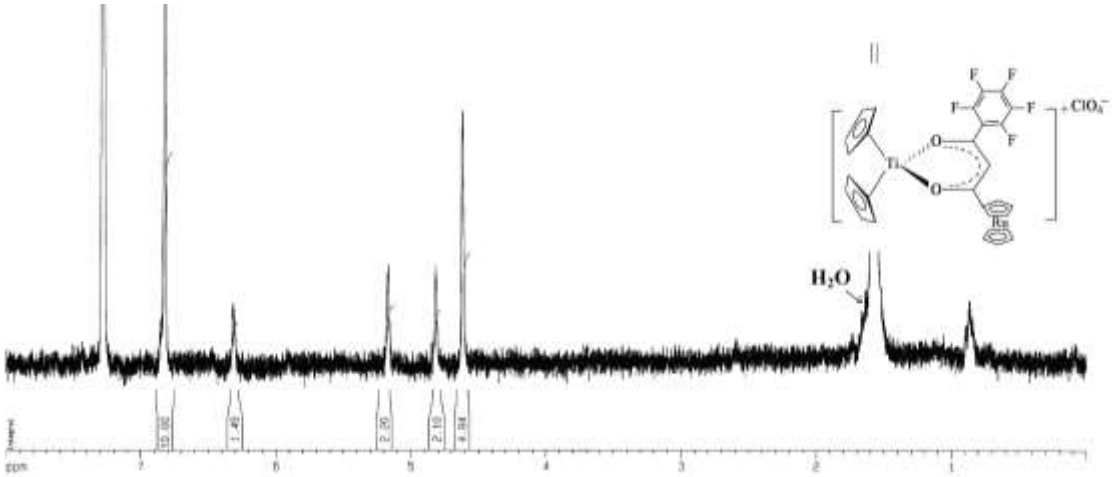

Spectrum 78: 1-Ruthenocenyl-3-undecylprop-1,3-dionato-κ^2O,O'-bis(η^5-cyclopentadienyl)titanium(IV) perchlorate, 198 in $CDCl_3$

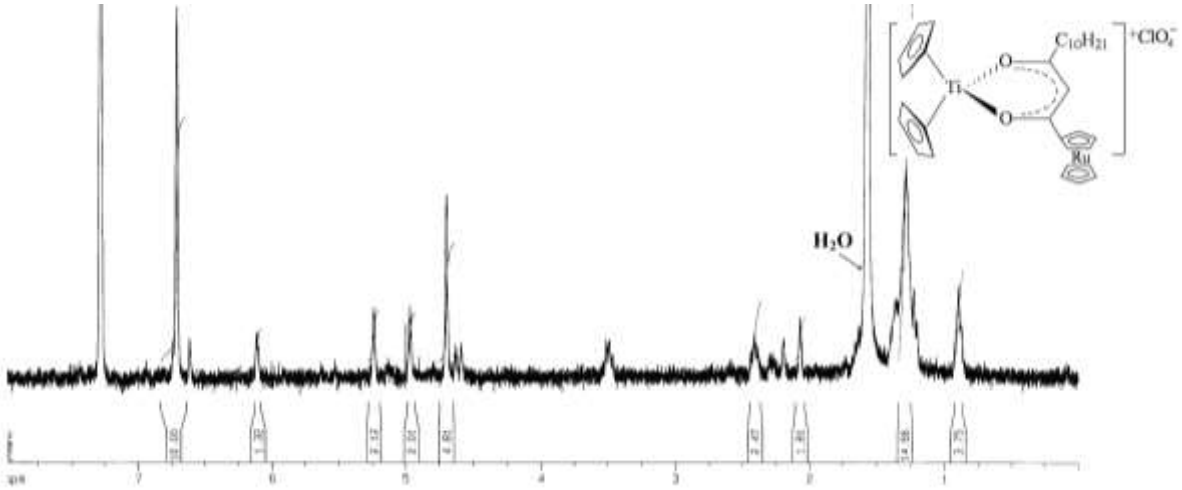

Spectrum 78(a): 1-Ruthenocenyl-3-undecylprop-1,3-dionato-κ^{2}O,O'-bis(η^5-cyclopentadienyl)titanium(IV) perchlorate, 198 in acetone d_6

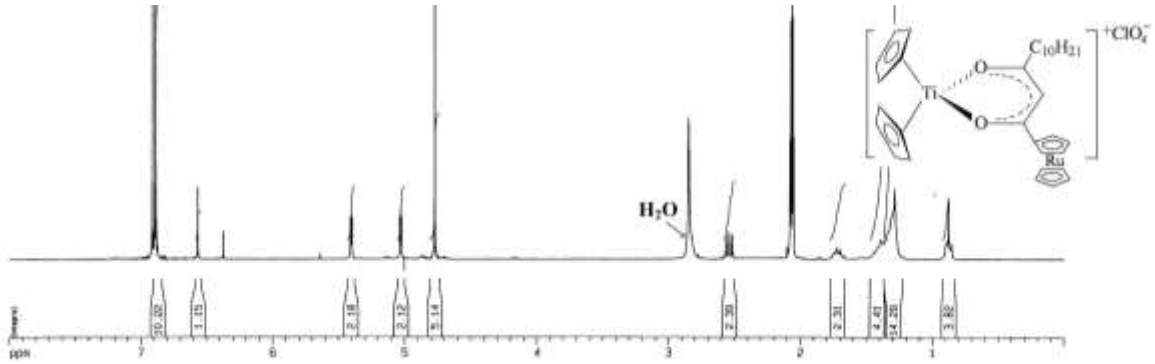

Spectrum 79: 1-Ruthenocenyl-3-perfluoroundecylprop-1,3-dionato-κ^{2}O,O'-bis(η^5-cyclopentadienyl)titanium(IV) perchlorate, 195 in $CDCl_3$

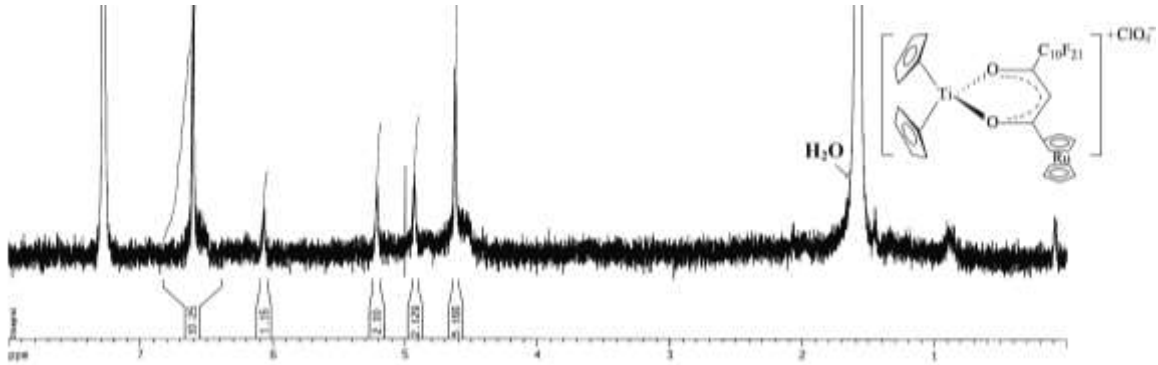

Spectrum 79(a): 1-Ruthenocenyl-3-perfluoroundecylprop-1,3-dionato-κ^{2}O,O'-bis(η^5-cyclopentadienyl)titanium(IV) perchlorate, 195 in acetone d_6

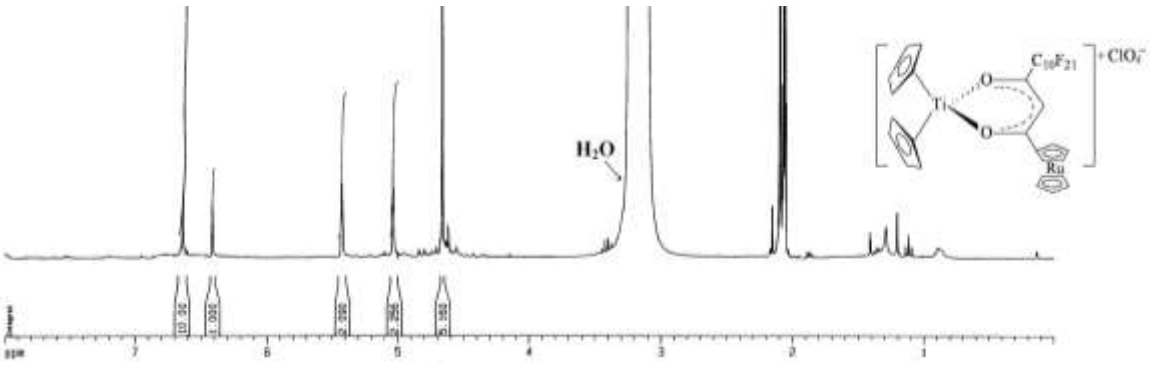

Spectrum 80: Methyl perfluoroundecanoate, 236

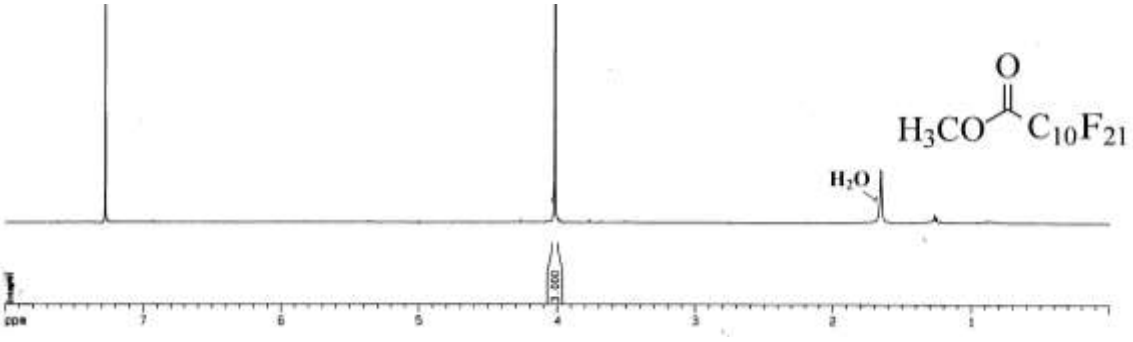

Spectrum 81: 1-H-1,2,3-Benzotriazol-1-ylethanone, 181

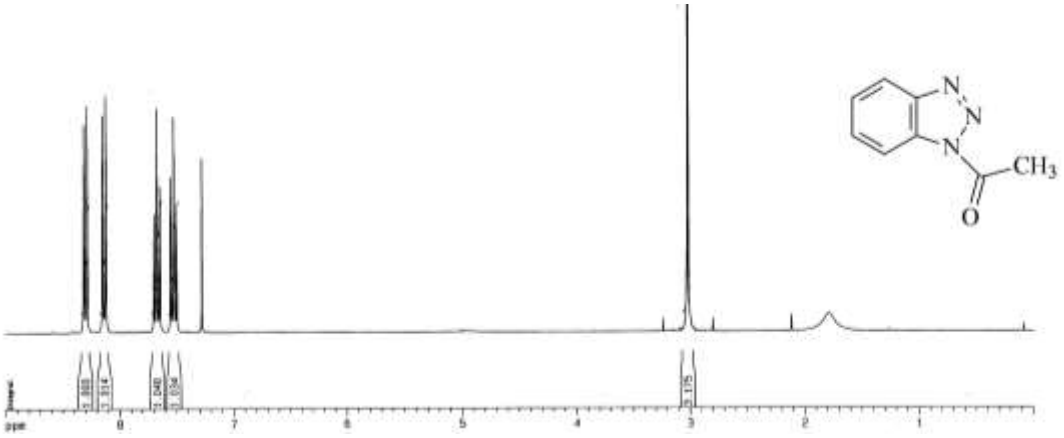

Spectrum 82: Tetrabutylammonium tetrakis[pentafluorophenyl]borate, 243

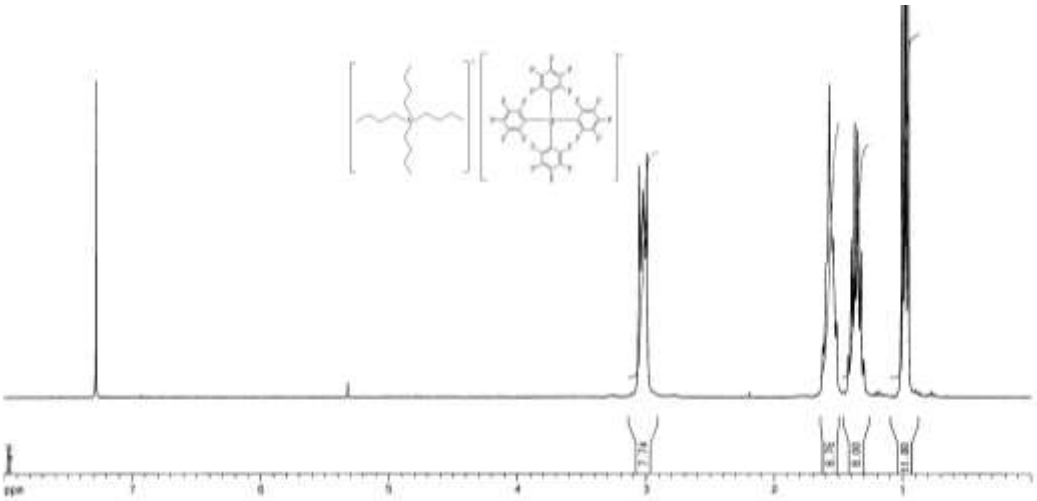

Abstract

In this study, ruthenocene-containing β-diketones, ruthenocene-, cobalticenium- and/or ferrocene- containing enaminones and ruthenocenyl and/or ferrocenyl containing titanium(IV) complexes were synthesised. Forty seven of these compounds were previously unknown.

The keto-enol isomerization kinetics of the β-diketones $RcCOCH_2COR$ with R = $C_{10}F_{21}$, CF_3, C_6F_5, $C_{10}H_{21}$, CH_3, Rc and Fc have been studied by ^1H NMR spectroscopy in CD_3CN. The influence of the solvent on this equilibrium has also been investigated utilising CD_2Cl_2 and $CDCl_3$ as different solvents.

The substitution reactions of the monodentate ferrocene-containing alkoxy groups of $[Ti(O(CH_2)_nFc)_2(RcCOCHCOCH_3)_2]$ {n = 1, 2, 3} with $HO(CH_2)_nFc$ {n = 2, 3, 4} and the substitution of the bi-dentate β-diketonato ligand of $[Ti(O(CH_2)_4Fc)_2(RcCOCHCOR)_2]$ {R = CH_3, CF_3} with $RcCOCH_2COR$ {R = CH_3, CF_3} is reported. Both revealed large positive entropy values, which suggest a dissociative substitution mechanism.

Electrochemical studies were conducted in dichloromethane in the presence of $[NBu_4][B(C_6F_5)_4]$ as uncoordinating supporting electrolyte. All ruthenocene-containing complexes exhibited chemically and electrochemically irreversible behaviour for the Ru^{3+}/Ru^{2+} and Ti^{4+}/Ti^{3+} couples. In contrast, the Fc/Fc^+ couples were mostly found to be electrochemically quasi-reversible and chemically reversible. It was found that E^{01}, E_{pa} and E_{pc} are dependent on either the alkyl chain length of the ferrocene-containing alkoxy group or the group electronegativity of the R-group of the β-diketonato ligand in all complexes.

Cytotoxic studies revealed that complexes $[(C_5H_5)_2Ti(RcCOCHCOR)]^+ClO_4^-$, $TiCl_2(RcCOCHCOR)_2$ and $Ti(O(CH_2)_4Fc)_2(RcCOCHCOR)_2$, (R = $C_{10}F_{21}$, CF_3, C_6F_5 or Fc), which contains more than one antineoplastic moiety, were the most effective in killing CoLo and HeLa cancer cell lines. These results are probably due to a synergistic effect between different fragments possessing anti-cancer activity in the same molecule.

Phase change studies of the complexes containing the long alkyl chains (R = $C_{10}H_{21}$, $C_{10}F_{21}$) and the crystal structure of $[(C_5H_5)_2Ti(RcCOCHCOCH_3)]^+ClO_4^-$ are also reported.

***Keywords*:** Titanium, ruthenocene, ferrocene, β-diketones, electrochemistry and cytotoxicity.

Opsomming

In hierdie studie is ferroseenbevattende alkohole, rutinoseenbevattende β-diketone, rutinoseen-, kobaltisenium- en/of ferroseenbevattende enaminone en rutinoseen- en/of ferroseenbevattende titanium(IV) komplekse gesintetiseer. Sewe-en-veertig van hierdie verbindings, was tot nog toe totaal onbekend.

Die keto-enol isomerisasie kinetika van die β-diketone $RcCOCH_2COR$ met R = $C_{10}F_{21}$, CF_3, C_6F_5, $C_{10}H_{21,}$ CH_3, Rc en Fc is met behulp van ^1H KMR spektroskopie in CD_3CN bestudeer. ‘n Oplosmiddel invloed op hierdie ewewig is ook met behulp van CD_2Cl_3 en $CDCl_3$ as oplosmiddels nagevors.

Die subsitutusie reaksies van die monodentate ferroseenbevattende alkoksiegroepe vanaf $[Ti(O(CH_2)_nFc)_2(RcCOCHCOCH_3)_2]$ {n = 1, 2, 3} met $HO(CH_2)_nFc$ {n = 2, 3, 4}asook die bi-dentate β-diketonato ligande van $[Ti(O(CH_2)_4Fc)_2(RcCOCHCOR)_2]$ {R = CH_3, CF_3} met $RcCOCH_2COR$ {R = CH_3, CF_3}is gerapporteer. In beide gevalle is groot positiewe entropie waardes gekry. Hierdie resultaat impliseer ‘n dissosiatiewe substitusie meganisme.

Elektrochemiese studies is uitgevoer in dichlorometaan in die teenwoordigheid van $[NBu_4][B(C_6F_5)_4]$ as nie-koordinerende ondersteuningselektroliet. Alle rutinoseen- en titaniumbevattende komplekse vertoon chemiese en elektrochemiese onomkeerbaarheid vir die Ru^{2+}/Ru^{3+} en Ti^{4+}/Ti^{3+} koppels. Daarteenoor het die meeste van die Fc/Fc^+ koppels elektrochemiese quasi-omkeerbare en chemiese omkeerbare gedrag getoon. Dit is bevind dat E^{01}, E_{pa} en E_{pc} afhanklik is van óf die alkiel ketting lengte van die ferroseenbevattende alkoksie groep óf die groep elektronegatiwiteit van die R-groep van die β-diketonato ligand in alle komplekse.

Sitotoksiese studies het getoon dat komplekse soos $[(C_5H_5)_2Ti(RcCOCHCOR)]^+ClO_4^-$, $TiCl_2(RcCOCHCOR)_2$ en $Ti(O(CH_2)_4Fc)_2(RcCOCHCOR)_2$, (waar R = $C_{10}F_{21}$, CF_3, C_6F_5 of Fc) wat meer as een antineoplastiese fragment bevat, meer effektief CoLo en HeLa kankersellyne dood. Hierdie resultaat is moontlik toe te skryf aan ‘n sinergistiese effek wat tussen die verskillende kankerbestrydende molekulere fragmente bestaan.

Fase eienskappe van die komplekse wat lang kettings bevat (R = $C_{10}H_{21,}$ $C_{10}F_{21}$) is ook bestudeer en die kristal struktuur van $(C_5H_5)_2Ti(RcCOCHCOCH_3)]^+ClO_4^-$ is gerapporteer.

Sleutelwoorde: Titanium, rutinoseen, ferroseen, β-diketone, elektrochemie en sitotoksisiteit.

I, Elizabeth Erasmus, declare that the dissertation hereby submitted by me for the Philosophiae Doctor degree at the University of the Free State is my own independent work and has not previously been submitted by me at another university/facility. I therefore cede copyright of the dissertation in favour of the University of the Free State.

Signed …….. Date ……...